Dissertation zur Erlangung des Doktorgrades
der Fakultät für Chemie und Pharmazie
der Ludwig-Maximilians-Universität München

Energetic Materials Based on 1,2,3-Triazoles and Open-Chain Nitramines

Carolin Pflüger

aus

Wuppertal, Deutschland

2016

Erklärung

Diese Dissertation wurde im Sinne von § 7 der Promotionsordnung vom 28. November 2011 von Herrn Prof. Dr. Thomas M. Klapötke betreut.

Eidesstattliche Versicherung

Diese Dissertation wurde eigenständig und ohne unerlaubte Hilfe erarbeitet.

München, den 10. Mai 2016

Carolin Pflüger

Dissertation eingereicht am:	10. Mai 2016
1. Gutachter:	Prof. Dr. Thomas M. Klapötke
2. Gutachter:	Prof. Dr. Konstantin Karaghiosoff
Mündliche Prüfung am:	09. Juni 2016

Meiner geliebten Familie

und im Gedenken
an meinen Großvater
Eugen C. H. Schnabel
1928–2003

Danksagung

Mein Dank gilt zuallererst meinem Doktorvater Herrn Prof. Dr. Thomas M. Klapötke für die Aufnahme in seinen Arbeitskreis, die interessante Themenstellung sowie uneingeschränkte Unterstützung und Freiheiten in der Forschung. Für die finanzielle Unterstützung, die Teilnahme an Fortbildungen und die Möglichkeit meine Ergebnisse auf internationalen Konferenzen vorzustellen, möchte ich meine Dankbarkeit für das in mich gesetzte Vertrauen aussprechen.

Herrn Prof. Dr. Konstantin Karaghiosoff danke ich für die Übernahme des Zweitgutachtens der Dissertation und besonders für die Einführung und Einarbeitung in die faszinierende Welt der Kristallographie, seinen unerschütterlichen Optimismus und seine Hilfsbereitschaft sowie etliche Anekdoten zur Auflockerung des Alltags.

Die Erstellung dieser Arbeit wurde durch ein Promotionsstipendium der Konrad-Adenauer-Stiftung gefördert. Mein Dank richtet sich daher an die Konrad-Adenauer-Stiftung sowohl für die finanzielle als auch für die ideelle Förderung. Besonders die zahlreichen Seminare und Veranstaltungen zum Beispiel in Schloss Eichholz und Schloss Wendgräben werden mir in Erinnerung bleiben.

Herrn Dieter Ehlers und Herrn Dr. Hans-Albrecht Krug von Nidda vom Departement Physik der Universität Augsburg danke ich für die Durchführung der EPR Experimente.

Herrn Dr. Jörg Stierstorfer gilt mein Dank für unzählige Anregungen, Diskussionen und Hilfestellungen sowie die akribische Korrektur sämtlicher Schriftstücke. Des Weiteren danke ich ihm für die Durchführung teambildender Maßnahmen im Arbeitskreis, insbesondere der Kochrunde.

Herrn Prof. Dr. J. Evers danke ich für den Exkurs in die Festkörperchemie durch die Zusammenarbeit im Bereich der Hochdruck-Raman-Spektroskopie und seine Geduld bei der notwendigen Justierung für die Messungen. Seine Begeisterung für die Wissenschaft und seine zahllosen unterhaltsamen Geschichten zu deren Entwicklung verdienen eine besondere Erwähnung.

Herrn Dr. Burkhard Krumm gilt mein Dank für die Aufnahme aller ^{15}N NMR Spektren, sowie Anregungen und Hilfestellungen jeglicher Art.

Frau Irene Scheckenbach danke ich für ihr Organsationstalent und ihre Unterstützung in allen bürokratischen Angelegenheiten.

Allen im Laufe meiner Promotion anwesenden Kollegen im Arbeitskreis danke ich für die stets sehr gute freundschaftliche Arbeitsatmosphäre. Besonderer Dank geht an alle Doktoranden des Labors D3.100 Dr. Quirin Axthammer, Thomas Reith, Regina Scharf und Dr. Michael Weyrauther für diverse fachliche und weltanschauliche Diskussionen, die Einführung in die *boarische* Sprache und Kultur sowie das Vorhalten eines nahezu unerschöpflichen Vorrats an Süßigkeiten.

Dr. Alexander Dippold, Dr. Dániel Izsák und Dr. Alexander Penger danke ich für die gute Zusammenarbeit im Bereich der energetischen Materialien.
Des Weiteren danke ich Dr. Alexander Penger für die Einführung in das spannende Arbeiten mit hochenergetischen Materialien.
Dr. Quirin Axthammer danke ich für die gute Zusammenarbeit in unserer "Kältekammer" im Bereich der Kristallographie.
Außerdem möchte ich Dr. Quirin Axthammer, Dr. Dániel Izsák und Regina Scharf für das sorgfältige Korrekturlesen etlicher Kapitel danken. Dr. Dániel Izsák danke ich ebenfalls für die Einführung in ein alternatives Textverarbeitungsprogramm und Hilfe bei diversen Formatierungsfragen.

Ein besonderer Dank geht auch an meine Bacheloranden und Praktikanten Timo Brünger, Dominik Gelsheimer, Ferdinand Lutter, Markus Reintinger, Florian Speck und Stefan Strangmüller, die alle mit viel Engagement einen erheblichen Beitrag zu dieser Arbeit geleistet haben.

Meinen Freunden Annalena, Angi, Boba, Carina, Carla, Dajana, Diana, Fabian, 2x Felix, Gideon, Johannes, Harald, Henning, Katrin, Lars, Martina, Nicole, Rebekka, Sarah, Susanna, 2x Tobi und natürlich meinem "Hauskeis Schwabing" gilt mein Dank für alle Unterstützung und Ablenkung sowie Verständnis in den vergangenen Jahren.

Nicht zuletzt geht mein Dank an meine Familie, insbesondere an meine Eltern, die mir durch ihre Liebe und unermessliche Unterstützung dies alles ermöglicht haben. Meinen großartigen Brüdern Lars und Gero danke ich für jegliche Ablenkung und dafür, dass ich mich immer auf sie verlassen kann.

Table of Contents

List of Figures

List of Schemes

List of Tables

Introduction

1.1 Historical Background

The history of energetic materials is well chronicled and therefore only a brief review over selected milestones in their development is given.
In 220 BC Chinese alchemists wanted to separate gold from silver during a low-temperature reaction using potassium nitrate (saltpeter) and sulfur. But they forgot to add charcoal in the first step and tried to fix their mistake by adding it to the ore in the last step, which resulted in an explosion.[1] This accidental discovery of blackpowder, also known as gunpowder, was most likely the first energetic composition, containing charcoal and sulfur as fuel and potassium nitrate as oxidizer, and therefore the beginning of the chemistry of explosives, their development and application. In Western Europe the discovery of blackpowder was considerably later when the English monk Roger Bacon experimented with potassium nitrate in the 13th century and produced blackpowder.[1] The study of its properties by the German monk Berthold Schwartz starting in 1325 probably had a great impact on the adaption of blackpowder in Central Europe. At first blackpowder was used to breach walls for military purposes but later on also for civil applications, especially for blastings in mining.
By the middle of the 19th century with rapidly advancing industrialization the limitations of blackpowder, especially in coal mining, led to the development of new explosives. Ascanio Sobrero, an Italian chemist, discovered nitroglycerine and detected its explosive nature but he stopped further investigations.[1] In 1863 Immanuel Nobel and his son Alfred commercialized the synthesis of nitroglycerine. Nitroglycerine was difficult to handle because of its impact sensitivity and the initiation with blackpowder was often unreliable. Its drawbacks were unreliable initiation and accidental explosions. After the death of his brother Emil by an unintended explosion, Alfred Nobel focused on safety issues. His efforts led to the development of guhr dynamite, which was protected by a patent in 1867. In dynamite nitroglycerine is taken up in the absorbent clay called “kieselguhr” to reduce its sensitivity.
For military purposes blackpowder was first replaced by picric acid in 1888. Unfortunately, picric acid suffers from the formation of highly sensitive metal salts by corrosion of the shells. Picric acid was substituted by the much less sensitive trinitrotoluene (TNT), which became the standard explosive in World War I.
Research in the field of higher performing explosives for military use was ongoing and by World War II pentaerythritol tetranitrate (PETN) and 1,3,5-trinitro-1,3,5-triazine (RDX)

were widely used. RDX was synthesized and patented by Georg Friedrich Henning in 1898 for medical purposes with regard to cardiac insufficiency.[2] Its energetic properties were discovered by Edmund von Herz in 1920.[3] The most relevant process to obtain RDX was the Bachmann process, which afforded RDX in high yield but with impurities of octogen (HMX). The later Brockman process yielded pure RDX.
While other explosives had been investigated for special applications requiring higher performance or lower sensitivities, none had been used as widely as RDX in the 20th century.
A main approach in the last century had been the process of plastification to obtain polymer bonded explosives (PBX) with reduced sensitivities to enable safer handling of these materials.[4] In the beginning inert, non-energetic binders such as polystrene were used, while the recent trend is to replace the non-energetic with energetic binders, which are in most cases covalent azides or nitrate esters.
Nowadays, the applications for military and civilian uses in mining, oil production, demolition, construction, and safety equipment such as airbags, signal flares, and fire extinguishing systems are extensively studied. The most recent developments in research of energetic materials focuses on the synthesis of compounds with either outstanding thermal or mechanical stability or high performance. The academic research mainly investigates on the synthesis and properties of novel energetic materials to determine factors affecting thermal and mechanical stability and performance and to develop new strategies in the design of energetic materials.

1.2 Definition and Classification of Energetic Materials

Energetic materials are used in a wide variety of different applications. Therefore, a definition of these materials and their subsequent classification is necessary to distinguish the wide area of applications and development. In general, energetic materials are defined by the American Society for Testing and Material as “a compound or mixture of substances which contain both the fuel and the oxidizer and reacts readily with the release of energy and gas”.[5] The entirety of energetic materials is divided in three main categories:

i) explosives

ii) propellants

iii) pyrotechnics

The class of explosives is further divided into primary and secondary (high) explosives depending on their type of initiation and energetic behavior.

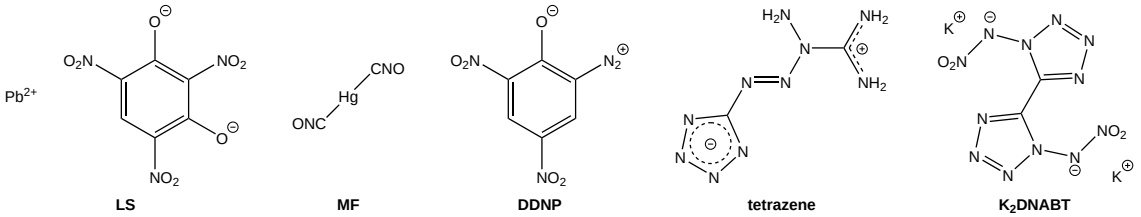

Figure 1.1: Molecular structures of lead styphnate (LS), mercury fulminate (MF), 2-diazo-4,6-dinitrophenol (DDNP), tetrazene, and dipotassium 1,1′-dinitramino-5,5′-bitetrazolate (K_2DNABT).

Primary Explosives are very sensitive explosives, which can be easily initiated by a simple initiating impulse (SII) and are therefore used as initiators for the main charges. In contrast to secondary explosives, they are able to detonate by thermal initiation even in an unconfined state. The initiation of primary explosives leads to a fast deflagration-to-detonation transition (DDT) in which the subsonic heat transfer of the decomposition becomes so fast that it transforms into a supersonic shock wave.[6] The shock wave is able to initiate the less sensitive main charge, typically a secondary explosive. Various external stimuli can serve as SII, mainly impact, friction, heat or an electric spark are applied. The impact sensitivity of primary explosives is usually less than 4 J and their friction sensitivity is less than 10 N.[4] The detonation velocities are in the range of 3500 to 5500 $m\,s^{-1}$ and considerably lower than the ones of secondary explosives. Historically common well known primary explosives are lead(II) azide (LA), lead(II) styphnate (LS), and mercury fulminate (MF) (Figure 1.1). Research is ongoing to replace these explosives, which suffer from the high toxicity of the heavy metal cations, by salts with less toxic metal cations (silver, copper, iron) or metal-free primary explosives. Representatives of these more environmental friendly explosives are 2-diazo-4,6-dinitrophenol (DDNP), tetrazene, and dipotassium 1,1′-dinitramino-5,5′-bitetrazolate.[7,8]

Secondary Explosives are much more stable toward outer stimuli than primary explosives and are usually kinetically (meta)stable compounds.[4] On account of this higher stability, they have to be initiated by much stronger stimuli. In general, a shock wave generated by a primary explosive is applied. After the initiation the shock wave propagates the reaction front through the unreacted material. Although secondary explosives are not as readily initiated as primary explosives, they exhibit much higher detonation performances with detonation velocities in the range of 6500 to 9000 $m\,s^{-1}$. Commonly used secondary explosives for mainly military applications are TNT, RDX, its higher homologue octogen (HMX), nitroguanidine (NQ), triaminotrinitrobenzene (TATB), and 1,1-diamino-2,2-dinitroethene (FOX-7) as well as hexanitrostilbene (HNS) and NG (in the form of dynamite for commercial use) for civil

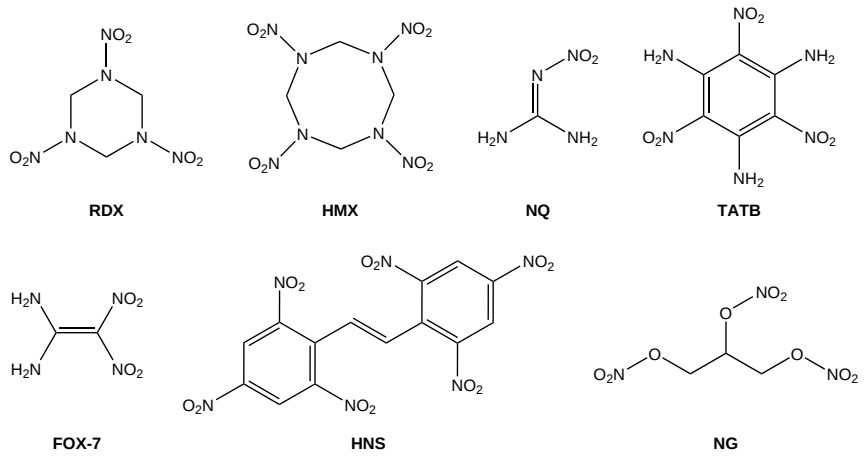

Figure 1.2: Molecular structures of common secondary explosives.

applications (Figure 1.2).

Propellants should not detonate, in contrast to primary and secondary explosives, but only burn or deflagrate. They are divided in two main classes, the propellant charges and rocket propellants.

Propellant charges are normally formulations containing both fuel and oxidizer. Single-based propellant charges for use in weapons from pistols to artillery weapons consist of nitrocellulose (NC).[4] Nitrocellulose shows an advantageous burning behavior, which leads to residue-free burning. To improve the performance, double-based and triple-based propellants were developed based on nitrocellulose and used for charges in tank and naval artillery ammunition. Double-based propellants containing nitrocellulose and nitroglycerin have an improved performance but unfortunately accompanied by higher combustion temperatures, which result in a higher rate of erosion of the gun barrel. For this reason triple-based propellants consisting of nitrocellulose, nitroglycerin and nitroguanidine were developed.

Since the insensitivity of propellant charges gains in importance, propellants with reduced sensitivities have been investigated under the purpose of low-vulnerability ammunition (LOVA).[4] In the worst case scenario they only should respond to bullet impact, shaped charged impact or fire with fire but not with a deflagration and in no case with a detonation. LOVA propellants contain mainly RDX or HMX as energetic fillers.

The scope of application and hence the required properties of rocket propellants differ from those of propellant charges. Similar to propellant charges, they combust in a controlled manner and do not detonate but they burn considerably slower.[4] Rocket propellants are distinguished in solid and liquid propellants. Solid rocket propellants are either homogeneous (e.g. nitrocellulose and nitroglycerin) or heterogeneous (composite propellants, e.g.

nitrocellulose and aluminum) mixtures. Liquid propellants are divided in monopropellants (hydrazine) and bipropellants, which are further divided into hypergolic containing both oxidizer and fuel (e.g. HNO_3 and hydrazine/monomethylhydrazine) and non-hypergolic propellants (O_2/H_2).
The most important characteristic of the performance of rocket propellants is the specific impulse, the change of the impulse (impulse = mass × velocity (or force) × time) per mass unit of the propellant.[4] It is a measure for the effectiveness of a propellant composition by showing the effective velocity of the combustion gases when leaving the nozzle. In English speaking areas the specific impulse (I_{sp}) is given based on the gravitation of the earth ($g = 9.81\,m\,s^{-1}$) and has the unit seconds (s). Therefore, the specific impulse is proportional to the square root of the ratio of the temperature of the combustion chamber (T_C) and the average molecular mass of the combustion products (M) (Equation 1.1). By an increase of the specific impulse by 20 s, the carried payload, for example warheads or satellites, can be approximately doubled.

$$I_{sp} \propto \sqrt{\frac{T_C}{M}} \tag{1.1}$$

Pyrotechnics are traditionally mixtures, which produce an effect by heat, light, sound, gas or smoke, or a combination of these, by a non-detonative self-sustaining exothermic chemical reaction.[4] In general, pyrotechnics consist of an oxidizer and a reducing agent. Furthermore, they could contain a binder, a propellant charge, a colorant, or noise and smoke generating additives depending on their intended application. The heat generating pyrotechnics are used for priming charges, detonators, and first fires in propellant charges. Smoke generating pyrotechnics are employed for signaling and camouflage purposes. The most popular use of light generating pyrotechnics is their application in fireworks but they are also used for military purposes such as illumination (visible and infrared) and decoy flares as aerial infrared countermeasure used by an aircraft to counter an infrared homing ("heat-seeking") surface-to-air missile or air-to-air missile.

1.3 Secondary Explosives: Performance and Physicochemical Properties

Energetic materials store relatively large amounts of energy, which are easily released upon initiation.[4] In a deflagration the propagation of the reaction occurs as a result of thermal processes, whereas in the faster detonation the reaction front propagates by a shock wave mechanism. In the detonation of an energetic compound an initial stimulus as input of energy is followed by a series of steps cumulating in a self-sustaining, highly exothermal

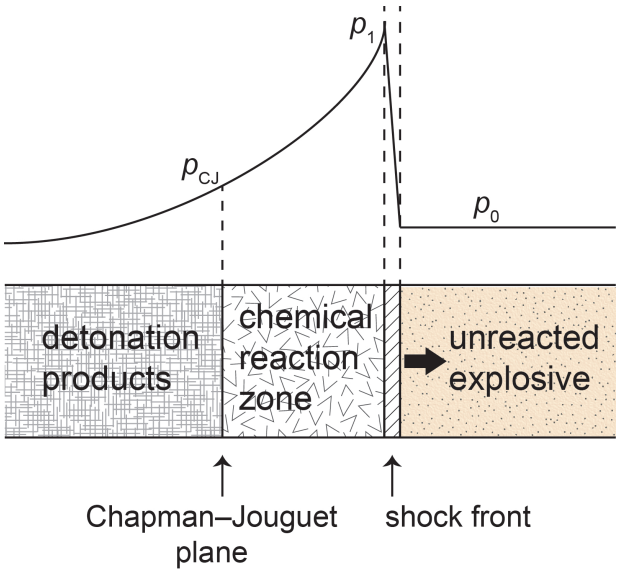

Figure 1.3: Schematic representation of the detonation process with regard to the pressure and the shock wave structure.

chemical decomposition releasing large amounts of energy and gaseous products. This results in a detonation by a supersonic shock wave propagating through the system.[9,10] Most of the energy of classical secondary explosives is either derived from oxidation of their carbon backbone, whereas the energy of modern explosives is mostly derived from their high enthalpies of formation.

In general, secondary explosives are initiated by the shock wave of a detonating primary explosive.[4] The shock wave compresses the secondary explosive, thereby increasing the temperature above the decomposition temperature through adiabatic heating, which results in a reaction of the explosive material directly behind the shock wave front, whereby the pressure increases from p_0 to p_1 (Figure 1.3). The shock wave accelerates due to the strongly exothermic reaction of the secondary explosive. Therefore, the density of the explosive shortly before the reaction zone increases to 1.3–1.5 times the maximum density of the crystal, while in the thin (up to ca. 0.2 mm) chemical reaction zone directly behind the shock wave front temperatures up to 3000 K and pressures above 330 kbar occur. If the shock wave propagates through the explosive with velocities faster than the speed of sound, the process is described as detonation. The shock wave propagates under constant acceleration until it reaches a stationary state. At the stationary state, the free energy released by the exothermic chemical reaction is the same as the sum of the energy, which is released to the surroundings as heat, and the energy, which is needed to compress and move the crystal, and thereby the propagation of the shock wave becomes a self-sustaining process.

The energy is released upon initiation as heat and can be described as difference of the enthalpies of formation of the energetic material and its decomposition products. The

heat of explosion (Q_v), which is normally given at constant volume, can be calculated applying the Hess's law, or it can be measured with a bomb calorimeter, and correlates to the released energy under adiabatic conditions. The composition of many explosives (appropriate numbers of carbon, hydrogen, nitrogen, and oxygen atoms) leads, apart from solid carbon, to very stable gaseous decomposition products e.g. dinitrogen, carbon monoxide and dioxide, and water.[11–13] Due to their low molecular masses high quantities of gaseous products can be released per gram of explosive, while their stabilities mean that a great amount of energy is released. The released volume of gaseous detonation products (V) is usually calculated for standard conditions (273 K and 1 bar) based on equations applying the ideal gas law.[4] The product of the heat of explosion and the volume of gaseous detonation products is defined as explosive power (Equation 1.2).

$$P = Q_v \times V \tag{1.2}$$

Furthermore, the heat of explosion usually depends on the oxygen balance Ω and becomes greater (more negative) for systems possessing a balanced oxygen content.[14] The oxygen balance is used to describe the relative amount of oxygen in excess or deficit to achieve the complete conversion of CHNO-containing explosives to carbon dioxide (or carbon monoxide, respectively), water and dinitrogen. For a compound with the general formula $C_aH_bN_cO_d$, the oxygen balance Ω (in %) is defined either with regard to CO_2 or CO as shown in Equation 1.3.

$$\begin{aligned} \Omega_{CO_2} &= \frac{\left(d - 2a - \frac{b}{2}\right) \times 1600}{M} \\ \Omega_{CO} &= \frac{\left(d - a - \frac{b}{2}\right) \times 1600}{M} \end{aligned} \tag{1.3}$$

The oxygen balance is not sufficient to estimate the thermodynamics of the reaction, but, particularly for compounds with highly negative oxygen balances, it is necessary to estimate how much of the oxygen is converted into CO, CO_2, and H_2O. An approximate scheme for the estimation of the detonation products in respect to the available oxygen content is given by the modified Springall–Roberts rules.[4]

Further characteristic parameters for the performance of energetic materials are their detonation velocity (D) and detonation pressure (p_{CJ}) at the Chapman–Jouguet point. The requirement of a chemical equilibrium between the reaction products is known as Chapman–Jouguet condition. This is described by the parameters at the Chapman–Jouguet point according to the classical Zel'dovich–Neumann–Döring (ZND) detonation model[4]

and can be regarded as a "stable" detonation, which can pass through the material in a stationary manner, that means at constant intensity and velocity.[10]
The detonation velocity is the rate of propagation of detonation in an explosive. It can be determined experimentally and it is characteristic for each explosive and not influenced by external factors, if the density of the explosive is at its maximum value and if it is charged into columns, which are wider than the critical diameter. Generally, the detonation velocity increases proportional to the density of the explosive.
Kamlet and Jacobsen suggested an empirical relationship between the detonation velocity and the detonation pressure (Equation 1.4). In this, the detonation velocity (D) is linear and the detonation pressure p_{CJ} even is exponentially dependent on the loading density (ρ_0). Therefore, the detonation pressure as well as the detonation velocity increase if the initial density of the explosive can be raised to its maximum (e.g. by casting or pressing) or if the crystal density, the limiting theoretically maximum density (TMD), is intrinsically high.

$$\begin{aligned} D &= \mathrm{A}\Phi^{0.5}(1 + \mathrm{B}\rho_0) \\ \rho_{\mathrm{CJ}} &= \mathrm{K}\rho_0^2\Phi \end{aligned} \tag{1.4}$$

with the constants A = 1.01, B = 1.30, and K = 15.88; $\Phi = N(M)^{0.5}(Q)^{0.5}$, where N is the number of moles of gas released per gram of explosive, M is the mass of gas in gram per mole of gas, and Q is the heat of explosion

The explosion temperature has to be distinguished from the detonation temperature.[10] The explosion temperature (T_{ex}) is the calculated temperature of the fumes of an explosive, which is supposed to have been detonated while confined in a shell assumed to be indestructible and impermeable to heat. The calculation is based on the heat of explosion (Q_{v}) and on the decomposition reaction regarding the formation of gases. On the other hand, the detonation temperature refers to the temperature of the front of the shock wave of a detonating explosive. It is higher than the calculated explosion temperature and can be estimated by the hydrodynamic shock wave theory.
The brisance, which is the destructive fragmentation effect of an explosive on its immediate surrounding, is determined mainly by its detonation pressure, and as a consequence by its loading density. The loading density ρ_0 is an important parameter in the performance characteristics of brisant explosives and propellant powders due to the necessity to ensure the strongest possible propellant effect in the loaded chamber. It refers to the ratio between the weight of the explosive and the space in which the explosive is detonated (explosion volume), whereas for powders the loading density is the maximum weight of the powder

and the space into which it is loaded.

In the context of energetic materials, the term sensitivity refers to the initiating capability of the material to result in a detonation. The sensitivities of energetic materials toward outer stimuli are important with respect to their safe synthesis, manipulation, transport, and storage as well as their scope of application. Since initiation by outer stimuli can also be caused accidentally, a main focus of research in the field of energetic materials is the challenge to diminish the sensitivity while maintaining reliable initiation and high performance. Various models and theories to correlate the sensitivities and initiating capability with specific molecular or crystal properties have been developed.[15,16] Therefore, the understanding and modelling of the initiation processes involves the areas of continuum mechanics, chemistry, and quantum chemistry.[17] However, it is important to keep in mind that a correlation does not necessarily imply a causal relationship because it may simply be symptomatic.[18]

According to the theory of Bowdern and Yoffe, the initiation of explosives is caused by the formation of the so-called "hot spots" that are leading to concentrated energy build-up at defect sites of the crystal lattice.[19] The stress delivered by outer stimuli like impact or friction can be regarded as thermal energy, which is located at areas with a diameter of 10^{-3} to 10^{-5} cm, temperatures of over 700 K, and a life span of 10^{-6} s. The transformation of the delivered energy from the lattice vibration to vibrations leads to an endothermic bond cleavage, which finally results in the exothermic decomposition. The requirement for such an exothermic decomposition is a sufficient diameter and temperature of the "hot spots", otherwise they would dissolve by thermal diffusion. They occur at lattice defects, which might be caused by vacant lattice positions, dislocations, inclusions of gas bubbles or impurities.

The multi-phonon up-pumping model, expects preferential "up-pumping" (or excitation) of specific vibrational modes at defect sites compared to the other sites in the crystal lattice.[17] This model is used to correlate the velocity of the energy transfer from "hot spots" to the molecular vibrational modes.

The trigger linkage concept takes into account the rupture of a specific type of bond as a key step in the initiation of a detonation.[20] The term "trigger linkage" is used for bonds that are expected to be the first to undergo a bond cleavage in a decomposition reaction. While considerable evidence points to the importance of trigger linkages such as C$-$NO$_2$ and N$-$NO$_2$ bonds in many nitroaromatic and nitroheterocyclic explosives, there are in some cases further indications of other initiating processes.

Especially the impact sensitivity, usually within a given class of structural related compounds, has been correlated with various features of certain bonds such as electronic energy levels, heats of fusion and sublimation, NMR chemical shifts, vibrational energy transfer,

and molecular stoichiometry.[15,18,21,22]

According to Murray and Politzer, the impact sensitivities within three classes of compounds (nitroaromatics, nitroheterocycles, and nitramines) correlate with features of their molecular surface electrostatic potentials (ESPs).[23–26] The molecular surface ESP can be either computed by quantum chemical calculations from the electron density or determined by diffraction measurements. The electrostatic potential ($V(r)$) is defined as shown in Equation 1.5, where Z_i and R_i denote the charge and position of the nucleus of atom i and $\rho(r)$ is the electronic density.

$$V(r) = \sum_i \frac{Z_i}{|R_i - r|} - \int \frac{\rho(r')dr'}{|r' - r|} \tag{1.5}$$

While an imbalance between stronger positive regions and weaker negative ones is uncommon for organic molecules in general, it is characteristic for the three previously mentioned classes of energetic compounds. According to these studies, larger electron-deficient areas above aromatic rings and C−NO_2 and N−NO_2 bonds indicate instability, which subsequently leads to more sensitive compounds.

The challenge in developing new explosives is based on three main demands which should be further improved: 1) performance, 2) safety, and 3) practicability (Figure 1.4).[27]

The requirements for new energetic materials for military as well as civil applications are manifold regarding performance and stability, meaning only a few explosives match all desired characteristics. High detonation performance can be achieved, as previously discussed, by materials with high density and high heats of formation, however, their sensitivity towards outer stimuli resulting in unintended detonation should be as low as possible to ensure their safe handling.

The main challenge is the combination of the desired high performance and low sensitivity

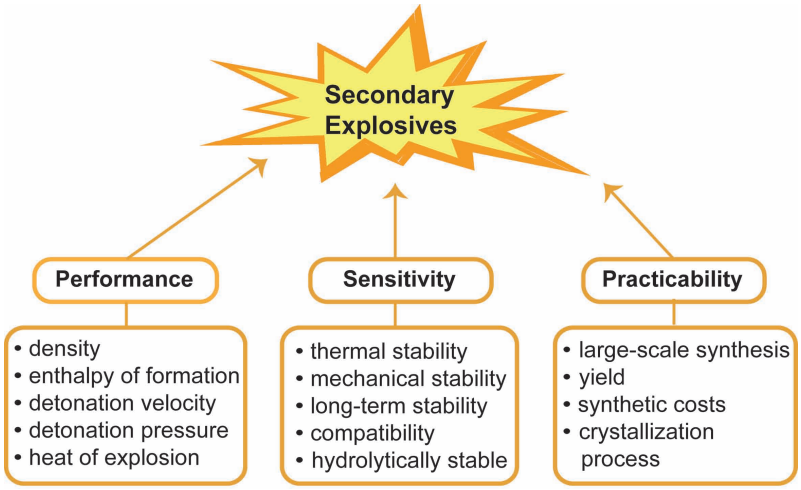

Figure 1.4: Demands for the development of new secondary explosives.

that are often contradictory.[28] The coherence of performance and sensitivity is for example established for the heat of explosion (Q), which rises with increasing sensitivity.[29] The potential for large-scale synthesis, yields, synthetic costs, and the crystallization process are included in the practicability. Furthermore, the environmental and toxicological acceptability is an increasing goal for secondary explosives.[1,4,30]

Many energetic materials, which are widely used nowadays, suffer from manifold drawbacks such as high toxicity, high sensitivity, or from a lack of performance for specialized applications. These drawbacks are the motivation for strong research efforts in the development of new secondary explosives. The widely used RDX as well as its degradation and decomposition products, which are found for example in the ground water in the vicinity of military training grounds and ammunition plants, are highly toxic towards plants, microrganisms, microbes, and also to organisms at the base of the food chain like the earthworm.[31–33] Furthermore, the US Environmental Protection Agency (EPA) categorized RDX as a potential carcinogen.[34] TNT and its degradation products are also ecologically toxic, causing damages for example in the liver and blood system and TNT itself is additionally classified as a potential carcinogen.[35]

Besides the improved environmental acceptability, enhanced physicochemical properties such as the detonation parameters and sensitivities towards outer stimuli are the goal in the design of new secondary explosives. The desired properties for new secondary explosives as RDX replacements are summarized in Table 1.1. The detonation velocity should exceed $8500\,\mathrm{m\,s^{-1}}$ and the detonation pressure should be higher than 340 kbar to ensure high performance. Besides the detonation parameters, the sensitivities toward impact, friction, and electrostatic discharge should be improved in comparison to RDX. Additionally, a thermal stability above 180 °C as well as a high long-term stability for the safe storage of the explosives are requested. Several selected chemical properties such as stability toward hydrolysis, compatibility with binder and plasticizer, smoke-free combustion as well as environmental acceptability are requested affecting their scope of application, their incorporation in mixtures, and exposure to the environment.

1.4 Motivation and Objectives

The benefits of developing new high-energy dense materials with a high nitrogen content combined with high positive enthalpies of formation are improved detonation performances and environmental acceptability. Furthermore, a large volume of nontoxic N_2 is produced upon detonation. The high enthalpies of formation result from the higher stability of the N≡N triple bond ($946\,\mathrm{kJ\,mol^{-1}}$) in comparison to the double ($418\,\mathrm{kJ\,mol^{-1}}$) and single ($159\,\mathrm{kJ\,mol^{-1}}$) bonds.[36] Therefore, suitable backbones are nitrogen-rich heterocycles such as

Table 1.1: Goals for the development of new high-energy dense materials (HEDMs).

Performance	detonation velocity	$D > 8500\,\mathrm{m\,s^{-1}}$
	detonation pressure	$p_{\mathrm{CJ}} > 340\,\mathrm{kbar}$
	heat of explosion	$-Q_{\mathrm{v}} > 6000\,\mathrm{kJ\,kg^{-1}}$
Stability	thermal stability	$T_{\mathrm{dec}} \geq 180\,^{\circ}\mathrm{C}$
	impact sensitivity	IS $> 7\,\mathrm{J}$
	friction sensitivity	FS $> 120\,\mathrm{N}$
	electrostatic discharge sensitivity	ESD $> 0.2\,\mathrm{J}$
Chemical properties	hydrolytically stable	
	compatible with binder and plasticizer	
	low water solubility (or nontoxic)	
	smoke-free combustion	
	long-term stability ($>$ 15 years under normal conditions)	

tetrazoles, triazoles and diazoles (Figure 1.5).[37] Additionally, new secondary explosives must exhibit high thermal stability and lower sensitivities to impact, friction, and electrostatic discharge to ensure safe handling. This concept of reduced sensitivity towards outer stimuli is particularly considered in the development of insensitive munitions (IM).

In regard to the requirements of detonation performance and safety the tetrazole and 1,2,3- as well as 1,2,4-triazole rings are the most promising backbones. The energetic properties of a large variety of tetrazoles and 1,2,4-triazoles are extensively studied. Only a relative small amount of energetic derivatives of 1,2,3-triazoles has been investigated, although the 1,2,3-triazole ring ($\Delta_f H(\mathrm{g})_{\mathrm{CBS4M}} = 231\,\mathrm{kJ\,mol^{-1}}$) possesses a higher enthalpy of formation than the 1,2,4-triazole ring ($\Delta_f H(\mathrm{g})_{\mathrm{CBS4M}} = 178\,\mathrm{kJ\,mol^{-1}}$) and therefore being more "energetic". The focus of this thesis is therefore on the synthesis and characterization of energetic materials composed of 1,2,3-triazole rings, which were either condensed to a benzene ring or linked with tetrazoles and 1,2,4-oxadiazole rings (Figure 1.6).

The dinitrobenzotriazole derivatives combine the characteristics of traditional explosives, which derive their energy by oxidation of the carbon backbone, and modern explosives, which derive their energy from the high enthalpies of formation. To improve the stability, amino groups should be introduced in *ortho* position of the nitro groups and thereby stabilize the C−NO_2 bonds by mesomerism.

Very promising is the combination of tetrazoles with 1,2,3-triazole rings. In general, tetrazoles are more energetic but also more sensitive towards external stimuli, whereas triazoles are less sensitive. The connectivity of the azoles is either established over an azo functionality or by a direct C−C linkage of both heterocycles. Thereby, symmetrically and asymmetrically substituted 1,2,3-triazoles are available. The introduction of various groups like amino and

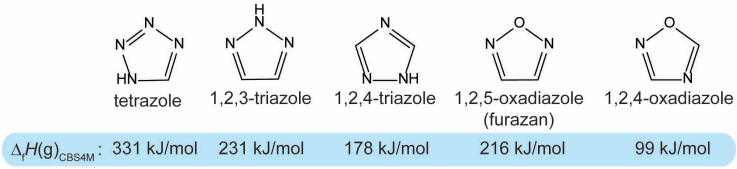

Figure 1.5: Promising nitrogen-rich heterocycles for the design of secondary explosives.

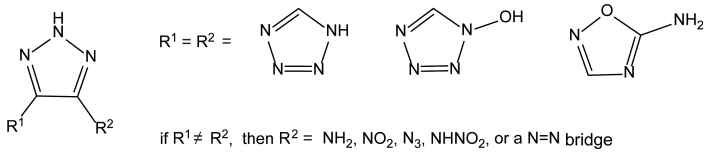

Figure 1.6: Possible symmetrically and asymmetrically substituted 1,2,3-triazoles.

the more energetic nitro, azido as well as a diazene bridge at the second carbon atom of the asymmetrically substituted 1,2,3-triazole enables the selective tailoring of energetic properties (Figure 1.6).

The energetic properties can be further tailored by introduction of an *N*-oxide to the heterocycle. It has recently been shown that the energetic performance of tetrazoles can be improved by formation of the corresponding *N*-hydroxy compounds.[38–40] Thereby the oxygen balance is increased and higher crystal densities and detonation performances are achieved. Furthermore, tetrazole *N*-oxides are usually less sensitive toward impact and friction.

The effect of the formation of energetic salts with nitrogen-rich cations on the thermochemical and physical properties as well as on the detonation parameters has been extensively studied and compared to known secondary explosives. Energetic salts show many advantages over conventional nonionic energetic compounds such as lower vapor pressures, reduced sensitivities, and often improved performances.[30,41,42] In general, the use of nitrogen-rich cations leads to higher enthalpies of formation, which thereby improve the detonation performance. Furthermore, the high acidity of the heterocyclic protons can cause compatibility problems in explosive charges,[43] which can be avoided by salt formations.

In addition to the salt formation, the drawbacks of the high acidity can be overcome by alkylation of the heterocyclic N−H function. Alkylation using nitramine containing side groups instead of alkyl groups is an interesting strategy to improve the energetic properties because the nitramine group may take part in intermolecular interactions as acceptor and donor for hydrogen bonds as well as for dipolar N···O and C···O interactions, which should cause higher densities in comparison to the methylated derivatives.[44,45] These open-chain nitramines often show promising thermal behavior and therefore being of interest as melt-cast explosives as potential TNT replacements. They additionally offer better performances than TNT, the most commonly used melt-cast matrix. In the second

part of this thesis this strategy is applied to various nitroazoles to enhance their stability, while introducing another energetic group.
The development of new high-energy dense materials with high performance as potential RDX replacements, guaranteed through high enthalpies of formation and high densities, is the major scope of this study. Due to their physicochemical and energetic properties, they are not exclusively used as explosives but for example like RDX also incorporated in propellant charges. Therefore, the attention may briefly turn to the application of these materials in propellant charges. The academic research interest mainly focuses on gaining a deeper understanding of factors affecting stability and performance as key to a more rational design of novel HEDMs with tailored properties for specialized applications.

Publications Most of the following chapters have been published as articles, or as parts thereof, in peer-reviewed scientific journals (*Chemistry – A European Journal*, *Dalton Transactions*, *European Journal of Inorganic Chemistry*, *Journal of Organic Chemistry*, *New Journal of Chemistry*) and as poster contributions at the annual international seminar *New Trends in Research of Energetic Materials* (2013–2015). The published articles were slightly modified to properly fit together as a thesis including additional minor improvements.

1.5 General Methods and Characterization

Caution! *Most compounds prepared herein are energetic compounds sensitive to impact, friction and electrostatic discharge. Although there were rarely any problems in handling the compounds, proper protective measures (ear protection, Kevlar® gloves, face shield, body armor and earthed equipment) and a plastic spatula should be used, especially when working with the oftentimes highly sensitive silver salts.*

Analytical Methods

NMR spectra were recorded using the spectrometers JEOL Eclipse 270, JEOL Eclipse 400, JEOL ECX 400, Bruker Avance III 400, Bruker 400 TR. The measurements were conducted in regular glass NMR tubes (⌀ 5 mm) and, if not stated otherwise, at 25 °C. Tetramethylsilane (^{1}H, ^{13}C) and nitromethane ($^{14/15}$N) were used as external standards. As additional internal standard the reference values of the partially deuterated solvent impurity (^{1}H) and the fully deuterated solvent (^{13}C) were used.[46]
Infrared (IR) spectra were recorded on a PerkinElmer BX FT IR spectrometer equipped with a Smiths DuraSamplIR II diamond ATR unit with pure samples. Transmittance values are qualitatively described as “very strong” (vs), “strong” (s), “medium” (m), “weak” (w) and “very weak” (vw).

Raman spectra were recorded on a Bruker RAM II spectrometer equipped with a Nd:YAG laser operating at 1064 nm and a reflection angle of 180° in open glass tubes (⌀ 5 mm). The intensities are reported as percentages of the most intense peak and are given in parentheses.
Low resolution mass spectra were recorded on a JEOL MStation JMS-700, with 4-nitrobenzyl alcohol as matrix for FAB measurements.
Determination of the carbon, hydrogen and nitrogen contents was carried out by combustion analysis using an Elementar Vario EL Analyser. The determined nitrogen values are often lower than the calculated ones, which is common for nitrogen-rich compounds and cannot be avoided. Highly energetic compounds, especially primary explosives, also often tend to give generally unsatisfactory measurements due to their explosive behavior.
Differential scanning calorimetry (DSC) was conducted with a Linseis DSC-PT10 in closed aluminum pans, equipped with a hole (⌀ 0.1 mm) for gas release, and a heating rate of 5 °C min^{-1}. Differential thermal analysis (DTA) was conducted with an OZM Research DTA 552-Ex in open glass tubes (diameter 4 mm, length about 47 mm) at a heating rate of 5 °C min^{-1}. The reported temperatures are not the extrapolated onsets (second derivation of the curve) but the beginning point of the signal for better comparison due to mostly broad signals. Melting points were checked with a Büchi Melting Point B-540 in open glass capillaries.
Crystal structures were determined by single-crystal X-ray diffraction on an Oxford Diffraction Xcalibur 3 diffractometer equipped with a Sapphire CCD detector, four circle kappa platform operating with molybdenum K_α radiation source (λ = 0.710 73 Å) and Oxford Cryosystems Cryostream cooling unit. Data collection and reduction were performed with CrysAlisPro.[47] Very small single-crystals were measured on a Bruker D8 Venture diffractometer with a fixed-chi three-circle platform using enhance molybdenum Kα radiation (λ = 0.710 73 Å). The data collection was realized by using Bruker SAINT software.[48]
The structures were solved with SIR97,[49] or SHELXS-97,[50] refined with SHELXL-97,[50] or SHELXL-2013,[51] and finally checked with PLATON,[52] all integrated into the WinGX software suite.[53] The finalized CIF files were checked with checkCIF,[54] and deposited at the Cambridge Crystallographic Data Centre (CCDC).[55] Intra- and intermolecular contacts were analyzed with Mercury.[56] The illustrations of molecular structures were drawn with Diamond.[57]

Sensitivities

Sensitivities to impact (IS) and friction (FS) were determined according to BAM standards,[58] using a BAM drop hammer and a BAM friction apparatus.[59–64] The compounds

were classified in compliance with UN guidelines.[65] Impact: insensitive > 40 J, less sensitive ≥ 35 J, sensitive ≥ 4 J, very sensitive ≤ 3 J; Friction: insensitive > 360 N, less sensitive $= 360$ N, sensitive < 360 N and > 80 N, very sensitive ≤ 80 N, extremely sensitive ≤ 10 N. Sensitivities to electrostatic discharge (ESD) were determined with an OZM Research ESD 2010 EN.

Calculated Heats of Formation

Nitrogen-rich highly energetic compounds tend to burn incompletely in bomb calorimetric measurements due to the trend of explosion. Therefore, oftentimes wrong enthalpies of combustion ($\Delta_c H$) and finally wrong enthalpies of formation ($\Delta_f H°$) are obtained. Thus, the enthalpies and energies of formation were calculated at the CBS-4M level of theory as implemented in Gaussian 09,[66–68] using the atomization energy method and utilizing experimental data.[69–73]

The initial geometries of the structures were taken, if available, from the corresponding, experimentally determined crystal structures. Structure optimization and frequency analyses were performed with Becke's B3 three parameter hybrid function using the LYP correlation functional (B3LYP). For C, H, N, and O a correlation consistent polarized double-ξ basis set was used (cc-pVDZ). The structures were optimized with symmetry constraints and the energy is corrected with the zero point vibrational energy. The enthalpies (H) and free energy (G) were calculated using the complete basis set (CBS) method in order to obtain accurate values. The CBS model uses the known asymptotic convergence of pair natural orbital expressions to extrapolate from calculations using a finite basis set to estimate the complete basis set limit. CBS-4 starts with a HF/3-21G(d) geometry optimization, which is the initial guess for the following SCF calculation as a base energy and final MP2/6-31+G calculation with a CBS extrapolation to correct the energy in second order. The used CBS-4M method additionally implements a MP4(SDQ)/631+(d,p) calculation to approximate higher order contributions and also includes some additional empirical corrections. The enthalpies of the gas-phase species were estimated according to the atomization energy method.

Gas phase enthalpies were transformed to solid state enthalpies by using Trouton's rule for neutral compounds,[74,75] and Jenkin's method for ionic compounds.[76–78] The complete method is extensively described in the literature. The molar energy ΔU and enthalpy of formation ΔH of a compound $C_aH_bN_cO_d$ are connected according to

$$\Delta H = \Delta U + \Delta nRT, \tag{1.6}$$

in which Δn is the change of moles of the gaseous components in the equation of formation,

$$a\,\mathrm{C} + \frac{b}{2}\,\mathrm{H_2} + \frac{c}{2}\,\mathrm{N_2} + \frac{d}{2}\,\mathrm{O_2} \longrightarrow \mathrm{C}_a\mathrm{H}_b\mathrm{N}_c\mathrm{O}_d. \tag{1.7}$$

Calculated Performances

All calculations affecting the detonation or combustion (gun propellants) parameters were carried out using the program package Explo5 v.6.02 (EOS BKWG-S).[79,80] The detonation parameters were calculated at the Chapman-Jouguet (CJ) point based on the steady-state detonation model using a modified Becker-Kistiakowski-Wilson equation of state for modeling the system. The CJ point is found from the Hugoniot curve of the first derivative.

1.6 References

[1] J. Akhavan, *The Chemistry of Explosives*, 2nd ed., RSC Paperbacks, Cambridge, United Kingdom, **2004**.

[2] G. F. Henning, DE104280 **1898**.

[3] E. von Herz, CH88759A **1921**.

[4] T. M. Klapötke, *Chemistry of High-Energy Materials*, 3rd ed., de Gruyter, Berlin, Germany **2015**.

[5] ASTM International, www.astm.org (accessed March 13, 2016).

[6] P. M. Dickson, J. E. Field, *Proc. R. Soc. Lond. A* **1993**, *441*, 359–375.

[7] R. Matyáš, J. Pachman, *Primary Explosives*, Springer, Heidelberg, Germany, **2013**.

[8] D. Fischer, T. M. Klapötke, J. Stierstorfer, *Angew. Chem., Int. Ed.* **2014**, *53*, 8172–8175; *Angew. Chem.* **2014**, *126*, 8311–8314.

[9] D. D. Dlott, *Fast Molecular Processes in Energetic Materials*, in *Energetic Materials, Part 2, Detonation, Combustion*, Eds. P. Politzer, J. S. Murray, Elsevier, Amsterdam, The Netherlands, **2003**, pp. 125–191.

[10] R. Meyer, J. Köhler, A. Homburg, *Explosives*, 5th ed., Wiley-VCH, Weinheim, Germany, **2002**.

[11] M. J. Kamlet, S. J. Jacobs, *J. Chem. Phys.* **1968**, *48*, 23–35.

[12] C. L. Mader, *Numerical Modeling of Explosives and Propellants*, 2nd ed., CRC Press, Boca Raton, FL (USA), **1998**.

[13] P. Politzer, J. S. Murray, *Cent. Eur. J. Energ. Mater.* **2011**, *8*, 209–220.

[14] T. Urbanski, *Chemistry and Technology of Explosives*, Vol. 4, Pergamon Press, Oxford, United Kingdom, **1984**.

[15] S. Zeeman, *Sensitivities of High Energy Compounds*, in *Structure and Bonding - High Energy Density Materials*, *125*th, Ed. T. M. Klapötke, Springer, Berlin, Germany, **2007**, pp. 195–271.

[16] R. W. Shaw, T. B. Brill, D. L. Thompson (Eds.), *Overviews of Recent Research on Energetic Materials*, *Adv. Ser. Phys. Chem.*, *16*, World Scientific, Singapore, **2005**.

[17] D. D. Dlott, *Multi-phonon up-pumping in energetic material*, in *Overviews of Recent Research on Energetic Materials*, Eds. R. W. Shaw, T. B. Brill, D. L. Thompson, *Adv. Ser. Phys. Chem.*, *16*, World Scientific, Singapore, **2005**, pp. 303–334.

[18] T. B. Brill, K. James, *Chem. Rev.* **1993**, *93*, 2667–2692.

[19] F. P. Bowden, A. D. Yoffe, *Initiation and Growth of Explosion in Liquids and Solids*, Cambridge University Press, United Kingdom, **1952**.

[20] M. J. Kamlet, H. G. Adolph, *Propellants, Explos., Pyrotech.* **1979**, *4*, 30–34.

[21] P. Politzer, J. S. Murray, *Energetic Materials, Part 2, Detonation, Combustion*, Elsevier, Amsterdam, The Netherlands, **2003**.

[22] S. A. Shackelford, *Cent. Eur. J. Energ. Mater.* **2008**, *5*, 75–101.

[23] J. S. Murray, P. Lane, P. Politzer, P. R. Bolduc, *Chem. Phys. Lett.* **1990**, *168*, 135–139.

[24] F. J. Owens, K. Jayasuriya, L. Abrahmsen, P. Politzer, *Chem. Phys. Lett.* **1985**, *116*, 434–438.

[25] J. S. Murray, M. C. Concha, P. Politzer, *Mol. Phys.* **2009**, *107*, 89–97.

[26] J. S. Murray, P. Lane, P. Politzer, *Mol. Phys.* **1995**, *85*, 1–8.

[27] D. Fischer, T. M. Klapötke, M. Reymann, J. Stierstorfer, *Chem. Eur. J.* **2014**, *20*, 6401–6411.

[28] H.-H. Licht, *Propellants, Explos., Pyrotech.* **2000**, *25*, 126–132.

[29] T. M. Klapötke (Ed.), *Structure and Bonding - High Energy Density Materials*, *125*, Springer, Berlin, Germany, **2007**.

[30] H. Gao, J. M. Shreeve, *Chem. Rev.* **2011**, *111*, 7377–7436.

[31] E. L. Etnier, *Regul. Toxicol. Pharmcol.* **1989**, *9*, 147–157.

[32] P. Y. Robidoux, J. Hawari, G. Bardai, L. Paquet, G. Ampleman, S. Thiboutot, G. I. Sunahara, *Arch. Environ. Contam. Toxicol.* **2002**, *43*, 379–388.

[33] Agency for Toxic Substances and Disease Registry (ATSDR), *Toxicological Profile for RDX*, **2012**, www.atsdr.cdc.gov./toxprofiles/tp78.pdf (accessed March 27, 2016).

[34] United States Environmental Protection Agency (EPA), *Technical Fact Sheet - Hexahydro-1,3,5-trinitro-1,3,5-triazine (RDX)*, **2014**.

[35] United States Environmental Protection Agency (EPA), *Technical Fact Sheet - 2,4,6-Trinitrotoluene (TNT)*, **2012**.

[36] A. F. Holleman, E. Wiberg, N. Wiberg, *Lehrbuch der Anorganischen Chemie*, 102nd ed., de Gruyter, Berlin, **2007**.

[37] T. M. Klapötke, J. Stierstorfer, in *Green Energetic Materials* (Ed. T. Brinck), Wiley, Hoboken, NJ (USA), **2014**, pp. 133–178.

[38] T. M. Klapötke, D. G. Piercey, J. Stierstorfer, *Chem. Eur. J.* **2011**, *17*, 13068–13077.

[39] A. A. Dippold, T. M. Klapötke, *J. Am. Chem. Soc.* **2013**, *135*, 9931–9938.

[40] J. C. Bottaro, M. Petrie, P. E. Penwell, A. L. Dodge, R. Malhontra, NANA/HEDM Technology: Late Stage Exploratory Effort, Report No. A466714; SRI International: Menlo Park, CA, **2003**; DARPA/AFOSOR funded, Contact No. F49629-02-C-0030.

[41] R. P. Singh, R. D. Verma, D. T. Meshri, J. M. Shreeve, *Angew. Chem., Int. Ed.* **2006**, *45*, 3584–3601; *Angew. Chem.* **2006**, *118*, 3664–3682.

[42] K. Wang, D. A. Parrish, J. M. Shreeve, *Chem. Eur. J.* **2011**, *17*, 14485–14492.

[43] P. F. Pagoria, G. S. Lee, A. R. Mitchell, R. D. Schmidt, *Thermochim. Acta* **2002**, *384*, 187–204.

[44] G. L. Starova, O. V. Frank-Kamenetskaya, M. S. Pevzner, *J. Struct. Chem.* **1989**, *29*, 799–801.

[45] Y.-X. Li, X.-J. Wang, J.-L. Wang, *Acta Crystallogr. Sect. E Struct. Rep. Online* **2009**, *65*, o3073-o3073.

[46] G. R. Fulmer, A. J. M. Miller, N. H. Sherden, H. E. Gottlieb, A. Nudelman, B. M. Stoltz, J. E. Bercaw, K. I. Goldberg, *Organometallics* **2010**, *29*, 2176–2179.

[47] *CrysAlisPro 1.171.37.33*, Agilent Technologies, Santa Clara, CA (USA), **2014**.

[48] Saint, V.8.18C, Bruker AXS GmbH, Karlsruhe, Germany, **2011**.

[49] A. Altomare, M. C. Burla, M. Camalli, G. L. Cascarano, C. Giacovazzo, A. Guagliardi, A. G. G. Moliterni, G. Polidori, R. Spagna, *J. Appl. Cryst.* **1999**, *32*, 115–119.

[50] G. M. Sheldrick, *Acta Cryst.* **2008**, *A64*, 112–122.

[51] G. M. Sheldrick, *Acta Cryst.* **2015**, *C71*, 3–8.

[52] L. Spek, *PLATON*, Utrecht University, Utrecht, Netherlands, **2015**.

[53] L. J. Farrugia, *J. Appl. Cryst.* **1999**, *32*, 837–838.

[54] (IUCr)checkCIF/PLATON, http://journals.iucr.org/services/cif/checkcif.html (accessed April 24, 2016).

[55] The Cambridge Crystallographic Data Centre, http://www.ccdc.cam.ac.uk (accessed April 24, 2016).

[56] C. F. Macrae, P. R. Edgington, P. McCabe, E. Pidcock, G. P. Shields, R. Taylor, M. Towler, J. van de Streek, *J. Appl. Crystallogr.* **2006**, *39*, 453–457.

[57] Klaus Brandenburg, DIAMOND, 3.2k ed., Crystal Impact GbR, Berlin, Germany, **2014**.

[58] Bundesanstalt für Materialforschung und -prüfung, http://www.bam.de (accessed December 31, 2012).

[59] M. Sućeska, *Test Methods for Explosives*, Springer, New York · Berlin · Heidelberg, **1995**.

[60] NATO, *Standardization Agreement 4489 (STANAG 4489), Explosives, Impact Sensitivity Tests* **1999**.

[61] *WIWeB-Standardarbeitsanweisung 4-5.1.02* **2002**.

[62] NATO, *Standardization Agreement 4487 (STANAG 4487), Explosives, Friction Sensitivity Tests* **2002**.

[63] *WIWeB-Standardarbeitsanweisung 4-5.1.03* **2002**.

[64] Reichel & Partner GmbH, http://www.reichel-partner.de (accessed December 31, 2012).

[65] *Recommendations on the Transport of Dangerous Goods, Manual of Tests and Criteria*, 4th edition, United Nations, New York · Geneva, **1999**.

[66] M. J. Frisch, G. W. Trucks, H. B. Schlegel, G. E. Scuseria, M. A. Robb, J. R. Cheeseman, G. Scalmani, V. Barone, B. Mennucci, G. A. Petersson, H. Nakatsuji, M. Caricato, X. Li, H. P. Hratchian, A. F. Izmaylov, J. Bloino, G. Zheng, J. L. Sonnenberg, M. Hada, M. Ehara, K. Toyota, R. Fukuda, J. Hasegawa, M. Ishida, T. Nakajima, Y. Honda, O. Kitao, H. Nakai, T. Vreven, J. A. Montgomery, Jr., J. E. Peralta, F. Ogliaro, M. Bearpark, J. J. Heyd, E. Brothers, K. N. Kudin, V. N. Staroverov, T. Keith, R. Kobayashi, J. Normand, K. Raghavachari, A. Rendell, J. C. Burant, S. S. Iyengar, J. Tomasi, M. Cossi, N. Rega, J. M. Millam, M. Klene, J. E. Knox, J. B. Cross, V. Bakken, C. Adamo, J. Jaramillo, R. Gomperts, R. E. Stratmann, O. Yazyev, A. J. Austin, R. Cammi, C. Pomelli, J. W. Ochterski, R. L. Martin, K. Morokuma, V. G. Zakrzewski, G. A. Voth, P. Salvador, J. J. Dannenberg, S. Dapprich, A. D. Daniels, O. Farkas, J. B. Foresman, J. V. Ortiz, J. Cioslowski, D. J. Fox, Gaussian 09 Revision C.01, Gaussian, Inc., Wallingford, CT, USA, **2010**.

[67] J. W. Ochterski, G. A. Petersson, J. A. Montgomery, *J. Chem. Phys.* **1996**, *104*, 2598–2619.

[68] J. A. Montgomery, M. J. Frisch, J. W. Ochterski, G. A. Petersson, *J. Chem. Phys.* **2000**, *112*, 6532–6542.

[69] B. M. Rice, S. V. Pai, J. Hare, *Combust. Flame* **1999**, *118*, 445–458.

[70] B. M. Rice, J. J. Hare, *J. Phys. Chem. A* **2002**, *106*, 1770–1783.

[71] E. F. C. Byrd, B. M. Rice, *J. Phys. Chem. A* **2006**, *110*, 1005–1013.

[72] P. J. Linstrom, W. G. Mallard (Eds.), *NIST Standard Reference Database Number 69*, http://webbook.nist.gov/chemistry/ (accessed December 31, 2012).

[73] J. D. Cox, D. D. Wagman, V. A. Medvedev, *CODATA Key Values for Thermodynamics*, Hemisphere Publishing Corp., New York, USA, **1984**.

[74] F. Trouton, *Philos. Mag.* **1884**, *18*, 54–57.

[75] M. S. Westwell, M. S. Searle, D. J. Wales, D. H. Williams, *J. Am. Chem. Soc.* **1995**, *117*, 5013–5015.

[76] H. D. B. Jenkins, H. K. Roobottom, J. Passmore, L. Glasser, *Inorg. Chem.* **1999**, *38*, 3609–3620.

[77] H. D. B. Jenkins, D. Tudela, L. Glasser, *Inorg. Chem.* **2002**, *41*, 2364–2367.

[78] H. D. B. Jenkins, J. F. Liebman, *Inorg. Chem.* **2005**, *44*, 6359–6372.

[79] M. Sućeska, *Propellants, Explos., Pyrotech.* **1991**, *16*, 197–202.

[80] M. Sućeska, Explo5, v.6.02, Zagreb, Croatia, **2013**.

Investigations of the Vicarious *C*-Aminations of 5,7-Dinitrobenzotriazole and 4,6-Dinitrobenzotriazol-3-ium-1-oxide and Their Energetic Properties

D. Ehlers, T. M. Klapötke, and C. Pflüger

Chem. Eur. J. **2015**, *21*, 16073–16082.

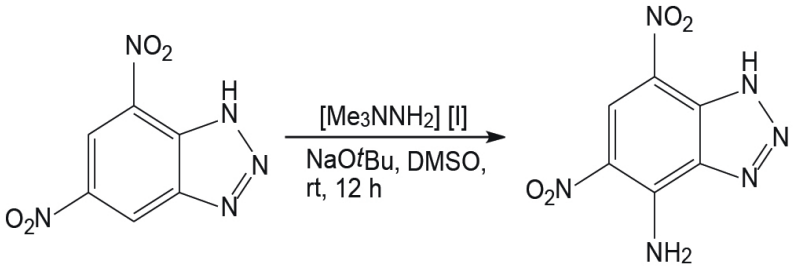

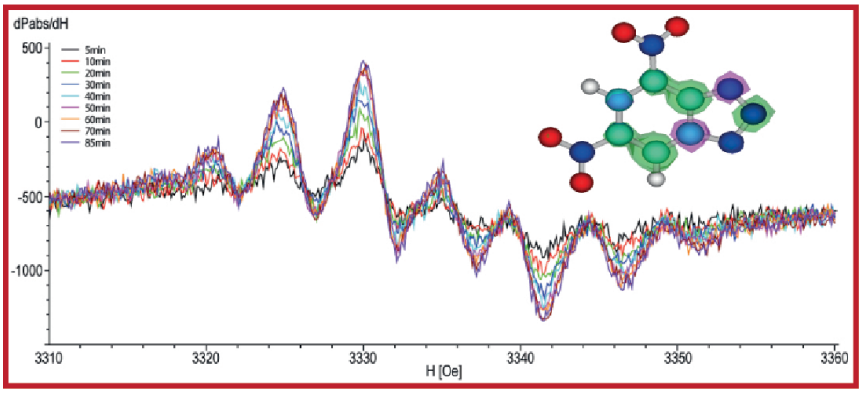

Investigations of the Vicarious *C*-Aminations of 5,7-Dinitrobenzotriazole and 4,6-Dinitrobenzotriazol-3-ium-1-oxide and Their Energetic Properties

D. Ehlers, T. M. Klapötke, and C. Pflüger
Chem. Eur. J. **2015**, *21*, 16073–16082.

Abstract

This combined experimental and theoretical study details the vicarious nucleophilic substitution by amination of 5,7-dinitrobenzotriazole (**1**) and 4,6-dinitrobenzotriazol-3-ium-1-oxide (**4**) with trimethylhydrazinium iodide to afford the new corresponding one- and two-time aminated compounds and investigations of its mechanism by EPR spectroscopy. The preferred position for the first amination is computed by spin density population and verified by X-ray crystallography. The zwitterionic structure of **4** is investigated in solution by ^{1}H NMR spectroscopy and in solid state by X-ray diffraction. Furthermore, the crystal structure of **1** is presented. The energetic behavior of the aminated products as well as the starting materials **1** and **4** was investigated, regarding sensitivities and performance.

2.1 Introduction

Energetic materials store relatively large amounts of energy that is easily released by initiation.[1] Explosives are employed when very rapid rates of energy applications and high pressures are desired, for example, to produce highly powerful shock waves in air, rock, and water as needed for mining, oil production, and other civil applications or for military purposes. Most commonly employed explosives are RDX (hexogen), HMX (octogen), TNT (trinitrotoluene), and nitroglycerin. Research is ongoing worldwide to discover high-energy dense materials (HEDMs) with high performances and substantially reduced sensitivities towards external stimuli as impact, friction, and heat. Unfortunately, these parameters often have a contradictory effect on each other.[4] Most of the energy of HEDMs is derived either from their very high positive heats of formation or from oxidation of the carbon backbone as seen for traditional explosives.[5,6] High-nitrogen heterocycles are mostly investigated because of their higher heats of formation, density, and oxygen balance in comparison to their carbocyclic analogues due to their larger number of inherently energetic N−N and C−N bonds.[7] By introduction of a benzene ring as carbon backbone to the heterocycles, their thermal stabilities are usually increased and the sensitivities reduced.

For fused-rings like benzimidazoles[8,9] and benzofuroxans[10,11] their energetic properties have been evaluated. 1,2,3-Triazoles are promising nitrogen-rich heterocycles, especially regarding the higher heat of formation of 1,2,3-triazoles ($\Delta_f H(\mathrm{g})_{\mathrm{CBS4M}} = 231\,\mathrm{kJ\,mol^{-1}}$) as compared with 1,2,4-triazoles ($\Delta_f H(\mathrm{g})_{\mathrm{CBS4M}} = 178\,\mathrm{kJ\,mol^{-1}}$). Benzotriazole derivatives as energetic materials have not been widely studied until now, although some evaluations of the energetic properties of 1*H*-benzotriazole[12] and of some nitro derivatives of 1-picryl-benzotriazole[13] have been carried out. In the last years also Ghule et al. investigated some nitrobenzotriazoles containing further energetic groups starting from 5-chloro-1*H*-benzotriazole.[14] But no investigations of the 5,7-dinitrobenzotriazole itself and the new 4-amino and diamino derivates have been performed.

Nitro groups contribute to a higher density and oxygen balance, whereas amino groups lead to higher thermal stabilities and improved sensitivities. By introduction of amino groups adjacent to nitro groups, the C−NO_2 bonds are strengthened by reducing the electropositive potential above and below aromatic C−NO_2 bonds by resonance and by formation of hydrogen bonds.[15–19] Furthermore, the density and stability rises due to intermolecular interactions involving the amino and nitro groups. This stabilization can, for example, be seen from the very insensitive explosive triaminotrinitrobenzene (TATB).[15–19]

A convenient way to introduce an amino group is the use of 1,1,1-trimethylhydrazinium iodide as amination reagent.[20,21] A proposed reaction mechanism involves the formation of radicals as studied by the amination of alkylated heterocycles.[21]

Furthermore, *N*-oxides have been widely studied in organic and biological chemistry for a long time.[22–24] The introduction of *N*-oxides to energetic heterocyclic compounds is a recent strategy to increase the energetic properties due to higher heats of formation and higher crystal densities.[25–27] The corresponding 4,6-dinitrobenzotriazol-3-ium-1-oxide was first prepared as precursor for coupling reagents in peptide synthesis.[28] The explosive properties of this compound have not been investigated yet, although energetic properties of 1-hydroxybenzotriazole and some of its derivatives were described.[29]

In this contribution the new amino derivatives are synthesized. The energetic properties of 5,7-dinitrobenzotriazole, 4,6-dinitrobenzotriazol-3-ium-1-oxide, and their aminated derivatives are investigated. In addition, the nucleophilic substitution in the amination reaction with trimethylhydrazinium iodide in the presence of acidic protons is studied, and the preferred first position for the amination is computed by spin density population.

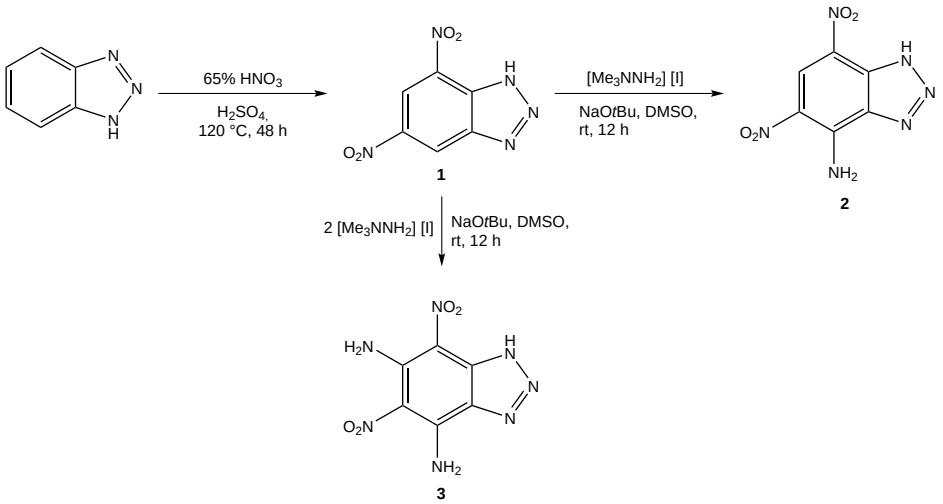

Scheme 2.1: 5,7-Dinitrobenzotriazole (**1**) and its amination products **2** and **3**.

2.2 Results and Discussion

2.2.1 Syntheses

5,7-Dinitro-1*H*-benzotriazole (**1**) was synthesized according to McHugh et al. by nitration of 1*H*-benzotriazole with 65% nitric acid and concentrated sulfuric acid at 120 °C.[30] The *C*-aminations of **1** were carried out with one respective two equivalents of trimethylhydrazinium iodide and sodium *tert*-butoxide as base to afford 4-amino-5,7-dinitrobenzotriazole (**2**) and 4,6-diamino-5,7-dinitrobenzotriazole (**3**) as depicted in Scheme 2.1.
4,6-Dinitrobenzotriazol-3-ium-1-oxide (**4**) was synthesized according to an improved synthesis from picryl chloride (Scheme 2.2).[28] The *C*-aminations by vicarious nucleophilic substitution (VNS) were carried out similar to the ones of **1** to yield 7-amino-4,6-dinitrobenzotriazol-3-ium-1-oxide (**5**) and 5,7-diamino-4,6-dinitrobenzotriazol-3-ium-1-oxide (**6**). The zwitterionic structures of **4** and **5** are confirmed by X-ray studies and in case of **4** also by ^{1}H NMR spectroscopy.
For the VNS of hydrogen of many *N*-alkylated nitroazoles (imidazoles, nitrobenzimidazoles, pyrazoles), Lopyrev et al. proposed a radical reaction mechanism.[21,31] The vicarious nucleophilic amination involves successive stages with electron transfer as shown in Scheme 2.3 from the anion of the reagent to the anion of the substrate.
First, hydrogen iodide is separated from 1,1,1-trimethylhydrazinium iodide by sodium *tert*-butoxide. Then, an ion radical pair is formed by the zwitterionic amination reagent and the nitroazole. This electron transfer takes place quickly, whereas the formation of the σ^H-complex is slower, which is proved by the observation of the primary radical anions of the nitroazoles. Because of the slow formation of the σ^H-complex, radical ions could escape from the ion radical pair, the so-called cage, before the σ^H-complex is formed.

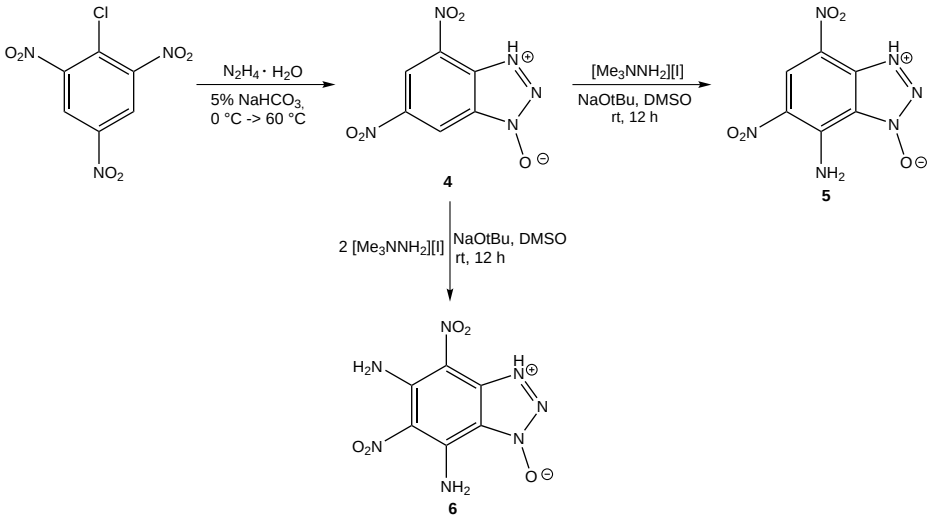

Scheme 2.2: 4,6-Dinitrobenzotriazol-3-ium-1-oxide (**4**) and its amination products **5** and **6**.

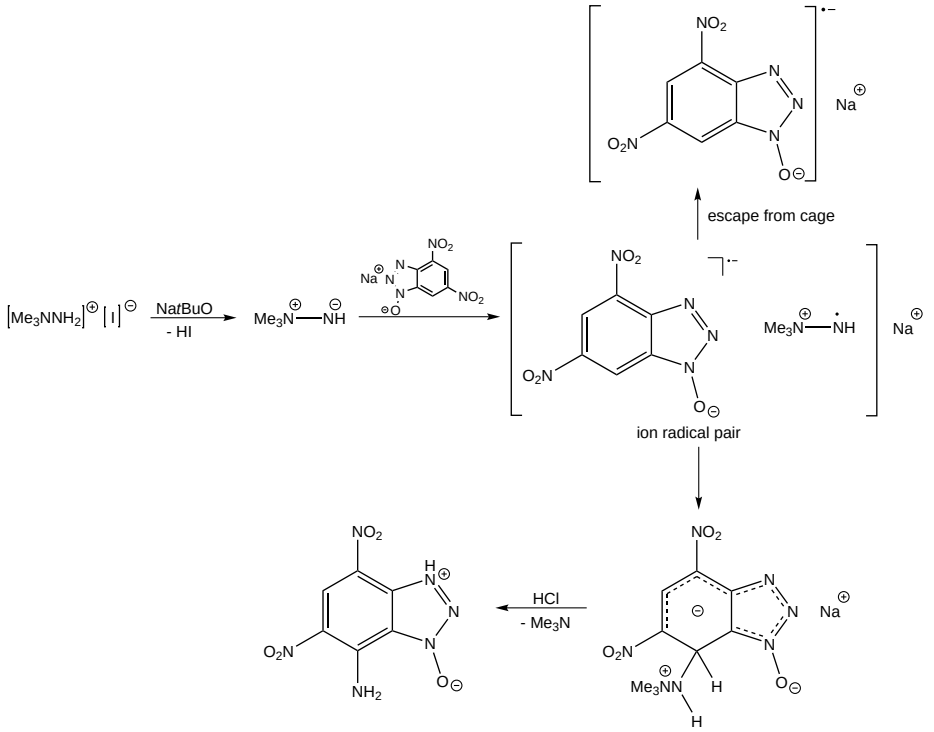

Scheme 2.3: Reaction mechanism of the vicarious nucleophilic substitution.

Trimethylamine is released from the σ^H-complex to afford the amination product. The presence of free radicals is monitored by EPR measurements for the two-time amination reactions of **1** and **4**. The amination reaction of **1** was monitored for several hours to evaluate the time dependence of the reaction. The reaction mixtures show the typical blue-violet color and a spectrum of the radical anions was observed by EPR measurements (Figure 2.1 and the Appendix, Figure A.1 and Figure A.2).

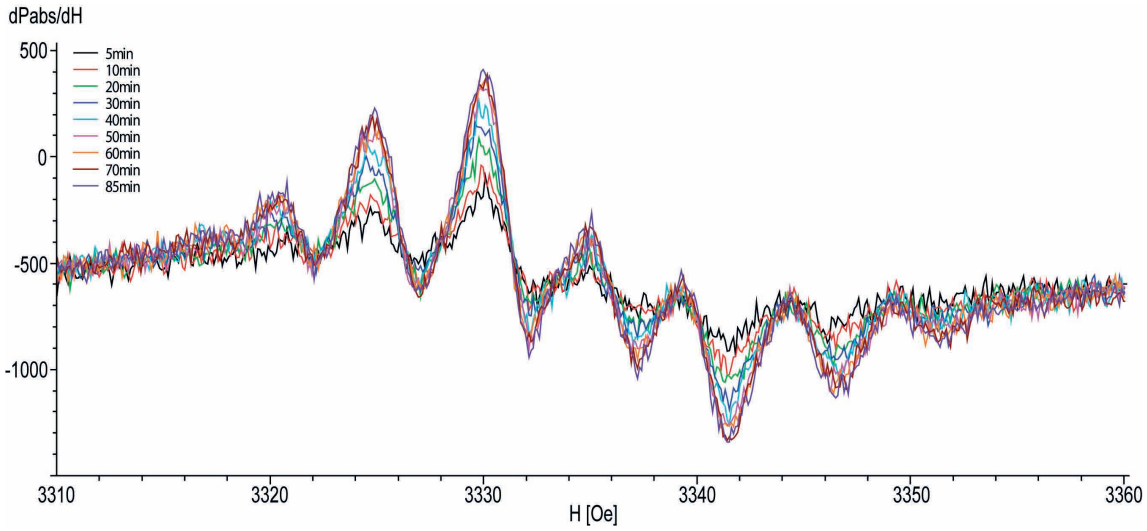

Figure 2.1: EPR spectra of the amination of 5,7-dinitrobenzotriazole (**1**).

The concentration of the in situ-formed radicals of **1** increases gradually as the EPR spectra of the amination of **1** show (Figure 2.1). Unambiguous assignment of the septet structure of the EPR spectrum of **1** presents some difficulties because of the low resolution and the two different formed radical anions. The septet structure may be caused by hyperfine interactions of the unpaired electron with the three nitrogen ^{14}N-nuclei of the triazole ring considering that their overlap parameters are statistically very similar giving a spin of three. Therefore, the septet structure with a coupling constant $\alpha_N = 5Œ$ may be formed. It was stated by Lopyrev et al. that the aminations only take place at the carbon atoms showing a positive spin density population. The preferred position is the one with the highest spin density population.[21,31] Therefore, the spin density population, the electron density applied to free radicals, was calculated for the corresponding free radicals to verify if the experimental results fit to the theoretical calculations. The spin density is defined as the total electron density of electrons of one spin minus the total electron density of the electrons of the other spin. Thus, in contrast to the total electron density defined as the sum of alpha and beta densities, the spin density is defined as the difference:

$$p^s(r) = p^\alpha(r) - p^\beta(r) \tag{2.1}$$

All calculations were carried out using the HyperChem code[32] at semi empirical PM3 level of theory. The structures of all radical anions were fully optimized at UHF/PM3 level and the total spin density populations were displayed as 3D isosurfaces at the 0.005 e bohr^{-3} contour value. Positive spin density population is shown in green and the negative spin density population is shown in red (Figure 2.2).

For the first amination the calculations reveal the preference of the C3 position in the

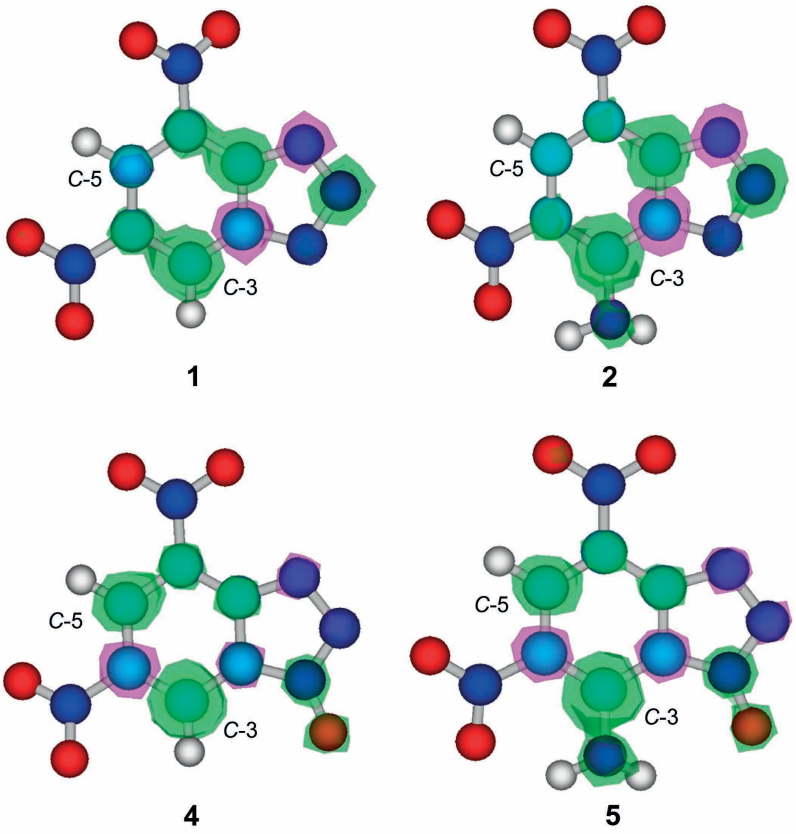

Figure 2.2: Calculated spin density population of the radical ions of **1**, **2**, **4**, and **5**. Positive spin density population is shown in green and negative spin density population is shown in red.

radical ion of **1** and C3 position in the radical ion of **4**, which possess the higher positive spin density populations as depicted in Figure 2.2. Interestingly, there is no or only a very small spin density population at the C5 in the radical ion **2**, but it could be aminated. The second amination of **4** is also possible because of the positive spin density population at the C5 carbon atom in the first formed radical ion of **2**. Therefore, the calculations and the obtained experimental results are consistent with the proposed radical mechanism.

2.2.2 NMR spectroscopy

All NMR spectra were recorded in DMSO-d_6 unless stated otherwise. The ^{1}H NMR spectra of compounds **1** and **4** recorded in acetone-d_6 show two doublets of the aromatic protons at $\delta = 9.47$ and 9.20 ppm and $\delta = 9.14$ and 9.05 ppm, respectively, with ^4J coupling constants of 1.9 Hz. In the ^{1}H NMR spectra of compounds **1** and **4** recorded in DMSO-d_6, two slightly downfield shifted multiplets of the aromatic protons and the triazole protons at $\delta = 16.02$ and 13.55 ppm, respectively, were observed. The downfield shift of the acidic proton of **4** indicates that in solution the zwitterionic structure with the proton at the triazole nitrogen

is also formed. The aromatic protons of the one-time aminated compounds **2** and **5** are seen at $\delta = 8.92$ and 8.88 ppm, whereas the protons of the amino group are observed downfield either as two singlets ($\delta = 9.71$, 9.07 ppm) or as multiplet ($\delta = 9.38$ ppm). The ^{1}H NMR spectra of **3** and **6** exhibit one multiplet for the protons of both amino groups in a range from $\delta = 10.33$–9.44 and 10.37–9.79 ppm. For **6** also the proton of the triazole ring is observed as very small and broad signal at $\delta = 15.31$ ppm.
In the ^{13}C NMR spectra of the presented compounds the resonance signals of all carbon atoms are observed.
The resonance signal of the nitrogen atoms of nitro groups are seen in the ^{14}N NMR spectra of all compounds mostly as one signal at $\delta = -15$ to -20 ppm. The NMR spectroscopic characterization of **1** and **4** was extended to ^{15}N NMR spectroscopy (Figure 2.3). Although the ^{15}N NMR measurements were performed with the highest possible concentrations, some signals of the triazole ring were still not observed. Because of the low solubility of **1**, two ^{15}N NMR spectra were recorded with different concentrations at 25 °C and 50 °C, respectively. In the ^{15}N NMR spectra of **1** and **4** two different signals at $\delta = -16.1$ and -18.8 ppm and $\delta = -17.1$ and -19.0 ppm, respectively, are observed, which could be unambiguously assigned to the corresponding nitro groups due to their coupling patterns. The only resonance signal of the triazole ring, which could be observed for compound **1**, at $\delta = 11.7$ ppm is assigned to the nitrogen N3, which is furthest away from the NH. For the triazole-1-oxide ring of **4** two signals are seen at $\delta = -1.2$ and -71.3 ppm. The broadened resonance signal that is shifted to higher field is therefore assigned to N2, whereas the other signal is assigned to the *N*-oxide nitrogen.

2.2.3 Crystal Structures

Compounds **1**, **2**, **4**, and **5** were also characterized by low-temperature single-crystal X-ray diffraction. The data and parameters of the measurements and refinements are summarized in the Appendix, Table A.1 and Table A.2.
5,7-Dinitrobenzotriazole (**1**) crystallizes in the orthorhombic space group $Pna2_1$. In comparison with the density of the unsubstituted benzotriazole (1.37 g cm^{-3}),[33] the density of **1** increases to 1.694 g cm^{-3} at 173 K and 1.645 g cm^{-3} at 293 K, respectively. The structure of **1** is shown in Figure 2.4. One strong classical hydrogen bond and one weaker non-classical hydrogen bond are formed, which connect the wave-like layers. Furthermore, the twisting of the nitro groups lead to dipolar N4···O3^{iii} and C3···O3^{iii} interactions of 2.879(4) and 2.935(4) Å, which are below the sum of their van der Waals radii.[34]
4-Amino-5,7-dinitrobenzotriazole (**2**) crystallizes as DMSO adduct in the monoclinic space group $P2_1/c$ with four formula units per unit cell and a density of 1.673 g cm^{-3}. The

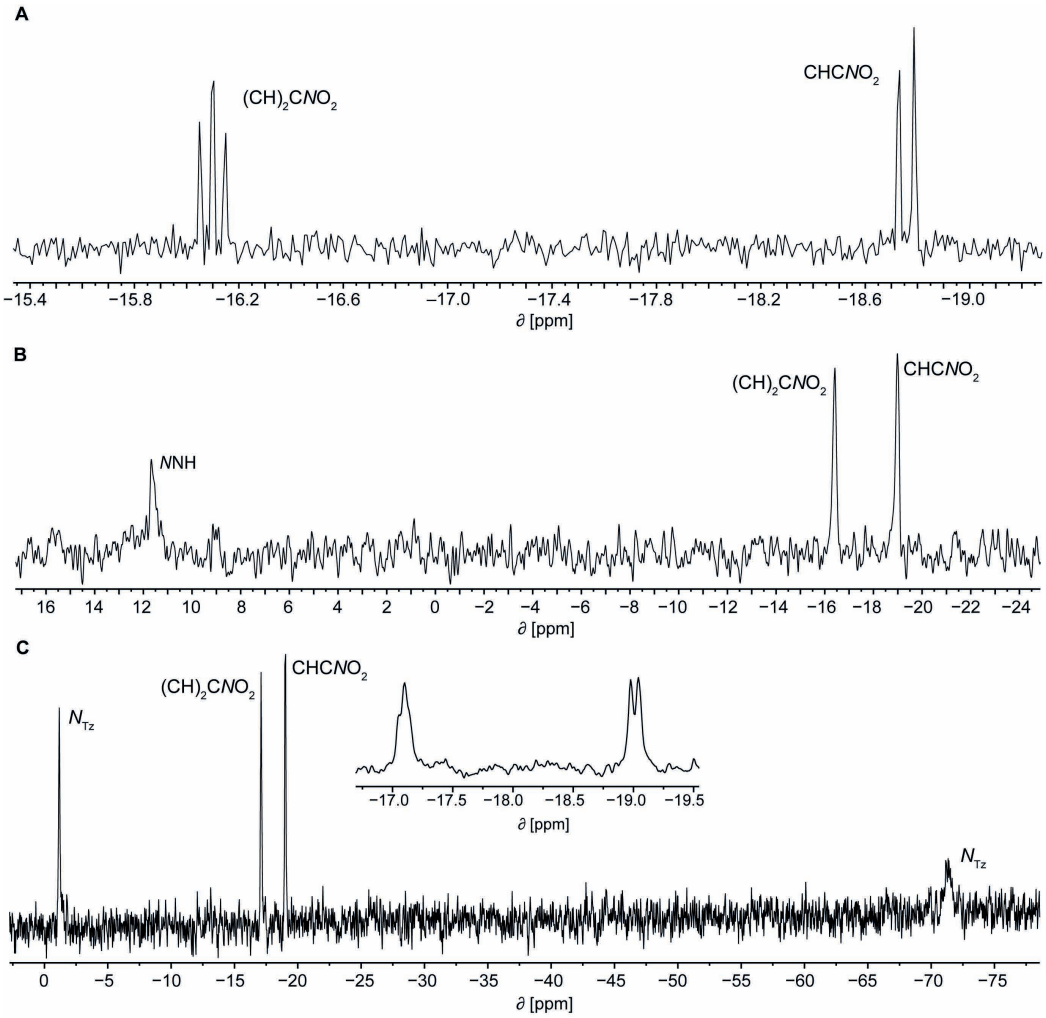

Figure 2.3: ^{15}N NMR spectra of **1** in DMSO-d_6 at 25 °C (A) and 50 °C (B) and of **4** in DMSO-d_6 at 25 °C (C).

diagonal layers along the *c* axis (Figure 2.5A) are connected by hydrogen bonds formed between the methyl groups of DMSO and the nitro groups. One nitro group is almost in plane (1.24(6)°) with the benzotriazole ring, whereas the nitro group of N5 is twisted out of plane by 12.66(6)°. With exception of the aromatic hydrogen atom, the other protons of the amino group and the triazole ring are involved in hydrogen bonding. Beside the hydrogen bonds of one layer along the *b* axis, intermolecular dipolar N6···O5^{iii} interactions are observed as displayed in Figure 2.5B.

The zwitterionic **4** crystallizes from acetonitrile as orange blocks (Figure A.4) in the orthorhombic space group *Pbca* with eight formula units per unit cell. Compound **4** shows a significantly higher density (1.723 g cm^{-3}) than that of **1**, which nicely confirms the concept of increasing the density by *N*-oxide introduction. The *N*-oxide N−O bond length of 1.30 Å is extended in comparison to the N−O bond lengths of the nitro groups (1.22–1.23 Å), but

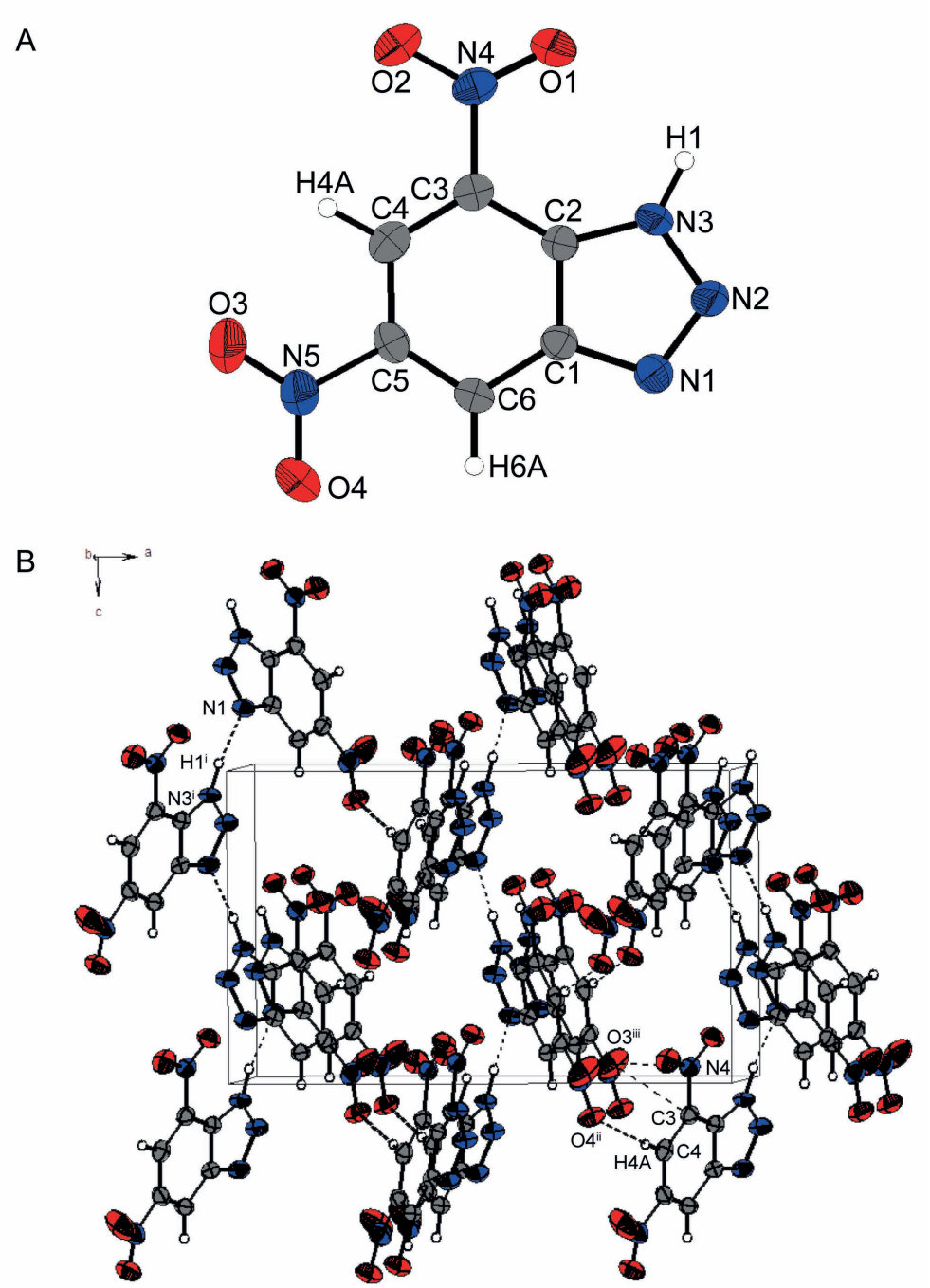

Figure 2.4: Crystal structure of 5,7-dinitrobenzotriazole (**1**); ellipsoids are set at 50% probability. Selected hydrogen bond lengths [Å] and angles [°] (D−H···A, d(D−H), d(H···A), d(D···A), ∠(D−H···A): N3−H1···N1^{i}: 0.93(4), 1.91(3), 2.781(4), 156(3); C4−H4A···O4^{ii}: 0.99(3), 2.56(3), 3.542(4), 169(3). Symmetry codes: (i) $-x, -y, 0.5+z$; (ii) $0.5-x, 0.5+y, 0.5+z$; (iii) $1-x, -y, 0.5+z$.

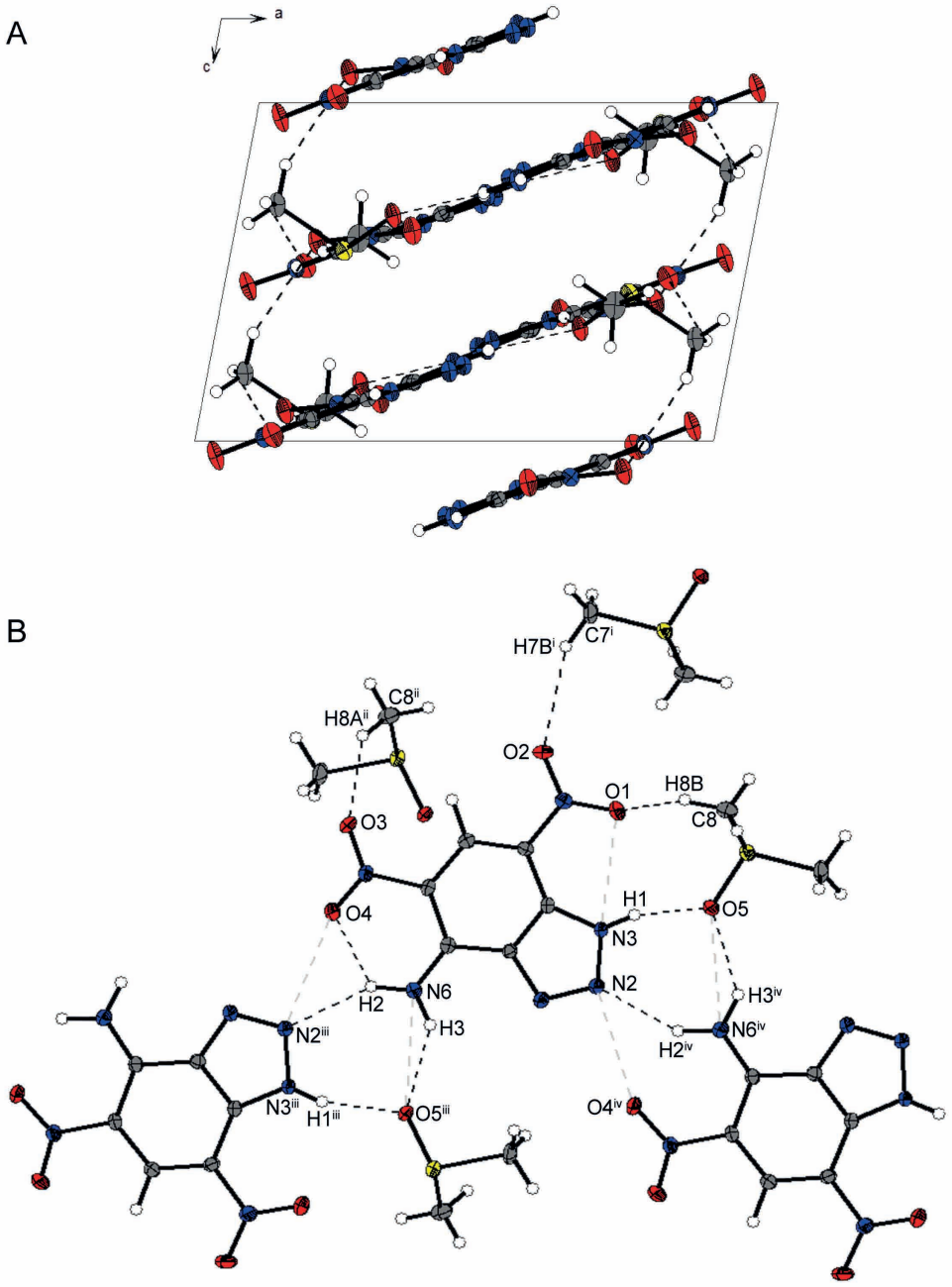

Figure 2.5: A) View through the layer structure of compound **2** as DMSO adduct along the *b* axis; B) View of one layer in the structure of **2**·DMSO. Selected hydrogen bond lengths [Å] and angles [°] (D−H···A, d(D−H), d(H···A), d(D···A), ∠(D−H···A): N3−H1···O5: 0.84(3), 1.87(3), 2.690(2), 163(3); C8−H8B···O1: 0.97(3), 2.52(3), 3.216(3), 129(2); C7^{i}−H7B^{i}···O2: 0.99(3), 2.70(2), 3.625(3), 155(2); C8^{ii}−H8A^{ii}···O3: 0.98(3), 2.46(3), 3.319(3), 146(2); N6−H2···N2^{iii}: 0.96(3), 2.19(3), 3.050(2), 148(2); N6−H2···O4: 0.96(3), 2.01(3), 2.655(2), 123(2); N6−H3···O5^{iii}: 0.91(2), 2.17(2), 2.907(2), 138(2). Symmetry codes: (i) $-x, 0.5+y, 0.5-z$; (ii) $-x, -y, -z$; (iii) $x, 0.5-y, 0.5+z$. Ellipsoids are drawn at the 50% probability level.

Table 2.1: Selected interactions within the crystal structure of **5**·H_2O.

D−H···A	d(D−H) [Å]	d(H···A) [Å]	d(D···A) [Å]	∠(D−H···A) [°]
N6−H2···O1	1.02(4)	2.04(4)	2.862(4)	136(3)
N6−H3···O5	0.94(4)	2.04(4)	2.666(4)	123(3)
N3−H1···O6^{iii}	0.88(4)	1.85(4)	2.728(4)	174(4)
N6−H3···O2^{i}	0.94(4)	2.24(4)	3.017(5)	139(3)
O6−H5O···O1^{ii}	0.80(5)	1.99(4)	2.782(4)	170(5)
O6−H4O···O3^{v}	0.81(5)	2.23(5)	2.893(4)	139(4)
O6−H4O···O5^{i}	0.81(5)	2.67(4)	3.209(4)	125(4)
dipolar interactions ΣvdW radii (N···O) < 3.07 Å N3···O6 2.728(4) Å				

Symmetry codes: (i) $1+x, 0.5-y, 0.5+z$; (ii) $1-x, 0.5+y, 0.5-z$; (iii) $x, 1.5-y, 0.5+z$; (iv) $-1+x, 0.5-y, 0.5+z$; (v) $x, 0.5-y, 0.5+z$.

in the range of pyridine *N*-oxides.[35] The other bond lengths of the triazole ring are in the same range as the ones of **1**. In contrast to **1** several intermolecular interactions are formed, which may be a reason for the higher density. The nitro groups N4 and N5 are twisted out of the benzotriazol-1-oxide plane by 6.34(4) and 12.42(3)°, respectively, thereby forming the hydrogen bonds and dipolar interactions shown in Figure 2.6B. Because of the zwitterionic structure of **4**, an intramolecular hydrogen bond between H1 of the protonated N1 and oxygen O5 of 2.401(18) Å is formed, whereas the negative charged oxygen O1 is involved in dipolar interactions and an intermolecular hydrogen bond to H1. The interactions lead to an undulated, opposed staggered packing of tilted layers along the *b* axis as displayed in Figure 2.6A.

7-Amino-4,6-dinitrobenzotriazol-3-ium-1-oxide (**5**) crystallizes as hydrate in the monoclinic space group $P2_1/c$ with four formula units per unit cell. Its crystal density is 1.834 g cm^{-3} at 100 K. The densities of the amino-substituted derivatives could not be compared because they crystallize either as hydrate or as DMSO adduct. The crystal structure of compound **5**·H_2O consists of four different layers along the *c* axis as shown in Figure 2.7A. The N−O bond length (1.292(4) Å) of the *N*-oxide of **5** is in the same range than the corresponding bond length of **4**.

The nitro groups of N4 and N5 as well as the amino group are turned out of the benzotriazol-1-oxide plane with twisting of 2.79(9), 5.22(9), and 4.05(9)°, respectively. These spatial arrangements afford several intramolecular classical and non-classical hydrogen bonds and dipolar N···O interactions, which are presented in Table 2.1.

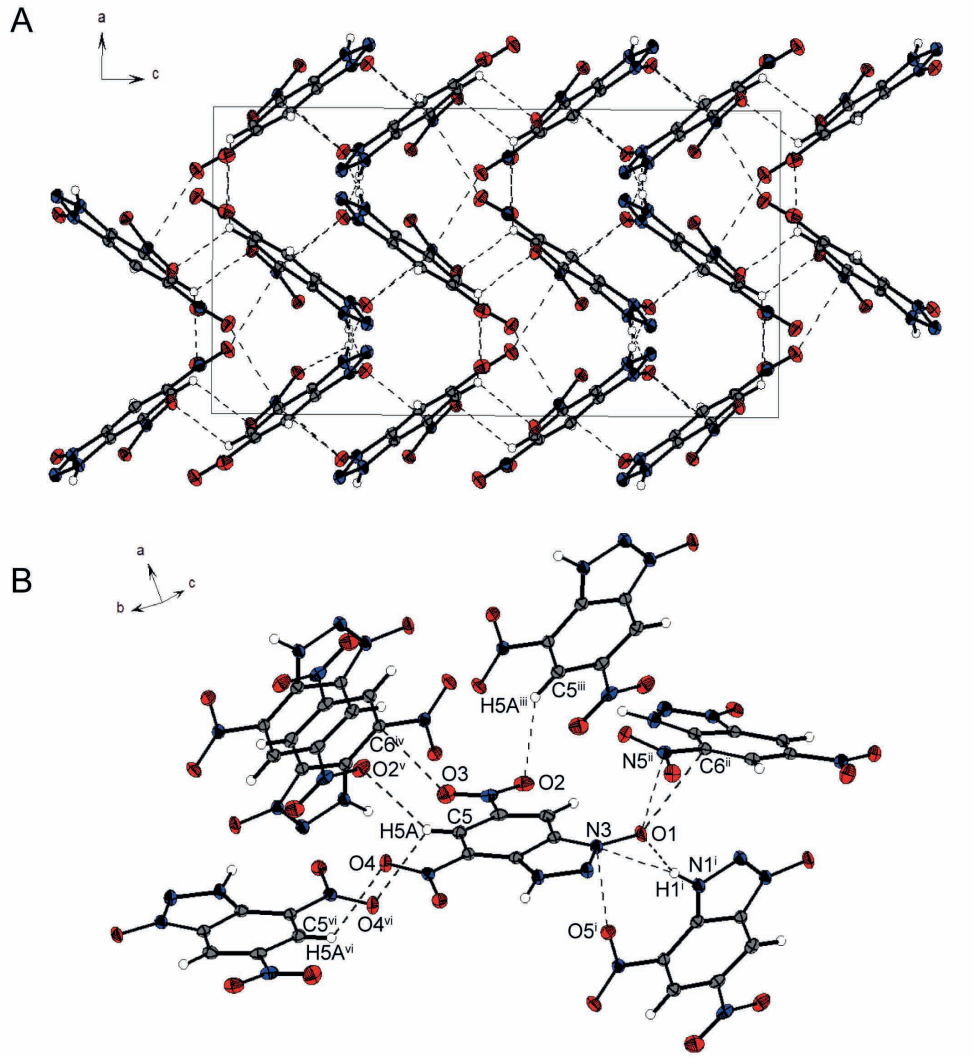

Figure 2.6: A) View through the layer structure of **4** along the *b* axis. B) View of selected interactions of **4**. Selected hydrogen bond lengths [Å] and angles [°] (D−H···A, *d*(D−H), *d*(H···A), *d*(D···A), ∠(D−H···A): N1^{i}−H1^{i}···O1: 0.928(18), 1.685(18), 2.5779(14), 160(1); C5−H5A···O2^{v}: 0.947(17), 2.499(17), 3.1906(16), 130(1); C5−H5A···O4^{vi}: 0.947(17), 2.573(17), 3.2150(16), 125(1). Selected dipolar N···O interactions (ΣvdW radii <3.07 Å): N5^{ii}···O1^{ii} 2.7430(14) Å; N3···O5^{ii} 2.7969(14) Å. Selected dipolar C···O interactions (ΣvdW radii <3.22 Å): C6^{ii}···O1^{iv} 2.9210(16) Å; C6^{iv}···O3 3.0118(16) Å. Symmetry codes: (i) $0.5 - x, -y, 0.5 + z$; (ii) $0.5 + x, 0.5 - y, -z$; (iii) $-x, 0.5 + y, 0.5 - z$; (iv) $-x, -y, -z$; (v) $0.5 + x, y, 0.5 - z$; (vi) $0.5 - x, 0.5 + y, z$; (vii) $x, 0.5 - y, 0.5 + z$. Ellipsoids are drawn at the 50% probability level.

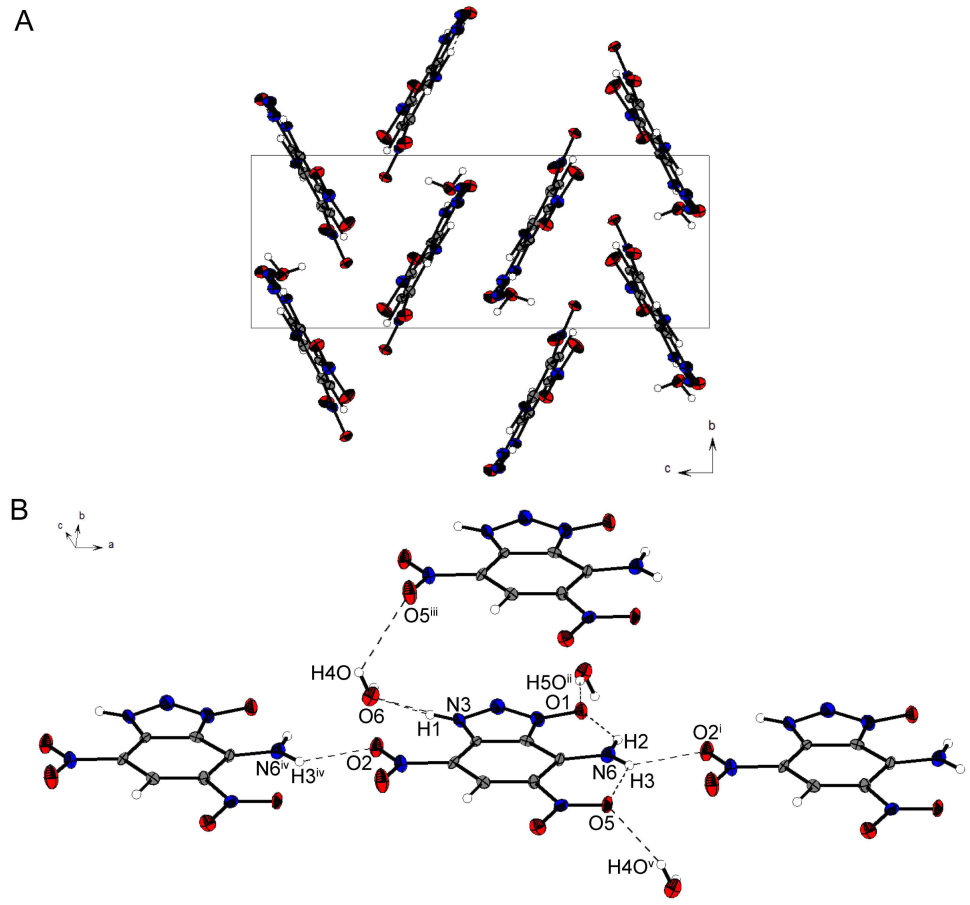

Figure 2.7: A) Unit cell of **5**·H_2O along the *a* axis, which consists of four different layers; B) Selected interactions of 7-amino-4,6-dinitrobenzotriazol-3-ium-1-oxide (**5**). Symmetry codes: (i) $1+x, 0.5-y, 0.5+z$; (ii) $1-x, 0.5+y, 0.5-z$; (iii) $x, 1.5-y, 0.5+z$; (iv) $-1+x, 0.5-y, 0.5+z$; (v) $x, 0.5-y, 0.5+z$. Ellipsoids are drawn at the 50% probability level.

2.2.4 Stabilities, Sensitivities, and Energetic properties

The thermal behaviors of all synthesized compounds were investigated on a Linseis PT10 DSC with a heating rate of 5 °C min^{-1} by using approximately 1.0 mg of material. All DSC curves are shown in Figure 2.8.

5,7-Dinitrobenzotriazole (**1**) and its one-time aminated derivative **2** melt before decomposition at 193 and 337 °C. The thermal stabilities of the successively *C*-aminated derivatives **2** and **3** are increased to 341 and 322 °C, respectively, in comparison to the decomposition point of 291 °C of **1**. The *N*-oxidations at the triazole lead to decreased thermal stabilities. The zwitterionic compound **4** decomposes already at 182 °C, whereas each *C*-amination results in an increase in the thermal stabilities by about 30 °C because of the strengthening of the C–NO_2 bonds by mesomerism and hydrogen bonding. Compound **5** loses its crystal water at 107 °C.

Because of the energetic nature of all synthesized compounds **1**–**6** and for initial safety

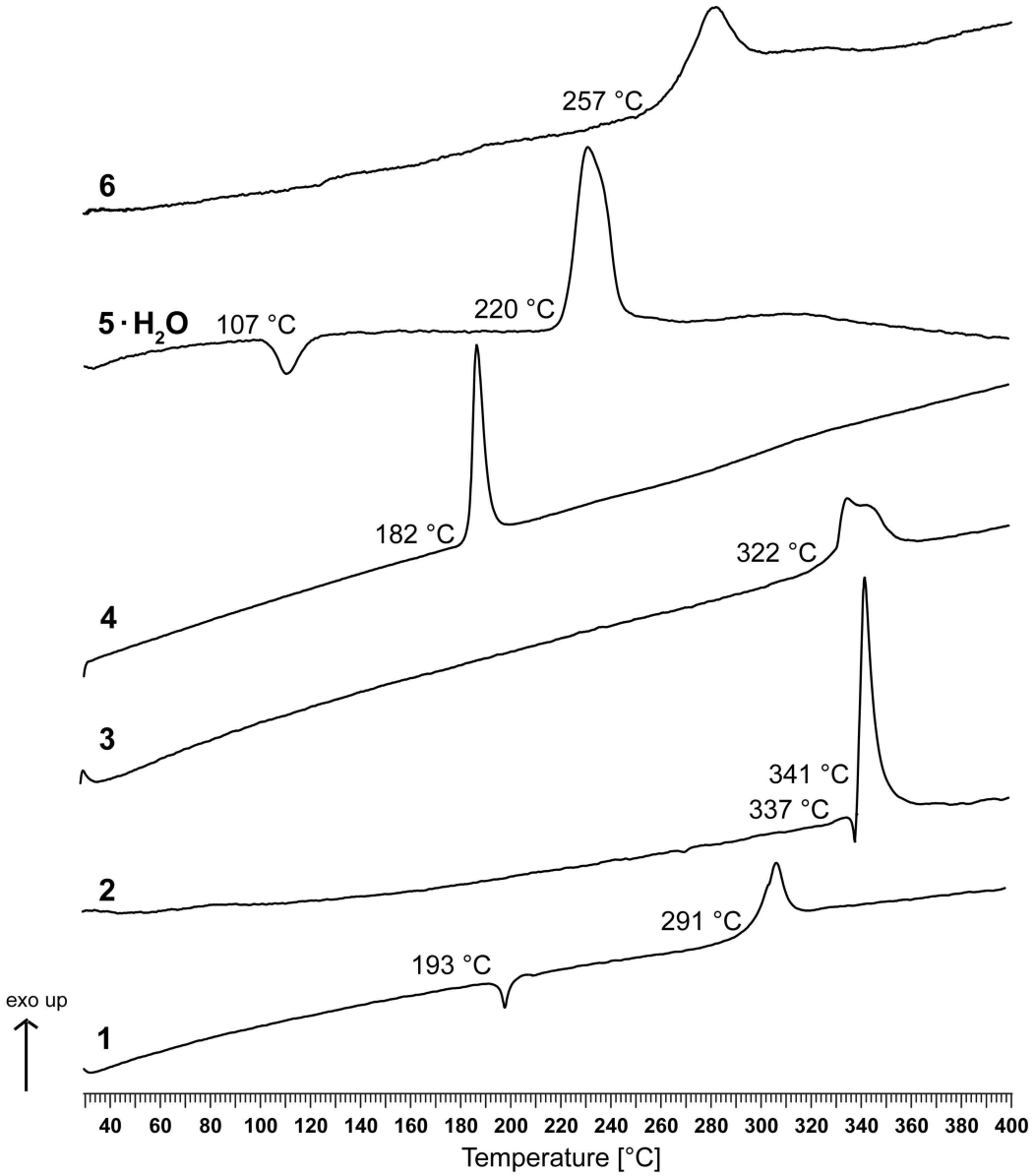

Figure 2.8: DSC plots of compounds **1**–**6**.

testing, their sensitivities and energetic behavior were determined. Their investigated physical and thermodynamic properties are summarized in Table 2.2.

The sensitivities towards impact and friction were determined experimentally according to the BAM standards and classified according to the UN recommendations for the transport of dangerous goods.[36–38] Compounds **1** and **2** are insensitive towards impact and friction, whereas the two-time aminated **3** is classified as less sensitive. The introduction of an *N*-oxide afforded the very impact sensitive 4,6-dinitrobenzotriazol-3-ium-1-oxide (**4**) with an impact sensitivity of 2 J but anyhow it is insensitive towards friction. The monohydrate of **4** is also insensitive towards impact. The impact sensitivity is improved by the one-time *C*-amination to 5 J for compound **5** and by the two-time *C*-aminations even further to

Table 2.2: Physical and energetic properties of **1**–**6**.

	1	**2**	**3**	**4**	**5**	**6**
Formula	$C_6H_3N_5O_4$	$C_6H_4N_6O_4$	$C_6H_5N_7O_4$	$C_6H_3N_5O_5$	$C_6H_4N_6O_5$	$C_6H_5N_7O_5$
M $[\mathrm{g\,mol^{-1}}]$	209.13	224.14	239.16	225.12	240.14	255.15
IS [J][a]	>40	>40	35	2	5	20
FS [N][b]	>360	>360	>360	>360	>360	>360
ESD [J][c]	0.3	0.85	1.5	0.2	1.0	1.5
N [%][d]	33.49	37.50	41.00	31.11	35.00	38.43
Ω [%][e]	-72.7	-71.4	-70.2	-60.4	-60.0	-59.6
T_{dec} [°C][f]	291	341	322	182	220	257
ρ $[\mathrm{g\,cm^{-3}}]$[g]	1.65	1.66	1.78	1.69	1.76	1.75
$\Delta_f H_m$ $[\mathrm{kJ\,mol^{-1}}]$[h]	179	128	115	202	163	140
$\Delta_f U$ $[\mathrm{kJ\,kg^{-1}}]$[i]	930	649	565	967	756	630
Calculated detonation parameters (EXPLO5 v. 6.02)						
$-Q_{\mathrm{v}}$ $[\mathrm{kJ\,kg^{-1}}]$[j]	4633	4283	4149	5154	4879	4639
T_{Ex} [K][k]	3406	3149	2959	3736	3461	3279
p_{CJ} [kbar][l]	199	198	239	233	255	247
D $[\mathrm{m\,s^{-1}}]$[m]	7252	7302	7916	7637	7930	7941
V_0 $[\mathrm{L\,kg^{-1}}]$[n]	638	667	687	649	662	693

[a] Impact sensitivity (BAM drophammer 1 of 6). [b] Friction sensitivity (BAM friction tester 1 of 6). [c] Electrostatic discharge (OZM Research). [d] Nitrogen content. [e] Oxygen balance ($\Omega = (x\mathrm{O} - 2y\mathrm{C} - 0.5z\mathrm{H})1600/M$). [f] Decomposition temperature. [g] Density at ambient temperature. [h] Calculated enthalpy of formation. [i] Calculated energy of formation. [j] Energy of explosion. [k] Detonation temperature. [l] Detonation pressure. [m] Detonation velocity. [n] Volume of detonation gases.

20 J for **6**. Thus, the compared sensitivities are increased by the *N*-oxide introduction with regards to **1**–**3**. The electrostatic discharges of all herein investigated compounds are greater than the human body can release.[1]

The densities from **1**–**6** as obtained from ambient temperature pycnometer or X-ray (**1**, 293 K) measurements range between 1.65–1.78 g cm^{-3}. The heats of formation were computed by ab initio calculations by using the Gaussian 09 program package[39] at the CBS-4M level of theory. The detonation parameters are calculated with Explo5 computer code (version 6.02)[40] based on the calculated solid state heats of formation and attributed to the corresponding densities at ambient temperature. The physicochemical properties as well as energetic properties are presented in Table 2.2. The *N*-oxidations lead to improved detonation performances of the zwitterionic *N*-oxides **4**–**6** in comparison to the corresponding **1**–**3**. Furthermore, the calculated detonation velocities as well as the volumes of gaseous products increase by gradual amination from 7252 up to 7941 m s^{-1} and 638 to 693 L kg^{-1}. On the other hand, the detonation temperatures of **1** to **6** decrease by gradual amination up to 3279 K.

2.3 Conclusions

5,7-Dinitrobenzotriazole (**1**) and 4,6-dinitrobenzotriazol-3-ium-1-oxide (**4**) have been successfully aminated with trimethylhydrazinium iodide in vicarious nucleophilic substitution reactions. The vicarious nucleophilic substitution reactions of these compounds containing acidic hydrogen atoms proceed through a radical reaction mechanism as evaluated by EPR spectroscopy. The selectivity of the position for the first introduced amino groups was computed by quantum mechanical calculations of the spin density population and fit to the experimental results as proven by crystal structures. Compounds **4** and **5** have zwitterionic structures, which were proved by their X-ray structure analysis and for **4** also in solution by ^{1}H NMR spectroscopy. All presented compounds were characterized comprehensively by vibrational, NMR spectroscopy, and mass spectrometry and selected energetic properties were investigated. The thermal stabilities, the sensitivities towards impact as well as the calculated detonation performance were improved by successive amination. In general, the *N*-oxide derivatives **4**–**6** show higher calculated detonation performances than the corresponding benzotriazoles **1**–**3**.

2.4 Experimental Section

Caution! *Most compounds prepared herein are energetic compounds sensitive to impact, friction and electrostatic discharge. Although there were no problems in handling the*

compounds, proper protective measures (ear protection, Kevlar® gloves, face shield, body armor and earthed equipment) should be used.

5,7-Dinitro-1*H*-benzotriazole (1)

1*H*-Benzotriazole (4.884 g, 41.00 mmol) was dissolved in sulfuric acid (96%, 60 mL) at 0 °C. Nitric acid (65 %, 63 mL) was added dropwise to the clear solution at 0 °C under vigorous stirring. The solution was stirred for 15 min at 0 °C and then heated to 120 °C for 48 h. The solution was cooled to room temperature and poured onto ice (200 mL). A colorless solid precipitated upon cooling in an ice bath, which was collected by suction filtration and was washed with cold water to afford a colorless powder (3.98 g, 19.02 mmol, 46%).
DSC (5 °C min^{-1}): T_{melt} = 193 °C, T_{dec} = 291 °C. ^{1}H NMR (400 MHz, acetone-d_6): δ = 9.47 (d, ^{4}J = 1.9 Hz, 1H, C*H*), 9.20 (d, ^{4}J = 1.9 Hz, 1H, C*H*) ppm. ^{1}H NMR (400 MHz, DMSO-d_6): δ = 16.02 (s, 1H, N*H*), 9.31 (m, 1H, C*H*), 8.91 (m, 1H, C*H*) ppm. ^{13}C{^{1}H} NMR (101 MHz, acetone-d_6): δ = 146.9 (C_{q}), 143.9 (CNO$_2$), 133.1 (CNO$_2$), 129.7 (C_{q}), 122.8 (*C*H), 118.8 (*C*H) ppm. ^{13}C{^{1}H} NMR (101 MHz, DMSO-d_6): δ = 146.6 (C_{q}), 143.7 (CNO$_2$), 133.2 (CNO$_2$), 130.0 (C_{q}), 123.3 (*C*H), 119.0 (*C*H) ppm. ^{14}N{^{1}H} NMR (29 MHz, acetone-d_6): δ = −14 (NO$_2$) ppm. ^{14}N{^{1}H} NMR (29 MHz, DMSO-d_6): δ = −17 (NO$_2$), −19 (NO$_2$) ppm. ^{15}N NMR (41 MHz, DMSO-d_6): δ = −16.1 (t, (CH)$_2$CNO$_2$), −18.8 (d, CHCNO$_2$) ppm. ^{15}N NMR (41 MHz, 50 °C, DMSO-d_6): δ = 11.7 (N_{tri}), −16.4 ((CH)$_2$CNO$_2$), −19.0 (CHCNO$_2$) ppm. IR (ATR): $\tilde{\nu}$ = 3100 (m), 2875 (m), 2755 (m), 1813 (w), 1641 (m), 1599 (w), 1536 (vs), 1487 (s), 1443 (m), 1386 (m), 1339 (vs), 1286 (s), 1275 (vs), 1227 (vs), 1190 (s), 1086 (s), 1068 (s), 988 (s), 968 (vs), 933 (s), 923 (s), 908 (vs), 877 (s), 851 (s), 838 (s), 801 (vs), 778 (s), 742 (vs), 733 (vs), 726 (vs), 688 (vs), 673 (s) cm^{-1}. Raman (1064 nm, 300 mW): $\tilde{\nu}$ = 3120 (1), 3103 (3), 3072 (1), 2687 (1), 1642 (4), 1601 (13), 1555 (3), 1543 (10), 1489 (4), 1437 (16), 1420 (9), 1392 (6), 1352 (100), 1290 (5), 1278 (5), 1235 (2), 1193 (3), 1064 (18), 936 (7), 926 (2), 853 (3), 803 (15), 728 (3), 691 (2), 473 (6), 363 (2), 348 (5), 266 (2) cm^{-1}. MS (DEI^{+}) m/z (%) = 209.1 (100) [M^{+}], 118.1 (3) [C$_6$H$_4$N$_3^{+}$]. EA (C$_6$H$_3$N$_5$O$_4$, 209.12 g mol^{-1}): calcd C 34.46, H 1.45, N 33.49%; found C 34.33, H 1.48, N 33.26%. Sensitivities (grain size: < 100 µm): IS: > 40 J; FS: > 360 N; ESD: 0.3 J.

General procedure for the amination by a VNS reaction:
The heterocyclic compound (0.5 g, 1 equiv) was dissolved in dimethyl sulfoxide (30 mL). 1,1,1-Trimethylhydrazinium iodide (TMHI) (1 or 2 equiv) and sodium *tert*-butoxide (2 equiv) were added to the prepared solution. The violet solution was stirred overnight at ambient temperature, whereby the color changed to dark red. The solution was poured onto ice (25 g) and was acidified to pH2. The precipitate was filtered off to yield the desired

aminated compound.

4-Amino-5,7-dinitro-1*H*-benzotriazole (2)

Following the general procedure by using one equivalent of TMHI a brown solid of **2** was obtained (108 mg, 0.48 mmol, 20%).
DSC (5 °C min^{-1}): T_{melt} = 337 °C, T_{dec} = 341 °C. ^{1}H NMR (270 MHz, DMSO-d_6): δ = 9.71 (s, 1H, NH_2), 9.07 (s, 1H, NH_2), 8.92 (s, 1H, CH) ppm. ^{13}C{^{1}H} NMR (68 MHz, DMSO-d_6): δ = 144.5, 137.4, 125.4 (*C*H), 124.6, 122.1 ppm. ^{14}N{^{1}H} NMR (29 MHz, DMSO-d_6): δ = −15 (NO_2) ppm. IR (ATR): $\tilde{\nu}$ = 3399 (w), 3293 (w), 3261 (w), 3179 (m), 3083 (w), 1642 (s), 1614 (m), 1597 (m), 1543 (m), 1489 (m), 1444 (w), 1396 (w), 1300 (vs), 1261 (s), 1229 (vs), 1215 (vs), 1084 (m), 1045 (m), 990 (s), 940 (m), 893 (w), 814 (m), 780 (vw), 756 (vw), 734 (w), 719 (w), 699 (m), 662 (m) cm^{-1}. Raman (1064 nm, 300 mW): $\tilde{\nu}$ = 3241 (1), 1639 (9), 1600 (2), 1540 (9), 1513 (17), 1490 (1), 1446 (8), 1418 (1), 1398 (1), 1325 (21), 1300 (100), 1246 (5), 1234 (53), 1218 (12), 1161 (2), 1087 (2), 1025 (2), 997 (15), 898 (5), 815 (10), 768 (1), 735 (16), 705 (2), 474 (4), 433 (2), 376 (5), 334 (10), 217 (2) cm^{-1}. MS (DEI$^+$): m/z (%) = 224.2 (100) [M$^+$]. EA ($C_6H_4N_6O_4$, 224.13 g mol^{-1}): calcd C 32.15, H 1.80, N 37.50%; found C 32.19, H 1.85, N 37.35%. Sensitivities (grain size: < 100 µm): IS: > 40 J; FS: > 360 N; ESD: 0.85 J.

4,6-Diamino-5,7-dinitro-1*H*-benzotriazole (3)

Following the general procedure by using 2 equiv of TMHI a brown solid of **3** was obtained as a DMSO adduct (583 mg, 1.84 mmol, 80%).
EA ($C_8H_{11}N_7O_5S$, 317.28 g mol^{-1}): calcd C 29.85, H 3.68, N 29.76, S 10.34%; found C 30.28, H 3.49, N 30.06, S 10.11%.
Without DMSO: Potassium salt of **3** (67 mg, 0.23 mmol) was added to water (20 mL). This suspension was acidified with 2M hydrochloric acid to pH2 and was stirred for 1 h at room temperature. The solid was filtered off to afford a brown solid (26 mg, 0.11 mmol, 47%).
DSC (5 °C min^{-1}): T_{dec} = 322 °C. ^{1}H NMR (400 MHz, DMSO-d_6): δ = 10.33–9.44 (m, 4H, NH_2) ppm. ^{13}C{^{1}H} NMR (101 MHz, DMSO-d_6): δ = 149.2, 147.4, 131.9, 129.2, 116.7, 108.6 ppm. ^{14}N{^{1}H} NMR (29 MHz, DMSO-d_6): δ = −16 (NO_2) ppm. IR (ATR): $\tilde{\nu}$ = 3381 (w), 3291 (w), 3186 (w), 3077 (vw), 1639 (m), 1615 (m), 1543 (w), 1487 (w), 1417 (w), 1396 (w), 1288 (vs), 1262 (s), 1230 (vs), 1193 (s), 1162 (w), 1085 (w), 1046 (w), 1024 (vw), 991 (s), 937 (vw), 896 (vw), 815 (m), 781 (w), 737 (m), 702 (m), 659 (m) cm^{-1}. Raman (1064 nm, 300 mW): $\tilde{\nu}$ = 1636 (15), 1599 (7), 1540 (13), 1511 (18), 1484 (9), 1446 (17), 1417 (14), 1399 (15), 1325 (79), 1301 (100), 1264 (20), 1234 (63), 1217 (25), 1196 (17), 1022 (7), 996 (19), 895 (8), 815 (19), 735 (19), 707 (7), 476 (9), 368 (11), 335 (14) cm^{-1}. MS (DEI$^+$)

m/z (%) = 239.0 (100) [M^+]. EA ($C_6H_5N_7O_4$, 239.15 g mol^{-1}): calcd C 30.13, H 2.11, N 41.00%; found C 29.85, H 2.35, N 39.44%. Sensitivities (grain size: < 100 µm): IS: 35 J; FS: > 360 N; ESD: 1.5 J.

4,6-Dinitrobenzotriazol-3-ium-1-oxide (4)

Picryl chloride (0.738 g, 2.98 mmol) was added to a solution of hydrazine hydrate (0.75 mL, 15.46 mmol) in 5% aqueous sodium hydrogen carbonate solution (80 mL) at 0 °C. The solution was stirred for 20 min at 0 °C and then for 2 h at room temperature. After heating for 1 h at 60 °C, activated charcoal (1 g) was added to the hot solution. It was filtered hot, cooled to 0 °C, and acidified to pH2 with conc. hydrochloric acid. The solvent was concentrated in vacuum until a precipitate occurred. The brown precipitate was filtered off to yield **4** as hydrate (392 mg, 1.61 mmol, 54%).
^{1}H NMR (270 MHz, DMSO-d_6): δ = 9.11 (d, ^4J = 1.9 Hz, 1H, C*H*), 8.89 (d, ^4J = 1.9 Hz, 1H, C*H*) ppm. ^{13}C{^{1}H} NMR (68 MHz, DMSO-d_6): δ = 136.7, 129.8, 117.1 (*C*H), 114.8 (*C*H) ppm. EA ($C_6H_3N_5O_5 \cdot H_2O$, 243.13 g mol^{-1}): calcd C 29.64, H 2.07, N 28.80%; found C 29.61, H 2.04, N 28.52%. Sensitivities (grain size: < 100 µm): IS: > 40 J; FS: > 360 N; ESD: 0.3 J.
Recrystallization from acetonitrile afforded pure 4,6-dinitrobenzotriazol-3-ium-1-oxide as an orange solid:
DSC (5 °C min^{-1}): T_{dec} = 182 °C. ^{1}H NMR (400 MHz, acetone-d_6): δ = 9.14 (d, ^4J = 1.9 Hz, 1H, C*H*), 9.05 (d, ^4J = 1.9 Hz, 1H, C*H*) ppm. ^{1}H NMR (400 MHz, DMSO-d_6) δ = 13.55 (s, 1H, N*H*), 9.06 (m, 1H, C*H*), 8.84 (m, 1H, C*H*) ppm. ^{13}C{^{1}H} NMR (101 MHz, acetone-d_6): δ = 146.0, 138.1, 136.7, 131.7, 118.5 (*C*H), 115.5 (*C*H) ppm. ^{14}N{^{1}H} NMR (29 MHz, acetone-d_6): δ = −20 (NO_2) ppm. ^{15}N NMR (29 MHz, DMSO-d_6): δ = −1.2 (N_{tri}), −17.1 (m, $(CH)_2CNO_2$), −19.0 (d, $CHCNO_2$), −71.3 (m, N_{tri}NH) ppm. IR (ATR): $\tilde{\nu}$ = 3105 (vw), 2654 (vw), 2296 (br, vw), 2230 (vw), 2142 (vw), 1783 (vw), 1703 (vw), 1641 (m), 1557 (m), 1542 (m), 1506 (m), 1434 (s), 1383 (vw), 1368 (vw), 1337 (vs), 1278 (s), 1245 (m), 1189 (m), 1184 (m), 1176 (m), 1156 (s), 1055 (m), 982 (m), 934 (vw), 916 (m), 895 (w), 884 (m), 827 (m), 805 (vs), 769 (m), 752 (s), 734 (vs), 723 (s), 704 (s) cm^{-1}. Raman (1064 nm, 300 mW): $\tilde{\nu}$ = 3104 (7), 3089 (4), 1645 (16), 1620 (17), 1565 (5), 1546 (9), 1508 (5), 1464 (6), 1418 (7), 1374 (20), 1342 (100), 1290 (8), 1284 (8), 1249 (6), 1191 (7), 1180 (7), 1159 (28), 1059 (10), 984 (5), 935 (3), 917 (4), 828 (3), 809 (27), 707 (3), 687 (4), 609 (11), 430 (6), 414 (7), 358 (6), 347 (8), 314 (9), 306 (7) cm^{-1}. MS (DEI$^+$): m/z (%) = 225.0 (39) [M^+], 209.0 (41) [$C_6H_3N_5O_4$+H^+]. EA ($C_6H_3N_5O_5$, 225.12 g mol^{-1}): calcd C 32.01, H 1.34, N 31.11%; found C 32.19, H 1.37, N 31.05%. Sensitivities (grain size: < 100 µm): IS: 2 J; FS: > 360 N; ESD: 0.2 J.

7-Amino-4,6-dinitrobenzotriazol-3-ium-1-oxide (5)

The compound was synthesized according to the general procedure with 1 equiv of TMHI to yield an ocher solid (162 mg, 0.62 mmol, 46%).
DSC (5 °C min^{-1}): T_{dehyd} = 107 °C, T_{dec} = 220 °C. ^{1}H NMR (400 MHz, DMSO-d_6): δ = 9.38 (m, 2H, NH_2), 8.88 (s, 1H, CH) ppm. ^{13}C{^{1}H} NMR (101 MHz, DMSO-d_6): δ = 142.4, 131.6, 126.3, 122.7, 121.8, 119.1 ppm. ^{14}N{^{1}H} NMR (29 MHz, DMSO-d_6): δ = −16 (NO_2) ppm. IR (ATR): $\tilde{\nu}$ = 3561 (vw), 3397 (w), 3275 (w), 3226 (w), 3067 (vw), 2913 (vw), 2658 (br, vw), 2361 (vw), 1644 (s), 1608 (s), 1544 (m), 1501 (m), 1449 (w), 1426 (m), 1413 (m), 1388 (m), 1321 (m), 1293 (vs), 1232 (vs), 1183 (s), 1151 (m), 1130 (m), 1056 (w), 986 (m), 934 (w), 888 (w), 819 (m), 782 (m), 771 (m), 762 (m), 740 (vw), 729 (vw), 718 (vw), 700 (w) cm^{-1}. Raman (1064 nm, 300 mW): $\tilde{\nu}$ = 3278 (6), 3065 (5), 2859 (10), 2735 (4), 2492 (4), 1868 (4), 1653 (22), 1587 (6), 1546 (17), 1510 (16), 1450 (11), 1430 (15), 1399 (11), 1382 (9), 1327 (87), 1299 (100), 1241 (75), 1192 (13), 1156 (6), 1138 (7), 1064 (7), 1057 (9), 989 (9), 977 (4), 894 (6), 819 (8), 781 (11), 736 (27), 704 (12), 432 (5), 365 (6), 332 (7) cm^{-1}. MS (DCI^{+}): m/z (%) = 241 (7) [M^{+}]. EA ($C_6H_4N_6O_5 \cdot 1.25\,H_2O$, 262.65 g mol^{-1}): calcd C 27.44, H 2.49, N 32.00%; found C 27.86, H 2.51, N 32.31%. Sensitivities (grain size: < 100 µm): IS: > 40 J; FS: > 360 N; ESD: 0.5 J.
5 · 1.25 H_2O was dried at 120 °C for five days yielding waterfree **5**.
IR (ATR): $\tilde{\nu}$ = 3410 (vw), 3271 (w), 3058 (vw), 2918 (vw), 1655 (br, vw), 1645 (s), 1606 (m), 1544 (w), 1497 (w), 1423 (w), 1380 (m), 1289 (s), 1226 (vs), 1179 (m), 1149 (m), 1129 (m), 1107 (m), 1053 (w), 982 (m), 945 (w), 886 (w), 818 (w), 779 (m), 770 (w), 761 (w), 730 (w), 714 (vw), 699 (w), 660 (vw) cm^{-1}. Raman (1064 nm, 300 mW): $\tilde{\nu}$ = 3268 (4), 2702 (1), 2718 (5), 1648 (18), 1549 (15), 1513 (19), 1439 (12), 1317 (7), 1299 (100), 1231 (68), 1183 (15), 1148 (6), 1060 (8), 986 (10), 889 (7), 816 (8), 786 (5), 733 (25), 702 (7), 509 (5), 403 (4), 332 (7) cm^{-1}. EA ($C_6H_4N_6O_5$, 240.13 g mol^{-1}): calcd C 30.01, H 1.68, N 35.00%; found C 30.09, H 2.06, N 34.57%. Sensitivities (grain size: < 100 µm): IS: 5 J; FS: > 360 N; ESD: 1.0 J.

5,7-Diamino-4,6-dinitrobenzotriazol-3-ium-1-oxide (6)

The general procedure was performed with 2 equiv of TMHI. Recrystallization from water afforded an orange solid (0.525 g, 2.06 mmol, 64%).
DSC (5 °C min^{-1}): T_{dec} = 257 °C. ^{1}H NMR (270 MHz, DMSO-d_6): δ = 15.31 (br s, 0.2H, NH), 10.37–9.79 (m, 4H, NH_2) ppm. ^{13}C{^{1}H} NMR (68 MHz, DMSO-d_6): δ = 149.3, 146.0, 145.2, 131.6, 114.8, 110.9 ppm. ^{14}N{^{1}H} NMR (29 MHz, DMSO-d_6): δ = −15 (NO_2) ppm. IR (ATR): $\tilde{\nu}$ = 3362 (w), 3244 (w), 3197 (vw), 1648 (s), 1608 (s), 1533 (m), 1441 (w), 1371 (m), 1338 (m), 1287 (vs), 1254 (vs), 1229 (vs), 1191 (vs), 1157 (s), 1096 (m), 976 (w), 879

(vw), 817 (w), 778 (m), 745 (w), 692 (m), 672 (m) cm^{-1}. Raman (1064 nm, 300 mW): $\tilde{\nu}$ = 3239 (10), 2111 (20), 1645 (27), 1606 (26), 1586 (18), 1510 (14), 1449 (24), 1390 (64), 1384 (64), 1285 (59), 1255 (38), 1233 (45), 1193 (100), 1180 (84), 1162 (24), 1122 (11), 1090 (12), 1057 (14), 977 (41), 885 (22), 819 (15), 782 (36), 755 (10), 640 (18), 571 (40), 420 (21), 406 (18), 366 (36), 354 (36) cm^{-1}. MS (DEI$^+$): m/z (%) = 255 (8) [M^+], 239 (28) [$C_6H_5N_7O_4^+$], 209 (10) [$C_6H_3N_5O_4^+$]. EA ($C_6H_5N_7O_5$, 255.15 g mol^{-1}): calcd C 28.24, H 1.98, N 38.43%; found C 28.78, H 2.10, N 37.53%. Sensitivities (grain size: < 100 µm): IS: 20 J; FS: > 360 N; ESD: 1.5 J.

2.5 References

[1] T. M. Klapötke, *Chemie der hochenergetischen Materialien*, 1st ed., de Gruyter, Berlin, **2009**.

[2] T. M. Klapötke, C. Pflüger, M. W. Reintinger, in *New Trends Res. Energ. Mater., Proc. Semin.* 16th, Pardubice, Czech Republic, **2013**, *2*, pp. 842–856.

[3] T. M. Klapötke, C. Pflüger, M. Sućeska, in *New Trends Res. Energ. Mater., Proc. Semin.*, 17th, Pardubice, Czech Republic, **2014**, *2*, pp. 754–768.

[4] J. P. Agrawal, *High Energy Materials, Propellants Explosives and Pyrotechnics*, Wiley-VCH, Weinheim, Germany, **2010**.

[5] H. Feuer, A. Nielsen, *Nitro Compounds: Recent Advances in Synthesis and Chemistry*, Wiley-VCH, Weinheim, Germany, **1990**.

[6] A. Nielsen, *Nitrocarbons*, Wiley-VCH, Weinheim, Germany, **1995**.

[7] M. A. Hiskey, D. E. Chavez, D. L. Naud, S. F. Son, H. L. Berghout, C. A. Bolme, in *Proc. Int. Pyrotech. Semin. 27*, 3–14, Grand Junction, CO (USA), **2000**.

[8] J. Šarlauskas, in *New Trends Res. Energ. Mater., Proc. Semin.*, 13th, Pardubice, Czech Republic, **2010**, *2*, pp. 730–737.

[9] T. M. Klapötke, A. Preimesser, J. Stierstorfer, *Propellants, Explos., Pyrotech.* **2015**, *40*, 60–66.

[10] W. Naixing, C. Boren, O. Yuxiang, *Propellants, Explos., Pyrotech.* **1994**, *19*, 145–148.

[11] L. Türker, S. Variş, *Polycyclic Aromat. Compd.* **2009**, *29*, 228–266.

[12] M. Malow, K. D. Wehrstedt, S. Neuenfeld, *Tetrahedron Lett.* **2007**, *48*, 1233–1235.

[13] A. Freyer, C. Lowema, R. Nissan, W. Wilson, *Aust. J. Chem.* **1992**, *45*, 525–539.

[14] D. Srinivas, V. D. Ghule, S. P. Tewari, K. Muralidharan, *Chem. Eur. J.* **2012**, *18*, 15031–15037.

[15] J. P. Agrawal, *Prog. Energy Combust. Sci.* **1998**, *24*, 1–30.

[16] J. S. Murray, P. Politzer, in *Chemistry and Physics of Energetic Materials* (Ed.: S. N. Bulusu), Kluwer, Dordrecht, Netherlands, **1990**, pp. 157–173.

[17] C. J. Wu, L. E. Fried, *J. Phys. Chem. A* **2000**, *104*, 6447–6452.

[18] M. R. Manaa, R. H. Gee, L. E. Fried, *J. Phys. Chem. A* **2002**, *106*, 8806–8810.

[19] J. Li, *J. Phys. Chem. B* **2010**, *114*, 2198–2202.

[20] R. D. Schmidt, G. S. Lee, P. F. Pagoria, A. R. Mitchell, R. Gilardi, *J. Heterocycl. Chem.* **2001**, *38*, 1227–1230.

[21] T. I. Vakul'skaya, I. A. Titova, G. V. Dolgushin, V. A. Lopyrev, *Magn. Reson. Chem.* **2005**, *43*, 1023–1027.

[22] A. Albini, S. Pietra, *Heterocyclic N-Oxides*, CRC, Boca Raton, FL (USA), **1991**.

[23] A. R. Katritzky, J. N. Lam, *Heterocycles* **1992**, *33*, 1011–1049.

[24] M. Begtrup, in *Advances in Heterocyclic Chemistry, Vol. 106* (Ed.: A. R. Katritzky), Academic Press, San Diego, CA (USA) **2012**, pp. 1–109.

[25] J. Šarlauskas, Ž. Anusevičius, A. Misiūnas, *Cent. Eur. J. Energ. Mater.* **2012**, *9*, 365–386.

[26] T. M. Klapötke, D. G. Piercey, J. Stierstorfer, *Chem. Eur. J.* **2011**, *17*, 13068–13077.

[27] A. A. Dippold, T. M. Klapötke, *J. Am. Chem. Soc.* **2013**, *135*, 9931–9938.

[28] J. Kehler, A. Püschl, O. Dahl, *Acta Chem. Scand.* **1996**, *50*, 1171–1173.

[29] K. D. Wehrstedt, P. A. Wandrey, D. Heitkamp, *J. Hazard. Mater.* **2005**, *126*, 1–7.

[30] C. J. McHugh, D. R. Tackley, D. Graham, *Heterocycles* **2002**, *57*, 1461–1470.

[31] T. I. Vakul'skaya, I. A. Titova, L. I. Larina, O. N. Verkhozina, G. V. Dolgushin, V. A. Lopyrev, *Chem. Heterocycl. Compd.* **2006**, *42*, 1427–1434.

[32] HyperChem™, version 7.0, HyperCube Inc., **2002**.

[33] A. Escande, J. L. Galigne, J. Lapasset, *Acta Crystallogr. B* **1974**, *30*, 1490–1495.

[34] A. Bondi, *J. Phys. Chem.* **1964**, *68*, 441–451.

[35] P. Politzer, P. Lane, J. S. Murray, *Mol. Phys.* **2013**, *112*, 719–725.

[36] Test methods according to the *UN Manual of Test and Criteria, Recommendations on the Transport of Dangerous Goods*, United Nations Publication, New York, Geneva, 4th revised ed., **2003**: Impact: Insensitive >40 J, less sensitive ≥ 35 J, sensitive ≥ 4 J, very sensitive ≤ 3 J; Friction: Insensitive >360 N, less sensitive $= 360$ N, sensitive <360 N a. >80 N, very sensitive ≤ 80 N, extremely sensitive ≤ 10 N.

[37] NATO, *Standardization Agreement 4489 (STANAG 4489)*, *Explosives, Impact Sensitivity Tests* **1999**.

[38] NATO, *Standardization Agreement 4487 (STANAG 4487)*, *Explosives, Friction Sensitivity Tests* **2002**

[39] M. J. Frisch, G. W. Trucks, H. B. Schlegel, G. E. Scuseria, M. A. Robb, J. R. Cheeseman, G. Scalmani, V. Barone, B. Mennucci, G. A. Petersson, H. Nakatsuji, M. Caricato, X. Li, H. P. Hratchian, A. F. Izmaylov, J. Bloino, G. Zheng, J. L. Sonnenberg, M. Hada, M. Ehara, K. Toyota, R. Fukuda, J. Hasegawa, M. Ishida, T. Nakajima, Y. Honda, O. Kitao, H. Nakai, T. Vreven, J. J. A. Montgomery, J. E. Peralta, F. Ogliaro, M. Bearpark, J. J. Heyd, E. Brothers, K. N. Kudin, V. N. Staroverov, R. Kobayashi, J. Normand, K. Raghavachari, A. Rendell, J. C. Burant, S. S. Iyengar, J. Tomasi, M. Cossi, N. Rega, J. M. Millam, M. Klene, J. E. Knox, J. B. Cross, V. Bakken, C. Adamo, J. Jaramillo, R. Gomperts, R. E. Stratmann, O. Yazyev, A. J. Austin, R. Cammi, C. Pomelli, J. W. Ochterski, R. L. Martin, K. Morokuma, V. G. Zakrzewski, G. A. Voth, P. Salvador, J. J. Dannenberg, S. Dapprich, A. D. Daniels, O. Farkas, J. B. Foresman, J. V. Ortiz, J. Cioslowski, D. J. Fox, Gaussian 09, Revision A.02, Inc., Wallingford CT, **2009**.

[40] M. Sućeska, Explo5 program, 6.02 ed., Zagreb, Croatia, **2014**.

Energetic Materials based on 5,7-Dinitrobenzotriazole and 4,6-Dinitrobenzotriazol-3-ium-1-oxide Derivatives

T. M. Klapötke, C. Pflüger, and M. W. Reintinger

Eur. J. Inorg. Chem. **2016**, *1*, 136–147.

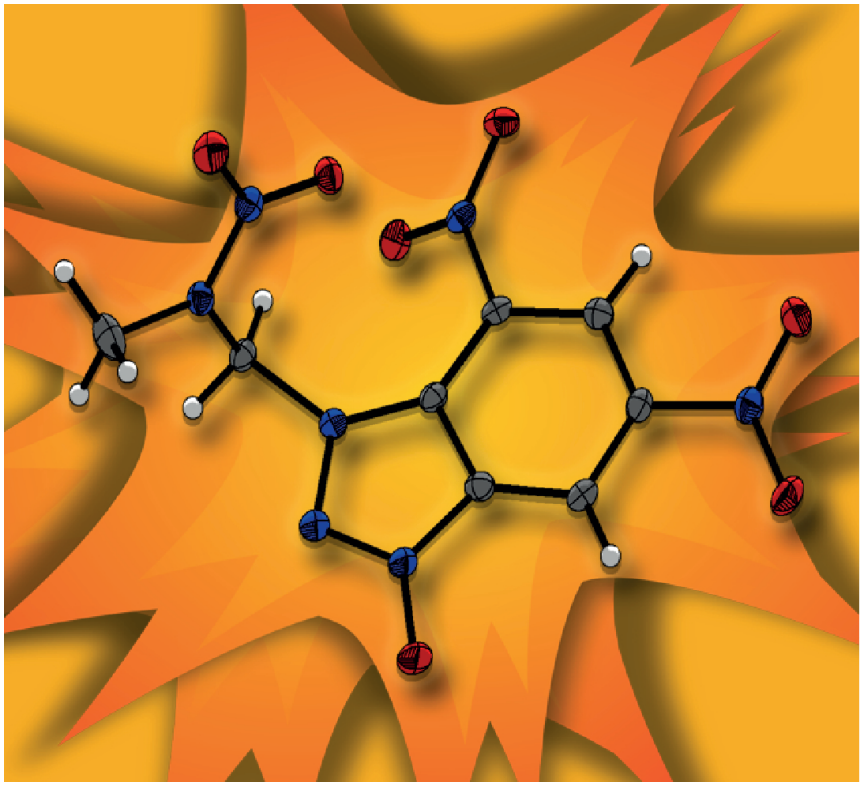

Energetic Materials based on 5,7-Dinitrobenzotriazole and 4,6-Dinitrobenzotriazol-3-ium-1-oxide Derivatives

T. M. Klapötke, C. Pflüger, and M. W. Reintinger
Eur. J. Inorg. Chem. **2016**, *1*, 136–147.

Abstract

Tailoring the properties of energetic materials is an ongoing challenge in the development of new materials. Various nitrogen-rich salts of 5,7-dinitrobenzotriazole, 4,6-dinitrobenzotriazol-1-oxide, and 5,7-diamino-4,6-dinitrobenzotriazol-1-oxide were synthesized to improve the energetic properties and stabilities of the corresponding nonionic parent compounds. Furthermore, the acidic N−H group was derivatized by alkylation to introduce nitramines as another energetic group. All presented compounds were comprehensively characterized by NMR and vibrational spectroscopy, mass spectrometry, and elemental analysis. The energetic properties were also explored and their detonation performances calculated with the EXPLO5 code. Several compounds were additionally investigated by single-crystal X-ray diffraction.

3.1 Introduction

The challenge to investigate new explosives is based on three main demands which should be further improved: 1) performance, 2) safety, and 3) practicability.[1] The performance of secondary explosives is well characterized, for example, by important quantities such as their density, heat of formation, detonation pressure, detonation velocity, and energy of explosion. The term safety refers to aspects such as thermal and long-term stability, sensitivity to impact, friction, and electrostatic discharge, and compatibility. The potential for large-scale synthesis, yields, synthetic costs, and the crystallization process are included in the practicability. Furthermore, the environmental and toxicological acceptability is an increasing goal for both secondary and primary explosives.[2–4]

Secondary explosives are used in large amounts in mixtures for military and civil applications. In these mixtures the high acidity of the heterocyclic protons causes compatibility problems in formulations of explosive charges,[5] which can be avoided by salt formation or by alkylation of the N−H group.

Energetic salts show many advantages over conventional nonionic energetic compounds. They often offer promising properties as energetic materials and thereby have lower vapor pressures.[6–8] Especially decreased sensitivities to friction, impact, and electrostatic discharge are required, but unfortunately high performance and low sensitivities seem to

be contradictory.[2,3] Thus, the choice of proper cations and anions has an impact on the desired properties of energetic salts and their applications.
Primary explosives are simply initiated by, for example, heat or shock and therefore used as initiators for secondary explosives to enable controlled detonations. In the 1980s primary explosives such as the potassium salts of 4,6-dinitrobenzofuroxan (KDNBF)[9] and hydroxyaminodinitrobenzofuroxan[10] as well as other amino- and dinitrobenzofuroxans[11,12] attracted attention as potential replacements for the toxic lead azide. The most promising, potassium 4,6-dinitrobenzofuroxan, was first synthesized by Drost in 1899.[13] Over the past century many efforts have been undertaken in the chemistry of benzofuroxans to evaluate their potential as energetic materials. Therefore, it is well known that the replacement of a nitro group by a furoxan ring yields higher density, detonation velocity, and insensitivity.[14]
Energetic salts of the related 4,6-dinitrobenzotriazol-3-ium-1-oxide had not been investigated until now, although they may offer interesting energetic properties. 4,6-Dinitrobenzotriazol-3-ium-1-oxide is very sensitive towards impact, as shown in a previous study by us.[15]
In general, deprotonation of azoles such as triazoles positively influences the sensitivities towards outer stimuli (impact, friction, electrostatic discharge) and thermal stability.[4] Furthermore, the use of nitrogen-containing anions and cations leads to higher heats of formation and higher densities.
Herein, energetic salts of 5,7-dinitrobenzotriazole, 4,6-dinitrobenzotriazol-3-ium-1-oxide, and 5,7-diamino-4,6-dinitrobenzotriazol-3-ium-1-oxide are presented and investigated with respect to stability and performance.
Additionally, 5,7-dinitrobenzotriazole and 4,6-dinitrobenzotriazol-3-ium-1-oxide were alkylated with 1-chloro-2-nitrazapropane to introduce another energetic group, namely, a nitramine, which leads to higher densities than methylation due to intermolecular interactions.[16–18]

3.2 Results and Discussion

3.2.1 Syntheses

The syntheses of the parent compounds starting from benzotriazole or picryl chloride are described in the literature (Scheme 3.1).[15,19,20]
Nitrogen-rich salts of 5,7-dinitrobenzotriazole (**1**), 4,6-dinitrobenzotriazol-3-ium-1-oxide (**4**), and 5,7-diamino-4,6-dinitrobenzotriazol-3-ium-1-oxide (**6**) were synthesized. The nitrogen-rich (**a**–**d**) and the potassium (**f**) salts depicted in Scheme 3.1 were synthesized by adding 1 equiv. of the corresponding base (potassium hydroxide, ammonia, hydroxylamine, guanidine, aminoguanidine; typically a carbonate) to a suspension of the parent compound in

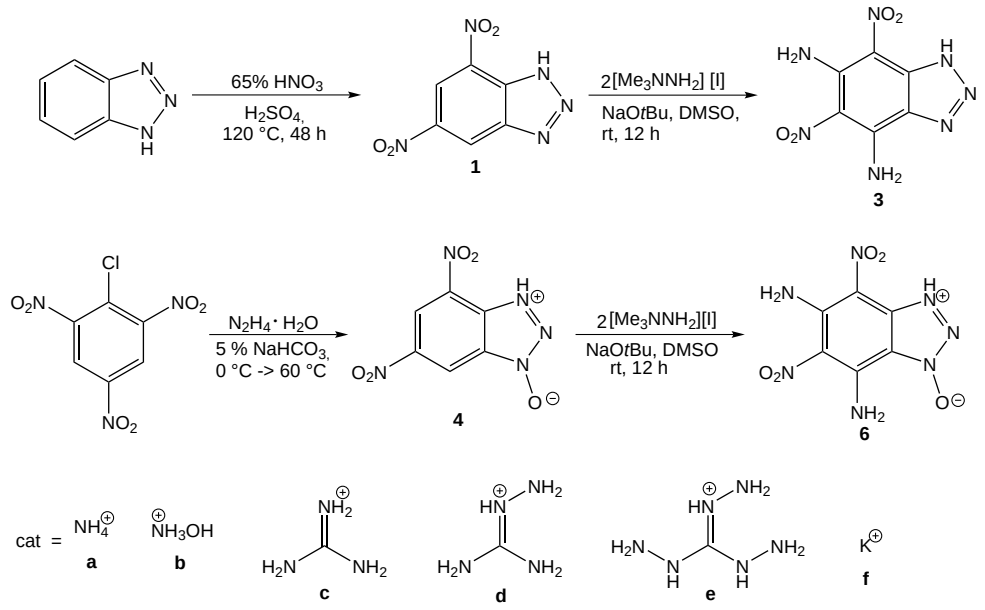

Scheme 3.1: Synthesis of **1**, **3**, **4**, and **6**, their nitrogen-rich salts **1a**–**e**, **4a**–**4e**, and **6a**–**6d**, and their potassium salts **1f**–**6f**.

water. The triaminoguanidinium salts (**e**) were obtained by metathesis reaction from the corresponding potassium salts and triaminoguanidinium chloride.

The acidity of 4,6-diamino-5,7-dinitrobenzotriazole (**3**) is too low for it to be deprotonated by the nitrogen-rich bases. Several attempts to obtain nitrogen-rich salts starting from the free acid **3** or the potassium salt **3f** failed. In both cases only the free acid was recovered. The reaction of the potassium salts **1f** and **4f** with 1-chloro-2-nitrazapropane yielded the isomeric alkylation products (Scheme 3.2). The alkylation of **1f** led to the formation of the three isomeric products of **7** in a ratio of 1:0.2:0.1, as determined from the ^{1}H NMR spectrum of the mixture of isomers. Two different isomers were formed by the alkylation of **4f**, whereby the alkylation mainly took place at the nitrogen atom, affording the zwitterionic **8x**, instead of the oxygen atom of the *N*-oxide, in a ratio of 1:0.3, as determined by ^{1}H NMR spectroscopy.

3.2.2 NMR Spectroscopy

In general, all compounds were characterized by ^{1}H, ^{13}C{^{1}H}, and ^{14}N{^{1}H} spectroscopy with D_2O, acetone-d_6, or DMSOd_6 as solvent. Due to the low solubility of several synthesized salts, especially those of **6**, some signals of the carbon atoms and nitrogen atoms could not be observed in the ^{13}C{^{1}H} and ^{14}N{^{1}H} NMR spectra, respectively.

The resonances of the aromatic protons of salts **1a**–**1f** were observed as doublets with coupling constants around 2 Hz or as multiplets, both in the range from 9.20 to 8.69 ppm. For the potassium salt **3f** two different shifts of the protons of the amino groups are

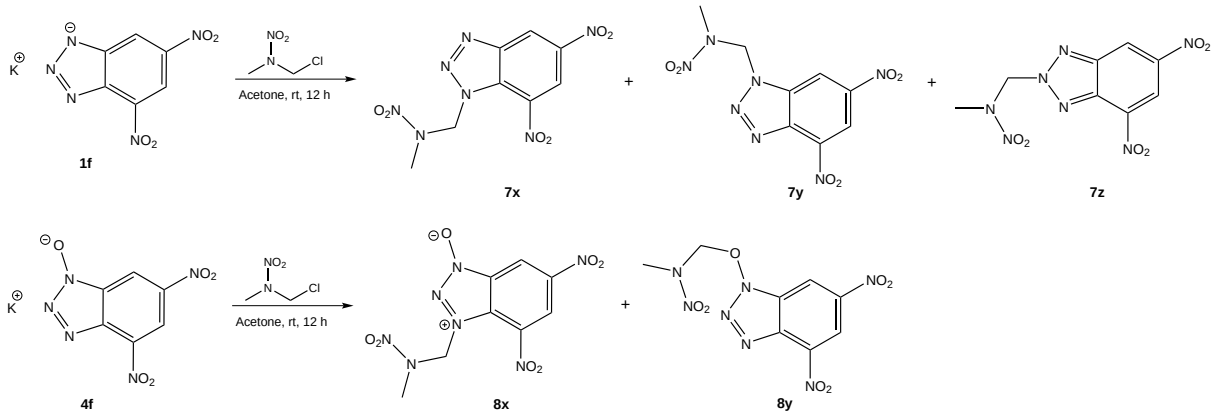

Scheme 3.2: Alkylation of **1f** and **4f** with 1-chloro-2-nitrazapropane.

observed (10.28 and 8.96 ppm). The same trend is observed in the ^{1}H NMR spectra of salts **4a**–**4f**, **6a**–**6d**, and **6f**. The resonances of protons of the nitrogen-rich guanidinium based cations are observed as broad signals at higher field in the range of 6.94–4.46 ppm.
The ^{13}C{^{1}H} NMR spectra show the expected resonances of the aromatic and guanidinium-based carbon atoms (see Experimental Section). For the two different nitro groups of the aromatic ring systems only one signal is observed in the ^{14}N{^{1}H} NMR spectra around −15 ppm. Furthermore, the signal of the positive charged nitrogen atoms of the ammonium (**1a**, **4a**, **6a**), hydroxylammonium (**1b**, **4b**), aminoguanidinium (**4d**), and triaminoguanidinium (**1e**) cations are observed around −359 ppm.
The reactions of **1f** and **4f** with 1-chloro-2-nitrazapropane yielded three and two constitutional isomers of the corresponding nitramines, respectively. The isomers of **7** were formed in a 1:0.2:0.1 ratio, as seen from the resonances in the ^{1}H NMR spectrum. The ^{1}H NMR spectrum of **8** shows the formation of two constitutional isomers in the ratio 1:0.3, derived from the different shifts of the aromatic protons, while the methylene (δ = 6.71 ppm) and methyl protons (δ = 3.60 ppm) show the same shifts. The signals of the methylene carbon atoms are observed at δ = 80.5 and 65.6 ppm, and those of the methyl carbon atoms at δ = 39.7 and 38.2 ppm. The signal at δ = 80.5 ppm corresponds to the minor *O*-alkylated isomer **8y** and the signal at δ = 65.6 ppm to the *N*-alkylated **8x**. The resonances of the nitrogen atoms of the different nitro groups of **7** and **8** are observed in the ranges between −19 to −31 ppm and −13 to −26 ppm, respectively.

3.2.3 Crystal Structures

Several herein described salts (**1b**, **1c**, **1e**, **1l**, **1f**, **4c**, **4e**, **6c**, **6d**) and the nitramines **7x** and **8x** were characterized by single-crystal X-ray diffraction (Figure 3.1). Selected data and parameters of the measurements and refinements are gathered in Table A.7–Table

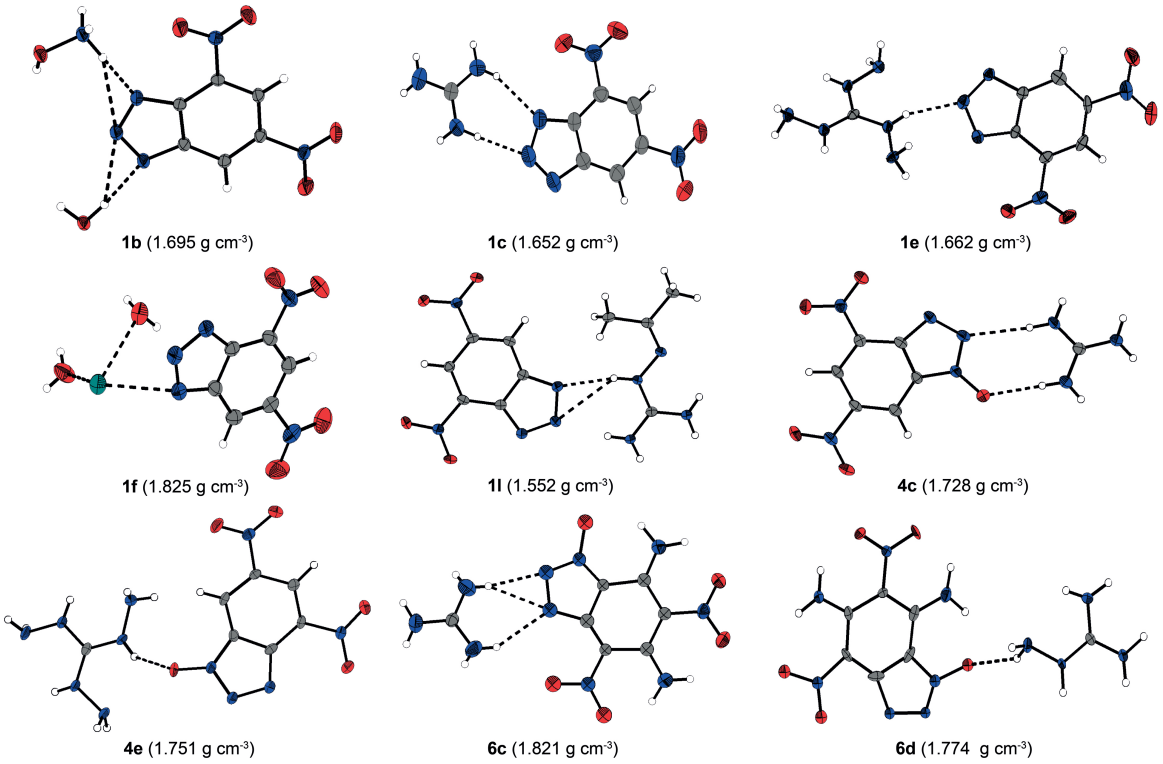

Figure 3.1: Molecular structures of salts **1b**, **1c**, **1e**, **1f**, **1l**, **4c**, **4e**, **6c**, and **6d**. Ellipsoids are drawn at 50% probability.

A.10.

Compound **1d** crystallizes from hot acetone as 1-(propan-2-ylidene)aminoguanidinium 5,7-dinitrobenzotriazolate (**1l**) in the triclinic space group $P\bar{1}$. The guanidinium (**6c**) and aminoguanidinium (**6d**) salts of 5,7-diamino-4,6-dinitrobenzotriazol-1-oxide crystallize in the triclinic space group $P\bar{1}$ and the monoclinic space group $C2/c$, respectively. Unfortunately, the structures of both **6c** and **6d** are disordered with different orientations of the triazol-1-oxide and the neighboring nitro group, as shown in the Appendix (Figure A.5 and Figure A.6). The disorder could not be completely resolved, and therefore the structures are not discussed.

The crystal structures of the hydroxylammonium salt **1b**·H_2O and the guanidinium salt **1c** are supported by various hydrogen bonds involving all nitrogen atoms of the deprotonated triazole rings and the cations and, in the case of **1b**, also the water of crystallization, and they show crystal densities of 1.695 g cm^{-3} (173 K) and 1.652 g cm^{-3} (293 K), respectively. The interactions are discussed in detail for the triaminoguanidinium salt **1e**. Triaminoguanidinium 5,7-dinitrobenzotriazolate (**1e**) crystallizes in the monoclinic space group $P2_1/c$ with four formula units per unit cell and a density of 1.662 g cm^{-3} at 100 K. The density is decreased in comparison to the parent 5,7-dinitrobenzotriazole (ρ = 1.694 g cm^{-3} at 173 K).[15] The structure of **1e** shows alternating layers of anions and cations along the c

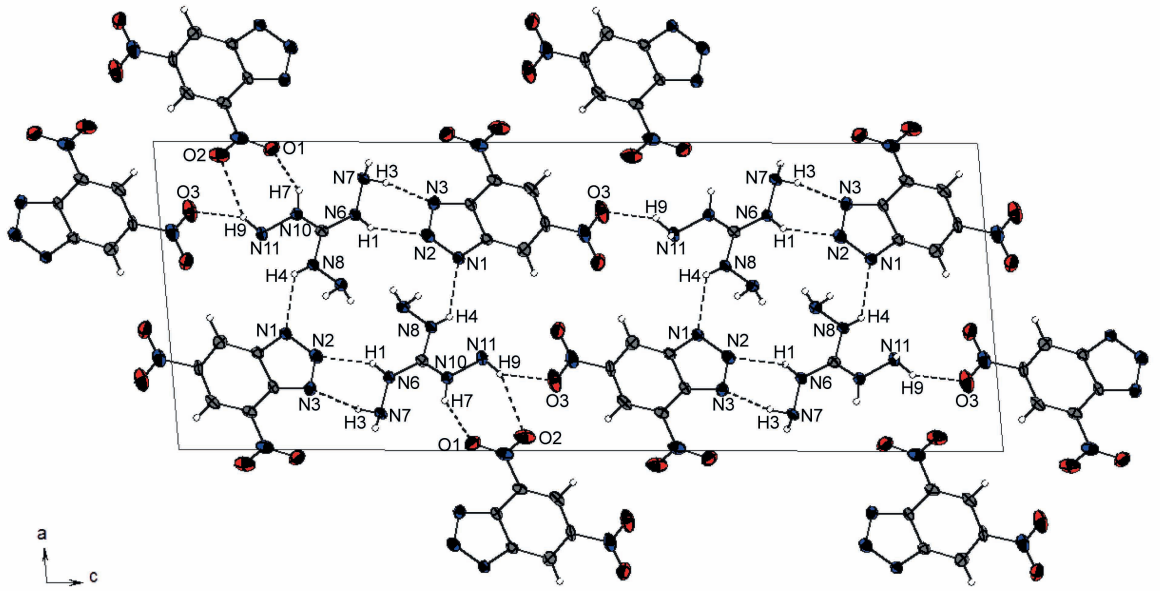

Figure 3.2: View of the layer structure of **1e** along the *b* axis. Hydrogen bonds are shown as black dotted lines. Ellipsoids are drawn at 50% probability.

axis and opposed layers along the *a* axis (Figure 3.2). The layers are connected by various hydrogen bonds between the cations and anions. The twisting of the nitro group of N4 out of the benzotriazole plane by 10.1(1)° supports the N10−H7···O1 and N11−H9···O2 hydrogen bonds (Table A.3). The proton H9 takes part in a bifurcated hydrogen bond by also interacting with the oxygen atom O3 from the other nitro group, which is turned out of plane by 6.2(1)°. All nitrogen atoms of the triazole ring participate in hydrogen bonds, and thereby a wavelike layer is formed along the *c* axis. The aromatic protons show no interactions. A weak intramolecular N···O interaction of 2.828(4) Å is observed between N3 and O1.

Guanidinium 4,6-dinitrobenzotriazol-1-oxide (**4c**) crystallizes in the monoclinic space group $P2_1/c$. It was obtained with a significantly higher density of 1.728 g cm^{-3} at 100 K than the corresponding 5,7-dinitrobenzotriazole salt **1c** (1.652 g cm^{-3} at 293 K). This result, which is more clearly observed for the triaminoguanidinium salts **1e** (1.662 g cm^{-3} at 100 K) and **4e** (1.751 g cm^{-3} at 100 K), nicely confirms the concept of increasing the density by introduction of *N*-oxide moieties. The bond lengths of the triazol-1-oxide rings of the salts **4c** and **4e** are similar to those of the zwitterionic parent compound **4**[15] and lie between those of single and double bonds.[21] The bond lengths of the *N*-oxide moieties of the salts and compound **4** differ only by 0.01 Å. The nitro N atom N4 of **4c** lies almost in the ring plane (C2−C3−N4−O2: 5.0(3)°), and therefore its oxygen atom O2 participates in an N···O interaction with the triazole nitrogen atom N3. The other nitro group is twisted out of plane by 8.1(3)° (C4−C5−N5−O4). Therefore, weaker non-classical hydrogen bonds are

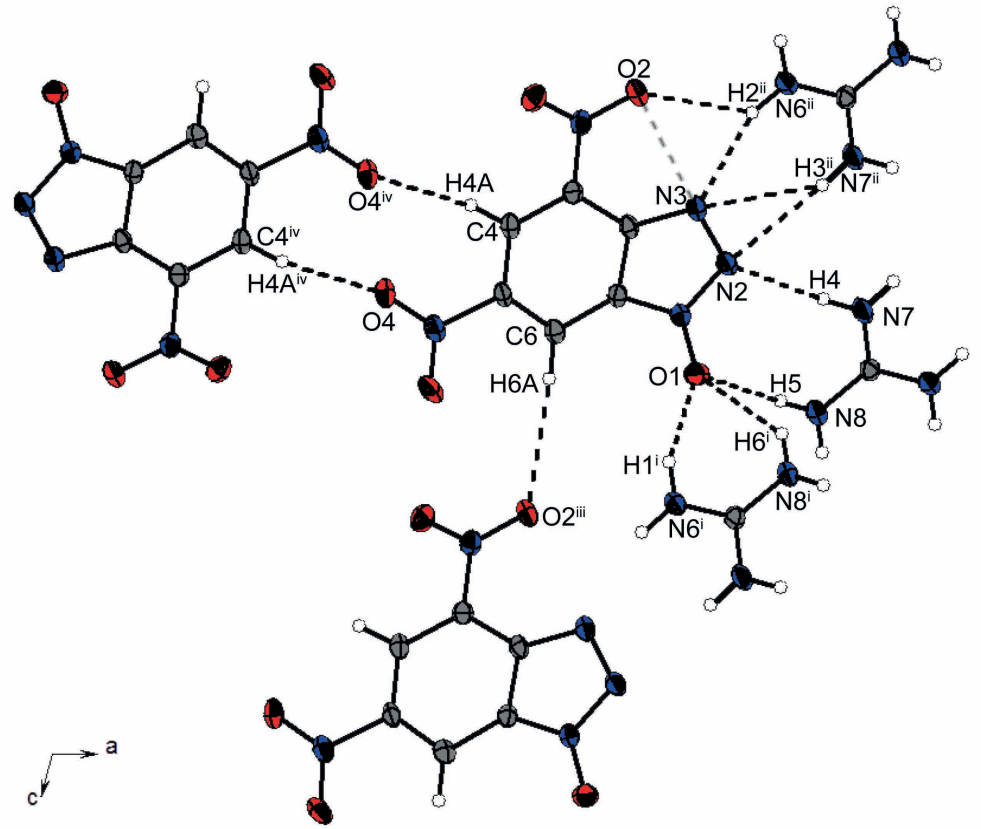

Figure 3.3: Selected interactions in the crystal structure of **4c**. Hydrogen bonds are shown as black dotted lines and the intramolecular dipolar N···O interaction is shown as a gray dotted line. Ellipsoids are drawn at 50% probability.

found for the two aromatic protons interacting with the nitro groups (Table A.4). Several classical hydrogen bonds are observed between the cations and anions. Selected interactions in the crystal structure of **4c** are shown in Figure 3.3. The hydrogen atoms H2 and H3 take part in three-center hydrogen bonds to the triazole nitrogen atom N3 and oxygen atom O2 or nitrogen atom N2, and thereby the molecules are connected along the *c* axis.

1-(5,7-Dinitrobenzotriazol-1-yl)-2-nitrazapropane (**7x**) crystallizes in the orthorhombic space group $P2_12_12_1$ with four formula units per unit cell and a crystal density of 1.746 g cm^{-3} at 123 K. Its molecular structure is shown in Figure 3.4. The methyl and methylene protons of the nitramine group are involved in several non-classical hydrogen bonds, as summarized in Table A.5. The twisting of the nitro N atom N5 of 35.8(2)° leads to an intramolecular N···O interaction (2.724(2) Å) to the oxygen atom O5 of the nitramine nitro group.

Nitramine **8x** crystallizes as an acetonitrile adduct in the orthorhombic space group *Pbca* with eight formula units per unit cell and a crystal density of 1.623 g cm^{-3} at 100 K. Its molecular structure is depicted in Figure 3.5. The N−O bond length of 1.2693(16) Å of the *N*-oxide is comparatively short in comparison to that of 4,6-dinitro-3*H*-benzotriazol-3-ium-

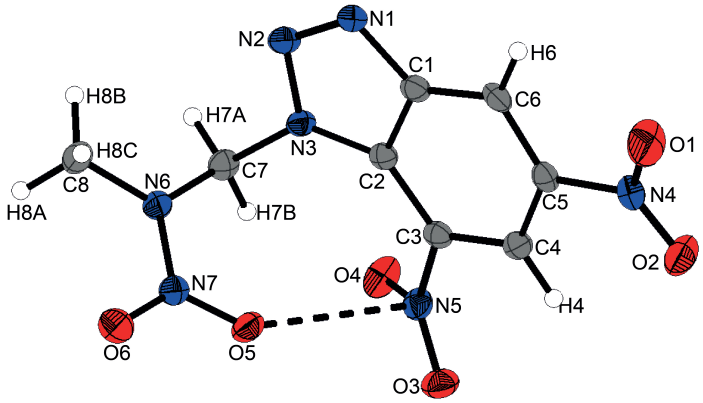

Figure 3.4: Molecular structure of **7x**. Thermal ellipsoids are drawn at 50% probability and the N···O interaction is shown as a black dotted line.

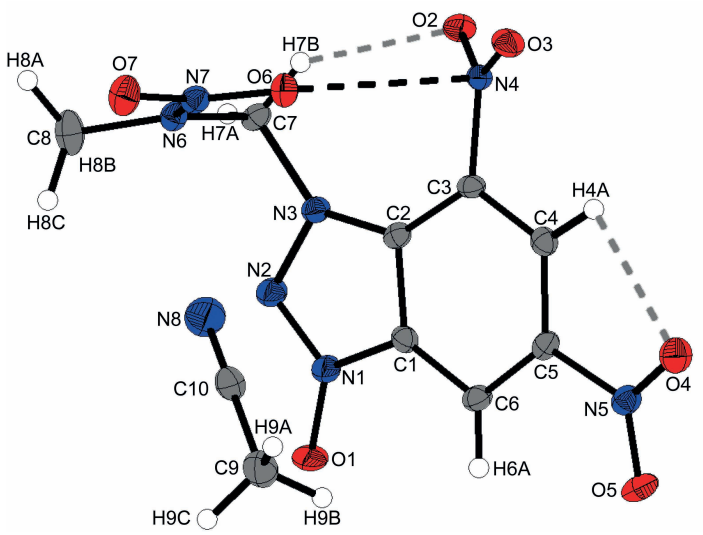

Figure 3.5: Molecular structure of **8x** as acetonitrile adduct. Thermal ellipsoids are drawn at 50% probability. Intramolecular non-classical hydrogen bonds are shown as gray dotted lines and the N···O interaction is shown as a black dotted line.

1-oxide (1.3004(14) Å).[15] The nitramine group is turned out of the benzotriazol-1-oxide plane by 80.93(5)° and from the plane of the neighboring nitro group of N4 by 37.62(4)°. These twists are supported by a non-classical hydrogen bond between the methylene proton H7B and the oxygen atom O2 of 2.230(16) Å, a dipolar N···O interaction, and intermolecular dipolar C···O interactions (Table A.6). The crystal structure consists of two different orientated pairs along the *c* axis with the nitramine group pointing up or down the *b* axis. The space between one pair is occupied by acetonitrile molecules, which interact with oxygen atom O5 by a non-classical hydrogen bond.

3.2.4 Sensitivities and Thermal Stabilities

For initial safety testing, impact, friction, and electrostatic discharge sensitivity tests were carried out. The impact sensitivity tests were performed according to STANAG 4489[22] by using a BAM drop hammer. The friction sensitivity tests were carried out according to STANAG 4487[23] by using a BAM friction tester. The sensitivity data are listed in Table 3.1–Table 3.3.

The salts of 5,7-dinitrobenzotriazole **1a**–**1f** are insensitive towards friction and impact, except for the hydroxylammonium salt **1b**, which is classified as sensitive with an impact sensitivity of 30 J (Table 3.1).[24] With the exception of the triaminoguanidinium salt **1e**, they all show high thermal stability up to 316 °C. The salts **1a** and **1b** melt before decomposition. Astonishingly, the thermal stability of the potassium salt **3f** (276 °C) is decreased in comparison to **1f** (316 °C), although it has two amino groups next to the nitro groups, which could participate in hydrogen bonds and thus increase the thermal stability.

The sensitivities towards impact of the salts of 4,6-dinitrobenzotriazol-1-oxide differ strongly (Table 3.2). The potassium salt **4f** and the hydroxylammonium salt **4b** are very sensitive towards impact with an impact sensitivity of 2 J. Salt **4f** is also sensitive to friction (288 N), while the other salts are insensitive. The impact sensitivity of the neutral parent compound (2 J)[15] could be decreased by formation of the salts **4a**, **4c**–**4e**, which are less sensitive or even insensitive. With the exception of **4b**, the salts show high thermal stabilities by decomposing at 207–295 °C (Figure 3.6).

The introduction of two amino groups adjacent to the nitro groups leads to less sensitive salts **6a**–**6d** and **6f** compared to the salts of 4,6-dinitrobenzotriazole-1-oxide **4a**–**4f**. The ammonium salt **6a** and the hydroxylammonium salt **6b** are the most sensitive salts towards impact with impact sensitivities of 20 and 9 J, respectively. The other salts are classified as less sensitive towards impact (35 J) according to the NATO standardization agreement.[22,23] The thermal stabilities of the nitrogen-rich salts of **6** are at least in the same range as the ones of **4** (Figure 3.6).

The nitramine **7** decomposes at 179 °C and the introduction of an *N*-oxide group leads to decreased thermal stability of 147 °C. Furthermore, a great difference is observed for the sensitivities. Whereas the mixture of isomeric nitramines **7** and **8** are insensitive to friction and **7** also towards impact, the zwitterionic nitramine **8** is very sensitive to impact (1 J).

3.2.5 Calculated Detonation Performances

To evaluate the utility of new energetic materials, their performance characteristics are usually calculated by computer codes. The detonation parameters of the salts were calculated with the EXPLO5 (version 6.02)[25] computer code. The program is based on the steady-state

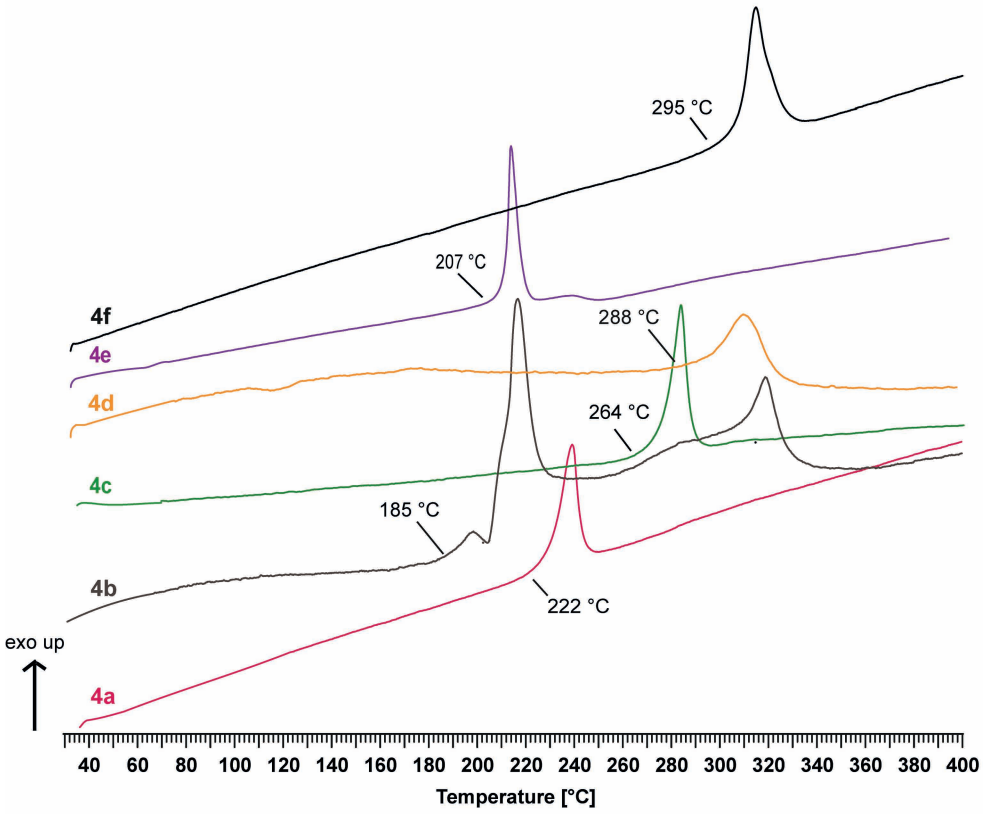

Figure 3.6: Differential scanning calorimetry (DSC) curves of the salts of 4,6-dinitrobenzotriazol-1-oxide (**4**).

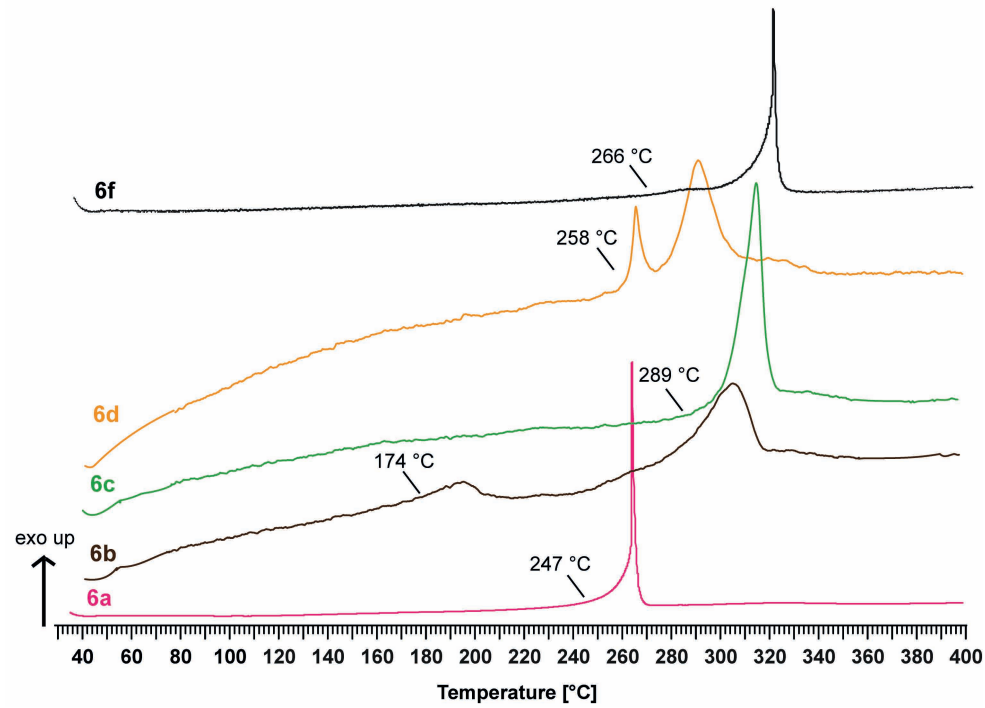

Figure 3.7: Differential scanning calorimetry (DSC) curves of the salts of 5,7-diamino-4,6-dinitrobenzotriazol-1-oxide (**6**).

model of equilibrium and uses the Becker–Kistiakowsky–Wilson equation of state (BKW EOS) for gaseous detonation products and Murnaghan EOS for both solid and liquid products.[26,27] It is designed to enable the calculation of detonation parameters at the Chapman–Jouguet point. The calculations were performed by using the maximum densities and calculated enthalpies of formation. The maximum densities were obtained from the crystal structures and if necessary recalculated to room temperature or measured with an He pycnometer from Linseis, if no crystal structure was available. The densities at 298 K were calculated from the corresponding crystal densities by Equation 3.1 and the coefficient of volume expansion α_v of the nitramine HMX (octogen) ($\alpha_v = 1.6\times10^{-4}\mathrm{K}$[28]) as first approximation.

$$\rho_{298K} = \frac{\rho_\mathrm{T}}{1 + \alpha_v(298 - \mathrm{T})} \tag{3.1}$$

The enthalpies of formation were calculated by using the CBS-4M quantum chemical method[29,30] with Gaussian 09 A.02.[31] Gas-phase enthalpies were converted to solid-state enthalpies by means of Trouton's rule.[32,33]

The calculated detonation performances of the 5,7-dinitrobenzotriazole salts **1a**–**1e** are improved in comparison to those of their free acid and trinitrotoluene (TNT). They show detonation velocities up to 7985 m s^{-1} and volumes of gaseous detonation products up to 803 L kg^{-1} (Table 3.1). The other detonation parameters are in the same range as those of TNT. The detonation performances of the corresponding 4,6-dinitrobenzotriazol-1-oxide salts (**4a**–**4e**) are improved by introduction of an *N*-oxide group (Table 3.2). The highest performance was calculated for **4e**, which showed a detonation pressure of 256 kbar, a detonation velocity up to 8334 m s^{-1}, and a large volume of gaseous detonation products (801 L kg^{-1}), which are comparable to the performance of 1,1-diamino-2,2-dinitroethene (FOX-7) (Table 3.3).

The ignitability of the potassium salt **4f** and the aminoguanidinium salt **4d** by laser radiation was tested because both of these salts decomposed audibly on attempting to record a Raman spectrum. Therefore, the substances were mixed with 2.5% polyethylene, slightly compressed in a small glass vessel, and irradiated with a laser pulse. For further information on the ignition testing, see the Appendix. The salt **4f** could be initiated by laser radiation, as it destroyed the glass vessel (Figure 3.8A), whereas **4d** only decomposed. Hence, ignition tests of hexogen (RDX) and pentaerythritol tetranitrate (PETN) were carried out with **4f**. RDX or PETN was filled in a small aluminum tube and slightly compressed. Then **4f** (50 or 100 mg) was added on top, slightly compressed, and ignited with a pyrotechnical igniter. Unfortunately, **4f** only deflagrated and could ignite neither RDX nor PETN (Figure 3.8). In general, silver salts are more potent than potassium

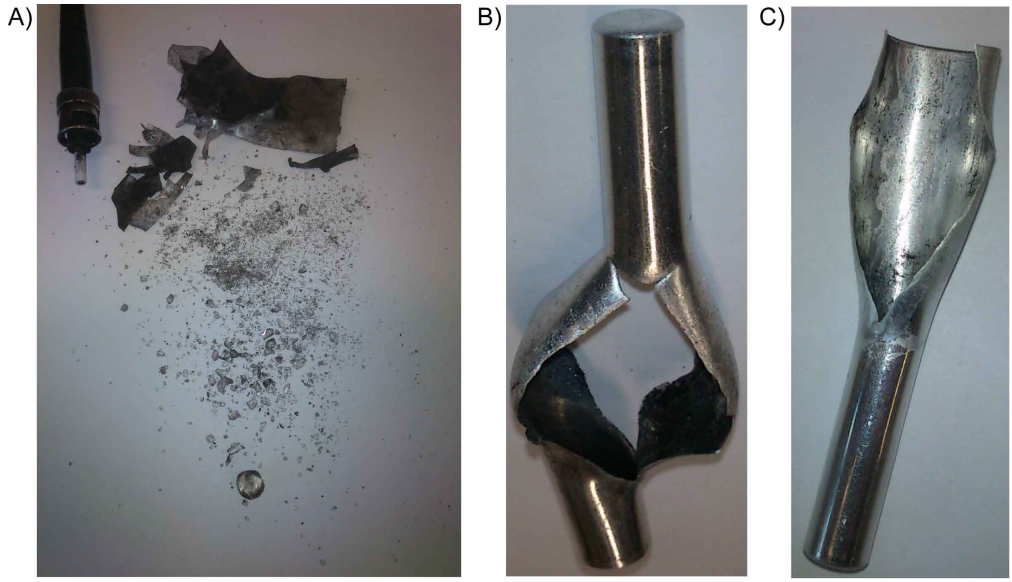

Figure 3.8: A) Glass vessel destroyed by successful laser ignition of **4f**. B) Tube filled with 300 mg of RDX and 50 mg of **4f**. C) Tube filled with 300 mg of PETN and 50 mg of **4f**.

salts, and therefore the ignition test of PETN was also carried out with the silver salt of **4**. Nevertheless, the silver salt **4g**·0.5 H_2O, which could not be completely dehydrated at 120 °C in vacuo, was also not able to ignite PETN.

Twofold amination of the 4,6-dinitrobenzotriazol-1-oxide core further increases the calculated detonation performance of the corresponding salts **6a**–**6d** due to the considerably higher densities (Table 3.3). The calculated detonation performances are comparable to that of FOX-7, with detonation velocities up to 8384 m s^{-1} and detonation pressures up to 271 kbar. The introduction of the nitramine group leads to improved detonation performance in comparison to the unmodified parent compounds due to the higher densities. The same trend for the performances of **7x** and **8x** as for the salts of 5,7-dinitrobenzotriazolate and 4,6-dinitrobenzotriazole-1-oxide was observed, with improved detonation performance of **8x** in comparison to **7x** (Table 3.1 and Table 3.2).

3.2.6 Conclusions

Nitrogen-rich salts of 5,7-dinitrobenzotriazolate (**1**), 4,6-dinitrobenzotriazol-1-oxide (**4**) and 5,7-diamino-4,6-dinitrobenzotriazol-1-oxide (**6**) could be synthesized. Only the potassium salt **3f** was obtained from 4,6-diamino-5,7-dinitrobenzotriazole, while its acidity was too low to be deprotonated by nitrogen-rich bases.

The derivatization of the acidic heterocyclic proton by alkylation with 1-chloro-2-nitrazapropane afforded the corresponding nitramine isomers of **7** and **8**, the ratios of which were determined by ^{1}H NMR spectroscopy. The crystal structures of the nitramines **7x** and

Table 3.1: Physical and energetic properties of 5,7-dinitrobenzotriazole (**1**), its salts **1a**–**1e**, and its nitramine **7x**.

	1	**1a**	**1b**	**1c**	**1d**	**1e**	**7x**
Molecular formula	$C_6H_3N_5O_4$	$C_6H_6N_6O_4$	$C_6H_6N_6O_5$	$C_7H_8N_8O_4$	$C_7H_9N_9O_4$	$C_7H_{11}N_{11}O_4$	$C_8H_7N_7O_6$
M [g mol^{-1}]	209.13	226.15	242.15	268.19	283.20	313.23	297.19
IS [J][a]	>40	30	>40	>40	>40	>40	>40*
FS [N][b]	>360	>360	>360	>360	>360	>360	>360*
ESD [J][c]	0.3	0.6	1.5	0.75	0.5	0.4	0.25*
Grain size [µm]	<100	<100	<100	<100	<100	<100	<100
N [%][d]	33.49	37.16	34.71	41.78	44.51	49.19	32.99
Ω [%][e]	−72.7	−77.8	−66.1	−83.5	−81.9	−79.2	−72.7
T_{melt} [°C][f]	193	189	195	–	–	–	–
T_{dec} [°C][g]	291	266	253	316	223	168	179
ρ [g cm^{-3}][h]	1.65	1.65	1.64	1.65	1.65	1.61	1.70
$\Delta_f H_m$ [kJ mol^{-1}][i]	179	198	251	156	260	475	213
$\Delta_f U$ [kJ kg^{-1}][j]	930	962	1125	673	1016	1620	800
Calculated detonation parameters (Explo5 v. 6.02)							
$-Q_v$ [kJ kg^{-1}][k]	4633	4803	5361	4169	4396	4762	4985
T_{det} [K][l]	3406	3256	3614	2873	2948	3079	3380
p_{CJ} [kbar][m]	199	211	230	196	209	222	231
D [m s^{-1}][n]	7252	7554	7709	7473	7726	7985	7723
V_0 [L kg^{-1}][o]	638	711	717	734	759	803	682

[a] Impact sensitivity (BAM drophammer 1 of 6). [b] Friction sensitivity (BAM friction tester 1 of 6). [c] Electrostatic discharge (OZM Research). [d] Nitrogen content. [e] Oxygen balance ($\Omega = (x\mathrm{O} - 2y\mathrm{C} - 0.5z\mathrm{H})1600/M$). [f] Melting point. [g] Decomposition temperature. [h] Density at ambient temperature. [i] Calculated enthalpy of formation. [j] Calculated energy of formation. [k] Energy of explosion. [l] Detonation temperature. [m] Detonation pressure. [n] Detonation velocity. [o] Volume of detonation gases. * Values for the isomeric mixture.

Table 3.2: Physical and energetic properties of 4,6-dinitrobenzotriazol-3-ium-1-oxide (**4**), its salts **4a**–**4f**, and its nitramine(**8x**).

	4	**4a**	**4b**	**4c**	**4d**	**4e**	**4f**	**8x**
Molecular formula	$C_6H_3N_5O_5$	$C_6H_6N_6O_5$	$C_6H_6N_6O_6$	$C_7H_8N_8O_5$	$C_7H_9N_9O_5$	$C_7H_{11}N_{11}O_5$	$C_6H_2KN_5O_5$	$C_8H_7N_7O_7$
M [g mol^{-1}]	225.12	242.15	258.15	284.19	299.20	329.23	263.21	313.19
IS [J][a]	2	5	2	>40	20	>40	2	1*
FS [N][b]	>360	>360	>360	>360	>360	288	>360	>360*
ESD [J][c]	0.2	0.3	0.15	1.5	0.3	0.5	0.08	0.08*
Grain size [µm]	<100	<100	<100	<100	<100	100–500	<100	<100
N [%][d]	31.11	34.71	32.55	39.43	42.13	46.80	26.61	31.31
Ω [%][e]	−60.4	−66.1	−55.8	−73.2	−72.2	−70.5	−51.7	−63.9
T_{dec} [°C][f]	182	222	185	262	288	207	295	147*
ρ [g cm^{-3}][g]	1.69	1.67	1.66	1.67	1.56	1.69	1.71	1.72
$\Delta_f H_m$ [kJ mol^{-1}][h]	202	194	252	152	257	470	62	246
$\Delta_f U$ [kJ kg^{-1}][i]	967	889	1064	626	953	1528	292	870
Calculated detonation parameters (Explo5 v. 6.02)								
$-Q_v$ [kJ kg^{-1}][j]	5154	5163	5674	4534	4708	5137	4920	5365
T_{det} [K][k]	3736	3494	3828	3097	3220	3280	3475	3607
p_{CJ} [kbar][l]	233	235	251	215	192	256	175	253
D [m s^{-1}][m]	7637	7764	7893	7664	7357	8334	6980	7926
V_0 [L kg^{-1}][n]	649	712	718	735	768	801	475	682

[a] Impact sensitivity (BAM drophammer 1 of 6). [b] Friction sensitivity (BAM friction tester 1 of 6). [c] Electrostatic discharge (OZM Research). [d] Nitrogen content. [e] Oxygen balance ($\Omega = (x\mathrm{O} - 2y\mathrm{C} - 0.5z\mathrm{H})1600/M$). [f] Decomposition temperature. [g] Density at ambient temperature. [h] Calculated enthalpy of formation. [i] Calculated energy of formation. [j] Energy of explosion. [k] Detonation temperature. [l] Detonation pressure. [m] Detonation velocity. [n] Volume of detonation gases. * Values for the isomeric mixture.

Table 3.3: Physical and energetic properties of 5,7-diamino-4,6-dinitrobenzotriazol-1-oxide (**6**), its salts **6a**–**6d** and FOX-7.

	6	**6a**	**6b**	**6c**	**6d**	FOX-7
Molecular formula	$C_6H_5N_7O_5$	$C_6H_8N_8O_5$	$C_6H_8N_8O_6$	$C_7H_{10}N_{10}O_5$	$C_7H_{11}N_{11}O_5$	$C_2H_4N_4O_4$
M [g mol^{-1}]	255.15	239.15	288.18	314.23	329.23	148.08
IS [J][a]	20	20	9	35	35	25
FS [N][b]	>360	>360	>360	>360	>360	>360
ESD [J][c]	1.5	1.5	1.5	1.5	1.25	1.0
Grain size [µm]	<100	<100	<100	<100	<100	<100
N [%][d]	38.43	41.17	38.88	44.58	46.80	37.84
Ω [%][e]	−59.6	−64.7	−55.5	−71.3	−70.5	−21.6
T_{dec} [°C][f]	257	247	174	289	258	228
ρ [g cm^{-3}][g]	1.75	1.77	1.73	1.79	1.72	1.76
$\Delta_f H_m$ [kJ mol^{-1}][h]	140	176	233	127	235	−134
$\Delta_f U$ [kJ kg^{-1}][i]	630	742	904	503	817	−805
Calculated detonation parameters (Explo5 v. 6.02)						
$-Q_v$ [kJ kg^{-1}][j]	4639	4838	5321	4275	4461	4733
T_{det} [K][k]	3279	3184	3496	2855	2952	3312
p_{CJ} [kbar][l]	247	268	271	262	248	291
D [m s^{-1}][m]	7941	8348	8281	8384	8248	8350
V_0 [L kg^{-1}][n]	693	758	757	777	799	800

[a] Impact sensitivity (BAM drophammer 1 of 6). [b] Friction sensitivity (BAM friction tester 1 of 6). [c] Electrostatic discharge (OZM Research). [d] Nitrogen content. [e] Oxygen balance ($\Omega = (x\mathrm{O} - 2y\mathrm{C} - 0.5z\mathrm{H})1600/M$). [f] Decomposition temperature. [g] Density at ambient temperature. [h] Calculated enthalpy of formation. [i] Calculated energy of formation. [j] Energy of explosion. [k] Detonation temperature. [l] Detonation pressure. [m] Detonation velocity. [n] Volume of detonation gases.

8x showed the main alkylation sites, and furthermore the structure of **8x** revealed its zwitterionic character due to *N*-alkylation instead of *O*-alkylation. Additionally, several crystal structures of salts from **1**, **4**, and **6** were presented. Most of the nitrogen-rich salts show high thermal stability up to 316 °C. The potassium salt **4f** could be initiated by laser radiation, but unfortunately this salt as well as the silver salt **4g**·0.5 H_2O are not able to ignite RDX or PETN; the salts only deflagrate. The salts of **1**, **4**, and **6** show, as expected, better detonation performances than their neutral parent compounds. Furthermore, the performance is increased by introduction of the *N*-oxide group and then further by introduction of two amino groups.

3.3 Experimental Section

Caution! *Most compounds prepared herein are energetic compounds sensitive to impact, friction and electrostatic discharge. Although there were no problems in handling the compounds, proper protective measures (ear protection, Kevlar® gloves, face shield, body armor and earthed equipment) should be used.*

Ammonium 5,7-Dinitrobenzotriazolate (1a)

To 2M ammonia (2 mL, 4.00 mmol) was added 5,7-dinitro-1*H*-benzotriazole (**1**) (206 mg, 0.99 mmol). The reaction mixture was stirred overnight. The precipitate was filtered off to afford a slightly yellow powder (166 mg, 0.73 mmol, 74%).
DSC (5 °C min^{-1}): T_{melt} = 189 °C, T_{dec} = 266 °C. ^{1}H NMR (400 MHz, acetone-d_6): δ = 9.20 (d, ^4J = 2.0 Hz, 1H, C*H*), 8.96 (d, ^4J = 2.0 Hz, 1H, C*H*) ppm. ^{1}H NMR (400 MHz, DMSO-d_6): δ = 9.05 (m, 1H, C*H*), 8.69 (m, 1H, C*H*), 7.35 (s, 4H, NH_4^+) ppm. ^{13}C{^{1}H} NMR (101 MHz, acetone-d_6): δ = 148.0 (C_q), 134.2 (C_q), 121.0 (*C*H), 115.5 (*C*H) ppm. ^{13}C{^{1}H} NMR (101 MHz, DMSO-d_6): δ = 148.1 (C_q), 140.1 (*C*NO_2), 139.2 (*C*NO_2), 134.4 (C_q), 119.8 (*C*H), 113.4 (*C*H) ppm. ^{14}N{^{1}H} NMR (29 MHz, acetone-d_6): δ = −12 (NO_2), −359 (NH_4^+) ppm. ^{14}N{^{1}H} NMR (29 MHz, DMSO-d_6): δ = −11 (NO_2), −359 (NH_4^+) ppm. IR (ATR): $\tilde{\nu}$ = 3346 (vw), 3325 (w), 3272 (w), 3094 (w), 3024 (vw), 2879 (w), 2732 (br), 1858 (vw), 1705 (vw), 1678 (vw), 1604 (w), 1575 (m), 1528 (w), 1510 (s), 1476 (s), 1441 (s), 1427 (m), 1406 (m), 1381 (w), 1353 (s), 1336 (vs), 1328 (vs), 1291 (vs), 1271 (m), 1201 (w), 1188 (m), 1172 (s), 1108 (m), 1099 (m), 1068 (m), 1051 (m), 1024 (w), 1013 (w), 994 (m), 972 (vw), 847 (vw), 935 (m), 924 (s), 902 (w), 804 (s), 782 (w), 751 (w), 748 (m), 734 (vs), 727 (vs), 692 (s) cm^{-1}. Raman (1064 nm, 300 mW): $\tilde{\nu}$ = 3096 (3), 1610 (6), 1578 (17), 1530 (1), 1520 (6), 1445 (20), 1383 (3), 1346 (100), 1336 (9), 1295 (39), 1203 (1), 1190 (2), 1174 (3), 1070 (6), 1053 (11), 1025 (3), 1015 (12), 996 (15), 937 (7), 806 (17), 739 (1), 730 (5), 693 (2), 479 (6), 365 (1), 355 (2), 275 (1), 239 (2) cm^{-1}. MS

(FAB$^-$): m/z (%) = 208.2 (100) [$C_6H_2N_5O_4^-$]. MS (FAB$^+$): m/z (%) = 18.1 (4) [NH_4^+]. EA ($C_6H_6N_6O_4$, 226.15 g mol^{-1}): calcd C 31.87, H 2.67, N 37.16%; found C 31.70, H 2.60, N 37.14%. Sensitivities (grain size: <100 µm): IS: >40 J; FS: >360 N; ESD: 0.6 J.

Hydroxylammonium 5,7-dinitrobenzotriazolate (1b)

5,7-Dinitro-1*H*-benzotriazole (**1**) (226 mg, 1.90 mmol) was dissolved in Et_2O (25 mL). Hydroxylamine dissolved in water (50% *w*/*w*, 0.12 mL, 1.96 mmol) was added. The mixture was stirred for 1 h and the precipitate was filtered off and was air-dried to afford 275 mg of crude product. Recrystallization from methyl *tert*-butyl ether (5 mL) and ethanol (6 mL) yielded a yellow powder (180 mg, 0.74 mmol, 39%).
DSC (5 °C min^{-1}): T_{melt} = 195 °C, T_{dec} = 253 °C. ^{1}H NMR (400 MHz, DMSO-d_6): δ = 9.12 (m, 1H, C*H*), 8.75 (m, 1H, C*H*) ppm. ^{13}C{^{1}H} NMR (101 MHz, DMSO-d_6): δ = 147.7 (C_q), 139.7 (CNO$_2$), 138.3 (CNO$_2$), 134.1 (C_q), 120.2 (*C*H), 114.0 (*C*H) ppm. ^{14}N{^{1}H} NMR (29 MHz, DMSO-d_6): $\delta = -14$ (NO$_2$), -359 (NH$_3$OH$^+$) ppm. IR (ATR): $\tilde{\nu}$ = 3100 (br), 2772 (br), 1815 (br), 1640 (w), 1613 (w), 1600 (w), 1580 (w), 1536 (m), 1488 (m), 1441 (m), 1386 (m), 1337 (s), 1286 (m), 1276 (m), 1228 (m), 1192 (m), 1109 (w), 1086 (m), 1069 (m), 987 (m), 970 (m), 934 (m), 923 (m), 909 (m), 838 (m), 803 (m), 778 (m), 742 (m), 726 (m), 687 (m) cm^{-1}. Raman (1064 nm, 300 mW): $\tilde{\nu}$ = 3102 (4), 3096 (3), 3088 (3), 1602 (19), 1582 (8), 1542 (10), 1523 (3), 1491 (7), 1438 (18), 1420 (10), 1401 (7), 1392 (8), 1352 (100), 1297 (10), 1278 (7), 1238 (4), 1193 (4), 1063 (15), 1036 (5), 936 (8), 804 (14), 727 (4), 473 (6), 360 (4), 348 (5), 267 (2) cm^{-1}. MS (FAB$^-$): m/z (%) = 208.3 (100) [$C_6H_2N_5O_4^-$]. EA ($C_6H_6N_6O_5 \cdot H_2O$, 260.16 g mol^{-1}): calcd C 27.70, H 3.10, N 32.30%; found C 28.06, H 2.89, N 31.99%. EA ($C_6H_6N_6O_5$, 242.15 g mol^{-1}): calcd C 29.76, H 2.50, N 34.71%; found C 29.70, H 2.56, N 33.98%. Sensitivities (grain size: <100 µm): IS: 30 J; FS: >360 N; ESD: 1.5 J.

Guanidinium 5,7-dinitrobenzotriazolate (1c)

Potassium salt **1f** (206 mg, 0.75 mmol) and guanidinium hydrochloride (86 mg, 0.78 mmol) were dissolved in a minimal amount of water at 100 °C. By cooling a yellow solid precipitated. It was recrystallized from ethanol to afford a yellow powder (141 mg, 0.53 mmol, 70%).
DSC (5 °C min^{-1}): T_{dec} = 316 °C. ^{1}H NMR (400 MHz, acetone-d_6): δ = 9.04 (m, 1H, C*H*), 8.69 (m, 1H, C*H*), 6.93 (s, 6H, NH_2) ppm. ^{13}C{^{1}H} NMR (101 MHz, DMSO-d_6): δ = 158.6 (C(NH$_2$)$_3$), 148.7 (C_q), 140.7 (CNO$_2$), 139.7 (CNO$_2$), 135.0 (C_q), 120.3 (*C*H), 113.8 (*C*H) ppm. ^{14}N{^{1}H} NMR (29 MHz, acetone-d_6): $\delta = -11$ (NO$_2$) ppm. IR (ATR): $\tilde{\nu}$ = 3472 (w), 3424 (w), 3356 (w), 3169 (br), 3099 (w), 1818 (vw), 1797 (wv), 1645 (s), 1605 (m), 1573 (m), 1562 (w), 1517 (m), 1500 (m), 1445 (m), 1377 (w), 1332 (s), 1296 (s), 1271 (m), 1184

(m), 1177 (m), 1096 (m), 1053 (m), 1015 (m), 979 (m), 933 (m), 916 (s), 901 (s), 845 (m), 805 (s), 781 (m), 745 (m), 729 (vs), 690 (m) cm^{-1}. Raman (1064 nm, 300 mW): $\tilde{\nu}$ = 3104 (3), 1657 (1), 1610 (12), 1579 (15), 1516 (9), 1448 (23), 1383 (6), 1347 (101), 1329 (65), 1298 (33), 1186 (4), 1048 (23), 1019 (14), 981 (24), 938 (7), 851 (5), 809 (17), 729 (5), 478 (7) cm^{-1}. MS (FAB^-): m/z (%) = 208.3 (71) [$C_6H_2N_5O_4^-$], 46.0 (11) [NO_2^-]. MS (FAB^+): m/z (%) = 60.1 (27) [$CH_6N_3^+$]. EA ($C_7H_8N_8O_4$, 268.19 g mol^{-1}): calcd C 31.35, H 3.01, N 41.78%; found C 31.47, H 2.89, N 41.57%. Sensitivities (grain size: < 100 µm): IS: > 40 J; FS: > 360 N; ESD: 0.75 J.

Aminoguanidinium 5,7-dinitrobenzotriazolate (1d)

5,7-Dinitro-1*H*-benzotriazole (**1**) (294 mg, 1.41 mmol) was dissolved in ethanol (20 mL) and aminoguanidinium hydrogen carbonate (191 mg, 1.40 mmol) was added. The solution was stirred for 1 h at room temperature. The precipitate was filtered off to afford a yellow solid (279 mg, 0.99 mmol, 70%).
DSC (5 °C min^{-1}): T_{dec} = 223 °C. ^{1}H NMR (400 MHz, DMSO-d_6): δ = 9.04 (m, 1H, C*H*), 8.69 (m, 2H, C*H*, N*H*), 7.31–6.88 (m, 4H, NH_2), 4.70 (s, 2H, NNH_2) ppm. ^{13}C{^{1}H} NMR (101 MHz, DMSO-d_6): δ = 158.8 ($C(NH_2)_2NH$), 148.0 (C_q), 140.1 (CNO_2), 139.0 (CNO_2), 134.4 (C_q), 119.6 (*C*H), 113.1 (*C*H) ppm. ^{14}N{^{1}H} NMR (29 MHz, DMSO-d_6): δ = −13 (NO_2) ppm. IR (ATR): $\tilde{\nu}$ = 3489 (m), 3366 (w), 3318 (w), 3254 (w), 3163 (m), 3111 (m), 3019 (m), 2829 (w), 2792 (w), 1822 (vw), 1795 (vw), 1682 (m), 1660 (m), 1619 (s), 1607 (s), 1576 (m), 1548 (vw), 1512 (vs), 1455 (m), 1439 (m), 1380 (m), 1333 (vs), 1292 (vs), 1270 (s), 1185 (m), 1175 (s), 1158 (s), 1119 (m), 1104 (s), 1063 (s), 1045 (s), 1022 (s), 990 (s), 935 (s), 914 (s), 898 (s), 843 (w), 803 (vs), 782 (s), 746 (m), 725 (vs), 688 (vs) cm^{-1}. Raman (1064 nm, 300 mW): $\tilde{\nu}$ = 3115 (2), 3084 (3), 2995 (2), 2954 (2), 2921 (10), 1650 (4), 1611 (9), 1581 (16), 1531 (10), 1459 (2), 1445 (18), 1382 (8), 1349 (100), 1331 (66), 1295 (27), 1276 (2), 1187 (4), 1119 (4), 1066 (32), 1024 (9), 991 (8), 937 (7), 806 (19), 727 (5), 476 (5), 356 (5) cm^{-1}. MS (FAB^-): m/z (%) = 208.3 (64) [$C_6H_2N_5O_4^-$]. MS (FAB^+): m/z (%) = 75.1 (28) [$CH_7N_4^+$]. EA ($C_7H_9N_9O_4$, 283.21 g mol^{-1}): calcd C 29.73, H 3.20, N 44.51%; found C 29.73, H 3.15, N 44.29%. Sensitivities (grain size: < 100 µm): IS: >40 J; FS: > 360 N; ESD: 0.5 J.

Triaminoguanidinium 5,7-dinitrobenzotriazolate (1e)

The potassium salt **1f** (225 mg, 0.82 mmol) and triaminoguanidinium chloride (120 mg, 0.85 mmol) were dissolved in a minimal amount of water at 100 °C. The solution was heated under reflux for 1 h. The clear solution was cooled to room temperature and was stored in the refrigerator for 48 h. The precipitate was suction filtered to afford an orange solid

(132 mg, 0.42 mmol, 51%).
DSC (5 °C min^{-1}): T_{dec} = 168 °C. ^{1}H NMR (400 MHz, DMSO-d_6): δ = 9.03 (d, ^{4}J = 2.0 Hz, 1H, C*H*), 8.68 (m, 4H, C*H*, N*H*), 4.46 (s, 6H, NH_2) ppm. ^{13}C{^{1}H} NMR (101 MHz, DMSO-d_6): δ = 159.0 (C(NHNH$_2$)$_3$), 148.1 (C_q), 140.2 (CNO$_2$), 138.9 (CNO$_2$), 134.4 (C_q), 119.5 (*C*H), 112.9 (*C*H) ppm. ^{14}N{^{1}H} NMR (29 MHz, DMSO-d_6): δ = −13 (NO$_2$), −359 (NH$^+$) ppm. IR (ATR): $\tilde{\nu}$ = 3306 (w), 3155 (w), 3100 (w), 1703 (w), 1682 (m), 1603 (w), 1573 (w), 1502 (m), 1443 (w), 1376 (w), 1336 (s), 1292 (m), 1275 (w), 1227 (w), 1186 (w), 1168 (w), 1133 (m), 1096 (w), 1057 (w), 1026 (m), 1005 (m), 983 (m), 930 (m), 913 (m), 893 (m), 846 (w), 803 (m), 781 (w), 746 (m), 727 (m), 688 (m) cm^{-1}. Raman (1064 nm, 300 mW): $\tilde{\nu}$ = 1679 (3), 1607 (10), 1578 (14), 1521 (11), 1447 (27), 1378 (13), 1349 (100), 1333 (67), 1292 (33), 1186 (3), 1169 (4), 1133 (4), 1055 (23), 1019 (18), 996 (3), 984 (20), 933 (10), 915 (3), 902 (4), 887 (4), 846 (3), 807 (28), 727 (7), 688 (3), 487 (4), 473 (8), 414 (3), 352 (9), 272 (4), 230 (3) cm^{-1}. MS (FAB$^-$): m/z (%) = 208.3 (100) [C$_6$H$_2$N$_5$O$_4^-$]. MS (FAB$^+$): m/z (%) = 105.1 (100) [CH$_9$N$_6^+$]. EA (C$_7$H$_{11}$N$_{11}$O$_4$, 313.23 g mol^{-1}): calcd C 26.84, H 3.54, N 49.19%; found C 26.97, H 3.43, N 48.90%. Sensitivities (grain size: < 100 µm): IS: > 40 J; FS: > 360 N; ESD: 0.4 J.

Potassium 5,7-dinitrobenzotriazolate (1f)

5,7-Dinitro-1*H*-benzotriazole (**1**) (433 mg, 2.07 mmol) was dissolved in ethanol (20 mL). Potassium hydroxide (114 mg, 2.03 mmol) dissolved in a minimal amount of water was added dropwise. A yellow solid precipitated. After 30 min of stirring the precipitate was filtered off and was dried at high vacuum to yield a yellow powder (466 mg, 1.70 mmol, 82%).
DSC (5 °C min^{-1}): T_{dehyd} = 86 °C, T_{dec} = 316 °C. ^{1}H NMR (400 MHz, acetone-d_6): δ = 9.01 (d, ^{4}J = 1.9 Hz, 1H, C*H*), 8.80 (d, ^{4}J = 1.9 Hz, 1H, C*H*) ppm. ^{13}C{^{1}H} NMR (101 MHz, acetone-d_6): δ = 148.2 (C_q), 140.5 (CNO$_2$), 138.1 (CNO$_2$), 134.5 (C_q), 120.2 (*C*H), 114.3 (*C*H) ppm. ^{14}N{^{1}H} NMR (29 MHz, acetone-d_6): δ = −14 (NO$_2$). IR (ATR): $\tilde{\nu}$ = 3609 (w), 3384 (w), 3104 (w), 3079 (w), 1680 (w), 1607 (m), 1576 (m), 1507 (s), 1448 (m), 1382 (w), 1330 (vs), 1300 (s), 1274 (m), 1221 (w), 1193 (m), 1175 (s), 1098 (m), 1056 (s), 1018 (m), 992 (m), 963 (w), 933 (m), 924 (m), 912 (m), 900 (m), 804 (s), 782 (m), 749 (s), 729 (vs), 689 (s) cm^{-1}. Raman (1064 nm, 300 mW): $\tilde{\nu}$ = 3108 (4), 3082 (3), 1607 (11), 1579 (17), 1524 (12), 1513 (9), 1449 (27), 1385 (14), 1351 (100), 1331 (57), 1304 (24), 1295 (24), 1287 (28), 1274 (9), 1203 (6), 1164 (3), 1101 (3), 1056 (20), 1047 (15), 1019 (14), 993 (15), 984 (9), 971 (13), 924 (3), 937 (8), 845 (4), 807 (27), 727 (8), 693 (3), 487 (3), 474 (8), 363 (4), 356 (3), 289 (4), 232 (3) cm^{-1}. MS (FAB$^-$): m/z (%) = 208.3 (100) [C$_6$H$_2$N$_5$O$_4^-$], 162 (1) [C$_6$H$_2$N$_4$O$_2^-$]. MS (FAB$^+$): m/z (%) = 39.0 (26) [K$^+$]. EA

($C_6H_2KN_5O_4 \cdot 1.5\,H_2O$, 274.23 g mol^{-1}): calcd C 26.28, H 1.84, N 25.54%; found C 26.19, H 1.83, N 25.12%. Sensitivities (grain size: < 100 µm): IS: > 40 J; FS: > 360 N; ESD: 0.3 J.

Potassium 4,6-diamino-5,7-dinitrobenzotriazolate (3f)

Compound **3** (315 mg, 0.99 mmol) was suspended in ethanol (10 mL) and potassium hydroxide (59 mg, 1.05 mmol) dissolved in a small amount of water was added dropwise. The suspension turned to dark brown. The suspension was stirred for 4 h at room temperature. The brown solid was filtered off and dried at high vacuum to afford a brown powder (268 mg, 0.94 mmol, 95%).
DSC (5 °C min^{-1}): T_{dec} = 276 °C. ^{1}H NMR (400 MHz, DMSO-d_6): δ = 10.28 (s, 2H, NH_2), 8.96 (s, 2H, NH_2) ppm. ^{13}C{^{1}H} NMR (101 MHz, DMSO-d_6): δ = 148.4, 147.4, 141.3, 129.9, 115.6, 112.6 ppm. ^{14}N{^{1}H} NMR (29 MHz, DMSO-d_6): $\delta = -16$ (NO_2) ppm. IR (ATR): $\tilde{\nu}$ = 3532 (vw), 3327 (vw), 3085 (br), 1634 (vw), 1568 (w), 1503 (w), 1341 (w), 1287 (m), 1218 (w), 1191 (m), 1157 (m), 1091 (w), 1054 (w), 1019 (w), 990 (w), 909 (vw), 886 (vw), 803 (vw), 781 (w), 748 (w), 692 (w) cm^{-1}. Raman (1064 nm, 300 mW): $\tilde{\nu}$ = 3274 (11), 3081 (11), 2808 (10), 2701 (11), 2241 (11), 2138 (11), 1582 (36), 1509 (28), 1480 (16), 1467 (17), 1413 (48), 1406 (51), 1356 (27), 1326 (83), 1281 (56), 1271 (61), 1238 (96), 1195 (48), 1182 (23), 1168 (25), 1070 (27), 1016 (28), 994 (32), 889 (26), 818 (34), 810 (32), 736 (15), 706 (12), 637 (20), 503 (22), 478 (25), 364 (53) cm^{-1}. MS (FAB$^-$): m/z (%) = 238.3 (51) [$C_6H_4N_7O_4^-$], 222 (12) [$C_6H_2N_6O_4^-$], 46.0 (8) [NO_2^-]. MS (FAB$^+$): m/z (%) = 39.0 (17) [K^+]. EA ($C_6H_4KN_7O_4 \cdot 0.5\,H_2O$, 286.25 g mol^{-1}): calcd C 25.18, H 1.76, N 34.25%; found C 25.28, H 1.97, N 31.65%. Sensitivities (grain size: < 100 µm): IS: > 40 J; FS: > 360 N; ESD: 1.5 J.

Ammonium 4,6-dinitrobenzotriazol-1-oxide (4a)

4,6-Dinitrobenzotriazol-3-ium-1-oxide (**4**) (205 mg, 0.84 mmol) was added to 2M ammonia (4 mL) in one portion. The red mixture was stirred for 30 min at room temperature. The solvent was removed in vacuum to yield a fine red powder (167 mg, 0.69 mmol, 82%).
DSC (5 °C min^{-1}): T_{dec} = 222 °C. ^{1}H NMR (400 MHz, D_2O): δ = 8.94–8.90 (m, 2H, CH) ppm. ^{13}C{^{1}H} NMR (101 MHz, D_2O): δ = 142.1, 136.6, 136.0, 129.7, 118.1 (CH), 116.9 (CH) ppm. ^{14}N{^{1}H} NMR (29 MHz, D_2O): $\delta = -12$ (NO_2), -357 (NH_4^+) ppm. IR (ATR): $\tilde{\nu}$ = 3310 (vw), 3098 (w), 2821 (w), 2760 (w), 1818 (vw), 1686 (vw), 1608 (w), 1583 (w), 1530 (m), 1519 (m), 1492 (w), 1468 (w), 1438 (m), 1420 (m), 1405 (m), 1379 (vw), 1340 (s), 1327 (vs), 1282 (s), 1210 (w), 1190 (w), 1178 (m), 1083 (m), 1064 (m), 997 (vw), 935 (w), 909 (m), 861 (w), 803 (m), 769 (w), 739 (m), 704 (m), 681 (w) cm^{-1}. Raman (1064 nm, 300 mW): $\tilde{\nu}$ = 1611 (13), 1533 (6), 1471 (7), 1431 (15), 1379 (23), 1329 (100),

1287 (41), 1217 (8), 1180 (19), 1074 (24), 999 (7), 808 (22) cm^{-1}. MS (FAB^+): m/z (%) = 18.1 [NH_4^+]. MS (FAB^-): m/z (%) = 224.1 [$C_6H_2N_5O_5^-$]. EA ($C_6H_6N_6O_5$, 242.15 g mol^{-1}): calcd C 29.76, H 2.50, N 34.71%; found C 29.74, H 2.43, N 34.45%. Sensitivities (grain size: < 100 µm): IS: 5 J; FS: > 360 N; ESD: 0.3 J.

Hydroxylammonium 4,6-dinitrobenzotriazol-1-oxide (4b)

4,6-Dinitrobenzotriazol-3-ium-1-oxide hydrate (**4**·H_2O) (257 mg, 1.05 mmol) was dissolved in ethanol (15 mL) and hydroxylamine solution (50% w/w, ρ = 1.078 g cm^{-3}, 0.6 mL, 9.79 mmol) was added. The dark red solution was stirred at room temperature for 30 min. The precipitate was filtered off to afford a dark red solid (90 mg, 0.34 mmol, 32%).
DSC (5 °C min^{-1}): T_{dec} = 185 °C. ^{1}H NMR (400 MHz, DMSO-d_6): δ = 9.87 (br s, 3H, NH_3OH$^+$), 8.74–8.71 (m, 2H, CH) ppm. $^{13}C\{^1H\}$ NMR (101 MHz, DMSO-d_6): δ = 143.6, 135.9, 122.8, 117.6 (*C*H), 116.7 (*C*H) ppm. $^{14}N\{^1H\}$ NMR (29 MHz, DMSO-d_6): δ = −16 (NO_2), −359 (NH_3OH^+) ppm. IR (ATR): $\tilde{\nu}$ = 3411 (vw), 3290 (vw), 3205 (w), 3142 (w), 3093 (w), 2883 (w), 2611 (w), 2363 (w), 2341 (w), 2063 (vw), 1815 (vw), 1616 (m), 1591 (m), 1524 (m), 1509 (m), 1471 (w), 1435 (m), 1416 (m), 1329 (vs), 1286 (vs), 1234 (m), 1216 (m), 1180 (m), 1099 (s), 1064 (s), 999 (m), 937 (vw), 911 (w), 886 (vw), 861 (w), 823 (w), 806 (m), 771 (m), 743 (m), 727 (m), 706 (m), 688 (m), 663 (w), 638 (vw) cm^{-1}. Raman (1064 nm, 300 mW): $\tilde{\nu}$ = 3077 (2), 1621 (6), 1583 (5), 1537 (4), 1519 (3), 1472 (4), 1437 (20), 1380 (25), 1330 (100), 1286 (41), 1224 (3), 1213 (3), 1183 (6), 1174 (6), 1102 (15), 1067 (5), 1054 (4), 1004 (3), 996 (5), 809 (15) cm^{-1}. EA ($C_6H_6N_6O_6$, 284.19 g mol^{-1}): calcd C 27.92, H 2.34, N 32.55%; found C 27.91, H 2.68, N 33.36%. Sensitivities (grain size: < 100 µm): IS: 2 J; FS: > 360 N; ESD: 0.15 J.

Guanidinium 4,6-dinitrobenzotriazol-1-oxide (4c)

Potassium 4,6-dinitrobenzotriazol-1-oxide (**4f**) (137 mg, 0.52 mmol) was dissolved in water (15 mL) and guanidinium chloride (50 mg, 0.52 mmol) was added. The reaction mixture was heated under reflux and then slowly cooled to room temperature. The crystalline brown solid was filtered off to afford **4c** (71 mg, 0.25 mmol, 48%).
DSC (5 °C min^{-1}): T_{dec} = 262 °C. ^{1}H NMR (400 MHz, DMSO-d_6): δ = 8.72 (m, 1H, CH), 8.70 (d, ^4J = 2.0 Hz, CH), 6.94 (s, 6H, NH_2) ppm. $^{13}C\{^1H\}$ NMR (101 MHz, DMSO-d_6): δ = 157.9 ($C(NH_2)_3$), 135.3, 130.3, 117.2 (*C*H), 116.3 (*C*H) ppm. $^{14}N\{^1H\}$ NMR (29 MHz, DMSO-d_6): δ = −15 (NO_2) ppm. IR (ATR): $\tilde{\nu}$ = 3455 (w), 3350 (w), 3265 (w), 3145 (w), 3091 (w), 3080 (w), 1826 (vw), 1670 (m), 1634 (m), 1610 (m), 1585 (m), 1552 (vw), 1523 (s), 1469 (w), 1434 (m), 1330 (vs), 1288 (s), 1210 (w), 1195 (w), 1179 (m), 1086 (m), 1061 (m), 1011 (w), 997 (w), 933 (w), 914 (m), 874 (vw), 859 (w), 804 (m), 772 (w), 742 (w), 707

(m), 686 (w) cm^{-1}. Raman (1064 nm, 300 mW): $\tilde{\nu}$ = 3081 (3), 1611 (19), 1588 (2), 1533 (13), 1472 (9), 1436 (4), 1427 (20), 1375 (22), 1334 (100), 1287 (47), 1214 (10), 1195 (2), 1179 (17), 1087 (33), 1063 (5), 1012 (14), 998 (3), 934 (4), 917 (1), 862 (3), 808 (22), 773 (2), 710 (3), 687 (1), 597 (2), 534 (5), 426 (6), 356 (4), 322 (3), 305 (2) cm^{-1}. MS (FAB^+): m/z (%) = 60.1 (48) [$CH_6N_3^+$]. MS (FAB^-): m/z (%) = 224.1 (100) [$C_6H_2N_5O_5^-$], 208.0 (20) [$C_6H_2N_5O_4^-$]. EA ($C_7H_8N_8O_5$, 284.19 g mol^{-1}): calcd C 29.58, H 2.84, N 39.43%; found C 29.62, H 2.76, N 38.82%. Sensitivities (grain size: < 100 µm): IS: > 40 J; FS: > 360 N; ESD: 1.5 J.

Aminoguanidinium 4,6-dinitrobenzotriazol-1-oxide (4d)

4,6-Dinitrobenzotriazol-3-ium-1-oxide hydrate (**4**·H_2O) (255 mg, 1.05 mmol) was dissolved in ethanol (10 mL) and aminoguanidinium hydrogen carbonate (147 mg, 1.08 mmol) was added. The mixture was stirred for 30 min at room temperature. Then the precipitate was filtered off to afford an orange solid (257 mg, 0.86 mmol, 82%).
DSC (5 °C min^{-1}): T_{dec} = 288 °C. ^{1}H NMR (270 MHz, DMSO-d_6): δ = 8.73 (d, ^4J = 2.1 Hz, C*H*), 8.70 (d, ^4J = 2.1 Hz, C*H*), 7.23–6.84 (m, 4H, CNH_2), 4.69 (s, 2H, NH_2) ppm. ^{13}C{^{1}H} NMR (68 MHz, DMSO-d_6): δ = 159.4 ($C(NH_2)_2NHNH_2$), 139.0, 135.9, 130.8, 117.7 (*C*H), 116.8 (*C*H) ppm. ^{14}N{^{1}H} NMR (29 MHz, D_2O): δ = −16 (NO_2), −316 ($NHNH_2^+$) ppm. IR (ATR): $\tilde{\nu}$ = 3450 (w), 3377 (w), 3339 (w), 3194 (w), 3085 (w), 3071 (w), 1837 (vw), 1682 (w), 1659 (m), 1615 (m), 1592 (m), 1540 (w), 1522 (m), 1477 (w), 1438 (m), 1427 (m), 1330 (vs), 1304 (m), 1289 (m), 1218 (w), 1196 (w), 1183 (m), 1128 (w), 1069 (m), 1005 (m), 998 (m), 965 (w), 936 (m), 921 (m), 864 (w), 808 (m), 773 (m), 742 (m), 730 (w), 710 (m), 689 (w) cm^{-1}. MS (FAB^+): m/z (%) = 75.0 (27) [$CH_7N_4^+$]. MS (FAB^-): m/z (%) = 224.2 (100) [$C_6H_2N_5O_5^-$]. EA ($C_7H_9N_9O_5$, 299.07 g mol^{-1}): calcd C 28.10, H 3.03, N 42.13%; found C 27.99, H 3.14, N 41.55%. Sensitivities (grain size: < 100 µm): IS: 20 J; FS: > 360 N; ESD: 0.3 J.

Triaminoguanidinium 4,6-dinitrobenzotriazol-1-oxide (4e)

Potassium 4,6-dinitrobenzotriazol-1-oxide (**4f**) (243 mg, 0.92 mmol) was dissolved in water (25 mL) and triaminoguanidinium chloride (130 mg, 0.93 mmol) was added. The dark red mixture was heated under reflux for 90 min and then cooled to room temperature. The formed dark red crystals were filtered off and dried at air to yield **4e** (166 mg, 0.50 mmol, 55%).
DSC (5 °C min^{-1}): T_{dec} = 207 °C. ^{1}H NMR (270 MHz, D_2O): δ = 8.98 (d, ^4J = 1.6 Hz, C*H*), 8.91 (d, ^4J = 2.0 Hz, C*H*) ppm. ^{13}C{^{1}H} NMR (68 MHz, D_2O): δ = 118.2 (*C*H), 117.0 (*C*H) ppm. IR (ATR): $\tilde{\nu}$ = 3355 (w), 3318 (m), 3177 (m), 3103 (w), 3078 (w), 2785 (vw),

2646 (vw), 1817 (vw), 1682 (s), 1599 (w), 1578 (m), 1513 (s), 1465 (m), 1438 (m), 1422 (m), 1374 (vw), 1327 (vs), 1284 (vs), 1204 (m), 1192 (w), 1172 (m), 1130 (m), 1069 (m), 1059 (s), 963 (m), 932 (m), 912 (m), 904 (s), 854 (m), 803 (m), 769 (m), 741 (m), 725 (w), 705 (m), 687 (w) cm^{-1}. Raman (1064 nm, 300 mW): $\tilde{\nu}$ = 1609 (16), 1531 (13), 1470 (11), 1444 (36), 1427 (13), 1376 (35), 1332 (100), 1286 (49), 1205 (10), 1177 (21), 1073 (25), 996 (13), 936 (9), 806 (43), 709 (6), 425 (9), 350 (8) cm^{-1}. MS (FAB^+): m/z (%) = 105.1 [$CH_9N_6^+$]. MS (FAB^-): m/z (%) = 224.1 [$C_6H_2N_5O_5^-$]. EA ($C_7H_{11}N_{11}O_5$, 329.23 g mol^{-1}): calcd C 25.54, H 3.37, N 46.80%; found C 25.75, H 3.17, N 46.72%. Sensitivities (grain size: 100–500 µm): IS: > 40 J; FS: > 360 N; ESD: 0.5 J.

Potassium 4,6-dinitrobenzotriazol-1-oxide (4f)

4,6-Dinitrobenzotriazol-3-ium-1-oxide monohydrate (**4**·H_2O) (305 mg, 1.25 mmol) was dissolved in ethanol (50 mL) and potassium hydroxide (72 mmol, 1.28 mmol) dissolved in a minimal amount of water was added dropwise. The solution was stirred at room temperature for 1 h. Then the solvent was removed in vacuo and the residue was washed with diethyl ether and filtered off to afford potassium 4,6-dinitrobenzotriazol-1-oxide (287 mg, 1.09 mmol, 87%) as black powder.
DSC (5 °C min^{-1}): T_{dec} = 295 °C. ^{1}H NMR (400 MHz, D_2O): δ = 8.96 (d, ^4J = 1.9 Hz, 1H, C*H*), 8.92 (d, ^4J = 1.9 Hz, 1H, C*H*) ppm. $^{13}C\{^1H\}$ NMR (101 MHz, D_2O): δ = 142.2, 136.6, 136.0, 129.7, 118.1 (*C*H), 117.0 (*C*H) ppm. $^{14}N\{^1H\}$ NMR (29 MHz, D_2O): δ = −17 (NO_2) ppm. IR (ATR): $\tilde{\nu}$ = 3102 (vw), 3071 (vw), 1604 (w), 1578 (w), 1535 (w), 1511 (m), 1463 (w), 1433 (m), 1375 (vw), 1327 (vs), 1282 (vs), 1208 (m), 1189 (w), 1173 (m), 1050 (s), 993 (w), 936 (w), 927 (w), 907 (w), 855 (w), 805 (m), 784 (w), 768 (w), 744 (m), 732 (m), 705 (s), 685 (w) cm^{-1}. MS (FAB^+): m/z (%) = 39.0 (14) [K^+]. MS (FAB^-): m/z (%) = 224.2 (100) [$C_6H_2N_7O_5^-$]. EA ($C_6H_2KN_7O_5$, 263.21 g mol^{-1}): calcd C 27.38, H 0.77, N 26.61%; found C 27.54, H 0.87, N 26.56%. Sensitivities (grain size: < 100 µm): IS: 2 J; FS: 288 N; ESD: 80 mJ.

Silver 4,6-dinitrobenzotriazol-1-oxide semihydrate (4g·0.5 H_2O)

4f (111 mg, 0.42 mmol) was dissolved in water (5 mL) and silver nitrate (86 mg, 0.51 mmol) was added in the dark. Immediately a brown precipitate occurred. The suspension was stirred for 3 h. The precipitate was filtered off and washed with ethanol and diethyl ether to afford a fine brown solid (109 mg, 0.33 mmol, 79%).
DTA (5 °C min^{-1}): T_{dec} = 205 °C. IR (ATR): $\tilde{\nu}$ = 3585 (vw), 3103 (vw), 1834 (vw), 1616 (w), 1590 (w), 1524 (m), 1477 (w), 1432 (m), 1375 (vw), 1341 (vs), 1330 (vs), 1291 (m), 1211 (vw), 1195 (w), 1177 (w), 1098 (m), 1061 (m), 1004 (vw), 935 (vw), 925 (w),

919 (w), 869 (vw), 803 (m), 776 (w), 739 (m), 726 (w), 704 (m), 685 (m) cm^{-1}. EA ($C_6H_2AgN_5O_5 \cdot 0.5\,H_2O$, 340.99 g mol^{-1}): calcd C 21.13, H 0.89, N 20.54%; found C 21.19, H 1.29, N 20.09%. Sensitivities (grain size: <100 µm): IS: 1 J; FS: >360 N; ESD: 0.1 J.

Ammonium 5,7-diamino-4,6-dinitrobenzotriazol-1-oxide (6a)

6 (250 mg, 0.98 mg) was suspended in 2M aqueous ammonia (14 mL) and stirred for 2 h at room temperature. The solvent was removed in vacuo. A reddish-brown solid (246 mg, 0.90 mmol, 92%) was obtained.
DSC (5 °C min^{-1}): $T_{dec} = 247$ °C. ^{1}H NMR (270 MHz, DMSO-d_6): $\delta = 10.68$–9.40 (m, 4H, NH_2), 7.20 (s, 4H, NH_4^+) ppm. ^{13}C{^{1}H} NMR (101 MHz, DMSO-d_6): $\delta = 149.1$, 145.9, 136.9, 122.5, 113.6, 110.4 ppm. ^{14}N{^{1}H} NMR (29 MHz, DMSO-d_6): $\delta = -14$ (NO_2), -359 (NH_4^+). IR (ATR): $\tilde{\nu} = 3344$ (vw), 3222 (w), 2752 (br, w), 2359 (vw), 1620 (m), 1603 (m), 1558 (m), 1512 (vw), 1388 (m), 1363 (m), 1332 (m), 1276 (s), 1209 (s), 1193 (s), 1172 (s), 1162 (s), 1111 (m), 1080 (m), 1051 (m), 987 (m), 880 (w), 819 (m), 763 (m), 705 (vw), 688 (m), 672 (w) cm^{-1}. Raman (1064 nm, 300 mW): $\tilde{\nu} = 1623$ (23), 1577 (22), 1550 (21), 1510 (36), 1496 (17), 1456 (17), 1394 (80), 1343 (34), 1313 (43), 1282 (94), 1236 (36), 1208 (24), 1194 (50), 1177 (100), 1166 (67), 1114 (19), 1085 (23), 1056 (22), 1046 (14), 1039 (10), 989 (89), 900 (10), 884 (34), 821 (24), 772 (31), 693 (9), 687 (11), 641 (11), 631 (22), 564 (39), 488 (10), 465 (14), 421 (15), 403 (24), 372 (53), 356 (43) cm^{-1}. MS (FAB$^+$): m/z (%) = 16 (1) [NH_4^+]. MS (FAB$^-$): m/z (%) = 254 (3) [$C_6H_4N_7O_5^-$]. EA ($C_6H_8N_8O_5$, 272.18 g mol^{-1}): calcd C 26.48, H 2.98, N 41.17%; found C 26.84, H 2.98, N 39.67%. Sensitivities (grain size: <100 µm): IS: 20 J; FS: >360 N; ESD: 1.5 J.

Hydroxylammonium 5,7-diamino-4,6-dinitrobenzotriazol-1-oxide (6b)

To a suspension of **6** (242 mg, 0.95 mmol) in water (30 mL) was added aqueous hydroxylamine solution (50% w/w, 0.30 mL, 160 mg, 4.90 mmol) and heated under reflux for 1 h. The precipitate was filtered off and washed with diethyl ether to yield a yellow solid (219 mg, 0.76 mmol, 80%).
DSC (5 °C min^{-1}): $T_{dec1} = 174$ °C, $T_{dec2} = 248$ °C. ^{1}H NMR (400 MHz, DMSO-d_6): $\delta = 10.60$–9.46 (m, 4H, NH_2) ppm. ^{13}C{^{1}H} NMR (101 MHz, DMSO-d_6): $\delta = 149.1$, 145.8, 136.2, 113.8, 110.0 ppm. IR (ATR): $\tilde{\nu} = 3355$ (w), 3225 (w), 3029 (w), 2679 (br, w), 1605 (s), 1545 (m), 1512 (m), 1394 (w), 1358 (m), 1335 (s), 1281 (s), 1216 (vs), 1172 (vs), 1094 (s), 1050 (s), 1001 (m), 987 (m), 879 (w), 823 (m), 764 (w), 759 (w), 704 (vw), 685 (w), 663 (vw) cm^{-1}. Raman (1064 nm, 300 mW): $\tilde{\nu} = 1620$ (13), 1582 (9), 1515 (14), 1404 (55), 1378 (45), 1361 (41), 1284 (40), 1246 (14), 1209 (13), 1178 (100), 1166 (99), 1126 (16), 1054 (16), 992 (44), 884 (29), 826 (20), 771 (21), 686 (11), 635 (13), 566 (30), 459 (7), 420 (9), 404

(13), 373 (49), 353 (42) cm^{-1}. MS (DEI^+): m/z (%) = 256.1 (16) [$C_6H_5N_7O_5$+H^+], 17.1 (8) [NH_3^+]. EA ($C_6H_8N_8O_6$, 288.18 g mol^{-1}): calcd C 25.01, H 2.80, N 38.88%; found C 25.15, H 2.76, N 37.98%. Sensitivities (grain size: < 100 µm): IS: 9 J; FS: > 360 N; ESD: 1.5 J.

Guanidinium 5,7-diamino-4,6-dinitrobenzotriazol-1-oxide (6c)

6 (250 mg, 0.98 mmol) and guanidinium carbonate (88 mg, 0.49 mmol) were suspended in water (30 mL) and heated under reflux for 1 h. The precipitate was filtered off. The orange solid was resuspended in water (20 mL) and heated under reflux for 30 min. The precipitate was filtered off and washed with diethyl ether to afford an orange solid (231 mg, 0.74 mmol, 75%).

DSC (5 °C min^{-1}): T_{dec} = 289 °C. ^{1}H NMR (270 MHz, DMSO-d_6): δ = 10.70–9.39 (m, 4H, NH_2), 6.93 (s, 6H, C(NH_2)$_3$) ppm. ^{13}C{^{1}H} NMR (101 MHz, DMSO-d_6): δ = 157.9 (C(NH$_2$)$_3$), 149.1, 145.9, 137.0, 113.6, 110.4, 109.8 ppm. ^{14}N{^{1}H} NMR (29 MHz, DMSO-d_6): δ = −16 (NO_2) ppm. IR (ATR): $\tilde{\nu}$ = 3742 (br, vw), 3471 (w), 3384 (m), 3334 (m), 3145 (w), 3058 (m), 1650 (s), 1619 (s), 1583 (s), 1565 (s), 1503 (m), 1407 (m), 1381 (m), 1349 (m), 1273 (vs), 1220 (vs), 1197 (vs), 1175 (vs), 1163 (s), 1076 (s), 1061 (s), 1005 (m), 988 (s), 887 (w), 818 (m), 778 (m), 768 (s), 732 (vw), 690 (w) cm^{-1}. Raman (1064 nm, 300 mW): $\tilde{\nu}$ = 1623 (14), 1558 (6), 1504 (7), 1415 (25), 1352 (8), 1342 (9), 1273 (100), 1237 (13), 1201 (13), 1181 (28), 1167 (25), 1065 (34), 1007 (23), 987 (40), 893 (36), 818 (18), 772 (16), 625 (8), 567 (13), 539 (6), 460 (8), 422 (6), 402 (6), 359 (50), 234 (5) cm^{-1}. MS (FAB^+): m/z (%) = 60 (2) [$CH_6N_3^+$]. MS (FAB^-): m/z (%) = 254 (1) [$C_6H_4N_7O_5^-$]. EA ($C_7H_{10}N_{10}O_5$, 314.23 g mol^{-1}): calcd C 26.76, H 3.21, N 44.58%; found C 26.94, H 3.20, N 44.39%. Sensitivities (grain size: < 100 µm): IS: 35 J; FS: > 360 N; ESD: 1.5 J.

Aminoguanidinium 5,7-diamino-4,6-dinitrobenzotriazol-1-oxide (6d)

6 (250 mg, 0.98 mmol) and aminoguanidinium hydrogen carbonate (133 mg, 0.98 mmol) were suspended in water (30 mL) and heated under reflux for 1 h. The precipitate was filtered off and washed with diethyl ether to yield an orange solid (250 mg, 0.76 mmol, 78%).

DSC (5 °C min^{-1}): T_{dec1} = 258 °C, T_{dec2} = 275 °C. ^{1}H NMR (270 MHz, DMSO-d_6): δ = 10.70–9.38 (m, 4H, NH_2), 8.56 (s, 1H, NH), 7.25–6.73 (m, 4H, NH_2), 4.68 (s, 2H, NNH_2) ppm. ^{13}C{^{1}H} NMR (101 MHz, DMSO-d_6): δ = 158.7 (C(NH$_2$)$_2$NHNH$_2$), 149.0, 145.9, 137.0, 113.6, 109.8 ppm. IR (ATR): $\tilde{\nu}$ = 3744 (br, vw), 3437 (m), 3343 (m), 3303 (m), 3213 (m), 3159 (m), 3013 (m), 2945 (m), 2845 (m), 1676 (m), 1658 (s), 1623 (s), 1587 (s), 1552 (m), 1500 (m), 1446 (w), 1396 (m), 1370 (m), 1357 (m), 1330 (m), 1270 (vs), 1220 (vs), 1194 (vs), 1170 (vs), 1158 (vs), 1108 (s), 1054 (s), 987 (m), 949 (m), 875 (m), 814 (m), 769 (m), 761 (m), 732 (w), 686 (m), 676 (m) cm^{-1}. Raman (1064 nm, 300 mW):

$\tilde{\nu}$ = 1626 (14), 1589 (11), 1543 (7), 1502 (13), 1406 (38), 1384 (29), 1359 (21), 1275 (100), 1233 (23), 1197 (26), 1177 (33), 1164 (71), 1082 (12), 1060 (24), 986 (53), 881 (49), 821 (21), 771 (27), 631 (21), 561 (21), 420 (14), 401 (13), 266 (59), 247 (11) cm^{-1}. MS (FAB^+): m/z (%) = 75 (5) [$CH_7N_4^+$]. MS (FAB^-): m/z (%) = 254 (1) [$C_6H_4N_7O_5^-$]. EA ($C_7H_{11}N_{11}O_5$, 329.23 g mol^{-1}): calcd C 25.54, H 3.37, N 46.80%; found C 25.91, H 3.36, N 46.11%. Sensitivities (grain size: < 100 µm): IS: 35 J; FS: > 360 N; ESD: 1.25 J.

Potassium 5,7-diamino-4,6-dinitrobenzotriazol-1-oxide (6f)

To a suspension of **6** (321 mg, 1.26 mmol) in ethanol (15 mL) a solution of potassium hydroxide (710 mg, 1.27 mmol) dissolved in water (1.5 mL) was added dropwise. The suspension was stirred for 5 h at room temperature and filtered off to yield an orange solid (344 mg, 1.25 mmol, 99%).
DTA (5 °C min^{-1}): T_{dec} = 266 °C. ^{1}H NMR (400 MHz, DMSO-d_6): δ = 10.61–9.42 (m, 4H, NH_2) ppm. ^{13}C{^{1}H} NMR (101 MHz, DMSO-d_6): δ = 149.1, 145.8 ppm. IR (ATR): $\tilde{\nu}$ = 3341 (vw), 3233 (vw), 1624 (m), 1607 (m), 1557 (w), 1505 (vw), 1391 (m), 1364 (m), 1341 (s), 1278 (vs), 1211 (vs), 1191 (vs), 1177 (vs), 1111 (w), 1069 (vw), 1054 (w), 986 (m), 881 (vw), 817 (w), 778 (vw), 763 (w), 749 (w), 689 (s), 676 (m) cm^{-1}. MS (FAB^+): m/z (%) = 39 (3) [K^+]. MS (FAB^-): m/z (%) = 254 (5) [$C_6H_4N_7O_5^-$]. EA ($C_6H_4KN_7O_5$, 272.18 g mol^{-1}): calcd C 24.58, H 1.37, N 33.44%; found C 25.31, H 1.70, N 33.07%. Sensitivities (grain size: < 100 µm): IS: 35 J; FS: > 360 N; ESD: 0.75 J.

1-(5,7-Dinitrobenzotriazol-1-yl)-2-nitrazapropane (7)

1-Chloro-2-nitrazapropane (106 mg, 0.85 mmol) was dissolved in acetone (25 mL) and the potassium salt **1f** (201 mg, 0.73 mmol) was added. The reaction mixture was stirred at room temperature overnight. The precipitate was filtered off and the solvent was removed in vacuo to afford a colorless solid (156 mg, 0.53 mmol, 72%).
DSC (5 °C min^{-1}): T_{dec} = 179 °C. ^{1}H NMR (400 MHz, acetone-d_6): δ = 9.46 (d, ^4J = 1.9 Hz, 0.2H, CH), 9.44–9.43 (m, 1.1H, CH), 9.15–9.13 (m, 1.1H, CH), 9.02 (d, ^4J = 1.9 Hz, 0.2H, CH), 7.10 (s, 0.5H, CH_2), 7.03 (s, 2H, CH_2), 6.99 (s, 0.6H, CH_2), 3.79 (s, 0.8H, CH_3), 3.73 (s, 0.8H, CH_3), 3.67 (s, 3H, CH_3) ppm. ^{13}C{^{1}H} NMR (101 MHz, acetone-d_6): δ = 149.3 (C_q), 144.6(CNO$_2$), 129.0 (C_q), 124.0 (CH), 123.3 (CH), 121.6 (CH), 120.2 (CH), 117.1 (CH), 115.8 (CH), 71.0 (CH$_2$), 66.3 (CH$_2$), 63.3 (CH$_2$), 39.8 (CH$_3$), 39.7 (CH$_3$), 39.3 (CH$_3$) ppm. ^{14}N{^{1}H} NMR (29 MHz, acetone-d_6): δ = −14 (CNO$_2$), −25 (NNO$_2$), −26 (NNO$_2$) ppm. IR (ATR): $\tilde{\nu}$ = 3085 (w), 3061 (w), 1628 (w), 1600 (w), 1578 (w), 1529 (vs), 1451 (m), 1417 (m), 1388 (w), 1379 (w), 1340 (vs), 1312 (m), 1282 (m), 1239 (s), 1210 (m), 1165 (w), 1086 (m), 1062 (m), 1037 (m), 962 (w), 943 (m), 930 (m), 917 (m), 902

(w), 884 (w), 870 (w), 858 (w), 849 (w), 818 (s), 801 (m), 781 (w), 758 (s), 745 (m), 737 (m), 707 (m), 675 (w), 666 (m) cm^{-1}. Raman (1064 nm, 300 mW): $\tilde{\nu}$ = 3103 (4), 3088 (3), 3079 (4), 3075 (4), 3063 (5), 3042 (4), 3033 (2), 3006 (13), 2979 (3), 2960 (7), 2956 (7), 2931 (3), 2685 (3), 1631 (11), 1600 (10), 1582 (7), 1547 (14), 1483 (4), 1461 (9), 1434 (11), 1420 (5), 1405 (5), 1393 (9), 1381 (20), 1351 (100), 1307 (8), 1252 (8), 1086 (5), 1065 (16), 1016 (5), 999 (9), 944 (7), 932 (7), 861 (6), 850 (21), 804 (13), 761 (7), 650 (4), 612 (4), 487 (4), 355 (6), 292 (5), 238 (7) cm^{-1}. MS (DEI^+): m/z (%) = 297.1 (1) [M^+], 222.1 (11) [$C_7H_4N_5O_4^+$], 89.1 (100) [$C_2H_5N_2O_2^+$]. EA ($C_8H_7N_7O_6$, 297.19 g mol^{-1}): calcd C 32.33, H 2.37, N 32.99%; found C 32.25, H 2.37, N 32.22%. Sensitivities (grain size: < 100 µm): IS: > 40 J; FS: > 360 N; ESD: 0.25 J.

1-(4,6-Dinitrobenzotriazol-3-ium-1-oxide-3-yl)-2-nitrazapropane (8)

1-Chloro-2-nitrazapropane (101 mg, 0.81 mmol) was dissolved in acetone (30 mL) and potassium 4,6-dinitrobenzotriazol-1-oxide (**4f**) (209 mg, 0.79 mmol) was added in one portion. The dark red solution was stirred at room temperature overnight. The precipitate was filtered off and the solvent was removed in vacuo. The crude product was washed with diethyl ether and filtered off to afford an ocher solid (216 mg, 0.70 mmol, 87%).
DSC (5 °C min^{-1}): T_{dec1} = 147 °C, T_{dec2} = 185 °C. ^{1}H NMR (400 MHz, acetone-d_6): δ = 9.17 (d, ^4J = 2.0 Hz, 1H, C*H*), 9.15 (d, ^4J = 1.9 Hz, 0.3H, C*H*), 9.05 (d, ^4J = 1.7 Hz, 0.3H, C*H*), 9.04 (d, ^4J = 2.1 Hz, 1H, C*H*), 6.71 (s, 2.4H, CH_2), 3.60 (s, 3.7H, CH_3) ppm. ^{13}C{^{1}H} NMR (101 MHz, acetone-d_6): δ = 130.2, 124.3 (*C*H), 118.7 (*C*H), 80.5 (*C*H_2), 65.6 (*C*H_2), 39.7 (*C*H_3), 38.2 (*C*H_3) ppm. ^{14}N{^{1}H} NMR (29 MHz, acetone-d_6): δ = −19 (C*N*O_2), −27 (N*N*O_2), −28 (N*N*O_2), −31 (N*N*O_2) ppm. IR (ATR): $\tilde{\nu}$ = 3104 (vw), 3083 (vw), 3060 (vw), 2361 (br, vw), 1642 (w), 1624 (w), 1609 (w), 1541 (m), 1532 (m), 1508 (m), 1438 (m), 1383 (vw), 1371 (vw), 1337 (vs), 1282 (m), 1246 (m), 1220 (m), 1190 (m), 1175 (w), 1157 (m), 1120 (m), 1067 (w), 1056 (w), 1042 (vw), 1030 (vw), 982 (w), 968 (w), 956 (w), 933 (vw), 916 (w), 911 (w), 895 (w), 884 (w), 829 (m), 805 (m), 792 (w), 763 (m), 733 (s), 702 (m), 682 (m) cm^{-1}. Raman (1064 nm, 300 mW): $\tilde{\nu}$ = 3105 (3), 3006 (5), 2961 (3), 1645 (1), 1626 (18), 1560 (1), 1546 (7), 1509 (4), 1454 (3), 1418 (25), 1391 (2), 1375 (8), 1342 (100), 1304 (1), 1291 (2), 1270 (1), 1250 (2), 1213 (3), 1180 (3), 1159 (11), 1070 (5), 1059 (2), 856 (8), 808 (14), 795 (2), 705 (3), 691 (2), 609 (5), 412 (4), 348 (3), 315 (3) cm^{-1}. MS (DEI^+): m/z (%) = 313.0 (1) [M^+], 225.0 (1) [$C_6H_2N_5O_5$+H^+], 209.0 (44) [$C_6H_2N_5O_4$+H^+], 89.1 (100) [$C_2H_5N_2O_2^+$]. EA ($C_8H_7N_7O_7$, 313.18 g mol^{-1}): calcd C 30.68, H 2.25, N 31.31%; found C 30.36, H 2.33, N 30.84%. Sensitivities (grain size: < 100 µm): IS: 1 J; FS: > 360 N; ESD: 80 mJ.

3.4 References

[1] D. Fischer, T. M. Klapötke, M. Reymann, J. Stierstorfer, *Chem. Eur. J.* **2014**, *20*, 6401–6411.

[2] J. Akhavan, *The Chemistry of Explosives*, 2nd ed., RSC, Cambridge, UK, **2004**.

[3] T. M. Klapötke, *Chemie der hochenergetischen Materialien*, 1st ed., de Gruyter, Berlin, Germany, **2009**.

[4] H. Gao, J. M. Shreeve, *Chem. Rev.* **2011**, *111*, 7377–7436.

[5] P. F. Pagoria, G. S. Lee, A. R. Mitchell, R. D. Schmidt, *Thermochim. Acta* **2002**, *384*, 187–204.

[6] R. P. Singh, R. D. Verma, D. T. Meshri, J. M. Shreeve, *Angew. Chem., Int. Ed.* **2006**, *45*, 3584–3601; *Angew. Chem.* **2006**, *118*, 3664–3682.

[7] A. A. Dippold, T. M. Klapötke, N. Winter, *Eur. J. Inorg. Chem.* **2012**, 3474–3484.

[8] K. Wang, D. A. Parrish, J. M. Shreeve, *Chem. Eur. J.* **2011**, *17*, 14485–14492.

[9] J. W. Fronabarger, M. D. Williams, W. B. Sanborn, D. A. Parrish, M. Bichay, *Propellants, Explos., Pyrotech.* **2011**, *36*, 459–470.

[10] W. P. Norris, US4529801 **1985**.

[11] W. Norris, R. Spear, R. Read, *Aust. J. Chem.* **1983**, *36*, 297–309.

[12] J. Šarlauskas, Ž. Anusevičius, A. Misiūnas, *Cent. Eur. J. Energ. Mater.* **2012**, *9*, 365–386.

[13] P. Drost, *Justus Liebigs Ann. Chem.* **1899**, *307*, 49–69.

[14] L. Türker, S. Variş, *Polycyclic Aromat. Compd.* **2009**, *29*, 228–266.

[15] D. Ehlers, T. M. Klapötke, C. Pflüger, *Chem. Eur. J.* **2015**, *21*, 16073–16082.

[16] R. Damavarapu, C. R. Surapaneni, N. Gelber, R. G. Duddu, M.-X. Zhang, P. R. Dave, US7304164 **2007**.

[17] S. S. Novikov, L. I. Khmelnitskii, O. V. Levedev, V. V. Sevastyanova, L. V. Epishina, *Khim. Geterotsikl. Soedin.* **1970**, *6*, 503.

[18] J. R. Cho, K. J. Kim, S. G. Cho, J. K. Kim, *J. Heterocycl. Chem.* **2002**, *39*, 141–147.

[19] J. Kehler, A. Püschl, O. Dahl, *Acta Chem. Scand.* **1996**, *50*, 1171–1173.

[20] C. J. McHugh, D. R. Tackley, D. Graham, *Heterocycles* **2002**, *57*, 1461–1470.

[21] F. H. Allen, O. Kennard, D. G. Watson, L. Brammer, A. G. Orpen, R. Taylor, *J. Chem. Soc., Perkin Trans. 2* **1987**, S1–S19.

[22] NATO, *Standardization Agreement 4489 (STANAG 4489), Explosives, Impact Sensitivity Tests* **1999**.

[23] NATO, *Standardization Agreement 4487 (STANAG 4487), Explosives, Friction Sensitivity Tests* **2002**.

[24] Test methods according to the *UN Manual of Test and Criteria, Recommendations on the Transport of Dangerous Goods*, United Nations Publication, New York, Geneva, 4th revised ed., **2003**: Impact: Insensitive >40 J, less sensitive ≥ 35 J, sensitive ≥ 4 J, very sensitive ≤ 3 J; Friction: Insensitive >360 N, less sensitive $= 360$ N, sensitive <360 N a. >80 N, very sensitive ≤ 80 N, extremely sensitive ≤ 10 N.

[25] M. Sućeska, Explo5 program, v. 6.02, Zagreb, Croatia, **2014**.

[26] M. Sućeska, *Propellants, Explos., Pyrotech.* **1991**, *16*, 197–202.

[27] M. Sućeska, *Propellants, Explos., Pyrotech.* **1999**, *24*, 280–285.

[28] C. Xue, J. Sun, B. Kang, Y. Liu, X. Liu, G. Song, Q. Xue, *Propellants, Explos., Pyrotech.* **2010**, *35*, 333–338.

[29] J. W. Ochterski, G. A. Petersson, J. J. A. Montgomery, *J. Chem. Phys.* **1996**, *104*, 2598–2619.

[30] J. J. A. Montgomery, M. J. Frisch, J. W. Ochterski, G. A. Petersson, *J. Chem. Phys.* **2000**, *112*, 6532–6542.

[31] M. J. Frisch, G. W. Trucks, H. B. Schlegel, G. E. Scuseria, M. A. Robb, J. R. Cheeseman, G. Scalmani, V. Barone, B. Mennucci, G. A. Petersson, H. Nakatsuji, M. Caricato, X. Li, H. P. Hratchian, A. F. Izmaylov, J. Bloino, G. Zheng, J. L. Sonnenberg, M. Hada, M. Ehara, K. Toyota, R. Fukuda, J. Hasegawa, M. Ishida, T. Nakajima, Y. Honda, O. Kitao, H. Nakai, T. Vreven, J. A. Montgomery Jr., J. E. Peralta, F. Ogliaro, M. Bearpark, J. J. Heyd, E. Brothers, K. N. Kudin, V. N. Staroverov, R. Kobayashi, J. Normand, K. Raghavachari, A. Rendell, J. C. Burant, S. S. Iyengar, J. Tomasi, M. Cossi, N. Rega, J. M. Millam, M. Klene, J. E. Knox, J. B.

Cross, V. Bakken, C. Adamo, J. Jaramillo, R. Gomperts, R. E. Stratmann, O. Yazyev, A. J. Austin, R. Cammi, C. Pomelli, J. W. Ochterski, R. L. Martin, K. Morokuma, V. G. Zakrzewski, G. A. Voth, P. Salvador, J. J. Dannenberg, S. Dapprich, A. D. Daniels, Ö. Farkas, J. B. Foresman, J. V. Ortiz, J. Cioslowski, D. J. Fox, Gaussian 09, revision A.02, Gaussian, Inc., Wallingford CT, **2009**.

[32] M. S. Westwell, M. S. Searle, D. J. Wales, D. H. Williams, *J. Am. Chem. Soc.* **1995**, *117*, 5013–5015.

[33] F. Trouton, *Philos. Mag.* **1884**, *18*, 54–57.

Energetic Derivatives of 5-(5-Amino-2*H*-1,2,3-triazol-4-yl)-1*H*-tetrazole

D. Izsák, T. M. Klapötke, and C. Pflüger

Dalton Trans. **2015**, *44*, 17054-17063.

Energetic Derivatives of 5-(5-Amino-2*H*-1,2,3-triazol-4-yl)-1*H*-tetrazole

D. Izsák, T. M. Klapötke, and C. Pflüger
Dalton Trans. **2015**, *44*, 17054-17063.

Abstract

This study presents the preparation of the novel nitrogen-rich compound 5-(5-amino-2*H*-1,2,3-triazol-4-yl)-1*H*-tetrazole (**13**) from commercially available chemicals in a five step synthesis. The more energetic derivatives with azido (**14**) and nitro (**15**) groups, as well as a diazene bridge (**16**) were also successfully prepared. The energetic compounds were comprehensively characterized by various means, including vibrational (IR, Raman) and multinuclear (^{1}H, ^{13}C, ^{14}N, ^{15}N) NMR spectroscopy, mass spectrometry and differential thermal analysis. The sensitivities towards important outer stimuli (impact, friction, electrostatic discharge) were determined according to BAM standards. The enthalpies of formation were calculated on the CBS-4M level of theory, revealing highly endothermic values, and were utilized to calculate the detonation parameters using EXPLO5 (v. 6.02).

4.1 Introduction

Poly-azole compounds have been the focus of several research groups worldwide working in the field of energetic materials in the recent years. These feature two, or even more, linked azoles (furazan, 1,2,4-triazole, tetrazole, etc.), which can be either directly linked,[1–21] or through energetic bridging moieties like a diazene bridge.[22–30]

The detonation performance of energetic compounds depends strongly on the enthalpy of formation and the density, with higher values resulting in more powerful explosives. The high nitrogen content of azole based compounds results in high positive enthalpies of formation due to the large number of inherent N−N and C−N bonds and thereby showing high potential as explosive.[31] Furthermore, the nitrogen-rich heterocycles mainly release nontoxic dinitrogen gas upon decomposition, whereby the environmental pollution might be diminished.

The design of new high explosives should consider improved thermal and mechanical sensitivities as well as an increased detonation performance, but unfortunately, these parameters often have contradictory impact to each other.[32]

The combination of multiple different heterocycles is advantageous due to the vast possibilities of tailoring the energetic performances. An interesting example combining the

frequently utilized tetrazole and 1,2,4-triazole moieties are the derivatives of 5-(5-amino-1*H*-1,2,4-triazol-3-yl)tetrazole with the energetic azido, nitro and nitramino groups, which have been investigated recently.[33] This C−C linkage of the two heterocycles benefits from the energetic tetrazole ring, the higher stability of the triazole ring and the second carbon atom of the triazole, which carries various energetic groups. Another option would be the utilization of a 1,2,3-triazole instead of the 1,2,4-triazole, which should result in higher enthalpies of formation and thus improved energetic performances, although potentially at the expense of thermal and mechanical stability. A suitable nitrile precursor had already been reported in 1956,[34] but no studies concerning the binary combination of a tetrazole and a 5-amino-1,2,3-triazole by means of a C−C link could be found.
The goal of this study has therefore been the synthesis of the novel 5-(5-amino-2*H*-1,2,3-triazol-4-yl)-1*H*-tetrazole (**13**) and its derivatives with azido (**14**) and nitro (**15**) groups as well as diazene bridging (**16**), their comprehensive characterization and the comparison of the compounds with the respective 1,2,4-triazole isomers and analogues.

4.2 Results and Discussion

4.2.1 Syntheses

There are two possible routes to the intermediate 5-amino-1-benzyl-1,2,3-triazole-4-carbonitrile (**11**). The first one is the direct synthesis from benzyl azide (**9**) and malononitrile with sodium in ethanol,[34] but this reaction suffers from low yields and the formation of 5-amino-1-benzyl-4-carbiminoethoxy-1,2,3-triazole as a byproduct, due to the presence of the second nitrile, which can react with the formed ethoxide. The second option is the well working synthesis (80%) of 5-amino-1-benzyl-1,2,3-triazole-4-carboxamide (**10**) from benzyl azide (**9**) and cyanoacetamide with sodium in ethanol,[34] which can then be further processed in two different ways. The first one would be the debenzylation to 4-amino-2*H*-1,2,3-triazole-5-carboxamide with sodium in liquid ammonia,[34] followed by the dehydration of the amide to a nitrile. Although the debenzylation is working well (96%), the dehydration did not result in a complete conversion with various reagents (phosphorus pentoxide, phosphoryl chloride, phosphorus pentachloride, thionyl chloride). Therefore, the benzyl protective group was left on the triazole and thus enabling the use of trifluoroacetic anhydride by protecting the ring from its acylation properties, resulting in a complete conversion of **10** into **11** in high yields (86%). The next step, the formation of 5-(5-amino-1-benzyl-1,2,3-triazol-4-yl)tetrazole (**12**) from **11** and sodium azide, proved to be quite difficult due to the frequent hydrolysis of the nitrile, in addition to the desired product, when zinc chloride was employed in a protic solvent (water, ethanol, methanol).

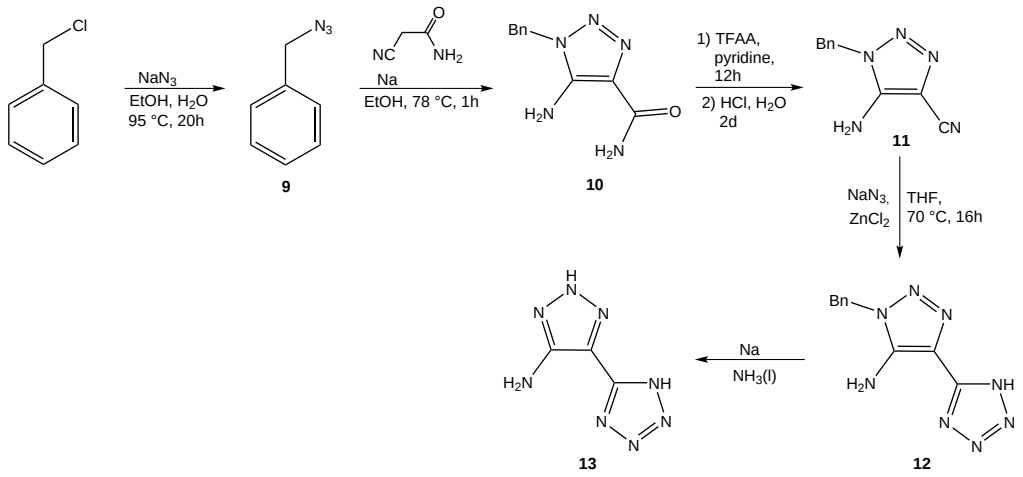

Scheme 4.1: Synthetic route towards 5-(5-amino-2*H*-1,2,3-triazol-4-yl)-1*H*-tetrazole (**13**) from commercially available benzyl chloride.

Hydrochloric acid and ammonium chloride in the same solvents did not result in partial hydrolysis, but also did not yield any product, and neither did acetic acid (both as acid and as solvent). Utilization of the polar, aprotic tetrahydrofuran and zinc chloride finally yielded pure **12** (97%). Debenzylation was again carried out with sodium in liquid ammonia to obtain the title compound 5-(5-amino-2*H*-1,2,3-triazol-4-yl)-1*H*-tetrazole (**13**) in high yield (95%). The optimized route is shown in Scheme 4.1

The amine of **13** was then converted into different energetic moieties as illustrated in Scheme 4.2. The azido derivative **14** was obtained in high yield (87%) by diazotation with sodium nitrite in sulfuric acid, followed by a diazo azide exchange with sodium azide. The nitro derivative **15** could not be obtained by the common reaction with an excess of sodium nitrite in sulfuric acid, a method which works well with 5-(5-amino-1*H*-1,2,4-triazol-3-yl)tetrazole for example,[33] but it was obtained by oxidation of the amine with potassium superoxide in tetrahydrofuran in a fair yield (68%). Azo coupling with potassium permanganate in water yielded 1,2-bis(4-(1*H*-tetrazol-5-yl)-2*H*-1,2,3-triazol-5-yl)diazene (**16**) also only in a fair yield (48%) as a dihydrate.

4.2.2 NMR Spectroscopy

All compounds prepared herein were investigated by multinuclear NMR spectroscopy (^{1}H and ^{13}C, some additionally ^{14}N and ^{15}N). ^{13}C NMR spectroscopy is well suited to differentiate between the precursor molecules **10**–**12**, the title compound **13** and its further derivatives **14**–**16**. While **10**–**12** all show the signals of the benzyl group (phenyl: 135.2–136.0, 128.7, 127.8–127.9, 127.4–127.5 ppm; methylene: 48.4–48.8 ppm), those are completely gone in the spectrum of **13**. The signal of the triazole carbon atom attached to the exocyclic

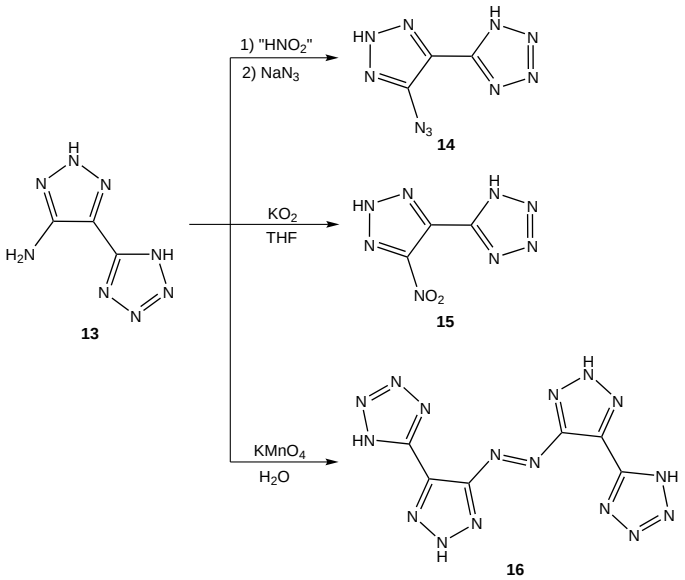

Scheme 4.2: Synthetic route towards the more energetic derivatives 5-(5-azido-2*H*-1,2,3-triazol-4-yl)-1*H*-tetrazole (**14**), 5-(5-nitro-2*H*-1,2,3-triazol-4-yl)-1*H*-tetrazole (**15**), and 1,2-bis(4-(1*H*-tetrazol-5-yl)-2*H*-1,2,3-triazol-5-yl)diazene (**16**).

carbon is at 121.8 (**10**), 113.7 (**11**), and 114.4 ppm (**12**). The carbon atom carrying the amine shows a signal at 144.9 (**10**), 148.0 (**11**), and 148.6 ppm (**12**). While the spectrum of **10** shows a signal at 164.5 ppm, stemming from the amide, **11** has the signal of the nitrile at 101.3 ppm and shows no signs of the former. Pure **12** finally exhibits a new signal at 142.9 ppm, belonging to the newly formed tetrazole. The signals of compounds **13**–**16** (^{1}H, ^{13}C and ^{14}N) are compiled in Table 4.1. While **14**–**16** show three sharp signals for the two triazole and one tetrazole carbon atoms in their corresponding ^{13}C NMR spectra, **13** shows only one sharp signal at 149.0 ppm, attributed to the tetrazole, and two small and broad signals at 147.6 and 111.6 ppm, attributed to the triazole. The carbon resonances of the rings are assigned due to their signal shapes and intensities, and in comparison to ^{13}C NMR spectra of corresponding salts. The corresponding ^{14}N NMR spectra show the signals of the central azide nitrogen atom (N_β) of **14** at −138 ppm as a broad signal and the nitro group of **15** at −21 ppm.

Compounds **14** and **15** were further investigated by ^{15}N and ^{15}N{^{1}H} NMR spectroscopy. The proton coupled ^{15}N NMR spectra are depicted in Figure 4.1. The proton decoupled ^{15}N NMR spectra can be found in the Appendix (Figure A.9). All nitrogen atoms display clearly visible resonances in the ^{15}N NMR spectra of both **14** (eight signals) and **15** (six signals). The tetrazole emits only two signals due to the enabled proton exchange in DMSO-d_6, equalizing the four nitrogen atoms to one protonated (−101.9 ppm in **14**, −65.4 ppm in **15**) and one non-protonated (−11.1 ppm in **14**, −14.4 ppm in **15**), similar to 5-(5-azido-1*H*-1,2,4-triazol-3-yl)tetrazole and 5-(3-nitro-1*H*-1,2,4-triazol-5-yl)-2*H*-tetrazole for example.[33]

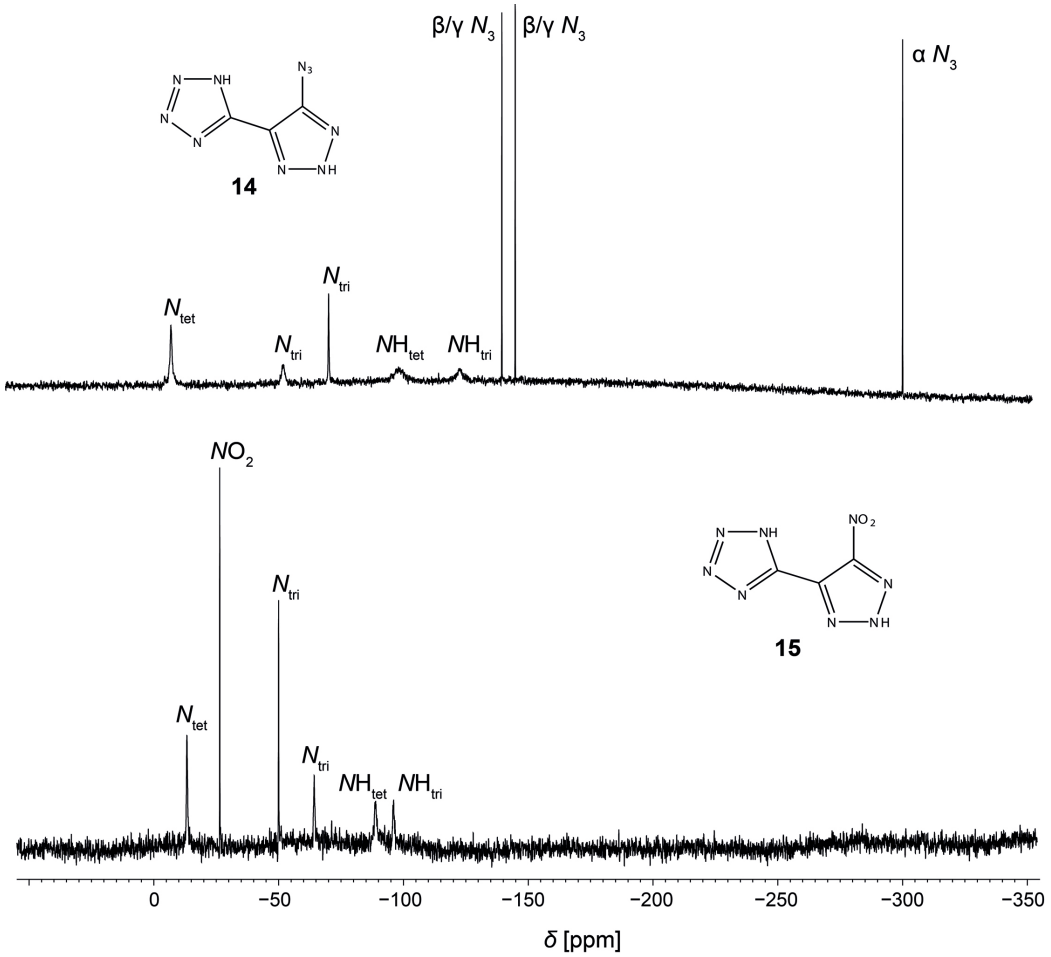

Figure 4.1: ^{15}N NMR spectra of 5-(5-azido-2*H*-1,2,3-triazol-4-yl)-1*H*-tetrazole (**14**) and 5-(5-nitro-2*H*-1,2,3-triazol-4-yl)-1*H*-tetrazole (**15**) in DMSO-d_6 at room temperature.

The triazole shows three signals in both compounds, with one being strong and sharp (−74.1 ppm in **14**, −51.1 ppm in **15**) and the other two being weaker and broad (−55.7 and −126.3 ppm in **14**, −65.4 and −97.2 ppm in **15**). The ^{15}N{^{1}H} NMR spectra confirm that the signals at −126.3 and −97.2 ppm carry the protons, in addition to their high field shift. The signal of the protonated nitrogen atom of the tetrazole ring is in all spectra broader than that of the triazole. The remaining signals are belonging to the azide (−143.2, −148.6 and −303.3 ppm) of **14** and the nitro group (−27.5 ppm) of **15**. While the signal at −303.3 ppm in the spectrum of **14** can be clearly attributed to the alpha nitrogen atom of the azide, the signals at −143.2 and −148.6 ppm have nearly identical intensities and are thus preventing an unambiguous assignment to the beta and gamma nitrogen atoms.

Table 4.1: NMR signals of **13**–**16** in DMSO-d_6 at room temperature.

	δ			
	^{1}H	^{13}C (triazole)	^{13}C (tetrazole)	^{14}N
13	16.19[i], 14.64[i], 6.03[ii]	147.6, 111.6	149.0	—
14	15.81[i]	147.7, 123.0	143.1	−138[iii]
15	9.93[i]	151.1, 127.7	147.7	−21[iv]
16	10.09[i]	153.7, 126.6	147.2	—

(i) aromatic NH; (ii) NH_2; (iii) azide N_β; (iv) NO_2.

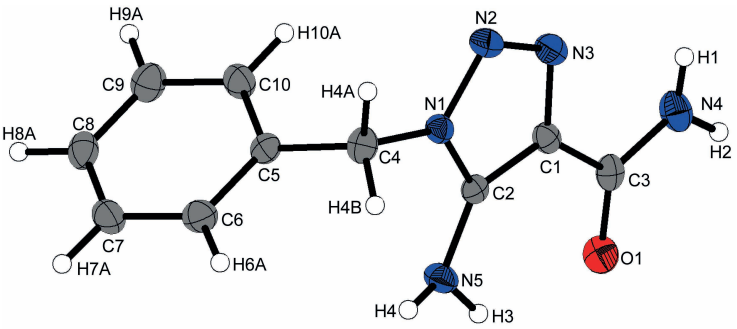

Figure 4.2: Molecular structure of 5-amino-1-benzyl-1,2,3-triazole-4-carboxamide (**10**). Thermal ellipsoids at 50% probability.

4.2.3 Crystal Structures

The precursor molecule 5-amino-1-benzyl-1,2,3-triazole-4-carboxamide (**10**) crystallizes in the monoclinic space group $P2_1/c$ with four formula units per unit cell. The molecular unit is depicted in Figure 4.2.

The bond lengths of the 1,2,3-triazole ring are between the length of the corresponding single and double bonds,[35] with the N1−N2 bond being significantly longer (1.376(1) Å) than the N2−N3 bond (1.304(1) Å), which is quite common for 1,4,5-substituted 1,2,3-triazoles.[36–39] The bond lengths of the amino group attached to the triazole (1.351(2) Å), as well as the amide N4−C3 bond (1.346(2) Å) are considerably shorter than the corresponding single bonds, caused by an involvement of the nonbinding electron pair of the nitrogen atoms, with both groups being almost planar. The amide group and the triazole ring are practically in plane (C2−C1−C3−O1: 1.66(2)°). The molecule features one weak and undirected intramolecular hydrogen bond between the ring amine and the amide oxygen as N5−H3···O1 (D···A: 2.956(1) Å; ∠D−H···A: 125(1)°), and a long but directed intermolecular hydrogen bond N4−H2···O1[i] (D···A: 3.070(2) Å; ∠D−H···A: 171(2)°) resulting in dimers (see Figure 4.3 for both). The dimers are connected by undulated ribbons through a π–π stacking interaction of the phenyl groups, depicted in Figure 4.3. The distance between the

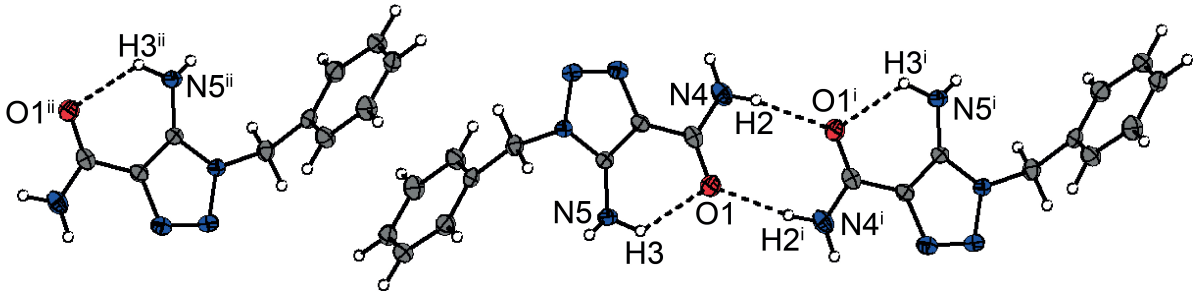

Figure 4.3: Hydrogen bonds and π–π stacking interactions of **10**. Thermal ellipsoids at 50% probability. Symmetry codes: (i) $-x+1, -y+3, -z+1$; (ii) $-x, 1-y, 1-z$.

Table 4.2: Hydrogen bonds present in 5-amino-1-benzyl-1,2,3-triazole-4-carboxamide (**10**).

D−H···A	d(D−H) [Å]	d(H···A) [Å]	d(D···A) [Å]	∠(D−H···A) [°]
N5−H3···O1	0.88(2)	2.36(1)	2.956(1)	125(1)
N4−H2···O1^{i}	0.90(2)	2.17(2)	3.070(2)	171(2)
N5−H4···N2^{ii}	0.91(2)	2.24(2)	3.128(2)	164(1)

Symmetry codes: (i) $-x+1, -y+3, -z+1$; (ii) $x, -y+1.5, z-0.5$.

two aromatic moieties is 3.531(2) Å, which is characteristic for these interactions.[40] The second intermolecular interaction, which connects the ribbons is formed by a very long but directed hydrogen bond N5−H4···N2^{ii} between the amino moiety and a nitrogen atom of a neighboring triazole (D···A: 3.128(2) Å; ∠D−H···A: 164(1)°), slightly above the sum of the van der Waals radii ($\sum r_w$(N,N) = 3.10 Å).[41] The resulting crystal structure, presented in Figure 4.4, has two areas, which are either dominated by polar hydrogen bonds or by nonpolar π–π stacking interactions. The parameters of the described hydrogen bonds are summarized in Table 4.2. Further information regarding the crystal structure determination has been compiled in the Appendix (Table A.11).

The title compound 5-(5-amino-2*H*-1,2,3-triazol-4-yl)-1*H*-tetrazole (**13**) crystallizes in the monoclinic space group $P2_1/n$ with four formula units per unit cell and a calculated density of 1.705 g cm^{-3} at 100 K. The molecular unit is depicted in Figure 4.5.

The bond lengths are again between formal single and double bonds. The triazole ring is more symmetrical than that of **10** with N1−N2 and N2−N3 bond lengths of 1.350(2) and 1.311(2) Å, respectively. The length of the C1−C3 bond (1.442(2) Å) is comparable to similar bisazole compounds.[33] Both rings form an almost planar system with a N3−C1−C3−N4 torsion angle of −1.1(2)°. The amino group is similar to that of **10** and is also in plane with both rings, leading to the assumption of a conjugated π-system across the whole molecule. Additionally, the molecule features an intramolecular N8−H4···N7 hydrogen bond between the amino group and the tetrazole ring. The structure is dominated by an

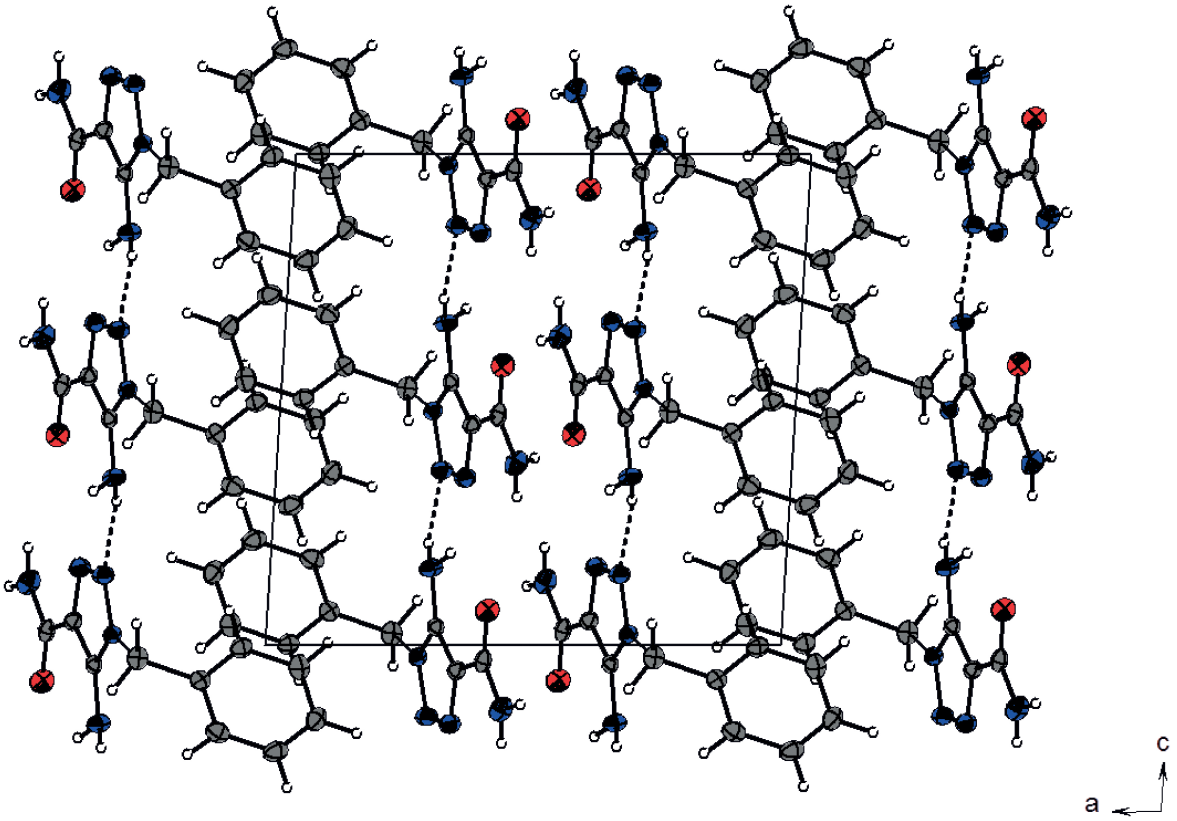

Figure 4.4: Unit cell of **10** along the *b* axis, illustrating the intermolecular N5−H4···N2^{ii} hydrogen bond. Thermal ellipsoids at 50% probability.

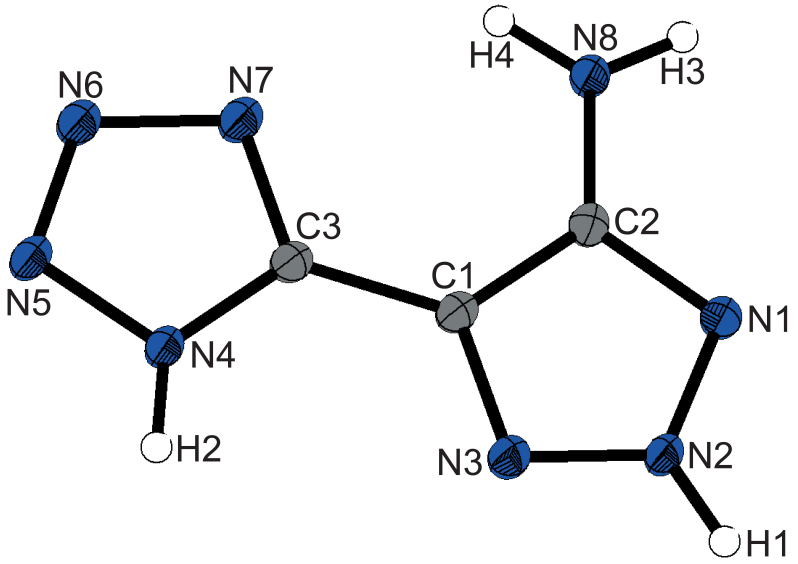

Figure 4.5: Molecular structure of 5-(5-amino-2*H*-1,2,3-triazol-4-yl)-1*H*-tetrazole (**13**). Thermal ellipsoids at 50% probability.

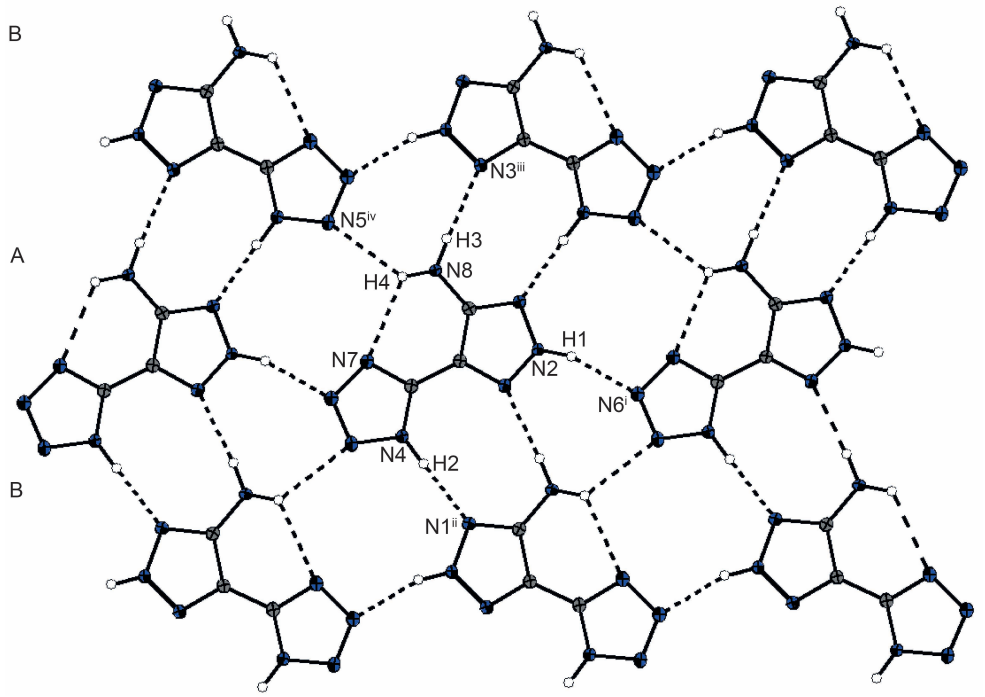

Figure 4.6: Hydrogen bonds of **13**, illustrating the two anti-parallel chains (A) and (B). Thermal ellipsoids at 50% probability. Symmetry codes: (i) $x, y, z+1$; (ii) $-x+0.5, y+0.5, -z+0.5$; (iii) $-x+0.5, y-0.5, -z+0.5$; (iv) $-x+0.5, y-0.5, -z-0.5$.

Table 4.3: Hydrogen bonds present in 5-(5-amino-2*H*-1,2,3-triazol-4-yl)-1*H*-tetrazole (**13**).

D−H···A	d(D−H) [Å]	d(H···A) [Å]	d(D···A) [Å]	∠(D−H···A) [°]
N2−H1···N6^{i}	0.90(2)	2.00(2)	2.875(2)	163(1)
N4−H2···N1^{ii}	0.91(2)	1.98(2)	2.891(2)	178(2)
N8−H3···N3^{iii}	0.89(2)	2.12(2)	3.011(2)	175(2)
N8−H4···N7	0.88(3)	2.41(2)	3.004(2)	125(2)
N8−H4···N5^{iv}	0.88(3)	2.42(2)	3.081(2)	131(2)

Symmetry codes: (i) $x, y, z+1$; (ii) $-x+0.5, y+0.5, -z+0.5$; (iii) $-x+0.5, y-0.5, -z+0.5$; (iv) $-x+0.5, y-0.5, -z-0.5$.

extensive hydrogen bonding network involving all eight nitrogen atoms, which is illustrated in Figure 4.6. The strong and quite directed N2−H1···N6^{i} hydrogen bond (D···A: 2.875(2) Å; ∠D−H···A: 163(1)°) results in the formation of a chain (A), which is connected to the anti-parallel chain (B) through the N4−H2···N1^{ii}, N8−H3···N3^{iii}, and N8−H4···N5^{iv} contacts (see Figure 4.6 and Table 4.3). The arrangement of the anti-parallel chains overall results in a layer structure with no special interactions between the layers.

4.2.4 Theoretical Calculations, Performances, and Stabilities

The thermal behaviors of the synthesized compounds were investigated by differential thermal analysis (DTA). The amino derivative **13** displays, as expected, the highest thermal stability of the neutral compounds (241 °C), while the nitro derivative **15** (188 °C), azido derivative **14** (152 °C) and especially the diazene bridged derivative **16** (128 °C) are significantly less thermally stable. It is interesting to note that, while the isomer 5-(5-amino-1*H*-1,2,4-triazol-3-yl)tetrazole (347 °C) and its nitro derivative (211 °C) display higher thermal stabilities than **13** and **15**,[33] respectively, due to the 1,2,4-triazole, the azido derivative exhibits the same decomposition temperature as **14**, as does the third isomer 1-(5-azido-1*H*-1,2,4-triazol-3-yl)tetrazole.[42] The azo bridged 1,2-bis(4-(1*H*-tetrazol-5-yl)-2*H*-1,2,3-triazol-5-yl)diazene (**16**), which was obtained as a dihydrate according to elemental analysis, shows no sign of water loss before decomposition at 128 °C. Dehydration thus proved to be unsuccessful at 100 °C and high vacuum for two days. Higher temperatures were not desirable due to the low decomposition point.

For initial safety testing the impact and friction sensitivities as well as the electrostatic discharge sensitivities were determined and assigned according to the UN recommendations on the transport of dangerous goods.[43] The parent compound **13** is the least sensitive of the neutral compounds, although it is still sensitive to impact (10 J), but insensitive to friction (360 N). While the azido derivative **14** is very sensitive to impact (3 J) and to friction (10 N), the nitro derivative **15** is only sensitive to impact (4 J) and to friction (108 N). Interestingly, the diazene **16** is very sensitive to both impact (2 J) and friction (28 N), although it is a dihydrate. 5-(5-Amino-1*H*-1,2,4-triazol-3-yl)tetrazole and its derivatives show the same trends, although the amine itself is additionally insensitive to impact, while its nitro derivative displays likewise lower sensitivities (25 J, 288 N) than its isomer **15**.[33]

The enthalpies and energies of formation were calculated on the CBS-4M level of theory as implemented in Gaussian 09,[44–46] using the atomization energy method and utilizing experimental data.[47–51] Gas phase enthalpies were transformed to solid state enthalpies by using Trouton's rule for neutral compounds.[52,53] The complete method is extensively described in the literature.[54] Calculations with the various isomers regarding the position of the proton revealed the 1*H*-tetrazole to be the most stable, albeit the difference to the 2*H*-tetrazole is only marginally. Detonation parameters of the neutral compounds were calculated with Explo5 v. 6.02.[55] The program is based on the steady-state model of equilibrium and uses the Becker–Kistiakowsky–Wilson equation of state (BKW EOS) for gaseous detonation products and the Murnaghan EOS for both solid and liquid products. The parameters of the BKW EOS in Explo5 6.02 are calibrated particularly for the formation of nitrogen gas, which is the main detonation product for compounds with a high

Table 4.4: Energetic properties and detonation parameters of **13**–**15** and RDX.

	13	**14**	**15**	RDX
Formula	$C_3H_4N_8$	$C_3H_2N_{10}$	$C_3H_2N_8O_2$	$C_6H_5N_7O_4$
M [g mol^{-1}]	152.13	178.13	182.11	222.12
IS [J][a]	10	3	4	7.4
FS [N][b]	> 360	10	108	120
ESD [mJ][c]	800	250	250	200
N [%][d]	73.66	78.64	61.53	37.84
Ω [%][e]	−84.1	−60.0	−43.9	−21.6
T_{dec} [°C][f]	241	152	188	204
ρ [g cm^{-3}][g]	1.66	1.56	1.69	1.80
$\Delta_f H°_{(s)}$ [kJ mol^{-1}][h]	460	846	516	85
$\Delta_f U°_{(s)}$ [kJ kg^{-1}][i]	3120	4833	2915	481
Calculated detonation parameters (EXPLO5 v. 6.02)				
$-Q_v$ [kJ kg^{-1}][j]	3481	4929	5064	5903
T_{det} [K][k]	2479	3678	3816	3849
p_{CJ} [kbar][l]	237	220	263	347
D [m s^{-1}][m]	8397	7963	8251	8854
V_0 [L mol^{-1}][n]	772	758	753	785

[a] Impact sensitivity (BAM drophammer 1 of 6). [b] Friction sensitivity (BAM friction tester 1 of 6). [c] Electrostatic discharge (OZM Research). [d] Nitrogen content. [e] Oxygen balance ($\Omega = (x\mathrm{O} - 2y\mathrm{C} - 0.5z\mathrm{H})1600/M$). [f] Decomposition temperature. [g] Density at ambient temperature. [h] Calculated enthalpy of formation. [i] Calculated energy of formation. [j] Energy of explosion. [k] Detonation temperature. [l] Detonation pressure. [m] Detonation velocity. [n] Volume of detonation gases.

nitrogen content. It is designed to enable the calculation of detonation parameters at the Chapman-Jouguet point. The calculations were performed using the maximum densities at room temperature, measured with a helium pycnometer.

The calculated detonation performances of **13**–**15** and RDX are summarized in Table 4.4. The computed detonation velocities range from 7963 m s^{-1} (**14**) up to 8397 m s^{-1} (**13**). The calculated detonation pressures are in the range of 237 to 263 kbar and the volume of gaseous reaction products amounts up to 772 L kg^{-1} (**13**). The detonation temperature of **15** (3816 K) is similar to RDX. The parameters of compound **16** were not calculated due to the unsuccessful dehydration.

4.3 Conclusions

The goal of this study has been the preparation and thorough characterization of the novel nitrogen-rich compound 5-(5-amino-2*H*-1,2,3-triazol-4-yl)-1*H*-tetrazole (**13**) and the

further derivatization of the amino moiety into the more energetic azido (**14**) and nitro (**15**) groups, as well as the connection by means of a diazene bridge (**16**). Low-temperature single-crystal X-ray diffraction revealed the position of the benzyl group of the precursor molecule 5-amino-1-benzyl-1,2,3-triazole-4-carboxamide (**10**), and likewise the position of the protons of the title compound **13**. The compounds were comprehensively characterized by multinuclear NMR (including ^{15}N for **14** and **15**) as well as vibrational spectroscopy and mass spectrometry. While the amino derivate exhibits a very good thermal stability (241 °C), as evidenced by DTA, the more energetic derivatives **14**–**16** are less thermally stable (128 to 188 °C). With the exception of the friction insensitive **13**, the main compounds **13**–**16** all have to be classified as sensitive or even very sensitive to both impact and friction, as determined by BAM standards. Although, compounds **13**–**15** are superior to the commonly used TNT regarding their calculated detonation parameters (EXPLO5, v. 6.02), the performance of RDX is not reached. On the other hand, taking into account the high nitrogen contents of 73.66 (**13**), 78.64 (**14**), 61.53 (**15**) and 74.65% (**16**) and high enthalpies of formation the compounds might be of interest as anions for primary as well as secondary explosives, or gun propellants in combination with metal (**14**) or nitrogen-rich cations (**13**, **15**, and **16**), respectively.[56]

4.4 Experimental Section

Caution! *Most compounds prepared herein are energetic compounds sensitive to impact, friction and electrostatic discharge. Although there were no problems in handling the compounds, proper protective measures (ear protection, Kevlar® gloves, face shield, body armor and earthed equipment) should be used.*

Benzyl azide (9)

Benzyl chloride (106 g, 840 mmol) and sodium azide (82.0 g, 1.26 mol) were stirred in a mixture of ethanol (400 mL) and water (50 mL) for 20 h at 95 °C. The suspension was afterwards poured in water (2 L), divided into four portions and each was extracted with diethyl ether (2 × 200 mL). The combined organic phases were dried over magnesium sulfate and evaporated under reduced pressure at 50 °C to obtain a clear, yellow liquid (106 g, 796 mmol, 95%).
^{1}H NMR (400 MHz, DMSO-d_6): δ = 7.44–7.34 (m, 5H, C*H*), 4.44 (s, 2H, CH_2) ppm.
^{13}C{^{1}H} NMR (101 MHz, DMSO-d_6): δ = 135.6, 128.7, 128.4, 128.1, 53.6 (*C*H$_2$) ppm.
^{14}N{^{1}H} NMR (29 MHz, DMSO-d_6): δ = −127 (N_β), −164 (N_γ), −300 (N_α) ppm.

5-Amino-1-benzyl-1,2,3-triazole-4-carboxamide (10)

Cyanoacetamide (16.8 g, 200 mmol) and **9** (26.6 g, 200 mmol) were added to sodium (4.60 g, 200 mmol) in ethanol (500 mL) and the mixture was refluxed for 1 h. The precipitate was filtered off and washed with water and ethanol, then suspended in ethanol/water (4:1, 500 mL) and heated for half an hour. The precipitate was filtered off again, and washed with water, ethanol, and diethyl ether to yield a colorless solid (34.5 g, 159 mmol, 80%).
^{1}H NMR (400 MHz, DMSO-d_6): δ = 7.50 (br, 2H, NH_2), 7.39–7.20 (m, 5H, CH), 5.45 (s, 2H, CH_2) ppm. ^{13}C{^{1}H} NMR (101 MHz, DMSO-d_6): δ = 164.5 (CONH$_2$), 144.9 (C_{tri}), 136.0, 128.7, 127.8, 127.4, 121.8 (C_{tri}), 48.4 (CH$_2$) ppm. MS (DEI$^+$): m/z = 217.2 [M$^+$]. EA ($C_{10}H_{11}N_5O$, 217.23 g mol^{-1}): calcd C 55.29, H 5.10, N 32.24%; found C 55.17, H 4.93, N 32.11%.

5-Amino-1-benzyl-1,2,3-triazole-4-carbonitrile (11)

Trifluoroacetic anhydride (26.0 mL, 184 mmol) was carefully added to a suspension of **10** (20.0 g, 92.1 mmol) in dry pyridine (210 mL), while cooled with an ice/water bath. The flask was sealed and the deep red solution was stirred for 16 h without removing or refreshing the cooling bath. The reaction mixture was poured on ice (250 g) and stirred for about 24 h at room temperature. Concentrated hydrochloric acid (220 mL) was added dropwise, then stirred for about 48 h at room temperature until a completely homogenized, light brown suspension was obtained. The precipitate was filtered off, washed with diluted hydrochloric acid and water, then suspended in toluene and stirred for 1 h. The solvent was evaporated under reduced pressure and the residue was suspended in *n*-pentane, filtered off and washed with *n*-pentane to yield a pale brownish powder (15.7 g, 78.8 mmol, 86%).
^{1}H NMR (400 MHz, DMSO-d_6): δ = 7.40–7.30 (m, 3H, CH), 7.25–7.23 (m, 2H, CH), 7.18 (s, 2H, NH_2), 5.43 (s, 2H, NH_2) ppm. ^{13}C{^{1}H} NMR (101 MHz, DMSO-d_6): δ = 148.0 (C_{tri}), 135.2, 128.7, 127.9, 127.5, 113.7 (C_{tri}), 101.3 (CN), 48.8 (CH$_2$) ppm. MS (DEI$^+$): m/z = 199.1 [M$^+$]. EA ($C_{10}H_9N_5$, 199.22 g mol^{-1}): calcd C 60.29, H 4.55, N 35.16%; found C 60.29, H 4.47, N 34.97%.

5-(5-Amino-1-benzyl-1,2,3-triazol-4-yl)-1*H*-tetrazole (12)

A suspension of **11** (15.9 g, 80.0 mmol), sodium azide (10.4 g, 160 mmol) and zinc chloride (13.6 g, 100 mmol) in dry tetrahydrofuran (250 mL) was stirred for 16 h at 70 °C. Concentrated hydrochloric acid (14 mL) was added to the cooled down solution, which was then stirred for half an hour. The solvent was evaporated under reduced pressure and the residue was suspended in half concentrated hydrochloric acid (300 mL) and stirred for several hours. The precipitate was filtered off and washed with diluted hydrochloric acid and water to

yield a pale yellow powder (18.8 g, 77.6 mmol, 97%).
^{1}H NMR (400 MHz, DMSO-d_6): δ = 7.37–7.26 (m, 5H, C*H*), 6.61 (s, 2H, NH_2), 5.55 (s, 2H, CH_2) ppm. ^{13}C{^{1}H} NMR (101 MHz, DMSO-d_6): δ = 148.6 (C_{tri}), 142.9 (C_{tet}), 135.8, 128.7, 127.9, 127.5, 114.4 (C_{tri}), 48.8 (CH$_2$) ppm. MS (DEI$^+$): m/z = 242.2 [M$^+$]. EA ($C_{10}H_{10}N_8$, 242.25 g mol^{-1}): calcd C 49.58, H 4.16, N 46.26%; found C 48.95, H 4.05, N 45.32%.

5-(5-Amino-2*H*-1,2,3-triazol-4-yl)-1*H*-tetrazole (13)

Sodium was added in small pieces to a clear red solution of **12** (37.6 g, 155 mmol) in liquid ammonia (about 150 mL) until a deep blue suspension was obtained, carefully followed by the addition of ammonium chloride until the blue color was completely gone. The solvent was allowed to slowly evaporate and the residue was dissolved in water (about 200 mL), then filtered. The filtrate was evaporated under reduced pressure and the residue was dissolved again in water (200 mL), then acidified with concentrated hydrochloric acid (40 mL). The precipitate was filtered off and washed with water to yield a yellow powder (22.5 g, 148 mmol, 95%).
DTA (5 °C min^{-1}): T_{dec} = 235 °C. ^{1}H NMR (400 MHz, DMSO-d_6): δ = 16.19 and 14.64 (br, 2H, N*H*), 6.03 (br, 2H, NH_2) ppm. ^{13}C{^{1}H} NMR (101 MHz, DMSO-d_6): δ = 149.0 (C_{tet}), 147.6 (br, C_{tri}), 111.6 (br, C_{tri}) ppm. IR (ATR): $\tilde{\nu}$ = 3437 (m), 3317 (m), 3227 (w), 3138 (m), 3036 (m), 2976 (m), 2895 (m), 2796 (m), 2700 (m), 2553 (m), 1624 (vs), 1564 (s), 1503 (m), 1467 (m), 1404 (w), 1372 (m), 1332 (w), 1250 (w), 1240 (s), 1214 (m), 1185 (m), 1145 (m), 1090 (s), 1019 (m), 1003 (s), 971 (vs), 866 (vs), 764 (m), 749 (vs), 691 (m) cm^{-1}. Raman (1064 nm, 300 mW): $\tilde{\nu}$ = 1646 (24), 1627 (100), 1571 (8), 1474 (5), 1406 (21), 1250 (8), 1178 (6), 1151 (9), 1104 (13), 1020 (23), 747 (9), 421 (12), 334 (15), 172 (14), 140 (24), 121 (31), 63 (10) cm^{-1}. MS (DEI$^+$): m/z = 152.1 [M$^+$]. EA ($C_3H_4N_8$, 152.12 g mol^{-1}): calcd C 23.69, H 2.65, N 73.66%; found C 24.07, H 2.76, N 73.29%. Sensitivities (grain size: < 100 µm): IS: 10 J, FS: 360 N, ESD: 800 mJ.

5-(5-Azido-2*H*-1,2,3-triazol-4-yl)-1*H*-tetrazole (14)

Sodium nitrite (2.07 g, 30.0 mmol) was added to a suspension of **13** (3.04 g, 20.0 mmol) in sulfuric acid (20%, 200 mL) at 0 °C. The cooling was removed and the yellow reaction mixture was stirred for 3 h at room temperature. Sodium azide (2.60 g, 40.0 mmol) was then added in small portions and stirred for 30 min at room temperature. The resulting colorless foamy suspension was refluxed until a clear solution was obtained. The resulting suspension after cooling down was extracted with ethyl acetate (4 × 150 mL). The combined organic phases were dried over magnesium sulfate and evaporated under reduced pressure. The

residue was suspended in toluene, evaporated again and washed with *n*-pentane to yield a colorless solid (3.08 g, 17.3 mmol, 87%).
DTA (5 °C min^{-1}): T_{dec} = 152 °C. ^{1}H NMR (400 MHz, DMSO-d_6): δ = 15.81 (br) ppm. ^{13}C{^{1}H} NMR (101 MHz, DMSO-d_6): δ = 147.7 (C_{tri}), 143.1 (C_{tet}), 123.0 (C_{tri}) ppm. ^{14}N{^{1}H} NMR (29 MHz, DMSO-d_6): δ = −138 (N_β). ^{15}N NMR (41 MHz, DMSO-d_6): δ = −11.1 (N_{tet}), −55.7 (N_{tri}), −74.1 (N_{tri}), −101.9 (NH$_{tet}$), −126.3 (NH$_{tri}$), −143.2 (N_γ/N_β), −148.6 (N_β/N_γ), −303.3 (N_α) ppm. IR (ATR): $\tilde{\nu}$ = 3524 (w), 3227 (w), 3132 (w), 2923 (w), 2800 (w), 2677 (w), 2426 (w), 2331 (w), 2147 (vs), 1915 (w), 1628 (s), 1525 (vs), 1407 (w), 1356 (w), 1345 (w), 1322 (m), 1308 (w), 1295 (w), 1250 (w), 1209 (s), 1160 (w), 1121 (w), 1103 (w), 1067 (m), 1019 (s), 1006 (m), 977 (s), 835 (m), 795 (m), 769 (m), 757 (s), 717 (w), 703 (w), 694 (w) cm^{-1}. Raman (1064 nm, 300 mW): $\tilde{\nu}$ = 2163 (12), 1631 (100), 1534 (22), 1445 (5), 1409 (17), 1357 (18), 1326 (9), 1299 (5), 1252 (8), 1219 (11), 1168 (17), 1126 (5), 1022 (16), 978 (9), 797 (6), 760 (11) cm^{-1}. MS (DEI$^+$): m/z = 178.1 [M$^+$]. EA ($C_3H_2N_{10}$, 178.12 g mol^{-1}): calcd C 20.23, H 1.13, N 78.64%; found C 19.83, H 1.89, N 73.11%. Sensitivities (grain size: < 100 µm): IS: 3 J, FS: 10 N, ESD: 250 mJ.

5-(5-Nitro-2*H*-1,2,3-triazol-4-yl)-1*H*-tetrazole (15)

Potassium superoxide (4.75 g, 66.9 mmol) and **13** (1.00 g, 6.57 mmol) were stirred in tetrahydrofuran (50 mL) for 72 h at 60 °C. The solvent was evaporated under reduced pressure and ice (80 g) was added to the dry residue, followed by sulfuric acid (98%, 11 mL). The resulting yellow suspension was stirred for 1 h, then extracted with methyl ethyl ketone (5 × 75 mL). The combined organic phases were washed with a saturated sodium chloride solution (2 × 50 mL), dried over magnesium sulfate and evaporated under reduced pressure. The resulting green solid was dried in fine vacuum overnight, pestled, resuspended in dichloromethane, sonicated for a few minutes and filtered off to yield a pale green solid (814 mg, 4.47 mmol, 68%).
DTA (5 °C min^{-1}): T_{melt} = 180 °C, T_{dec} = 188 °C. ^{1}H NMR (400 MHz, DMSO-d_6): δ = 9.93 (br) ppm. ^{13}C{^{1}H} NMR (101 MHz, DMSO-d_6): δ = 151.1 (C_{tri}), 147.7 (C_{tet}), 127.7 (C_{tri}) ppm. ^{14}N{^{1}H} NMR (29 MHz, DMSO-d_6): δ = −21 (NO$_2$) ppm. ^{15}N NMR (41 MHz, DMSO-d_6): δ = −14.4 (N_{tet}), −27.5 (NO$_2$), −51.1 (N_{tri}), −65.4 (N_{tri}), −89.6 (NH$_{tet}$), −97.2 (NH$_{tri}$) ppm. IR (ATR): $\tilde{\nu}$ = 3221 (w), 3113 (w), 3055 (w), 2908 (w), 1630 (w), 1547 (vs), 1500 (vw), 1472 (w), 1383 (s), 1350 (m), 1244 (w), 1197 (vw), 1138 (m), 1097 (m), 1065 (s), 1021 (w), 1008 (s), 991 (m), 845 (m), 835 (vs), 744 (m), 726 (m), 707 (m) cm^{-1}. Raman (1064 nm, 300 mW): $\tilde{\nu}$ = 1652 (12), 1630 (100), 1546 (6), 1470 (16), 1414 (7), 1387 (23), 1340 (23), 1284 (8), 1244 (6), 1201 (7), 1014 (11), 987 (8), 833 (5), 504 (7), 383 (5), 166 (5), 137 (9), 92 (40), 79 (24) cm^{-1}. MS (DEI$^+$): m/z = 182.2 [M$^+$], 30.1 [NO$^+$]. EA

($C_3H_2N_8O_2$, 182.10 g mol^{-1}): calcd C 19.79, H 1.11, N 61.53%; found C 19.88, H 1.63, N 59.98%. Sensitivities (grain size: <100 µm): IS: 4 J, FS: 108 N, ESD: 250 mJ.

1,2-Bis(4-(1*H*-tetrazol-5-yl)-2*H*-1,2,3-triazol-5-yl)diazene dihydrate (16)

Potassium permanganate (1.05 g, 6.67 mmol) was added in small portions to **13** (1.52 g, 10.0 mmol) in aqueous sodium hydroxide (10%, 40 mL) at 70 °C. After stirring for 2 h at 100 °C, ethanol (10 mL) was added and stirred for further 15 min. The suspension was filtered through kieselgur and washed until the filtrate was colorless. The combined filtrates were evaporated under reduced pressure, the residue was suspended in hydrochloric acid (2M, 100 mL) and stirred for several hours. The precipitate was filtered off and washed with diluted hydrochloric acid and water to yield a yellow solid (700 mg, 2.08 mmol, 42%).
DTA (5 °C min^{-1}): T_{dec} = 128 °C. ^{1}H NMR (400 MHz, DMSO-d_6): δ = 10.09 (br) ppm. ^{13}C{^{1}H} NMR (101 MHz, DMSO-d_6): δ = 153.7 (C_{tri}), 147.2 (C_{tet}), 126.6 (C_{tri}) ppm. IR (ATR): $\tilde{\nu}$ = 3522 (w), 3422 (w), 3232 (s), 2824 (w), 2748 (w), 2613 (w), 2501 (m), 2360 (m), 2000 (vw), 1877 (w), 1637 (m), 1611 (m), 1498 (m), 1428 (vw), 1406 (m), 1369 (s), 1344 (m), 1298 (vw), 1245 (w), 1220 (w), 1207 (w), 1178 (w), 1143 (w), 1125 (vs), 1076 (vs), 1030 (vs), 1004 (s), 977 (s), 960 (s), 903 (m), 822 (vs), 772 (w), 726 (m), 672 (vw) cm^{-1}. Raman (1064 nm, 300 mW): $\tilde{\nu}$ = 1638 (37), 1613 (16), 1503 (16), 1492 (17), 1469 (100), 1432 (21), 1404 (8), 1369 (56), 1344 (69), 1329 (31), 1298 (10), 1245 (7), 1200 (14), 1182 (5), 1151 (4), 1125 (6), 980 (14), 903 (8), 621 (7), 353 (4) cm^{-1}. MS (FAB$^-$): m/z = 299.1 [M$^+$]. EA ($C_3H_4N_8 \cdot 2\,H_2O$, 336.24 g mol^{-1}): calcd C 21.43, H 2.40, N 66.65%; found C 22.68, H 2.32, N 66.07%. Sensitivities (grain size: <100 µm): IS: 2 J, FS: 28 N, ESD: 700 mJ.

4.5 References

[1] T. M. Klapötke, A. Preimesser, J. Stierstorfer, *Z. Anorg. Allg. Chem.* **2012**, *638*, 1278–1286.

[2] D. E. Chavez, D. Parrish, D. N. Preston, I. W. Mares, *Propellants, Explos., Pyrotech.* **2012**, *37*, 647–652.

[3] R. Wang, H. Xu, Y. Guo, R. Sa, J. M. Shreeve, *J. Am. Chem. Soc.* **2010**, *132*, 11904–11905.

[4] A. A. Dippold, T. M. Klapötke, *Chem. Eur. J.* **2012**, *18*, 16742–16753.

[5] A. A. Dippold, T. M. Klapötke, *J. Am. Chem. Soc.* **2013**, *135*, 9931–9938.

[6] A. A. Dippold, T. M. Klapötke, M. Oswald, *Dalton Trans.* **2013**, *42*, 11136–11145.

[7] T. M. Klapötke, P. C. Schmid, S. Schnell, J. Stierstorfer, *J. Mater. Chem. A* **2015**, *3*, 2658–2668.

[8] C. He, J. M. Shreeve, *Angew. Chem., Int. Ed.* **2015**, *54*, 6260–6264; *Angew. Chem.* **2015**, *127*, 6358–6362.

[9] D. E. Chavez, M. A. Hiskey, D. L. Naud, *J. Pyrotech.* **1999**, *10*, 17–36.

[10] N. Fischer, D. Izsák, T. M. Klapötke, S. Rappenglück, J. Stierstorfer, *Chem. Eur. J.* **2012**, *18*, 4051–4062.

[11] I. V. Tselinskii, S. F. Mel'nikova, T. V. Romanova, *Russ. J. Org. Chem.* **2001**, *37*, 430–436.

[12] N. Fischer, D. Fischer, T. M. Klapötke, D. G. Piercey, J. Stierstorfer, *J. Mater. Chem.* **2012**, *22*, 20418–20422.

[13] D. Fischer, T. M. Klapötke, M. Reymann, P. C. Schmid, J. Stierstorfer, M. Sućeska, *Propellants, Explos., Pyrotech.* **2014**, *39*, 550–557.

[14] T. M. Klapötke, M. Q. Kurz, R. Scharf, P. C. Schmid, J. Stierstorfer, M. Sućeska, *ChemPlusChem* **2015**, *80*, 97–106.

[15] K. Hafner, T. M. Klapötke, P. C. Schmid, J. Stierstorfer, *Eur. J. Inorg. Chem.* **2015**, 2794–2803.

[16] D. Fischer, T. M. Klapötke, J. Stierstorfer, *Angew. Chem., Int. Ed.* **2014**, *53*, 8172–8175; *Angew. Chem.* **2014**, *126*, 8311–8314.

[17] H. Tanaka, K. Shimamoto, A. Onishi (Toyo Kasei Kogyo Co. Ltd., Osaka, Japan), US6300498B1 **2001**.

[18] S. Date, N. Itadzu, T. Sugiyama, Y. Miyata, K. Iwakuma, M. Abe, K. Hasue, *38th International Annual Conference of ICT*, Karlsruhe, Germany, June 26–29, **2007**.

[19] N. Fischer, D. Izsák, T. M. Klapötke, J. Stierstorfer, *Chem. Eur. J.* **2013**, *19*, 8948–8957.

[20] S. Nimesh, H.-G. Ang, *Propellants, Explos., Pyrotech.* **2015**, *40*, 426–432.

[21] C. Bian, M. Zhang, C. Lia, Z. Zhou, *J. Mater. Chem. A* **2015**, *3*, 163–169.

[22] P. Yin, D. A. Parrish, J. M. Shreeve, *Chem. Eur. J.* **2014**, *20*, 6707–6712.

[23] M. A. Hiskey, N. Goldman, J. R. Stine, *J. Energ. Mater.* **1998**, *16*, 119–127.

[24] N. Fischer, K. Hüll, T. M. Klapötke, J. Stierstorfer, G. Laus, M. Hummel, C. Froschauer, K. Wurst, H. Schottenberger, *Dalton Trans.* **2012**, *41*, 11201–11211.

[25] D. Fischer,T. M. Klapötke, D. G. Piercey, J. Stierstorfer, *Chem. Eur. J.* **2013**, *19*, 4602–4613.

[26] E. G. Francois, D. E. Chavez, M. M. Sandstrom, *Propellants, Explos., Pyrotech.* **2010**, *35*, 529–534.

[27] D. Fischer, T. M. Klapötke, M. Reymann, J. Stierstorfer, *Chem. Eur. J.* **2014**, *20*, 6401–6411.

[28] J. Zhang, J. M. Shreeve, *J. Phys. Chem. C* **2015**, *119*, 12887–12895.

[29] P. W. Leonard, D. E. Chavez, P. F. Pagoria, D. A. Parrish, *Propellants, Explos., Pyrotech.* **2011**, *36*, 233–239.

[30] V. Thottempudi, J. Zhang, C. He, J. M. Shreeve, *RSC Adv.* **2014**, *4*, 50361–50364.

[31] M. A. Hiskey, D. E. Chavez, D. L. Naud, S. F. Son, H. L. Berghout, C. A. Bolme, *27th International Pyrotechnics Seminar*, Grand Junction, CO, USA, July 16–21, **2000**.

[32] J. P. Agrawal, *High Energy Materials*, Wiley-VCH, Weinheim, **2010**.

[33] A. A. Dippold, T. M. Klapötke, *Chem. Asian J.* **2013**, *8*, 1463–1471.

[34] J. R. E. Hoover, A. R. Day, *J. Am. Chem. Soc.* **1956**, *78*, 5832–5836.

[35] A. F. Holleman, E. Wiberg, N. Wiberg, *Lehrbuch der Anorganischen Chemie*, 102nd ed., de Gruyter, Berlin, Germany, **2007**.

[36] D.-F. Pan, X.-B. Chen, H.-T. Gao, C. Feng, P. Chen, *Acta Crystallogr., Sect. E: Struct. Rep. Online* **2011**, *67*, o3326.

[37] E. S. Gladkov, S. M. Desenko, I. S. Konovalova, U. Groth, O. V. Shishkin, E. V. Vashchenko, V. A. Chebanov, *J. Heterocycl. Chem.* **2013**, *50*, E189–E192.

[38] H. A. Michaels, J. T. Simmons, R. J. Clark, L. Zhu, *J. Org. Chem.* **2013**, *78*, 5038–5044.

[39] A. Al-Azmi, A. K. Kalarikkal, *Tetrahedron* **2013**, *69*, 11122–11129.

[40] C. Janiak, *J. Chem. Soc., Dalton Trans.* **2000**, 3885–3896.

[41] A. Bondi, *J. Phys. Chem.* **1964**, *68*, 441–451.

[42] D. Izsák, T. M. Klapötke, *Cent. Eur. J. Energ. Mater.* **2015**, *12*, 403–416.

[43] Test methods according to the *UN Manual of Test and Criteria, Recommendations on the Transport of Dangerous Goods*, United Nations Publication, New York, Geneva, 4th revised ed., **2003**: Impact: Insensitive $>40\,\mathrm{J}$, less sensitive $\geq 35\,\mathrm{J}$, sensitive $\geq 4\,\mathrm{J}$, very sensitive $\leq 3\,\mathrm{J}$; Friction: Insensitive $>360\,\mathrm{N}$, less sensitive $= 360\,\mathrm{N}$, sensitive $<360\,\mathrm{N}$ a. $>80\,\mathrm{N}$, very sensitive $\leq 80\,\mathrm{N}$, extremely sensitive $\leq 10\,\mathrm{N}$.

[44] M. J. Frisch, G. W. Trucks, H. B. Schlegel, G. E. Scuseria, M. A. Robb, J. R. Cheeseman, G. Scalmani, V. Barone, B. Mennucci, G. A. Petersson, H. Nakatsuji, M. Caricato, X. Li, H. P. Hratchian, A. F. Izmaylov, J. Bloino, G. Zheng, J. L. Sonnenberg, M. Hada, M. Ehara, K. Toyota, R. Fukuda, J. Hasegawa, M. Ishida, T. Nakajima, Y. Honda, O. Kitao, H. Nakai, T. Vreven, J. A. Montgomery Jr., J. E. Peralta, F. Ogliaro, M. Bearpark, J. J. Heyd, E. Brothers, K. N. Kudin, V. N. Staroverov, T. Keith, R. Kobayashi, J. Normand, K. Raghavachari, A. Rendell, J. C. Burant, S. S. Iyengar, J. Tomasi, M. Cossi, N. Rega, J. M. Millam, M. Klene, J. E. Knox, J. B. Cross, V. Bakken, C. Adamo, J. Jaramillo, R. Gomperts, R. E. Stratmann, O. Yazyev, A. J. Austin, R. Cammi, C. Pomelli, J. W. Ochterski, R. L. Martin, K. Morokuma, V. G. Zakrzewski, G. A. Voth, P. Salvador, J. J. Dannenberg, S. Dapprich, A. D. Daniels, O. Farkas, J. B. Foresman, J. V. Ortiz, J. Cioslowski, D. J. Fox, Gaussian 09 Revision C.01, Gaussian, Inc., Wallingford, CT, USA, **2010**.

[45] J. W. Ochterski, G. A. Petersson, J. A. Montgomery, *J. Chem. Phys.* **1996**, *104*, 2598–2619.

[46] J. A. Montgomery, M. J. Frisch, J. W. Ochterski, G. A. Petersson, *J. Chem. Phys.* **2000**, *112*, 6532–6542.

[47] B. M. Rice, S. V. Pai, J. Hare, *Combust. Flame* **1999**, *118*, 445–458.

[48] B. M. Rice, J. J. Hare, *J. Phys. Chem. A* **2002**, *106*, 1770–1783.

[49] E. F. C. Byrd, B. M. Rice, *J. Phys. Chem. A* **2006**, *110*, 1005–1013.

[50] P. J. Linstrom, W. G. Mallard (Eds.), *NIST Standard Reference Database Number 69*, http://webbook.nist.gov/ chemistry/ (accessed February 9, 2015).

[51] J. D. Cox, D. D. Wagman, V. A. Medvedev, *CODATA Key Values for Thermodynamics*, Hemisphere Publishing Corp., New York, USA, **1984**.

[52] F. Trouton, *Philos. Mag.* **1884**, *18*, 54–57.

[53] M. S. Westwell, M. S. Searle, D. J. Wales, D. H. Williams, *J. Am. Chem. Soc.* **1995**, *117*, 5013–5015.

[54] T. M. Klapötke, *Chemistry of High-Energy Materials*, 2nd ed., de Gruyter, Berlin, Germany, **2011**.

[55] M. Sućeska, EXPLO5, v. 6.02, Zagreb, Croatia, **2014**.

[56] D. Izsák, T. M. Klapötke, C. Pflüger, in *New Trends Res. of Energ. Mater., Proc. Semin.*, 18th, Pardubice, Czech Republic, **2015**, *2*, pp. 573–592.

Tailoring the Energetic Properties of 5-(5-Amino-1,2,3-triazol-4-yl)tetrazole and Its Derivatives by Salt Formation: From Sensitive Primary to Insensitive Secondary Explosives

D. Izsák, T. M. Klapötke, F. H. Lutter, and C. Pflüger

Eur. J. Inorg. Chem. **2016**, 1720–1729.

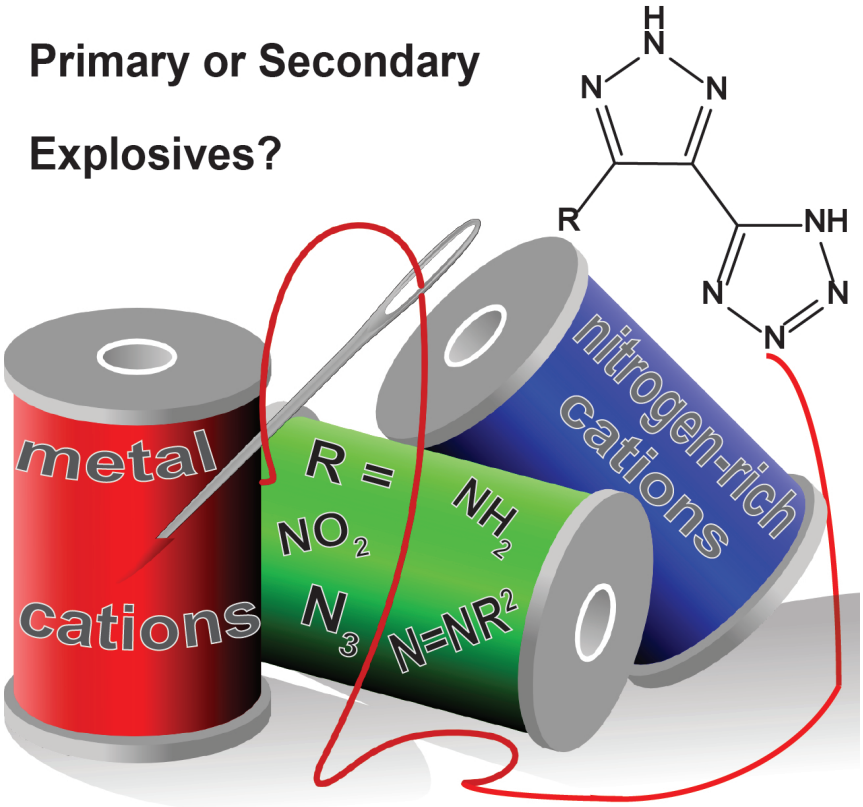

Tailoring the Energetic Properties of 5-(5-Amino-1,2,3-triazol-4-yl)tetrazole and Its Derivatives by Salt Formation: From Sensitive Primary to Insensitive Secondary Explosives

D. Izsák, T. M. Klapötke, F. H. Lutter, and C. Pflüger

Eur. J. Inorg. Chem. **2016**, 1720–1729.

Abstract

The main challenge in the development of energetic materials is the combination of high energy content with chemical and mechanical stability, two properties that are often contradictory. The energetic properties of 5-(5-amino-1,2,3-triazol-4-yl)tetrazole and its derivatives, in which the amino group is substituted by an azido and a nitro group as well as a diazene bridge, should be improved and tailored for possible applications by formation of various nitrogen-rich and metal salts thereof. The thermal and mechanical sensitivities were determined and the detonation performances of the nitrogen-rich salts were calculated. Furthermore, the combustion performances of erosion-reduced gun propellant mixtures of the most promising salts were computed due to their high nitrogen content and energetic performance. Metal salts of 5-(5-azido-1,2,3-triazol-4-yl)tetrazole were investigated to test their capability as primary explosives.

5.1 Introduction

The increasing need for energetic materials for highly specified applications in military and civil use present various challenges for the development of improved explosives. The design of explosives should consider improved thermal and mechanical stabilities as well as an increased detonation performance, and furthermore, their impact on the environment should be diminished.[1,2] Therefore, the main challenge in the design of modern explosives is the combination of a large energy content, which supplies high performance, and thermal and mechanical stability for safety reasons, because these parameters often have a contradictory impact on each other.[3] The performance of secondary explosives is well characterized by their detonation velocity, detonation pressure, and energy of explosion, which are determined by their density and enthalpies of formation.

Nitrogen-rich heterocycles have high positive enthalpies of formation and release a large amount of energy upon detonation because the stability of the N≡N bond ($946\,\mathrm{kJ\,mol^{-1}}$) is higher than that of the N=N bond ($418\,\mathrm{kJ\,mol^{-1}}$) and the N−N bond ($159\,\mathrm{kJ\,mol^{-1}}$).[4] The enthalpies of formation of azoles increase as the number of catenated nitrogen atoms

increases.[5] In regard to the requirements of detonation performance and safety, tetrazoles as well as 1,2,3- and 1,2,4-triazoles are promising azoles. In general, tetrazole is more energetic but also more sensitive towards external stimuli, whereas triazoles are less sensitive. A large variety of energetic materials based on biheterocylic systems of tetrazoles and 1,2,4-triazoles, their combinations, and salts have been investigated,[6–11] but only a few heterocyclic substituted 1,2,3-triazoles and salts thereof are known.[12–14] The 1,2,3-Triazole linked with only one tetrazole ring offers the possibility to introduce another energetic group attached to the second carbon atom to specify the energetic properties.

The binary combination of 5-amino-1,2,3-triazole and tetrazole by means of a C−C linkage was recently investigated by us.[15] Furthermore, the amino group was converted into a nitro group, an azido group, as well as a diazene bridge to design the performance of explosives depending on the energetic groups. The energetic properties can be further specified for applications by the kind of explosive or they can be tailored to particular requirements by formation of metal or nitrogen-rich salts.

Energetic salts show many advantages over conventional nonionic energetic compounds such as lower vapor pressures, reduced sensitivities, and often improved performances.[16–18] In general, the use of nitrogen-rich cations leads to higher enthalpies of formation, which thereby improves the detonation performance. Furthermore, the high acidity of the heterocyclic protons can cause compatibility problems in explosive charges,[19] which can be avoided by salt formation.

Herein, selected metal and nitrogen-rich salts of 5-(5-amino-1,2,3-triazol-4-yl)tetrazole and its more energetic derivatives (nitro, azido, and diazene-bridged) are presented to take the different requirements of specific applications into account.

Such a specific application might be the possible incorporation of their nitrogen-rich salts in erosion-reduced gun propellant mixtures owing to their high nitrogen contents. Two challenges in the development of gun propellant mixtures are the enhancement in performance and the reduction of gun barrel erosion to elongate its lifespan.[20–23] In low-vulnerability (LOVA) propellants, 1,3,5-trinitro-1,3,5-triazine (RDX) is included as an energetic filler to enhance the combustion performance.[24–26] Unfortunately, an increase in the amount of RDX also leads to higher combustion temperatures, which thus causes problems concerning erosion of the gun barrel.[27,28] Therefore, the amount of RDX has to be reduced, and instead, high nitrogen-rich compounds are added to afford erosion-reduced propellant mixtures.[29,30]

This study presents the energetic properties and calculated detonation performances as well as calculated combustion performance of selected nitrogen-rich salts of 5-(5-amino-1,2,3-triazol-4-yl)tetrazole, its derivatives with azido and nitro groups, and its diazene-bridged analogue 1,2-bis(5-(tetrazol-5-yl)-1,2,3-triazol-4-yl)diazene for possible use in gun

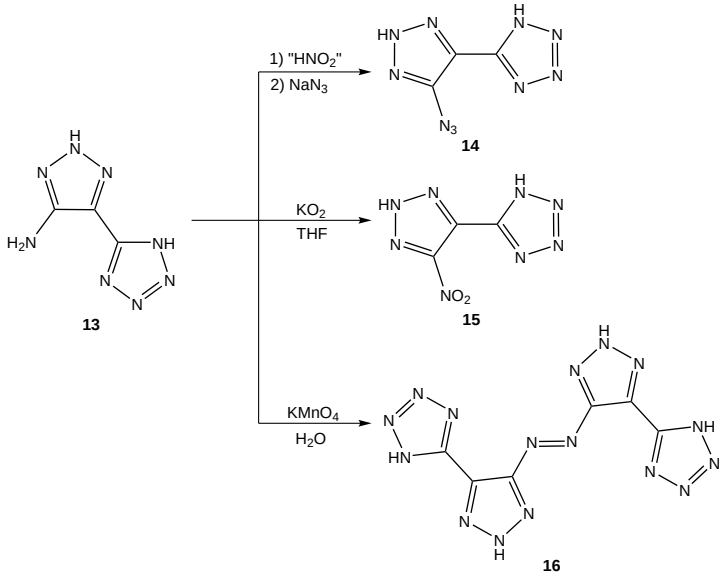

Scheme 5.1: Synthetic route towards 5-(5-azido-2*H*-1,2,3-triazol-4-yl)-1*H*-tetrazole (**14**), 5-(5-nitro-2*H*-1,2,3-triazol-4-yl)-1*H*-tetrazole (**15**), and 1,2-bis(4-(1*H*-tetrazol-5-yl)-2*H*-1,2,3-triazol-5-yl)diazene (**16**) starting from 5-(5-amino-2*H*-1,2,3-triazol-4-yl)-1*H*-tetrazole (**13**).

propellant formulations. Additionally, metal salts of 5-(5-azido-1,2,3-triazol-4-yl)tetrazole were investigated to test their ability to form primary explosives. Primary explosives often consist of metal salts and are simply initiated by, for example, heat or shock and are, therefore, used as initiators for the less sensitive secondary explosives.

5.2 Results and Discussion

5.2.1 Syntheses

5-(5-Amino-2*H*-1,2,3-triazol-4-yl)-1*H*-tetrazole (**13**) was synthesized starting from commercially available benzyl chloride in a well-working five-step synthesis.[15] The more energetic derivatives with azido (see compound **14**) and nitro (see compound **15**) groups as well as a diazene bridge (see compound **16**) were also prepared according to Scheme 5.1, as described in the literature.[15]

Derivatives **13**, **15**, and **16** are promising anions for nitrogen-rich salts as secondary explosives, whereas the more sensitive **14** is a promising anion for metal salts as primary explosives. Nitrogen-rich and alkali metal salts with ammonium (see compounds **13a**, **14a**, and **15a**), hydroxylammonium (see compounds **13b**, **15b**, and **16-2b**), guanidinium (see compounds **13c**, **15c**, and **16-2c**), aminoguanidinium (see compounds **13d**, **15d**, and **16-2d**), potassium (see compounds **13f**, **14f**, **15f**, **16-2f**, and **16-4f**), and cesium (see compound **14h**) were prepared in ethanol or aqueous solution by using **13**, **14**, **15**, or **16** and

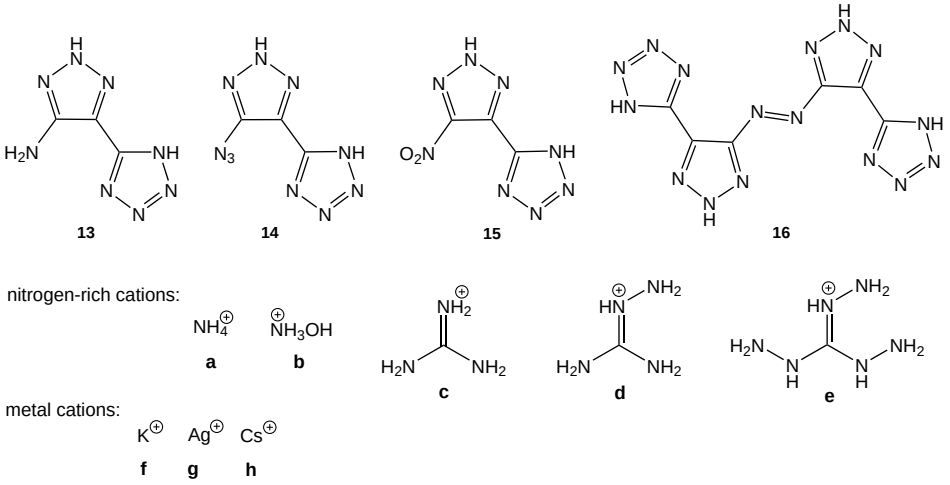

Figure 5.1: Nitrogen-rich salts **13a**–**e**, **14a**, **15a**–**e**, and **16-2b**–**16-2d**, and the mixed salt **16-e,f**, and metal salts **13f**–**16f**, **14g**, and **14h**.

the corresponding carbonates, hydrogen carbonates, or free bases (Figure 5.1). The deprotonation of azene-bridged **16** with potassium hydroxide (4 equiv.) yielded the tetrapotassium salt **16-4f**·0.5 H_2O. Triaminoguanidinium salts **13e** and **15e** were synthesized by metathesis reactions of the corresponding potassium salts with triaminoguanidinium chloride and subsequent precipitation of the salt or removal of the solvent under reduced pressure. The reaction of potassium **16-2f** with triaminoguanidinium chloride (2 equiv.) yielded only double salt **16-e,f** consisting of one potassium cation and one triaminoguanidinium cation. The solubility of **16** and its doubly deprotonated salts was very low in organic solvents and in water, whereby heating of the reaction mixtures was required to obtain a clear solution and to facilitate the reaction. With the exception of the aminoguanidinium salt **16-2d**, all of the salts precipitated as hydrates and their dehydration at 120 °C and 5×10^{-3} mbar (1 mbar = 100 Pa) was not successful. The silver salt **14g** was obtained by the reaction of **14** with silver nitrate in water.

5.2.2 NMR Spectroscopy

All compounds prepared herein were investigated by multinuclear NMR spectroscopy (^{1}H and ^{13}C, some additionally ^{14}N). Their ^{1}H NMR and ^{13}C NMR shifts are summarized in Table 5.1.

The remaining acidic proton of several salts of **13** is observed at a low field around 14 ppm. In the ^{13}C NMR spectra, all salts exhibit three signals for the anion. The resonance signal of the triazole carbon atom of **13** carrying the amino group is strongly affected by deprotonation and shifts from 111.6 ppm to about 123 ppm. With the exception of the salts of azido derivative **14**, the other triazole resonances as well as the tetrazole carbon

Table 5.1: ^{1}H and ^{13}C{^{1}H} NMR shifts of the salts either in DMSO-d_6 or in case of **16-4f** in D_2O.

	^{1}H NMR shifts [ppm]	^{13}C{^{1}H} NMR shifts [ppm]
13a	8.52[⁇], 5.40[*]	154.5[†], 148.7[‡], 122.8[‡]
13b	9.31[⁇], 5.68[⁇]	153.5[†], 148.3[‡], 121.2[‡]
13c	13.97[#], 7.35[⁇], 5.45[*]	158.6[⁇], 155.0[†], 148.7[‡], 123.2[‡]
13d	13.77[#], 8.91[⁇], 7.25[⁇], 5.41[*], 4.74[⁇]	159.9[⁇], 155.1[†], 148.9[‡], 123.3[‡]
13e	13.57[#], 8.61[⁇], 5.37[*], 4.51[⁇]	159.7[⁇], 154.9[†], 149.2[‡], 123.9[‡]
13f	13.61[#]	155.1[†], 149.0[‡], 124.1[‡]
14a	8.09, 7.42	150.0[‡], 140.8[†], 123.6[‡]
14f	5.60[#]	150.8[‡], 139.5[†], 123.7[‡]
14h	n.o.	150.7[‡], 139.5[†], 123.6[‡]
15a	7.13[⁇]	153.8, 151.4, 133.5[‡]
15b	9.37	151.8, 151.4, 129.9[‡]
15c	7.01[⁇]	158.0[⁇], 151.5, 149.1, 126.9[‡]
15d	8.79[⁇], 7.18[⁇], 5.03[⁇]	158.9[⁇], 151.5, 149.7, 127.7[‡]
15e	8.60[⁇], 4.56[⁇]	159.1[⁇], 151.6, 148.8, 126.5[‡]
15f	n.o.	151.5, 148.8, 126.5[‡]
16-2b	7.99[⁇]	154.5, 149.6, 127.4[‡]
16-2c	7.17[⁇], 5.04[#]	158.8[⁇], 155.1, 150.2, 126.3[‡]
16-2d	8.71[⁇], 7.35[⁇], 6.90[⁇], 4.71[⁇#]	158.8[⁇], 154.9, 149.6, 125.9[‡]
16e,f	8.62[⁇], 7.27[⁇#]	159.0[⁇], 154.4, 149.0, 126.2[‡]
16-2f	6.53[#]	154.0, 147.9, 125.7[‡]
16-4f	–	153.5, 153.2, 133.2[‡]

[⁇]cation; [*] NH_2; [#] aromatic NH; [†] tetrazole carbon atom; [‡] triazole carbon atom.

atom resonances are around 150 ppm. The tetrazole carbon atom signals of **13a-f** are shifted to lower fields than the triazole resonances. For **14a** and **14f-h**, the tetrazole carbon atom resonance is observed around 140 ppm, whereas the triazole resonance is still around 150 ppm. Unambiguous assignment of the second triazole and the tetrazole signals of the salts of **15** and **16** was not possible. No irregularities in the NMR shifts of the ^{1}H and ^{13}C resonances of the nitrogen-rich cations were observed.

In the ^{14}N NMR spectra of **14f** and **14h**, the three resonances of the azido group are found around 20, −40, and −130 ppm, but they could not be unambiguously assigned. The signals around −20 ppm in the ^{14}N NMR spectra of **15a-f** are attributed to the nitrogen atom resonance of the nitro group. Furthermore, the nitrogen resonance of the ammonium cations was assigned in the ^{14}N NMR spectra of ammonium salts **13-15a**.

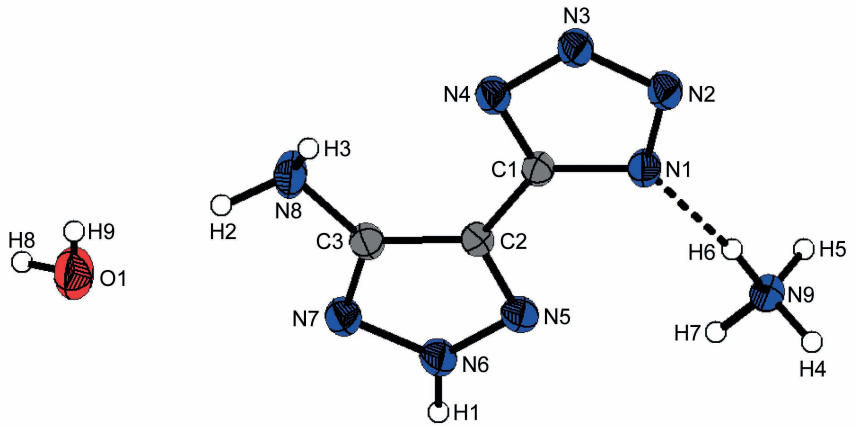

Figure 5.2: Molecular structure of ammonium 5-(5-amino-2*H*-1,2,3-triazol-4-yl)tetrazolate monohydrate (**13a**·H_2O). Thermal ellipsoids are drawn at the 50% probability level.

5.2.3 Crystal Structures

Several salts were characterized by low-temperature single-crystal X-ray diffraction. Selected data and parameters of the measurements and refinements as well as selected bond lengths and angles are summarized in the Appendix (Table A.17 and Table A.18).

The ammonium salt **13a** crystallizes as a monohydrate in the orthorhombic space group *Fdd*2 with 16 formula units per cell and a crystal density of 1.553 g cm^{-3} at 173 K. Its molecular structure is depicted in Figure 5.2.

The C−C bond length (1.40 Å) of the triazole ring and the N−C (1.33–1.34 Å) and N−N (1.31–1.34 Å) bond lengths of both the triazole and the tetrazole rings are in the range of formal single and double bonds because of their aromaticity.[4,32] The C−N bond (1.38 Å) of the amino moiety to the triazole is slightly shorter than a normal C−N bond, which is caused by conjunctive involvement of the nonbonding electron pair. The tetrazole and triazole rings are twisted by 1.92(9)°, whereas the amino group is turned out of the triazole plane by 42(2)°, which enables an intramolecular interaction between the amino H3 atom and N4 (H···A 2.48(3) Å, D···A 3.027(3) Å, ∠D−H···A 122(2)°). The N1 atom of the deprotonated tetrazole rings interacts with the ammonium cation by forming a strong hydrogen bond (N9−H6···N1, H···A 1.96(3) Å, D···A 2.932(3) Å, ∠D−H···A 173(3)°). The alternated anion layers along the *b* axis (Figure A.10) are connected by the strong N6−H1···N3 hydrogen bond of 1.91(3) Å (D···A 2.819(3) Å, ∠D−H···A 169(3)°). Several other hydrogen bonds involving all hydrogen atoms are found within the crystal structure of **13a**·H_2O and are summarized in Table A.12.

The crystal structure of the hydroxylammonium salt **13b** has orthorhombic symmetry (*Pbca*) with eight molecules in the unit cell and a crystal density of 1.720 g cm^{-3} at 173 K. Its molecular structure is depicted in Figure 5.3A. The azoles are twisted by 18.9(1)°, and

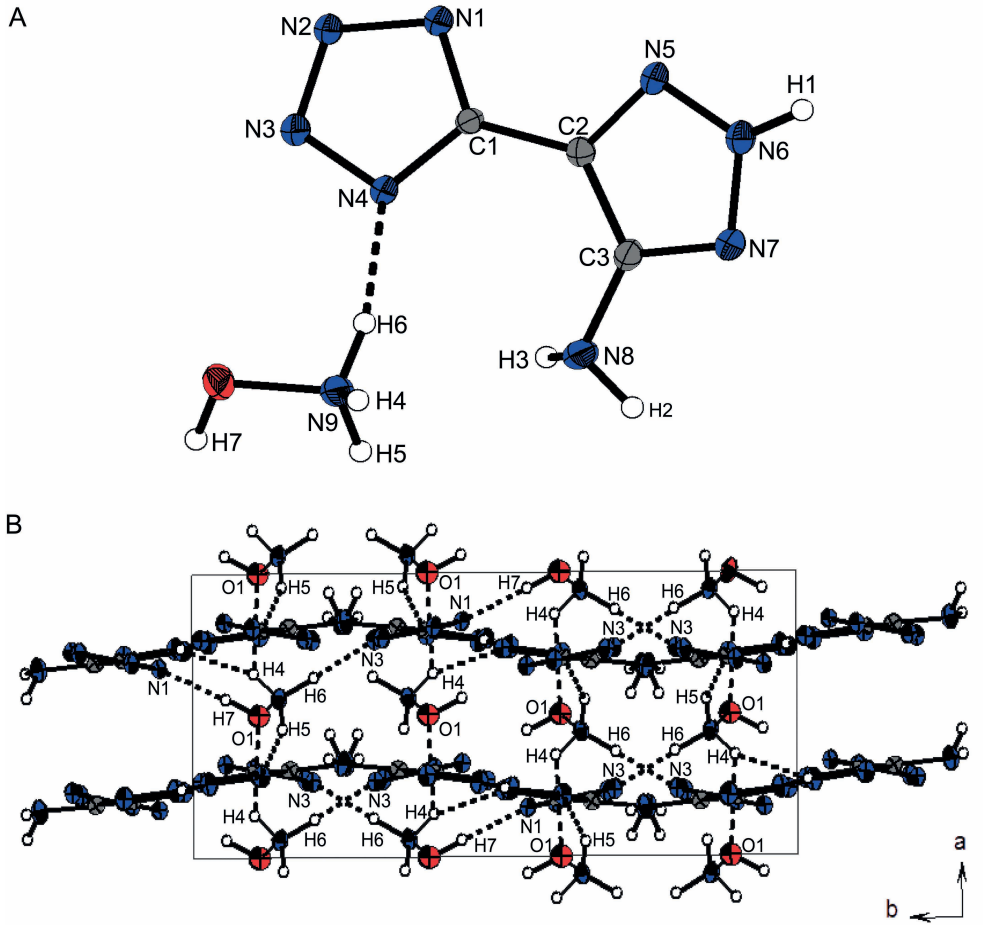

Figure 5.3: A) Molecular structure of hydroxylammonium 5-(5-amino-2*H*-1,2,3-triazol-4-yl)tetrazolate (**13b**). B) Crystal structure of **13b** along the *c* axis. Thermal ellipsoids are displayed at the 50% probability level.

the tetrazole ring is deprotonated. The crystal structure consists of an alternating layer structure of anions and cations (Figure 5.3B) that are linked by the various hydrogen bonds summarized in Table A.13. Each hydrogen atom of the hydroxylammonium cation forms hydrogen bonds either to the nitrogen atoms of the tetrazole/triazole ring or to the oxygen atom of another cation. The H4 atom is involved in a three-center hydrogen bond to the O1 atom and the N5 atom (N9−H4···O1, H···A 2.50(2) Å, D···A 2.936(3) Å, ∠D−H···A 110(1)°; N9−H4···N5, H···A 2.11(2) Å, D···A 2.986(2) Å, ∠D−H···A 158(2)°), which connects the cation layer with another cation and the anion layer.

In contrast to the structures of **13a** and **13b**, the proton of the triazole ring is not located at the centered nitrogen atom in the crystal structure of the guanidinium salt **13c** (Figure 5.4A). It crystallizes in the monoclinic space group *P*21 with two formula units per unit cell and a crystal density of 1.661 g cm^{-3}. The bonds lengths of the triazole vary from the corresponding bond lengths of the other salts because of the different position of the

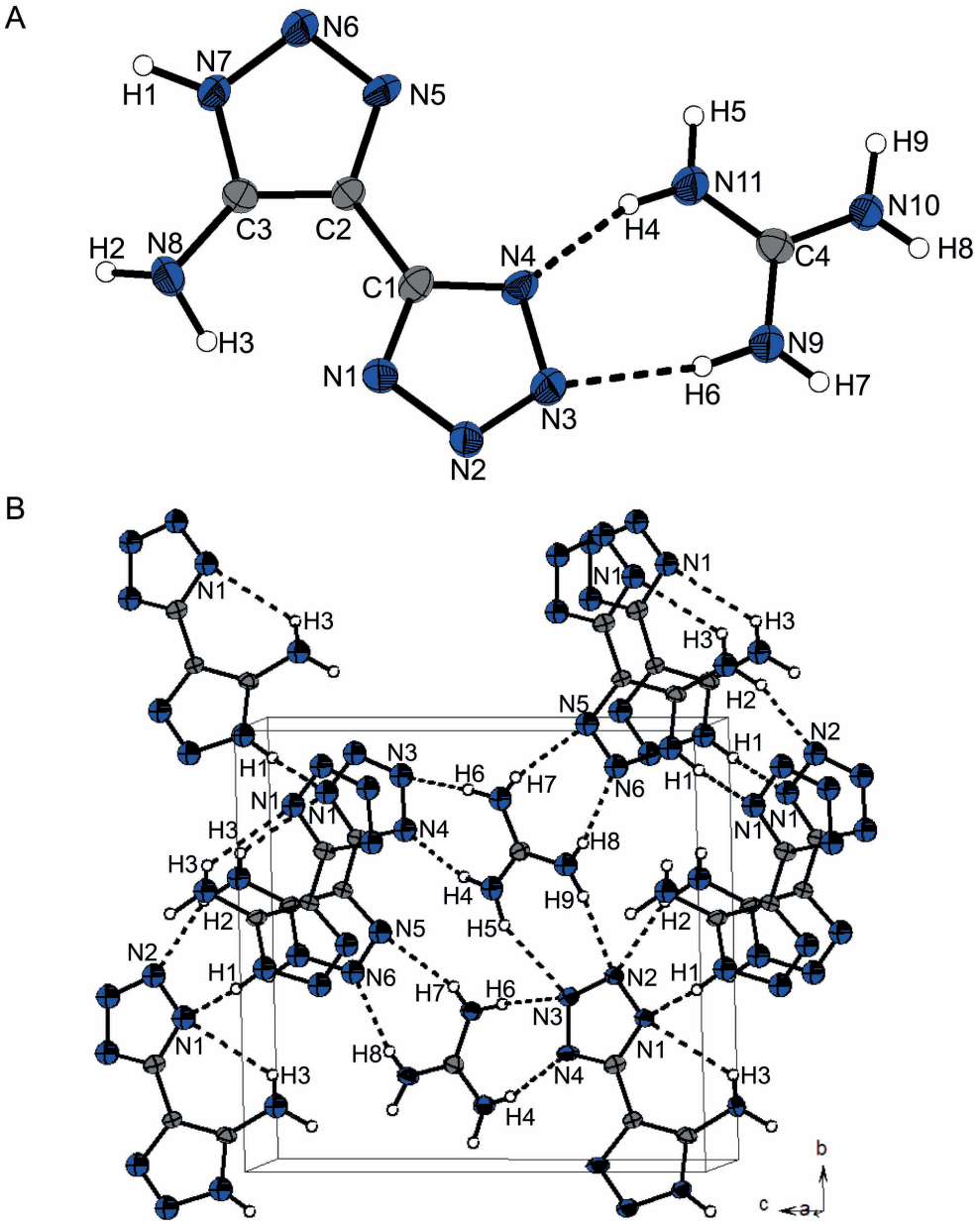

Figure 5.4: A) Molecular structure of guanidinium 5-(5-amino-1*H*-1,2,3-triazol-4-yl)-tetrazolate (**13c**). B) Unit cell of **13c**. Selected hydrogen bonds are shown as black dashed lines. Thermal ellipsoids are displayed at the 50% probability level.

heterocyclic proton. Whereas the C2−N5 (1.355(7) Å) and N6−N7 bonds (1.356(6) Å) are significantly shorter, the C2−C3 bond is elongated (1.378(7) Å) relative to the corresponding bonds of the other salts. The anions are connected by two hydrogen bonds of 1.93(6) and 2.17(5) Å either from the heterocyclic H1 proton (N7−H1···N1, D···A 2.866(7) Å, ∠D−H···A 165(5)°) or the amino H2 proton (N8−H2···N2, D···A 3.105(6) Å, ∠D−H···A 158(4)°). The crystal structure of **13c** depicted in Figure 5.4B shows that each donor and acceptor atom is embedded in hydrogen bonds. The hydrogen bonds are listed in Table A.14.

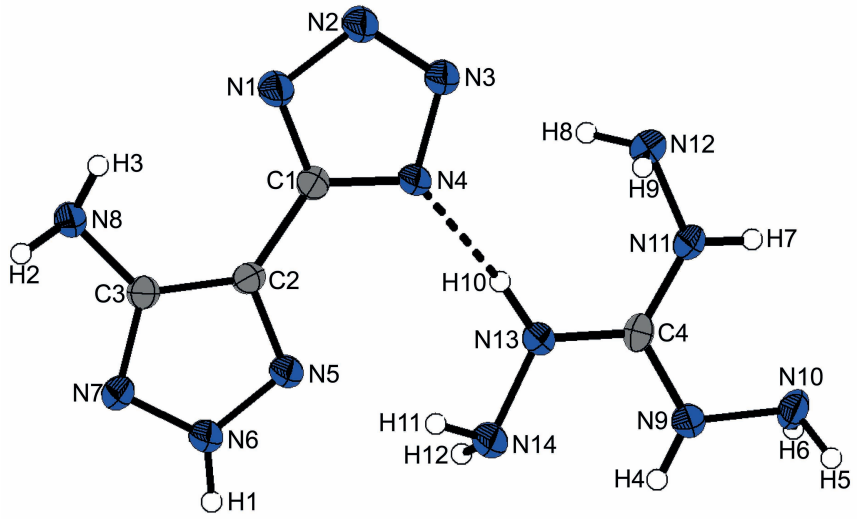

Figure 5.5: Molecular structure of triaminoguanidinium 5-(5-amino-2*H*-1,2,3-triazol-4-yl)tetrazolate (**13e**). Thermal ellipsoids are drawn at the 50% probability level.

The triaminoguanidinium salt **13e** shows monoclinic symmetry (*Cc*) and crystallizes from water with four formula units per unit cell and a crystal density of 1.682 g cm^{-3} at 173 K. The molecular structure of **13e** is shown in Figure 5.5.

The crystal structure of **13e** is formed by various hydrogen bonds from the amino groups of the cation to the azole rings as depicted in Figure A.11. The anions are linked to each other by a strong intermolecular hydrogen bond of 1.949(3) Å between the H1 proton attached to the triazole and N2 (D···A 2.788(4) Å, ∠D−H···A 164.5(2)°). The crystal structure consists of alternating cation and anion layers along the *b* axis that are linked by various hydrogen bonds involving the protons of the triaminoguanidinium cation. The hydrogen bonds are listed in Table A.15.

Potassium salt **13f** crystallizes as a sesquihydrate in the monoclinic space group $P2/n$ with four formula units per unit cell and a crystal density of 1.664 g cm^{-3}. Its molecular structure is shown in Figure 5.6. The anions are connected by a strong hydrogen bond of 1.98(3) Å between the heterocyclic proton and N2 (D···A 2.867(3) Å, ∠D−H···A 174(3)°), thereby forming a diagonal layer in the *ac* plane (Figure A.12). The potassium ion is distorted octahedral and coordinated by three water molecules, two nitrogen atoms of the tetrazole ring, and the amino N8 atom. The K···O and K···N interactions are below the sum of the corresponding van der Waals (vdW) radii.[4] The coordination interactions to the oxygen atoms are in the range of 2.67 to 2.79 Å and are, therefore, slightly stronger than the corresponding interactions to the nitrogen atoms, which are summarized in Table 5.2.

Compound **15d**, the aminoguanidinium salt of 5-(5-nitro-1,2,3-triazolate-4-yl)-1*H*-tetrazole, crystallizes in the monoclinic space group $I2/a$ with eight formula units per unit cell and a

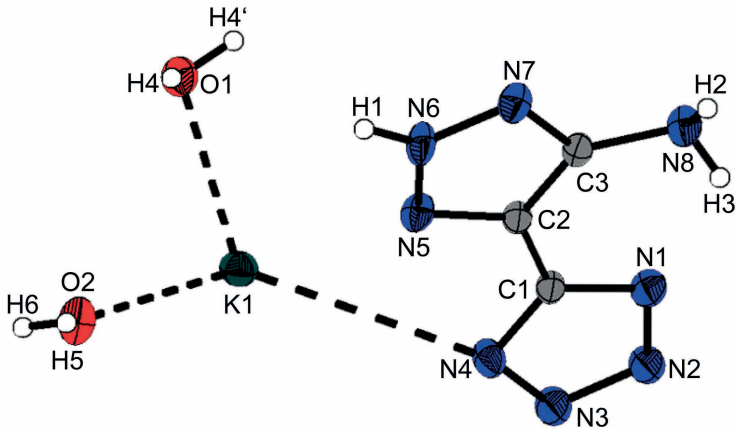

Figure 5.6: Molecular structure of potassium 5-(5-amino-2*H*-1,2,3-triazol-4-yl)tetrazolate sesquihydrate (**13f**·1.5 H_2O). Thermal ellipsoids are drawn at the 50% probability level.

Table 5.2: Coordination interactions of the potassium ion.

Coordination interactions below ΣvdW radii (K···O: < 3.02 Å, K···N: < 3.05 Å)[31]		
K1···O2 2.690(2) Å	K1···O2 2.791(2) Å	K1···O1 2.672(2) Å
K1···N7 2.878(2) Å	K1···N8 2.987(3) Å	K1···N5 2.900(2) Å

crystal density of 1.708 g cm^{-3} at 173 K. In contrast to the salts of 5-(5-amino-1,2,3-triazol-4-yl)tetrazole, the triazole ring is deprotonated instead of the tetrazole ring (Figure 5.7). The rings are twisted by about 4°, whereas the nitro group is turned out of the triazole plane by 8°. Twisting of the nitro group leads to an intermolecular dipolar N···O interaction (2.915(1) Å) between N8 and O2. Furthermore, the anions are connected by a hydrogen bond between the triazole proton and the triazole N5 atom by forming dimers. The cation is almost perpendicular to the anion. Therefore, the crystal structure is formed by alternating layers of cations and anions along the *c* axis, as shown in Figure 5.7. The ions of one layer are staggered along the *a* axis. This structure is supported by various hydrogen bonds between the cations and anions involving the azole nitrogen atoms as acceptors. The hydrogen bonds are summarized in Table A.16. Additionally, a dipolar C···O interaction of 3.045(1) Å is observed between the tetrazole C1 atom and the O1 atom, which is below the sum of their van der Waals radii (3.22 Å).[4]

5.2.4 Thermal Stabilities and Sensitivities

For initial safety testing, the thermal behavior of the salts was investigated by differential thermal analysis (DTA), and the impact (IS), friction (FS), and electrostatic discharge (ESD) sensitivities, which were assigned according to the United Nations recommendations

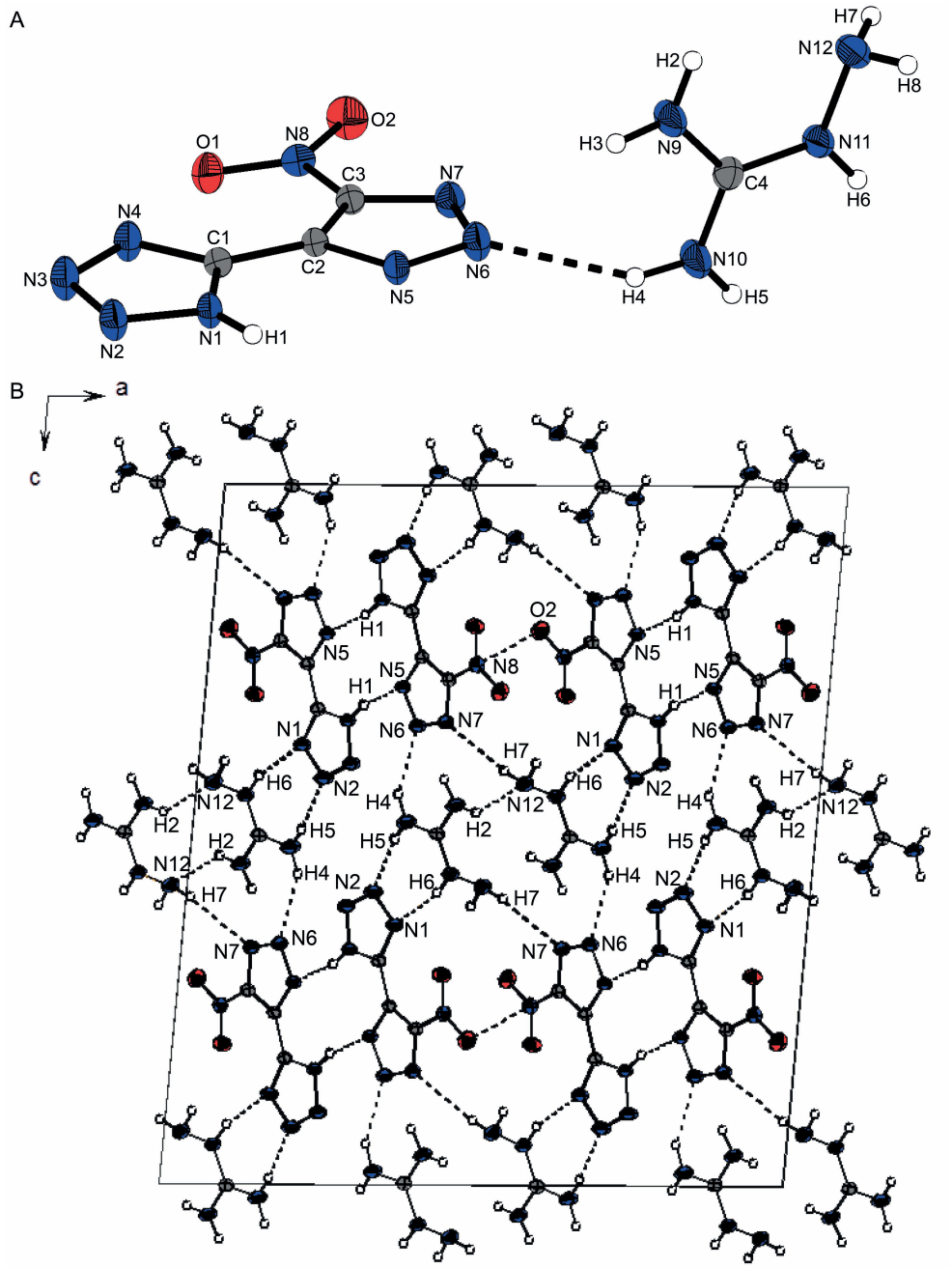

Figure 5.7: A) Molecular structure of aminoguanidinium 5-(5-nitro-1,2,3-triazolate-4-yl)-1*H*-tetrazole (**15d**). B) Crystal structure of **15d** along the *b* axis. Thermal ellipsoids are drawn at the 50% probability level.

Table 5.3: Energetic properties of 5-(5-azido-1,2,3-triazol-4-yl)tetrazole (**14**) and metal salts **14f**–**h**.

Compound	IS[a] [J]	FS[b] [N]	ESD[c] [J]	T_{dec}[d] [°C]	DDT[e]	Fast heating
14	3	10	250	152	–	–
14f	2	60	40	135	yes	detonation
14g	1	⋘5	–	121	yes	detonation
14h	1	5	14	148	yes	detonation

[a] Impact sensitivity (BAM drophammer, 1 of 6). [b] Friction sensitivity (BAM drophammer, 1 of 6). [c] Electrostatic discharge. [d] Decomposition temperature. [e] Deflagration-to-detonation transition.

on the transport of dangerous goods, were also evaluated.[33–35]

Amino derivative **13** had the highest thermal stability of the neutral molecules (241 °C), whereas the thermal stability of nitro derivative **15** (188 °C) and especially those of azido derivative **14** (152 °C) and diazene bridged **16** (128 °C) were well below.[15] Unfortunately, the formation of salts **13a**–**e** did not raise the thermal stabilities (181–240 °C; Table 5.4), as was generally expected for such compounds relative to their neutral parent compounds. Although the thermal stabilities of salts **13a**–**e** did not increase, the impact sensitivities were improved relative to that of **13** (Table 5.4). Their impact sensitivities varied between sensitive (for **13b** and **13e**: 25 J), less sensitive (for **13a**·H_2O: 40 J), and insensitive (for **13c** and **13d**: > 40 J), and they were all insensitive towards friction (> 360 N) and, therefore, less sensitive than RDX.

Ammonium salt **14a** (132 °C), potassium salt **14f** (135 °C), silver salt **14g** (121 °C), as well as cesium salt **14h** (148 °C) were also thermally less stable than the parent compound (Table 5.3). Whereas azido derivative **14** was the most sensitive of the parent compounds (IS: 3 J, FS: 10 N), the same trend was observed for its salts, which were all very sensitive to impact (2 J and lower) and very sensitive (for **14a** and **14f**: < 60 N) or extremely sensitive (for **14g** and **14h**: ⋘5 N and 5 N) to friction. Specifically, silver salt **14g** was found to be an extremely dangerous compound and could be detonated by the slightest amount of friction when dry. Whereas the electrostatic discharge sensitivity of silver salt **14g** was not determined, cesium salt **14h** had a sensitivity of 14 mJ, which is in the range of primary explosives such as lead azide (5 mJ). Both the silver and cesium salts were the only ones to always detonate (impact, friction, and electrostatic discharge), whereas ammonium salt **14a** merely only vanished without sound.

Salts **15a**–**e** of the nitro derivative showed higher thermal stabilities up to 220 °C (Table 5.4 and Table 5.5), with exception of hydroxylammonium salt **15b** (168 °C) and triaminoguanidinium salt **15e** (174 °C). With the exception of hydroxylammonium salt **15b** (2 J), the impact sensitivities were improved to a much lesser extent of 8 to 20 J relative to that of

15 (4 J) (Table 5.4 and Table 5.5). All salts of **15** were insensitive to friction, whereas **15** was classified as sensitive.
The thermal stabilities of nitrogen-rich salts **16-2b** to **16-e,f** were in the range of 145 to 192 °C and were therefore improved relative to that of **16**. The only anhydrous salt of **16**, which is therefore the most interesting of this kind, is the aminoguanidinium salt **16-2d** (Table 5.5). It decomposed at 192 °C and showed improved sensitivities relative to RDX and its very sensitive parent compound **16**·2 H_2O (IS: 2 J, FS: 28 N),[15] being insensitive towards friction and impact sensitive (12.5 J).
The electrostatic discharge sensitivities of the nitrogen-rich salts were in the range of 300 to 1500 mJ and are therefore greater than the human body can release.

5.2.5 Primary Explosives

Metal salts **14g** and **14h** containing the silver and cesium cations were tested for their potential of being true primary explosives and not just highly sensitive compounds (Table 5.3). In separate experiments, a small amount (approx. 5 mg) of **14g** and **14h** was heated on a spatula by using a lighter, without direct flame contact. Both compounds detonated upon reaching their corresponding ignition temperatures. Next, a small sample (again approx. 5 mg) of **14h** was fixed to a surface with a bit of transparent tape and poked with a preheated needle, which resulted in detonation. This compound was therefore tested for its ability to initiate a commonly used secondary explosive. RDX was loaded in a copper tube (6.50 mm × 57.70 mm), layered with **14h**, and slightly pressed. For the ignition, a commercial type A electrical igniter[36] was used on top with direct contact to the primary explosive. Both 50 and 25 mg of **14h** were able to initiate 300 mg of RDX, which resulted in destruction of the copper tube (Figure 5.8). A test with only 100 mg of **14h** and no RDX resulted in deflagration.

5.2.6 Detonation Performances

In the first instance, the performance characteristics of new energetic materials are calculated to evaluate their potential for possible applications. Enthalpies of formation were computed at the CBS-4M level of theory[37,38] with Gaussian 09, revision A.02,[39] by using the atomization energy method[40–42] and utilizing experimental data.[43,44] Gas-phase enthalpies were transformed into solid-state enthalpies by using Trouton's rule[45,46] for neutral compounds and Jenkins method for ionic compounds.[47] The complete method is extensively described in the literature.[1] Detonation parameters were calculated by using the Explo5 version 6.02.[48] The program is based on the steady-state model of equilibrium and uses the Becker–Kistiakowsky–Wilson equation of state (BKW EOS) for

Figure 5.8: Copper tube test of **14h**. (Top) Type A igniter; (left) empty copper tube; (middle) damaged copper tube after deflagration of pure **14h** (100 mg); (right) remnants after detonation (300 mg of RDX, 50 mg of **14h**).

gaseous detonation products and the Murnaghan EOS for both solid and liquid products. The parameters of the BKW EOS in EXPLO5 v. 6.02 are calibrated particularly for the formation of nitrogen gas, which is the main detonation product for compounds with a high nitrogen content. It is designed to enable the calculation of detonation parameters at the Chapman–Jouguet point. The calculations were performed by using the maximum densities at room temperature. The densities at 298 K (ρ_{rt}) were either calculated from the corresponding crystal densities by Equation 5.1 and the coefficient of volume expansion (α_{v}) from the nitramine HMX (octogen) ($\alpha_{\mathrm{v}} = 1.6 \times 10^{-4}\,\mathrm{K}$[49]) or measured with a helium pycnometer from Linseis.

$$\rho_{298K} = \frac{\rho_{\mathrm{T}}}{1 + \alpha_v(298 - \mathrm{T})} \tag{5.1}$$

The physical parameters of nitrogen-rich salts **13a**, **16-2b**, **16-2c**, and **16-e,f** are not discussed, because they could not be obtained as anhydrous compounds.

In general, the detonation parameters regarding detonation pressure and velocity as well as the volume of gaseous products were increased by the formation of the nitrogen-rich salts, whereas the heats of explosion and the detonation temperatures were reduced (Table 5.4 and Table 5.5). On the basis of these calculations, compounds **13b**, **13d**, **13e**, and **15e** have higher detonation velocities than RDX. Compound **13e** even has a higher detonation velocity than bistriaminoguanidinium 5,5′-azobistetrazolate (TAGzT, $D = 9371\,\mathrm{m\,s^{-1}}$) of $9571\,\mathrm{m\,s^{-1}}$.

Table 5.4: Physical and energetic properties of **13b**–**13e**, **14a**, and **15a**–**15c**.

	13b	**13c**	**13d**	**13e**	**14a**	**15a**	**15b**	**15c**
Molecular formula	$C_3H_7N_9O$	$C_4H_9N_{11}$	$C_4H_{10}N_{12}$	$C_4H_{12}N_{14}$	$C_3H_5N_{11}$	$C_3H_5N_9O_2$	$C_3H_5N_9O_3$	$C_4H_7N_{11}O_2$
M [g mol^{-1}]	185.15	211.19	226.21	256.24	195.15	199.13	215.13	241.18
IS [J][a]	25	>40	>40	25	20	>9	2	>20
FS [N][b]	>360	>360	>360	>360	>360	>360	>360	>360
ESD [mJ][c]	300	1500	1500	400	1000	1250	600	1500
Grain size [µm]	<100	<100	<100	<100	<100	<100	<100	<100
N [%][d]	68.09	72.96	74.31	76.53	78.95	63.31	58.60	63.89
Ω [%][e]	−73.4	−94.7	−91.9	−87.4	−69.7	−52.2	−40.9	−52.4
T_{melt} [°C][f]	–	188	211	203	–	–	142	–
T_{dec} [°C][g]	181	249	232	215	132	207	168	220
ρ [g cm^{-3}][h]	1.70	1.63	1.63	1.66	1.63	1.62	1.67	1.67
$\Delta_f H_m$ [kJ mol^{-1}][i]	540	350	554	773	859	463	514	426
$\Delta_f U$ [kJ kg^{-1}][j]	3032	2366	2571	3140	4501	2425	2488	1868
Calculated detonation parameters (EXPLO5 v. 6.02)								
$-Q_{\text{v}}$ [kJ kg^{-1}][k]	4691	2976	3201	3802	4830	4830	5535	4010
T_{det} [K][l]	2871	2050	2132	2326	3181	3369	3799	2804
p_{CJ} [kbar][m]	307	241	255	300	277	4241	279	244
D [m s^{-1}][n]	9350	8706	8926	9571	8903	8200	8513	8340
V_0 [L kg^{-1}][o]	860	837	855	884	822	832	827	828

[a] Impact sensitivity (BAM drophammer 1 of 6). [b] Friction sensitivity (BAM friction tester 1 of 6). [c] Electrostatic discharge (OZM Research). [d] Nitrogen content. [e] Oxygen balance ($\Omega = (x\text{O} - 2y\text{C} - 0.5z\text{H})1600/M$). [f] Melting point. [g] Decomposition temperature. [h] Density at ambient temperature. [i] Calculated enthalpy of formation. [j] Calculated energy of formation. [k] Energy of explosion. [l] Detonation temperature. [m] Detonation pressure. [n] Detonation velocity. [o] Volume of detonation gases.

Table 5.5: Physical and energetic properties of **15d** and **15e**, **16-2d** and for comparison of **13**, **15**, RDX, and TAGzT.

	15d	**15e**	**16-2d**	**13**	**15**	RDX	TAGzT
Molecular formula	$C_4H_8N_{12}O_2$	$C_4H_{10}N_{14}O_2$	$C_8H_{16}N_{24}$	$C_3H_4N_8$	$C_3H_2N_8O_2$	$C_6H_5N_7O_4$	$C_4H_{18}N_{22}$
M [g mol^{-1}]	256.19	286.21	448.38	152.13	182.11	222.12	374.36
IS [J][a]	10	8	12.5	10	4	7.4	4
FS [N][b]	>360	>360	>360	>360	108	120	60
ESD [mJ][c]	1000	500	300	800	250	200	150
Grain size [µm]	<100	<100	<100	<100	<100	<100	<100
N [%][d]	65.61	68.51	74.97	73.66	61.53	37.84	82.32
Ω [%][e]	−62.4	−61.4	−85.6	−84.1	−43.9	−21.6	−72.7
T_{melt} [°C][f]	198	150	–	–	180	–	–
T_{dec} [°C][g]	214	174	192	241	188	204	202
ρ [g cm^{-3}][h]	1.67	1.65	1.63	1.66	1.69	1.80	1.60
$\Delta_f H_m$ [kJ mol^{-1}][i]	532	748	1340	460	516	85	1070
$\Delta_f U$ [kJ kg^{-1}][j]	2181	2725	3099	3120	2915	481	2990
Calculated detonation parameters (Explo5 v. 6.02)							
$-Q_{\mathrm{v}}$ [kJ kg^{-1}][k]	4251	4669	3598	3481	5064	5903	3670
T_{det} [K][l]	2874	3001	2415	2479	3816	3849	2316
p_{CJ} [kbar][m]	261	280	253	237	263	347	282
D [m s^{-1}][n]	8597	8918	8740	8397	8251	8854	9371
V_0 [L kg^{-1}][o]	847	879	826	772	753	785	943

[a] Impact sensitivity (BAM drophammer 1 of 6). [b] Friction sensitivity (BAM friction tester 1 of 6). [c] Electrostatic discharge (OZM Research). [d] Nitrogen content. [e] Oxygen balance ($\Omega = (x\mathrm{O} - 2y\mathrm{C} - 0.5z\mathrm{H})1600/M$). [f] Melting point. [g] Decomposition temperature. [h] Density at ambient temperature. [i] Calculated enthalpy of formation. [j] Calculated energy of formation. [k] Energy of explosion. [l] Detonation temperature. [m] Detonation pressure. [n] Detonation velocity. [o] Volume of detonation gases.

5.2.7 Gun Propellant Evaluation

The improved sensitivities of salts **13c**–**e** and **16-2d** to external stimuli relative to that of TAGzT[50] as well as their high thermal stabilities (> 200 °C) and especially their high nitrogen contents (> 70%) make them promising replacements for TAGzT in gun propellant mixtures. TAGzT is used in erosion-reduced formulations derived from the formulation EX-99, which is applied for large naval guns and contains a high amount of RDX.[29] The amount of RDX is reduced by adding TAGzT to achieve a lower combustion temperature and less erosion, which thereby elongates the lifespan because of the higher nitrogen content. These formulations are referred to as high-nitrogen 1 and 2 (HN-1 and HN-2). Therefore, the combustion performances of selected salts **13c**–**e**, and **16-2d** were computed for a first evaluation as potential ingredients.

The computed combustion performances of the genuine HN-1 and HN-2 formulations and the corresponding formulations in which TAGzT was replaced by the selected salts are listed in Table 5.6. The enthalpies of formation of the other ingredients were either taken from the EXPLO5[48] or ICT database.[51] In general, the HN-1-based formulations showed higher combustion performances than the formulations based on HN-2. On the other hand, the addition of FOX-12 led to higher N_2/CO ratios and lower combustion temperatures, which are advantageous in terms of improved lifespan by avoiding gun-barrel corrosion The specific energy (f_E), the force constant, is related to the muzzle velocity and should be as high as possible to achieve a higher possible muzzle velocity.[25]

Especially, formulations containing **13e** showed advantageous higher specific energies. Therefore, the HN-1 and HN-2 formulations containing triaminoguanidinium salt **13e** are the most promising formulations for further investigations concerning optimized propellant formulations, processing, and ballistics. These formulations show the highest specific energies but also the highest combustion temperatures. However, the combustion temperature of each formulation is below the critical temperature of 3273 K to ensure the safety of the gun.[25]

5.3 Conclusions

The formation of selected metal and nitrogen-rich salts of 5-(5-amino-1,2,3-triazol-4-yl)tetrazole (**13**) and its derivatives with an azido group (see compound **14**), a nitro group (see compound **15**), and a diazene bridge (see compound **16**) resulted in primary and secondary explosives. Deprotonation of the salts of **13** and **15** took place either at the tetrazole ring or the triazole ring, as identified by single-crystal X-ray crystallography. Relative to that shown by the parent compounds, the nitrogen-rich salts showed reduced

Table 5.6: Calculated performances of the gun propellant charges assuming isochoric combustion and loading densities of $0.2\,\mathrm{g\,cm^{-3}}$ with Explo5 (v. 6.02).

	HN-1[a]					HN-2[b]				
	T_C [K][c]	p_{max} [bar][d]	f_E [kJ g^{-1}][e]	b_E [cm^3 g^{-1}][f]	N_2/CO [w/w][g]	T_C [K][c]	p_{max} [bar][d]	f_E [kJ g^{-1}][e]	b_E [cm^3 g^{-1}][f]	N_2/CO [w/w][g]
HN-1	2574	3063	1.071	1.505	0.82	–	–	–	–	–
HN-2	–	–	–	–	–	2387	2860	0.996	1.517	0.89
13c	2591	3029	1.062	1.493	0.76	2395	2820	0.985	1.506	0.83
13d	2626	3072	1.078	1.491	0.78	2429	2864	1.001	1.504	0.84
13e	2708	3170	1.114	1.487	0.81	2509	2965	1.037	1.501	0.87
16-2d	2697	3099	1.092	1.477	0.78	2496	2896	1.016	1.491	0.84

[a] HN-1: RDX/bistriaminoguanidinium 5,5′-bisazotetrazolate (TAGzT)/cellulose acetate butyrate (CAB)/1:1 mixture of bis(2,2-dinitropropyl)acetal and -formal (BDNPA-F)/nitrocellulose (NC) (13.25) 56/20/12/8/4. [b] HN-2: RDX/TAGzT/FOX-12/CAB/BDNPA-F/NC (13.25) 40/20/16/12/8/4. [c] Adiabatic combustion temperature. [d] Pressure in closed vessel. [e] Specific energy. [f] Co-volume of gaseous products. [g] N_2/CO ratio

sensitivities towards mechanical stimuli such as impact, friction, and electrostatic discharge. Unfortunately, the thermal stabilities were not, in general, improved by salt formation; however, most salts still showed sufficient thermal stability. The calculated detonation performances of the secondary explosives were improved relative to those of the nonionic parent molecules. The most promising high explosives for potential application as RDX replacements are the guanidinium derived salts **13c**–**e** and **16-2d**, which showed performances and thermal stabilities similar to those shown by RDX, while exhibiting better mechanical stabilities.

These four salts were further investigated as potential replacements of the more sensitive TAGzT by calculation of their combustion performances in nitrogen-rich, thereby erosion-reduced, LOVA gun propellants HN-1 and HN-2. Their computed combustion performances were at least in the same range as those of the genuine mixtures and in the case of **13e** they were even improved. Although their combustion temperatures were higher, they were below the critical temperature.

Potassium salt **14f**, silver salt **14g**, and cesium salt **14h** were found to be very sensitive true primary explosives with deflagration to detonation transitions, and they detonated even if directly burned, similar to lead azide. Specifically, silver salt **14g** was found to be extremely sensitive and could be detonated by the slightest amount of friction when dry. Furthermore, **14h** was able to initiate RDX.

5.4 Experimental Section

Caution! *Most compounds prepared herein are energetic compounds sensitive to impact, friction and electrostatic discharge. Although there were no problems in handling the compounds, proper protective measures (ear protection, Kevlar® gloves, face shield, body armor and earthed equipment) should be used, especially when working with the primary explosives **14f**–**14h**.*

Ammonium 5-(5-amino-2*H*-1,2,3-triazol-4-yl)tetrazolate monohydrate (13a·H_2O)

13 (250 mg, 1.64 mmol) was suspended in 2M NH_3 (10 mL) and stirred for 18 h at 60 °C. The solvent was removed under reduced pressure to obtain **13a** (261 mg, 1.40 mmol, 85%) as a yellow powder.

DTA (5 °C min^{-1}): T_{dehyd} = 103 °C, T_{melt} = 165 °C, T_{dec} = 240 °C. ^{1}H NMR (400 MHz, DMSO-d_6): δ = 8.52 (br, 4H, NH_4^+), 5.40 (s, 2H, NH_2) ppm. ^{13}C{^{1}H} NMR (101 MHz, DMSO-d_6): δ = 154.5, 148.7, 122.8 (C_{tri}) ppm. ^{14}N{^{1}H} NMR (29 MHz, DMSO-d_6): δ = −359 (NH$_4^+$) ppm. IR (ATR): $\tilde{\nu}$ = 3392 (w), 3298 (w), 3172 (m), 3004 (m), 2812 (s), 2364 (w), 2121 (vw), 1844 (vw), 1694 (vw), 1644 (w), 1603 (m), 1549 (m), 1509 (m), 1432 (vs),

1380 (s), 1313 (w), 1262 (vw), 1213 (w), 1162 (m), 1133 (m), 1113 (m), 1095 (m), 1042 (m), 1030 (vs), 977 (vs), 822 (s), 769 (w), 725 (w) cm^{-1}. Raman (1064 nm, 300 mW): $\tilde{\nu}$ = 1606 (100), 1429 (7), 1172 (16), 1161 (12), 1032 (13), 426 (6), 168 (6), 136 (19), 95 (11), 78 (11) cm^{-1}. MS (FAB^+): m/z (%) = 18 (2) [NH_4^+]. MS (FAB^-): m/z (%) = 151 (43) [$C_3H_3N_8^-$]. EA ($C_3H_7N_9 \cdot H_2O$, 187.17 g mol^{-1}): calcd C 19.25, H 4.85, N 67.35%; found C 20.09, H 4.76, N 67.14%. Sensitivities (grain size: < 100 µm): IS: > 40 J; FS: > 360 N; ESD: 1.5 J.

Hydroxylammonium 5-(5-amino-2*H*-1,2,3-triazol-4-yl)tetrazolate (13b)

13 (250 mg, 1.64 mmol) was suspended in ethanol (20 mL). A solution of hydroxylamine in water (50% *w*/*w*, 0.10 mL, 1.64 mmol) was added and the mixture was stirred for 3 h at 60 °C. The precipitate was filtered off and air-dried to obtain **13b** (245 mg, 1.39 mmol, 85%) as yellow powder.
DTA (5 °C min^{-1}): T_{dec1} = 178 °C, T_{dec2} = 240 °C. ^{1}H NMR (400 MHz, DMSO-d_6): δ = 9.31 (br, NH_3OH), 5.68 (br, 2H, NH_2) ppm. $^{13}C\{^1H\}$ NMR (101 MHz, DMSO-d_6): δ = 153.5, 148.3, 121.2 (C_{tri}) ppm. IR (ATR): $\tilde{\nu}$ = 3382 (w), 3308 (vw), 3119 (2982 (w), 2834 (m), 2677 (m), 2470 (m), 2116 (vw), 1918 (vw), 1603 (m), 1576 (m), 1546 (m), 1520 (s), 1415 (w), 1391 (w), 1257 (w), 1225 (m), 1220 (s), 1177 (s), 1129 (m), 1106 (w), 1038 (s), 997 (s), 974 (s), 822 (s), 783 (vs), 705 (vs) cm^{-1}. Raman (1064 nm, 300 mW): $\tilde{\nu}$ = 1607 (100), 1556 (5), 1420 (10), 1322 (5), 1179 (18), 1166 (14), 1045 (13), 1000 (8), 769 (5), 718 (6), 439 (8), 412 (5), 174 (11), 130 (17), 113 (39), 103 (27), 87 (25), 74 (5) cm^{-1}. MS (FAB^-): m/z (%) = 151 (43) [$C_3H_3N_8^-$]. EA ($C_3H_7N_9O$, 185.15 g mol^{-1}): calcd C 19.46, H 3.81, N 68.09%; found C 20.02, H 3.82, N 67.18%. Sensitivities (grain size: < 100 µm): IS: 25 J; FS: > 360 N; ESD: 0.3 J.

Guanidinium 5-(5-amino-1*H*-1,2,3-triazol-4-yl)tetrazolate (13c)

13 (250 mg, 1.64 mmol) was suspended in ethanol (20 mL). Bisguanidinium carbonate (148 mg, 0.83 mmol) was added and the mixture was stirred for 3 h at 60 °C. The precipitate was filtered off and air-dried to obtain **13c** (294 mg, 1.40 mmol, 85%) as yellow powder.
DTA (5 °C min^{-1}): T_{melt} = 188 °C, T_{dec} = 249 °C. ^{1}H NMR (400 MHz, DMSO-d_6): δ = 13.97 (br, 1H, NH), 7.35 (s, 6H, C(NH_2)$_3$), 5.45 (s, 2H, NH_2) ppm. $^{13}C\{^1H\}$ NMR (101 MHz, DMSO-d_6): δ = 158.6 (C(NH_2)$_3$), 155.0, 148.7, 123.2 (C_{tri}) ppm. IR (ATR): $\tilde{\nu}$ = 3397 (m), 3293 (w), 3196 (m), 3081 (m), 2925 (w), 2765 (w), 1682 (m), 1642 (vs), 1607 (m), 1582 (m), 1443 (w), 1428 (w), 1375 (w), 1253 (s), 1216 (vw), 1165 (m), 1123 (w), 1094 (w), 1034 (w), 987 (s), 819 (m), 768 (m), 714 (w), 693 (w), 667 (m) cm^{-1}. Raman (1064 nm, 300 mW): $\tilde{\nu}$ = 3206 (5), 1681 (5), 1633 (47), 1610 (49), 1587 (57), 1448 (30), 1432 (10), 1380 (5), 1257

(10), 1217 (5), 1169 (15), 1122 (10), 1094 (7), 1072 (7), 1044 (56), 1033 (15), 1011 (71), 988 (17), 768 (21), 716 (9), 553 (17), 545 (16), 425 (14), 411 (22), 325 (11), 302 (5), 179 (17), 142 (100), 111 (97), 99 (81), 80 (85) cm^{-1}. MS (FAB^+): m/z (%) = 60 (100) [$CH_6N_3^+$]. MS (FAB^-): m/z (%) = 151 (100) [$C_3H_3N_8^-$]. EA ($C_4H_{10}N_{12}$, 212.20 g mol^{-1}): calcd C 22.75, H 4.30, N 72.96%; found C 23.35, H 4.30, N 72.26%. Sensitivities (grain size: < 100 µm): IS: > 40 J; FS: > 360 N; ESD: 1.5 J.

Aminoguanidinium 5-(5-amino-2*H*-1,2,3-triazol-4-yl)tetrazolate (13d)

13 (250 mg, 1.64 mmol) was suspended in ethanol (20 mL). Aminoguanidinium bicarbonate (224 mg, 1.65 mmol) was added and the mixture was stirred for 18 h at 60 °C. The precipitate was filtered off and air-dried to obtain **13d** (341 mg, 1.51 mmol, 92%) as yellow powder.
DTA (5 °C min^{-1}): T_{melt} = 211 °C, T_{dec} = 232 °C. ^{1}H NMR (400 MHz, DMSO-d_6): δ = 13.77 (br, 1H, N*H*), 8.91 (s, 1H, CN*H*), 7.25 (m, 4H, C(NH_2)$_2$), 5.41 (s, 2H, NH_2), 4.74 (s, 2H, NNH_2) ppm. ^{13}C{^{1}H} NMR (101 MHz, DMSO-d_6): δ = 159.5 (*C*NH(NH$_2$)$_2$), 155.1, 148.9, 123.3 (C_{tri}) ppm. IR (ATR): $\tilde{\nu}$ = 3426 (w), 3361 (m), 3334 (m), 3149 (m), 2979 (w), 2881 (w), 2675 (w), 2617 (w), 2106 (vw), 1809 (vw), 1684 (vs), 1675 (vs), 1647 (s) 1613 (m), 1599 (m), 1562 (w), 1530 (m), 1464 (vw), 1417 (vw), 1378 (vw), 1319 (vw), 1231 (m), 1215 (w), 1174 (m), 1148 (w), 1136 (w), 1117 (w), 1099 (m), 1041 (w), 1025 (w), 974 (vs), 916 (w), 769 (m), 690 (vw) cm^{-1}. Raman (1064 nm, 300 mW): $\tilde{\nu}$ = 1600 (100), 1539 (6), 1413 (11), 1320 (5), 1175 (26), 1026 (32), 974 (13), 770 (12), 746 (5), 721 (5), 512 (5), 434 (13), 419 (13), 335 (8), 314 (5), 179 (8), 141 (38), 105 (46), 93 (36), 116 (39) cm^{-1}. MS (FAB^+): m/z (%) = 75 (20) [$CH_7N_4^+$]. MS (FAB^-): m/z (%) = 151 (43) [$C_3H_3N_8^-$]. EA ($C_4H_{10}N_{12}$, 262.21 g mol^{-1}): calcd C 21.24, H 4.46, N 74.31%; found C 21.80, H 4.35, N 73.72%. Sensitivities (grain size: < 100 µm): IS: > 40 J; FS: > 360 N; ESD: 1.5 J.

Triaminoguanidinium 5-(5-amino-2*H*-1,2,3-triazol-4-yl)tetrazolate (13e)

13f (200 mg, 1.05 mmol) was dissolved in a minimal amount of water. Triaminoguanidinium chloride (149 mg, 1.06 mmol) was added and the mixture was stirred for 1.5 h at room temperature. The precipitate was filtered off and air-dried to obtain **13e** (163 mg, 0.64 mmol, 61%) as colorless powder.
DTA (5 °C min^{-1}): T_{melt} = 203 °C, T_{dec} = 215 °C. ^{1}H NMR (270 MHz, DMSO-d_6): δ = 13.57 (br, 1H, N*H*), 8.61 (s, 3H, NH$_2$N*H*), 5.37 (s, 2H, NH_2), 4.51 (s, 6H, C(NHNH_2)$_3$) ppm. ^{13}C{^{1}H} NMR (101 MHz, DMSO-d_6): δ = 159.7 (*C*(NHNH$_2$)$_3$), 154.9, 149.2, 123.9 (C_{tri}) ppm. IR (ATR): $\tilde{\nu}$ = 3351 (m), 3340 (m), 3265 (s), 3183 (br), 2940 (m), 2848 (m), 2776 (m), 2617 (m), 1680 (s), 1647 (s), 1631 (s), 1596 (vs), 1541 (s), 1489 (w), 1418 (s), 1378 (m), 1327 (w), 1240 (w), 1213 (s), 1180 (s), 1173 (s), 1127 (m), 1112 (m), 1086 (s), 1036 (s), 1026

(s), 981 (s), 958 (m), 934 (s), 878 (m), 850 (m), 768 (m), 715 (m) cm^{-1}. Raman (1064 nm, 300 mW): $\tilde{\nu}$ = 1599 (100), 1421 (13), 1181 (24), 1130 (5), 1037 (11), 1024 (13), 983 (6), 850 (5), 796 (5), 769 (9), 723 (8), 422 (8), 323 (8) cm^{-1}. MS (FAB^+): m/z (%) = 75 (19) [$CH_9N_6^+$]. MS (FAB^-): m/z (%) = 151 (40) [$C_3H_3N_8^-$]. EA ($C_4H_{12}N_{14}$, 256.24 g mol^{-1}): calcd C 18.75, H 4.72, N 76.53%; found C 19.39, H 4.60, N 75.86%. Sensitivities (grain size: < 100 µm): IS: 25 J; FS: > 360 N; ESD: 0.4 J.

Potassium 5-(5-amino-2*H*-1,2,3-triazol-4-yl)tetrazolate (13f)

13 (500 mg, 3.28 mmol) was suspended in ethanol (40 mL). KOH (186 mg, 3.32 mmol) was added and the mixture was stirred for 2 h at 60 °C. The precipitate was filtered off and air-dried to obtain **13f** (498 mg, 2.63 mmol, 80%) as yellow powder.
DTA (5 °C min^{-1}): T_{dec} = 234 °C. ^{1}H NMR (400 MHz, DMSO-d_6): δ = 13.61 (br, 1H, N*H*), 5.37 (s, 2H, NH_2) ppm. $^{13}C\{^1H\}$ NMR (101 MHz, DMSO-d_6): δ = 155.1, 149.0, 124.1 (C_{tri}) ppm. IR (ATR): $\tilde{\nu}$ = 3403 (m), 3372 (m), 3325 (m), 3293 (m), 3124 (br), 2939 (m), 2855 (m), 2354 (w), 1600 (s), 1545 (s), 1513 (s), 1410 (m), 1316 (w), 1227 (m), 1204 (s), 1162 (s), 1125 (m), 1106 (m), 1080 (m), 1023 (s), 973 (vs), 783 (br), 720 (m), 702 (br) cm^{-1}. Raman (1064 nm, 300 mW): $\tilde{\nu}$ = 1602 (100), 1419 (9), 1164 (14), 1031 (8), 1025 (11), 973 (5), 417 (11) cm^{-1}. MS (FAB^+): m/z (%) = 39 (19) [K^+]. MS (FAB^-): m/z (%) = 151 (98) [$C_3H_3N_8^-$], 108 (9) [$C_2N_6^-$], 16 (5) [NH_2^-]. EA ($C_3H_3KN_8$, 190.21 g mol^{-1}): calcd C 18.94, H 1.59, N 58.91%; found C 18.79, H 1.82, N 56.65%. Sensitivities (grain size: < 100 µm): IS: 40 J; FS: > 360 N; ESD: 0.75 J.

Ammonium 5-(5-azido-2*H*-1,2,3-triazol-4-yl)tetrazolate (14a)

Aqueous ammonia solution (2M, 1 mL, 2.00 mmol) and **14** (356 mg, 2.00 mmol) were refluxed in ethanol (20 mL) for 30 min. The solvent was evaporated under reduced pressure and the yellow residue was washed with a low amount of ethanol and diethyl ether, then dried in fine vacuum to yield a pale yellow solid (348 mg, 1.77 mmol, 80%).
DTA (5 °C min^{-1}): T_{dec} = 132 °C. ^{1}H NMR (400 MHz, DMSO-d_6): δ = 8.09 (br), 7.42 (br) ppm. $^{13}C\{^1H\}$ NMR (101 MHz, DMSO-d_6): δ = 150.0 (C_{tri}), 140.8 (C_{tet}), 123.6 (C_{tri}) ppm. $^{14}N\{^1H\}$ NMR (29 MHz, DMSO-d_6): δ = −135 (*N*), −353 (NH_4^+) ppm. IR (ATR): $\tilde{\nu}$ = 3043 (s), 2819 (s), 2366 (w), 2155 (vs), 1881 (w), 1705 (w), 1622 (m), 1604 (m), 1524 (s), 1505 (s), 1433 (vs), 1393 (m), 1372 (m), 1318 (m), 1301 (w), 1216 (s), 1167 (w), 1155 (w), 1132 (w), 1101 (w), 1031 (m), 980 (vs), 872 (w), 819 (w), 796 (s), 769 (m), 758 (w), 689 (w), 658 (w) cm^{-1}. MS (FAB^+): m/z (%) = 18.1 [NH_4^+]. MS (FAB^-): m/z (%) = 177.3 [$C_3HN_{10}^-$]. EA ($C_3H_5N_{11}$, 195.15 g mol^{-1}): calcd C 18.46, H 2.58, N 78.95%; found C 18.64, H 2.86, N 72.88%. Sensitivities (grain size: < 100 µm): IS: 20 J; FS: 360 N; ESD: 1.0 J.

Potassium 5-(5-azido-2*H*-1,2,3-triazol-4-yl)tetrazolate monohydrate (14f·H_2O)

Potassium carbonate (138 mg, 1.00 mmol) and **14** (356 mg, 2.00 mmol) were refluxed in water (30 mL) for 30 min. The solvent was left to evaporate and the yellow residue was dried in fine vacuum to yield a yellow solid (341 mg, 1.58 mmol, 79%).
DTA (5 °C min^{-1}): T_{dec} = 135 °C. ^{1}H NMR (400 MHz, DMSO-d_6): δ = 5.60 (br) ppm. $^{13}C\{^{1}H\}$ NMR (101 MHz, DMSO-d_6): δ = 150.8, 139.5, 123.7 (C_{tri}) ppm. $^{14}N\{^{1}H\}$ NMR (29 MHz, DMSO-d_6): δ = 25, −42, −136 (N) ppm. IR (ATR): $\tilde{\nu}$ = 3361 (w), 3053 (m), 2911 (m), 2868 (m), 2789 (m), 2157 (s), 2135 (vs), 1625 (m), 1604 (s), 1516 (vs), 1471 (s), 1386 (m), 1368 (m), 1316 (m), 1297 (m), 1235 (vs), 1203 (m), 1121 (s), 1026 (s), 976 (vs), 865 (m), 812 (w), 789 (m), 771 (m), 737 (w), 691 (w), 656 (w) cm^{-1}. MS (FAB^+): m/z (%) = 39.0 [K^+]. MS (FAB^-): m/z (%) = 177.2 [$C_3HN_{10}^-$]. EA ($C_3HKN_{10} \cdot H_2O$, 234.22 g mol^{-1}): calcd C 15.38, H 1.29, N 59.80%; found C 15.87, H 1.51, N 53.93%. Sensitivities (grain size: < 100 µm): IS: 2 J; FS: 60 N; ESD: 40 mJ.

Silver 5-(5-azido-2*H*-1,2,3-triazol-4-yl)tetrazolate (14g)

Silver nitrate (85 mg, 0.50 mmol) in water (20 mL) was added dropwise to **14** (89 mg, 0.50 mmol) in water (20 mL) at 80 °C and the resulting suspension was refluxed in the dark for 30 min. After cooling down the precipitate was filtered off and washed with water, ethanol, and diethyl ether to yield a pale yellow solid. The yield was not determined due to the extremely high friction sensitivity.
DTA (5 °C min^{-1}): T_{dec} = 121 °C. Sensitivities (grain size: < 100 µm): IS: < 1 J; FS: ⋘ 5 N.

Cesium 5-(5-azido-2*H*-1,2,3-triazol-4-yl)tetrazolate (14h)

Cesium carbonate (326 mg, 1.00 mmol) and **14** (356 mg, 2.00 mmol) were refluxed in water (30 mL) for 30 min. The solvent was left to evaporate and the yellow residue was dried in fine vacuum to yield a green-yellow solid (505 mg, 1.63 mmol, 82%).
DTA (5 °C min^{-1}): T_{dec} = 148 °C. $^{13}C\{^{1}H\}$ NMR (101 MHz, DMSO-d_6): δ = 150.7, 139.5, 123.6 (C_{tri}) ppm. $^{14}N\{^{1}H\}$ NMR (29 MHz, DMSO-d_6): δ = 20, −44, −135 (N) ppm. IR (ATR): $\tilde{\nu}$ = 3149 (w), 2948 (w), 2811 (w), 2706 (w), 2483 (m), 2443 (m), 2411 (m), 2340 (m), 2248 (w), 2130 (vs), 1815 (m), 1755 (w), 1704 (w), 1595 (s), 1573 (m), 1537 (w), 1499 (s), 1489 (vs), 1429 (w), 1384 (m), 1365 (s), 1325 (w), 1295 (m), 1222 (vs), 1194 (vs), 1157 (m), 1132 (m), 1119 (s), 1075 (m), 1030 (m), 1016 (vs), 970 (vs), 939 (s), 848 (w), 821 (w), 798 (vs), 767 (s), 688 (w), 663 (w) cm^{-1}. MS (FAB^+): m/z (%) = 133.1 [Cs^+]. MS (FAB^-): m/z (%) = 177.2 [$C_3HN_{10}^-$]. EA (C_3HCsN_{10}, 310.02 g mol^{-1}): calcd C 11.62, H 0.33, N 45.18%; found C 11.63, H 0.98, N 38.24%. Sensitivities (grain size: < 100 µm): IS: 1 J; FS: 5 N; ESD: 14 mJ.

Ammonium 5-(5-nitro-1,2,3-triazolate-4-yl)-1*H*-tetrazole (15a)

15 (250 mg, 1.37 mmol) was suspended in 2M NH_3 (10 mL) and stirred for 6 h at room temperature. The solvent was removed under reduced pressure to obtain **15a** (273 mg, 1.37 mmol, quantitative) as a green-yellow powder.
DTA (5 °C min^{-1}): T_{dec} = 207 °C. ^{1}H NMR (400 MHz, DMSO-d_6): δ = 7.13 (br, 4H, NH_4^+) ppm. ^{13}C{^{1}H} NMR (101 MHz, DMSO-d_6): δ = 153.8, 151.4, 133.5 (C_{tri}) ppm. ^{14}N{^{1}H} NMR (29 MHz, DMSO-d_6): δ = −12 (NO_2), −353 (NH_4) ppm. IR (ATR): $\tilde{\nu}$ = 3282 (w), 3161 (w), 2994 (m), 2798 (m), 2349 (vw), 2282 (vw), 1874 (vw), 1707 (vw), 1682 (w), 1616 (w), 1588 (vw), 1514 (m), 1423 (s), 1376 (vs), 1356 (s), 1264 (w), 1211 (w), 1195 (m), 1140 (w), 1123 (w), 1061 (w), 1020 (m), 972 (m), 835 (s), 753 (w), 716 (w), 694 (vw) cm^{-1}. Raman (1064 nm, 300 mW): $\tilde{\nu}$ = 1616 (41), 1589 (100), 1545 (7), 1515 (9), 1216 (22), 1378 (55), 1357 (58), 1308 (13), 1267 (8), 1211 (6), 1197 (13), 1109 (25), 1054 (15), 1021 (27), 1003 (15), 840 (18), 512 (6), 773 (10), 390 (8), 231 (9), 179 (13), 86 (35) cm^{-1}. MS (FAB$^+$): m/z (%) = 18 (4) [NH_4^+]. MS (FAB$^-$): m/z (%) = 181 (100) [$C_3H_3N_8^-$], 94 (1) [$C_2N_5^-$]. EA ($C_3H_5N_9O_2$, 199.13 g mol^{-1}): calcd C 18.09, H 2.53, N 63.31%; found C 17.77, H 3.23, N 63.18%. Sensitivities (grain size: < 100 µm): IS: > 9 J; FS: > 360 N; ESD: 1.25 J.

Hydroxylammonium 5-(5-nitro-1,2,3-triazolate-4-yl)-1*H*-tetrazole (15b)

15 (350 mg, 1.77 mmol) was dissolved in ethanol (15 mL). A solution of hydroxylamine in water (50% *w*/*w* in H_2O, 0.11 mL, 1.77 mmol) was added and the mixture was stirred for 3 h at room temperature. The precipitate was filtered off to obtain **15b** (215 mg, 1.00 mmol, 56%) as green powder.
DTA (5 °C min^{-1}): T_{melt} = 142 °C, T_{dec} = 168 °C. ^{1}H NMR (400 MHz, DMSO-d_6): δ = 9.37 (br) ppm. ^{13}C{^{1}H} NMR (101 MHz, DMSO-d_6): δ = 151.8, 151.4, 129.9 (C_{tri}) ppm. ^{14}N{^{1}H} NMR (29 MHz, DMSO-d_6): δ = −13 (NO_2), −354 (NH_3OH^+) ppm. IR (ATR): $\tilde{\nu}$ = 3530 (w), 3197 (m), 2947 (m), 2683 (br), 2149 (w), 1641 (w), 1616 (w), 1600 (w), 1502 (vs), 1433 (m), 1385 (s), 1370 (vs), 1340 (m), 1281 (m), 1262 (m), 1227 (s), 1215 (s), 1190 (w), 1154 (w), 1142 (m), 1093 (w), 1056 (w), 1031 (m), 1007 (m), 993 (m), 898 (vw), 838 (vs), 758 (w), 748 (w), 712 (w), 698 (w) cm^{-1}. Raman (1064 nm, 300 mW): $\tilde{\nu}$ = 3136 (5), 2907 (6), 1630 (88), 1560 (8), 1500 (19), 1486 (20), 1436 (46), 1394 (100), 1340 (36), 1289 (12), 1271 (19), 1242 (15), 1138 (20), 1030 (26), 1009 (19), 835 (13), 773 (13), 751 (6), 500 (13), 411 (15), 384 (16), 229 (26), 191 (34), 142 (48), 108 (76), 607 (5), 89 (72) cm^{-1}. MS (FAB$^+$): m/z (%) = 34 (3) [NH_4OH^+]. MS (FAB$^-$): m/z (%) = 181 (98) [$C_3HN_8O_2^-$]. EA ($C_3H_5N_9O_3$, 215.05 g mol^{-1}): calcd C 16.75, H 2.34, N 58.60%; found C 16.57, H 2.85, N 55.09%. Sensitivities (grain size: < 100 µm): IS: 2 J; FS: > 360 N; ESD: 0.6 J.

Guanidinium 5-(5-nitro-1,2,3-triazolate-4-yl)-1*H*-tetrazole (15c)

15 (252 mg, 1.38 mmol) was dissolved in ethanol (20 mL). Bisguanidinium carbonate (125 mg, 0.69 mmol) was added and the mixture was stirred for 2 h at room temperature. The solvent was removed under reduced pressure to obtain **15c** (275 mg, 1.14 mmol, 83%) as yellow powder.
DTA (5 °C min^{-1}): T_{dec} = 220 °C. ^{1}H NMR (400 MHz, DMSO-d_6): δ = 7.01 (s, 6H, NH_2) ppm. ^{13}C{^{1}H} NMR (101 MHz, DMSO-d_6): δ = 158.0 (C(NH$_2$)$_3$), 151.5, 149.1, 126.9 (C_{tri}) ppm. ^{14}N{^{1}H} NMR (29 MHz, DMSO-d_6): δ = −14 (NO$_2$), −309 (NH$_2$) ppm. IR (ATR): $\tilde{\nu}$ = 3476 (m), 3438 (m), 3365 (s), 3254 (m), 3151 (br), 3013 (m), 2937 (w), 2885 (w), 2785 (w), 2718 (w), 2587 (w), 2364 (w), 2222 (w), 1756 (vw), 1652 (vs), 1573 (m), 1518 (vs), 1488 (m), 1436 (w), 1385 (s), 1359 (s), 1245 (w), 1202 (m), 1141 (m), 1099 (m), 1069 (m), 1013 (s), 897 (w), 833 (vs), 750 (w), 708 (w) cm^{-1}. Raman (1064 nm, 300 mW): $\tilde{\nu}$ = 1626 (100), 1518 (7), 1491 (20), 1438 (13), 1386 (45), 1325 (21), 1250 (9), 1203 (11), 1115 (27), 1013 (37), 837 (12), 546 (6), 509 (5), 383 (5), 152 (28), 122 (21), 93 (24) cm^{-1}. MS (FAB$^+$): m/z (%) = 60 (44) [CH$_6$N$_3^+$], 57 (4) [CH$_3$N$_3^+$]. MS (FAB$^-$): m/z (%) = 181 (100) [C$_3$HN$_8$O$_2^-$]. EA (C$_4$H$_7$N$_{11}$O$_2$, 241.18 g mol^{-1}): calcd C 19.92, H 2.93, N 63.89%; found C 20.71, H 3.03, N 65.23%. Sensitivities (grain size: < 100 µm): IS: > 20 J; FS: > 360 N; ESD: 1.5 J.

Aminoguanidinium 5-(5-nitro-1,2,3-triazolate-4-yl)-1*H*-tetrazole (15d)

15 (250 mg, 1.34 mmol) was suspended in ethanol (20 mL). Aminoguanidinium bicarbonate (183 mg, 1.35 mmol) was added and the mixture was stirred for 18 h at room temperature. The precipitate was filtered off and air-dried to obtain **15d** (252 mg, 1.51 mmol, 73%) as yellow powder.
DTA (5 °C min^{-1}): T_{melt} = 198 °C, T_{dec} = 214 °C. ^{1}H NMR (400 MHz, DMSO-d_6): δ = 8.79 (s, 2H, NHNH_2), 7.18 (m, 4H, C(NH_2)$_2$), 5.03 (br, 1H, NH) ppm. ^{13}C{^{1}H} NMR (101 MHz, DMSO-d_6): δ = 158.9 (C(NH$_2$)$_2$), 151.5, 149.7, 127.7 (C_{tri}) ppm. ^{14}N{^{1}H} NMR (29 MHz, DMSO-d_6): δ = −20 (NO$_2$) ppm. IR (ATR): $\tilde{\nu}$ = 3448 (w), 3335 (m), 3282 (m), 3234 (m), 3210 (m), 3071 (v), 3028 (m), 2885 (w), 2825 (w), 2770 (w), 2718 (w), 2675 (w), 1661 (vs), 1623 (s), 1548 (s), 1502 (m), 1494 (m), 1449 (w), 1441 (m), 1381 (s), 1358 (s), 1316 (m), 1274 (s), 1257 (m), 1213 (w), 1190 (m), 1138 (w), 1120 (w), 1105 (m), 1067 (m), 828 (vs), 769 (vw), 750 (m), 713 (vw), 658 (vw) cm^{-1}. Raman (1064 nm, 300 mW): $\tilde{\nu}$ = 1628 (100), 1548 (5), 1524 (6), 1495 (16), 1438 (15), 1429 (8), 1381 (77), 1320 (18), 1277 (5), 1262 (10), 1191 (17), 1121 (16), 1109 (38), 1010 (28), 999 (13), 968 (12), 832 (10), 769 (8), 832 (10), 769 (8), 516 (6), 508 (6), 404 (5), 380 (8), 369 (6), 231 (11) cm^{-1}. MS (FAB$^+$): m/z (%) = 75 (33) [CH$_7$N$_4^+$], 55 (10) [CHN$_3^+$], 43 (7) [CH$_3$N$_2^+$]. MS (FAB$^-$): m/z (%) = 181 (74) [C$_3$HN$_8$O$_2^-$], 112 (40) [C$_2$N$_4$O$_2^-$], 69 (10) [CHN$_4^-$]. EA (C$_4$H$_8$N$_{12}$O$_2$, 256.19 g mol^{-1}):

calcd C 18.75, H 3.15, N 65.61%; found C 19.25, H 3.36, N 63.28%. Sensitivities (grain size: $< 100\,\mu m$): IS: 10 J; FS: > 360 N; ESD: 1.0 J.

Triaminoguanidinium 5-(5-nitro-1,2,3-triazolate-4-yl)-1*H*-tetrazole (15e)

15f (287 mg, 1.30 mmol) was dissolved in a minimal amount of water. Triaminoguanidinium chloride (180 mg, 1.28 mmol) was added and the mixture was stirred for 3 h at room temperature until the desired product precipitated. It was filtered off and air-dried to obtain **15e** (284 mg, 0.99 mmol, 76%) as green powder.
DTA (5 °C min^{-1}): $T_{melt} = 150$ °C, $T_{dec} = 174$ °C. ^{1}H NMR (400 MHz, DMSO-d_6): $\delta = 8.60$ (s, 3H, N*H*NH$_2$), 4.56 (br, 6H, N*H*$_2$) ppm. ^{13}C{^{1}H} NMR (101 MHz, DMSO-d_6): $\delta = 159.1$ (*C*(NH$_2$)$_2$), 151.6, 148.8, 126.5 (C_{tri}) ppm. ^{14}N{^{1}H} NMR (29 MHz, DMSO-d_6): $\delta = -14$ (*N*O$_2$) ppm. IR (ATR): $\tilde{\nu} = 3321$ (w), 3298 (m), 3200 (m), 3016 (w), 2687 (w), 1878 (vw), 1683 (s), 1659 (m), 1613 (m), 1596 (m), 1524 (s), 1509 (s), 1411 (w), 1380 (vs), 1325 (s), 1286 (w), 1267 (vw), 1244 (w), 1217 (w), 1188 (m), 1138 (m), 1112 (m), 1060 (m), 1025 (m), 1000 (m), 958 (vs), 859 (w), 832 (s), 767 (w), 751 (w), 715 (vw), 703 (vw), 664 (vw) cm^{-1}. Raman (1064 nm, 300 mW): $\tilde{\nu} = 3238$ (7), 1614 (100), 1528 (12), 1481 (10), 1466 (9), 1426 (21), 1420 (21), 1381 (99), 1327 (27), 1268 (11), 1247 (12), 1206 (5), 1193 (8), 1135 (16), 1089 (30), 1016 (7), 990 (18), 860 (8), 833 (26), 768 (6), 752 (5), 639 (5), 510 (10), 501 (9), 401 (8), 382 (9), 373 (6), 219 (5) cm^{-1}. MS (FAB$^+$): m/z (%) = 105 (99) [CH$_9$N$_6^+$]. MS (FAB$^-$): m/z (%) = 181 (100) [C$_3$HN$_8$O$_2^-$]. EA (C$_4$H$_8$N$_{12}$O$_2$, 256.19 g mol^{-1}): calcd C 16.79, H 3.52, N 68.51%; found C 16.85, H 3.34, N 66.04%. Sensitivities (grain size: 100–500 µm): IS: 8 J; FS: > 360 N; ESD: 0.5 J.

Potassium 5-(5-nitro-1,2,3-triazolate-4-yl)-1*H*-tetrazole (15f)

15 (604 mg, 3.32 mmol) was dissolved in ethanol (25 mL). K$_2$CO$_3$ (205 mg, 1.48 mmol) was added and the mixture was stirred for 2 h at room temperature. The precipitate was filtered off to obtain **15f** (487 mg, 2.21 mmol, 67%) as yellow powder.
DTA (5 °C min^{-1}): $T_{dec1} = 233$ °C, $T_{dec2} = 301$ °C. ^{13}C{^{1}H} NMR (101 MHz, DMSO-d_6): $\delta = 151.5$, 148.8, 126.5 (C_{tri}) ppm. ^{14}N{^{1}H} NMR (29 MHz, DMSO-d_6): $\delta = -15$ (*N*O$_2$) ppm. IR (ATR): $\tilde{\nu} = 3107$ (w), 2996 (w), 2900 (w), 2798 (w), 1893 (vw), 1651 (vw), 1619 (m), 1520 (s), 1505 (vs), 1483 (m), 1471 (m), 1414 (w), 1384 (vs), 1343 (m), 1327 (m), 1261 (w), 1230 (w), 1184 (m), 1139 (m), 1104 (m), 1064 (m), 1019 (vw), 1000 (m), 987 (m), 887 (m), 835 (vs), 752 (m), 722 (vw), 701 (w) cm^{-1}. Raman (1064 nm, 300 mW): $\tilde{\nu}$ = 1620 (100), 1506 (5), 1472 (16), 1388 (95), 1345 (13), 1326 (16), 1263 (11), 1231 (6), 1186 (10), 1139 (5), 1103 (18), 1093 (21), 1061 (6), 1021 (5), 995 (17), 837 (13) cm^{-1}. MS (FAB$^+$): m/z (%) = 39 (16) [K$^+$]. MS (FAB$^-$): m/z (%) = 219 (7) [C$_3$KN$_8$O$_2^-$], 181 (100)

[$C_3HN_8O_2^-$]. EA ($C_3HKN_8O_2$, 220.19 g mol^{-1}): calcd C 16.36, H 0.46, N 50.89%; found C 16.53, H 0.88, N 49.36%. Sensitivities (grain size: < 100 µm): IS: 15 J; FS: 324 N; ESD: 0.75 J.

Bishydroxylammonium 1,2-bis(5-(tetrazolate-5-yl)-1,2,3-triazol-4-yl)diazene sesquihydrate (16-2b·1.5 H_2O)

16·2 H_2O (250 mg, 0.74 mmol) was suspended in a mixture of ethanol (50 mL) and water (50 mL) under heating. Hydroxylamine (50% *w*/*w*, 0.1 mL, 1.63 mmol, 2.3 eq.) was added and the suspension was stirred under heating until it became a clear solution. The solvent was partly boiled away over night at room temperature. The precipitate was filtered off and dried at air to obtain **16-2b**·1.5 H_2O (193 mg, 0.49 mmol, 66%) as a yellow solid.
DTA (5 °C min^{-1}): T_{dec} = 163 °C. ^{1}H NMR (400 MHz, DMSO-d_6): δ = 7.99 (br) ppm. $^{13}C\{^1H\}$ NMR (101 MHz, DMSO-d_6): δ = 154.5, 149.6, 127.4 (C_{tri}) ppm. IR (ATR): $\tilde{\nu}$ = 3113 (m), 3023 (m), 2950 (m), 2848 (m), 2699 (s), 2633 (m), 2591 (m), 2359 (w), 1848 (w), 1776 (vw), 1627 (w), 1597 (w), 1570 (w), 1526 (m), 1494 (w), 1386 (vs), 1318 (vw), 1296 (vw), 1217 (m), 1206 (m), 1181(w), 1157(w), 1112 (vw), 1098 (vw), 1079 (w), 1037 (m), 992 (vs), 951 (m), 908 (m), 843 (m), 771 (w), 734 (w), 703 (w) cm^{-1}. Raman (1064 nm, 300 mW): $\tilde{\nu}$ = 1635 (55), 1500 (9), 1470 (6), 1437 (100), 1336 (89), 1226 (33), 1144 (2), 1114 (2), 1101 (2), 1082 (14), 1055 (5), 1008 (2), 973 (4), 909 (10), 762 (3), 561 (2), 304 (4) cm^{-1}. MS (FAB$^+$): *m*/*z* = 33.0 [NH_2OH^+]. MS (FAB$^-$): *m*/*z* (%) = 299.1 (10) [$C_6H_3N_{16}^-$]. EA ($C_6H_{10}N_{18}O_2 \cdot 1.5\,H_2O$, 393.29 g mol^{-1}): calcd C 18.32, H 3.33, N 64.11%; found C 18.37, H 3.52, N 61.67%. Sensitivities (grain size: < 100 µm): IS: > 8 J; FS: > 360 N; ESD: 0.2 J.

Bisguanidinium 1,2-bis(5-(tetrazolate-5-yl)-1,2,3-triazol-4-yl)diazene sesquihydrate (16-2c·1.5 H_2O)

16·2 H_2O (276 mg, 0.82 mmol) was suspended in water (100 mL) under heating. Bisguanidinium carbonate (148 mg, 0.82 mmol, 1 eq) was added and the suspension was stirred under heating until it became a clear solution. The solvent was partly boiled away over night at room temperature. The precipitate was filtered off and dried at air to obtain **16-2c**·1.5 H_2O (118 mg, 0.26 mmol, 32%) as a yellow solid.
DTA (5 °C min^{-1}): T_{dec} = 192 °C. ^{1}H NMR (400 MHz, DMSO-d_6): δ = 7.17 (s, 12H, NH_2), 5.04 (br, 2H, NH) ppm. $^{13}C\{^1H\}$ NMR (101 MHz, DMSO-d_6): δ = 158.8 ($C(NH_2)_3$), 155.1, 150.2, 126.3 (C_{tri}) ppm. IR (ATR): $\tilde{\nu}$ = 3484 (m), 3455 (s), 3339 (m), 2754 (w), 2643 (w), 2552 (w), 2464 (w), 2349 (vw), 2067 (vw), 1994 (vw) 1966 (vw), 1938 (vw), 1925 (vw), 1905 (vw), 1689 (vs), 1642 (vs), 1598 (m), 1574 (w), 1550 (w), 1445 (w), 1380 (m), 1353 (m), 1302 (vw), 1265 (w), 1207 (w), 1191 (w), 1157 (m), 1148 (m), 1081 (w), 1040 (w), 994

(s), 977 (m), 912 (vw), 815 (vw), 801 (vw), 766 (w), 727 (w), 720 (w), 698 (vw), 660 (vw) cm^{-1}. Raman (1064 nm, 300 mW): $\tilde{\nu}$ = 1607 (84), 1547 (3), 1463 (9), 1411 (63), 1373 (100), 1351 (96), 1306 (4), 1265 (3), 1222 (3), 1202 (11), 1161 (4), 1132 (22), 1085 (16), 1042 (2), 1015 (8), 994 (6), 912 (8), 769 (4), 712 (2), 538 (2), 413 (4), 301 (4) cm^{-1}. MS (ESI^-): m/z (%) = 299.1 (100) [$C_6H_3N_{16}^-$]. EA ($C_8H_{14}N_{22} \cdot 1.5\,H_2O$, 445.37 g mol^{-1}): calcd C 21.57, H 3.85, N 69.19%; found C 21.59, H 3.92, N 63.22%. Sensitivities (grain size: < 100 µm): IS: 40 J; FS: > 360 N; ESD: 1.2 J.

Bisaminoguanidinium 1,2-bis(5-(tetrazolate-5-yl)-1,2,3-triazol-4-yl)diazene (16-2d)

16·2 H_2O (250 mg, 0.74 mmol) was suspended in water (100 mL) under heating. Aminoguanidinium bicarbonate (201 mg, 1.48 mmol, 2 eq) was added and the suspension was stirred under heating until it became a clear solution. The solvent was partly boiled away over night at room temperature. The precipitate was filtered off and dried at air to obtain **16-2d** (252 mg, 0.56 mmol, 76%) as a yellow solid.
DTA (5 °C min^{-1}): T_{dec} = 192 °C. ^{1}H NMR (400 MHz, DMSO-d_6): δ = 8.71 (s, 2H, CN*H*), 7.35 (s, 4H, CNH_2), 6.90 (s, 4H, CNH_2), 4.71 (br, 6H, N*H*, NNH_2) ppm. $^{13}C\{^1H\}$ NMR (101 MHz, DMSO-d_6): δ = 158.8 (CNHNH$_2$), 154.9, 149.6, 125.9 (C_{tri}) ppm. IR (ATR): $\tilde{\nu}$ = 3420 (w), 3329 (m), 3289 (m), 3170 (m), 3015 (m), 2857 (w), 2748 (w), 1887 (vw), 1668 (vs), 1591 (m), 1553 (w), 1534 (vw), 1502 (vw), 1482 (vw), 1454 (vw), 1415 (vw), 1385 (m), 1357 (w), 1308 (vw), 1272 (vw), 1201 (w), 1145 (w), 1117 (w), 1094 (w), 1073 (m), 1037 (m), 992 (m), 981 (m), 926 (m), 895 (m), 764 (vw), 730 (w), 682 (vw) cm^{-1}. Raman (1064 nm, 300 mW): $\tilde{\nu}$ = 1627 (29), 1591 (24), 1494 (10), 1477 (29), 1438 (100), 1360 (46), 1340 (57), 1300 (20), 1221 (29), 1146 (14), 1110 (19), 1000 (9), 971 (8), 906 (11), 419 (3) cm^{-1}. MS (FAB^+) m/z (%) = 75.2 (9) [$CH_7N_4^+$]. MS (FAB^-) m/z (%) = 299.1 (3) [$C_6H_3N_{16}^-$]. EA ($C_8H_{16}N_{24}$, 448.37 g mol^{-1}): calcd C 21.43, H 3.60, N 74.97%; found C 21.21, H 3.93, N 70.03%. Sensitivities (grain size: < 100 µm): IS: 12.5 J; FS: > 360 N; ESD 0.3 J.

Potassium triaminoguanidinium 1,2-bis(5-(tetrazolate-5-yl)-1,2,3-triazol-4-yl)diazene semihydrate (16-e,f·0.5 H_2O)

16-2f·2 H_2O (250 mg, 0.61 mmol) was dissolved in water (30 mL) under heating. Triaminoguanidinium chloride (171 mg, 1.22 mmol, 2 eq.) was added and the solution was stirred for several hours. The solvent was partly boiled away over night at room temperature. The precipitate was filtered off and dried at air to obtain **16-e,f**·0.5 H_2O (123 mg, 0.27 mmol, 44%) as a yellow solid.
DTA (5 °C min^{-1}): T_{dec} = 145 °C. ^{1}H NMR (400 MHz, DMSO-d_6): δ = 8.62 (s, 3H, N*H*), 7.27

(br, 8H, NH_2, CNH) ppm. ^{13}C{^{1}H} NMR (101 MHz, DMSO-d_6): δ = 159.0 (C(NHNH$_2$)$_3$), 154.4, 149.0, 126.2 (C_{tri}) ppm. IR (ATR): $\tilde{\nu}$ = 3358 (w), 3287 (w), 3028 (w), 2844 (w), 2751 (w), 2681 (w), 2681 (w), 2637 (w), 2588 (w), 1823 (vw), 1683 (w), 1626 (w), 1583 (vw), 1514 (w), 1491 (w), 1430 (vw), 1386 (s), 1320 (vw), 1275 (vw), 1234 (w), 1212 (w), 1165 (vw), 1152 (w), 1106 (vw), 1075 (w), 1035 (m), 992 (vs), 942 (m), 769 (m), 753 (m), 685 (vw) cm^{-1}. Raman (1064 nm, 300 mW): $\tilde{\nu}$ = 1635 (27), 1589 (4), 1501 (7), 1468 (35), 1439 (100), 1372 (12), 1342 (79), 1314 (9), 1233 (25), 1143 (8), 1112 (3), 1078 (7), 1056 (4), 972 (5), 915 (7) cm^{-1}. MS (FAB$^+$) m/z (%) = 105.1 (12) [$CH_{11}N_6^+$], 39.0 [K$^+$]. MS (FAB$^-$): m/z (%) = 299.1 (20) [$C_6H_3N_{16}^-$]. EA ($C_7H_{11}KN_{22} \cdot 0.5\,H_2O$, 451.42 g mol^{-1}): calcd C 19.00, H 2.51, N 69.65%; found C 19.14, H 2.65, N 56.98%. Sensitivities (grain size: < 100 µm): IS: > 40 J; FS: > 360 N; ESD: 0.75 J.

Bispotassium 1,2-bis(5-(tetrazolate-5-yl)-1,2,3-triazol-4-yl)diazene dihydrate (16-2f·2 H_2O)

16·2 H_2O (500 mg, 1.49 mmol) was suspended in water (30 mL) under heating. Potassium hydroxide (167 mg, 2.98 mmol, 2 eq.) was added and the suspension was stirred under heating until it became a clear solution. The solvent was partly boiled away over night at room temperature. The precipitate was filtered off and dried at air to obtain **16-2f**·2 H_2O as a yellow solid (522 mg, 1.27 mmol, 85%).
DTA (5 °C min^{-1}): T_{dehyd} = 113 °C, T_{dec} = 178 °C. ^{1}H NMR (400 MHz, DMSO-d_6): δ = 6.53 (br, 2H, NH) ppm. ^{13}C{^{1}H} NMR (101 MHz, DMSO-d_6): δ = 154.0, 147.9, 125.7 (C_{tri}) ppm. IR (ATR): $\tilde{\nu}$ = 3608 (vw), 3436 (w), 3279 (w), 3017 (w), 2839 (w), 2755 (w), 2688 (w), 2628 (w), 2584 (w), 2360 (w), 1827 (vw), 1622 (w), 1506 (w), 1486 (w), 1469 (w), 1384 (s), 1344 (w), 1316 (vw), 1287 (vw), 1230 (w), 1202 (w), 1172 (w), 1146 (m), 1108 (vw), 1071 (w), 1058 (w), 1034 (m), 1025 (m), 995 (vs), 920 (m), 772 (w), 753 (w), 735 (m), 686 (vw) cm^{-1}. Raman (1064 nm, 300 mW): $\tilde{\nu}$ = 1631 (40), 1590 (22), 1501 (11), 1435 (100), 1405 (24), 1340 (93), 1231 (32), 1136 (9), 1094 (7), 1071 (16), 1036 (4), 998 (7), 969 (4), 913 (9) cm^{-1}. MS (FAB$^+$) m/z (%) = 39.0 (75) [K$^+$]. MS (FAB$^-$) m/z (%) = 299.1 (13) [$C_6H_3N_{16}^-$]. EA ($C_6H_2K_2N_{16} \cdot 2\,H_2O$, 412.41 g mol^{-1}): calcd C 17.47, H 1.47, N 54.34%; found C 17.54, H 1.58, N 51.11%. Sensitivities (grain size: < 100 µm): IS: 40 J; FS: > 360 N; ESD: 0.75 J.

Tetrapotassium 1,2-bis(5-(tetrazolate-5-yl)-1,2,3-triazolate-4-yl)diazene semihydrate (16-4f·0.5 H_2O)

16·2 H_2O (417 mg, 1.24 mmol) was suspended in water (30 mL) under heating. Potassium hydroxide (279 mg, 4.98 mmol, 4 eq.) was added and the suspension was stirred under

heating until it became a clear solution. The solvent was partly boiled away over night at room temperature. The precipitate was filtered off and dried at air to obtain **16-4f**·0.5 H_2O (539 mg, 1.17 mmol, 94%) as a yellow solid.
DTA (5 °C min^{-1}): T_{dec} = 355 °C. $^{13}C\{^1H\}$ NMR (101 MHz, D_2O): δ = 153.5, 153.2, 133.2 (C_{tri}) ppm. IR (ATR): $\tilde{\nu}$ = 3383 (vw), 1670 (vw), 1654 (vw), 1599 (w), 1467 (s), 1380 (w), 1343 (m), 1286 (m), 1174 (m), 1144 (m), 1124 (w), 1060 (m), 1024 (m), 994 (w), 775 (w), 733 (vs), 711 (w), 657 (w), 626 (s), 600 (w), 587 (w), 570 (m) cm^{-1}. Raman (1064 nm, 300 mW): $\tilde{\nu}$ = 1638 (37), 1612 (16), 1502 (16), 1492 (17), 1469 (100), 1432 (21), 1404 (8), 1369 (56), 1344 (69), 1329 (31), 1298 (10), 1244 (7), 1200 (14), 1182 (5), 1151 (4), 1125 (6), 980 (14), 903 (8), 621 (7), 353 (4) cm^{-1}. EA ($C_6K_4N_{16} \cdot 0.5\,H_2O$, 461.58 g mol^{-1}): calcd C 15.61, H 0.22, N 48.55%; found C 16.36, H 0.63, N 47.60%. Sensitivities (grain size: < 100 µm): IS: > 40 J; FS: > 360 N; ESD: 1.5 J.

5.5 References

[1] T. M. Klapötke, *Chemistry of High-Energy Materials*, 3rd ed., de Gruyter, Berlin, Germany, **2015**.

[2] J. Akhavan, *The Chemistry of Explosives*, 2nd ed., RSC, Cambridge, United Kingdom, **2004**.

[3] J. P. Agrawal, *High Energy Materials, Propellants Explosives and Pyrotechnics*, Wiley-VCH, Weinheim, Germany, **2010**.

[4] A. F. Holleman, E. Wiberg, N. Wiberg, *Lehrbuch der Anorganischen Chemie*, 102nd ed., de Gruyter, Berlin, Germany, **2007**.

[5] T. M. Klapötke, J. Stierstorfer, in *Green Energetic Materials* (Ed.: T. Brinck), Wiley, Hoboken, NJ (USA), **2014**, pp. 133–178.

[6] A. A. Dippold, T. M. Klapötke, *Chem. Asian J.* **2013**, *8*, 1463–1471.

[7] M. Dachs, A. A. Dippold, J. Gaar, M. Holler, T. M. Klapötke, *Z. Anorg. Allg. Chem.* **2013**, *639*, 2171–2180.

[8] D. Izsák, T. M. Klapötke, S. Reuter, *Eur. J. Inorg. Chem.* **2013**, 5641–5651.

[9] A. A. Dippold, D. Izsák, T. M. Klapötke, *Chem. Eur. J.* **2013**, *19*, 12042–12051.

[10] R. Wang, H. Xu, Y. Guo, R. Sa, J. M. Shreeve, *J. Am. Chem. Soc.* **2010**, *132*, 11904–11905.

[11] A. A. Dippold, T. M. Klapötke, M. Oswald, *Dalton Trans.* **2013**, *42*, 11136–11145.

[12] C. Bian, K. Wang, L. Liang, M. Zhang, C. Li, Z. Zhou, *Eur. J. Inorg. Chem.* **2014**, 6022–6030.

[13] H. Tanaka, T. Toda (Toyo Kasei Kogyo Co. Ltd., Osaka), WO20070133323 A1 **2007**.

[14] A. A. Dippold, D. Izsák, T. M. Klapötke, C. Pflüger, *Chem. Eur. J.* **2016**, *22*, 1768–1778.

[15] D. Izsák, T. M. Klapötke, C. Pflüger, *Dalton Trans.* **2015**, *44*, 17054–17063.

[16] H. Gao, J. M. Shreeve, *Chem. Rev.* **2011**, *111*, 7377–7436.

[17] R. P. Singh, R. D. Verma, D. T. Meshri, J. M. Shreeve, *Angew. Chem., Int. Ed.* **2006**, *45*, 3584–3601; *Angew. Chem.* **2006**, *118*, 3664–3682.

[18] K. Wang, D. A. Parrish, J. M. Shreeve, *Chem. Eur. J.* **2011**, *17*, 14485–14492.

[19] P. F. Pagoria, G. S. Lee, A. R. Mitchell, R. D. Schmidt, *Thermochim. Acta* **2002**, *384*, 187–204.

[20] A. W. Horst, P. J. Baker, B. M. Rice, P. J. Kaste, J. W. Colburn, J. J. Hare, *ARL-TR-2584*, Army Research Labratory, Aberdeen, Maryland, **2001**.

[21] L. H. Caveny, *ARLCD-CR-80016*, US Army Armament Research and Development Command, Dover, New Jersey, **1980**.

[22] A. A. Juhasz, G. H. Lushington, *34th AIAA/ASME/SAE/ASEE Joint Propulsion Conference & Exhibit*, Cleveland, Ohio, July 13-15, **1998**.

[23] A. C. Hordijk, C. A. van Driel, M. J. G. Bakker, *23rd International Symposium on Ballistics*, Tarragona, Spain, April 16-20, **2007**, pp. 449–456.

[24] H. J. Maag, G. Klingenberg, *Propellants, Explos., Pyrotech.* **1996**, *21*, 1–7.

[25] R. S. Damse, A. Singh, H. Singh, *Propellants, Explos., Pyrotech.* **2007**, *32*, 52–60.

[26] R. R. Sanghavi, P. J. Kamale, M. A. R. Shaikh, S. D. Shelar, K. S. Kumar, A. Singh, *J. Hazard. Mater.* **2007**, *143*, 532–534.

[27] R. S. Damse, H. Singh, *Defence Sci.* **2000**, *50*, 75–81.

[28] V. Rosenband, Y. Schneebaum, A. Gany, *Wear* **1998**, *221*, 109–115.

[29] N. Fischer, D. Izsák, T. M. Klapötke, S. Rappenglück, J. Stierstorfer, *Chem. Eur. J.* **2012**, *18*, 4051–4062.

[30] D. E. Chavez, B. C. Tappan, B. A. Mason, D. Parrish, *Propellants, Explos., Pyrotech.* **2009**, *34*, 475–479.

[31] A. Bondi, *J. Phys. Chem.* **1964**, *68*, 441–451.

[32] F. H. Allen, O. Kennard, D. G. Watson, L. Brammer, A. G. Orpen, R. Taylor, *J. Chem. Soc., Perkin Trans. 2* **1987**, *0*, S1–S19.

[33] Test methods according to the *UN Manual of Test and Criteria, Recommendations on the Transport of Dangerous Goods*, United Nations Publication, New York, Geneva, 4th revised ed., **2003**: Impact: Insensitive $>40\,\mathrm{J}$, less sensitive $\geq 35\,\mathrm{J}$, sensitive $\geq 4\,\mathrm{J}$, very sensitive $\leq 3\,\mathrm{J}$; Friction: Insensitive $>360\,\mathrm{N}$, less sensitive $= 360\,\mathrm{N}$, sensitive $<360\,\mathrm{N}$ a. $>80\,\mathrm{N}$, very sensitive $\leq 80\,\mathrm{N}$, extremely sensitive $\leq 10\,\mathrm{N}$.

[34] NATO, *Standardization Agreement 4489 (STANAG 4489), Explosives, Impact Sensitivity Tests* **1999**.

[35] NATO, *Standardization Agreement 4487 (STANAG 4487), Explosives, Friction Sensitivity Tests* **2002**.

[36] Schaffler GmbH & Co. KG, http://www.schaffler.co.at (accessed December 29, 2012).

[37] J. W. Ochterski, G. A. Petersson, J. J. A. Montgomery, *J. Chem. Phys.* **1996**, *104*, 2598–2619.

[38] J. J. A. Montgomery, M. J. Frisch, J. W. Ochterski, G. A. Petersson, *J. Chem. Phys.* **2000**, *112*, 6532–6542.

[39] M. J. Frisch, G. W. Trucks, H. B. Schlegel, G. E. Scuseria, M. A. Robb, J. R. Cheeseman, G. Scalmani, V. Barone, B. Mennucci, G. A. Petersson, H. Nakatsuji, M. Caricato, X. Li, H. P. Hratchian, A. F. Izmaylov, J. Bloino, G. Zheng, J. L. Sonnenberg, M. Hada, M. Ehara, K. Toyota, R. Fukuda, J. Hasegawa, M. Ishida, T. Nakajima, Y. Honda, O. Kitao, H. Nakai, T. Vreven, J. J. A. Montgomery, J. E. Peralta, F. Ogliaro, M. Bearpark, J. J. Heyd, E. Brothers, K. N. Kudin, V. N. Staroverov, R. Kobayashi, J. Normand, K. Raghavachari, A. Rendell, J. C. Burant, S. S. Iyengar, J. Tomasi, M. Cossi, N. Rega, J. M. Millam, M. Klene, J. E. Knox, J. B. Cross, V. Bakken, C. Adamo, J. Jaramillo, R. Gomperts, R. E. Stratmann, O. Yazyev, A. J. Austin, R. Cammi, C. Pomelli, J. W. Ochterski, R. L. Martin, K. Morokuma, V. G. Zakrzewski, G. A. Voth, P. Salvador, J. J. Dannenberg, S. Dapprich, A. D.

Daniels, O. Farkas, J. B. Foresman, J. V. Ortiz, J. Cioslowski, D. J. Fox, Gaussian 09, Revision A.02, Inc., Wallingford CT, **2009**.

[40] B. M. Rice, S. V. Pai, J. Hare, *Combust. Flame* **1999**, *118*, 445–458.

[41] B. M. Rice, J. J. Hare, *J. Phys. Chem. A* **2002**, *106*, 1770–1783.

[42] E. F. C. Byrd, B. M. Rice, *J. Phys. Chem. A* **2006**, *110*, 1005–1013.

[43] P. J. Linstrom, W. G. Mallard, *NIST Standard Reference Database Number 69*, http://webbook.nist.gov/chemistry (accessed December 31, 2012).

[44] J. D. Cox, D. D. Wagman, V. A. Medvedev, *CODATA Key Values for Thermodynamics*, Hemisphere Publishing Corp., New York, **1984**.

[45] F. Trouton, *Philos. Mag.* **1884**, *18*, 54–57.

[46] M. S. Westwell, M. S. Searle, D. J. Wales, D. H. Williams, *J. Am. Chem. Soc.* **1995**, *117*, 5013–5015.

[47] H. D. B. Jenkins, H. K. Roobottom, J. Passmore, L. Glasser, *Inorg. Chem.* **1999**, *38*, 3609–3620.

[48] M. Sućeska, Explo5 program, 6.02 ed., Zagreb, Croatia, **2014**.

[49] C. Xue, J. Sun, B. Kang, Y. Liu, X. Liu, G. Song, Q. Xue, *Propellants, Explos., Pyrotech.* **2010**, *35*, 333–338.

[50] A. Hammerl, M. A. Hiskey, G. Holl, T. M. Klapötke, K. Polborn, J. Stierstorfer, J. J. Weigand, *Chem. Mater.* **2005**, *17*, 3784–3793.

[51] Fraunhofer Institut für Chemische Technologie, *ICT Thermodynamic Data Base*, Pfinztal, Germany, **1998-2000**.

Isolation of a Moderately Stable but Sensitive Zwitterionic Diazonium Tetrazolyl-1,2,3-triazolate

T. M. Klapötke, B. Krumm, and C. Pflüger

J. Org. Chem. **2016**, *81*, 6123–6127.

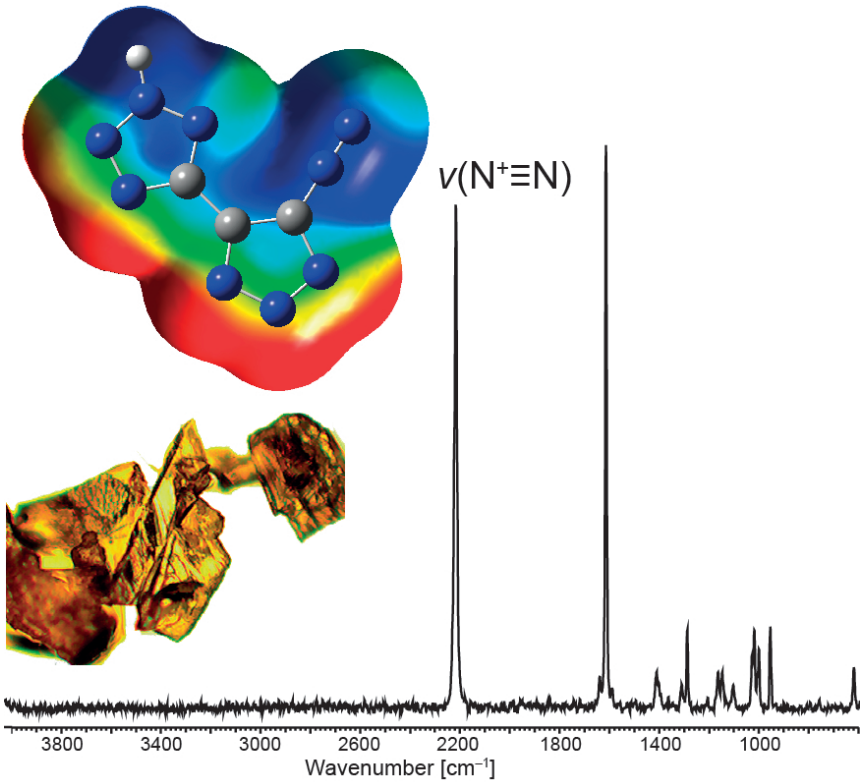

Isolation of a Moderately Stable but Sensitive Zwitterionic Diazonium Tetrazolyl-1,2,3-triazolate

T. M. Klapötke, B. Krumm, and C. Pflüger
J. Org. Chem. **2016**, *81*, 6123–6127.

Abstract

An unexpected formation of a diazonium compound was observed by nitration of an amino substituted triazolyl tetrazole with mixed acid. The crystal structure determination revealed a zwitterionic diazonium tetrazolyl-1,2,3-triazolate, whose constitution was supported by NMR and vibrational spectroscopic analysis. The thermal stability and sensitivity toward impact and friction, were determined. In contrast, diazotriazoles are rather unstable and are mainly handled in solution and/or low temperatures, which is not the case for this diazonium tetrazolyl-1,2,3-triazolate, being stable as a solid at ambient temperature.

6.1 Introduction

Diazoazoles have found wide application as key intermediates in various coupling reactions but also in biological applications.[1] Furthermore, diazonium compounds are important reagents such as for the conversion into fluoroaromatic compounds according to Balz-Schiemann,[2,3] or for the preparation of azo compounds in the synthetic dye industry.
The formation of diazonium compounds was first reported in 1858 by Griess, who has subsequently discovered various reactions of this compound class.[4,5] The most common method for the synthesis of diazonium compounds is the diazotation of aromatic amines with in situ generated nitrous acid from sodium nitrite and a mineral acid, which was developed in 1875 by Meyer.[5]
Several years later, in 1892, the first diazoazole, the highly sensitive diazotetrazole, was synthesized by Thiele, who reported explosions during the synthesis in aqueous solutions at 0 °C.[6] The isolation of 3-diazoindazole by Bamberger in 1899 initiated a considerable interest in the properties and reactivity of diazoindoles and diazopyrroles.[7] Furthermore, diazotriazoles, -imidazoles and -pyrazoles were investigated. Especially, the improvement of techniques for isolation and purification had a great influence in the chemistry of diazoazoles in the second half of the 20th century. On the other hand, diazonium moieties are known to be highly energetic and detonations can be initiated by shock, heat or exposure to concentrated acids, and therefore, they are often not isolated for safety reasons but directly used in further reactions.[8,9] The stability and reactivity of diazoazoles depend strongly on the mutual influence of the azole ring and the diazo moiety.[1] Especially, the properties

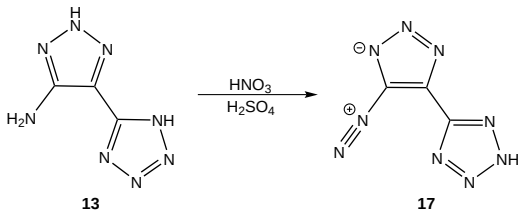

Scheme 6.1: Nitration of 5-(5-amino-2*H*-1,2,3-triazol-4-yl)-1*H*-tetrazole (**13**) with mixed acid to form the diazonium 1,2,3-triazolate (**17**).

differ according to the azole rings because they range from an electron-rich azole, such as pyrrole, to very electron-deficient azoles, such as tetrazole.
Pyrazole-3-diazonium derivatives are the most extensive studied diazoazoles in regard of stability and reactivity.[10] The more energetic diazo 1,2,3- and 1,2,4-triazoles are much less studied because of their lower stability, and hence difficulties in isolation and safe handling (mainly only in solution) remain challanges.[8] The resonance stabilization of the diazoazoles determines their stability and reactivity due to the delocalization of the negative charge over the azole ring.[1,11] Two crystal structures of diazo 1,2,4-triazoles[12,13] are reported, showing the zwitterionic character of the diazotriazole in accordance to other diazoazole structures.[14] However, to the best of our knowledge, no crystal structures of diazo-1,2,3-triazoles have been reported so far.

6.2 Results and Discussion

6.2.1 Synthesis

5-(5-Amino-2*H*-1,2,3-triazol-4-yl)-1*H*-tetrazole (**13**) was synthesized in five steps as reported recently by us starting from commercially available benzyl chloride.[15] The nitration of **13** with nitric acid (100%, traces of NO_2) in concentrated sulfuric acid at 5 °C and stirring for 12 h at room temperature did not yield the expected corresponding nitramine ($RNHNO_2$, but the inner diazonium salt **17** (Scheme 6.1). This could be due to the presence of NO_2 in the nitration mixture.
The synthesis of the diazonium salt by direct diazotation in concentrated sulfuric acid using sodium nitrite was not successful. The use of another mineral acid or diluted sulfuric acid was not possible due to the low solubility of the amine **13**.

6.2.2 Crystal structure

The formation of the inner diazonium salt 5-diazonium-4-(2*H*-tetrazol-5-yl)-1,2,3-triazolate (**17**) is proven by its crystal structure showing a deprotonated triazole ring (Figure 6.1). It crystallizes as a monohydrate in the monoclinic space group $P2_1/n$ with four formula

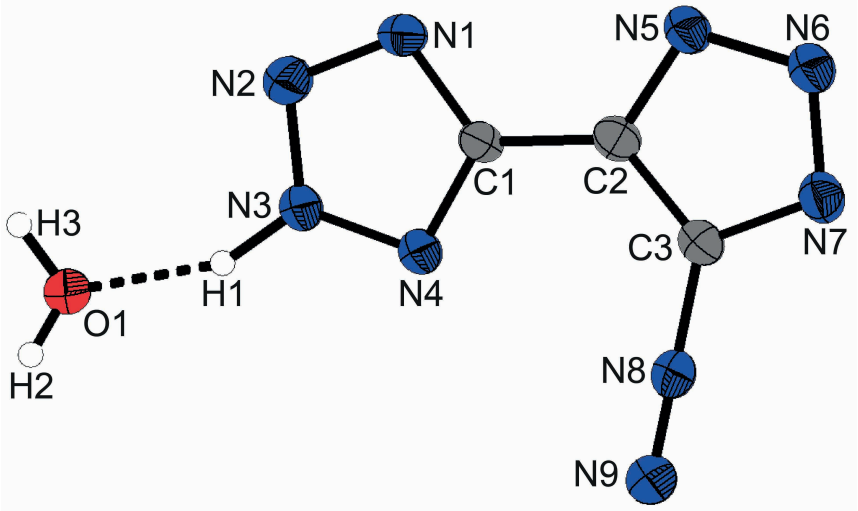

Figure 6.1: Molecular structure of 5-diazonium-4-(2*H*-tetrazol-5-yl)-1,2,3-triazolate monohydrate (**17**·H_2O). Thermal ellipsoids are drawn at the 50% probability level.

units per unit cell and a crystal density of 1.716 g cm^{-3} at 173 K. Selected crystallographic data and bond lengths and angles are summarized in the Appendix (Table A.19 and Table A.21).

The triazole and tetrazole rings are twisted by an angle of 8° (◁N5−C2−C1−N4: 172.3(2)°). The diazonium group N9−N8−C3 is in plane with the triazole ring showing an angle of almost 180° (∠N9−N8−C3: 179.9(2)°).

The diazonium N8−N9 bond length of 1.096(3) Å is virtually identical to the analogous bond lengths found in various diazonium cations[14,16,17] and inner diazonium salts[12,18] clearly indicating a N≡N triple bond (1.10 Å[19]). The C3−N8 bond length (1.365(3) Å) is in the range of common Csp^2−N bond lengths (1.34–1.37 Å).[20]

The crystal structure consists of diagonal layers along the *b* axis (Figure 6.2). The arrangement of the molecules within one layer is supported by hydrogen bonds involving all protons. The heterocyclic proton H1 interacts with the oxygen O1 of the crystal water over a distance of 1.68(3) Å. From each proton of the crystal water, hydrogen bonds are observed to the tetrazole nitrogen N1 and the triazole nitrogen N7, respectively (Table A.20). Furthermore, the diazonium nitrogen N9 shows a dipolar N···N interaction to the tetrazole nitrogen N2 (2.884(3) Å). The layers are connected by weak intermolecular dipolar C···N interactions between C3 and N6 of 3.076(2) Å and a dipolar N···O interaction (N8···O1 2.909(2) Å), which are below the sum of their van der Waals radii.[20]

The computed electrostatic potential (ESP) of the molecular surface (Figure 6.3) clearly shows a large electron-deficient area above the diazonium group and an electron-rich area above the triazole nitrogens thus confirming the zwitterionic structure.

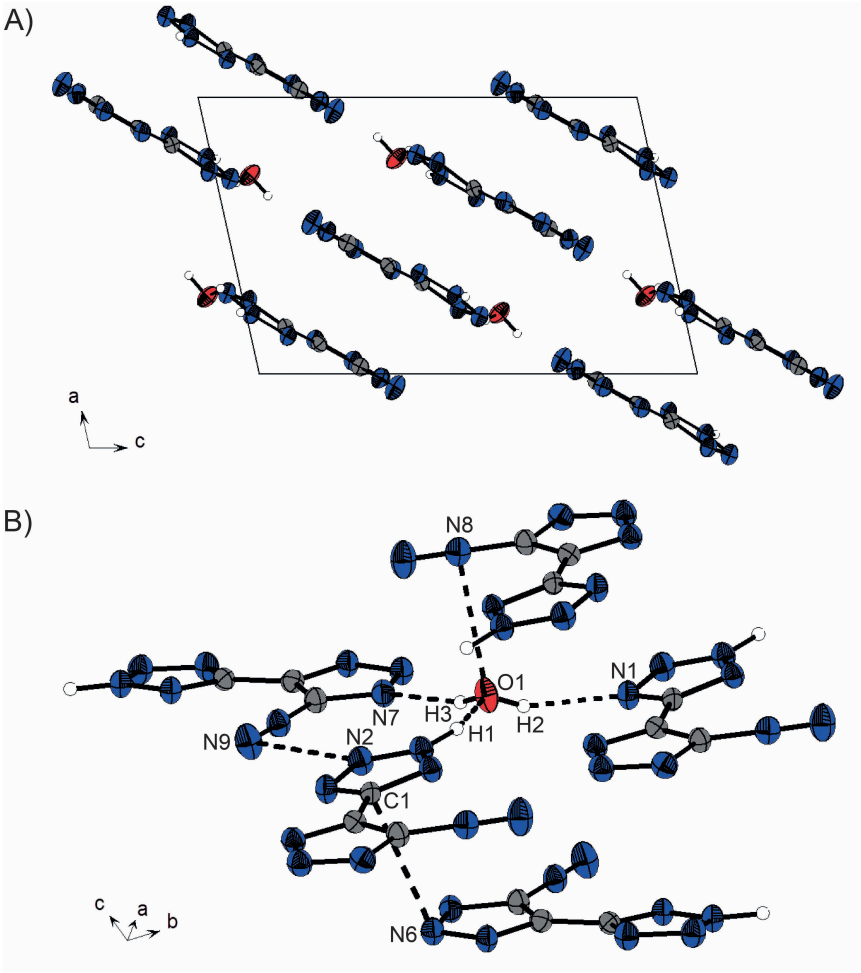

Figure 6.2: A) Unit cell of **17**·H_2O along the *b* axis. B) Interactions within the crystal structure of **17**·H_2O.

6.2.3 NMR and Vibrational Spectroscopy

The solubility of **17** only in DMSO-d_6 is sufficiently good to allow thorough NMR characterization, especially the meaningful ^{15}N NMR spectroscopy. However, after few days in DMSO-d_6 a color change from yellow via orange to finally red indicates significant decomposition.

In the ^{1}H NMR spectrum at 6.5 ppm the broadened resonance of the acidic proton of the tetrazole ring is observed. In the ^{13}C NMR spectrum (Figure 6.4, bottom) the tetrazole carbon resonance is shifted to lower field (148.3 ppm) in comparison to the carbon resonances of the triazole ring. The resonance signal of the triazole carbon atom attached to the tetrazole is observed at 141.1 ppm, whereas the resonance signal of the diazonium bonded carbon is shifted to higher field and broadened (111.5 ppm). This large upfield shift in comparison to other triazole carbon atoms is characteristic for the *ipso* carbon atom of the diazo group.[1] In the proton-coupled ^{15}N NMR spectrum all seven nitrogen resonances are observed

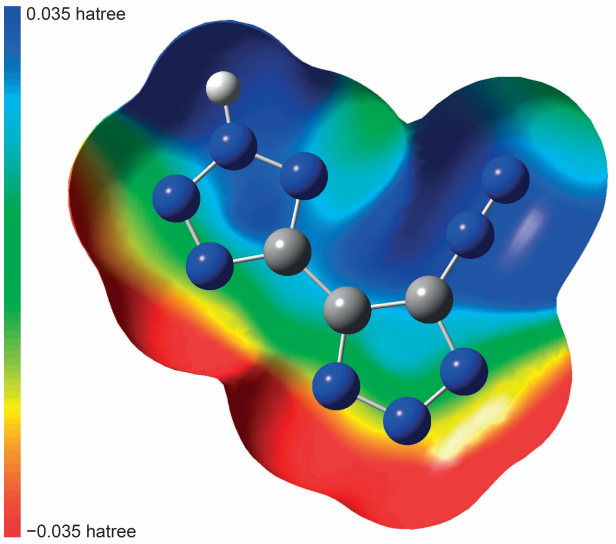

Figure 6.3: *Z*-clipped molecular surface electrostatic potential (ESP) of **17** calculated at B3LYP/6-31G(d,p) level at the 0.001 e/bohr^3 hypersurface.[21] The legend for the color range is given on the left and range from −0.035 (red, electron-rich) to 0.035 (blue, electron-deficient) hartrees.

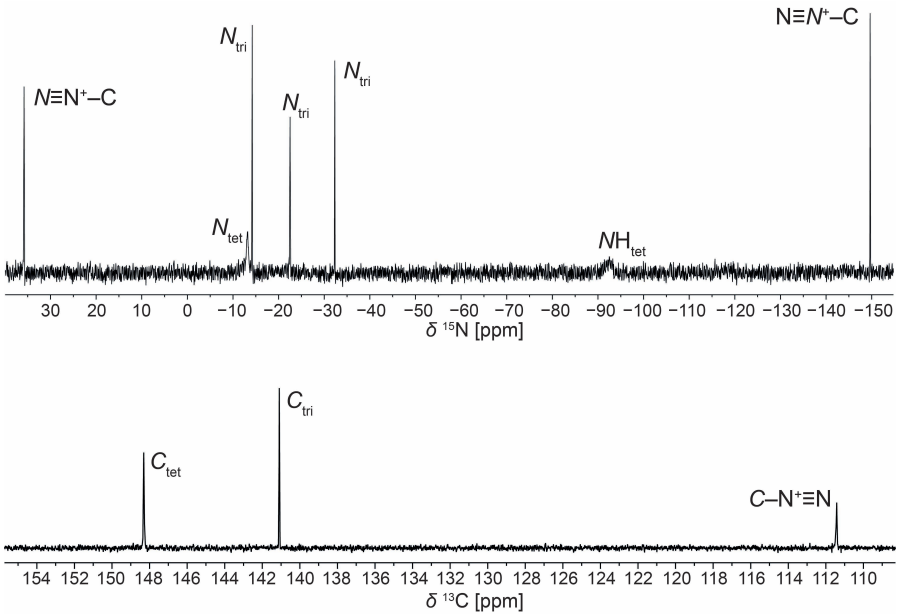

Figure 6.4: ^{13}C and ^{15}N NMR spectra of 5-diazonium-4-(2*H*-tetrazol-5-yl)-1,2,3-triazolate (**17**) in DMSO-d_6.

(Figure 6.4, top). For the tetrazole only two signals are observed, due to the proton exchange in DMSO-d_6, one signal of the protonated nitrogen at −92.5 ppm (*N*H) and one of the non-protonated nitrogen at −13.0 ppm. Both resonances are nicely identified by the broadened appearance due to the direct coupling to hydrogen, respectively over two bonds. A definite assignment of the location of the tetrazole hydrogen atom is not possible, because in solution the NH_{tet} can be found at position 1 or 2 of the tetrazole ring. The resonances of the triazole unit cannot be unambiguously assigned with regard to the specific position of the 1,2,3-triazole. The resonance signal of the positive charged diazonium nitrogen is found at higher field (−149.6 ppm) in the ^{15}N NMR (proven also by the appearance of one visible resonance in the ^{14}N NMR spectrum, which has to be assigned to the positively charged nitrogen at the same position). The terminal diazonium nitrogen atom is unusually detected at low field at +35.8 ppm. The few existing ^{15}N NMR data for diazonium salts report resonances at around −60 ppm for the terminal nitrogen, whereas that of the positively charged nitrogen appears within a narrow range around −150 ppm.[22] The ^{15}N NMR resonances for the terminal nitrogen in diazoalkanes of the type RR′C=N=N seem to be rather flexible, but some exhibit resonances in the range of +60 to +30 ppm,[23] depending on the substituents, and thus, are in the same region as the observed terminal nitrogen resonance in **17**.

In the IR and Raman spectra of **17** the characteristic valence vibration of the diazonium N≡N bond is observed in the expected region as strong bands at 2206 cm^{-1} and 2210 cm^{-1}, respectively.

6.2.4 Thermal Stability and Sensitivities

The loss of the crystal water molecule is observed at 90 °C over a broad temperature range and directly afterwards **17** decomposes. The diazonium salt **17** is thermally stable up to 141 °C, which is comparable to other diazonium 1,2,3-triazoles such as 4-diazonium-1,2,3-triazolate-5-carboxamide (175 °C) and 4-diazonium-1,2,3-triazolate-5-(phenyl)methanone (134 °C).[9,24]

Furthermore, the mechanical sensitivity to impact and friction were determined and classified according to the UN recommendations for the transport of dangerous goods.[25] The diazonium compound **17** is classified as very sensitive to impact (< 1 J) and friction (40 N). However, it is less sensitive than 3-diazo- and 4-diazotriazoles, which are light and shock sensitive and explode when scratched.[1]

6.3 Conclusions

The inner diazonium salt 5-diazonium-4-(2*H*-tetrazol-5-yl)-1,2,3-triazolate (**17**) was isolated from the reaction mixture of 5-(5-amino-1,2,3-triazol-4-yl)tetrazole (**13**) in mixed acid. The zwitterionic structure with the delocalized negative charge at the triazole ring was confirmed by single-crystal X-ray analysis. NMR spectroscopic investigation reveals an unusual low-field shift of the terminal nitrogen of the diazonium unit. The diazonium triazolate **17** is very sensitive to outer stimuli such as impact and friction and is thermally rather stable. Therefore, this diazonium compound **17** seems to be a promising diazonium material for further chemistry, such as cycloadditions with dipolarophiles, which could lead to a variety of new C,N-heterocycles.

6.4 Experimental Section

Caution! *This diazonium salt is an energetic compound with very high sensitivity to various stimuli. While no issues in the synthesis and handling of this material were encountered, proper protective measures (ear protection, Kevlar® gloves, face shield, body armor and earthed equipment) as well as a plastic spatula should be used all the time.*

5-Diazonium-4-(2*H*-tetrazol-5-yl)-1,2,3-triazolate (17)

5-(5-Amino-1,2,3-triazol-4-yl)tetrazole (**13**) (388 mg, 2.55 mmol) was dissolved in concentrated H_2SO_4 (2.5 mL). The yellow solution was cooled to 0 °C and HNO_3 (100%, 0.4 mL) was added in small portions and stirred for 2 h at 0 °C. Then the mixture was allowed to slowly warm up to room temperature and stirred over night. The mixture was poured onto ice (10 g) and stored at 4 °C to obtain yellow crystals of **17**·H_2O (102 mg, 22%).
DSC (5 °C min^{-1}): T_{dehyd} = 90 °C, T_{dec} = 141 °C. ^{1}H NMR (400 MHz, DMSO-d_6): δ = 6.5 (vbr, 1H, NH/H_2O) ppm. ^{13}C{^{1}H} NMR (101 MHz, DMSO-d_6): δ = 148.3 (C_{tet}), 141.1 (C_{tri}), 111.5 (br, CN$_2^+$) ppm. ^{14}N{^{1}H} NMR (29 MHz, DMSO-d_6): δ = −150 (N^+≡N) ppm. ^{15}N NMR (41 MHz, DMSO-d_6): δ = 35.8 (CN$^+$≡N), −13.0 (N_{tet}), −14.2/ −22.5/ −32.3 (N_{tri}), −92.5 (NH$_{tet}$), −149.6 (CN^+≡N). IR (ATR): $\tilde{\nu}$ = 3433 (m), 3342 (w), 3230 (w), 3019 (w), 2833 (w), 2730 (w), 2640 (w), 2353 (vw), 2206 (vs), 1867 (vw), 1724 (vw), 1612 (w), 1499 (w), 1464 (vw), 1400 (w), 1365 (vw), 1351 (vw), 1312 (s), 1289 (m), 1246 (vw), 1209 (m), 1166 (m), 1147 (m), 1125 (w), 1074 (w), 1037 (vs), 1004 (m), 981 (w), 958 (m), 937 (m), 903 (w), 826 (vw), 764 (vw), 727 (vw), 685 (vw), 673 (vw) cm^{-1}. Raman (1064 nm, 300 mW): $\tilde{\nu}$ = 2210 (90), 1638 (6), 1613 (100), 1589 (4), 1412 (7), 1404 (6), 1396 (4), 1366 (3), 1312 (5), 1290 (15), 1209 (3), 1168 (7), 1151 (7), 1137 (3), 1107 (5), 1033 (10), 1024 (15), 1005 (11), 960 (15), 765 (2), 628 (8), 578 (4), 505 (3), 428 (3), 385 (5), 377 (7),

207 (13) cm^{-1}. MS (DCI^+): m/z (%) = 273.2 (3) [$C_6H_4N_{14}^+$], 138.1 (9) [$C_3H_3N_7^+$]. EA ($C_3HN_9 \cdot H_2O$, 181.12 g mol^{-1}): calcd C 19.89, H 1.67, N 69.60%; found C 19.77, H 2.20, N 65.91%. Sensitivities (grain size: < 100 µm): IS: < 1 J; FS: 40 N; ESD: 40 mJ.

6.5 References

[1] G. Cirrincione, A. M. Almerico, E. Aiello, G. Dattolo, *Diazoazoles*, in *Adv. Heterocycl. Chem.*, *48* (Ed.: A. R. Katritzky), Academic Press, **1990**, pp. 65–175.

[2] G. Balz, G. Schiemann, *Ber. Dtsch. Chem. Ges. B* **1927**, *60*, 1186–1190.

[3] C. G. Swain, R. J. Rogers, *J. Am. Chem. Soc.* **1975**, *97*, 799–800.

[4] P. Griess, *Ann. Chem. Pharm.* **1858**, *106*, 123–125.

[5] R. Wizinger-Aust, *Angew. Chem.* **1958**, *70*, 199–204.

[6] J. Thiele, *Liebigs Ann. Chem.* **1892**, *270*, 1–63.

[7] E. Bamberger, *Ber. Dtsch. Chem. Ges.* **1899**, *32*, 1773–1797.

[8] H. K. W. Hui, H. Shechter, *Tetrahedron Lett.* **1982**, *23*, 5115–5118.

[9] Y. F. Shealy, R. F. Struck, L. B. Holum, J. A. Montgomery, *J. Org. Chem.* **1961**, *26*, 2396–2401.

[10] I. V. Ledenyova, V. V. Didenko, K. S. Shikhaliev, *Chem. Heterocycl. Compd.* **2014**, *50*, 1214–1243.

[11] M. Tišler, B. Stanovnik, *Chem. Heterocycl. Compd.* **1980**, *16*, 443–463.

[12] A. A. Dippold, T. M. Klapötke, F. A. Martin, S. Wiedbrauk, *Eur. J. Inorg. Chem.* **2012**, 2429–2443.

[13] T. M. Klapötke, A. Nordheider, J. Stierstorfer, *New J. Chem.* **2012**, *36*, 1463–1468.

[14] R. P. Brint, D. J. Coveney, F. L. Lalor, G. Ferguson, M. Parvez, P. Y. Siew, *J. Chem. Soc., Perkin Trans. 2* **1985**, 139–145.

[15] D. Izsák, T. M. Klapötke, C. Pflüger, *Dalton Trans.* **2015**, *44*, 17054–17063.

[16] N. W. Alcock, T. J. Greenhough, D. M. Hirst, T. J. Kemp, D. R. Payne, *J. Chem. Soc., Perkin Trans. 2* **1980**, 8–12.

[17] M. Cygler, M. Przybylska, R. M. Elofson, *Can. J. Chem.* **1982**, *60*, 2852–2855.

[18] D. Izsák, T. M. Klapötke, A. Preimesser, J. Stierstorfer, *Z. Anorg. Allg. Chem.* **2016**, *642*, 48–55.

[19] A. F. Holleman, E. Wiberg, N. Wiberg, *Lehrbuch der Anorganischen Chemie*, 102nd ed., de Gruyter, Berlin, Germany, **2007**.

[20] A. Bondi, *J. Phys. Chem.* **1964**, *68*, 441–451.

[21] M. J. Frisch, G. W. Trucks, H. B. Schlegel, G. E. Scuseria, M. A. Robb, J. R. Cheeseman, G. Scalmani, V. Barone, B. Mennucci, G. A. Petersson, H. Nakatsuji, M. Caricato, X. Li, H. P. Hratchian, A. F. Izmaylov, J. Bloino, G. Zheng, J. L. Sonnenberg, M. Hada, M. Ehara, K. Toyota, R. Fukuda, J. Hasegawa, M. Ishida, T. Nakajima, Y. Honda, O. Kitao, H. Nakai, T. Vreven, J. J. A. Montgomery, J. E. Peralta, F. Ogliaro, M. Bearpark, J. J. Heyd, E. Brothers, K. N. Kudin, V. N. Staroverov, R. Kobayashi, J. Normand, K. Raghavachari, A. Rendell, J. C. Burant, S. S. Iyengar, J. Tomasi, M. Cossi, N. Rega, J. M. Millam, M. Klene, J. E. Knox, J. B. Cross, V. Bakken, C. Adamo, J. Jaramillo, R. Gomperts, R. E. Stratmann, O. Yazyev, A. J. Austin, R. Cammi, C. Pomelli, J. W. Ochterski, R. L. Martin, K. Morokuma, V. G. Zakrzewski, G. A. Voth, P. Salvador, J. J. Dannenberg, S. Dapprich, A. D. Daniels, O. Farkas, J. B. Foresman, J. V. Ortiz, J. Cioslowski, D. J. Fox, Gaussian 09, Revision A.02, Inc., Wallingford CT, **2009**.

[22] C. Casewit, J. D. Roberts, R. A. Bartsch, *J. Org. Chem.* **1982**, *47*, 2875–2878.

[23] S. Berger, S. Braun, H.-O. Kalinowski, *NMR Spektroskopie von Nichtmetallen Bd 2, ^{15}N-NMR-Spektroskopie*, Thieme, Stuttgart · New York, **1992**.

[24] D. Stadler, W. Anschütz, M. Regit, G. Keller, D. van Assche, J.-P. Fleury, *Liebigs Ann. Chem.* **1975**, 2159–2168.

[25] Test methods according to the *UN Manual of Test and Criteria, Recommendations on the Transport of Dangerous Goods*, United Nations Publication, New York, Geneva, 4th revised ed., **2003**: Impact: Insensitive > 40 J, less sensitive ≥ 35 J, sensitive ≥ 4 J, very sensitive ≤ 3 J; Friction: Insensitive > 360 N, less sensitive $= 360$ N, sensitive < 360 N a. > 80 N, very sensitive ≤ 80 N, extremely sensitive ≤ 10 N.

Combining the Advantages of Tetrazoles and 1,2,3-Triazoles: 4,5-Bis(tetrazol-5-yl)-1,2,3-triazole, 4,5-Bis(1-hydroxytetrazol-5-yl)-1,2,3-triazole and Their Energetic Derivatives

A. A. Dippold, D. Izsák, T. M. Klapötke, and C. Pflüger

Chem. Eur. J. **2016**, *22*, 1768–1778.

HOT PAPER

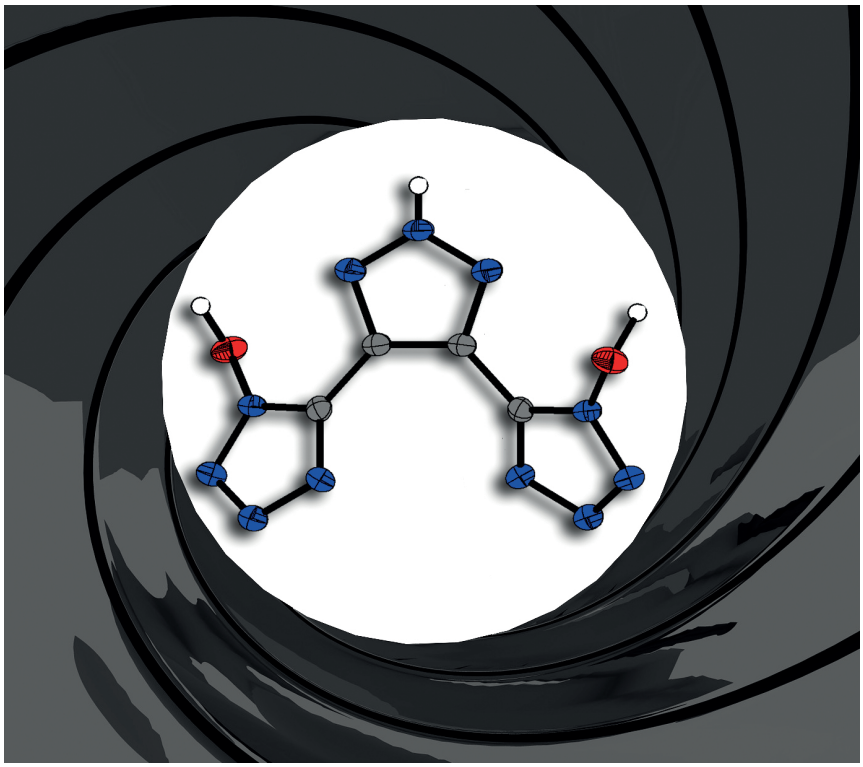

Combining the Advantages of Tetrazoles and 1,2,3-Triazoles: 4,5-Bis(tetrazol-5-yl)-1,2,3-triazole, 4,5-Bis(1-hydroxytetrazol-5-yl)-1,2,3-triazole and Their Energetic Derivatives

A. A. Dippold, D. Izsák, T. M. Klapötke, and C. Pflüger

Chem. Eur. J. **2016**, *22*, 1768–1778.

HOT PAPER

Abstract

In the development of new energetic materials, the main challenge is the combination of high energy content with chemical and mechanical stability, two properties that are often contradictory. In this study, the syntheses and comprehensive characterizations of 4,5-bis(tetrazol-5-yl)-1,2,3-triazole and the novel 4,5-bis(1-hydroxytetrazol-5-yl)-1,2,3-triazole, as well as their energetic properties, are presented, combining the advantages of the more energetic tetrazole and the more stable 1,2,3-triazole rings. Nitrogen-rich salts of both compounds were synthesized to investigate their detonation performances and combustion behavior calculated by computer codes for potential application in erosion-reduced gun propellant mixtures due to their high nitrogen content. The structures of several compounds were studied by single-crystal X-ray diffraction and, especially in the case of 4,5-bis(tetrazol-5-yl)-1,2,3-triazole, revealed the site of deprotonation.

7.1 Introduction

The demands on explosives are increasing, particularly with regards to performance and safety for both military and civil applications. Therefore, strong research efforts are ongoing to meet these requirements. 1,3,5-Trinitro-1,3,5-triazine (RDX), which is currently the most used secondary explosive in energetic formulations, shows very good performance and energetic properties but it suffers from high toxicity.[1,2] Modern explosives should exhibit high performance, low sensitivity to external stimuli such as impact or friction, high thermal stability, and low environmental impact.[3,4] The main challenge is the combination of high energy content with chemical and mechanical stability, two properties that are often contradictory.

One strategy in the synthesis of possible RDX replacements is the investigation of nitrogen-rich compounds that have high positive enthalpies of formation leading to a large released

amount of energy upon detonation. Furthermore, a large volume of nontoxic N_2 is produced on detonation. The high enthalpies of formation result from the higher stability of the N≡N triple bond (946 kJ mol^{-1}) in comparison to the double (418 kJ mol^{-1}) and single (159 kJ mol^{-1}) bonds.[5] Therefore, suitable backbones are nitrogen-rich heterocycles such as pentazoles, tetrazoles, triazoles, and diazoles.[6] Their enthalpies of formation increase with the number of catenated nitrogen atoms, but unfortunately pentazole has not been isolated in macroscopic quantities and alkylated pentazoles are usually thermally not very stable and extremely sensitive towards outer stimuli.[7] In regard to the requirements of detonation performance and safety the tetrazole and 1,2,3- as well as 1,2,4-triazole rings are the most promising backbones. A large number of energetic materials based on monoheterocyclic, biheterocyclic and triheterocyclic systems have been investigated.[8–17] Very promising is the combination of tetrazoles with 1,2,3-triazole rings ($\Delta_f H(g)_{\mathrm{CBS4M}} = 231$ kJ mol^{-1}), which possess higher enthalpies of formation than the 1,2,4-triazoles ($\Delta_f H(g)_{\mathrm{CBS4M}} = 178$ kJ mol^{-1}). 4,5-Bis(tetrazol-5-yl)-2*H*-1,2,3-triazole has been first described and patented by Tanaka and Toda in 2007 and since then some salts have been reported, albeit without any characterization.[18,19]

It has recently been shown that the energetic performance of tetrazoles can be improved by formation of the corresponding *N*-hydroxy compounds.[20–22] Thereby the oxygen balance, the relative amount of oxygen in excess or deficit for conversion of the molecule or mixture into its fully oxidized products without external oxygen, is increased, leading to higher crystal densities and detonation performances. Furthermore, tetrazole *N*-oxides are usually less sensitive towards impact and friction. Henceforth, this selective synthesis of the corresponding novel *N*-oxide 4,5-bis(1-hydroxytetrazol-5-yl)-2*H*-1,2,3-triazole is presented. Nitrogen-rich salts of these two heterocyclic systems are promising ingredients in solid gun propellant mixtures due to their high nitrogen content. Conventional gun propellants are classified as single- [nitrocellulose (NC)], double- [NC, nitroglycerin (NG)], and triple-base [NC, NG, nitroguanidine (NQ)] propellants, which furthermore contain additives such as plasticizers, stabilizers, deterring agents, and flash-suppressors.[23] The primary challenges are the ongoing enhancement of the gun propellant performance and performance issues such as gun barrel erosion, blast, environmental issues, and lifespan.[24] In low-vulnerability (LOVA) propellants, the amounts of NC, NG, and NQ are reduced and an energetic filler (mostly RDX) is incorporated in the NC matrix, whereby the energy output is improved.[23,25] Unfortunately, the higher percentage of RDX leads to higher combustion temperatures and thus leading to problems with erosion of the gun barrel.[26] Therefore, the amount of RDX is reduced and instead high nitrogen-rich compounds are added to afford erosion-reduced propellant mixtures.[27,28]

This contribution reports the syntheses and comprehensive characterization of 4,5-bis-

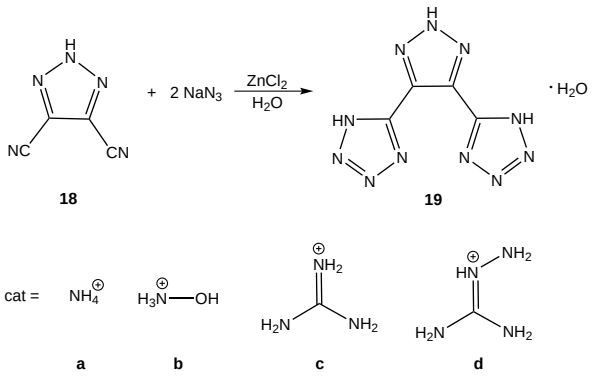

Scheme 7.1: Synthesis of 4,5-bis(1*H*-tetrazol-5-yl)-2*H*-1,2,3-triazole (**19**) and selected nitrogen-rich cations for its doubly deprotonated salts **19a**–**d**.

(tetrazol-5-yl)-1,2,3-triazole and 4,5-bis(1-hydroxytetrazol-5-yl)-1,2,3-triazole, their nitrogen-rich salts as well as their calculated detonation performances and gun propellant evaluation. Furthermore, metal salts of 4,5-bis(tetrazol-5-yl)-1,2,3-triazole were investigated to test their ability to form primary explosives, similar to other nitrogen-rich polycyclic tetrazole compounds like 5-(tetrazol-1-yl)-2*H*-tetrazole,[29] bis(1*H*-tetrazol-5-yl)amine,[30] 1,2-bis(1*H*-tetrazol-5-yl)diazene[31] or 1,3-bis(1*H*-tetrazol-5-yl)triazene[32].

7.2 Results and Discussion

7.2.1 Syntheses

The reaction of 4,5-dicyano-2*H*-1,2,3-triazole with sodium azide and zinc chloride in a 1,3-dipolar cycloaddition yielded 4,5-bis(1*H*-tetrazol-5-yl)-2*H*-1,2,3-triazole hydrate (**19**·H_2O), similar to previously reported procedures[18] (Scheme 7.1).

The synthesis of the novel heterocyclic system 4,5-bis(1-hydroxytetrazol-5-yl)-2*H*-1,2,3-triazole was carried out from 4,5-dicyano-2*H*-1,2,3-triazole by reaction with hydroxylamine followed by diazotization in aqueous hydrochloric acid, resulting in the formation of the chloroxime **21**. The chloro-azide exchange afforded **22**, which was not isolated but directly converted into **23** by ring closure in diethyl ether saturated with gaseous hydrogen chloride. The ring closure could not be carried out in concentrated hydrochloric acid due to the formation of amide groups instead of the tetrazole rings. The optimized synthesis route, based on previously reported reactions for similar compounds,[8] is shown in Scheme 7.2.

Salts of **19** and **23** with selected nitrogen-rich cations were synthesized from the neutral compounds and nitrogen-rich bases in aqueous solutions. Attempts to synthesize the triaminoguanidinium salts by salt metathesis from the corresponding potassium salts **19f** and **23f** were not successful. Astonishingly, the reaction of **23** with an excess of triaminoguani-

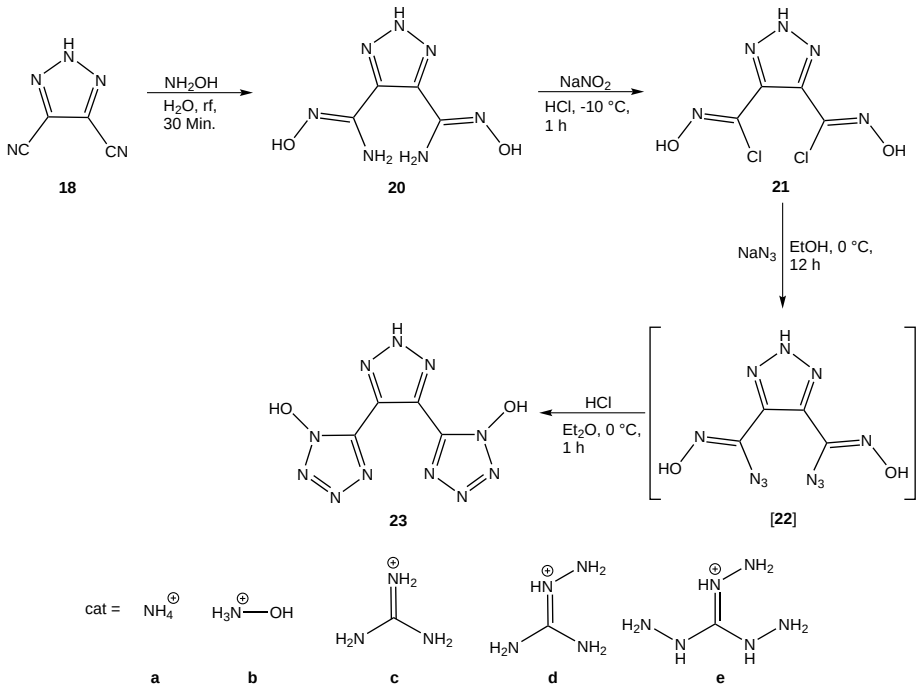

Scheme 7.2: Synthesis of 4,5-bis(1-hydroxytetrazol-5-yl)-2*H*-1,2,3-triazole (**23**) and selected nitrogen-rich cations for its doubly deprotonated salts **23a**–**d**, the singly deprotonated **23e**, and the trisguanidinium salt **23k**.

dinium chloride only yielded the mono triaminoguanidinium salt **23e**. Nevertheless, the deprotonation of all three acidic protons of **23** is also possible, as shown by the synthesis of the trisguanidinium salt **23k**. Due to its low density, no efforts were undertaken to synthesize further triply deprotonated salts because the detonation performances increased with higher densities of the energetic materials.

The ability of **19** to form primary explosives was tested by the reaction of **19** with selected metal bases to afford the corresponding silver (**g**), cesium (**h**), copper(II) (**i**) and zinc (**j**) salts. Silver nitrate was able to deprotonate both tetrazole and the triazole rings to form the triply deprotonated salt **19g**.

7.2.2 NMR Spectroscopy

All compounds were characterized by ^{1}H and ^{13}C{^{1}H} NMR spectroscopy, and some additionally by ^{14}N and ^{15}N NMR spectroscopy in DMSO-d_6 at room temperature. 4,5-Dicyano-2*H*-1,2,3-triazole (**18**) was previously characterized by NMR spectroscopy, albeit with incorrect assignments.[33] The acidic proton is shifted downfield to $\delta = 16.92$ ppm, whereas the carbon resonances of the aromatic carbon atoms are observed at $\delta = 124.4$ ppm and the exocyclic carbon atoms of the nitrile groups at $\delta = 110.8$ ppm. In the ^{15}N NMR spectrum of **18** (Figure 7.1), three signals are observed, which correspond to the N–H nitrogen

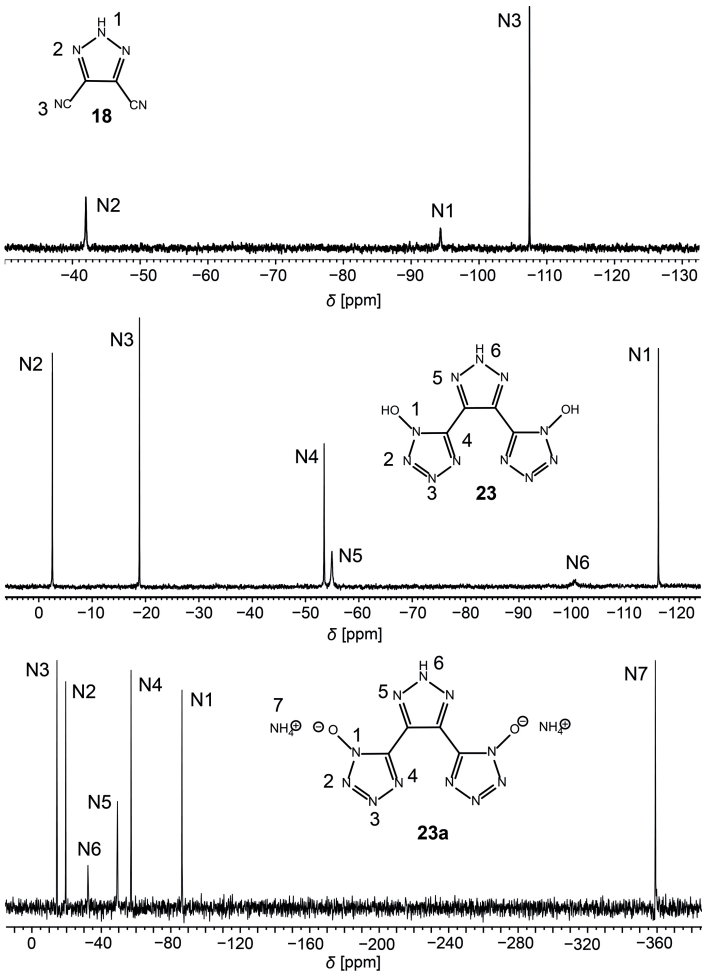

Figure 7.1: ^{15}N NMR spectra of 4,5-dicyano-2*H*-1,2,3-triazole (**18**), 4,5-bis(1-hydroxytetrazol-5-yl)-2*H*-1,2,3-triazole (**23**), and its ammonium salt **23a** recorded in DMSO-d_6 at room temperature.

($\delta = -94.21$ ppm), the two equivalent ring nitrogen atoms ($\delta = -42.0$ ppm), and the two equivalent nitrogen atoms of the nitrile groups ($\delta = -107.5$ ppm).
The formation of the tetrazole rings of **19** leads to a downfield shift of the triazole carbon resonances ($\delta = 131.8$ ppm). The carbon resonances of the tetrazole rings are detected at $\delta = 148.1$ ppm. The signals of salts **19a**–**d** and **19f** are compiled in Table 7.1. Whereas the triazole carbon atoms of **19a**–**d** and **19f** are shifted by about 2 ppm in comparison to the parent molecule **19**, the salt formation strongly affects the shift of the tetrazole carbon atoms by up to 5 ppm downfield. The proton resonances of the cations of **19b**–**d** can also be observed, as can the carbon resonances of the guanidinium-based cations (Table 7.1). Additionally, the resonances of the positively charged nitrogen atoms of **19a** ($\delta = -359$ ppm), **19c** ($\delta = -304$ ppm), and **19d** ($\delta = -311$ ppm) can be observed in the ^{14}N NMR spectrum recorded in D_2O.

Table 7.1: NMR signals of the neutral compound **19** and its salts **19a**–**d** and **19f**.

	δ in DMSO-d_6[a]				
	$^{13}C\{^1H\}$ (tetrazole)	$^{13}C\{^1H\}$ (triazole)	^1H (cation)	$^{13}C\{^1H\}$ (cation)	^{14}N (cation)
19	148.1	131.8	–	–	–
19a	(153.2)	(133.3)	n.o.	–	(−359)
19b	150.0	130.2	10.33[b]	–	n.o.
19c	155.2 (153.0)	133.2 (131.7)	7.65[c]	158.3 (155.7)	(−304)
19d	152.0 (150.8)	131.7 (131.0)	9.06[d], 7.18[c], 4.71[e]	158.9 (156.7)	(−311)
19f	153.1	133.3	n.o.	–	–

[a] Values in parentheses are signals in D_2O; [b] not possible to assign; [c] CNH_2; [d] CNH; [e] NNH_2; n.o. = no signals observed.

Table 7.2: NMR signals of the neutral compound **23** and its salts **23a**–**f** and **23k**.

	δ in DMSO-d_6[a]			
	$^{13}C\{^1H\}$ (tetrazole)	$^{13}C\{^1H\}$ (triazole)	^1H	$^{13}C\{^1H\}$ (cation)
23	138.9	129.1	9.11[a]	–
23a	138.5	130.2	7.10[b]	–
23b	137.8	129.9	9.06[c]	–
23c	138.4	130.0	7.16[d]	158.6
23d	139.7	130.3	7.35[c]	159.6
23e	139.4	129.7	8.60[c]	159.6
23f	139.6	128.6	n.o.	–
23k	139.6	130.7	7.40[d]	158.8

[a] NOH; [b] NH_4^+; [c] not possible to assign; [d] NNH_2; n.o. = no signals observed.

2*H*-1,2,3-Triazole-4,5-bis(carboxamidoxime) (**20**) gives rise to two resonance signals, corresponding to the amino group (δ = 6.67 ppm) and the *N*-hydroxy group (δ = 9.91 ppm), in the ^1H NMR spectrum. In the ^1H NMR spectrum of **21**, the signal of the amino group has completely disappeared, whereas the triazole proton resonance and the proton resonance of the oxime groups are observed at δ = 15.74 and 12.74 ppm, respectively. The carbon resonances of chloroxime **21** (δ = 137.9 and 126.5 ppm) are shifted to higher field in comparison to amidoxime **20** (146.7 and 133.6 ppm). The signals of **23** and its salts **23a**–**f** and **23k** are summarized in Table 7.2.

The carbon of the newly formed hydroxytetrazole rings of **23** has its signal at δ = 138.9 ppm, whereas the second signal at 129.1 ppm corresponds to the triazole carbon atoms. In the ^1H NMR spectrum, only the resonance of the *N*-hydroxy protons at δ = 9.11 ppm is

visible. Additionally, the ^{15}N NMR spectra of **23** and its ammonium salt **23a** were recorded and are depicted in Figure 7.1. The assignments are based on comparison with similar molecules[34] in addition to theoretical calculations using Gaussian 09 [OP86/SVP NMR scrf=(solvent=dmso)].[35] The resonances corresponding to the triazole nitrogen atoms of **23** and **23a** could be assigned, due to their coupling with the hydrogen atom, to the peaks at $\delta = -54.9$ (N5) and -100.3 ppm (N6) in **23** and at $\delta = -32.7$ (N6) and -49.6 ppm (N5) in **23a**, respectively. The signal corresponding to the nitrogen carrying the hydroxy group is shifted by deprotonation from $\delta = -116.1$ to -86.8 ppm. The other tetrazole resonances of **23** are observed at $\delta = -2.3$ (N2), -18.9 (N3), and -53.5 ppm (N4), whereas the corresponding resonances of **23a** are found at $\delta = -14.8$ (N3), -19.8 (N2), and -57.5 ppm (N4). The ammonium salt **23a** gives rise to the ammonium resonance at $\delta = -355$ ppm in the ^{14}N NMR spectrum and at $\delta = -359.3$ ppm in the ^{15}N NMR spectrum. The deprotonation of the *N*-hydroxy groups does not strongly affect the shift of either the tetrazole carbon atoms or the triazole carbon atoms of **23a**–**k** (Table 7.2) in the ^{13}C NMR spectra. The cation resonances of **23a**–**e** and **23k** are also compiled in Table 7.2.

7.2.3 Crystal Structures

Several compounds were characterized by low-temperature single-crystal X-ray diffraction. Selected data and parameters of the measurements and refinements are summarized in the Appendix (Table A.27 and Table A.28).

Compound **19** crystallizes as the dimethylammonium salt (Figure 7.2) from hot dimethylformamide in the monoclinic space group $P2_1/c$ with four formula units per unit cell. The ring system is almost planar, with torsion angles below 3° for the tetrazole rings [$\sphericalangle$C3−C2−C1−N1: 2.7(2)°; $\sphericalangle$C2−C3−C4−N11: −2.5(2)°]. An intramolecular hydrogen bond N1−H1···N11 is formed between the tetrazole rings (see the Appendix, Table A.22). The hydrogen atom of the triazole ring is located at N7, adjacent to the deprotonated tetrazole ring, instead of at the center nitrogen atom.

The crystal structure of the bisaminoguanidinium salt **19d** monohydrate has monoclinic symmetry ($P2_1/n$) with four molecular moieties in the unit cell and a crystal density of 1.623 g cm^{-3} at 100 K. Its molecular structure is shown in Figure 7.3. Instead of both tetrazole rings, one tetrazole and the triazole are deprotonated and a strong hydrogen bond of 1.86(3) Å is formed between the tetrazole rings. The non-deprotonated tetrazole ring is twisted by −177.9(2)° ($\sphericalangle$C2−C3−C4−N8), whereas the deprotonated ring is twisted by 176.7(2)° ($\sphericalangle$C3−C2−C1−N1).

These twistings allow the formation of hydrogen bonds between the cations and the heterocyclic anion. From each cation, two hydrogen bonds are formed to the counterion

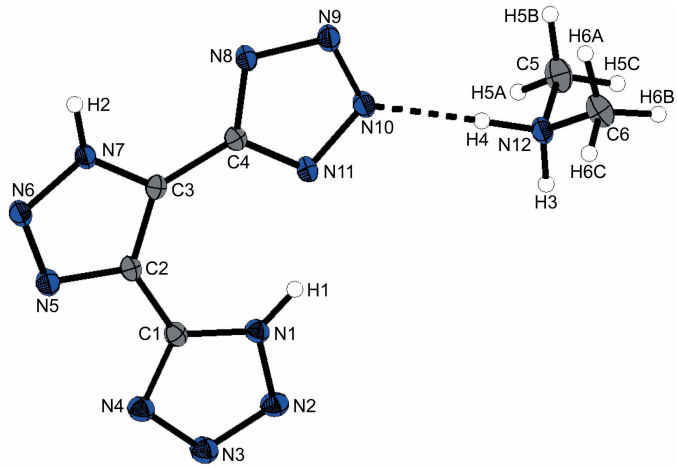

Figure 7.2: Molecular structure of dimethylammonium 5-(4-(1*H*-tetrazol-5-yl)-1*H*-1,2,3-triazol-5-yl)tetrazolate. Thermal ellipsoids are drawn at the 50% probability level.

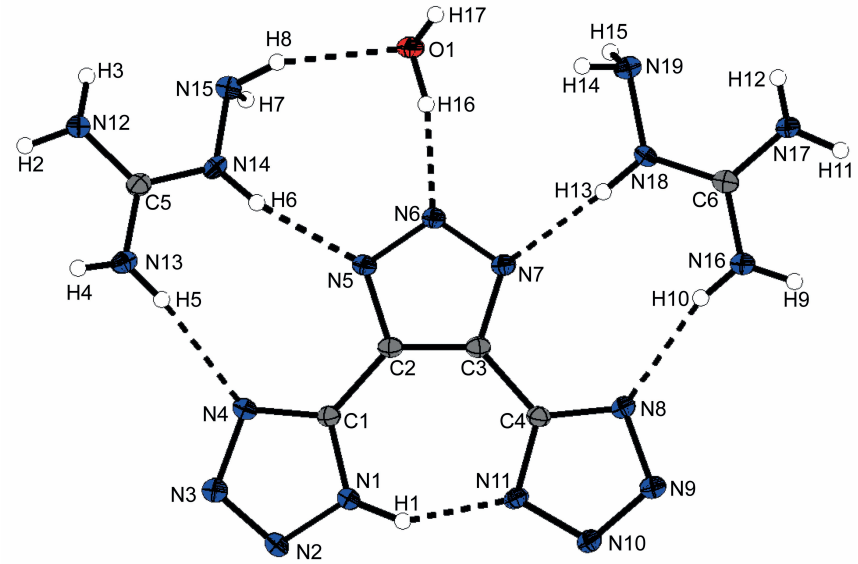

Figure 7.3: Molecular structure of bisaminoguanidinium 5-(5-(1*H*-tetrazol-5-yl)-1,2,3-triazolate-4-yl)tetrazolate (**19d**) as hydrate. Thermal ellipsoids are drawn at the 50% probability level.

with lengths ranging from 1.86–2.21 Å, forming nine-membered rings. The crystal structure is supported by various intermolecular hydrogen bonds, as shown in the Appendix (Figure A.14 and Table A.23). Furthermore, one molecule of water interacts with the center nitrogen of the triazole over a distance of 1.83(3) Å and with an amino group of one cation. The molecules are opposed staggered along the *c* axis and also staggered along the *a* axis, forming a diagonal layer structure.

4,5-Bis(1-hydroxytetrazol-5-yl)-2*H*-1,2,3-triazole (**23**) crystallizes as a dihydrate in the orthorhombic space group *Pbcn*, with four formula units per unit cell, a crystal density of 1.804 g cm^{-3} (Figure 7.4A), and a twofold screw axis and a glide plane through the

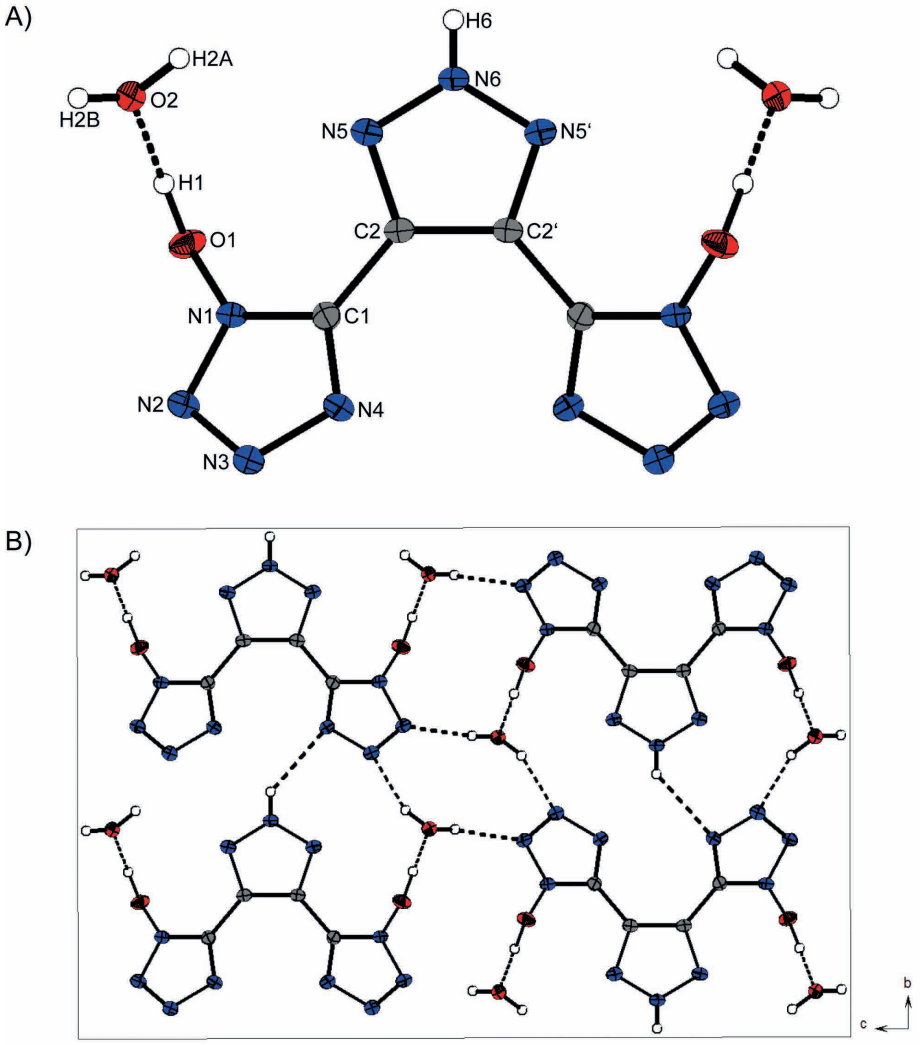

Figure 7.4: A) Molecular structure of 4,5-bis(1-hydroxytetrazol-5-yl)-2*H*-1,2,3-triazole dihydrate (**23**·2 H_2O); B) unit cell of **23**·2 H_2O along the *a* axis. Thermal ellipsoids are shown at the 50% probability level.

center of the molecule. The bond lengths and angles within the azole rings are all within the range of formal C−N, N−N, and C−C single and double bonds (C−N: 1.34, 1.33 Å; C−C: 1.41 Å; N−N: 1.36, 1.30 Å)[5,36] and in the same range as the corresponding bonds of the non-deprotonated azole rings of the dimethylammonium salt of **19**. The N−O bond length of 1.3515(18) Å is slightly elongated in comparison to other tetrazole *N*-hydroxy bond lengths (mean length: 1.34 Å).[34,37,38]

The *N*-hydroxy protons participate in a strongly directed hydrogen bond to the crystal water with an O1−H1···O2 angle of 172° (Table 7.3). Furthermore, the same orientation of the *N*-hydroxy group and the triazole ring leads to a weak intramolecular N5···O1 interaction of 3.030(2) Å, within the sum of the van der Waals radii (r_w(O)+r_w(N) = 3.07 Å).[39] The tetrazole rings are twisted out of the triazole plane by 32.2(3)°, whereby each nitrogen

Table 7.3: Hydrogen bonds within the crystal structure of **23**·2 H_2O.

D−H···A	d(D−H) [Å]	d(H···A) [Å]	d(D···A) [Å]	∠(D−H···A) [°]
O1−H1···O2	1.06(3)	1.40(3)	2.4558(18)	172(2)
O2−H2A···N3^{i}	0.92(3)	1.98(3)	2.866(2)	160(3)
O2−H2B···N2^{ii}	0.83(2)	2.13(2)	2.959(2)	172(2)
N6−H6···N4^{iii}	0.76(4)	2.56(3)	3.122(2)	132.25(3)

Symmetry codes: (i) $0.5-x, 0.5+y, z$; (ii) $-0.5+x, 0.5-y, 1-z$; (iii) $1.5-x, 0.5+y, z$.

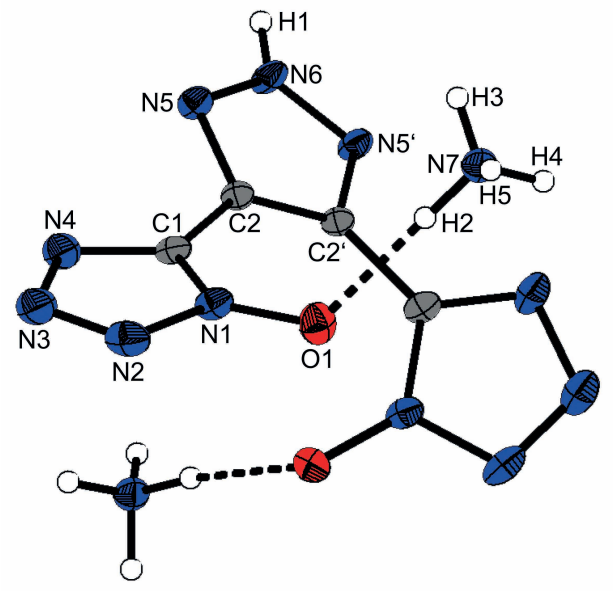

Figure 7.5: Molecular structure of **23a**. Thermal ellipsoids are drawn at the 50% probability level.

atom except for that carrying the hydroxy group is involved in hydrogen bonding either to the crystal water or to the triazole proton. The crystal structure is formed from oppositely aligned layers with staggered molecules along the c axis (Figure 7.4B). The layers are connected by hydrogen bonds involving the crystal water molecules. Additionally, a weak three-center hydrogen bond between the triazole proton and nitrogen N4 is observed.

As expected, the N−O bond lengths in the corresponding anions of the ammonium (**23a**), hydroxylammonium (**23b**) and guanidinium (**23k**) salts are significantly shorter upon deprotonation. The ammonium salt **23a** crystallizes in the monoclinic space group $C2/c$ with a crystal density of 1.736 g cm^{-3} and a twofold axis going through the center of the molecule (Figure 7.5). Therefore, both N−O bonds have the same lengths (1.314(2) Å), the other salts **23b** and **23k** the two N−O bonds differ by around 0.01 Å.

The tetrazole rings of **23a** are twisted by 36.8(3)° and the torsion angle between the triazole and the N-oxide (◁N5−C2−N1−O1) is −134.4(2)°. The orientation of the tetrazole

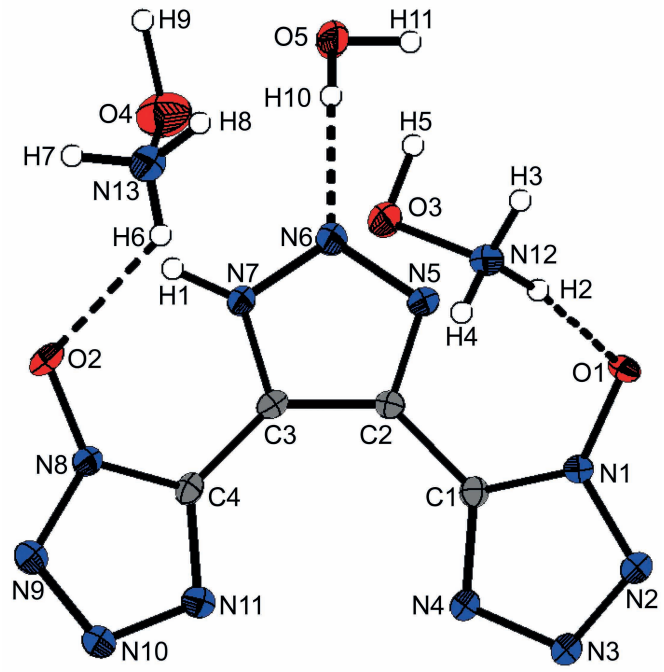

Figure 7.6: Molecular structure of **23b** as monohydrate. Thermal ellipsoids are drawn at the 50% probability level.

N-oxides leads to the formation of several strong and directed hydrogen bonds (see the Appendix, Table A.24). The crystal structure is composed of staggered molecules along the *b* axis and opposed alternating layers along the *c* axis (Figure A.15). The anions of one column along the *b* axis are connected by weak three-center hydrogen bonds between the triazole proton and the negatively charged *N*-oxides (H···A: 2.24(3) Å; D···A: 2.923(2) Å; ∠DHA: 141(3)°). These columns are connected by directed hydrogen bonds to the ammonium cations.

The monohydrate of the hydroxylammonium salt **23b** shows monoclinic symmetry ($P2_1/c$) at 173 K. Its molecular structure is depicted in Figure 7.6. The tetrazole rings are twisted with torsion angles of 152.7(2)° (◁C2−C3−C4−N8) and −145.1(2)° (◁C3−C2−C1−N4), respectively, and the *N*-oxide bond lengths differ by around 0.02 Å. The N−O bond lengths of the hydroxylammonium cations (1.42 Å) are similar to previously reported values.[38] The crystal structure consists of a wave-like arrangement of the anions, which is supported by various hydrogen bonds involving the cations and the crystal water (summarized in Table A.25). Furthermore, the anions are connected by a hydrogen bond from the proton of the triazole ring and the *N*-oxide oxygen O2 (H···A: 1.81(3) Å; D···A: 2.657(2) Å; ∠DHA: 157(2)°).

The trisguanidinium salt **23k** crystallizes as a monohydrate in the triclinic space group $P\bar{1}$ at 173 K (Figure 7.7A). Its *N*-oxide groups are orientated differently to those in the structures of its parent compound and the salts **23a** and **23b**. The tetrazole rings

are twisted by −164.0(2)° (◁C3−C2−C1−N1) and −134.4(2)° (◁C2−C3−C4−N8). The spatial arrangement enables the formation of numerous hydrogen bonds involving the guanidinium cations and the crystal water (see the Appendix, Table A.26). In particular, the *N*-oxide oxygen atoms O1 and O2 are involved in several hydrogen bonds. The crystal structure consists of four different layers alternating between cations and anions along the *c* axis (Figure 7.7B). Two layers are formed by oppositely orientated anions, whereas the other two layers consist either of the cations and the crystal water or only of the perpendicularly aligned cations. Although there are various hydrogen bonds, the crystal density is comparatively low (1.52 g cm^{-3} at 173 K) due to the spatial arrangement of the cations.

The molecular structure of the hydroxylammonium salt **24** of the side product of **23** is shown in Figure 7.8. It crystallizes in the monoclinic space group $P2_1/c$ with four formula units per unit cell and a crystal density of 1.824 g cm^{-3} at 100 K.

7.2.4 Thermal Stabilities, Sensitivities, and Toxicities

4,5-Bis(tetrazol-5-yl)-1,2,3-triazole (**19**) has high thermal stability up to 277 °C, whereas the introduction of the *N*-hydroxy groups in the tetrazole rings in **23** leads to a reduced but still satisfactory thermal stability up to 246 °C. Whereas the thermal stabilities of the nitrogen-rich salts **19a**–**d** are mostly above 260 °C, with the exception of the hydroxylammonium salt **19b**, the thermal stabilities of the metal salts **19f**–**j** are even higher up to 336 °C. The ammonium salt **19a** melts at 223 °C, whereas the guanidinium-based salts **19c** and **19d** undergo endothermic phase transitions at 201 and 185 °C, respectively.

The nitrogen-rich salts **23a**–**e** and **23k** show a similar trend in thermal stability as the nitrogen-rich salts of **19**. Their thermal stabilities are in the same range as those of the non-ionic **23** or even reduced. Furthermore, the salts **23c**, **23e**, and **23k** melt at temperatures 13–50 °C below those at which they decompose. The nitrogen-rich salts of **19** and **23** could be dehydrated at temperatures between 66 and 131 °C. Nevertheless, all compounds with the exception of **19b** meet the demands of 180 °C thermal stability requested for potential applications as new explosives.

Furthermore, the mechanical sensitivities to impact (IS), friction (FS), and electrostatic discharge (ESD) were investigated and classified according to the UN recommendations for the transport of dangerous goods.[40] The impact sensitivity tests were performed according to STANAG 4489[41] by using a BAM drophammer. The friction sensitivity tests were carried out according to STANAG 4487[42] by using a BAM friction tester. Surprisingly, compound **19** shows a high impact sensitivity of 2 J and a friction sensitivity of 240 N, whereas its nitrogen-rich salts are insensitive to impact and friction. The metal salts **19f**–**j**

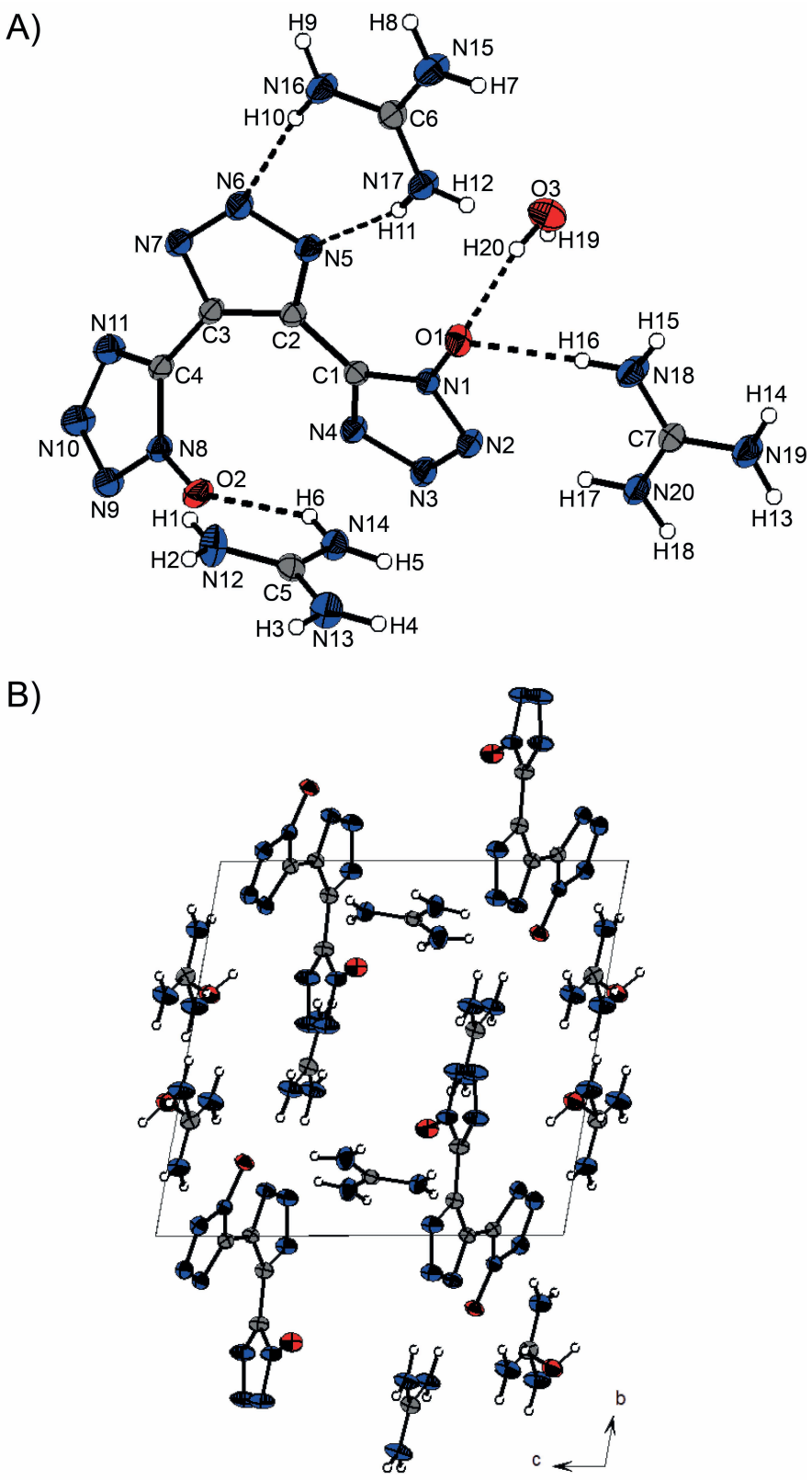

Figure 7.7: A) Molecular structure of **23k** monohydrate; B) unit cell of **23k**·H_2O along the *a* axis. Thermal ellipsoids are drawn at the 50% probability level.

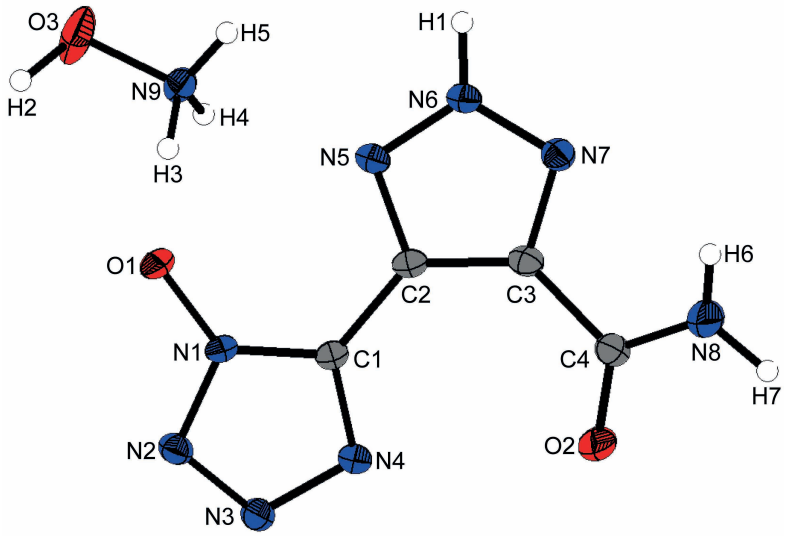

Figure 7.8: Molecular structure of hydroxylammonium 5-(2*H*-1,2,3-triazole-5-carboxamide-4-yl)tetrazole-1-oxide (**24**).

are also rather less sensitive to both impact and friction, with the silver salt **19g** being the most sensitive (12 J, 288 N).

The introduction of the *N*-hydroxy group to the tetrazole rings leads, in contrast to the general trend of tetrazole oxides, to the even more impact-sensitive compound **23** (1 J), while having the same friction sensitivity (Tables 7.5–7.7). The impact sensitivities of the nitrogen-rich salts of **23** are improved in comparison to the parent compound, but they vary strongly. The ammonium salt **23a** (10 J), the hydroxylammonium salt **23b** (> 7 J), and the mono triaminoguanidinium salt **23e** (10 J) are classified as sensitive to impact, whereas the other salts based on the guanidinium cations, **23c**, **23d**, and **23k**, are insensitive towards impact (> 40 J). In contrast to **23**, which is sensitive to friction (240 N), all salts are insensitive to friction (> 360 N). Thus, the sensitivities to impact could not be increased as intended by *N*-oxide introduction in comparison to **19** and its nitrogen-rich salts, but the nitrogen-rich salts show still better or at least sensitivities in the same range than RDX. The electrostatic discharge sensitivities of all herein investigated compounds are greater than the human body can release.[3]

The toxicity to aquatic organisms of the ammonium salt **19a**, due to the insolubility of **19** in water, and **23** were investigated by using the luminescent marine bacterium *Vibrio fischeri* (see the Appendix). The half-maximum effective concentration (EC_{50}) after 15 and 30 min of the ammonium salt **19a** and the nonionic **23** are higher than those of RDX, signifying that the two compounds are less toxic than RDX (Table 7.4) and that **19a** is considerably less toxic than **23**.

Table 7.4: EC_{50} values after 15 min and 30 min of compounds **19a**, **23**, and RDX.

Compound	EC_{50} values after 15 min [g L^{-1}]	EC_{50} values after 30 min [g L^{-1}]
19a	2.973	1.824
23	0.587	0.546
RDX (literature value)[43]	0.327 (0.322)	0.239 (0.266)

7.2.5 Energetic Properties

In the first instance the performance characteristics of new energetic materials are calculated to evaluate their utility for possible applications as an energetic material. Their enthalpies of formation were computed by ab initio calculations using the Gaussian 09 program package[35] at the CBS-4M level of theory. The detonation parameters are calculated with the Explo5 (version 6.02) computer code[44] based on the calculated solid-state enthalpies of formation and attributed to the corresponding densities at room temperature measured with a helium gas pycnometer from Linseis. For a complete discussion of the methods that were used for calculations, see the Introduction. The physicochemical and energetic properties of compounds **19** and **23** and their salts are presented in Tables 7.5–7.7.
Compound **19** and its corresponding *N*-hydroxy derivative **23** show similar calculated detonation performances with detonation velocities of around 8300 m s^{-1} and detonation pressures of 248 kbar and 260 kbar, respectively. The detonation performances are improved by the formation of the nitrogen-rich salts with exception of the guanidinium salts **19c**, **23c**, and **23k**. The other salts have detonation velocities in the range 8561–9022 m s^{-1} and detonation pressures up to 288 kbar. The aminoguanidinium salts **19d** and **23d**, as well as the ammonium salt **23a**, show calculated detonation performances in the same range or even superior to RDX, the most commonly used explosive.

7.2.6 Gun Propellant Evaluation

For gun propellants, the most important parameters are the combustion temperature T_c, the specific energy f_E ($f_E = nRT_c$), the co-volume b_E, and the pressure p_{max}, while assuming isochoric combustion. These parameters, as well as the N_2/CO ratio, were calculated with the program package Explo5 6.02 assuming isochoric conditions by using the virial equation of state with a loading density of 0.2 g cm^{-3}. The calculated parameters for two different kinds of gun propellant charges are presented in Table 7.8. The formulations referred to as High-Nitrogen 1 and 2 (HN-1 and HN-2) are erosion-reduced formulations derived from EX-99 due to their higher nitrogen content. EX-99 is a common formulation for large naval guns and contains a high amount of RDX. The amount of RDX is reduced in the HN-1

Table 7.5: Physical and energetic properties of **19** and its salts **19a**–**d**.

	19	**19a**	**19b**	**19c**	**19d**
Molecular formula	$C_4H_3N_{11}$	$C_4H_9N_{13}$	$C_4H_9N_{13}O_2$	$C_6H_{13}N_{17}$	$C_6H_{15}N_{19}$
M [g mol^{-1}]	205.14	239.20	271.20	323.28	353.33
IS [J][a]	2	>40	>40	>40	>40
FS [N][b]	240	>360	>360	>360	>360
ESD [J][c]	0.4	0.8	0.5	1.5	1.0
Grain size [µm]	<100	<100	<100	<100	<100
N [%][d]	75.11	76.12	67.14	73.66	75.32
Ω [%][e]	−74.1	−83.6	−61.9	−91.6	−88.3
T_{dec} [°C][f]	277	301	160	289	264
ρ [g cm^{-3}][g]	1.69	1.62	1.64	1.52	1.66
$\Delta_f H_m$ [kJ mol^{-1}][h]	801	591	745	615	846
$\Delta_f U$ [kJ kg^{-1}][i]	3989	2585	2857	2017	2515
Calculated detonation parameters (Explo5 v. 6.02)					
$-Q_v$ [kJ kg^{-1}][j]	4172	3118	4851	2598	3119
T_{det} [K][k]	3042	2187	3128	1966	2104
p_{CJ} [kbar][l]	248	237	273	184	263
D [m s^{-1}][m]	8360	8587	8798	7785	9022
V_0 [L kg^{-1}][n]	733	843	867	840	854

[a] Impact sensitivity (BAM drophammer 1 of 6). [b] Friction sensitivity (BAM friction tester 1 of 6). [c] Electrostatic discharge (OZM Research). [d] Nitrogen content. [e] Oxygen balance ($\Omega = (x\mathrm{O} - 2y\mathrm{C} - 0.5z\mathrm{H})1600/M$). [f] Decomposition temperature. [g] Density at room temperature. [h] Calculated enthalpy of formation. [i] Calculated energy of formation. [j] Energy of explosion. [k] Detonation temperature. [l] Detonation pressure. [m] Detonation velocity. [n] Volume of detonation gases.

and HN-2 formulations and, instead of that, bistriaminoguanidinium 5,5′-azobistetrazolate (TAGzT) is added. The synthesized compounds should replace the more sensitive TAGzT (IS 4 J, FS 60 N)[45] in the formulations HN-1 and HN-2. The enthalpies of formation of the other ingredients were either taken from the Explo5 or ICT databases.[46]

The HN-1-based formulations show generally higher performances than those based on HN-2 because of the higher content of RDX. However, they also have lower N_2/CO ratios by about 0.06 and higher combustion temperatures, which are undesirable with regard to the improvement of lifespans by avoiding gun barrel corrosion. Nevertheless, the combustion temperatures are still below the critical temperature of 3273 K. The most promising compounds as possible ingredients in gun propellants are **19b**, **23a**, **23b**, and **23e**, which have higher specific energies than the genuine HN-1 and HN-2 mixtures.

Table 7.6: Physical and energetic properties of **23** and its salts **23a**–**c**.

	23	**23a**	**23b**	**23c**
Molecular formula	$C_4H_3N_{11}O_2$	$C_4H_9N_{13}O_2$	$C_4H_9N_{13}O_4$	$C_6H_{13}N_{17}O_2$
M [g mol^{-1}]	237.14	271.21	303.20	355.28
IS [J][a]	1	10	7	>40
FS [N][b]	240	>360	>360	>360
ESD [J][c]	0.3	0.7	0.3	1.25
Grain size [µm]	<100	<100	<100	<100
N [%][d]	64.97	67.14	60.06	67.02
Ω [%][e]	−50.6	−61.9	−44.9	−74.3
T_{dec} [°C][f]	246	241	182	244
ρ [g cm^{-3}][g]	1.67	1.69	1.63	1.56
$\Delta_f H_m$ [kJ mol^{-1}][h]	823	682	722	331
$\Delta_f U$ [kJ kg^{-1}][i]	3555	2625	2486	1042
Calculated detonation parameters (Explo5 v. 6.02)				
$-Q_v$ [kJ kg^{-1}][j]	5309	4629	5574	2748
T_{det} [K][k]	3896	2989	3670	2112
p_{CJ} [kbar][l]	260	288	270	186
D [m s^{-1}][m]	8277	8991	8561	7659
V_0 [L kg^{-1}][n]	759	862	871	851

[a] Impact sensitivity (BAM drophammer 1 of 6). [b] Friction sensitivity (BAM friction tester 1 of 6). [c] Electrostatic discharge (OZM Research). [d] Nitrogen content. [e] Oxygen balance ($\Omega = (x\mathrm{O} - 2y\mathrm{C} - 0.5z\mathrm{H})1600/M$). [f] Decomposition temperature. [g] Density at room temperature. [h] Calculated enthalpy of formation. [i] Calculated energy of formation. [j] Energy of explosion. [k] Detonation temperature. [l] Detonation pressure. [m] Detonation velocity. [n] Volume of detonation gases.

7.2.7 Primary Explosives

The metal salts **19g**–**j** were tested for their potential suitability as primary explosives. A small amount (approximately 5 mg) was therefore heated on a spatula without direct flame contact by using a lighter. Whereas the copper(II) salt **19i** and the silver salt **19g** mildly detonated upon ignition, the cesium salt **19h** and the zinc salt **19j** were only deflagrated. Next, a small amount (again approximately 5 mg) was taped to a metal surface with transparent sticky tape and poked with a hot needle. Although the compounds are confined, which aids the formation of a shock wave, all four, including the water-free silver salt **19g**, were only deflagrated. The initiation capability of secondary explosives was thus not further investigated due to the low detonation performances.

Table 7.7: Physical and energetic properties of the nitrogen-rich salts **23d**, **23e**, **23k**, as well as RDX and TAGzT.

	23d	**23e**	**23k**	RDX	TAGzT
Molecular formula	$C_6H_{15}N_{19}O_2$	$C_5H_{11}N_{17}O_2$	$C_7H_{18}N_{20}O_2$	$C_3H_6N_6O_6$	$C_4H_{18}N_{22}$
M [g mol^{-1}]	385.32	341.26	414.35	222.12	374.36
IS [J][a]	>40	10	>40	7.5	4
FS [N][b]	>360	>360	>360	120	60
ESD [J][c]	1.2	0.5	1.0	0.2	0.15
Grain size [µm]	<100	<100	<100	<100	<100
N [%][d]	69.07	69.78	67.61	37.84	82.32
Ω [%][e]	−72.7	−63.3	−81.1	−21.6	−72.7
T_{dec} [°C][f]	215	212	240	205	202
ρ [g cm^{-3}][g]	1.63	1.60	1.52	1.80	1.602
$\Delta_f H_m$ [kJ mol^{-1}][h]	928	1128	357	70	1070
$\Delta_f U$ [kJ kg^{-1}][i]	2523	3414	981	417	2990
Calculated detonation parameters (Explo5 v. 6.02)					
$-Q_v$ [kJ kg^{-1}][j]	4156	5064	2624	5844	3670
T_{det} [K][k]	2677	3259	1991	3815	2316
p_{CJ} [kbar][l]	266	267	183	343	282
D [m s^{-1}][m]	8836	8726	7684	8838	9371
V_0 [L kg^{-1}][n]	873	866	877	786	943

[a] Impact sensitivity (BAM drophammer 1 of 6). [b] Friction sensitivity (BAM friction tester 1 of 6). [c] Electrostatic discharge (OZM Research). [d] Nitrogen content. [e] Oxygen balance ($\Omega = (x\mathrm{O} - 2y\mathrm{C} - 0.5z\mathrm{H})1600/M$). [f] Decomposition temperature. [g] Density at room temperature. [h] Calculated enthalpy of formation. [i] Calculated energy of formation. [j] Energy of explosion. [k] Detonation temperature. [l] Detonation pressure. [m] Detonation velocity. [n] Volume of detonation gases.

Table 7.8: Calculated performances of the gun propellant charges assuming isochoric combustion and loading densities of $0.2\,\mathrm{g\,cm^{-3}}$ with EXPLO5 (v. 6.02).

	HN-1[a]					HN-2[b]				
	T_C [K][c]	p_{max} [bar][d]	f_E [kJ g^{-1}][e]	b_E [cm^3 g^{-1}][f]	N_2/CO [w/w][g]	T_C [K][c]	p_{max} [bar][d]	f_E [kJ g^{-1}][e]	b_E [cm^3 g^{-1}][f]	N_2/CO [w/w][g]
HN-1	2574	3063	1.071	1.505	0.82	–	–	–	–	–
HN-2	–	–	–	–	–	2387	2860	0.996	1.517	0.89
19a	2479	2921	1.020	1.508	0.75	2295	2712	0.945	1.518	0.81
19b	2759	3137	1.112	1.454	0.73	2553	2934	1.036	1.469	0.79
19d	2452	2917	1.016	1.516	0.74	2275	2713	0.943	1.525	0.81
23a	2734	3108	1.102	1.454	0.73	2529	2905	1.026	1.469	0.79
23b	2934	3225	1.158	1.411	0.72	2723	3029	1.083	1.426	0.78
23d	2621	3047	1.073	1.479	0.73	2427	2844	0.998	1.492	0.79
23e	2774	3164	1.120	1.412	0.74	2570	2962	1.044	1.474	0.80

[a] HN-1: RDX/bistriaminoguanidinium 5,5′-bisazotetrazolate (TAGzT)/cellulose acetate butyrate (CAB)/1:1 mixture of bis(2,2-dinitropropyl)acetal and -formal (BDNPA-F)/nitrocellulose (NC) (13.25) 56/20/12/8/4. [b] HN-2: RDX/TAGzT/FOX-12/CAB/BDNPA-F/NC (13.25) 40/20/16/12/8/4. [c] Adiabatic combustion temperature. [d] Pressure in closed vessel. [e] Specific energy. [f] Co-volume of gaseous products. [g] N_2/CO ratio

7.3 Conclusions

Synthetic routes towards the novel 4,5-bis(1-hydroxytetrazol-5-yl)-2*H*-1,2,3-triazole (**23**), 4,5-bis(1*H*-tetrazol-5-yl)-2*H*-1,2,3-triazole (**19**), their salts and their comprehensive characterizations were reported. The deprotonation sites of **19d**, one tetrazole and the triazole rings, were revealed by its crystal structure. Furthermore, the crystal structures of the dimethylammonium salt of **19**, **23**, and its salts **23a**, **23b**, and **23k** were presented. The molecules **19** and **23** showed surprisingly high sensitivities towards impact, whereas their nitrogen-rich salts could be classified as less sensitive or even insensitive. All herein-investigated compounds, with the exception of the hydroxylammonium salts **19b** and **23b**, showed high thermal stabilities in the temperature range 215–301 °C. The calculated detonation performances are comparable to common secondary explosives such as RDX. Most promising was the aminoguanidinium salt **19d**, which shows a detonation velocity superior to RDX, while possessing lower sensitivities. With regard to their potential use in gun propellant mixtures, such as the erosion-reduced HN-1 or HN-2 mixtures, the mixtures containing the tetrazole oxide derivatives generally show better combustion characteristics.

7.4 Experimental Section

Caution! *Most compounds prepared herein are energetic compounds sensitive to impact, friction, and electrostatic discharge. Although there were no problems in handling the compounds, proper protective measures (ear protection, Kevlar® gloves, face shield, body armor and earthed equipment) should be used.*

4,5-Dicyano-2*H*-1,2,3-triazole (18)

Compound **18** was synthesized as reported previously.[33]
Diaminomaleodinitrile (10.400 g, 96.20 mmol) was dissolved in water (125 mL) and acidified with 1M hydrochloric acid (100 mL). Sodium nitrite (6.640 g, 96.20 mmol) was added to the mixture in portions at 0 °C while maintaining the temperature below 4 °C during the addition. The reaction mixture was then allowed to warm up to room temperature and stirred for 1 h. The brownish solution was filtrated and the pale brown filtrate was extracted five times with diethyl ether (600 mL). The combined organic layer was dried over $MgSO_4$, filtered and the solvent was removed in vacuo to yield the crude product (10.553 g). The crude product was sublimed at 90 °C under reduced pressure (3×10^{-3} mbar) to afford a colorless powder (9.602 g, 80.68 mmol, 84%).
^{1}H NMR (400 MHz, DMSO-d_6): δ = 16.92 (s, 1H, N*H*) ppm. ^{13}C{^{1}H} NMR (101 MHz, DMSO-d_6): δ = 124.4 (C_{tri}), 110.8 (*C*N) ppm. ^{15}N NMR (41 MHz, DMSO-d_6): δ = −42.0

(s, 2N, *N*NH), −94.2 (s, 1N, *N*H), −107.5 (s, 2N, C*N*) ppm.

4,5-Bis(1*H*-tetrazol-5-yl)-2*H*-1,2,3-triazole (19)

4,5-Dicyano-1,2,3-triazole (**18**) (2.227 g, 18.70 mmol) was dissolved in water (100 mL) and sodium azide (2.930 g, 45.10 mmol) and zinc chloride (3.469 g, 25.45 mmol) were added. The clear solution was heated under reflux for 3 h. After several minutes, a colorless precipitate was formed. The solution was then cooled to room temperature and concentrated hydrochloric acid (50 mL) was added while cooling to 0 °C. The precipitate was removed by filtration under suction and the crude product was washed with water, ethanol, and diethyl ether (each 10 mL) to afford 4,5-bis(1*H*-tetrazol-5-yl)-2*H*-1,2,3-triazole hydrate (3.532 g, 15.83 mmol, 85%) as colorless solid.
DSC (5 °C min^{-1}): T_{dehyd} = 153 °C, T_{dec} = 277 °C. ^{13}C{^{1}H} NMR (101 MHz, DMSO-d_6): δ = 148.1 (C_{tet}), 131.8 (C_{tri}) ppm. IR (ATR): $\tilde{\nu}$ = 3511 (w), 3401 (w), 3238 (m), 3013 (w), 2980 (w), 2520 (w), 2464 (w), 2424 (w), 1896 (vw), 1638 (m), 1604 (m), 1492 (w), 1470 (m), 1442 (vw), 1430 (vw), 1396 (w), 1339 (m), 1249 (vw), 1229 (w), 1188 (w), 1128 (s), 1114 (m), 1074 (s), 1037 (m), 1013 (m), 993 (m), 963 (vs), 894 (m), 836 (m), 772 (vw), 748 (m), 710 (vw), 672 (vw) cm^{-1}. Raman (1064 nm, 300 mW): $\tilde{\nu}$ = 3231 (1), 1639 (50), 1601 (25), 1507 (2), 1495 (2), 1470 (3), 1430 (11), 1391 (6), 1384 (8), 1339 (4), 1303 (10), 1268 (7), 1247 (6), 1203 (6), 1115 (3), 1125 (2), 1097 (2), 1083 (2), 1037 (6), 1019 (5), 993 (3), 773 (4), 749 (2), 489 (8), 428 (5) cm^{-1}. MS (DCI^{+}): m/z (%) = 206.2 (9) [M+H^{+}]. EA ($C_4H_3N_{11} \cdot H_2O$, 223.16 g mol^{-1}): calcd C 21.53, H 2.26, N 69.04%; found C 21.74, H 2.36, N 67.73%. Sensitivities (grain size: < 100 µm): IS: 40 J; FS: > 360 N; ESD: 0.4 J.
After dehydration at 120 °C and 3 × 10^{-3} mbar:
EA ($C_4H_3N_{11}$, 205.14 g mol^{-1}): calcd C 23.42, H 1.47, N 75.11%; found C 24.12, H 1.81, N 73.97%. Sensitivities (grain size: < 100 µm): IS: 2 J; FS: 240 N.

Bisammonium 5-(5-(1*H*-tetrazol-5-yl)-1,2,3-triazolate-4-yl)tetrazolate (19a)

In 2M NH_3 (30 mL) was dissolved 4,5-bis(tetrazol-5-yl)-1,2,3-triazole hydrate (280 mg, 1.25 mmol). The solution was stirred for 1 h at room temperature and then the solvent was removed in vacuo to afford a colorless solid (210 mg, 0.94 mmol, 75%).
DSC (5 °C min^{-1}): T_{melt} = 223 °C, T_{dec} = 301 °C. ^{13}C{^{1}H} NMR (101 MHz, D_2O): δ = 153.2 (C_{tet}), 133.3 (C_{tri}) ppm. ^{14}N{^{1}H} NMR (29 MHz, D_2O): δ = −359 ($N{H_4}^{+}$) ppm. IR (ATR): $\tilde{\nu}$ = 3162 (m), 3036 (s), 2845 (m), 2826 (m), 1886 (w), 1727 (vw), 1703 (m), 1659 (m), 1640 (m), 1562 (m), 1532 (vw), 1464 (s), 1440 (vs), 1413 (vs), 1390 (s), 1290 (vw), 1278 (vw), 1246 (m), 1228 (m), 1152 (m), 1134 (m), 1077 (vw), 1046 (vw), 1028 (vw), 999 (s), 981 (m), 957 (m), 756 (w), 716 (vw), 688 (vw) cm^{-1}. Raman (1064 nm, 300 mW): $\tilde{\nu}$ = 1705 (1),

1638 (100), 1562 (26), 1483 (7), 1464 (1), 1418 (9), 1388 (1), 1326 (8), 1249 (6), 1211 (6), 1189 (12), 1151 (5), 1135 (7), 1111 (6), 1078 (23), 1058 (5), 1046 (7), 999 (2), 981 (3), 775 (9), 757 (2), 688 (2), 489 (7), 431 (3), 382 (3), 325 (12) cm^{-1}. MS (FAB^+): m/z (%) = 18.0 (1) [NH_4^+]. MS (FAB^-): m/z (%) = 204.2 (35) [$C_4H_2N_{11}^-$]. EA ($C_4H_9N_{13}$, 239.20 g mol^{-1}): calcd C 20.08, H 3.79, N 76.12%; found C 20.22, H 3.88, N 73.47%. Sensitivities (grain size: < 100 µm): IS: > 40 J; FS: > 360 N; ESD: 0.8 J.

Bishydroxylammonium 5-(5-(1*H*-tetrazol-5-yl)-1,2,3-triazolate-4-yl)tetrazolate (19b)

4,5-Bis(tetrazol-5-yl)-1,2,3-triazole hydrate (245 mg, 1.10 mmol) was dissolved in water (20 mL) and hydroxylamine solution (50% w/w, ρ = 1.078 g mL^{-1}, 0.10 mL, 2.2 mmol) was added dropwise. The mixture was stirred until a clear solution was obtained. The solvent was removed in vacuo to afford a colorless solid (270 mg, 1.00 mmol, 91%).
DSC (5 °C min^{-1}): T_{dec1} = 160 °C, T_{dec2} = 218 °C. ^{1}H NMR (400 MHz, DMSO-d_6): δ = 10.33 (s) ppm. $^{13}C\{^1H\}$ NMR (101 MHz, DMSO-d_6): δ = 150.0 (C_{tet}), 130.2 (C_{tri}) ppm. IR (ATR): $\tilde{\nu}$ = 3067 (m), 2621 (m), 2508 (m), 2066 (w), 1677 (w), 1658 (w), 1622 (m), 1580 (m), 1556 (m), 1504 (m), 1474 (m), 1463 (m), 1444 (m), 1427 (m), 1407 (m), 1389 (m), 1334 (m), 1302 (w), 1257 (m), 1230 (m), 1187 (vw), 1166 (vw), 1146 (vw), 1122 (m), 1109 (m), 1086 (s), 1063 (vs), 1045 (s), 1018 (m), 998 (vs), 991 (vs), 946 (m), 911 (m), 868 (s), 849 (s), 760 (w), 752 (w), 716 (vw), 704 (vw), 669 (vw) cm^{-1}. Raman (1064 nm, 300 mW): $\tilde{\nu}$ = 1616 (100), 1583 (51), 1557 (14), 1541 (1), 1430 (12), 1398 (2), 1391 (10), 1382 (2), 1344 (9), 1306 (11), 1271 (9), 1258 (4), 1240 (5), 1220 (15), 1202 (1), 1194 (3), 1168 (7), 1120 (1), 1104 (9), 1082 (3), 1049 (3), 1019 (1), 1001 (3), 992 (14), 779 (9), 754 (2), 577 (2), 492 (22), 482 (4), 433 (7), 379 (3), 349 (15) cm^{-1}. MS (FAB^+): m/z (%) = 34.0 (1) [NH_3OH^+]. MS (FAB^-): m/z (%) = 204.3 (86) [$C_4H_2N_{11}^-$]. EA ($C_4H_9N_{13}O_2$, 271.20 g mol^{-1}): calcd C 17.72, H 3.35, N 67.14%; found C 18.65, H 2.83, N 67.88%. Sensitivities (grain size: < 100 µm): IS: > 40 J; FS: > 360 N; ESD: 0.5 J.

Bisguanidinium 5-(5-(1*H*-tetrazol-5-yl)-1,2,3-triazolate-4-yl)tetrazolate (19c)

4,5-Bis(tetrazol-5-yl)-1,2,3-triazole hydrate (235 mg, 1.05 mmol) and guanidinium hydrogen carbonate (256 mg, 2.11 mmol) were dissolved in water (20 mL) and heated under reflux for 1 h. The solvent was removed in vacuo to afford a colorless solid (323 mg, 1.00 mmol, 95%).
DSC (5 °C min^{-1}): T_{dehyd} = 74 °C, T_{endo} = 201 °C, T_{dec} = 289 °C. ^{1}H NMR (400 MHz, DMSO-d_6): δ = 7.65 (s, 12H, NH_2) ppm. $^{13}C\{^1H\}$ NMR (101 MHz, DMSO-d_6): δ = 158.3 ($C(NH_2)_3$), 155.2 (C_{tet}), 133.2 (C_{tri}) ppm. $^{13}C\{^1H\}$ NMR (101 MHz, D_2O): δ = 155.7 ($C(NH_2)_3$), 153.0 (C_{tet}), 131.7 (C_{tri}) ppm. $^{14}N\{^1H\}$ NMR (101 MHz, D_2O): δ = −304

(NH_2). IR (ATR): $\tilde{\nu}$ = 3463 (m), 3348 (m), 3035 (br, s), 2841 (m), 2224 (w), 1637 (vs), 1594 (m), 1435 (w), 1399 (m), 1320 (w), 1308 (w), 1279 (vw), 1236 (w), 1207 (vw), 1169 (m), 1149 (m), 1134 (m), 1102 (m), 1058 (m), 1041 (w), 998 (m), 768 (vw), 741 (vw), 717 (vw) cm^{-1}. Raman (1064 nm, 300 mW): $\tilde{\nu}$ = 1618 (100), 1562 (9), 1544 (21), 1446 (2), 1416 (2), 1402 (8), 1323 (4), 1309 (2), 1251 (6), 1206 (4), 1193 (7), 1148 (2), 1131 (12), 1103 (3), 1060 (15), 1040 (4), 1006 (39), 532 (7), 484 (11), 450 (2), 423 (3), 370 (4), 344 (9) cm^{-1}. MS (FAB^+): m/z (%) = 324.3 (19) [M+H^+], 265.3 (9) [$C_5H_7N_{14}^+$], 119.0 (19) [2(CN_3H_5)+H^+], 60.1 (100) [$CN_3H_6^+$]. MS (FAB^-): m/z (%) = 204.3 (100) [$C_6H_2N_{11}^-$]. EA ($C_6H_{13}N_{17}$·1.25 H_2O, 345.80 g mol^{-1}): calcd C 20.84, H 4.52, N 68.86%; found C 21.25, H 4.75, N 68.56%. Sensitivities (grain size: < 100 µm): IS: > 40 J; FS: > 360 N; ESD 1.5 J.
After dehydration at 120 °C and 3×10^{-3} mbar:
EA ($C_6H_{13}N_{17}$, 323.15 g mol^{-1}): calcd C 22.29, H 4.05, N 73.66%; found C 22.48, H 4.05, N 71.77%. Sensitivities (grain size: < 100 µm): IS: > 40 J; FS: > 360 N; ESD 1.5 J.

Bisaminoguanidinium 5-(5-(1*H*-tetrazol-5-yl)-1,2,3-triazolate-4-yl)tetrazolate (19d)

To **19**·H_2O (221 mg, 0.99 mmol) dissolved in water (20 mL) was added aminoguanidinium hydrogen carbonate (268 mg, 1.97 mmol). The solution was heated under reflux for 1 h and then the solvent was reduced in vacuo. The precipitate was filtered off to afford a colorless solid (288 mg, 0.82 mmol, 83%).
DSC (5 °C min^{-1}): T_{dehyd} = 74 °C, T_{endo} = 185 °C, T_{dec} = 264 °C. ^{1}H NMR (400 MHz, DMSO-d_6): δ = 9.06 (s, 2H, N*H*), 7.18 (m, 8H, CNH_2), 4.71 (s, 4H, NNH_2) ppm. $^{13}C\{^1H\}$ NMR (101 MHz, DMSO-d_6): δ = 158.9 ($C(NH_2)_2NH$), 152.0 (C_{tet}), 131.7 (C_{tri}) ppm. $^{13}C\{^1H\}$ NMR (101 MHz, D_2O): δ = 156.7 ($C(NH_2)_2NH$), 150.8 (C_{tet}), 131.0 (C_{tri}). $^{14}N\{^1H\}$ NMR (101 MHz, D_2O): δ = −311 (NH^+) ppm. IR (ATR): $\tilde{\nu}$ = 3468 (m), 3418 (m), 3390 (m), 3316 (m), 3150 (m), 2954 (m), 2783 (m), 1682 (vs), 1666 (vs), 1640 (vs), 1621 (m), 1592 (m), 1561 (s), 1468 (m), 1431 (w), 1416 (w), 1308 (w), 1252 (vw), 1230 (m), 1190 (w), 1152 (w), 1123 (w), 1096 (m), 1076 (m), 1059 (m), 1039 (m), 1008 (m), 994 (s), 917 (vw), 792 (w), 755 (w), 696 (m) cm^{-1}. Raman (1064 nm, 300 mW): $\tilde{\nu}$ = 1640 (65), 1621 (100), 1591 (30), 1568 (41), 1490 (13), 1442 (7), 1432 (6), 1417 (12), 1388 (8), 1316 (16), 1251 (10), 1224 (13), 1214 (18), 1194 (9), 1144 (15), 1118 (6), 1105 (5), 1098 (5), 1079 (11), 1062 (22), 1040 (15), 1023 (4), 985 (7), 960 (20), 922 (3), 775 (10), 626 (4), 621 (5), 504 (9), 499 (9), 489 (12), 475 (12), 424 (9), 376 (8), 342 (28) cm^{-1}. MS (FAB^+): m/z (%) = 354.4 (19) [M+H^+], 280.3 (14) [$C_5H_9N_{15}^+$], 75.1 (100) [$CH_7N_4^+$]. MS (FAB^-): m/z (%) = 204.3 (100) [$C_4H_2N_{11}^-$]. EA ($C_6H_{15}N_{19}$, 353.18 g mol^{-1}): calcd C 20.40, H 4.28, N 75.32%; found C 20.58, H 4.30, N 72.90%. Sensitivities (grain size: < 100 µm): IS: > 40 J; FS: > 360 N; ESD: 1.0 J.

Bispotassium 5-(5-(1*H*-tetrazol-5-yl)-1,2,3-triazolate-4-yl)tetrazolate (19f)

To 4,5-bis(tetrazol-5-yl)-1,2,3-triazole (**19**) (457 mg, 2.05 mmol) suspended in water (50 mL) potassium hydroxide (239 mg, 4.26 mmol) dissolved in water (10 mL) was added dropwise. The suspension turned into a clear solution after some minutes of stirring. The solution was stirred at 50 °C for 1 h. Then the solvent was removed in vacuo to afford a colorless solid (550 mg, 1.96 mmol, 96%).
DSC (5 °C min^{-1}): T_{dec} = 330 °C. $^{13}C\{^{1}H\}$ NMR (101 MHz, D_2O): δ = 153.1 (C_{tet}), 133.3 (C_{tri}) ppm. IR (ATR): $\tilde{\nu}$ = 3324 (w), 3010 (s), 1790 (vw), 1657 (w), 1650 (w), 1615 (w), 1581 (w), 1556 (w), 1462 (vw), 1440 (m), 1410 (m), 1344 (w), 1292 (vw), 1279 (vw), 1258 (vw), 1234 (vw), 1204 (vw), 1171 (m), 1134 (m), 1104 (s), 1046 (m), 994 (vs), 908 (m), 763 (w), 673 (w) cm^{-1}. Raman (1064 nm, 300 mW): $\tilde{\nu}$ = 1648 (2), 1626 (7), 1603 (100), 1558 (60), 1547 (19), 1473 (1), 1440 (7), 1412 (11), 1344 (5), 1294 (13), 1259 (17), 1207 (26), 1177 (13), 1134 (20), 1294 (13), 1259 (17), 1207 (26), 1177 (13), 1134 (20), 1080 (6), 1094 (16), 1047 (28), 1034 (4), 1001 (6), 786 (6), 764 (2), 719 (1), 581 (2), 493 (15), 440 (7), 388 (3), 338 (10), 212 (2) cm^{-1}. MS (FAB$^+$): m/z (%) = 39.0 (22) [K^+]. MS (FAB$^-$): m/z (%) = 204.2 (36) [$C_4H_2N_{11}^-$], 242.2 (39) [$C_4HKN_{11}^-$], 280.0 (5) [M−H^-]. EA ($C_4HK_2N_{11}$·0.2 H_2O, 284.57 g mol^{-1}): calcd C 16.86, H 0.50, N 54.08%; found C 17.32, H 0.97, N 53.99%. Sensitivities (grain size: < 100 µm): IS: > 40 J; FS: > 360 N; ESD: 0.5 J.

Trissilver 4,5-bis(tetrazolate-5-yl)-1,2,3-triazolate hydrate (19g·H_2O)

A solution of **19** (215 mg, 1.05 mmol) in a mixture of water (5 mL) and aqueous sodium hydroxide (2M, 1.0 mL) was added dropwise to a solution of silver nitrate (535 mg, 3.15 mmol) in water (14 mL) at 90 °C. The resulting suspension was refluxed for 30 min. After cooling to room temperature the precipitate was filtered off and washed with water, ethanol, and diethyl ether, then dried in air to yield a colorless powder (533 mg, 0.98 mmol, 98%).
DSC (5 °C min^{-1}): T_{dec} = 336 °C. IR (ATR): $\tilde{\nu}$ = 3356 (w), 1621 (w), 1544 (w), 1413 (s), 1320 (m), 1251 (w), 1189 (m), 1144 (s), 1109 (w), 1063 (w), 1042 (w), 1022 (w), 996 (vs), 870 (w), 756 (m), 718 (w), 702 (w) cm^{-1}. EA ($C_4Ag_3N_{11} \cdot H_2O$, 543.74 g mol^{-1}): calcd C 8.84, H 0.37, N 28.34%; found C 9.22, H 0.61, N 28.86%. Sensitivities (grain size: < 100 µm): IS: 12 J; FS: 288 N; ESD: 50 mJ.

Biscesium 5-(5-(1*H*-tetrazol-5-yl)-1,2,3-triazolate-4-yl)tetrazolate (19h)

19 (223 mg, 1.00 mmol) and cesium carbonate (325 mg, 1.00 mmol) were suspended in ethanol / water (3:1, 20 mL) and heated under stirring. Water was added dropwise until all solids were dissolved and the solution was further refluxed for 15 min. The solvent was removed under reduced pressure and the residue was washed with ethanol and diethyl ether,

then dried in air to yield a colorless powder (420 mg, 0.90 mmol, 90%).
DSC (5 °C min^{-1}): T_{dec} = 322 °C. IR (ATR): $\tilde{\nu}$ = 2651 (w), 1888 (w), 1628 (w), 1552 (w), 1472 (w), 1464 (w), 1412 (m), 1382 (m), 1315 (w), 1282 (w), 1240 (m), 1211 (w), 1140 (m), 1117 (m), 1067 (w), 1040 (w), 1031 (w), 990 (vs), 978 (vs), 758 (w), 715 (w), 688 (w) cm^{-1}. EA ($C_4HCs_2N_{11}$, 468.94 g mol^{-1}): calcd C 10.25, H 0.21, N 32.86%; found C 10.75, H 0.43, N 33.47%. Sensitivities (grain size: < 100 µm): IS: 25 J; FS: 360 N; ESD: 0.1 J.

Copper 5-(5-(1*H*-tetrazol-5-yl)-1,2,3-triazolate-4-yl)tetrazolate dihydrate (19i·2 H_2O)

Prepared similar to **19g** using copper(II) chloride dihydrate (179 mg, 3.15 mmol) yielding a blue powder (300 mg, 0.99 mmol, 99%).
DSC (5 °C min^{-1}): T_{dehyd} = 157 °C, T_{dec} = 305 °C. IR (ATR): $\tilde{\nu}$ = 3135 (m), 1675 (w), 1624 (m), 1588 (w), 1475 (w), 1452 (w), 1427 (s), 1350 (w), 1340 (w), 1286 (w), 1258 (w), 1249 (w), 1203 (w), 1168 (w), 1148 (s), 1110 (w), 1034 (w), 1003 (vs), 991 (s), 859 (s), 780 (w), 758 (w), 723 (w) cm^{-1}. EA ($C_4HCuN_{11} \cdot 2\,H_2O$, 302.71 g mol^{-1}): calcd C 15.87, H 1.66, N 50.90%; found C 15.56, H 1.89, N 48.45%. Sensitivities (grain size: < 100 µm): IS: 35 J; FS: 160 N; ESD: 0.2 J.

Zinc 5-(5-(1*H*-tetrazol-5-yl)-1,2,3-triazolate-4-yl)tetrazolate dihydrate (19j·2 H_2O)

Prepared similar to **19g** using zinc chloride (143 mg, 1.05 mmol) yielding a colorless powder (262 mg, 0.86 mmol, 86%).
DSC (5 °C min^{-1}): T_{dec1} = 272 °C, T_{dec2} = 370 °C. IR (ATR): $\tilde{\nu}$ = 3196 (s), 2298 (w), 1892 (w), 1634 (m), 1603 (m), 1566 (m), 1490 (w), 1466 (w), 1428 (m), 1418 (m), 1396 (w), 1357 (w), 1337 (m), 1326 (w), 1283 (w), 1268 (w), 1226 (m), 1178 (s), 1162 (s), 1128 (w), 1112 (w), 1079 (m), 1063 (m), 1038 (w), 1009 (vs), 994 (m), 962 (m), 896 (w), 886 (w), 833 (w), 796 (w), 762 (w), 748 (w), 732 (w), 694 (m), 674 (m) cm^{-1}. EA ($C_4HN_{11}Zn \cdot 2\,H_2O$, 304.54 g mol^{-1}): calcd C 15.78, H 1.65, N 50.59%; found C 15.43, H 1.67, N 48.25%. Sensitivities (grain size: < 100 µm): IS: 15 J; FS: 360 N; ESD: 0.2 J.

2*H*-1,2,3-Triazol-4,5-bis(carboxamidoxime) (20)

4,5-Dicyano-2*H*-1,2,3-triazole (**18**) (2.111 g, 17.73 mmol) was dissolved in water (100 mL) and hydroxylamine (50% *w*/*w*, 2.2 mL, 35.97 mmol) was added. The solution was heated under reflux for 2 h. Afterwards the solution was concentrated under reduced pressure to approximately 50 mL. The formed precipitate was filtered off to afford **20** (3.013 g, 16.27 mmol, 92%) as a colorless solid.

DSC (5 °C min^{-1}): T_{dec} = 252 °C. ^{1}H NMR (400 MHz, DMSO-d_6): δ = 9.91 (s, 2H, O*H*), 6.67 (s, 4H, NH_2) ppm. ^{13}C{^{1}H} NMR (101 MHz, DMSO-d_6): δ = 146.7 (*C*NOH), 133.6 (C_{tri}) ppm. IR (ATR): $\tilde{\nu}$ = 3467 (w), 3381 (m), 3349 (m), 3288 (br, w), 3242 (vw), 2540 (br, m), 1679 (vs), 1631 (vs), 1582 (vs), 1532 (w), 1463 (s), 1347 (m), 1257 (w), 1215 (m), 1148 (w), 1106 (s), 1029 (m), 1007 (s), 912 (m), 829 (s), 808 (s), 765 (m), 716 (vw), 684 (w) cm^{-1}. Raman (1064 nm, 300 mW): $\tilde{\nu}$ = 3352 (7), 2702 (5), 2238 (17), 1673 (16), 1575 (100), 1539 (14), 1438 (8), 1338 (15), 1260 (7), 1218 (23), 1154 (22), 1133 (14), 1088 (18), 1017 (29), 826 (7), 757 (19), 589 (35), 560 (63), 500 (16), 474 (14), 450 (22), 420 (22), 380 (27), 368 (26), 353 (12), 338 (20), 231 (35) cm^{-1}. MS (DEI$^+$): m/z (%) = 185 (100) [M$^+$], 152 (18) [$C_4H_4N_6O^+$], 110 (45) [$C_3H_2N_4O^+$], 67 (56) [$C_2HN_3^+$]. EA ($C_4H_7N_7O_2$, 185.15 g mol^{-1}): calcd C 25.95, H 3.81, N 52.96%; found C 26.41, H 3.68, N 52.56%. Sensitivities (grain size: < 100 µm): IS: > 40 J; FS: > 360 N; ESD: 0.75 J.

2*H*-1,2,3-Triazol-4,5-bis(carboxoxime dichloride) (21)

20 (2.010 g, 10.84 mmol) was dissolved in a solution of concentrated hydrochloric acid (25 mL) and water (25 mL). The solution was cooled down to −10 °C and then sodium nitrite (3.730 g, 54.09 mmol) dissolved in water (15 mL) was added dropwise while maintaining the temperature at −10 °C. After complete addition, the solution was stirred at room temperature overnight. It was extracted three times with diethyl ether (25 mL). The combined organic layer was washed with brine (20 mL), dried over magnesium sulfate, and insolubles were filtered off. The solvent was evaporated to yield a colorless solid (2.155 g, 9.62 mmol, 89%).
DSC (5 °C min^{-1}): T_{dec} = 114 °C. ^{1}H NMR (400 MHz, DMSO-d_6): δ = 15.74 (s, 1H, N*H*), 12.73 (s, 2H, O*H*) ppm. ^{13}C{^{1}H} NMR (101 MHz, DMSO-d_6): δ = 137.9 (*C*NOH), 126.1 (C_{tri}) ppm. MS (DEI$^+$): m/z (%) = 223 (4) [M$^+$]. EA ($C_4H_3Cl_2N_5O_2$, 224.00 g mol^{-1}): C 21.45, H 1.35, N 31.26%; found C 22.40, H 1.40, N 30.78%. Sensitivities (grain size: < 100 µm): IS: 15 J; FS: > 360 N; ESD: 0.4 J.

4,5-Bis(1-hydroxytetrazol-5-yl)-2*H*-1,2,3-triazole (23)

A solution of **21** (2.817 g, 12.58 mmol) in ethanol (35 mL) was cooled to 0 °C and sodium azide (5.747 g, 88.40 mmol) dissolved in water (25 mL) was added dropwise while the temperature was maintained below 5 °C. The clear yellow solution was then stirred overnight. It was then acidified with 2M hydrochloric acid (30 mL) and extracted four times with diethyl ether (100 mL). The combined organic layers were washed with brine and dried over magnesium sulfate, which was then filtered off to afford a solution of **22** in diethyl ether. The solution of **22** was cooled to 0 °C and hydrogen chloride was bubbled through

intermittently while the temperature should not exceed 10 °C. The saturated solution was stirred for 3 d. The solvent was then evaporated in air and the colorless residue was recrystallized in water. After suction filtration, **23** (1.126 g, 4.75 mmol, 38%) was obtained as a colorless solid.

DSC (5 °C min^{-1}): T_{dec} = 246 °C. ^{1}H NMR (400 MHz, DMSO-d_6): δ = 9.11 (s, 2H, O*H*) ppm. ^{13}C{^{1}H} NMR (101 MHz, DMSO-d_6): δ = 138.9 (C_{tet}), 129.1 (C_{tri}) ppm. ^{15}N NMR (41 MHz, DMSO-d_6): δ = −2.6 (*N*NOH), −18.9 (*N*N$_{tet}$), −53.5 (C*N*$_{tet}$), −54.9 (*N*NH), −100.3 (*NOH*), −116.1 (*N*OH) ppm. IR (ATR): $\tilde{\nu}$ = 3507 (br, w), 2978 (m), 2099 (vw), 1815 (vw), 1624 (w), 1453 (m), 1409 (m), 1351 (w), 1302 (m), 1273 (w), 1225 (m), 1193 (w), 1099 (vs), 1017 (s), 990 (w), 982 (w), 916 (br), 758 (w), 733 (m), 686 (s), 669 (m) cm^{-1}. Raman (1064 nm, 300 mW): $\tilde{\nu}$ = 1625 (100), 1594 (65), 1359 (6), 1291 (24), 1261 (19), 1220 (75), 1189 (8), 1152 (10), 1004 (13), 989 (10), 765 (13), 746 (22), 718 (6), 467 (17), 450 (11), 351 (5), 281 (11), 221 (5) cm^{-1}. MS (DEI^{+}): m/z (%) = 238 (1) [M+H^{+}], 67 (24) [$C_2HN_3^{+}$], 28 (100) [N_2^{+}]. EA ($C_4H_3N_{11}O_2 \cdot 2\,H_2O$, 273.17 g mol^{-1}): calcd C 17.59, H 2.58, N 56.40%; found C 18.06, H 2.56, N 55.94%. Sensitivities (grain size: < 100 µm): IS: 40 J; FS: > 360 N; ESD: 1.50 J.

After dehydration at 120 °C and 3 × 10^{-3} mbar:

EA ($C_4H_3N_{11}O_2$, 237.14 g mol^{-1}): calcd C 20.26, H 1.28, N 64.97%; found C 20.33, H 1.83, N 63.09%. Sensitivities (grain size: < 100 µm): IS: 1 J; FS: 240 N; ESD: 0.3 J.

Bisammonium 4,5-bis(tetrazol-1-oxide-5-yl)-2*H*-1,2,3-triazole (23a)

23 (109 mg, 0.40 mmol) was dissolved in 2M aqueous ammonia (10 mL) and stirred for 1 h at room temperature. The reaction mixture was suction filtered and a brownish solid (107 mg, 0.39 mmol, 97%) was obtained.

DTA (5 °C min^{-1}): T_{dehyd} = 80 °C, T_{dec} = 241 °C. ^{1}H NMR (400 MHz, DMSO-d_6): δ = 7.10 (s, 8H, N*H*$_4^{+}$) ppm. ^{13}C{^{1}H} NMR (101 MHz, DMSO-d_6): δ = 138.5 (C_{tet}), 130.2 (C_{tri}) ppm. ^{14}N{^{1}H} NMR (29 MHz, DMSO-d_6): δ = −355 (*N*H$_4^{+}$) ppm. ^{15}N NMR (41 MHz, DMSO-d_6): δ = −14.8 (N*N*$_{tet}$), −19.8 (*N*NO^{-}), −32.7 (*N*H), −49.6 (N_{tri}), −57.5 (C*N*$_{tet}$), −86.8 (*N*O^{-}), −359.3 (*N*H$_4^{+}$) ppm. IR (ATR): $\tilde{\nu}$ = 3176 (br, w), 3087 (br, w), 2962 (br, m), 2811 (br, m), 2188 (vw), 2105 (vw), 2042 (vw), 1984 (vw), 1680 (br, vw), 1575 (m), 1412 (vs), 1391 (s), 1294 (m), 1264 (w), 1231 (vs), 1213 (m), 1194 (m), 1176 (w), 1132 (w), 1092 (vw), 1032 (m), 1011 (m), 985 (s), 759 (m), 741 (m) cm^{-1}. Raman (1064 nm, 300 mW): $\tilde{\nu}$ = 1586 (100), 1547 (15), 1257 (26), 1238 (8), 1206 (4), 1181 (33), 1162 (23), 1128 (15), 1005 (11), 752 (11), 464 (4) cm^{-1}. MS (FAB^{+}): m/z (%) = 18 (1) [NH$_4^{+}$]. MS (FAB^{-}): m/z (%) = 236 (9) [$C_4H_2N_{11}O_2^{-}$]. EA ($C_4H_9N_{13}O_2 \cdot 2\,H_2O$, 307.24 g mol^{-1}): calcd C 15.64, H 4.27, N 59.27%; found C 16.26, H 4.50, N 60.19%. Sensitivities (grain size: < 100 µm):

IS: 10 J; FS: > 360 N; ESD: 1.00 J.
After dehydration at 120 °C:
EA ($C_4H_9N_{13}O_2$, 271.21 g mol^{-1}): calcd C 17.72, H 3.35, N 67.14%; found C 17.50, H 3.72, N 64.51%. Sensitivities (grain size: < 100 µm): IS: 10 J; FS: > 360 N; ESD: 0.7 J.

Bishydroxylammonium 4,5-bis(tetrazol-1-oxide-5-yl)-2*H*-1,2,3-triazole (23b)

An aqueous hydroxylamine solution (50% *w*/*w*, 71 mg, 0.14 mL, 2.14 mmol) was added to a solution of **23** (253 mg, 1.07 mmol) in water (20 mL) and stirred for 1.5 h at room temperature. The solvent was then removed under reduced pressure to obtain a colorless solid (319 mg, 0.99 mmol, 92%).
DSC (5 °C min^{-1}): T_{dehyd} = 131 °C, T_{dec} = 182 °C. ^{1}H NMR (400 MHz, DMSO-d_6): δ = 9.49 (br) ppm. ^{13}C{^{1}H} NMR (101 MHz, DMSO-d_6): δ = 137.8 (C_{tet}), 129.9 (C_{tri}) ppm. IR (ATR): $\tilde{\nu}$ = 3366 (vw), 3139 (br, m), 2693 (br, m), 1988 (vw), 1620 (m), 1580 (w), 1513 (m), 1404 (vs), 1317 (vw), 1276 (s), 1264 (w), 1227 (vs), 1189 (s), 1151 (s), 1081 (w), 1029 (m), 1002 (s), 988 (m), 890 (m), 757 (s), 687 (m) cm^{-1}. Raman (1064 nm, 300 mW): $\tilde{\nu}$ = 1643 (100), 1588 (23), 1494 (9), 1425 (4), 1405 (3), 1318 (3), 1286 (4), 1260 (10), 1242 (20), 1224 (5), 1191 (4), 1154 (15), 1137 (2), 1004 (16), 761 (10), 749 (2), 694 (6), 559 (3), 467 (6), 265 (3) cm^{-1}. MS (FAB$^-$): *m*/*z* (%) = 236 (14) [$C_4H_2N_{11}O_2^-$]. EA ($C_4H_9N_{13}O_4 \cdot H_2O$, 317.62 g mol^{-1}): calcd C 14.96, H 3.45, N 56.69%; found C 15.87, H 3.51, N 55.91%. Sensitivities (grain size: < 100 µm): IS: > 40 J; FS: > 360 N; ESD: 0.45 J.
After dehydration at 120 °C:
EA ($C_4H_9N_{13}O_4$, 303.20 g mol^{-1}): calcd C 15.85, H 2.99, N 60.06%; found C 16.67, H 3.57, N 59.26%. Sensitivities (grain size: < 100 µm): IS: > 7 J; FS: > 360 N; ESD: 0.3 J.

Bisguanidinium 4,5-bis(tetrazol-1-oxide-5-yl)-2*H*-1,2,3-triazole (23c)

To a solution of **23** (247 mg, 0.90 mmol) in ethanol (15 mL), bisguanidinium carbonate (165 mg, 0.92 mmol) was added and the reaction mixture was stirred for 15 min at room temperature. The colorless precipitate was then suction filtered, washed with diethyl ether and dried at air. **23c** (237 mg, 0.67 mmol, 74%) was obtained as a hydrate, which was then dried at 120 °C.
DTA (5 °C min^{-1}): T_{melt} = 190 °C, T_{endo} = 222 °C, T_{dec} = 244 °C. ^{1}H NMR (270 MHz, DMSO-d_6): δ = 7.16 (s, 12H, NH_2) ppm. ^{13}C{^{1}H} NMR (68 MHz, DMSO-d_6): δ = 158.6 (C(NH$_2$)$_3$), 138.4 (C_{tet}), 130.0 (C_{tri}) ppm. IR (ATR): $\tilde{\nu}$ = 3348 (br, m), 3234 (br, m), 3076 (br, m), 2812 (br, w), 2343 (vw), 1658 (vs), 1641 (vs), 1581 (w), 1448 (w), 1434 (w), 1420 (m), 1403 (w), 1314 (w), 1279 (m), 1252 (m), 1228 (s), 1192 (w), 1179 (w), 1141 (w), 1090 (w), 1066 (vw), 1032 (m), 998 (w), 984 (s), 869 (w), 764 (m) cm^{-1}. Raman

(1064 nm, 300 mW): $\tilde{\nu}$ = 1655 (22), 1642 (100), 1613 (4), 1584 (47), 1456 (22), 1283 (16), 1253 (9), 1230 (41), 1205 (5), 1194 (9), 1138 (33), 1013 (80), 991 (6), 765 (20), 744 (20), 538 (15), 476 (7), 453 (10), 383 (7), 301 (23) cm^{-1}. MS (FAB^+): m/z (%) = 60 (26) [$CH_6N_3^+$]. MS (FAB^-): m/z (%) = 236 (43) [$C_4H_2N_{11}O_2^-$]. EA ($C_6H_{13}N_{17}O_2$, 355.28 g mol^{-1}): calcd C 20.28, H 3.69, N 67.02%; found C 20.81, H 3.75, N 66.10%. Sensitivities (grain size: < 100 µm): IS: > 40 J; FS: > 360 N; ESD: 1.25 J.

Bisaminoguanidinium 4,5-bis(tetrazol-1-oxide-5-yl)-2*H*-1,2,3-triazole (23d)

A solution of **23** (296 mg, 1.25 mmol) in water (30 mL) was heated to 70 °C and aminoguanidinium hydrogen carbonate (347 mg, 2.55 mmol) was added. The reaction mixture was stirred for 1 h at room temperature. The solvent was removed under reduced pressure and the residue was recrystallized in water, which then was allowed to evaporate at air. A yellow solid (400 mg, 1.04 mmol, 83%) was obtained.
DSC (5 °C min^{-1}): T_{dehyd} = 84 °C, T_{dec} = 215 °C. ^{1}H NMR (270 MHz, DMSO-d_6): δ = 7.37 (s, 8H, NH_2), 4.67 (s, 4H, NNH_2) ppm. $^{13}C\{^1H\}$ NMR (101 MHz, DMSO-d_6): δ = 159.6 ($C(NH_2)_2NH$), 139.7 (C_{tet}), 130.3 (C_{tri}) ppm. IR (ATR): $\tilde{\nu}$ = 3355 (m), 3240 (br, m), 3134 (br, w), 3082 (m), 2849 (br, w), 2205 (vw), 1667 (vs), 1591 (m), 1431 (s), 1390 (w), 1378 (w), 1278 (w), 1262 (w), 1234 (s), 1196 (m), 1164 (vw), 1149 (w), 1128 (w), 1030 (w), 990 (vw), 982 (s), 905 (w), 762 (w), 745 (w), 681 (w) cm^{-1}. Raman (1064 nm, 300 mW): $\tilde{\nu}$ = 3260 (4), 1624 (100), 1592 (9), 1571 (26), 1437 (6), 1279 (6), 1236 (18), 1205 (9), 1151 (15), 1121 (19), 1107 (2), 1007 (15), 965 (19), 747 (18), 514 (8), 466 (6), 386 (13), 380 (4), 296 (5) cm^{-1}. MS (FAB^+): m/z (%) = 75 (100) [$CH_7N_4^+$]. MS (FAB^-): m/z (%) = 236 (100) [$C_4H_2N_{11}O_2^-$]. EA ($C_6H_{15}N_{19}O_2 \cdot H_2O$, 403.33 g mol^{-1}): calcd C 17.87, H 4.25, N 65.98%; found C 18.32, H 4.50, N 64.53%. Sensitivities (grain size: < 100 µm): IS: > 40 J; FS: > 360 N; ESD: 1.5 J.
After dehydration at 120 °C:
EA ($C_6H_{15}N_{19}O_2$, 385.32 g mol^{-1}): calcd C 18.70, H 3.92, N 69.07%; found C 19.75, H 4.24, N 66.90%. Sensitivities (grain size: < 100 µm): IS: > 40 J; FS: > 360 N; ESD: 1.2 J.

Triaminoguanidinium 4-(tetrazol-1-oxide-5-yl)-5-(1-hydroxytetrazol-5-yl)-2*H*-1,2,3-triazole (23e)

To a solution of **23** (253 mg, 1.07 mmol) in water (25 mL) triaminoguanidinium chloride (260 mg, 1.46 mmol) was added, and the reaction mixture was stirred overnight at 100 °C. After cooling to room temperature, the solution was stored at 8 °C and the crystalline precipitate was filtered off to afford a colorless solid (341 mg, 1.00 mmol, 93%).
DSC (5 °C min^{-1}): T_{melt} = 199 °C, T_{dec} = 212 °C. ^{1}H NMR (400 MHz, DMSO-d_6): δ = 8.59

(s, 1H), 4.41 (s, 9H, C(N*H*N*H*$_2$)$_3$) ppm. ^{13}C{^{1}H} NMR (101 MHz, DMSO-d_6): δ = 159.1 (*C*(NHNH$_2$)$_3$), 138.9 (C_{tet}), 129.0 (C_{tri}) ppm. IR (ATR): $\tilde{\nu}$ = 3351 (w), 3338 (w), 3211 (m), 3127 (vw), 2357 (w), 1856 (br, w), 1681 (s), 1609 (w), 1585 (w), 1451 (w), 1439 (w), 1384 (w), 1359 (w), 1300 (w), 1278 (m), 1261 (w), 1223 (m), 1194 (w), 1162 (w), 1130 (s), 1113 (s), 1035 (m), 975 (vs), 939 (s), 773 (m), 751 (m), 727 (m), 679 (m), 642 (m) cm^{-1}. Raman (1064 nm, 300 mW): $\tilde{\nu}$ = 3353 (3), 3341 (5), 3287 (6), 3277 (9), 1613 (100), 1579 (21), 1387 (4), 1367 (4), 1301 (12), 1259 (24), 1226 (6), 1139 (7), 899 (3), 890 (2), 878 (11), 778 (6), 743 (5), 731 (8), 649 (5), 635 (2), 598 (4), 553 (9) cm^{-1}. MS (FAB$^+$): *m*/*z* (%) = 105 (15) [$CH_9N_6^+$]. MS (FAB$^-$): *m*/*z* (%) = 236 (17) [$C_4H_2N_{11}O_2^-$]. EA ($C_5H_{11}N_{17}O_2$, 341.26 g mol^{-1}): calcd C 17.60, H 3.25, N 69.78%; found C 17.79, H 3.46, N 68.23%. Sensitivities (grain size: < 100 µm): IS: 10 J; FS: > 360 N; ESD: 0.5 J.

Trisguanidinium 4,5-bis(tetrazol-1-oxide-5-yl)-1,2,3-triazolate (23k)

To a solution of **23**·2 H_2O (249 mg, 0.91 mmol) in ethanol (15 mL) bisguanidinium carbonate (241 mg, 1.35 mmol) was added. The reaction mixture was then stirred for 45 min at room temperature. The yellowish precipitate was then suction filtered, washed with diethyl ether and dried in air. The crude product was two times recrystallized in water and dried at 120 °C to afford **23k** (106 mg, 0.26 mmol, 28%).
DTA (5 °C min^{-1}): T_{melt} = 190 °C, T_{dec} = 240 °C. ^{1}H NMR (270 MHz, DMSO-d_6): δ = 7.40 (s, 18H, N*H*$_2$) ppm. ^{13}C{^{1}H} NMR (68 MHz, DMSO-d_6): δ = 158.8 (*C*(NH$_2$)$_3$), 139.6 (C_{tet}), 130.7 (C_{tri}) ppm. IR (ATR): $\tilde{\nu}$ = 3431 (w), 3360 (br, m), 3127 (br, m), 3019 (br, m), 2811 (br, w), 2350 (w), 2227 (vw), 1641 (vs), 1577 (m), 1431 (m), 1416 (m), 1403 (m), 1277 (m), 1228 (s), 1166 (w), 1141 (m), 1084 (w), 1031 (m), 999 (w), 983 (s), 762 (m), 737 (vw) cm^{-1}. Raman (1064 nm, 300 mW): $\tilde{\nu}$ = 1640 (2), 1613 (100), 1562 (27), 1434 (18), 1422 (3), 1405 (58), 1333 (13), 1263 (11), 1231 (8), 1203 (6), 1166 (4), 1132 (14), 1089 (2), 1011 (39), 771 (5), 752 (33), 716 (2), 554 (7), 538 (11), 469 (3) cm^{-1}. MS (FAB$^+$): *m*/*z* (%) = 60 (26) [$CH_6N_3^+$]. MS (FAB$^-$): *m*/*z* (%) = 236 (43) [$C_4H_2N_{11}O_2^-$]. EA ($C_7H_{18}N_{20}O_2$, 414.35 g mol^{-1}): calcd C 20.29, H 4.38, N 67.61%; found C 20.83, H 4.79, N 66.99%. Sensitivities (grain size: < 100 µm): IS: > 40 J; FS: > 360 N; ESD: 1.0 J.

Bispotassium 4,5-bis(tetrazol-1-oxide-5-yl)-2*H*-1,2,3-triazole monohydrate (23f·H_2O)

23 (495 mg, 2.11 mmol) was dissolved in ethanol (30 mL) and a solution of potassium hydroxide (244 mg, 4.22 mmol) in water (10 mL) was added. The reaction mixture was heated to 70 °C for 1.5 h under reflux. After suction filtration the colorless precipitate was washed with diethyl ether and dried at air to obtain a colorless solid (433 mg, 1.38 mmol,

65%).
DTA (5 °C min^{-1}): T_{dec} = 283 °C. $^{13}C\{^1H\}$ NMR (68 MHz, DMSO-d_6): δ = 139.6 (C_{tet}), 128.6 (C_{tri}) ppm. IR (ATR): $\tilde{\nu}$ = 3465 (w), 3376 (vw), 3289 (vw), 3051 (br, m), 2361 (w), 1672 (m), 1569 (vw), 1526 (vw), 1435 (m), 1411 (vs), 1385 (w), 1289 (m), 1278 (m), 1236 (s), 1203 (w), 1125 (w), 1097 (s), 1076 (m), 1027 (w), 1010 (w), 994 (m), 978 (vs), 886 (m), 850 (w), 769 (w), 761 (m), 747 (w), 667 (vw) cm^{-1}. Raman (1064 nm, 300 mW): $\tilde{\nu}$ = 1623 (100), 1574 (18), 1465 (23), 1453 (4), 1413 (3), 1389 (47), 1293 (11), 1277 (4), 1250 (17), 1204 (7), 1135 (8), 1101 (16), 995 (8), 979 (14), 771 (6), 749 (4), 461 (5), 376 (2), 299 (3), 259 (2) cm^{-1}. MS (FAB$^+$): m/z (%) = 39 (3) [K^+]. MS (FAB$^-$): m/z (%) = 236 (6) [$C_4H_2N_{11}O_2^-$]. EA ($C_4HK_2N_{11}O_2 \cdot H_2O$, 331.34 g mol^{-1}): calcd C 14.50, H 0.91, N 46.50%; found C 14.84, H 1.24, N 45.56%. Sensitivities (grain size: < 100 µm): IS: > 40 J; FS: > 360 N; ESD: 1.00 J.

7.5 References

[1] E. L. Etnier, *Regul. Toxicol. Pharmcol.* **1989**, *9*, 147–157.

[2] P. Y. Robidoux, J. Hawari, G. Bardai, L. Paquet, G. Ampleman, S. Thiboutot, G. I. Sunahara, *Arch. Environ. Contam. Toxicol.* **2002**, *43*, 379–388.

[3] T. M. Klapötke, *Chemie der hochenergetischen Materialien*, 1st ed., de Gruyter, Berlin, Germany, **2009**.

[4] J. Akhavan, *The Chemistry of Explosives*, RSC, Cambridge, UK, **2004**.

[5] A. F. Holleman, E. Wiberg, N. Wiberg, *Lehrbuch der Anorganischen Chemie*, 102nd ed., de Gruyter, Berlin, Germany, **2007**.

[6] T. M. Klapötke, J. Stierstorfer, in *Green Energetic Materials* (Ed.: T. Brinck), Wiley, Hoboken, NJ (USA), **2014**, pp. 133–178.

[7] R. Huisgen, I. Ugi, *Angew. Chem.* **1956**, *68*, 705–706.

[8] A. A. Dippold, D. Izsák, T. M. Klapötke, *Chem. Eur. J.* **2013**, *19*, 12042–12051.

[9] Y. Guo, G.-H. Tao, Z. Zeng, H. Gao, D. A. Parrish, J. M. Shreeve, *Chem. Eur. J.* **2010**, *16*, 3753–3762.

[10] K. Y. Lee, C. B. Storm, M .A. Hiskey, M. D. Coburn, *J. Energ. Mater.* **1991**, *9*, 415–428.

[11] D. G. Piercey, D. E. Chavez, S. Heimsch, C. Kirst, T. M. Klapötke, J. Stierstorfer, *Propellants, Explos., Pyrotech.* **2015**, *40*, 491–497.

[12] Y. Zhang, D. A. Parrish, J. M. Shreeve, *J. Mater. Chem. A* **2013**, *1*, 585–593.

[13] J. Zhang, Q. Zhang, T. T. Vo, D. A. Parrish, J. M. Shreeve, *J. Am. Chem. Soc.* **2015**, *137*, 1697–1704.

[14] I. V. Tselinskii, S. F. Mel'nikova, T. V. Romanova, *Russ. J. Org. Chem.* **2001**, *37*, 430–436.

[15] D. Izsák, T. M. Klapötke, C. Pflüger, *Dalton Trans.* **2015**, *44*, 17054–17063.

[16] C. Bian, K. Wang, L. Liang, M. Zhang, C. Li, Z. Zhou, *Eur. J. Inorg. Chem.* **2014**, 6022–6030.

[17] D. E. Chavez, J. C. Bottaro, M. Petrie, D. A. Parrish, *Angew. Chem., Int. Ed.* **2015**, *54*, 12973–12975; *Angew. Chem.* **2015**, *127*, 13165–13167.

[18] H. Tanaka, T. Toda (Toyo Kasei Kogyo Co. Ltd., Osaka), WO20070133323A1 **2007**.

[19] P. Pagoria, M. Zhang, A. DeHope, G. Lee, A. Mitchell, P. Leonard, in *New Trends in Research of Energetic Materials*, *Procedding Semin.*, Pardubice, Czech Republic, **2012**, *1*, pp. 55–65.

[20] T. M. Klapötke, D. G. Piercey, J. Stierstorfer, *Chem. Eur. J.* **2011**, *17*, 13068–13077.

[21] A. A. Dippold, T. M. Klapötke, *J. Am. Chem. Soc.* **2013**, *135*, 9931–9938.

[22] J. C. Bottaro, M. Petrie, P. E. Penwell, A. L. Dodge, R. Malhontra, NANA/HEDM Technology: Late Stage Exploratory Effort, Report No. A466714; SRI International: Menlo Park, CA, **2003**; DARPA/AFOSOR funded, Contact No. F49629-02-C-0030.

[23] H. J. Maag, G. Klingenberg, *Propellants, Explos., Pyrotech.* **1996**, *21*, 1–7.

[24] A. W. Horst, P. J. Baker, B. M. Rice, P. J. Kaste, J. W. Colburn, J. J. Hare, *Vol. ARL-TR-2584*, Army Research Labratory, Aberdeen, Maryland, **2001**

[25] R. S. Damse, A. Singh, H. Singh, *Propellants, Explos., Pyrotech.* **2007**, *32*, 52–60.

[26] R. S. Damse, H. Singh, *Defence Sci.* **2000**, *50*, 75–81.

[27] N. Fischer, D. Izsák, T. M. Klapötke, S. Rappenglück, J. Stierstorfer, *Chem. Eur. J.* **2012**, *18*, 4051–4062.

[28] D. E. Chavez, B. C. Tappan, B. A. Mason, D. A. Parrish, *Propellants, Explos., Pyrotech.* **2009**, *34*, 475–479.

[29] N. Fischer, D. Izsák, T. M. Klapötke, J. Stierstorfer, *Chem. Eur. J.* **2013**, *19*, 8948–8957.

[30] A. Hahma, E. Karvinen, J. Stierstorfer, T. M. Klapötke (Diehl BGT Defece GmbH & Co. KG, Überlingen), EP2548857A1 **2013**.

[31] A. Hahma, E. Karvinen, T. M. Klapötke, J. Stierstorfer (Diehl BGT Defece GmbH & Co. KG, Überlingen), EP2377840A2 **2011**.

[32] A. Hahma, E. Karvinen (Diehl BGT Defece GmbH & Co. KG, Überlingen), EP2338863A2 **2010**.

[33] M.-J. Crawford, K. Karaghiosoff, T. M. Klapötke, F. A. Martin, *Inorg. Chem.* **2009**, *48*, 1731–1743.

[34] M. Dachs, A. A. Dippold, J. Gaar, M. Holler, T. M. Klapötke, *Z. Anorg. Allg. Chem.* **2013**, *639*, 2171–2180.

[35] M. J. Frisch, G. W. Trucks, H. B. Schlegel, G. E. Scuseria, M. A. Robb, J. R. Cheeseman, G. Scalmani, V. Barone, B. Mennucci, G. A. Petersson, H. Nakatsuji, M. Caricato, X. Li, H. P. Hratchian, A. F. Izmaylov, J. Bloino, G. Zheng, J. L. Sonnenberg, M. Hada, M. Ehara, K. Toyota, R. Fukuda, J. Hasegawa, M. Ishida, T. Nakajima, Y. Honda, O. Kitao, H. Nakai, T. Vreven, J. J. A. Montgomery, J. E. Peralta, F. Ogliaro, M. Bearpark, J. J. Heyd, E. Brothers, K. N. Kudin, V. N. Staroverov, R. Kobayashi, J. Normand, K. Raghavachari, A. Rendell, J. C. Burant, S. S. Iyengar, J. Tomasi, M. Cossi, N. Rega, J. M. Millam, M. Klene, J. E. Knox, J. B. Cross, V. Bakken, C. Adamo, J. Jaramillo, R. Gomperts, R. E. Stratmann, O. Yazyev, A. J. Austin, R. Cammi, C. Pomelli, J. W. Ochterski, R. L. Martin, K. Morokuma, V. G. Zakrzewski, G. A. Voth, P. Salvador, J. J. Dannenberg, S. Dapprich, A. D. Daniels, O. Farkas, J. B. Foresman, J. V. Ortiz, J. Cioslowski, D. J. Fox, Gaussian 09, Revision A.02, Inc., Wallingford CT, **2009**.

[36] F. H. Allen, O. Kennard, D. G. Watson, L. Brammer, A. G. Orpen, R. Taylor, *J. Chem. Soc., Perkin Trans. 2* **1987**, *0*, S1–S19.

[37] N. Fischer, L. Gao, T. M. Klapötke, J. Stierstorfer, *Polyhedron* **2013**, *51*, 201–210.

[38] D. Fischer, T. M. Klapötke, D. G. Piercey, J. Stierstorfer, *Chem. Eur. J.* **2013**, *19*, 4602–4613.

[39] A. Bondi, *J. Phys. Chem.* **1964**, *68*, 441–451.

[40] Test methods according to the *UN Manual of Test and Criteria, Recommendations on the Transport of Dangerous Goods*, United Nations Publication, New York, Geneva, 4th revised ed., **2003**: Impact: Insensitive >40 J, less sensitive ≥ 35 J, sensitive ≥ 4 J, very sensitive ≤ 3 J; Friction: Insensitive >360 N, less sensitive $= 360$ N, sensitive <360 N a. >80 N, very sensitive ≤ 80 N, extremely sensitive ≤ 10 N.

[41] NATO, *Standardization Agreement 4489 (STANAG 4489)*, *Explosives, Impact Sensitivity Tests* **1999**.

[42] NATO, *Standardization Agreement 4487 (STANAG 4487)*, *Explosives, Friction Sensitivity Tests* **2002**.

[43] J. C. Cheng, S. J. Mark, M. H. Margaret, T. M. Klapötke, *JANNAF* **2012**, *5*, 39–49.

[44] M. Sućeska, Explo5 program, 6.02 ed., Zagreb, Croatia, **2014**.

[45] A. Hammerl, M. A. Hiskey, G. Holl, T. M. Klapötke, K. Polborn, J. Stierstorfer, J. J. Weigand, *Chem. Mater.* **2005**, *17*, 3784–3793.

[46] Fraunhofer Institut für Chemische Technologie, ICT Thermodynamic Data Base, V1.00 Pfinztal, Germany, **1998**–**2000**.

High-pressure Raman Spectroscopy of Bisaminoguanidinium 5-(5-(1*H*-Tetrazol-5-yl)-1,2,3-triazolate-4-yl)tetrazolate

J. Evers, T. M. Klapötke, and C. Pflüger

unpublished results.

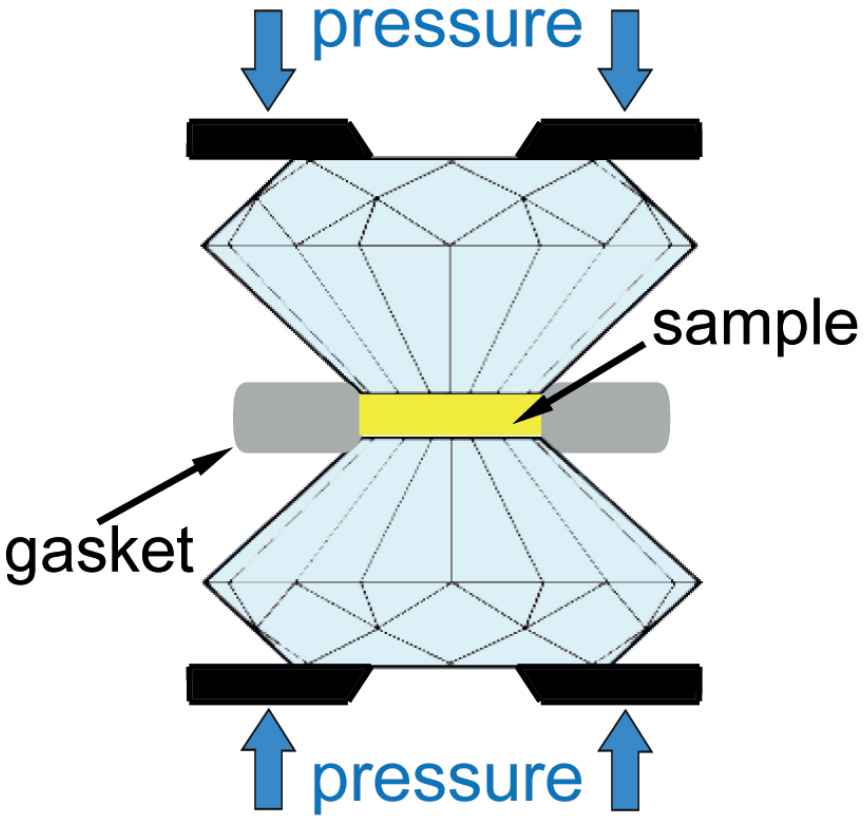

High-pressure Raman Spectroscopy of Bisaminoguanidinium 5-(5-(1*H*-Tetrazol-5-yl)-1,2,3-triazolate-4-yl)tetrazolate

J. Evers, T. M. Klapötke, and C. Pflüger
unpublished results

Abstract

The behavior of energetic materials under high-pressure is of interest regarding structural properties, which affect stability and sensitivity as well as the modeling of the detonative properties with high-pressure equations of state. In this study bisaminoguanidinium 5-(5-(1*H*-tetrazol-5-yl)-1,2,3-triazolate-4-yl)tetrazolate is compressed up to 19.5 GPa using diamond anvil cell techniques. The influence of the high-pressure on its structure is investigated by Raman spectroscopy.

8.1 Introduction

The behavior towards high pressure of a wide range of materials including metals, semiconductors, superconductors, minerals, and less extensive energetic materials has been studied. Energetic materials experience extreme conditions by deflagration or detonation in the high-pressure (10–50 GPa) and high-temperature (600–4000 °C) regime.[1] These extreme conditions result in polymorphic transitions. Polymorphism affects many properties such as melting and decomposition temperature, solubility, density, color, hygroscopicity, stability to pressure and temperature, sensitivity towards outer stimuli (impact, friction, electrostatic discharge), and solid-state chemistry.[2] Furthermore, the performance parameters of energetic materials, especially the detonation velocity and pressure, depend on the solid-state structure, in particular the crystal density. Therefore, the densest polymorph of an energetic compound should be selected when possible to benefit for example in improved performance, processing and packing of the polymorphs, and different crystal morphologies. Solid-state phase transitions in energetic materials are also relevant because the crystals may develop surface and internal defects and the crystal size may be reduced.[2]
According to the theory of initiation of energetic materials the formation of the so-called "hot spots" is envisaged, which are leading to concentrated energy at the defect sites due to cavitation and / or frictional heating caused by the initiation process and compression, or vacant lattice positions, dislocations, inclusions of gas bubbles or impurities.[3] Starting from these "hot spots" the reaction front propagates outward leading to a violent runaway reaction. Another model expects preferential "up-pumping" (or excitation) of specific

vibrational modes at defect sites in the crystal lattice resulting in greater local heating at the defect sites compared to the other sites in the lattice.[4,5] This model is used to correlate the velocity of the energy transfer from "hot spots" to the vibrational modes to the experimentally obtained sensitivities.[6,7]

Regarding these conditions polymorphism in molecular materials as well as various techniques to study these materials under pressure are gaining in importance. Useful techniques to study polymorphism are vibrational spectroscopy, differential scanning calorimetry, thermal gravimetric analysis, optical polarising microscopy, powder and single-crystal X-ray crystallography as well as solid-state NMR spectroscopy.[2]

Three general methods for the study of energetic materials at high pressures have been employed: i) direct static compression; ii) dynamic shock wave studies; iii) computational studies. Direct static compression generally involves compression of the sample in a diamond-anvil cell up to pressures of 30 GPa and temperatures up to 650 K.

Additionally, the behavior of energetic materials at high-pressure is of interest to model the detonative properties with high-pressure equations of state (EOS) and other pressure and temperature dependent thermodynamic parameters to investigate reaction mechanisms.[8]

High-pressure structural and spectroscopic studies of several common energetic materials like ammonium perchlorate (AP),[9–11] octogen (HMX),[12,13] hexogen (RDX),[1,14–16] hexanitrohexaazaisowurtzitane (CL-20),[17–19] pentaerythritol tetranitrate (PETN),[20–22] and 1,1-diamino-2,2-dinitroethene (FOX-7)[8,23–26] have been carried out, giving insights in their mechanical and energetic behavior.

This study deals with the effect of high-pressure on the salt bisaminoguanidinium 5-(5-(1*H*-tetrazol-5-yl)-1,2,3-triazolate-4-yl)tetrazolate and its influence on the vibrational modes observed in the Raman spectra.

8.2 Results and Discussion

8.2.1 Synthesis

Bisaminoguanidinium 5-(5-(1*H*-tetrazol-5-yl)-1,2,3-triazolate-4-yl)tetrazolate (**19d**) was synthesized by deprotonation of 4,5-bis(1*H*-tetrazol-5-yl)-2*H*-1,2,3-triazole with aminoguanidinium hydrogen carbonate in water (Scheme 8.1).[27] It was dehydrated by heating to 120 °C at 3×10^{-3} mbar for 2 d.

8.2.2 Structural Studies

At ambient pressure the bisaminoguanidinium salt **19d**·H_2O adopts monoclinic structure of $P2_1/n$ (Z = 4) as determined by single-crystal X-ray diffraction studies.[27] Its molecular

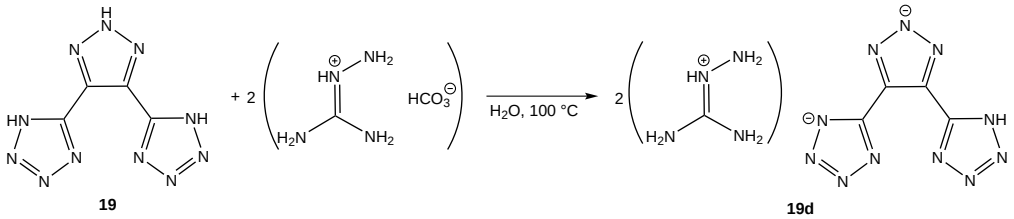

Scheme 8.1: Synthesis of the bisaminoguanidinium salt **19d**.

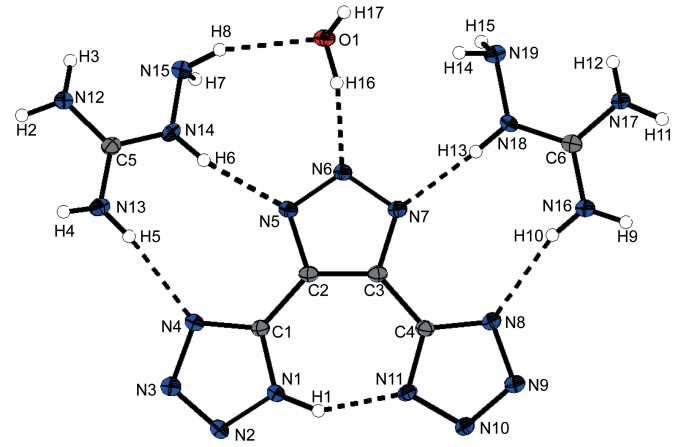

Figure 8.1: Molecular structure of bisaminoguanidinium 5-(5-(1*H*-tetrazol-5-yl)-1,2,3-triazolate-4-yl)tetrazolate (**19d**) as monohydrate. Thermal ellipsoids are drawn at the 50% probability level.

structure is shown in Figure 8.1. Instead of both tetrazole rings, one tetrazole and the triazole are deprotonated, whereby a strong hydrogen bond of 1.86(3) Å is formed between the tetrazole rings.

The high-pressure (HP) experiments were performed in a diamond anvil cell of Mao-Bell type[28] (culet: 300 µm; starting gasket thickness: 85 µm; gasket hole: 160 µm). Powdered sample of **19d** mixed with KBr (1:5) as pressure transmitter and pressure gauge was pestled and loaded in a diamond anvil cell with a stainless steel T301 gasket. For KBr specific volumes are tabulated in literature up to 165 GPa at room temperature.[29] Photographs of the gasket at 000 NG to 550 NG showing an increasing hole diameter are depicted in Figure 8.2.

The HP diffractograms were recorded with AgK_α radiation ($\lambda = 0.5609$ Å) in the range $\theta = 4.0$–$7.9°$ (increment: 0.03°; counting time per increment: 600 s) to determine the pressure. Structural data were obtained by the Rietveld method with both diffractometer zero point and asymmetry parameter fixed. Selected data of the HP diffractograms as well as the measured P–V points are listed in Table 8.1 and Table 8.2, respectively. The pressure calibration curve is shown in Figure 8.3. The diffractograms show a phase transition between 300 and 350 NG from the NaCl type to the CsCl type. The phase transition is accompanied

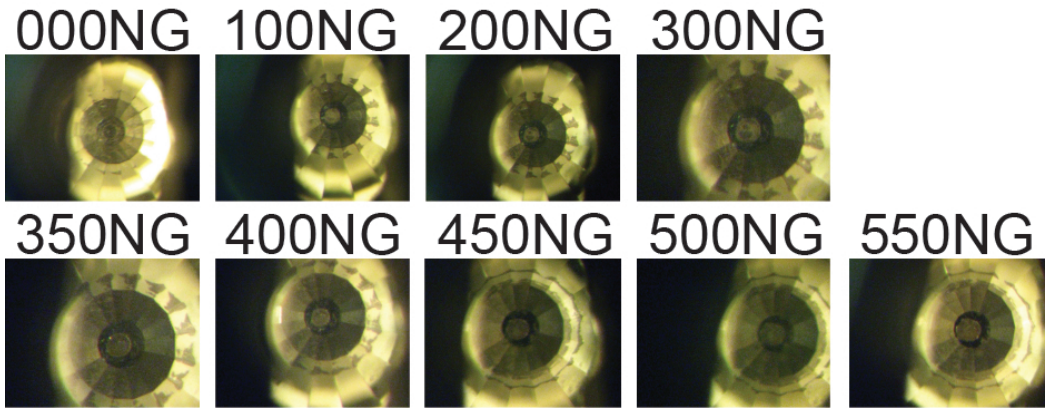

Figure 8.2: Filled gasket at 000 to 550 NG.

Table 8.1: Measured data of HP diffractograms (point of origin: 0.235).

Turning [NG]	Reflexes (hkl)	θ	θ_{cor}	$\sin 2\theta_{cor}$	$h^2+k^2+l^2$
000	200	5.116	4.881	0.00724	4
	220	7.125	6.890	0.01439	8
100	111	4.468	4.233	0.00545	3
	200	5.103	4.868	0.00720	4
	220	7.125	6.890	0.01439	8
200	111	4.463	4.228	0.00544	3
	200	5.107	4.872	0.00721	4
	220	7.133	6.898	0.01442	8
300	111	4.601	4.366	0.00580	3
	200	5.257	5.022	0.00766	4
	220	7.368	7.133	0.01542	8
350	100	4.487	4.252	0.00550	1
	110	6.254	6.019	0.01100	2
400	110	6.453	6.218	0.01173	2
450	110	6.540	6.305	0.01206	2
500	110	6.694	6.459	0.01265	2

by a strong decrease in the cell length and volume. The cell length a is calculated from the Bragg equation:

$$a = \sqrt{n^2\lambda^2\frac{1}{x}}$$
$$x = \frac{4\sin^2\theta}{(h^2+k^2+l^2)} \tag{8.1}$$

The Raman spectra were recorded for selected pressures using a Bruker BAN II spectrometer

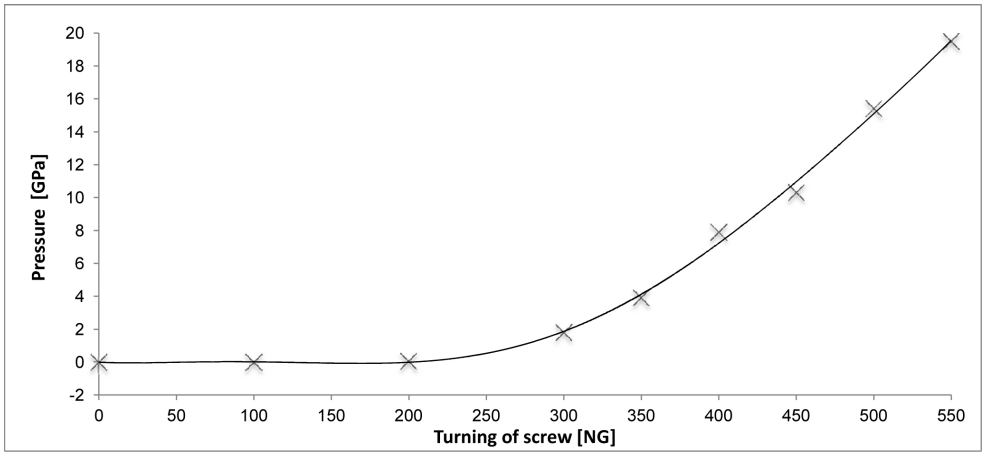

Figure 8.3: Pressure calibration curve.

Table 8.2: Measured P–V points.

Turning [NG]	000	100	200	300	350	400	450	500	550
a [Å]	6.606	6.606	6.601	6.392	3.782	3.662	3.612	3.525	3.473
V_{EZ} [Å^3]	72.07	72.07	71.91	65.29	13.53	12.28	11.78	10.95	10.47
p [GPa]	0.0001	0.0001	0.05	1.8	3.9	7.9	10.3	15.4	19.5

with a Nd:YAG laser ($\lambda = 1064\,\mathrm{nm}$) and a laser output of 1000 mW. The Raman spectrum of **19d** loaded in a glass tube is presented in Figure 8.4. At higher wavenumbers ($> 3000\,\mathrm{cm^{-1}}$) the N−H valence vibrations are observed. The two most intensive vibrational bands at 1640 and $1590\,\mathrm{cm^{-1}}$ are attributed to the valence vibrations of C=C, C=N, and N=N bonds.
In Figure 8.5 the Raman spectrum of the empty diamond anvil cell as well as the high-pressure Raman spectra of the mixture of **19d** and KBr in the diamond anvil cell from $1 \times 10^{-4}\,\mathrm{GPa}$ to 19.5 GPa are depicted. The signal to noise ratio and the intensities of the vibrational bands are very low due to the little amount of **19d**. Therefore, the discussion is focused on the two most intensive vibrational bands.
In the range of ambient pressure (0.0001 GPa) to 0.05 GPa no changes are observed in the Raman spectra. In the Raman spectrum recorded at 1.8 GPa the vibrational bands around 1640 and $1595\,\mathrm{cm^{-1}}$ are shifted to higher wavenumbers (1678 and $1619\,\mathrm{cm^{-1}}$, respectively). The increase in pressure leads to a further shift to higher wavenumbers of the vibrational band that was around $1640\,\mathrm{cm^{-1}}$ prior to the pressure increase. It is shifted up to $1712\,\mathrm{cm^{-1}}$ at 15.4 GPa before the compound is destroyed at 19.5 GPa. The second intensive vibrational band around $1590\,\mathrm{cm^{-1}}$ vanished by increasing the pressure up to 7.9 GPa which might be caused by an overlay with the band of the diamond anvil cell ($1658\,\mathrm{cm^{-1}}$) and line broadening. This shift to higher wavenumbers may indicate a phase transition. The change in the HP Raman spectrum at 1.8 GPa in comparison to the former spectra is accompanied

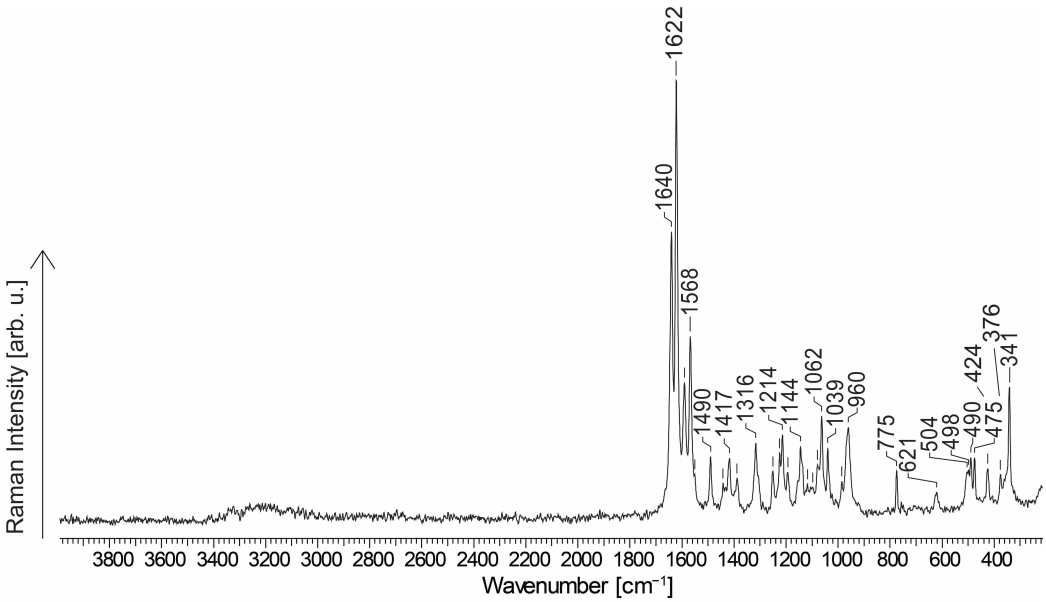

Figure 8.4: Raman spectrum of **19d** filled in a glass tube and recorded at 1 bar and room temperature.

by the first considerable change in the dimensions of the unit cell of KBr from 71.91 Å^3 to 65.29 Å^3 as determined by the powder diffractograms.
Although unit cell parameters and Raman spectra at different pressures are reported, no detailed structural information could be derived and the Raman spectra are generally not well resolved and therefore provide little insights into structural changes occurring in **19d** with increasing pressure.

8.3 Conclusions

Structural and molecular changes in bisaminoguanidinium 5-(5-(1*H*-tetrazol-5-yl)-1,2,3-triazolate-4-yl)tetrazolate (**19d**) compressed to high pressures up to 19.5 GPa were investigated using diamond anvil cell experiments. The experiments consisted of Rietveld powder diffraction and Raman spectroscopy. The Raman spectroscopy showed that the vibrational bands around 1640 and 1590 cm^{-1} were shifted to higher wavenumbers with increasing pressure. The first change was observed in the Raman spectrum at 1.8 GPa suggesting a transition to a new phase.

8.4 References

[1] J. A. Ciezak, T. A. Jenkins, Z. Liu, R. J. Hemley, *J. Phys. Chem. A* **2007**, *111*, 59–63.

[2] F. P. A. Fabbiani, C. R. Pulham, *Chem. Soc. Rev.* **2006**, *35*, 932–942.

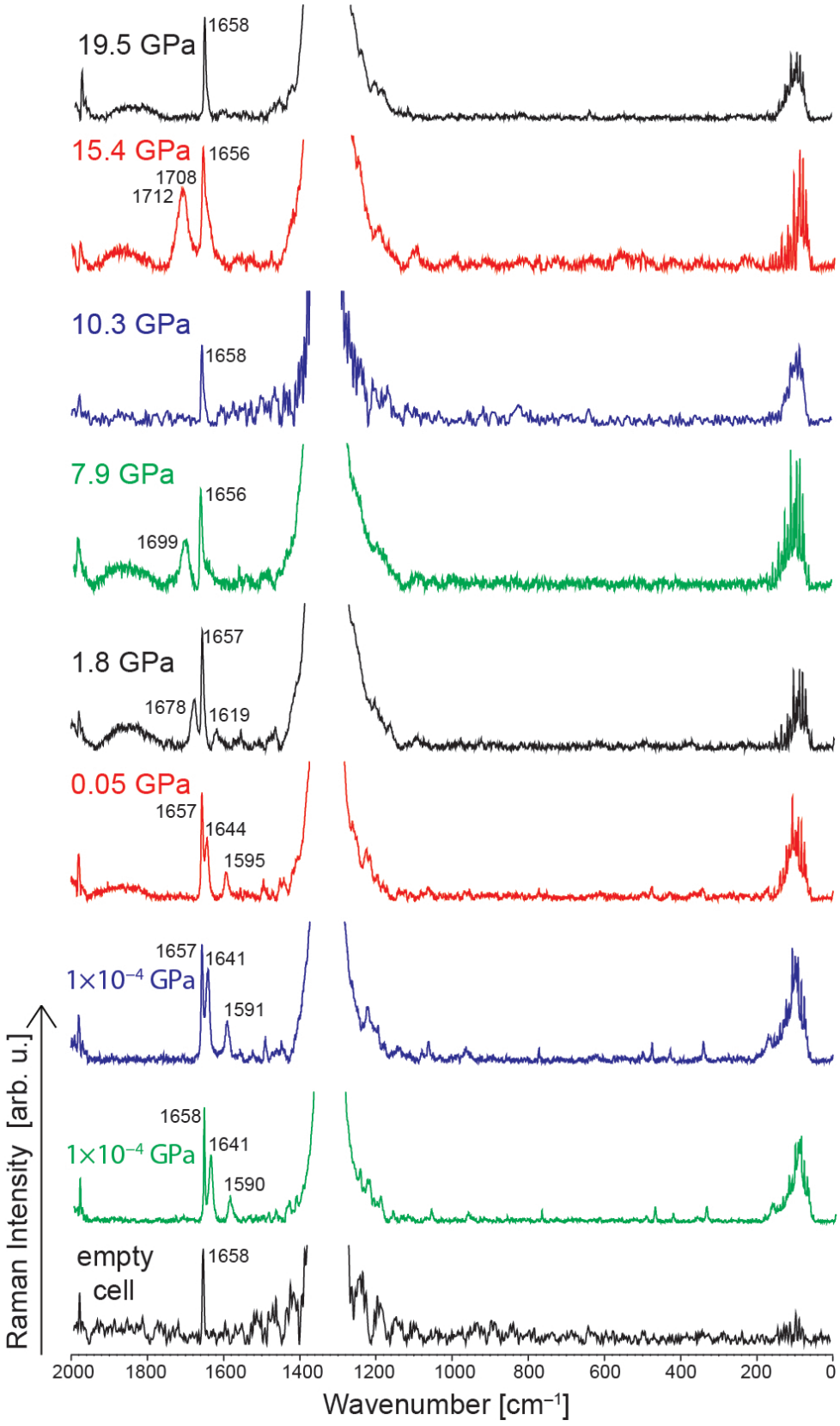

Figure 8.5: HP Raman spectra of **19d** mixed with KBr from 1×10^{-4} GPa to 19.5 GPa and the empty diamond anvil cell at 1×10^{-4} GPa for comparison.

[3] F. P. Bowden, A. D. Yoffe, *Initiation and Growth of Explosion in Liquids and Solids*, Cambridge University Press, Cambridge, United Kingdom, **1952**.

[4] D. D. Dlott, *Theor. Comput. Chem.* **2003**, *13*, 125–191.

[5] D. D. Dlott, *Adv. Ser. Phys. Chem.* **2005**, *16*, 303–333.

[6] L. E. Fried, A. J. Ruggiero, *J. Phys. Chem.* **1994**, *98*, 9786–9791.

[7] K. L. McNesby, C. S. Coffey, *J. Phys. Chem. B* **1997**, *101*, 3097–3104.

[8] S. M. Peiris, C. P. Wong, F. J. Zerilli, *J. Chem. Phys.* **2004**, *120*, 8060–8066.

[9] S. M. Peiris, G. I. Pangilinan, T. P. Russell, *J. Phys. Chem. A* **2000**, *104*, 11188–11193.

[10] P. W. Richter, C. W. F. T. Pistorius, *J. Solid State Chem.* **1971**, *3*, 434–439.

[11] M. F. Foltz, J. L. Maienschein, in *AIP Conference Proceedings*, *370*, **1996**, pp. 239–242.

[12] M. Pravica, M. Galley, E. Kim, P. Weck, Z. Liu, *Chem. Phys. Lett.* **2010**, *500*, 28–34.

[13] J. L. Maienschein, J. F. Wardell, M. R. DeHaven, C. K. Black, *Propellants, Explos., Pyrotech.* **2004**, *29*, 287–295.

[14] Z. A. Dreger, Y. M. Gupta, *J. Phys. Chem. A* **2010**, *114*, 7038–7047.

[15] Z. A. Dreger, Y. M. Gupta, *J. Chem. Phys. B* **2007**, *111*, 3893–3903.

[16] I. D. H. Oswald, D. I. A. Millar, A. J. Davidson, D. J. Francis, W. G. Marshall, C. R. Pulham, A. Cumming, A. R. Lennie, J. E. Warren, *High Pressure Res.* **2010**, *30*, 280–291.

[17] J. A. Ciezak, T. A. Jenkins, Z. Liu, *Propellants, Explos., Pyrotech.* **2007**, *32*, 472–477.

[18] D. I. A. Millar, H. E. Maynard-Casely, A. K. Kleppe, W. G. Marshall, C. R. Pulham, A. S. Cumming, in *New Tends Res. Energ. Mater., Proceedings Semin.*, 13th, Pardubice, Czech Republic, **2010**, *1*, pp. 223–235.

[19] J. A. Ciezak, E. F. C. Byrd, B. M. Rice, in *232nd ACS National Meeting*, San Francisco, CA (USA), **2006**.

[20] Z. A. Dreger, Y. M. Gupta, *J. Phys. Chem. A* **2013**, *117*, 5306–5313.

[21] M. Pravica, K. Lipinska-Kalita, Z. Quine, E. Romano, Y. Shen, M. F. Nicol, W. J. Pravica, *J. Phys. Chem. Solids* **2006**, *67*, 2159–2163.

[22] K. E. Lipinska-Kalita, M. G. Pravica, M. Nicol, *J. Chem. Phys. B* **2005**, *109*, 19223–19227.

[23] Z. A. Dreger, Y. Tao, Y. M. Gupta, *J. Phys. Chem. A* **2014**, *118*, 5002–5012.

[24] M. M. Bishop, N. Velisavljevic, R. Chellappa, Y. K. Vohra, *J. Phys. Chem. A* **2015**, *119*, 9739–9747.

[25] J. Evers, T. M. Klapötke, P. Mayer, G. Oehlinger, J. Welch, *Inorg. Chem.* **2006**, *45*, 4996–5007.

[26] Z. A. Dreger, A. I. Stash, Z.-G. Yu, Y.-S. Chen, Y. Tao, Y. M. Gupta, *J. Phys. Chem. C* **2016**, *120*, 1218–1224.

[27] A. A. Dippold, D. Izsák, T. M. Klapötke, C. Pflüger, *Chem. Eur. J.* **2016**, *22*, 1768–1778.

[28] H. K. Mao, *Science* **1978**, *200*, 1145–1147.

[29] A. Dewaele, A. B. Belonoshko, G. Garbarino, F. Occelli, P. Bouvier, M. Hanfland, M. Mezouar, *Phys. Rev. B* **2012**, *85*, 214105.

Combination of 1,2,4-Oxadiazoles and 1,2,3-Triazoles: Building Blocks for Energetic Material Design

T. M. Klapötke, and C. Pflüger

unpublished results.

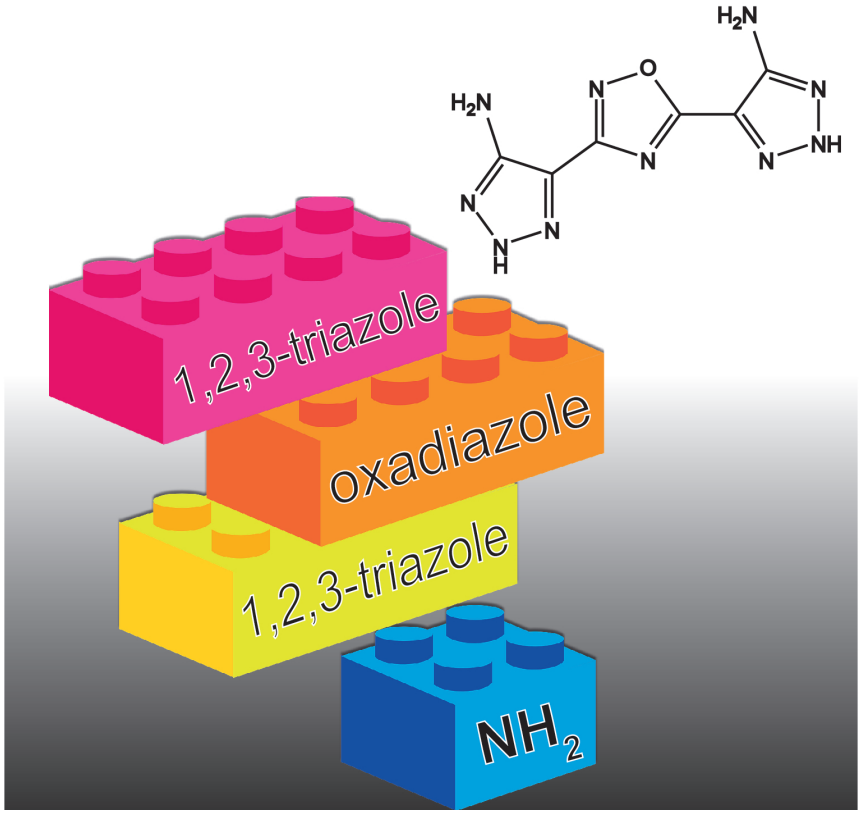

Combination of 1,2,4-Oxadiazoles and 1,2,3-Triazoles: Building Blocks for Energetic Material Design

T. M. Klapötke, and C. Pflüger
unpublished results.

Abstract

The development of new building blocks for the design of energetic materials offering both high performance and low sensitivity towards external stimuli is of growing interest worldwide. This study reports on the syntheses of basic energetic building blocks by C–C linkages of 1,2,3-triazoles and 1,2,4-oxadizoles. The oxadiazole rings were formed either by reaction of 5-amino-1,2,3-triazole-4-carboxamidoxime and 1,2,3-triazole-4,5-dicarboxamidoxime with cyanogen bromide or by reaction of 5-amino-1,2,3-triazole-4-carboxamidoxime with 5-amino-1,2,3-triazole-4-carbonitrile. They combine the advantages of the more energetic 1,2,3-triazole and the 1,2,4-oxadiazole, which contributes to a better oxygen balance likely accompanied by higher performance and density. Additionally, the derivatization of the amino groups enables the selective tailoring of the energetic properties of these building blocks.

9.1 Introduction

Energetic materials are widely used as explosives or as ingredients in propellant or pyrotechnic mixtures for military, industrial as well as civil applications. Due to the high requirements particularly concerning performance and stability, strong research efforts are ongoing worldwide to develop explosives, which combine high performance and high stability. Unfortunately, the structural patterns leading to high performance or stability often have contradictory impact to each other.

In the design of energetic materials, a common strategy is the combination of various energetic units composed of different backbones. Nitrogen-rich heterocycles such as tetrazole, triazoles, and oxdiazoles are suitable backbones due to their inherently high enthalpies of formation, which result in the release of a large amount of energy upon initiation.

Oxadiazoles found wide application as ingredients in drugs,[1,2] dyestuffs,[3,4] ionic liquids,[5,6] and energetic materials. The furazan ring (1,2,5-oxadiazole) is the most energetic and most investigated isomer of the oxadiazole family owing to its high enthalpy of formation (Figure 9.1) and high density, but its derivatives often suffer from low thermal stability and high sensitivity towards outer stimuli. A large number of various functionalized monofurazans[7–9] as well as linked and ring-fused furazans have been investigated with regard to their energetic

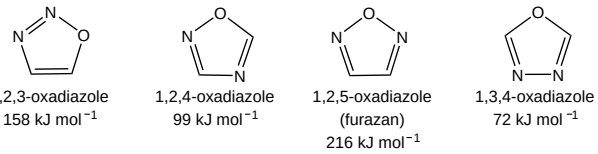

Figure 9.1: Computed gas-phase enthalpies of formation (CBS-4M) of the four isomers of the oxadiazole family.

properties and are promising for potential use in explosive formulations and propellant mixtures.[10–14]

The 1,2,3-oxadiazoles are generally unstable, unless they are sterically protected, because they readily tautomerize to the corresponding open-chain α-diazoketones.[15] The 1,2,4- and 1,3,4-oxadiazoles should be less sensitive towards outer stimuli due to the observation that a reduced number of readily cleaved N−O bonds in the heterocycle result in higher thermal stability. Nevertheless, they have been studied rarely as energetic materials in comparison to the furazans, thus only several studies report on the promising energetic properties of single 1,2,4-oxadiazole rings with various substituents or combinations with furazan rings.[16–20]

The replacement of the furazan ring by a 1,2,3-triazole should result in enhanced thermal stability and reduced sensitivity, while maintaining the high level of detonation performance. Moreover, the combination of 1,2,3-triazole rings with 1,2,4-oxadiazoles instead of only nitrogen containing heterocycles such as tetrazoles should lead to a less negative oxygen balance and higher density, thereby improving the detonation performance and sensitivities. Their energetic properties can then be further tailored by introduction of energetic groups such as nitro, nitramino, and azido either to the triazole or the oxadiazole ring or a diazene bridge as linker. This study presents the symmetrical and asymmetrical combination of amino-1,2,3-triazoles and amino-1,2,4-oxadiazoles as well as the linkage of two amino-1,2,3-triazoles via an 1,2,4-oxadiazole ring as energetic building blocks for further tailoring of their energetic properties by derivatization of their amino groups.

9.2 Results and Discussion

9.2.1 Syntheses

The attempted debenzylation of 5-amino-1-benzyl-1,2,3-triazole-4-carbonitrile, which was synthesized as recently reported,[21] in liquid ammonia according to the debenzylation of 5-(5-amino-1,2,3-triazol-4-yl)-1*H*-tetrazole resulted in the hydrolysis of the nitrile, yielding only the 5-amino-2*H*-1,2,3-triazole-4-carboxamide, whereas the benzyl-protected nitrile was reobtained by an attempted hydrogenation (H_2, Pd/C). Therefore, 5-amino-1-benzyl-1,2,3-

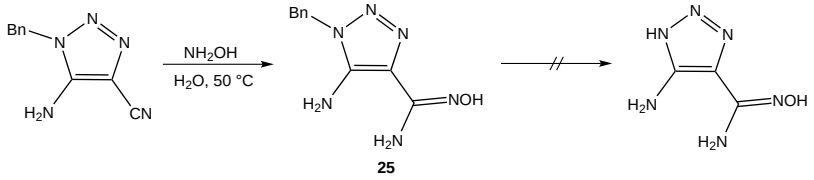

Scheme 9.1: Reaction of 5-amino-1-benzyl-1,2,3-triazole-4-carbonitrile with hydroxylamine and its attempted debenzylation.

triazole-4-carbonitrile was first reacted with hydroxylamine to obtain the corresponding amidoxime **25** (Scheme 9.1). Various debenzylation attempts either under reducing conditions (sodium in liquid ammonia; hydrogenation with Pd/C as catalyst in glacial acetic acid at 70 °C; hydrogenation using additionally $Pd(OH)_2$), or under oxidizing conditions ($Na_2S_2O_4$ in DMSO at 90 °C; KOtBu, O_2 in DMSO at room temperature) were not successful. Only the starting material was isolated or in the case of $Pd(OH)_2$ the reaction products could not be identified.

Finally, the debenzylation of 5-amino-1-benzyl-1,2,3-triazole-4-carbonitrile succeed by reduction with sodium in liquid ammonia using a modified literature procedure (Scheme 9.2).[22] Alkaline aqueous conditions have to be avoided in the workup after removal of the ammonia because otherwise the amide would be formed. Hence, the residue was cooled to 0 °C, acidified to pH2 with precooled 2M HCl and the solution had to be extracted rapidly. In several cases the formation of the amide could not be completely avoided, but due to its lower solubility it was filtered off and the extraction yielded pure 5-amino-1*H*-1,2,3-triazole-4-carbonitrile (**26**). The amidoxime **27** was formed by the reaction of **26** with hydroxylamine in water at 50 °C in a very good yield (93%). The ring closure to 5-amino-3-(5-amino-1,2,3-triazol-4-yl)-1,2,4-oxadiazole (**28**) was performed by in situ deprotonation of **27** with potassium hydrogen carbonate, followed by reaction with cyanogen bromide. Similar reaction conditions were used for the synthesis of 3,5-bis(5-amino-1,2,4-oxadiazol-4-yl)-1,2,3-triazole (**29**).

The combination of two aminotriazoles via an oxadiazole ring was accomplished by the reaction of **26** and **27** under acidic conditions using zinc chloride as catalyst to yield 3,5-bis(5-amino-2*H*-1,2,3-triazol-4-yl)-1,2,4-oxadiazole (**30**) (Scheme 3).

9.2.2 NMR Spectroscopy and Mass Spectrometry

All NMR spectra were recorded in DMSO-d_6. The signals of the benzyl group are completely gone in the NMR spectra of **26** and instead the resonance of the heterocyclic proton is observed at 14.61 ppm. Furthermore, the proton resonances of the amino group are observed at 6.70 ppm. The ^{13}C NMR spectrum of **26** shows the two signals of the triazole at 150.6

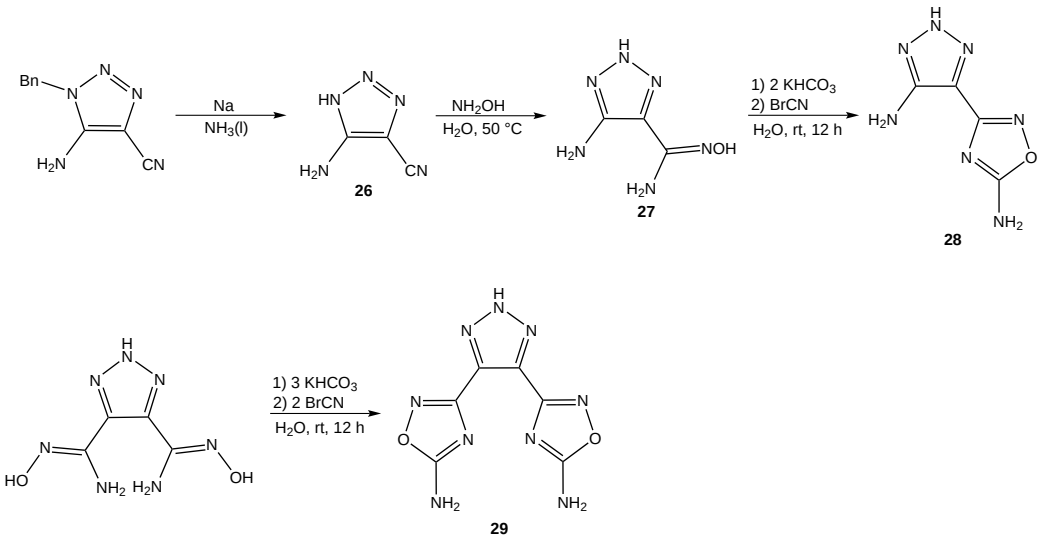

Scheme 9.2: Synthesis of 5-amino-3-(5-amino-2*H*-1,2,3-triazol-4yl)-1,2,4-oxadiazole (**28**) and 3,5-bis(5-amino-1,2,4-oxadiazol-4-yl)-1,2,3-triazole (**29**).

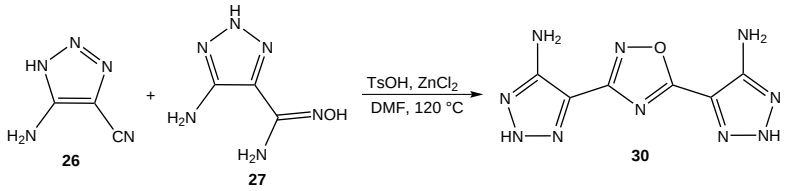

Scheme 9.3: Synthesis of 3,5-bis(5-amino-2*H*-1,2,3-triazol-4-yl)-1,2,4-oxadiazole (**30**).

and 101.7 ppm and the carbon resonance of the cyano group at 114.0 ppm. The reaction with hydroxylamine leads to a low-field shift of the triazole carbon formerly attached to the cyano group to 123.6 ppm. The resonances of the other triazole carbon and the carboxamide group of **27** are observed at 148.0 and 147.9 ppm. In the ^{1}H NMR spectrum of **27**, the proton resonances of the acidic protons of the triazole and the oxime show a low-field shift to 13.8 ppm (NH) and 9.49 ppm (NOH). The proton resonances of the amino groups are observed at similar shifts (5.61 and 5.34 ppm), thus preventing an unambiguous assignment. The solubility of the oxadiazole **28** was too low to observe any resonance signals of the quaternary carbon atoms, although the spectrum was recorded with an increased number of scans and pulse delay. Moreover, the proton resonances of the amino groups are not found in the ^{1}H NMR spectrum. The formation of the amino-1,2,4-oxadiazole **28** is therefore proven by its ESI mass spectrum showing the molecule ion peak respective the peaks of its agglomeration with water and/or another molecule of **28**, respectively.
Unfortunately, no resonance signals nor molecule ion peak or fragmentation products of the bisoxadiazole **29** could be observed in the NMR spectra or ESI or FAB mass spectra either because of its insolubility or it could not be ionized. The proton resonances of **30** are

Table 9.1: Selected hydrogen bonds within the crystal structure of 5-amino-1*H*-1,2,3-triazole-4-carbonitrile (**26**).

D−H···A	d(D−H) [Å]	d(H···A) [Å]	d(D···A) [Å]	∠(D−H···A) [°]
N4−H2···N3^{i}	0.928(18)	2.142(19)	3.0416(17)	163.3(16)
N4−H3···N5^{ii}	0.854(19)	2.193(19)	3.0462(18)	178.5(19)
N1−H1···N2^{iii}	1.004(19)	1.879(18)	2.8726(16)	169.9(17)
N1−H1···N3^{iii}	1.004(19)	2.693(18)	3.5614(16)	144.9(15)

Symmetry codes: (i) $x, -1+y, z$; (ii) $1-x, -0.5+y, 0.5-z$; (iii) $-x, -0.5+y, -0.5-z$.

observed as broad multiplet in the range from 8.54–7.66 ppm. In the ESI mass spectrum of **30** the peak of the molecule ion agglomerated with sodium and potassium was observed at $m/z = 295$.

9.2.3 Crystal Structures

5-Amino-1*H*-1,2,3-triazole-4-carbonitrile (**26**) and 5-amino-2*H*-1,2,3-triazole-4-carboxamidoxime (**27**) were characterized by low-temperature single-crystal X-ray diffraction. Selected data and parameters of the measurements and refinements are summarized in the Appendix. The nitrile **26** crystallizes in the monoclinic space group $P2_1/c$ with four formula units per unit cell and a crystal density of 1.565 g cm^{-3} at 173 K. The C−C bond length between the nitrile and the triazole ring of 1.4165(17) Å is as expected in the range of common C_{sp2}−C_{sp1} bonds (1.44 Å).[23] The nitrile C≡N bond (1.1457(17) Å) is in the range of CN triple bonds. The molecule is almost planar with a torsion angle of 177.83(14)° between the triazole and the nitrile, thereby forming a diagonal layer structure along the *ac* plane (Figure 9.2A). All nitrogen atoms participate in hydrogen bonds either as donor or acceptor, which lead to various hydrogen bonds in each layer (Figure 9.2B). The acidic proton is involved in a three-center hydrogen bond interacting with N2 and N3 (Table 9.1). The two protons of the amino group interact with the triazole nitrogen N3 and the nitrile nitrogen N5 as acceptor. No hydrogen bonds or dipolar interactions below the sum of their van der Waals radii could be observed between the layers.

The amidoxime **27** crystallizes as monohydrate with two formula units per unit cell with a crystal density of 1.568 g cm^{-3} at 173 K. The crystal structure shows monoclinic symmetry ($P2_1$). Its molecular structure is depicted in Figure 9.3A. The amidoxime moiety is turned out of the plane of the aminotriazole by 4.46(9)° due to the formation of a six-membered ring by an intramolecular hydrogen bond between H3 and N6 (D−H: 0.92(4) Å; H···A: 2.32(4) Å, D···A: 2.946(4) Å; ∠DHA: 126(3)°). The wave-like crystal structure is supported by various hydrogen bonds summarized in Table 9.2. The acidic protons of the triazole ring and the oxime form strong and directed hydrogen bonds to the crystal water molecule and

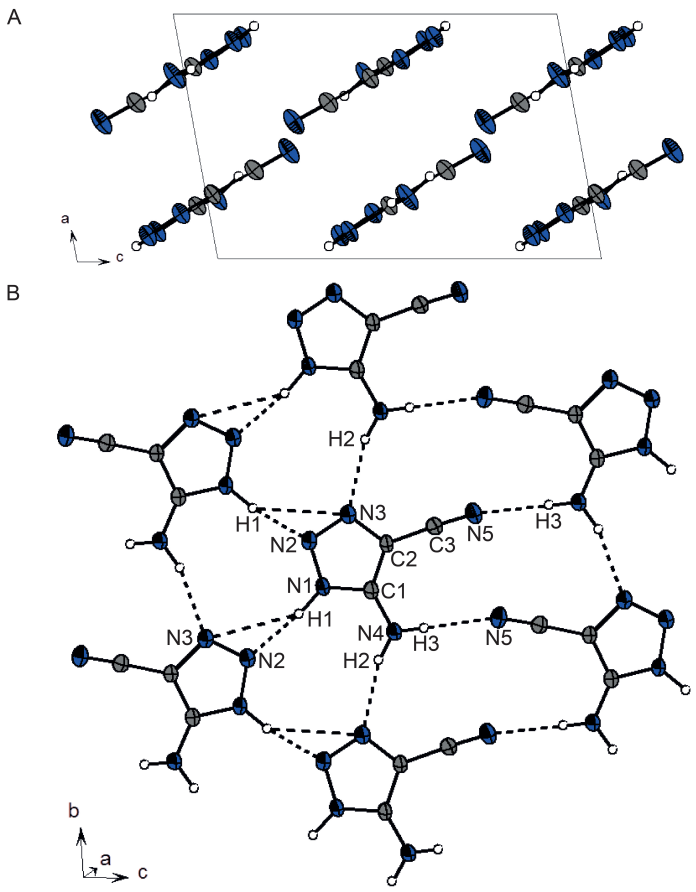

Figure 9.2: A) Unit cell of 5-amino-1*H*-1,2,3-triazole-4-carbonitrile (**26**) along the *b* axis. B) Hydrogen bonds (black dashed) within one layer in the crystal structure of **26**. Thermal ellipsoids are drawn at the 50% probability level.

to the nitrogen of the amino group attached to the triazole ring (Figure 9.3B). Furthermore, the nitrogen atoms N1, N3, and N5 as well as both oxygen atoms participate in hydrogen bonds.

9.2.4 Thermal Stability and Sensitivities

The nitrile **26** shows high thermal stability up to 205 °C, whereas the amidoxime **27** is thermally less stable (148 °C). The loss of the crystal water molecules of both compounds **28** and **30** is observed over a broad temperature range from 40 to 140 °C. The amino-1,2,4-oxadiazoles **28** and **29** are thermally stable up to 163 °C and 180 °C, respectively. The dehydration of **28** almost directly passes into decompostion. The thermal stability is considerably improved up to 243 °C for the oxadiazole **30** with two amino-1,2,3-triazole substituents.

The nitrile **26**, the amidoxime **27** as well as the oxadiazole **28**·H_2O are insensitive to impact and friction. The symmetrically substituted triazole **29**·H_2O is classified as sensitive towards

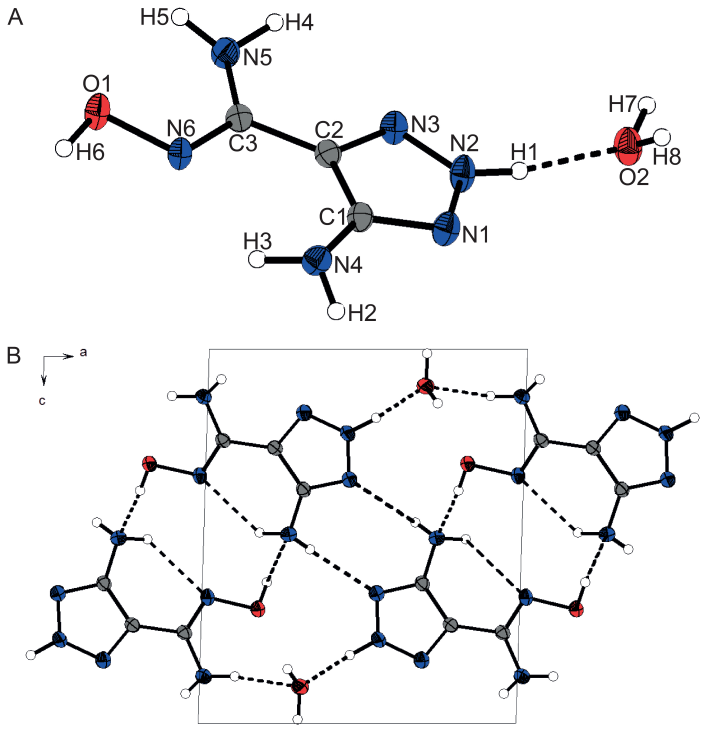

Figure 9.3: A) Molecular structure of 5-amino-2*H*-1,2,3-triazole-4-carboxamidoxime monohydrate (**27**·H_2O). B) Unit cell of **27**·H_2O along the *b* axis; hydrogen bonds are dashed. Thermal ellipsoids are drawn at the 50% probability level.

Table 9.2: Selected hydrogen bonds within the crystal structure of 5-amino-2*H*-1,2,3-triazole-4-carboxamidoxime monohydrate (**27**·H_2O).

D−H···A	*d*(D−H) [Å]	*d*(H···A) [Å]	*d*(D···A) [Å]	∠(D−H···A) [°]
N4−H3···N6^{i}	0.92(4)	2.32(4)	2.946(4)	126(3)
N2−H1···O2^{iii}	0.94(4)	1.81(4)	2.739(3)	170(3)
N4−H2···N1^{ii}	0.85(3)	2.29(3)	3.122(4)	165(3)
N5−H5···O2^{iii}	0.89(4)	2.17(4)	3.010(3)	158(3)
O1−H6···N4^{iv}	0.92(4)	1.89(5)	2.798(3)	171(4)
O2−H8···O1^{v}	0.83(5)	2.00(4)	2.777(3)	156(4)
O2−H7···N3^{vi}	0.98(4)	1.92(4)	2.884(3)	169(4)
N5−H4···N5^{vii}	0.92(4)	2.49(3)	3.227(3)	138(3)

Symmetry codes: (i) $x, 1+y, z$; (ii) $1-x, -0.5+y, 1-z$; (iii) $-1+x, 1+y, z$; (iv) $-x, -0.5+y, 1-z$; (v) $1+x, y, z$; (vi) $1-x, -0.5+y, -z$; (vii) $-x, 0.5+y, -z$.

impact (15 J), but also as insensitive towards friction. The sensitivities of **30** were not determined because it was only obtained as monohydrate with remaining traces of DMF.

9.3 Conclusions

The reaction of 5-amino-1,2,3-triazole-4-carboxamidoxime (**27**) and 1,2,3-triazole-4,5-dicarboxamidoxime **20** with cyanogen bromide under alkine conditions resulted in the formation of the corresponding asymmetrically and symmetrically substituted 1,2,3-triazolyl-1,2,4-oxadiazoles **28** and **29**, respectively. The oxadiazole **30** was formed by the reaction of the nitrile **26** with the amidoxime **27**. Their NMR spectroscopic characterization presented some difficulties concerning their low solubilities, their structures (only quaternary carbon atoms and amino protons) as well as their presumed isomerization in solution, which prevented the observation of the quaternary carbon resonances. Therefore, the compounds could be only identified by mass spectrometry and elemental analysis. Nevertheless, these oxadiazoles are promising backbones for the design of energetic materials due to the possibility of further tailoring of their energetic properties by derivatization of the amino group.

9.4 Experimental Section

Caution! *Most compounds prepared herein are energetic compounds sensitive to impact, friction and electrostatic discharge. Although there were no problems in handling the compounds, proper protective measures (ear protection, Kevlar® gloves, face shield, body armor and earthed equipment) should be used.*

5-Amino-1-benzyl-1,2,3-triazole-4-carboxamidoxime (25)

5-Amino-1-benzyl-1,2,3-triazole-4-carbonitrile (533 mg, 2.68 mmol) was dissolved in DMF (15 mL) and hydroxylamine (50% *w*/*w* in water, 0.20 mL, 3.69 mmol) was added. The solution was stirred at 80 °C for 1 h, whereby a precipitate occurred. The precipitate was filtered off and washed with ethanol (10 mL) to yield a colorless solid (497 mg, 2.14 mmol, 80%).
^{1}H NMR (400 MHz, DMSO-d_6): δ = 9.24 (s, 1H, NO*H*), 7.29 (m, 5H, C$_6$*H*$_5$), 5.98 (s, 2H, N*H*$_2$), 5.64 (s, 2H, N*H*$_2$), 5.41 (s, 2H, C*H*$_2$) ppm. ^{13}C{^{1}H} NMR (68 MHz, DMSO-d_6): δ = 147.7 (*C*NOH), 140.5 (*C*$_{tri}$NH$_2$), 136.0 (*C*H), 128.6 (*C*H), 127.7 (*C*H), 127.3 (*C*H), 120.8 (*C*$_{tri}$), 48.5 (*C*H$_2$) ppm. Raman (1064 nm, 300 mW): $\tilde{\nu}$ = 3057 (36), 3046 (14), 2976 (9), 2948 (20), 1622 (68), 1582 (101), 1546 (40), 1474 (21), 1428 (21), 1315 (29), 1253 (15), 1199 (13), 1186 (10), 1158 (12), 1115 (16), 1079 (21), 1029 (17), 1003 (68), 949 (12), 935 (25), 899 (5), 833 (5), 797 (38), 742 (21), 724 (8), 619 (9), 585 (5), 461 (4), 425 (9), 381

(12), 345 (11), 304 (5), 280 (12), 233 (8), 210 (21), 181 (8), 89 (319) cm^{-1}. MS (DEI^+): m/z (%) = 232.2 (25) [M^+], 187.2 (5) [$C_{10}H_{11}N_4^+$], 91.2 (100) [$C_7H_7^+$]. EA ($C_{10}H_{12}N_6O$, 232.24 g mol^{-1}): calcd C 51.72, H 5.21, N 36.19%; found C 51.71, H 5.20, N 36.23%.

Attempted debenzylation of 5-amino-1-benzyl-1,2,3-triazole-4-carboxamidoxime (25)

25 (612 mg, 2.64 mmol) was dissolved in glacial acetic acid (125 mL) in a preheated flask under nitrogen atmosphere. Then Pd/C (10% Pd, 150 mg) and $Pd(OH)_2/C$ (150 mg) were added. The mixture was heated to 70 °C and hydrogenated at 1 atm for 3 h. The mixture was further stirred for 9 h at 70 °C. Afterwards it was filtered hot over kieselguhr to remove the catalyst. The filtrate was concentrated in vacuo to yield a colorless solid (310 mg).
^1H NMR (400 MHz, DMSO-d_6): δ = 7.91 (s, 1H), 4.09 (br, 3H), 2.40 (s, 2H), 1.89 (s, 1H) ppm. $^{13}C\{^1H\}$ NMR (68 MHz, DMSO-d_6): δ = 155.5, 121.7, 25.3 ppm. MS (DEI^+): m/z (%) = 150.2 (100).

5-Amino-2*H*-1,2,3-triazole-4-carbonitrile (26)

Sodium was added in small pieces to a solution of **11** (3.00 g, 15.06 mmol) in liquid ammonia (60 mL) until a deep blue suspension was obtained. Then ammonium chloride was carefully added until the blue color was completely gone. The solvent was allowed to slowly evaporate and the residue was dissolved in cold 2M HCl (about 15 mL). The precipitate was then filtered off and the filtrate was extracted with ethyl acetate (3×20 mL). The combined organic layer was washed with brine, dried over $MgSO_4$ and the solvent was removed in vacuo to yield a yellow solid (687 mg, 6.30 mmol, 42%).
DTA (5 °C min^{-1}): T_{dec1} = 205 °C, T_{dec2} = 261 °C. ^1H NMR (400 MHz, DMSO-d_6): δ = 14.61 (s, 1H, N*H*), 6.70 (s, 2H, NH_2) ppm. $^{13}C\{^1H\}$ NMR (68 MHz, DMSO-d_6): δ = 150.6 (C_{tri}), 114.0 (*C*N), 101.7 (C_{tri}) ppm. IR (ATR): $\tilde{\nu}$ = 3362 (m), 3342 (m), 3251 (w), 3204 (m), 3122 (m), 3092 (m), 3012 (m), 2936 (m), 2847 (m), 2726 (m), 2683 (w), 2563 (w), 2505 (vw), 2236 (m), 1659 (vs), 1617 (vs), 1494 (vw), 1448 (m), 1323 (vw), 1291 (m), 1237 (w), 1104 (w), 1056 (m), 998 (m), 976 (m), 878 (w), 813 (s), 764 (w), 720 (vw), 655 (m), 614 (vw) cm^{-1}. Raman (1064 nm, 300 mW): $\tilde{\nu}$ = 3206 (8), 2254 (2), 2236 (100), 1664 (7), 1627 (9), 1496 (20), 1447 (4), 1296 (21), 1069 (10), 1057 (3), 978 (17), 766 (21), 614 (10), 552 (10), 511 (6), 397 (4), 3811 (4), 192 (17), 158 (4), 120 (18) cm^{-1}. MS (DEI^+): m/z (%) = 109.1 (100) [M^+]. EA ($C_3H_3N_5$, 109.09 g mol^{-1}): calcd C 33.03, H 2.77, N 64.20%; found C 32.71, H 3.18, N 63.14%. Sensitivities (grain size: < 100 µm): IS: > 40 J; FS: > 360 N; ESD: 1.0 J.

5-Amino-2*H*-1,2,3-triazole-4-carboxamidoxime (27)

To hydroxylamine (50% *w*/*w* in H_2O, 0.7 mL, 10.7 mmol) in water (40 mL) was added **26** (1.225 g, 11.23 mmol). The solution was heated to 50 °C for 2 h. The solvent was removed in vacuo and the residue was washed with diethyl ether (10 mL) to yield a yellow solid (1.238 g, 8.71 mmol, 93%).
DTA (5 °C min^{-1}): T_{dehyd} = 71 °C, T_{dec} = 148 °C. ^{1}H NMR (400 MHz, DMSO-d_6): δ = 13.76 (br, 1H, N*H*), 9.49 (s, 1H, NO*H*), 5.61 (s, 2H, NH_2), 5.34 (s, 2H, NH_2) ppm. ^{13}C{^{1}H} NMR (101 MHz, DMSO-d_6): δ = 148.0, 147.9 (C_{tri}), 123.6 (C_{tri}) ppm. IR (ATR): $\tilde{\nu}$ = 3426 (m), 3339 (m), 3250 (m), 3152 (m), 3031 (m), 2925 (m), 2809 (m), 2357 (vw), 2091 (vw), 1658 (s), 1596 (m), 1571 (m), 1548 (m), 1441 (m), 1399 (w), 1333 (vw), 1294 (vw), 1241 (m), 1192 (w), 1167 (vw), 1111 (w), 1086 (vw), 982 (s), 939 (vs), 793 (vs), 744 (m), 695 (w), 661 (vw) cm^{-1}. Raman (1064 nm, 300 mW): $\tilde{\nu}$ = 3243 (9), 1665 (40), 1603 (36), 1568 (100), 1544 (55), 1502 (11), 1489 (12), 1465 (18), 1458 (17), 1387 (25), 1332 (26), 1274 (5), 1244 (13), 1171 (36), 1116 (35), 1080 (26), 985 (22), 941 (9), 927 (10), 914 (10), 906 (10), 822 (28), 744 (18), 422 (39), 354 (25), 322 (15), 312 (13) cm^{-1}. MS (DEI$^+$): *m*/*z* (%) = 142.1 (48) [M$^+$]. EA ($C_3H_6N_6O \cdot 0.5\,H_2O$, 151.07 g mol^{-1}): calcd C 23.84, H 4.67, N 55.61%; found C 23.32, H 4.67, N 52.77%.
After dehydration at 60 °C and 3×10^{-3} mbar for 2 d:
EA ($C_3H_6N_6O$, 142.14 g mol^{-1}): calcd C 25.35, H 4.26, N 59.13%; found C 25.82, H 4.18, N 57.73%. Sensitivities (grain size: < 100 µm): IS: > 40 J; FS: > 360 N.

5-Amino-3-(5-amino-2*H*-1,2,3-triazol-4-yl)-1,2,4-oxadiazole monohydrate (28·H_2O)

To **27** (602 mg, 4.24 mmol) dissolved in water (50 mL) was added slowly $KHCO_3$ (848 mg, 7.70 mmol). Cyanogen bromide (540 mg, 5.10 mmol) was added in portions to the yellow solution, which turned to brown. It was stirred for 24 h at room temperature and then acidified to pH2 with 2M HCl. The precipitate was filtered off, washed with water (10 mL), ethanol (10 mL), and diethyl ether (10 mL) to yield a dark brown solid (283 mg, 1.69 mmol, 40%).
DTA (5 °C min^{-1}): T_{dehyd} = 41 °C, T_{dec} = 160 °C. IR (ATR): $\tilde{\nu}$ = 3324 (w), 3184 (w), 2361 (vw), 2333 (vw), 2170 (vw), 1631 (vs), 1546 (vs), 1536 (vs), 1385 (s), 973 (w), 900 (vw), 793 (w), 687 (vw) cm^{-1}. MS (ESI$^+$): *m*/*z* (%) = 186.1 (59) [M+H_2O+H$^+$]. MS (ESI$^-$): *m*/*z* (%) = 167.0 (83) [M$^-$], 184.1 (100) [M$^-$+H_2O], 352.1 (88) [M$^-$+H_2O+M]. EA ($C_4H_5N_7O \cdot H_2O$, 185.15 g mol^{-1}): calcd C 25.95, H 3.81, N 52.96%; found C 25.93, H 3.77, N 52.31%. Sensitivities (grain size: < 100 µm): IS: > 40 J; FS: > 360 N; ESD: 1.5 J.

3,5-Bis(5-amino-1,2,4-oxadiazol-4-yl)-1,2,3-triazole monohydrate (29·H_2O)

$KHCO_3$ (2.376 g, 21.58 mmol) was dissolved in water (200 mL) and 2*H*-1,2,3-triazole-4,5-bis(carboxamidoxime) (**20**) (1.322 g, 7.14 mmol) was added. The mixture was heated under reflux until a clear solution was obtained. It was then cooled below 40 °C and cyanogen bromide (1.510 g, 14.26 mmol) was added in portions. Immediately a precipitate occurred and the solution turned to orange. It was stirred for 24 h at room temperature and then acidified with 2M HCl to pH2. The precipitate was filtered off to yield a light brown solid (959 mg, 4.08 mmol, 57%).
DSC (5 °C min^{-1}): T_{dec} = 180 °C. IR (ATR): $\tilde{\nu}$ = 3460 (vw), 3376 (w), 3353 (w), 3187 (w), 2702 (w), 2553 (w), 2190 (w), 1672 (s), 1627 (vs), 1581 (vs), 1536 (s), 1469 (s), 1458 (s), 1349 (m), 1258 (m), 1215 (m), 1148 (w), 1105 (m), 1029 (w), 1005 (m), 908 (vw), 830 (w), 801 (w), 765 (m), 717 (vw), 683 (vw) cm^{-1}. Raman (1064 nm, 300 mW): $\tilde{\nu}$ = 2195 (21), 2186 (19), 1677 (31), 1596 (100), 1538 (66), 1479 (31), 1353 (28), 1260 (13), 1136 (13), 1218 (22), 1153 (23), 1088 (20), 1016 (21), 996 (12), 990 (12), 982 (11), 974 (12), 965 (13), 845 (2), 757 (15), 641 (6), 635 (7), 500 (24), 482 (6), 472 (6), 380 (10), 350 (13), 324 (3), 301 (5), 231 (12) cm^{-1}. EA ($C_6H_6N_{10}O \cdot H_2O$, 248.17 g mol^{-1}): calcd C 28.46, H 2.79, N 49.79%; found C 27.93, H 3.19, N 47.70%. Sensitivities (grain size: < 100 µm): IS: 15 J; FS: > 360 N; ESD: 1.0 J.

3,5-Bis(5-amino-2*H*-1,2,3-triazol-4-yl)-1,2,4-oxadiazole monohydrate (30·H_2O)

To **27** (439 mg, 3.09 mmol) dissolved in DMF (10 mL) was added $ZnCl_2$ (462 mg, 3.39 mmol), *p*-toluenesulfonic acid hydrate (663 mg, 3.49 mmol) and **26** (338 mg, 3.10 mmol). The orange solution was stirred at 120 °C for 3 d. It was then cooled to room temperature and poured onto ice (24 g). The brown precipitate was filtered off and washed with water (10 mL), ethanol (10 mL), and diethyl ether (10 mL) to yield a brown solid (230 mg). To remove traces of DMF and *p*-toluenesulfonic acid it was suspended in water (30 mL), heated to 100 °C for 1 h and filtered hot to afford a brown solid (146 mg, 0.62 mmol, 20%).
DTA (5 °C min^{-1}): T_{dehyd} = 47 °C, T_{dec} = 240 °C. ^{1}H NMR (400 MHz, DMSO-d_6): δ = 8.54–8.09 (m) ppm. IR (ATR): $\tilde{\nu}$ = 3328 (m), 3198 (m), 2358 (w), 2337 (w), 1642 (vs), 1633 (vs), 1609 (vs), 1597 (vs), 1563 (vs), 1556 (vs), 1365 (m), 1344 (m), 1272 (w), 1232 (w), 1177 (w), 1125 (vw), 1098 (vw), 1088 (vw), 983 (vw), 953 (vw), 800 (w), 774 (vw), 687 (vw) cm^{-1}. MS (ESI$^+$): m/z (%) = 295.1 (37) [M^-+K^++Na^+]. EA ($C_6H_6N_{10}O \cdot H_2O \cdot 0.4$ DMF, 281.44 g mol^{-1}): calcd C 30.73, H 3.87, N 51.76%; found C 30.89, H 3.28, N 50.47%.

9.5 References

[1] A. Pace, P. Pierro, *Org. Biomol. Chem.* **2009**, *7*, 4337–4348.

[2] L. Alexey, K. Ruben, I. Yan, K. Mikhail, *Lett. Drug Des. Discovery* **2016**, *13*, 198–204.

[3] Z. He, C.-W. Kan, C.-L. Ho, W.-Y. Wong, C.-H. Chui, K.-L. Tong, S.-K. So, T.-H. Lee, L. M. Leung, Z. Lin, *Dyes Pigm.* **2011**, *88*, 333–343.

[4] A. M. Breul, M. D. Hager, U. S. Schubert, *Chem. Soc. Rev.* **2013**, *42*, 5366–5407.

[5] J. A. Pedro, J. R. Mora, E. Westphal, H. Gallardo, H. D. Fiedler, F. Nome, *J. Mol. Struct.* **2012**, *1016*, 76–81.

[6] E. Westphal, D. H. de Silva, F. Molin, H. Gallardo, *RSC Adv.* **2013**, *3*, 6442–6454.

[7] A. B. Sheremetev, N. N. Makhova, W. Friedrichsen, in *Adv. Heterocycl. Chem.*, *78*, Academic Press, **2001**, pp. 65–188.

[8] Y. Tang, J. Zhang, L. A. Mitchell, D. A. Parrish, J. M. Shreeve, *J. Am. Chem. Soc.* **2015**, *137*, 15984–15987.

[9] A. Gunasekaran, T. Jayachandran, J. H. Boyer, M. L. Trudell, *J. Heterocycl. Chem.* **1995**, *32*, 1405–1407.

[10] T. M. Klapötke, T. G. Witkowski, *Propellants, Explos., Pyrotech.* **2015**, *40*, 366–373.

[11] R. L. Willer, *Synthesis of high-nitrogen content heterocyclic nitramines and energetic internal plasticizers*, Technical Report, ADA182898, Morton Thiokol, Elkton, MD (USA), **1987**.

[12] J. Guy, G. Herve, G. Cagnon, F. Alvarez (SNPE Materiaux Energetiques), FR2911339 A1 **2008**.

[13] L. V. Batog, L. S. Konstantinova, V. Y. Rozhkov, O. V. Lebedev, M. A. Margarita, N. N. Makhova, I. V. Ovchinnikov, L. I. Khmel'nitskii, in *29th International Annual Conference of ICT*, Karlsruhe, Germany, **1998**.

[14] J. M. Veauthier, D. E. Chavez, B. C. Tappan, D. A. Parrish, *J. Energ. Mater.* **2010**, *28*, 229–249.

[15] G. Romeo, U. Chiacchio, in Modern Heterocyclic Chemistry, Wiley-VCH, **2011**, pp. 1047–1252.

[16] Y. Tang, C. He, L. A. Mitchell, D. A. Parrish, J. M. Shreeve, *J. Mater. Chem. A* **2015**, *3*, 23143–23148.

[17] T. M. Klapötke, N. T. Mayr, S. Seel, in *New Trends Res. Energ. Mater.*, *Proceedings Semin.*, 12th, **2009**, *2*, pp. 596–607.

[18] T. M. Klapötke, M. H. Kunzmann, N. T. Mayr, S. Seel, in *New Trends Res. Energ. Mater.*, *Proceedings Semin.*, 12th, **2009**, *2*, pp. 581–595.

[19] Z. Fu, R. Su, Y. Wang, Y. Wang, W. Zeng, N. Xiao, Y. Wu, Z. Zhou, J. Chen, F. Chen, *Chem. Eur. J.* **2012**, *18*, 1886–1889.

[20] Y. Tang, H. Gao, L. A. Mitchell, D. A. Parrish, J. M. Shreeve, *Angew. Chem., Int. Ed.* **2016**, *55*, 1147–1150; *Angew. Chem.* **2016**, *128*, 1159–1162.

[21] D. Izsák, T. M. Klapötke, C. Pflüger, *Dalton Trans.* **2015**, *44*, 17054–17063.

[22] J. R. E. Hoover, A. R. Day, *J. Am. Chem. Soc.* **1956**, *78*, 5832–5836.

[23] F. H. Allen, O. Kennard, D. G. Watson, L. Brammer, A. G. Orpen, R. Taylor, *J. Chem. Soc., Perkin Trans. 2* **1987**, *0*, S1–S19.

Melt-cast Materials: Combining the Advantages of Highly Nitrated Azoles and Open-chain Nitramines

T. M. Klapötke, A. Penger, C. Pflüger, and J. Stierstorfer

New J. Chem. **2016**, *40*, 6059–6069.

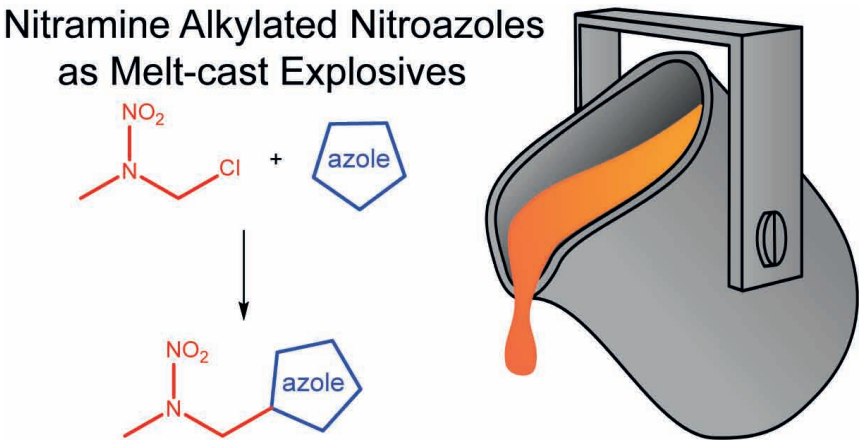

Melt-cast Materials: Combining the Advantages of Highly Nitrated Azoles and Open-chain Nitramines

T. M. Klapötke, A. Penger, C. Pflüger, and J. Stierstorfer

New J. Chem. **2016**, *40*, 6059–6069.

Abstract

Numerous efforts to substitute TNT as melt-cast matrix in explosive charges are ongoing due to its low performance and security issues. In this study the syntheses and full structural as well as spectroscopic characterization of 2-nitrazapropyl substituted polynitroazoles as potential melt-cast explosives are presented. This straightforward method of derivatization the heterocyclic N−H function by introducing a further energetic group improves the stability and energetic properties. X-ray crystallographic measurements were performed for all compounds and afforded insights into structural characteristics like strong intermolecular interactions. All compounds were characterized in terms of sensitivities towards impact, friction, and electrostatic discharge as well as thermal stabilities. The energetic properties were calculated with the EXPLO5 (v. 6.02) program.

10.1 Introduction

Melt-cast explosives are used in mortars, grenades, artillery shells but also for civil applications e.g. for mining and demolition. Nowadays, the melt-cast technology is based on 2,4,6-trinitrotoluene (TNT), 2,4-dinitroanisole (DNAN), and 1,3,3-trinitroazetidine (TNAZ), whose structures are depicted in Figure 10.1.

In general, the melt-cast explosives are molten in kettles heated at 80 to 120 °C with hot water or steam ingredients.[1] Therefore, an ideal melt-cast explosive or its formulations should have a low melting point (70–120 °C), a sufficient separation of melting and decomposition processes, low vapor pressure to diminish the inhalation toxicity, and a higher density and better performance than the ones already used. Furthermore, for processing the melt-cast explosives should show no shrinking and cracking on cooling and no separation from the shell on casing.

The drawback of TNT is its low performance ($D = 7300\,\mathrm{m\,s^{-1}}$) and its formulations are weak and brittle prone to cracking, which increase the impact sensitivities, exudation and they are dimensional instable in regard to thermal cycling.[2] DNAN did not show the toxicity drawback, which the manufacturing of TNT possesses and it is less sensitive, but also its performance is lower. Formulations of TNAZ show issues concerning the sensitivities

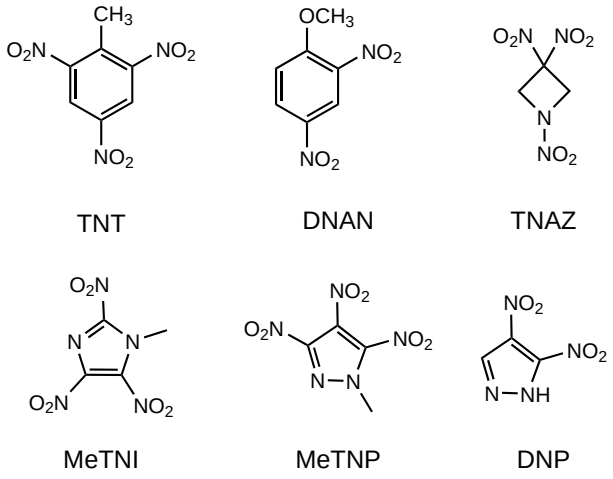

Figure 10.1: Melt-cast explosives.

and the melt-cast process to perform crack-free and tension-free castings.[1] Therefore, the development of new in all fields improved melt-cast explosives is still pursued.

Polynitrated azoles like 1-methyl-2,4,5-trinitroimidazole (MeTNI)[3,4] and 1-methyl-3,4,5-trinitropyrazole (MeTNP)[5,6] as well as 3,4-dinitropyrazole (DNP)[7] (Figure 10.1) show promising properties as replacement for TNT as melt-cast explosives due to their high positive enthalpies of formation, which results from the large number of C−N and N−N bonds as well as from ring/cage strain.[8] The nitro groups lead to an increased acidity of the heterocyclic proton which may result in problems concerning compatibility and storage. A common strategy to avoid the acidity and diminish the hygroscopicity is their *N*-alkylation by methylation or introduction of alkyl chains, which leads to better stabilities and compatibilities in formulations of explosive charges.[5,9–17]

Alkylation using nitramine containing side groups is an interesting strategy to improve the energetic properties because the nitramino group may take part in intermolecular interactions as acceptor and donor for hydrogen bonds as well as for dipolar N···O and C···O interactions, which should result in higher densities in comparison to the methylated derivatives.[18,19] The linkage of two equal azoles by nucleophilic substitution of 1,3-dichloro-2-nitrazapropane with the corresponding potassium salts of nitrated azoles has been investigated in different research groups[11,17,20,21] in analogy to studies of Bottaro and Highsmith.[22,23] The resulting open-chain nitramines show high thermal stabilities, high detonation performances, and varying sensitivities towards impact and friction, but unfortunately did not melt before decomposition. Therefore, a nitramine function should be introduced without linking the azoles. Preliminary results using 1-chloro-2-nitrazapropane and the doubly in situ deprotonated 3-nitro-1,2,4-triazol-5-one as well as various deprotonated tetrazole derivatives as azole building blocks reveal promising properties, especially

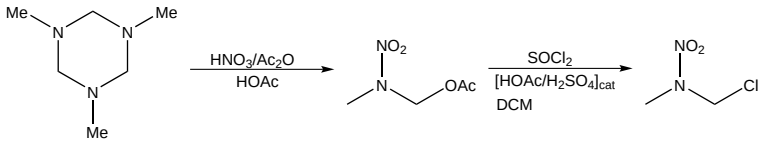

Scheme 10.1: Synthesis of 1-chloro-2-nitrazapropane starting from 1,3,5-trimethylhexahydro-1,3,5-triazine.

in regard to their thermal behavior with respect to melting before decomposition.[20,21,24] We now present an extended study of current work combing the advantages of highly nitrated azoles and nitramines by alkylation of the N−H function with 1-chloro-2-nitrazapropane to obtain potential melt-cast explosives.

10.2 Results and Discussion

10.2.1 Syntheses

1-Chloro-2-nitrazapropane was synthesized in two steps as shown in Scheme 10.1.[24] After the nitration of 1,3,5-trimethylhexahydro-1,3,5-triazine the conversion of 2-nitro-2-azapropyl acetate to 1-chloro-2-nitrazapropane was carried out by heating under reflux with thionyl chloride in dichloromethane and catalytic amounts of acetic acid and sulfuric acid.

The appropriate nitrogen-rich heterocycles were obtained from literature-known procedures[5,23,25–35] and generally converted to the corresponding potassium salts by using potassium hydroxide. The alkylation of the potassium salts with 1-chloro-2-nitrazapropane in aprotic solvents like acetone or acetonitrile yielded the desired energetic nitramines as depicted in Scheme 10.2.

In contrast to 1-(3-nitro-1*H*-1,2,4-triazol-5-on-4-yl)-2-nitrazapropane (**31**), which was synthesized from the monopotassium salt, the two times alkylated **32** was obtained from the in situ deprotonated free acid 3-nitro-1,2,4-triazol-5-one (NTO) using triethylamine as base. Various studies concerning the chemical stability of alkylated dinitrotriazoles show elimination of nitrite and formation of NTO derivatives and bistriazolyl systems under basic reaction conditions.[36–40] Thus, the alkylation of potassium 3,5-dinitro-1,2,4-triazolate was carried out at room temperature and in stoichiometric amounts to avoid elimination of nitrite. The nucleophilic substitution of 1-chloro-2-nitrazapropane with the potassium salt of 3-amino-5-nitro-1,2,4-triazole (ANTA) took place at the endocylic nitrogen atom to yield selectively nitramine **34**. Potassium 3,3′-dinitro-5,5′-bi(1,2,4-triazolate) was alkylated two times at the nitrogen atoms N1/N1′ to afford nitramine **35**.

Furthermore, the asymmetric and symmetric dinitroimidazole and symmetric dinitropyrazole derivatives were successfully alkylated to yield nitramines **36**, **37**, and **38**, respectively. The

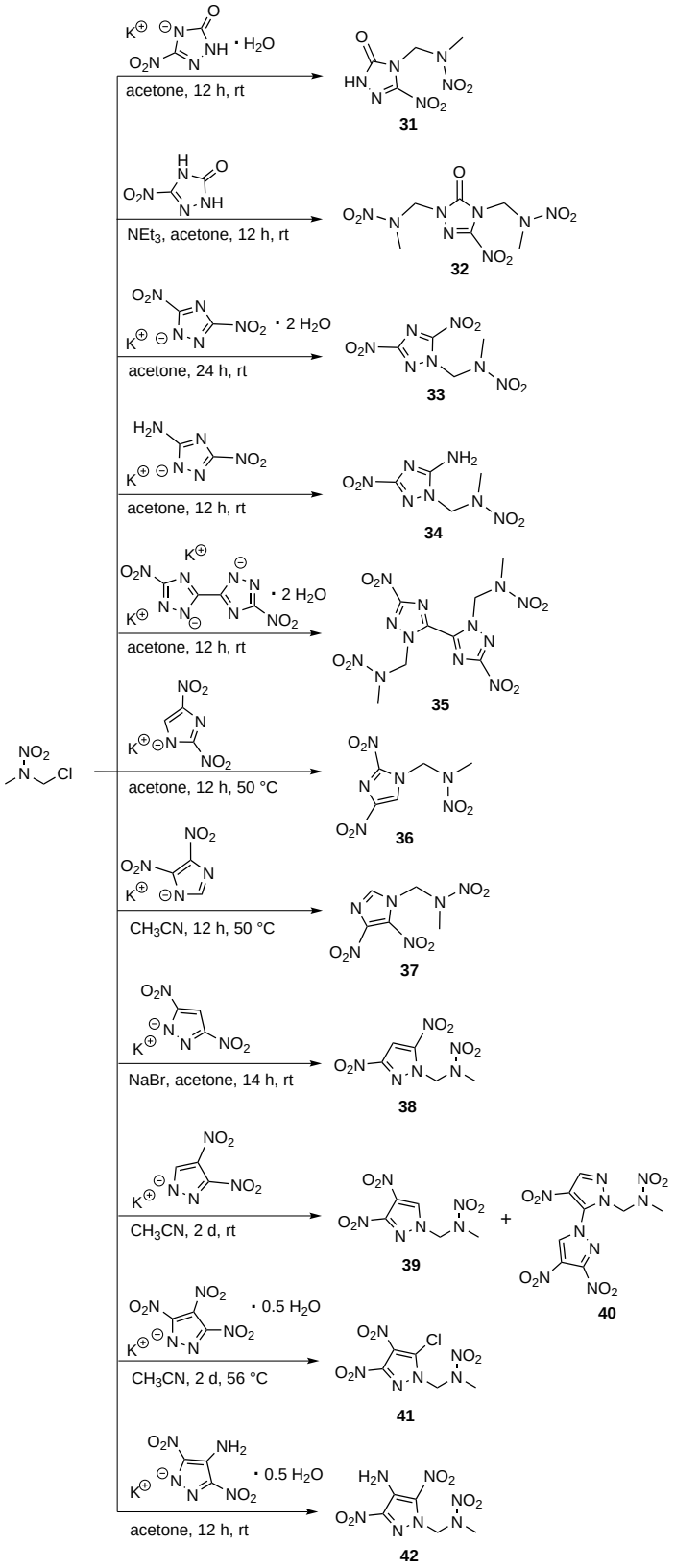

Scheme 10.2: Syntheses of the energetic nitramines **31**–**42** starting from 1-chloro-2-nitrazapropane.

reaction velocity of the synthesis of **38** was optimized by a Finkelstein halogen-exchange using sodium bromide. Two different substituted nitramines were formed by the alkylation of the potassium 3,4-dinitropyrazolate. The alkylation at N1 of 3,4-dinitropyrazole afforded the desired nitramine **39**. The formation of the other bipyrazolyl based nitramine **40** is caused by the high electrophilicity of the C3 position, which leads to a loss of the nitro group.[41] The supposed intermediate, the existing 3-chloro-4-nitro-pyrazolate,[42] reacted with another equivalent of potassium 3,4-dinitropyrazolate, thereby forming the 3,4,4′-trinitro-1,3′-bipyrazolyl system of nitramine **40**. The regioselectivity of the alkylation of 3,4-dinitropyrazole depending on the reaction temperature was studied revealing that the alkylation at N1 is preferred at low temperatures. The relative ratio of nitramines **39** and **40** was determined by the intensities of the ^{1}H NMR spectra with a reaction time of 24 h at 25 °C (84:16) and 82 °C (66:34), respectively. The isolated yields are not related to the reported ratio of intensities of the ^{1}H NMR due to partial decomposition during purification by column chromatography, which also leads to very low yields. The same reaction behavior was also observed for the nucleophilic substitution of 1,3-dichloro-2-nitrazapropane with potassium 3,4-dinitropyrazolate as reported previously.[11] Additionally to the presented synthesis route for bipyrazolyl systems, they were solely available by *cine*-substitutions starting from 1,4-dinitropyrazole derivatives.[43]

The nucleophilic substitution of 1-chloro-2-nitrazapropane with potassium 3,4,5-trinitropyrazolate afforded the 5-chloro-3,4-dinitropyrazolate substituted nitramine **41** due to the specific reactivity of the C5 position towards nucleophiles. This behavior was already studied by Dalinger et al. for nucleophilic substitution reactions with methylated 3,4,5-trinitropyrazole.[44] The reaction of 1-chloro-2-nitrazapropane with potassium 4-amino-3,5-dinitropyrazolate in acetone at ambient conditions afforded **42** in good yield.

10.2.2 NMR Spectroscopy

Vibrational spectroscopic studies of all synthesized compounds were performed with IR and Raman spectroscopy and the frequencies were assigned according to literature.[45] A detailed description is given in the Appendix. Compounds **31**–**42** were characterized by ^{1}H, ^{13}C and ^{14}N NMR spectroscopy in acetone-d_6. Selected chemical shifts of ^{1}H, ^{13}C and ^{14}N resonances of all presented compounds are summarized in Table 10.1.

The chemical shifts of methylene protons of open-chain nitramines were studied in the 1970th and identified in a range of 5.90–6.10 ppm.[46,47] By introduction of electron withdrawing substituents like nitro groups in the azoles the resonances of the methylene protons are shifted downfield. This effect is considerably observed for the 1,2,4-triazole based nitramines **33** and **35** with resonances of 6.81 ppm and 6.84 ppm, respectively. The resonance signals of

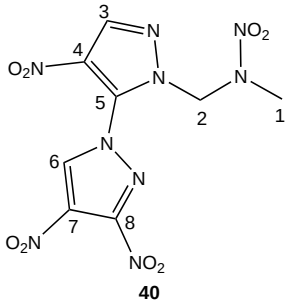

^{1}H NMR	
1	3.59 ppm
2	6.33 ppm
3	8.56 ppm
6	9.50 ppm

^{13}C NMR	
1	39.0 ppm
2	63.9 ppm
3	137.0 ppm
4	128.8 ppm
5	132.0 ppm
6	138.2 ppm
7	127.1 ppm
8	150.1 ppm

Figure 10.2: Assigned ^{1}H and ^{13}C{^{1}H} NMR resonances of **40** in acetone-d_6.

methyl protons are in a range of 3.50 ppm to 3.70 ppm. The CH resonances of the imidazolyl and pyrazolyl substituents show the characteristic downfield shifts of aromatic protons of nitrogen-rich heterocycles. The carbon resonances of the C−NO_2 functions are observed as small, broadened signals, because of their coupling to the nitrogen cores of the nitro groups. The chemical shifts of the ^{13}C methylene resonances are in a range of 58.0 ppm to 67.0 ppm and the methyl resonances are found in the range from 38.3 ppm to 39.9 ppm. The resonance signals of the aromatic C−NO_2 and the N−NO_2 nitro group nitrogens were observed in the ^{14}N NMR from −18 ppm to −37 ppm. An unambiguous assignment of these signals is difficult, because of their similar shifts.
Two-dimensional NMR spectra (HMBC) of **40** were recorded for an unambiguous assignment of the protons and carbon atoms of the 3,4,4′-trinitro-1,3′-bipyrazole system (Figure A.16). The assignment is given in Figure 10.2. The C−H resonance (No. 3) of the nitramine alkylated pyrazole ring is shifted upfield in comparison to the C−H resonance of **39**, whereas the other C−H resonance is shifted downfield, because of the neighboring electron withdrawing substituted pyrazolyl substituent. The methyl and methylene proton resonances of **40** are in the same range as the ones of **39**.

10.2.3 Crystal Structures

All presented compounds were also characterized by low-temperature single-crystal X-ray diffraction. Their molecular structures are depicted in Figure 10.3. Selected data and parameters of the measurements and refinements are summarized in Table A.41 to Table A.43 in the Appendix.
Nitramine **31** crystallizes from acetone / dichloromethane in the monoclinic space group $P2_1$ with two formula units per unit cell and a density of 1.721 g cm^{-3} at 173 K. Its unit cell is shown in Figure 10.4.
The two times alkylated nitramine **32** crystallizes as nitric acid adduct from diluted nitric acid in the monoclinic space group $P2_1$. The N−N bond length of the nitramine groups of **31** and **32** (1.34 Å) are shorter than the N−N bond lengths in the triazolone rings (1.37 Å).

Table 10.1: NMR signals of **31**–**42** in acetone-d_6 at room temperature.

	^{1}H NMR			^{13}C{^{1}H} NMR					^{14}N
	$C_{ar}H$	CH_2	CH_3	CNO_2	CH	C_q	CH_2	CH_3	NO_2
31	–	6.02	3.57	146.2	–	152.8	58.0	39.6	−30, −34
32	–	6.03, 5.90	3.57, 3.50	145.3	–	151.8	60.3, 58.4	39.8, 38.3	−31, −34
33	–	6.81	3.65	158.0, 151.2	–	–	67.0	39.0	−32, −37
34	–	6.11	3.60	n.o.[a]	–	156.9	61.6	38.5	−21, −25
35	–	6.84	3.68	n.o.[a]	–	143.7	65.4	39.1	−26
36	8.70	6.55	3.70	143.0	125.5	–	65.3	39.8	−23, −30, −32
37	8.28	6.43	3.66	142.3, 129.6	138.0	–	62.9	39.6	−24, −30, −34
38	7.91	6.72	3.64	154.1, 147.7	103.5	–	67.9	39.9	−25, −30
39	9.03	6.33	3.63	148.4, 126.9	134.0	–	66.9	38.8	−28, −31
40	9.50, 8.56	6.33	3.59	150.1, 129.7, 128.2	138.2, 137.0	132.0	63.9	39.0	−20, −25, −26
41	–	6.42	3.66	148.4, 123.9	–	130.0	64.4	39.0	−28, −31
42	–	6.64	3.59	130.5–130.4	–	130.5–130.4	67.3	38.8	−18, −23, −26

[a] Due to the low solubility in organic solvents some carbon signals could not be observed, although the measurements were performed with elongated pulse delays.

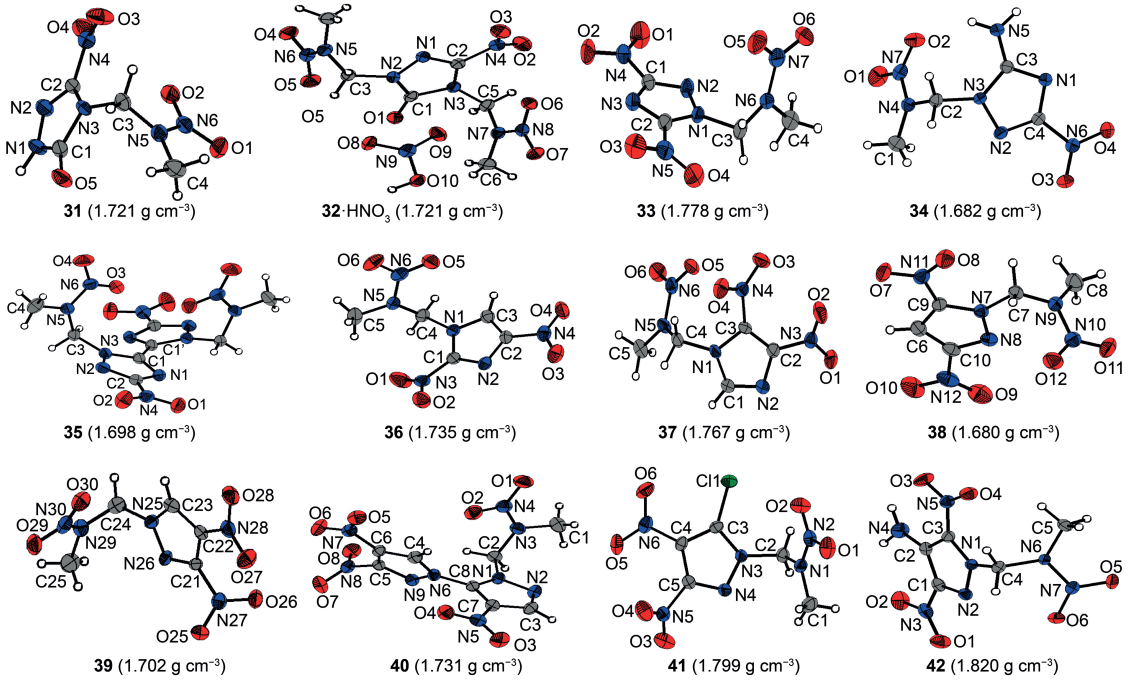

Figure 10.3: Molecular structures of the herein presented nitramines **31**–**42**.

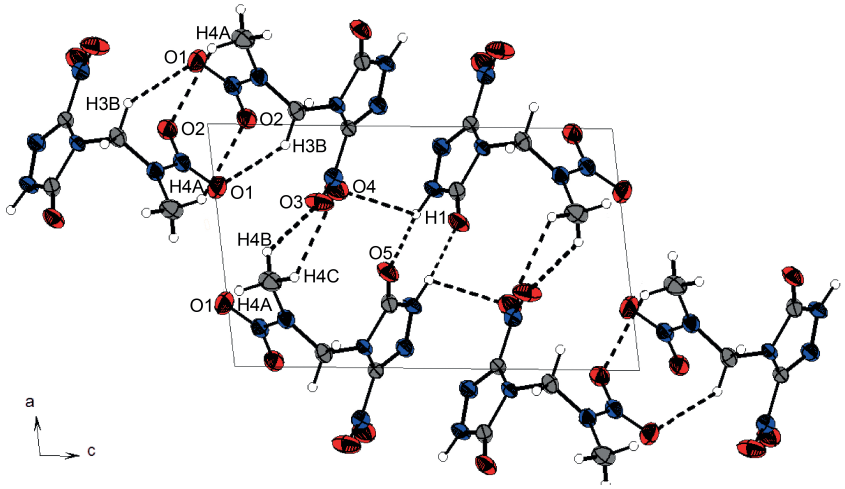

Figure 10.4: Unit cell of 1-(3-nitro-1*H*-1,2,4-triazol-5-on-4-yl)-2-nitrazapropane (**31**) along the *b* axis. Thermal ellipsoids are drawn at the 50% probability level. Selected hydrogen bonds are shown black dotted.

In comparison to the C−O bond length of γ–lactam systems (1.235 Å),[48] the C−O bond length of nitramine **31** (1.214(3) Å) is shorter, whereas the corresponding bond length of **32** is in the same range (1.230(3) Å). The C−N bond length to the nitro group is 1.457(3) Å and compared to the C−N bond lengths of the triazolone ring of 1.293(3)–1.400(3) Å considerably elongated. The significant differences in the bond lengths are an evidence for the localization of the double bond character. In analogy to β–NTO,[49] the C2−N2 bond

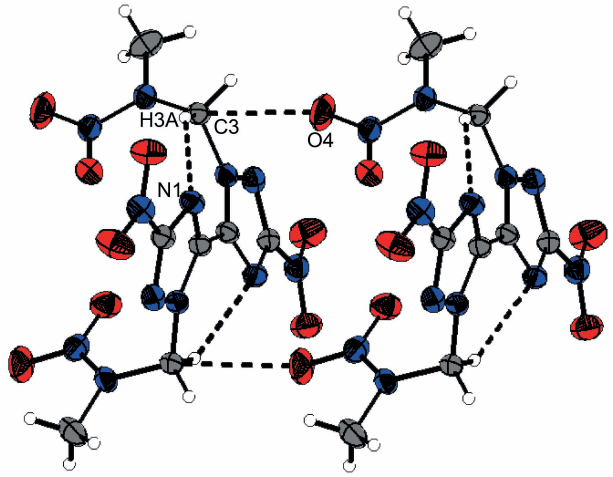

Figure 10.5: Selected structure forming dipolar intermolecular C···O interactions and non-classical hydrogen bonds within the crystal structure of **35** are shown black dotted.

length (1.293(3) Å) is the shortest one, whereas the alkylation leads to an elongated C1−N3 bond length of 1.400(3) Å instead of 1.378(2) Å.[49] The C−NO_2 function is twisted out of the triazole plane by 20.4° in contrast to the almost planar structure in NTO. This twisting enables various intermolecular interactions within the crystal structure of **31**. Due to the high acidity of the protons of the 2-nitrazapropyl substituent non-classical C−H···O and C−H···N hydrogen bonds are formed. Furthermore, high-grade directed dipolar N···O and C···O interactions are observed in a range from 2.87–2.97 Å. These dipolar interactions of O2 to the C2−N4 bond are supported by the twisting of the C−NO_2 group. The interactions are summarized in Table A.30. The layer-like packing of **31** is formed by an intermolecular hydrogen bond of the acidic N−H function and the oxygen of the γ–lactam system. The layers are connected by weak non-classical hydrogen bonds between the terminal methyl group and the nitro groups, whereas the non-classical hydrogen bond C3−H3A···N2 is found within one layer. The dipolar N6···O2 interaction of 2.970 Å is observed in between the layers. Similar interactions are observed in the crystal structure of nitramine **32** as listed in Table A.31.

The crystal structures of the other 1,2,4-triazole based nitramines **33**–**35** are supported by several non-classical hydrogen bonds and additionally either classical hydrogen bonds (**34**) or various dipolar interactions (nitramines **33** and **35**) as summarized in Table A.32 to Table A.34. The structure of nitramine **35** shows *C*2 symmetry perpendicular to the C1−$C1^{i}$ axis and its triazole rings are twisted by 26.1(1)°. Its crystal structure is depicted in Figure A.17. The molecules of one layer are connected by a dipolar C···O interaction (C3···O4: 2.920(2) Å) (Figure 10.5).

The 4,5-dinitroimidazolyl based nitramine **37** crystallizes with a higher crystal density of 1.767 g cm^{-3} than the 2,4-dinitroimidazole based **36** (1.735 g cm^{-3}) at 173 K. Furthermore,

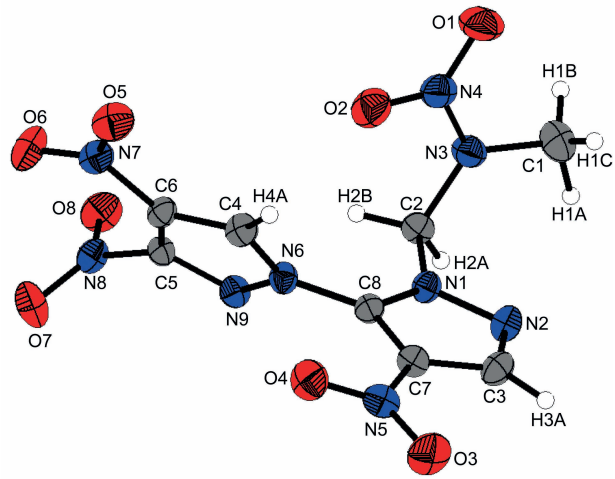

Figure 10.6: Molecular structure of 1-(3,4,4′-trinitro-1,3′-bipyrazol-2′-yl)-2-nitrazapropane (**40**). Thermal ellipsoids are drawn at the 50% probability level.

a greater extend of non-classical hydrogen bonds and dipolar interactions are observed within the crystal structure of **37** than in the one of **36** (Table A.35 and Table A.36).
The crystal structures of the two dinitropyrazolyl based nitramines **38** and **39** are supported by various non-classical hydrogen bonds, dipolar N···O and C···O interactions below the sum of the corresponding van der Waals radii (Table A.37 and Table A.38).
1-(3,4,4′-Trinitro-1,3′-bipyrazol-2′-yl)-2-nitrazapropane (**40**) crystallizes from dichloromethane in the triclinic space group $P\bar{1}$ with two formula units per unit cell and a crystal density of 1.731 g cm^{-3} at 173 K. The molecular structure of **40** is depicted in Figure 10.6. The pyrazole rings are twisted by 55.86(6)°. The almost perpendicular twistings of the nitro groups N7 and N8 are caused by steric repulsion of the neighbored nitro group, thereby taking part in intra- and intermolecular interactions. The pyrazole N−N bond lengths of 1.367(2) Å respective 1.379(2) Å are elongated in comparison to the nitramine N−N bond of 1.358(2) Å. The alignment of **40** within the crystal structure is formed by non-classical hydrogen bonds. The C−H functions of the bipyrazolyl system and the methylene protons interact with the nitro groups and the nitrogen atoms of the bipyrazole due to their high acidity (Table A.39). Additionally to the non-classical hydrogen bonds, dipolar high-grade directed N···O and C···O interactions of oxygen O8 are observed, which are shorter than the corresponding sum of the van der Waals radii.[50]
The neighbored nitro groups of nitramine **41** are less screwed than the ones of **40**. The oxygen atoms of the nitro group N6 as well as the nitramine group are involved in non-classical hydrogen bonds and additionally dipolar interactions are observed (Table A.40).
1-(4-Amino-3,5-dinitropyrazol-1-yl)-2-nitrazapropane (**42**) crystallizes from acetonitrile / dichloromethane in the monoclinic space group $P2_1/c$ with four formula units per unit cell. The bond lengths and angles in the pyrazole ring are similar to the corresponding ones

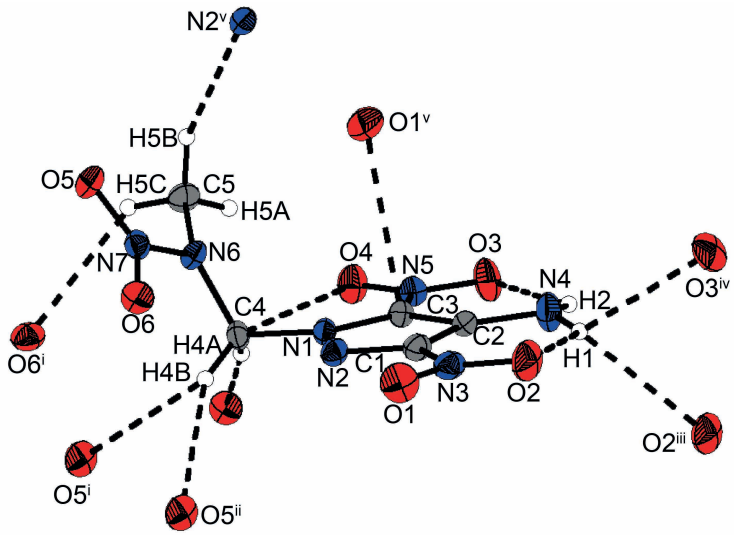

Figure 10.7: Selected hydrogen bonds in the structure of **42**, including the four-center hydrogen bond formed by proton H1 and two different oxygen atoms O2 and oxygen O3.

in the nitramine alkylated ring of the bipyrazolyl system **40**. In contrast to the crystal structure of 1-chloro-2-nitrazapropane,[51] the nitramine nitro group is nonplanar with the C4−C5−N7 plane, but twisted out of the plane by 5.9(1)°. The pyrazolyl ring is turned out of the CNC–plane by 58.11(5)°. Due to the spatial arrangement of the nitramine group, various intramolecular non-classical hydrogen bonds and electrostatic interactions are formed, involving the methyl and methylene groups as donor and the nitramine nitro group as well as the O4 of the *C*–bonded nitro group as acceptor (Figure 10.7). These and further selected interactions are listed in Table 10.2. The amino group is twisted out of the pyrazole ring by 3.65(3)°, whereas the nitro groups are almost in plane with a twist of less than 0.5°. These twistings enable two intramolecular classical hydrogen bonds of 2.1781(16) Å and 2.2521(17) Å. Furthermore, intramolecular dipolar N···O and C···O interactions considerably below the sum of the van der Waals radii are observed. The unit cell and crystal structure are shown in Figure A.18. The crystal structure consists of two different layers, which are opposed staggered to each other. The layers are connected by a great number of non-classical and classical hydrogen bonds in a range from 2.40–2.60 Å. Remarkable is a very uncommon four-center bond, which is formed by proton H1 of the amino group interacting intermolecular with the oxygen atoms O3 and O2 and also intramolecular with another O2. Additionally to the intermolecular hydrogen bonds, an intermolecular dipolar C···O interaction between C3 and O1 of 3.0179(17) Å is observed. The high number of intra- and intermolecular interactions leads to the high density of 1.820 g cm^{-3} at 173 K, which is the highest of the herein presented nitramines.

Table 10.2: Selected interactions within the crystal structure of **42**.

D−H···A	d(D−H) [Å]	d(H···A) [Å]	d(D···A) [Å]	∠(D−H···A) [°]
C5−H5A···O4	0.981(2)	2.3212(16)	3.174(3)	144.94(13)
N4−H2···O3	0.8954(7)	2.1781(16)	2.7687(18)	122.93(6)
N4−H1···O2	0.8763(7)	2.2521(17)	2.8219(18)	122.54(6)
C4−H4A···O6	0.9902(7)	2.4025(17)	3.3827(18)	170.31(6)
C5−H5C···O6^{i}	0.980(2)	2.5719(14)	3.293(2)	130.43(12)
C4−H4B···O5^{i}	0.9904(6)	2.5871(15)	3.2073(15)	120.66(5)
C4−H4B···O5^{ii}	0.9904(6)	2.6017(14)	3.5332(16)	156.74(5)
N4−H1···O2^{iii}	0.8763(7)	2.5768(17)	3.1444(18)	123.13(6)
N4−H1···O3^{iv}	0.8763(7)	2.4858(14)	3.0075(16)	118.79(5)
C5−H5B···N2^{v}	0.980(2)	2.5903(16)	3.479(3)	150.99(13)
dipolar interactions ΣvdW radii (N···O) < 3.07 Å [50] N4···O3 2.7687(18) Å; N4···O2 2.8219(18) Å				
dipolar interactions ΣvdW radii (C···O) < 3.22 Å [50] C4···O4 2.9061(17) Å; C3···O1^{v} 3.0179(17) Å				

Symmetry codes: (i) $1-x, 0.5+y, 0.5-z$; (ii) $x, -0.5-y, 0.5+z$; (iii) $-x, -y, 1-z$; (iv) $-x, -0.5+y, 0.5-z$; (v) $x, -0.5-y, -0.5+z$.

10.2.4 Thermal Stabilities, Sensitivities, and Energetic Properties

The thermal behavior of all presented compounds was investigated by differential scanning calorimetry (Table 10.3–Table 10.4). With the exception of 1-(3-nitro-1*H*-1,2,4-triazol-5-on-4-yl)-2-nitrazapropane (**31**) all nitramines melt before decomposition. For potential applications as energetic ingredients a thermal stability above 180 °C is desired, which is achieved by the majority of the compounds. They show thermal stabilities from 151 °C to 264 °C.

Especially for melt-cast applications the pyrazole based nitramines **38**–**41** and **32** are of great interest, which are melting below 140 °C and 80–150 °C before decomposition. In general, the pyrazole based nitramines **38**–**42** show higher thermal stabilities than the imidazole based nitramines **36** and **37**. The replacement of one nitro group in 1-(3,5-dinitro-1,2,4-triazol-1-yl)-2-nitrazapropane (**33**) by an amino group (**34**) leads to an increase in thermal stability of almost 60 °C. The same effect is observed for the thermal stability of the twice alkylated **32** in comparison to the mono alkylated **31**.

The impact, friction, and electrostatic discharge sensitivity tests were carried out for initial safety testing according to BAM methods.[52–54] All presented nitramines are sensitive towards friction with the exception of 1-(4-amino-3,5-dinitropyrazol-1-yl)-2-nitrazapropane (**42**). The impact sensitivities of the 1,2,4-triazolyl based nitramines differ strongly depending on the substituents and vary from sensitive to insensitive. Therefore, the twice alkylated

NTO derivative **32** as well as 1-(5-amino-3-nitro-1,2,4-triazol-1-yl)-2-nitrazapropane (**34**) and the bitriazole **35** are insensitive towards impact, whereas **31** and **33** show sensitivities of 10 J and 7 J. The 2,4-dinitroimidazolyl nitramine **36** is less sensitive than the 4,5-dinitroimidazolyl nitramine **37** showing impact sensitivities of 38 J and 25 J, respectively. The pyrazolyl based derivatives are insensitive towards impact with the exception of **38** (19 J). The electrostatic sensitivities of all presented compounds are within the range of 0.025–0.6 J and greater than the values (0.005–0.02 J) the human body can release.[55] In comparison to TNT the synthesized nitramines mainly show lower impact sensitivities, but increased sensitivities towards friction.

In the first instance the performance characteristics of new energetic materials are calculated to evaluate their utility for possible applications as an energetic material. The detonation parameters of all presented nitramines were calculated using the EXPLO5 (version 6.02) computer code.[56] The calculations were performed using the maximum densities at 25 °C and the calculated enthalpies of formation. Enthalpies of formation were calculated using the atomization method with CBS-4M[57,58] based electronic enthalpies computed with GAUSSIAN 09 A.02.[59] Gas phase enthalpies were transformed to solid state enthalpies by Trouton's rule by subtracting the gas-phase enthalpies with the corresponding enthalpies of sublimation.[60,61] If the compound has no melting point, the decomposition point was used instead to transform the gas phase enthalpy to the solid state enthalpy by Trouton's rule. The crystal densities at low-temperature were corrected to the corresponding crystal densities at 298 K by Equation 10.1 and the α_v coefficient of volume expansion from the related nitramine HMX ($\alpha_v = 1.6\times10^{-4}\,K$[62]).

$$\rho_{298K} = \frac{\rho_T}{1 + \alpha_v(298 - T)} \tag{10.1}$$

The energetic properties of all presented compounds are summarized in Table 10.3 and Table 10.3. The calculated detonation velocities (D) of all compounds range from 7788 m s^{-1} to 8482 m s^{-1}. The detonation pressures (p_{CJ}) of the nitramines at the Chapman–Jouguet point are calculated in the range from 235 kbar to 298 kbar. All nitramines show improved detonation performances in comparison to the widely used melt-cast explosives TNT and DNAN. Most promising for potential applications as TNT replacements in melt-cast formulations are nitramines **32**, **36**, **38**, and **39** with regard to their thermal behavior, sensitivities, and performance.

Furthermore, 1-(3,5-dinitro-1,2,4-triazol-1-yl)-2-nitrazapropane (**33**) and 1-(4-amino-3,5-dinitropyrazol-1-yl)-2-nitrazapropane (**42**) could be of potential use for energetic applications showing performances comparable to pentaerythritol tetranitrate (PETN), while possessing improved sensitivities.

Table 10.3: Physical and energetic properties of nitramines **31**–**38**.

	31	**32**	**33**	**34**	**35**	**36**	**37**	**38**
Molecular formula	$C_4H_6N_6O_5$	$C_6H_{10}N_8O_7$	$C_4H_5N_7O_6$	$C_4H_7N_7O_4$	$C_8H_{10}N_{12}O_8$	$C_5H_6N_6O_6$	$C_5H_6N_6O_6$	$C_5H_6N_6O_6$
M [g mol^{-1}]	218.13	306.20	247.13	217.15	402.25	246.14	246.14	246.14
IS [J][a]	10	>40	7	>40	>40	38	25	19
FS [N][b]	160	96	160	252	240	120	144	288
ESD [J][c]	0.025	0.10	0.15	0.60	0.15	0.13	0.15	0.1
Grain size [µm]	<100	<100	<100	<100	<100	100–500	<100	<100
N [%][d]	38.55	36.60	39.67	45.15	41.29	34.14	34.14	34.14
Ω [%][e]	−44.0	−52.3	−29.1	−55.3	−51.7	−45.5	−45.5	−45.5
T_{melt} [°C][f]	–	117	136	202	225	130	142	126
T_{dec} [°C][g]	151	211	167	224	228	183	190	210
ρ [g cm^{-3}][h]	1.69	1.66*	1.74	1.65	1.66	1.70	1.73	1.65
$\Delta_f H_m$ [kJ mol^{-1}][i]	−71	−51	216	105	311	71	90	111
$\Delta_f U$ [kJ kg^{-1}][j]	−229	−65	964	586	866	379	456	542
Calculated detonation parameters (Explo5 v. 6.02)								
$-Q_v$ [kJ kg^{-1}][k]	4598	4885	5701	4756	5017	5291	5374	5409
T_{det} [K][l]	3210	3258	3942	3205	3472	3610	3630	3713
p_{CJ} [kbar][m]	244	237	305	235	242	263	277	250
D [m s^{-1}][n]	7941	7925	8471	7983	7919	8046	8184	7899
V_0 [L kg^{-1}][o]	780	798	757	819	764	739	733	749

[a] Impact sensitivity (BAM drophammer 1 of 6). [b] Friction sensitivity (BAM friction tester 1 of 6). [c] Electrostatic discharge (OZM Research). [d] Nitrogen content. [e] Oxygen balance ($\Omega = (x\text{O} - 2y\text{C} - 0.5z\text{H})1600/M$). [f] Melting point. [g] Decomposition temperature. [h] Density at ambient temperature. [i] Calculated enthalpy of formation. [j] Calculated energy of formation. [k] Energy of explosion. [l] Detonation temperature. [m] Detonation pressure. [n] Detonation velocity. [o] Volume of detonation gases. * Density measured with a He pycnometer.

Table 10.4: Physical and energetic properties of nitramines **39**–**42** in comparison to TNT, DNAN, and PETN.

	39	**40**	**41**	**42**	TNT	DNAN	PETN
Molecular formula	$C_5H_6N_6O_6$	$C_8H_7N_9O_8$	$C_5H_5ClN_6O_6$	$C_5H_7N_7O_6$	$C_7H_5N_3O_6$	$C_7H_6N_2O_5$	$C_5H_8N_4O_{12}$
M [g mol^{-1}]	246.14	357.20	280.59	261.16	227.13	198.13	316.13
IS [J][a]	>40	>40	>40	>40	15	>40	3
FS [N][b]	n.d.	288	288	>360	>360	>360	60
ESD [J][c]	n.d.	0.2	0.1	0.4	0.7	n.d.	0.19
Grain size [µm]	<100	<100	<100	<100	<100	100–500	<100
N [%][d]	34.14	38.83	29.95	37.54	18.50	14.14	17.72
Ω [%][e]	−45.5	−51.5	−34.2	−45.9	−74.0	−96.9	−10.1
T_{melt} [°C][f]	80	133	82	141	81	94	141
T_{dec} [°C][g]	222	264	214	163	309	315	165
ρ [g cm^{-3}][h]	1.67	1.70	1.76	1.78	1.65*	1.59	1.78*
$\Delta_f H_m$ [kJ mol^{-1}][i]	136	331	111	108	−59*	−177	−534*
$\Delta_f U$ [kJ kg^{-1}][j]	643	1010	466	508	−185*	−813	−1594*
Calculated detonation parameters (Explo5 v. 6.02)							
$-Q_v$ [kJ kg^{-1}][k]	5512	5406	4872	5284	5022	4484	5994
T_{det} [K][l]	3747	3751	3761	3492	3452	3004	3971
p_{CJ} [kbar][m]	259	258	256	298	207	161	309
D [m s^{-1}][n]	8003	7986	7788	8482	7241	6705	8404
V_0 [L kg^{-1}][o]	746	707	715	753	633	636	743

[a] Impact sensitivity (BAM drophammer 1 of 6). [b] Friction sensitivity (BAM friction tester 1 of 6). [c] Electrostatic discharge (OZM Research). [d] Nitrogen content. [e] Oxygen balance ($\Omega = (x\text{O} - 2y\text{C} - 0.5z\text{H})1600/M$). [f] Melting point. [g] Decomposition temperature. [h] Density at ambient temperature. [i] Calculated enthalpy of formation. [j] Calculated energy of formation. [k] Energy of explosion. [l] Detonation temperature. [m] Detonation pressure. [n] Detonation velocity. [o] Volume of detonation gases. * Values obtained from the Explo5 database.

10.3 Conclusions

Nucleophilic substitution of 1-chloro-2-nitrazapropane with nitro-substituted azoles afforded various open-chain nitramines as reported herein. The alkylation of 3,4-dinitropyrazole yielded additionally to the desired nitramine **39** the alkylated bipyrazolyl system **40**. Prior to this reaction, bipyrazolyl-substituted systems were solely obtained by *cine*-substitutions. The crystal structures of all compounds were determined by low-temperature single-crystal X-ray diffraction and deliver insight into structural characteristics. A plurality of hydrogen bonds and dipolar C···O and N···O interactions is observed within each crystal structure, which leads to higher densities compared to the known crystal structures of methylated parent compounds. Especially, within the crystal structure of 1-(4-amino-3,5-dinitropyrazol-1-yl)-2-nitrazapropane (**42**) a high quantity of intra- and intermolecular interactions was observed, which leads to the highest density ($1.82\,\mathrm{g\,cm^{-3}}$) of the herein presented nitramines. With exception of **31**, all nitramines melt before decomposition. The decomposition temperatures range from 151 to 264 °C. The thermally most stable one is the bipyrazolyl nitramine **40**. Due to the comparatively low melting points of nitramines **32** and **38**–**41** ($< 135\,°\mathrm{C}$) and their considerably higher decomposition points, they are promising as potential melt-cast explosives.

Their sensitivities towards impact, friction, and electrostatic discharge were investigated by BAM methods. Compounds **31**, **33** and **36**–**38** are found to be sensitive towards impact, while the others are insensitive. All compounds are sensitive towards friction between 96 N to 288 N with the exception of **42** ($> 360\,\mathrm{N}$, insensitive). However, the sensitivities of the nitramines are mainly in the range of RDX and PETN or even improved. The nitramines show calculated performances with detonation velocities in the range from 7788–8482 $\mathrm{m\,s^{-1}}$ and detonation pressures between 237–305 kbar. Nitramines **33** and **42** exhibit performances comparable to PETN accompanied by improved sensitivities towards impact and friction. However, their thermal stabilities are lower than 180 °C. Therefore, the most promising compounds for potential application as energetic material are with regard to their sensitivities and performances the imidazolyl based nitramines **36** and **37**. The most promising potential TNT replacements are nitramines **32**, **36**, and **38** regarding their syntheses, sensitivities, energetic performance, and especially their thermal behavior.

10.4 Experimental Section

Caution! *Most compounds prepared herein are energetic compounds sensitive to impact, friction, and electrostatic discharge. Although there were no problems in handling the compounds, proper protective measures (ear protection, Kevlar® gloves, face shield, body*

armor and earthed equipment) should be used.

1-(3-Nitro-1*H*-1,2,4-triazol-5-on-4-yl)-2-nitrazapropane (31)

To a solution of potassium 3-nitro-1,2,4-triazolat-5-one monohydrate (2.86 g, 15.36 mmol) in acetone (30 mL) was added dropwise 1-chloro-2-nitrazapropane (1.91 g, 15.36 mmol) dissolved in acetone (10 mL). The reaction mixture was stirred overnight at room temperature and the inorganic solid was filtered off. The organic layer was concentrated in vacuo to afford a pale yellow solid. The crude product was washed with ethanol (10 mL) and hot water (10 mL) to yield a colorless solid (437 mg, 2.00 mmol, 13%).
DSC (5 °C min^{-1}): T_{dec} = 151 °C. ^{1}H NMR (400 MHz, acetone-d_6): δ = 12.00 (s, 1H, N*H*), 6.02 (s, 2H, CH_2), 3.57 (s, 3H, CH_3) ppm. ^{13}C{^{1}H} NMR (101 MHz, acetone-d_6): δ = 152.8 (*C*O), 146.2 (br, *C*NO$_2$), 58.0 (*C*H$_2$), 39.6 (*C*H$_3$) ppm. ^{14}N{^{1}H} NMR (29 MHz, acetone-d_6): δ = −30 (*N*O$_2$), −34 (*N*O$_2$) ppm. IR (ATR): $\tilde{\nu}$ = 3162 (w), 3094 (w), 3062 (w), 2960 (w), 2928 (vw), 2852 (vw), 2794 (vw), 1770 (vw), 1732 (s), 1716 (vs), 1690 (w), 1584 (vw), 1540 (vs), 1454 (m), 1414 (w), 1380 (w), 1340 (m), 1292 (m), 1278 (w), 1260 (m), 1184 (w), 1110 (vw), 1056 (w), 1026 (w), 934 (w), 860 (vw), 840 (w), 800 (w), 766 (w), 736 (w), 710 (w), 662 (w), 632 (vw), 610 (w), 736 (w), 710 (w), 662 (w), 632 (vw), 610 (w) cm^{-1}. Raman (1064 nm, 300 mW): $\tilde{\nu}$ = 3061 (14), 3012 (55), 2959 (32), 2910 (7), 2890 (6), 2856 (4), 1717 (5), 1578 (59), 1547 (39), 1469 (20), 1450 (29), 1413 (41), 1397 (56), 1341 (100), 1292 (10), 1273 (9), 1188 (29), 1108 (74), 1057 (12), 1026 (9), 936 (14), 862 (75), 842 (24), 801 (63), 739 (5), 716 (5), 663 (8), 608 (29), 591 (6), 478 (18), 450 (10), 426 (21), 416 (26), 409 (22), 329 (6), 253 (15), 197 (13), 131 (5), 109 (17) cm^{-1}. MS (DCI^{+}): m/z (%) = 219 (16) [M+H^{+}]. EA ($C_4H_6N_6O_5$, 218.13 g mol^{-1}): calcd C 22.03, H 2.77, N 38.55%; found C 23.44, H 2.85, N 36.08%. Sensitivities (grain size: < 100 µm): IS: 10 J; FS: 160 N; ESD: 0.25 J.

2,4-Bis(2-nitrazaprop-1-yl)-3-nitro-1,2,4-triazol-5-one (32)

To a solution of 5-nitro-2,4-dihydro-1,2,4-triazol-3-one (214 mg, 1.64 mmol) in acetone (10 mL) was added dropwise a solution of triethylamine (331 mg, 3.27 mmol) in acetone (1 mL). After 5 min of stirring, 1-chloro-2-nitrazapropane (610 mg, 4.90 mmol) was added. The reaction mixture was stirred overnight at room temperature and the formed inorganic solid was filtered off. The organic layer was concentrated in vacuo and the yellow oily crude product was treated with dichloromethane. The resulting solid was washed with diethyl ether and dried at air to afford colorless solid (166 mg, 0.54 mmol, 33%).
DSC (5 °C min^{-1}): T_{melt} = 117 °C, T_{dec} = 211 °C. ^{1}H NMR (400 MHz, acetone-d_6): δ = 6.03 (s, 2H, CH_2), 5.90 (s, 2H, CH_2), 3.57 (s, 3H, CH_3), 3.50 (s, 3H, CH_3) ppm. ^{13}C{^{1}H} NMR

(101 MHz, acetone-d_6): δ = 151.8 (*C*O), 145.3 (br, *C*NO_2), 60.3 (*C*H_2), 58.4 (*C*H_2), 39.8 (*C*H_3), 38.3 (*C*H_3) ppm. ^{14}N{^{1}H} NMR (29 MHz, acetone-d_6): δ = −31 (*N*O_2), −34 (*N*O_2) ppm. IR (ATR): $\tilde{\nu}$ = 3042 (vw), 3018 (vw), 3008 (vw), 2978 (vw), 2966 (vw), 2942 (vw), 1738 (vs), 1554 (s), 1540 (s), 1470 (m), 1452 (m), 1438 (w), 1430 (w), 1414 (m), 1386 (m), 1354 (w), 1334 (w), 1306 (s), 1292 (s), 1262 (m), 1218 (w), 1176 (w), 1126 (w), 1112 (w), 1088 (w), 1018 (m), 960 (vw), 896 (w), 864 (vw), 854 (vw), 816 (vw), 784 (m), 768 (w), 762 (w), 748 (w), 730 (w), 712 (w), 682 (w), 648 (vw), 632 (w), 610 (w) cm^{-1}. Raman (1064 nm, 300 mW): $\tilde{\nu}$ = 3044 (25), 3019 (26), 2978 (59), 2923 (12), 2902 (12), 2849 (6), 1753 (3), 1739 (10), 1586 (100), 1550 (49), 1496 (7), 1454 (97), 1429 (18), 1414 (23), 1390 (85), 1380 (53), 1357 (44), 1317 (68), 1289 (44), 1271 (22), 1245 (31), 1219 (57), 1176 (10), 1128 (62), 1114 (18), 1088 (14), 1033 (7), 1023 (9), 986 (29), 960 (16), 899 (17), 864 (35), 855 (70), 818 (43), 786 (8), 772 (2), 749 (5), 732 (5), 713 (3), 682 (5), 652 (12), 632 (6), 614 (20), 610 (19), 598 (15), 502 (12), 429 (19), 413 (23), 387 (8), 356 (4), 350 (4), 305 (10), 267 (12), 248 (2) cm^{-1}. MS (DCI$^+$): m/z (%) = 307 (6) [M+H$^+$]. EA ($C_6H_{10}N_8O_7$, 306.19 g mol^{-1}): calcd C 23.54, H 3.29, N 36.60%; found C 23.78, H 3.19, N 35.43%. Sensitivities (grain size: < 100 µm): IS: > 40 J; FS: 96 N; ESD: 0.10 J.

1-(3,5-Dinitro-1,2,4-triazol-1-yl)-2-nitrazapropane (33)

To a solution of 1-chloro-2-nitrazapropane (400 mg, 2.52 mmol) in acetonitrile (5 mL) was added potassium 3,5-dinitrotriazolate dihydrate (744 mg, 3.19 mmol). The reaction mixture was stirred for 24 h at room temperature. The formed precipitate was filtered off and the organic layer was removed in vacuo. The oily crude product was purified by washing with ethanol (10 mL). After filtration a colorless solid was obtained (494 mg, 2.39 mmol, 95%). DSC (5 °C min^{-1}): T_{melt} = 136 °C, T_{dec} = 165 °C. ^{1}H NMR (400 MHz, acetone-d_6): δ = 6.81 (s, 2H, C*H*$_2$), 3.65 (s, 3H, C*H*$_3$) ppm. ^{13}C{^{1}H} NMR (101 MHz, acetone-d_6): δ = 158.0 (br, *C*NO_2), 151.2 (br, *C*NO_2), 67.0 (*C*H_2), 39.0 (*C*H_3) ppm. ^{14}N{^{1}H} NMR (29 MHz, acetone-d_6): δ = −32 (*N*O_2), −37 (*N*O_2), −169 (br) ppm. IR (ATR): $\tilde{\nu}$ = 3062 (vw), 3036 (w), 2988 (vw), 2970 (vw), 2942 (vw), 2912 (vw), 2882 (vw), 1582 (vs), 1574 (vs), 1540 (s), 1516 (vs), 1476 (m), 1462 (m), 1438 (w), 1426 (m), 1412 (w), 1400 (w), 1382 (w), 1360 (w), 1334 (m), 1318 (s), 1300 (s), 1282 (vs), 1216 (m), 1188 (w), 1124 (w), 1042 (m), 1022 (w), 976 (w), 878 (w), 862 (m), 830 (m), 764 (w), 736 (w), 690 (m), 646 (w), 614 (w) cm^{-1}. Raman (1064 nm, 300 mW): $\tilde{\nu}$ = 3065 (4), 3037 (9), 2989 (16), 2969 (10), 2949 (3), 2913 (3), 2899 (3), 1583 (7), 1574 (9), 1568 (12), 1541 (4), 1520 (5), 1478 (7), 1462 (11), 1440 (96), 1429 (100), 1413 (28), 1402 (20), 1383 (42), 1361 (5), 1342 (16), 1321 (22), 1301 (7), 1285 (9), 1218 (21), 1191 (3), 1125 (13), 1051 (3), 1041 (4), 1025 (13), 978 (6), 878 (22), 864 (4), 830 (15), 770 (3), 760 (14), 736 (2), 691 (4), 644 (2), 617 (5), 601 (2), 521 (1), 485

(3), 420 (8), 379 (5), 357 (9), 335 (6), 305 (10), 289 (5), 206 (7), 185 (5), 164 (9), 116 (48), 88 (85) cm^{-1}. MS (DCI^+): m/z (%) = 248 (1) [M+H$^+$]. EA ($C_4H_5N_7O_6$, 247.13 g mol^{-1}): calcd C 19.44, H 2.04, N 39.67%; found C 19.11, H 1.95, N 38.73%. Sensitivities (grain size: < 100 µm): IS: 7 J; FS: 160 N; ESD: 0.15 J.

1-(5-Amino-3-nitro-1,2,4-triazol-1-yl)-2-nitrazapropane (34)

1-Chloro-2-nitrazapropane (215 mg, 1.73 mmol) was dissolved in acetone (20 mL) and potassium 5-amino-3-nitro-1,2,4-triazolate (289 mg, 1.73 mmol) was added. The reaction mixture was stirred overnight at room temperature. The precipitate was filtered off and the solvent was removed in vacuo to afford an orange solid. It was washed with ethanol (10 mL) and water (10 mL). Recrystallization in acetonitrile yielded a beige solid (67 mg, 0.31 mmol, 18%).
DSC (5 °C min^{-1}): T_{melt} = 202 °C, T_{dec} = 224 °C. ^{1}H NMR (400 MHz, acetone-d_6): δ = 6.58 (s, 2H, NH_2), 6.11 (s, 2H, CH_2), 3.60 (s, 3H, CH_3) ppm. ^{13}C{^{1}H} NMR (101 MHz, acetone-d_6): δ = 156.9, 61.6 (CH_2), 38.5 (CH_3) ppm. ^{14}N{^{1}H} NMR (29 MHz, acetone-d_6): δ = −21 (NO_2), −25 (NO_2) ppm. IR (ATR): $\tilde{\nu}$ = 3428 (s), 3298 (w), 3224 (w), 3176 (m), 3040 (w), 2359 (w), 2332 (w), 1641 (s), 1569 (m), 1538 (m), 1517 (vs), 1455 (m), 1447 (m), 1436 (m), 1426 (m), 1401 (m), 1384 (m), 1341 (w), 1306 (s), 1299 (vs), 1262 (m), 1246 (m), 1225 (m), 1102 (w), 1091 (w), 1021 (m), 949 (w), 856 (m), 844 (m), 797 (w), 762 (w), 730 (w), 712 (w), 656 (w) cm^{-1}. Raman (1064 nm, 300 mW): $\tilde{\nu}$ = 3432 (1), 3241 (1), 3225 (1), 3175 (2), 3167 (1), 3025 (1), 2997 (13), 2925 (1), 2795 (1), 1647 (6), 1576 (18), 1550 (7), 1514 (50), 1440 (6), 1427 (19), 1403 (100), 1345 (8), 1307 (39), 1262 (4), 1231 (30), 1105 (22), 1028 (14), 953 (13), 856 (18), 800 (18), 767 (3), 710 (4), 661 (2), 652 (1), 631 (1), 612 (5), 588 (1), 478 (1), 452 (1), 425 (6), 392 (2), 359 (2), 303 (2), 267 (6), 216 (4) cm^{-1}. MS (DCI^+): m/z (%) = 218.2 (64) [M+H$^+$], 130.1 (0.5) [$C_2H_3N_5O_2^+$], 89 (26) [$C_2H_5N_2O_2^+$]. EA ($C_4H_7N_7O_4$, 217.14 g mol^{-1}): calcd C 22.12, H 3.25, N 45.15%; found C 22.65, H 3.14, N 44.52%. Sensitivities (grain size: 100–500 µm): IS: > 40 J; FS: 252 N; ESD: 0.6 J.

5,5′-Bi(1-(2-nitrazapropan-1-yl)-3-nitro-1,2,4-triazole) (35)

1-Chloro-2-nitrazapropane (186 mg, 1.49 mmol) was dissolved in acetone (20 mL) and dipotassium 3,3′-dinitro-5,5′-bi(1,2,4-triazolate) dihydrate (252 mg, 0.75 mmol) was added. The reaction mixture was stirred overnight at room temperature. The precipitate was filtered off and the solvent was concentrated in vacuo. The crude product was washed with ethanol and water to afford beige solid (86 mg, 0.21 mmol, 28%).
DSC (5 °C min^{-1}): T_{melt} = 225 °C, T_{dec} = 228 °C. ^{1}H NMR (400 MHz, acetone-d_6): δ = 6.84 (s, 4H, CH_2), 3.68 (s, 6H, CH_3) ppm. ^{13}C{^{1}H} NMR (101 MHz, acetone-d_6): δ = 143.7,

65.4 (CH_2), 39.1 (CH_3) ppm. $^{14}N\{^1H\}$ NMR (29 MHz, acetone-d_6): $\delta = -26$ (NO_2) ppm. IR (ATR): $\tilde{\nu} = 3048$ (w), 2365 (vw), 2333 (vw), 1560 (s), 1552 (s), 1538 (vs), 1493 (w), 1473 (m), 1452 (m), 1412 (s), 1386 (m), 1360 (w), 1336 (w), 1312 (s), 1298 (vs), 1287 (vs), 1237 (vs), 1096 (w), 1050 (m), 1025 (s), 969 (w), 959 (w), 862 (vw), 836 (vs), 760 (m), 727 (w), 716 (m), 682 (w), 662 (w) cm^{-1}. Raman (1064 nm, 300 mW): $\tilde{\nu} = 3050$ (3), 3002 (23), 2961 (7), 1621 (6), 1598 (96), 1560 (5), 1492 (64), 1453 (5), 1435 (13), 1420 (22), 1388 (30), 1359 (4), 1339 (4), 1315 (16), 1278 (8), 1242 (8), 1222 (3), 1177 (5), 1129 (9), 1031 (13), 991 (3), 972 (3), 864 (18), 774 (6), 745 (3), 602 (5), 418 (4), 281 (4) cm^{-1}. MS (DCI$^+$): m/z (%) = 403.3 (45) [M+H$^+$], 89.1 (91) [$C_2H_5N_2O_2^+$], 43.1 (42) [$C_2H_5N^+$]. EA ($C_8H_{10}N_{12}O_8$, 402.24 g mol^{-1}): calcd C 23.89, H 2.51, N 41.29%; found C 24.36, H 2.46, N 40.79%. Sensitivities (grain size: < 100 µm): IS: > 40 J; FS: 240 N; ESD: 0.15 J.

1-(2,4-Dinitroimidazol-1-yl)-2-nitrazapropane (36)

To a solution of potassium 2,4-dinitroimidazolate (530 mg, 2.70 mmol) in acetone (10 mL) was added dropwise 1-chloro-2-nitrazapropane (333 mg, 2.67 mmol) in acetone (1 mL). The reaction mixture was stirred at 50 °C overnight and the formed precipitate was filtered off. The organic layer was concentrated in vacuo and the crude product was purified by washing with ethanol and filtered off to yield a yellow solid (390 mg, 1.58 mmol, 59%).
DSC (5 °C min^{-1}): $T_{melt} = 130$ °C, $T_{dec} = 183$ °C. ^1H NMR (400 MHz, acetone-d_6): $\delta =$ 8.70 (s, 1H, CH), 6.55 (s, 2H, CH_2), 3.70 (s, 3H, CH_3) ppm. $^{13}C\{^1H\}$ NMR (101 MHz, acetone-d_6): $\delta = 143.0$ (br, CNO_2), 125.5 (CH), 65.3 (CH_2), 39.8 (CH_3) ppm. $^{14}N\{^1H\}$ NMR (29 MHz, acetone-d_6): $\delta = -23$ (NO_2), -30 (NO_2), -32 (NO_2), -210 (br), -215 (br) ppm. IR (ATR): $\tilde{\nu} = 3146$ (w), 3068 (vw), 3004 (vw), 2948 (vw), 1542 (vs), 1514 (m), 1494 (s), 1464 (m), 1430 (m), 1408 (w), 1396 (w), 1378 (w), 1354 (m), 1334 (vs), 1302 (s), 1270 (m), 1256 (s), 1178 (w), 1128 (m), 1028 (m), 994 (w), 956 (w), 880 (vw), 862 (w), 850 (m), 836 (w), 820 (m), 766 (w), 750 (w), 724 (w), 680 (m), 648 (vw), 622 (vw), 610 (w), 680 (m), 648 (vw), 622 (vw), 610 (w) cm^{-1}. Raman (1064 nm, 300 mW): $\tilde{\nu} = 3148$ (4), 3069 (3), 3041 (1), 3005 (6), 2963 (3), 2896 (1), 1565 (3), 1548 (20), 1522 (17), 1514 (24), 1468 (3), 1433 (100), 1410 (33), 1386 (19), 1355 (21), 1338 (17), 1309 (8), 1296 (13), 1273 (24), 1180 (4), 1134 (7), 1109 (2), 1033 (2), 1015 (2), 996 (14), 957 (3), 863 (4), 854 (8), 838 (2), 820 (4), 757 (2), 752 (2), 726 (4), 612 (4) cm^{-1}. MS (DCI$^+$): m/z (%) = 247 (3) [M+H$^+$]. EA ($C_5H_6N_6O_6$, 246.14 g mol^{-1}): calcd C 24.40, H 2.46, N 34.14%; found C 24.50, H 2.29, N 33.83%. Sensitivities (grain size: < 100 µm): IS: 38 J; FS: 120 N; ESD: 0.13 J.

1-(4,5-Dinitroimidazol-1-yl)-2-nitrazapropane (37)

To a solution of 1-chloro-2-nitrazapropane (262 mg, 2.10 mmol) in acetonitrile (15 mL) was added potassium 4,5-dinitroimidazolate (412 mg, 2.10 mmol).The reaction mixture was stirred at 50 °C overnight and the precipitate was filtered off. The organic layer was removed in vacuo and the crude product was washed with ethanol. After drying at air a colorless solid was obtained (440 mg, 1.79 mmol, 85%).
DSC (5 °C min^{-1}): T_{melt} = 142 °C, T_{dec} = 190 °C. ^{1}H NMR (400 MHz, acetone-d_6): δ = 8.28 (s, 1H, C*H*), 6.43 (s, 2H, CH_2), 3.66 (s, 3H, CH_3) ppm. ^{13}C{^{1}H} NMR (101 MHz, acetone-d_6): δ = 142.3 (*C*NO$_2$), 138.0 (*C*H), 129.6 (*C*NO$_2$), 62.9 (*C*H$_2$), 39.6 (*C*H$_3$) ppm. ^{14}N{^{1}H} NMR (29 MHz, acetone-d_6): δ = −24 (*N*O$_2$), −30 (*N*O$_2$), −34 (*N*O$_2$), −135 (br), −210 (br) ppm. IR (ATR): $\tilde{\nu}$ = 3126 (m), 3052 (w), 3006 (vw), 2960 (vw), 1562 (w), 1528 (vs), 1518 (vs), 1494 (vs), 1466 (m), 1454 (m), 1426 (m), 1388 (w), 1356 (m), 1342 (s), 1314 (s), 1286 (s), 1252 (s), 1216 (m), 1164 (m), 1128 (w), 1032 (m), 1018 (w), 962 (w), 872 (vw), 856 (w), 846 (m), 814 (m), 766 (w), 754 (m), 714 (w), 696 (m), 638 (w), 622 (vw), 612 (w) cm^{-1}. Raman (1064 nm, 300 mW): $\tilde{\nu}$ = 3126 (20), 3053 (12), 3038 (6), 3005 (25), 2959 (13), 2897 (5), 1565 (45), 1544 (36), 1521 (31), 1498 (11), 1468 (4), 1457 (6), 1428 (16), 1413 (6), 1390 (51), 1371 (85), 1360 (62), 1344 (100), 1318 (16), 1289 (29), 1255 (5), 1221 (2), 1165 (5), 1130 (19), 1035 (6), 1018 (4), 966 (5), 874 (4), 857 (56), 819 (11), 764 (13), 757 (22), 715 (13), 698 (4), 649 (4), 613 (10), 501 (8), 459 (3), 448 (5), 402 (6), 363 (3), 342 (5), 300 (5), 231 (7), 205 (10), 198 (8), 149 (3), 113 (24) cm^{-1}. MS (DCI^{+}): m/z (%) = 247 (11) [M+H^{+}]. EA ($C_5H_6N_6O_6$, 246.14 g mol^{-1}): calcd C 24.40, H 2.46, N 34.14%; found C 24.51, H 2.52, N 33.98%. Sensitivities: (grain size: 100–500 µm): IS: 25 J; FS: 144 N; ESD: 0.15 J.

1-(3,5-Dinitropyrazol-1-yl)-2-nitrazapropane (38)

To a solution of 1-chloro-2-nitrazapropane (124 mg, 1.00 mmol) in acetone (5 mL) was added potassium 3,5-dinitropyrazolate (195 mg, 1.00 mmol) and sodium bromide (192 mg, 0.99 mmol). The reaction mixture was stirred at room temperature for 14 h and the precipitate was filtered off. The organic layer was concentrated in vacuo and the crude product was washed with ethanol. The colorless precipitate was filtered off to yield **38** (139 mg, 0.57 mmol, 57%).
DSC (5 °C min^{-1}): T_{melt} = 126 °C, T_{dec} = 210 °C. ^{1}H NMR (400 MHz, acetone-d_6): δ = 7.91 (s, 1H, C*H*), 6.72 (s, 2H, CH_2), 3.64 (s, 3H, CH_3) ppm. ^{13}C{^{1}H} NMR (101 MHz, acetone-d_6): δ = 154.1 (br, *C*NO$_2$), 147.7 (br, *C*NO$_2$), 103.5 (*C*H), 67.9 (*C*H$_2$), 39.9 (*C*H$_3$) ppm. ^{14}N{^{1}H} NMR (29 MHz, acetone-d_6): δ = −25 (*N*O$_2$), −30 (*N*O$_2$), −178 (br) ppm. IR (ATR): $\tilde{\nu}$ = 3174 (w), 3152 (w), 3066 (w), 3020 (w), 2954 (w), 2868 (w), 1564 (w), 1536 (m), 1514 (m), 1462 (w), 1430 (w), 1384 (w), 1344 (m), 1288 (m), 1240 (w), 1186 (w), 1110

(w), 1090 (w), 1050 (w), 1022 (w), 1000 (w), 972 (w), 852 (w), 834 (w), 764 (w), 742 (w), 684 (w), 658 (w), 636 (w), 624 (w) cm^{-1}. Raman (1064 nm, 300 mW): $\tilde{\nu}$ = 3175 (4), 3152 (4), 3069 (4), 3055 (4), 3021 (14), 3010 (10), 2954 (8), 2927 (3), 1567 (7), 1555 (8), 1542 (5), 1532 (5), 1516 (10), 1487 (6), 1467 (16), 1433 (29), 1409 (100), 1386 (30), 1355 (13), 1335 (7), 1320 (6), 1307 (6), 1286 (10), 1243 (10), 1186 (3), 1116 (3), 1052 (1), 1026 (1), 1003 (11), 977 (2), 971 (1), 875 (10), 863 (12), 818 (9), 760 (4), 747 (3), 739 (2), 685 (2), 641 (1), 608 (5), 574 (1), 531 (1), 496 (2), 485 (1), 434 (3), 402 (2), 384 (2), 352 (4), 343 (4), 298 (8), 272 (3) cm^{-1}. MS (DCI^+): m/z (%) = 247 (4) [$M+H^+$], 200 (2) [M^+-NO_2]. EA ($C_5H_6N_6O_6$, 246.14 g mol^{-1}): calcd C 24.40, H 2.46, N 34.14%; found C 24.82, H 2.41, N 33.75%. Sensitivities (grain size: < 100 µm): IS: 19 J; FS: 288 N; ESD: 0.10 J.

1-(3,4-Dinitropyrazol-1-yl)-2-nitrazapropane (39)

To a suspension of potassium 3,4-dinitropyrazolate (1.00 g, 4.31 mmol) and sodium bromide (0.44 g, 4.31 mmol) in acetonitrile (10 mL) was added 1-chloro-2-nitrazapropane (0.54 g, 4.31 mmol) dissolved in acetonitrile. After two days of stirring at room temperature the inorganic solid was filtered off. The organic layer was concentrated in vacuo and purified via column chromatography [silica gel, ethyl acetate/*i*-hexane (70:30)]. Due to decomposition by chromatography only a small amount of colorless solid (36 mg, 0.15 mmol, 3%) was obtained.

DSC (5 °C min^{-1}): T_{melt} = 82 °C, T_{dec} = 234 °C. ^{1}H NMR (400 MHz, acetone-d_6): δ = 9.03 (s, 1H, C*H*), 6.33 (s, 2H, CH_2), 3.63 (s, 3H, CH_3) ppm. $^{13}C\{^1H\}$ NMR (101 MHz, acetone-d_6): δ = 148.4 (br, *C*NO_2), 134.0 (*C*H), 126.9 (br, *C*NO_2), 66.9 (*C*H_2), 38.8 (*C*H_3) ppm. $^{14}N\{^1H\}$ NMR (29 MHz, acetone-d_6): δ = −28 (*N*O_2), −31 (*N*O_2), −176 (br) ppm. IR (ATR): $\tilde{\nu}$ = 3147 (w), 3122 (m), 3053 (w), 3008 (vw), 2959 (vw), 1544 (s), 1523 (vs), 1465 (m), 1448 (m), 1425 (w), 1388 (w), 1364 (m), 1324 (m), 1292 (m), 1275 (s), 1253 (m), 1186 (w), 1136 (m), 1119 (m), 1075 (m), 1017 (m), 1003 (m), 959 (w), 878 (w), 861 (m), 808 (m), 763 (w), 748 (m), 679 (w), 665 (w) cm^{-1}. Raman (1064 nm, 300 mW): $\tilde{\nu}$ = 3148 (9), 3132 (14), 3123 (20), 3056 (20), 3007 (42), 2957 (29), 2928 (9), 2887 (8), 1609 (6), 1567 (29), 1559 (31), 1543 (36), 1523 (86), 1465 (82), 1417 (96), 1389 (26), 1363 (75), 1353 (100), 1322 (65), 1280 (30), 1258 (14), 1160 (12), 1140 (10), 1119 (13), 1004 (61), 960 (18), 863 (90), 855 (76), 810 (12), 762 (19), 753 (14), 743 (16), 681 (6), 666 (8), 609 (29), 593 (11), 498 (16), 492 (17), 452 (13), 436 (12), 424 (12), 395 (23), 382 (21), 329 (20), 309 (15), 275 (9), 204 (45) cm^{-1}. MS (DCI^+): m/z (%) = 247 (73) [$M+H^+$], 200 (26) [M^+-NO_2]. EA ($C_5H_6N_6O_6$, 246.14 g mol^{-1}): calcd C 24.40, H 2.46, N 34.14%; found C 22.72, H 2.15, N 31.07%. Sensitivities (grain size: < 100 µm): IS: > 40 J. R_f value [silica gel, ethyl acetate/*i*-hexane (70:30)]: 0.72.

1-(3,4,4′-Trinitro-1,3′-bipyrazol-2′-yl)-2-nitrazapropane (40)

40 was obtained as side product by the synthesis of **39**. Isolation by column chromatography [silica gel, ethyl acetate/*i*-hexane (70:30)] yielded **40** as rose solid (103 mg, 0.29 mmol, 14%). DSC (5 °C min^{-1}): T_{melt} = 133 °C, T_{dec} = 264 °C. ^{1}H NMR (400 MHz, acetone-d_6): δ = 9.50 (s, 1H, C*H*), 8.56 (s, 1H, C*H*), 6.33 (s, 2H, CH_2), 3.59 (s, 3H, CH_3) ppm. ^{13}C{^{1}H} NMR (101 MHz, acetone-d_6): δ = 150.1 (br, *C*NO$_2$), 138.2 (*C*H), 137.0 (*C*H), 132.0 (C_q), 129.7 (br, *C*NO$_2$), 128.2 (br, *C*NO$_2$), 63.9 (*C*H$_2$), 39.0 (*C*H$_3$) ppm. ^{14}N{^{1}H} NMR (29 MHz, acetone-d_6): δ = −20 (*N*O$_2$), −25 (*N*O$_2$), −26 (*N*O$_2$), −170 (br) ppm. IR (ATR): $\tilde{\nu}$ = 3144 (w), 3053 (w), 3008 (w), 1599 (m), 1568 (m), 1528 (m), 1512 (m), 1501 (m), 1466 (m), 1451 (w), 1438 (w), 1416 (w), 1402 (m), 1365 (m), 1337 (m), 1315 (m), 1292 (m), 1248 (m), 1226 (w), 1185 (w), 1121 (w), 1041 (w), 1027 (w), 1012 (w), 945 (w), 877 (w), 869 (w), 856 (w), 826 (m), 807 (m), 762 (m), 747 (w), 697 (w), 664 (w) cm^{-1}. Raman (1064 nm, 300 mW): $\tilde{\nu}$ = 3143 (23), 3054 (9), 3035 (4), 3008 (22), 2951 (9), 2892 (3), 2855 (2), 2836 (2), 1599 (83), 1572 (13), 1552 (37), 1535 (39), 1518 (29), 1500 (52), 1478 (14), 1464 (19), 1454 (22), 1433 (34), 1415 (57), 1403 (100), 1380 (16), 1364 (45), 1338 (62), 1315 (25), 1291 (10), 1252 (16), 1227 (12), 1194 (15), 1126 (5), 1118 (9), 1043 (13), 1030 (2), 1013 (5), 952 (24), 942 (34), 869 (4), 858 (41), 827 (4), 807 (3), 764 (19), 755 (7), 748 (5), 700 (4), 662 (5), 638 (4), 631 (3), 617 (5), 606 (7), 579 (6), 476 (3), 461 (4), 450 (3), 442 (3), 383 (3), 370 (4), 353 (5), 313 (5), 294 (10), 278 (11), 241 (3) cm^{-1}. MS (DCI$^+$): m/z (%) = 358 (4) [M+H$^+$]. EA ($C_8H_7N_9O_8$, 357.20 g mol^{-1}): calcd C 26.90, H 1.98, N 38.83%; found C 26.84, H 1.87, N 34.48%. Sensitivities (grain size: < 100 µm): IS: > 40 J; FS: 288 N; ESD: 0.20 J. R_f value [silica gel, ethyl acetate/*i*-hexane (70:30)]: 0.83.

1-(5-Chloro-3,4-dinitropyrazol-1-yl)-2-nitrazapropane (41)

To a mixture of potassium 3,4,5-trinitropyrazolate semihydrate (575 mg, 2.30 mmol) in acetonitrile (10 mL) was added 1-chloro-2-nitrazapropane (286 mg, 2.30 mmol) dissolved in acetonitrile (5 mL). The reaction mixture was stirred under reflux for 2 d and the precipitate was filtered off. The organic layer was concentrated in vacuo and the crude oily product was dissolved in hot dichloromethane. The precipitate was filtered off and the filtrate was removed in vacuo. The resulting oil was overlaid with methanol and the formed precipitate was filtered off and dried at air to afford **41** (116 mg, 0.41 mmol, 18%).
DSC (5 °C min^{-1}): T_{melt} = 82 °C, T_{dec} = 214 °C. ^{1}H NMR (400 MHz, acetone-d_6): δ = 6.42 (s, 2H, CH_2), 3.66 (s, 3H, CH_3) ppm. ^{13}C{^{1}H} NMR (101 MHz, acetone-d_6): δ = 148.4 (br, *C*NO$_2$), 130.0 (*C*Cl), 123.9 (br, *C*NO$_2$), 64.4 (*C*H$_2$), 39.0 (*C*H$_3$) ppm. ^{14}N{^{1}H} NMR (29 MHz, acetone-d_6): δ = −28 (*N*O$_2$), −31 (*N*O$_2$), −176 (br) ppm. IR (ATR): $\tilde{\nu}$ = 3055 (vw), 2998 (vw), 2965 (vw), 1562 (m), 1533 (vs), 1498 (s), 1461 (m), 1452 (m), 1444 (m),

1426 (m), 1406 (m), 1384 (w), 1359 (m), 1339 (s), 1334 (m), 1292 (m), 1266 (s), 1235 (s), 1168 (w), 1128 (w), 1044 (w), 1027 (m), 961 (w), 888 (w), 852 (w), 814 (m), 774 (w), 762 (m), 752 (m), 710 (w), 681 (w) cm^{-1}. Raman (1064 nm, 300 mW): $\tilde{\nu}$ = 3056 (14), 3023 (7), 2998 (30), 2967 (20), 2892 (6), 2867 (4), 2857 (4), 1567 (21), 1544 (14), 1522 (14), 1501 (59), 1476 (18), 1461 (26), 1445 (100), 1430 (29), 1397 (22), 1366 (51), 1339 (83), 1293 (6), 1258 (24), 1170 (5), 1129 (15), 1044 (14), 1033 (8), 959 (7), 888 (7), 853 (40), 815 (9), 774 (20), 755 (11), 711 (2), 682 (2), 639 (4), 610 (11), 539 (7), 523 (4), 448 (11), 423 (5), 387 (9), 369 (15), 344 (18), 311 (12), 271(7), 223 (9), 199 (12), 171 (19), 126 (41), 105 (89), 82 (80) cm^{-1}. MS (DCI$^+$): m/z (%) = 281 (38) [M+H$^+$], 234 (3) [M$^+$−NO$_2$]. EA ($C_5H_5ClN_6O_6$, 280.58 g mol^{-1}): calcd C 21.40, H 1.80, N 29.95, Cl 12.64%; found C 21.71, H 1.78, N 29.78, Cl 12.77%. Sensitivities (grain size: < 100 µm): IS: > 40 J; FS: 288 N; ESD: 0.10 J.

1-(4-Amino-3,5-dinitropyrazol-1-yl)-2-nitrazapropane (42)

1-Chloro-2-nitrazapropane (115 mg, 0.92 mmol) was dissolved in acetone (15 mL) and potassium 4-amino-3,5-dinitropyrazolate semihydrate (187 mg, 0.85 mmol) was added. The reaction mixture was stirred overnight at room temperature. The precipitate was filtered off and the organic layer was concentrated in vacuo. The crude product was washed with ethanol and diethyl ether to afford a yellow solid (197 mg, 0.75 mmol, 88%).
DSC (5 °C min^{-1}): T_{melt} = 141 °C, T_{dec} = 165 °C. ^{1}H NMR (400 MHz, acetone-d_6): δ = 7.01 (s, 2H, NH_2), 6.66 (s, 2H, CH_2), 3.61 (s, 3H, CH_3) ppm. ^{13}C{^{1}H} NMR (101 MHz, acetone-d_6): δ = 130.5–130.4 (3C, CNH$_2$, CNO$_2$), 67.3 (CH$_2$), 38.8 (CH$_3$) ppm. ^{14}N{^{1}H} NMR (29 MHz, acetone-d_6): δ = −19 (NO_2), −23 (NO_2), −26 (NO_2), −184 (br), −318 (br) ppm. IR (ATR): $\tilde{\nu}$ = 3489 (w), 3383 (w), 3079 (vw), 2982 (vw), 2361 (vw), 2337 (vw), 1648 (m), 1612 (vw), 1581 (vw), 1547 (vw), 1516 (m), 1480 (s), 1429 (m), 1405 (w), 1385 (w), 1359 (w), 1318 (s), 1298 (vs), 1245 (vs), 1223 (m), 1152 (w), 1075 (w), 1025 (m), 974 (w), 889 (w), 849 (w), 827 (m), 790 (m), 758 (m), 748 (w), 705 (w), 665 (w), 649 (m), 614 (w) cm^{-1}. Raman (1064 nm, 300 mW): $\tilde{\nu}$ = 3373 (2), 2982 (5), 1654 (13), 1642 (9), 1572 (5), 1481 (3), 1433 (6), 1407 (11), 1378 (84), 1344 (51), 1325 (18), 1225 (9), 851 (7), 830 (17), 794 (9), 651 (5), 601 (3), 350 (7) cm^{-1}. MS (DCI$^+$): m/z (%) = 261 (8) [M$^+$]. EA ($C_5H_7N_7O_6$, 261.15 g mol^{-1}): calcd C 23.00, H 2.70, N 37.54%; found C 23.19, H 2.65, N 37.25%. Sensitivities (grain size: < 100 µm): IS: > 40 J; FS: > 360 N; ESD: 0.4 J.

10.5 References

[1] P. Ravi, D. M. Badgujar, G. M. Gore, S. P. Tewari, A. K. Sikder, *Propellants, Explos., Pyrotech.* **2011**, *36*, 393–403.

[2] D. W. Doll, J. M. Hanks, T. K. Highsmith, G. K. Lund, WO01/46092 A1 **2001**.

[3] R. Damavarapu, N. Gelber, R. Surapaneni, M. Zhang, R. Duddu, D. Parithosh, in *New Trends Res. Energ. Mater., Proceedings Semin.*, 12th, Pardubice, Czech Republic, **2009**, *1*, pp. 109–114.

[4] J. R. Cho, K. J. Kim, S. G. Cho, J. K. Kim, *J. Heterocycl. Chem.* **2002**, *39*, 141–147.

[5] G. Hervé, C. Roussel, H. Graindorge, *Angew. Chem., Int. Ed.* **2010**, *49*, 3177–3181; *Angew. Chem.* **2010**, *122*, 3245–3249.

[6] I. L. Dalinger, I. A. Vatsadze, T. K. Shkineva, G. P. Popova, S. A. Shevelev, Y. V. Nelyubina, *J. Heterocycl. Chem.* **2013**, *50*, 911–924.

[7] S. Ek, K. Dudek, J. Johansson, N. Latypov, in *New Trends Res. Energ. Mater., Proceedings Semin.*, 17th, Pardubice, Czech Republic, **2014**, *1*, pp. 180–188.

[8] M.-H. V. Huynh, M. A. Hiskey, E. L. Hartline, D. P. Montoya, R. Gilardi, *Angew. Chem., Int. Ed.* **2004**, *43*, 4924–4928; *Angew. Chem.* **2004**, *116*, 5032–5036.

[9] L. I. Bagal, M. S. Pevzner, A. N. Frolov, N. I. Sheludyakova, *Khim. Geterotsikl. Soedin.* **1970**, 259–264.

[10] P. F. Pagoria, G. S. Lee, A. R. Mitchell, R. D. Schmidt, *Thermochim. Acta* **2002**, *384*, 187–204.

[11] T. M. Klapötke, A. Penger, C. Pflüger, J. Stierstorfer, M. Sućeska, *Eur. J. Inorg. Chem.* **2013**, 4667–4678.

[12] M. A. Kettner, T. M. Klapötke, *Chem. Eur. J.* **2015**, *21*, 3755–3765.

[13] Y. Tang, C. He, H. Gao, J. M. Shreeve, *J. Mater. Chem. A* **2015**, *3*, 15576–15582.

[14] P. Yin, J. Zhang, D. A. Parrish, J. M. Shreeve, *Chem. Eur. J.* **2014**, *20*, 16529–16536.

[15] P. Yin, D. A. Parrish, J. M. Shreeve, *Angew. Chem., Int. Ed.* **2014**, *53*, 12889–12892; *Angew. Chem.* **2014**, *126*, 13103–13106.

[16] O. P. Shitov, V. L. Korolev, V. S. Bogdanov, V. A. Tartakovsky, *Russ. Chem. Bull.* **2003**, *52*, 695–699.

[17] J. Zhang, C. He, D. A. Parrish, J. M. Shreeve, *Chem. Eur. J.* **2013**, *19*, 8929–8936.

[18] G. L. Starova, O. V. Frank-Kamenetskaya, M. S. Pevzner, *J. Struct. Chem.* **1989**, *29*, 799–801.

[19] Y.-X. Li, X.-J. Wang, J.-L. Wang, *Acta Crystallogr. Sect. E Struct. Rep. Online* **2009**, *65*, o3073-o3073.

[20] T. M. Klapötke, A. Penger, C. Pflüger, in *New Trends Res. Energ. Mater., Proceedings Semin.*, 14th, Pardubice, Czech Republic, **2011**, *2*, pp. 753–761.

[21] A. Penger, *Offenkettige Nitramine als potentielle Ersatzstoffe für Cyclomethylentrinitramin (RDX)*, dissertation, Ludwig Maximilian University of Munich, **2011**.

[22] J. C. Bottaro, R. J. Schmitt, A. M. Petrie, P. E. Penwell, US62555112 **2001**.

[23] T. K. Highsmith, J. M. Hanks, S. P. Velarde, J. C. Bottaro, WO2002060881 A1 **2002**.

[24] N. Fischer, K. Karaghiosoff, T. M. Klapötke, J. Stierstorfer, *Z. Anorg. Allg. Chem.* **2010**, *636*, 735–749.

[25] K. Y. Lee, C. B. Storm, M. A. Hiskey, M. D. Coburn, *J. Energ. Mater.* **1991**, *9*, 415–428.

[26] R. D. Schmidt, G. S. Lee, P. F. Pagoria, A. R. Mitchell, R. Gilardi, *J. Heterocycl. Chem.* **2001**, *38*, 1227–1230.

[27] A. R. Katritzky, S. Singh, K. Kirichenko, M. Smiglak, J. D. Holbrey, W. M. Reichert, S. K. Spear, R. D. Rogers, *Chem. Eur. J.* **2006**, *12*, 4630–4641.

[28] G. Wüllner, F.-W. Herkenrath, A. Jülich, Y. Yamada, S. Kawabe, WO2010021409 **2010**.

[29] R. Hüttel, F. Büchele, *Chem. Ber.* **1955**, *88*, 1586–1590.

[30] J. W. A. M. Janssen, H. J. Koeners, C. G. Kruse, C. L. Habraken, *J. Org. Chem.* **1973**, *38*, 1777–1782.

[31] G. T. Morgan, I. Ackerman, *J. Chem. Soc. Trans.* **1923**, *123*, 1308–1318.

[32] Y. V. Serov, M. S. Pevzner, T. P. Kofman, I. V. Tselinskii, *Russ. J. Org. Chem.* **1990**, *26*, 773–777.

[33] L. I. Bagal, M. S. Pevzner, A. N. Frolov, N. I. Sheludyakova, *Chem. Heterocycl. Compd.* **1970**, *6*, 240–244.

[34] A. A. Dippold, T. M. Klapötke, N. Winter, *Eur. J. Inorg. Chem.* **2012**, 3474–3484.

[35] K.-Y. Lee, L. B. Chapman, M. D. Cobura, *J. Energ. Mater.* **1987**, *5*, 27–33.

[36] L. I. Bagal, M. S. Pevzner, V. Y. Samarenko, A. P. Egorov, *Khim. Geterotsikl. Soedin.* **1970**, 1701–1703.

[37] M. S. Pevzner, V. Y. Samarenko, L. I. Bagal, *Khim. Geterotsikl. Soedin.* **1972**, 117–119.

[38] T. P. Kofman, G. Y. Kartseva, V. I. Namestnikov, E. A. Paketina, *Russ. J. Org. Chem.* **1998**, *34*, 1032–1039.

[39] M. S. Pevzner, T. P. Kofman, E. N. Kibasova, L. F. Sushchenko, T. L. Uspenskaya, *Khim. Geterotsikl. Soedin.* **1980**, 257–261.

[40] T. P. Kofman, *Russ. J. Org. Chem.* **2001**, *37*, 1158–1168.

[41] I. L. Dalinger, I. A. Vatsadze, T. K. Shkineva, I. O. Kortusov, G. P. Popova, V. V. Kachala, S. A. Sheveleva, *Russ. Chem. Bull.* **2010**, *59*, 1786–1790.

[42] I. J. Ferguson, K. Schofield, J. W. Barnett, M. R. Grimmett, *J. Chem. Soc., Perkin Trans. 1* **1977**, *0*, 672–675.

[43] P. Cohen-Fernandes, C. Erkelens, C. G. M. Van Eendenburg, J. J. Verhoeven, C. L. Habraken, *J. Org. Chem.* **1979**, *44*, 4156–4160.

[44] I. L. Dalinger, I. A. Vatsadze, T. K. Shkineva, G. P. Popova, S. A. Shevelev, *Mendeleev Commun.* **2011**, *21*, 149–150.

[45] M. Hesse, H. Meier, B. Zeeh, *Spektroskopische Methoden in der organischen Chemie*, 7th ed., Thieme, Stuttgart, Germany **2005**.

[46] I. J. Solomon, R. K. Momii, F. H. Jarke, A. J. Kacmarek, J. K. Raney, P. C. Adlaf, *J. Chem. Eng. Data* **1973**, *18*, 335–337.

[47] A. R. Farminer, G. A. Webb, *Tetrahedron* **1975**, *31*, 1521–1526.

[48] F. H. Allen, O. Kennard, D. G. Watson, L. Brammer, A. G. Orpen, R. Taylor, *J. Chem. Soc., Perkin Trans. 2* **1987**, *0*, S1–S19.

[49] N. B. Bolotina, E. Zhurova, A. A. Pinkerton, *J. Appl. Crystallogr.* **2003**, *36*, 280–285.

[50] A. Bondi, *J. Phys. Chem.* **1964**, *68*, 441–451.

[51] B. Aas, M. A. Kettner, T. M. Klapötke, M. Sućeska, C. Zoller, *Eur. J. Inorg. Chem.* **2013**, 6028–6036.

[52] Test methods according to the *UN Manual of Test and Criteria, Recommendations on the Transport of Dangerous Goods*, United Nations Publication, New York, Geneva, 4th revised ed., **2003**: Impact: Insensitive >40 J, less sensitive ≥ 35 J, sensitive ≥ 4 J, very sensitive ≤ 3 J; Friction: Insensitive >360 N, less sensitive $= 360$ N, sensitive <360 N a. >80 N, very sensitive ≤ 80 N, extremely sensitive ≤ 10 N.

[53] NATO, *Standardization Agreement 4489 (STANAG 4489), Explosives, Impact Sensitivity Tests* **1999**.

[54] NATO, *Standardization Agreement 4487 (STANAG 4487), Explosives, Friction Sensitivity Tests* **2002**.

[55] T. M. Klapötke, *Chemistry of High-Energy Materials*, 3rd ed., de Gruyter, Berlin, Germany, **2015**.

[56] M. Sućeska, EXPLO5 program, 6.02 ed., Zagreb, Croatia, **2014**.

[57] J. J. A. Montgomery, M. J. Frisch, J. W. Ochterski, G. A. Petersson, *J. Chem. Phys.* **2000**, *112*, 6532–6542.

[58] J. W. Ochterski, G. A. Petersson, J. J. A. Montgomery, *J. Chem. Phys.* **1996**, *104*, 2598–2619.

[59] M. J. Frisch, G. W. Trucks, H. B. Schlegel, G. E. Scuseria, M. A. Robb, J. R. Cheeseman, G. Scalmani, V. Barone, B. Mennucci, G. A. Petersson, H. Nakatsuji, M. Caricato, X. Li, H. P. Hratchian, A. F. Izmaylov, J. Bloino, G. Zheng, J. L. Sonnenberg, M. Hada, M. Ehara, K. Toyota, R. Fukuda, J. Hasegawa, M. Ishida, T. Nakajima, Y. Honda, O. Kitao, H. Nakai, T. Vreven, J. J. A. Montgomery, J. E. Peralta, F. Ogliaro, M. Bearpark, J. J. Heyd, E. Brothers, K. N. Kudin, V. N. Staroverov, R. Kobayashi, J. Normand, K. Raghavachari, A. Rendell, J. C. Burant, S. S. Iyengar, J. Tomasi, M. Cossi, N. Rega, J. M. Millam, M. Klene, J. E. Knox, J. B. Cross, V. Bakken, C. Adamo, J. Jaramillo, R. Gomperts, R. E. Stratmann, O. Yazyev, A. J. Austin, R. Cammi, C. Pomelli, J. W. Ochterski, R. L. Martin, K. Morokuma, V. G. Zakrzewski, G. A. Voth, P. Salvador, J. J. Dannenberg, S. Dapprich, A. D. Daniels, O. Farkas, J. B. Foresman, J. V. Ortiz, J. Cioslowski, D. J. Fox, GAUSSIAN 09, Revision A.02, Inc., Wallingford CT, **2009**.

[60] M. S. Westwell, M. S. Searle, D. J. Wales, D. H. Williams, *J. Am. Chem. Soc.* **1995**, *117*, 5013–5015.

[61] F. Trouton, *Philos. Mag.* **1884**, *18*, 54–57.

[62] C. Xue, J. Sun, B. Kang, Y. Liu, X. Liu, G. Song, Q. Xue, *Propellants, Explos., Pyrotech.* **2010**, *35*, 333–338.

3-Nitramino-4-nitrofurazan: Enhancing the Stability and Energetic Properties by Introduction of Alkylnitramines

T. M. Klapötke, and C. Pflüger

unpublished results.

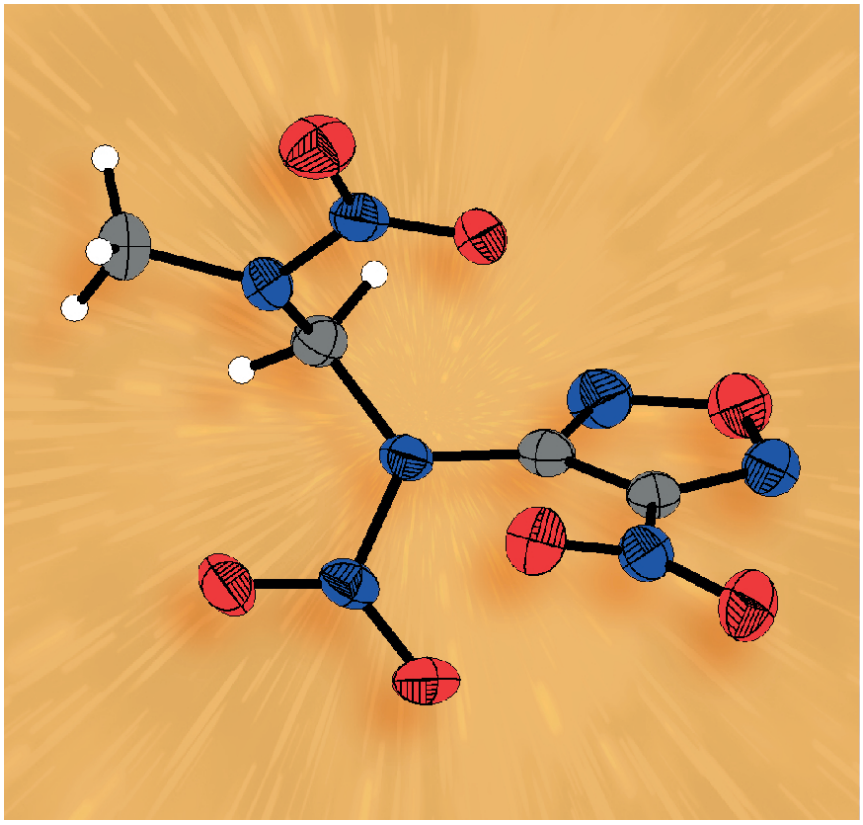

3-Nitramino-4-nitrofurazan: Enhancing the Stability and Energetic Properties by Introduction of Alkylnitramines

T. M. Klapötke, and C. Pflüger
unpublished results.

Abstract

Nitration of 3-amino-4-nitrofurazan with N_2O_5 yielded the corresponding nitramine. 3-Nitramino-4-nitrofurazan is a very promising explosive regarding detonation performance but it suffers from its hygroscopicity, low thermal stability, and high sensitivities to external stimuli. The introduction of other nitramine groups either by alkylation with 1-chloro-2-nitrazapropane or by combination of two 3-nitramino-4-nitrofurazans yielded the corresponding more stable and non-hygroscopic open-chain nitramines. Their molecular structures were investigated by single-crystal X-ray diffraction. The remarkable difference of their impact sensitivities were evaluated by calculation of their electrostatic potential of the molecular surfaces. Furthermore, the detonation parameters of the open-chain nitramines were computed with EXPLO5 (v. 6.02) computer code.

11.1 Introduction

The combination of mechanical and thermal stability with high energy content to ensure high performance is the main challenge in the design of energetic materials. The performance of a secondary explosive strongly depends on its density and enthalpy of formation. The term sensitivity refers to the ease of initiating a detonation or decomposition.[1] To prevent accidental initiations by unintended stimuli such as impact, friction, and heat, diminishing the sensitivities is a major challenge in the development of new energetic materials. Unfortunately, the structural patterns leading to higher stability or improved performance often have contradictory impact. Furthermore, the environmental acceptability of energetic materials as well as their degradation and decomposition products gains in importance due to the toxicity and ecological hazards of commonly used explosives and the contamination of drinking water in the vicinity of military training grounds and ammunition plants.[2–5] Aminofurazans are promising backbones for the design of energetic materials. Their energetic properties could be improved by introduction of more energetic groups (e.g. nitro, nitramino).[6–10] 3-Nitramino-4-nitrofurazan shows very promising detonation performance but it suffers from its hygroscopicity, low thermal stability, and high sensitivities to external stimuli.[6] The formation of energetic salts is a well known strategy to generally enhance the

stability without negative impact to the performance. 3-Nitramino-4-nitrofurazan as well as energetic salts thereof possess high densities and have been patented in 1995 as potentially useful ingredients in propellant, explosive, gasifier, and pyrotechnic compositions.[6]
Another possibility to enhance the mechanical stability and to overcome the hygroscopicity is the derivatization of the acidic nitramine group by alkylation. Several methylene-bis(nitraminofurazans) have already been prepared and characterized with respect to their spectroscopic properties and crystal structures, but no investigations of their energetic properties have been carried out.[11,12] Alkylation using nitramine containing side groups is an interesting strategy to improve the energetic properties in comparison to the introduction of a methyl group. The nitramine groups may take part in intermolecular interactions as acceptor and donor for hydrogen bonds as well as for dipolar N···O and C···O interactions, which should result in higher densities in comparison to the methylated derivatives. The derivatization of the NH function of various nitroazoles with nitramine containing alkylation agents was previously studied showing promising energetic properties.[13–16]
This contribution describes the alkylation of potassium 3-nitramino-4-nitrofurazan by the use of 1-chloro-2-nitrazapropane and 1,3-dichloro-2-nitrazapropane as alkylation agents to improve the mechanical and thermal stabilities of the nonionic 3-nitramino-4-nitrofurazan. Furthermore, the crystal structures of the open-chain nitramines are presented and their huge difference in the impact sensitivity is evaluated by calculation of their electrostatic potential of the molecular surfaces.

11.2 Results and Discussion

11.2.1 Syntheses

3-Amino-4-nitrofurazan was nitrated with dinitrogen pentoxide similar as described in literature and shown in Scheme 11.1 to yield 3-nitramino-4-nitrofurazan (**43**).[6,17] The nitramine **43** was deprotonated with potassium hydroxide to obtain the non-hygroscopic potassium salt **43f**. Another energetic group was introduced by alkylation with 1-chloro-2-nitrazapropane to yield 1-(4-nitrofurazan-3-yl)-1,3-dinitrazabutane (**44**). The use of 1,3-dichloro-2-nitrazapropane as alkylation reagent afforded the 1,5-bis(4-nitrofurazan-3-yl)-1,3,5-trinitrazapentane (**45**), in which two nitrofurazanes are linked by three nitramine groups. Sodium bromide was applied in the reaction toward **45** to facilitate the alkylation by a halogen exchange according to the Finkelstein reaction.[18] Recrystallization from acetonitrile yielded the pure nitramines **44** and **45**, respectively, in moderate yields.

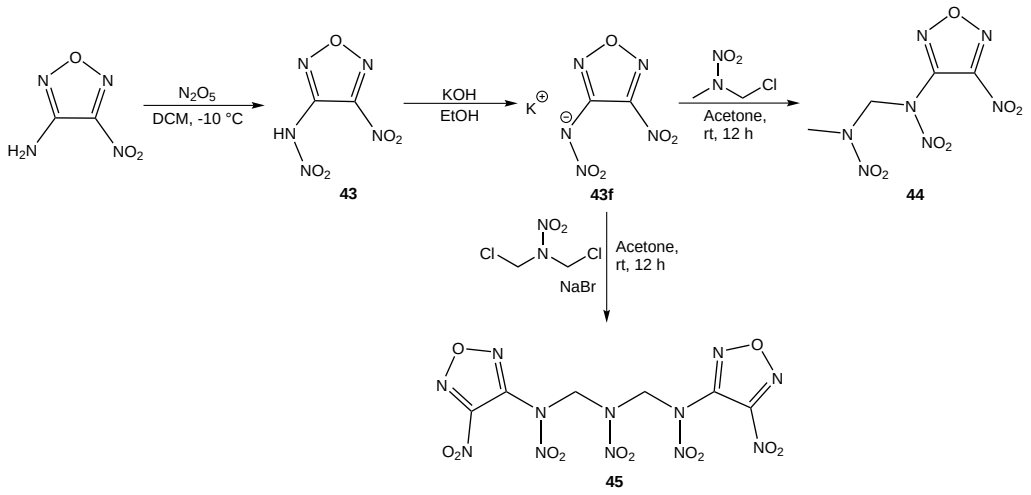

Scheme 11.1: Syntheses of 1-(4-nitrofurazan-3-yl)-1,3-dinitrazabutane (**44**) and 1,5-bis(4-nitrofurazan-3-yl)-1,3,5-trinitrazapentane (**45**).

11.2.2 NMR Spectroscopy

The nitramines **44** and **45** were characterized by multinuclear NMR spectroscopy (^{1}H, ^{13}C{^{1}H}, and ^{14}N) in acetonitrile-d_3 at room temperature. Their resonance signals are summarized in Table 11.1. The resonance signal of the methyl protons of **44** is observed at 3.58 ppm, whereas the resonance of the methylene protons of **44** and **45** are shifted to lower field. The same trend is observed for the corresponding carbon resonances in the ^{13}C NMR. The carbon resonances of the furazan rings of both nitramines **44** and **45** show similar shifts at low field around 157 and 147 ppm. In the ^{14}N NMR spectra the nitrogen resonances of the nitro groups are detected. The three nitrogen resonances of **44** could be assigned to the nitro group attached to the carbon (−30 ppm) and the signals at −38 and −43 ppm to the nitro groups of the nitramine groups. An unambiguous assignment of the nitrogen resonances of **45** is not possible due to very similar shifts.

Table 11.1: NMR shifts of nitramines **44** and **45** in acetonitrile-d_3.

	^{1}H NMR shifts [ppm]		^{13}C{^{1}H} NMR shifts [ppm]				^{14}N NMR shifts [ppm]
	CH_2	CH_3	CNO_2	$CNNO_2$	CH_2	CH_3	CNO_2 and NNO_2
44	5.95	3.58	157.0	147.6	68.3	40.6	−30 (CNO_2); −38, −43 (NNO_2)
45	6.27	–	156.8	147.2	66.9	–	−36, −37, −43†

† Unambiguous assignment not possible.

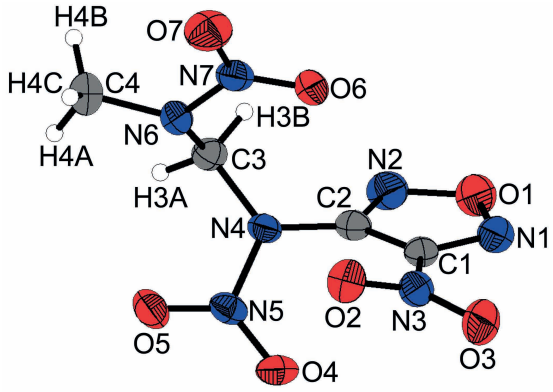

Figure 11.1: Molecular structure of 1-(4-nitrofurazan-3-yl)-1,3-dinitrazabutane (**44**). Thermal ellipsoids are drawn at the 50% probability.

11.2.3 Crystal Structures

Nitramines **44** and **45** were characterized by low-temperature single-crystal X-ray diffraction. Selected data and parameters of the measurements and refinements are summarized in the Appendix (Table A.46).

Nitramine **44** crystallizes from acetonitrile in the monoclinic space group $P2_1/c$ with four formula units per unit cell and a crystal density of 1.776 g cm^{-3} at 173 K. Its molecular structure is depicted in Figure 11.1. The N−N bond lengths of the nitramine groups differ slightly by 0.03 Å. The spatial arrangement of the nitramine groups, which are twisted by 60.65(5)°, is supported by intramolecular dipolar C···O (C2···O6: 2.7974(17) Å; ΣvdW radii: 3.22 Å) and intermolecular C···O (C1···O4: 2.9085(14) Å; ΣvdW radii: 3.22 Å) and N···O (N4···O6: 2.7571(15) Å; ΣvdW radii: 3.07 Å) interactions, which are below the sum of their corresponding van der Waals radii.[19] The twistings of the nitro group (17.79(5)°) and the nitramine N4 (55.30(5)°) out of the furazane plane enable the formation of non-classical hydrogen bonds and dipolar interactions supporting the arrangement in the crystal structure (Table A.44).

The crystal structure is formed by four different opposed and staggered layers along the *b* axis (Figure 11.2). The non-classical hydrogen bonds between the methylene proton H3B and O6 of 2.276(19) Å (D−H: 0.975(19) Å, D···A: 3.2193(16) Å, ∠DHA: 162.6(16)°) and the methyl proton H4C and O4 of 2.65(2) Å (D−H: 0.92(2) Å, D···A: 3.488(2) Å, ∠DHA: 152.1(17)°) alternately connect the different layers. Furthermore, dipolar intermolecular interactions between O3 and another O3 (2.7831(16) Å) along the *b* axis and C4 (2.9955(19) Å) connecting the layers along the *a* axis are observed supporting the layer-like structure.

The nitramine **45** crystallized as twin and was therefore refined as 2-component twin using TWINABS – Bruker AXS scaling for twinned crystals for the absorption process. It shows monoclinic symmetry ($P2_1/c$) and crystallizes with eight formula units per unit cell and a

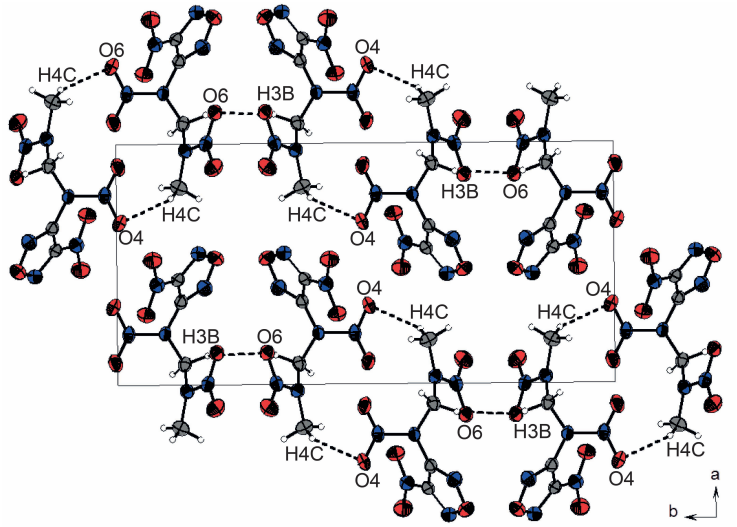

Figure 11.2: Unit cell of nitramine **44**. Non-classical hydrogen bonds are shown black dotted.

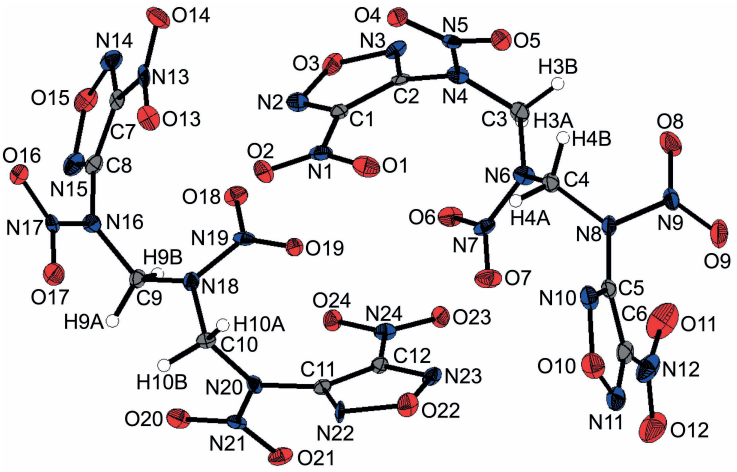

Figure 11.3: Asymmetric unit of the crystal structure of nitramine **45**. Thermal ellipsoids are drawn at the 50% probability.

density of 1.994 g cm^{-3} at 100 K. The asymmetric unit consists of two molecules as depicted in Figure 11.3. The spatial arrangement of the asymmetric unit is assisted by a dipolar N···O interaction of 2.956(6) Å (N2···O19). In contrast to the structure of **44**, the nitro groups are turned out of the furazan plane by less then 10°, whereas the nitramines are skewed in both structures.

The molecular structures are supported either by the intramolecular non-classical hydrogen bond C4−H4B···O5 (H···D: 2.342(4) Å, A···D: 3.036(7) Å, ∠DHA: 126.4(3)°) or a dipolar C···O interaction between C11 and O19 of 2.864(7) Å, which is below the sum of the corresponding van der Waals radii.[19] The crystal structure consists of two different layers along the *a* axis, which are formed by pairs of opposed and staggered molecules (Figure

A.19). Various non-classical hydrogen bonds are found within the crystal structure of **45** connecting the layers (Table A.45).

11.2.4 Thermal Stability, Sensitivities, and Energetic Properties

The thermal stability as well as the sensitivities to outer stimuli like impact, friction, and electrostatic discharge were investigated because they are very important for the safe handling of energetic materials. The thermal stability of **43** (65 °C) could be considerably improved by alkylation with 1-chloro-2-nitrazapropane and 1,3-bischloro-2-nitrazapropane to 108 °C (**44**) and 150 °C (**45**), respectively. Furthermore, the three nitramines melt before decomposition (Table 11.2).

The impact sensitivities of the nitramines differ strongly. Nitramine **44** is classified as sensitive (30 J), while being less sensitive than **43** (4 J), whereas nitramine **45** is very sensitive to impact (2 J). Nevertheless, the friction sensitivities for both **44** and **45** are improved in comparison to **43** (Table 11.2). Nitramine **45** shows an astonishing high electrostatic discharge sensitivity (50 mJ).

The remarkable difference in the impact sensitivities of nitramines **44** and **45** might be explained by their electrostatic potentials (ESPs) of the molecular surface. The ESPs were computed by quantum chemical calculations using Gaussian 09 program package[20] and consists of the evaluation of the electron density and electrostatic potential of the optimized structures for the gas phase. The calculations were carried out at the B3LYP/6-31G(d,p) level. While an imbalance between stronger positive regions and weaker negative ones is uncommon for organic molecules in general, it is characteristic for three classes of energetic compounds: nitroaromatics, nitramines and nitroheterocycles. According to several studies, larger electron-deficient areas above aromatic rings and C−N bonds indicate instability, which subsequently leads to more sensitive compounds.[21–25] The surface ESP of nitramine **45** shows a slightly larger electron-deficient area above the furazan ring, which can be regarded as aromatic, and especially above the C−N bond to the nitro group, in comparison to the surface ESP of nitramine **44** (Figure 11.4). These electron-deficient areas within the inner skeleton of **45** might explain the higher impact sensitivity in relation to **44**.

Their detonation performance parameters such as heat of explosion, detonation velocity, detonation temperature, detonation pressure, and the volume of gaseous detonation products are calculated with Explo5 (version 6.02)[26,27] in the first instance to evaluate their utility for possible applications as energetic materials. The enthalpies of formation were calculated by using the Gaussian 09 program package[20] at the CBS-4M level of theory. The Explo5 (version 6.02) computer code is based on the computed solid state enthalpies of formation and attributed to the corresponding densities at room temperature measured

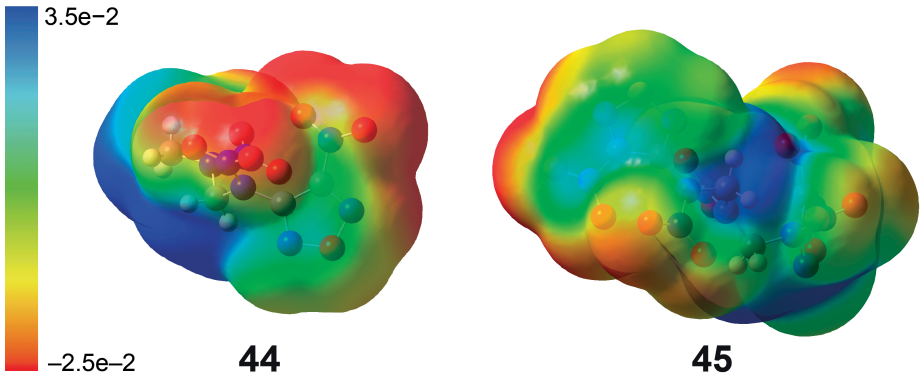

Figure 11.4: Electrostatic potentials (ESPs) of the molecular surfaces of nitramines **44** and **45** at 0.001 e bohr^{-1} calculated at B3LYP/6-31G(d,p) level. The legend for the color range is given on the left and range from −0.025 (red, electron-rich) to 0.035 (blue, electron-deficient) hatrees.

with a Helium gas pycnometer. Both nitramines **44** and **45** show similar or even improved detonation parameters than RDX (Table 11.2). In comparison to **44** and RDX, nitramine **45** shows an enhanced detonation velocity (9334 m s^{-1}), heat of explosion (−6723 kJ kg^{-1}), and detonation pressure (393 kbar) due to its higher density and enthalpy of formation, on which these values are depending. Unfortunately, the low thermal stability prevents possible applications as RDX replacement.

11.3 Conclusions

The alkylation of the potassium salt of 3-nitramino-4-nitrofurazan with 1-chloro-2-nitrazapropane and 1,3-dichloro-2-nitrazapropane yielded the non-hygroscopic nitramines **44** and **45**, respectively. Their molecular structures were investigated by single-crystal X-ray diffraction revealing their high densities and various hydrogen bonds and dipolar interactions, which support the spatial arrangement. The thermal stabilities of both **44** and **45** were considerably improved in comparison to the nonionic parent compound (**43**). Their impact sensitivities differ strongly, hence their electrostatic potential of the molecular surfaces were computed to reveal differences. The more sensitive **45** shows slightly larger and stronger electron-deficient areas above the furazan ring as well as the C−NO_2 bond, which might cause the higher sensitivity. The nitramines **44** and **45** show high calculated detonation performances. Especially, **45** exhibits excellent detonation parameters superior to RDX but it suffers from its low thermal stability and high sensitivities, which may prevent any application as explosive filler.

Table 11.2: Energetic properties and detonation parameters of **43**–**45** and RDX.

	43	**44**	**45**	RDX
Formula	$C_2HN_5O_5$	$C_4H_5N_7O_7$	$C_6H_4N_{12}O_{12}$	$C_3H_6N_6O_6$
M [g mol^{-1}]	175.06	263.13	436.17	316.14
IS [J][a]	4	30	2	7.5
FS [N][b]	120	> 360	324	120
ESD [mJ][c]	300	500	50	200
N [%][d]	40.01	37.26	38.54	37.84
Ω_{CO_2} [%][e]	4.6	−21.3	−7.3	−21.6
Ω_{CO} [%][f]	22.8	3.0	14.7	0.0
T_{melt} [°C][g]	58	96	128	–
T_{dec} [°C][h]	65	108	150	210
ρ [g cm^{-3}][i]	1.94	1.74	1.90	1.80
$\Delta_f H°_{(s)}$ [kJ mol^{-1}][j]	264	265	603	70
$\Delta_f U°_{(s)}$ [kJ kg^{-1}][k]	1584	1095	1463	417
Calculated detonation parameters (EXPLO5 v. 6.02)				
$-Q_v$ [kJ kg^{-1}][l]	6555	6153	6723	5844
T_{det} [K][m]	4768	4250	4725	3815
p_{CJ} [kbar][n]	398	322	393	343
D [m s^{-1}][o]	9438	8596	9334	8838
V_0 [L mol^{-1}][p]	733	759	728	786

[a] Impact sensitivity (BAM drophammer, 1 of 6). [b] Friction sensitivity (BAM friction tester, 1 of 6). [c] Electrostatic discharge (OZM Research). [d] Nitrogen content. [h] Oxygen balance to CO_2 ($\Omega = (x\mathrm{O} - 2y\mathrm{C} - 0.5z\mathrm{H})1600/M$). [g] Oxygen balance to CO ($\Omega = (x\mathrm{O} - y\mathrm{C} - 0.5z\mathrm{H})1600/M$). [e] Melting point. [f] Decomposition temperature. [i] Density at room temperature. [j] Enthalpy of formation. [k] Energy of formation. [l] Heat of explosion. [m] Detonation temperature. [n] Detonation pressure. [o] Detonation velocity. [p] Volume of gaseous detonation products.

11.4 Experimental Section

Caution! *Most compounds prepared herein are energetic compounds sensitive to impact, friction, and electrostatic discharge. Although there were no problems in handling the compounds, proper protective measures (ear protection, Kevlar® gloves, face shield, body armor and earthed equipment) should be used.*

Potassium 4-nitrofurazan-3-nitramide (43f)

Dichloromethane (30 mL) was cooled to −15 °C and N_2O_5 (1.81 g, 16.75 mmol) was added in small portions while maintaining the temperature below −10 °C. After complete dissolution 3-amino-4-nitrofurazan (**43**) (1.82 g, 14.00 mmol) was added in small portions at −10 °C. Then the solution was slowly warmed up to 0–5 °C and stirred for 3 h. The solvent was

removed under a constant nitrogen flow until most of the solvent was removed. Then ethanol (15 mL) and potassium hydroxide (785 mg, 14.00 mmol) dissolved in a minimal amount of water was added dropwise at room temperature. Immediately a yellow precipitate occurred. The mixture was stirred for 2 h and then the precipitate was filtered off to yield a yellow solid (1.74 g, 8.16 mmol, 58%).
$^{13}C\{^1H\}$ NMR (101 MHz, D_2O): δ = 151.5, 125.8 ppm. $^{14}N\{^1H\}$ NMR (29 MHz, acetonitrile-d_3): δ = −15 (NNO_2), −32 (CNO_2) ppm.

1-(4-Nitrofurazan-3-yl)-1,3-dinitrazabutane (44)

1-Chloro-2-nitrazapropane (202 mg, 1.62 mmol) was dissolved in acetone (30 mL) and potassium 4-nitrofurazan-3-nitramide (**43f**) (330 mg, 1.55 mmol) was added. The mixture was stirred overnight at room temperature. The inorganic solids were filtered off and the solvent was removed in vacuo. The crude product was recrystallized from acetonitrile to yield a colorless solid (191 mg, 0.73 mmol, 47%).
DTA (5 °C min^{-1}): T_{melt} = 96 °C, T_{dec} = 108 °C. ^1H NMR (400 MHz, acetonitrile-d_3): δ = 5.95 (s, 2H, CH_2), 3.58 (s, 3H, CH_3) ppm. $^{13}C\{^1H\}$ NMR (101 MHz, acetonitrile-d_3): δ = 157.0 (C_{fz}), 147.6 (C_{fz}), 68.3 (CH_2), 40.6 (CH_3) ppm. $^{14}N\{^1H\}$ NMR (29 MHz, acetonitrile-d_3): δ = −30 (CNO_2), −38 (NNO_2), −43 (NNO_2) ppm. IR (ATR): $\tilde{\nu}$ = 3261 (vw), 3030 (vw), 2980 (vw), 2953 (vw), 2920 (vw), 2866 (vw), 1594 (m), 1575 (m), 1536 (s), 1454 (m), 1423 (m), 1395 (m), 1375 (m), 1341 (m), 1281 (vs), 1255 (vs), 1204 (w), 1186 (w), 1102 (m), 1058 (m), 1011 (s), 925 (m), 906 (w), 887 (vw), 851 (w), 828 (s), 800 (vw), 776 (w), 764 (m), 748 (m), 702 (m), 669 (w), 646 (m), 615 (vw) cm^{-1}. Raman (1064 nm, 300 mW): $\tilde{\nu}$ = 3030 (20), 2980 (45), 2956 (17), 2901 (7), 1608 (8), 1589 (23), 1549 (33), 1534 (8), 1498 (91), 1427 (60), 1397 (12), 1376 (69), 1342 (28), 1293 (84), 1190 (6), 1107 (6), 1060 (15), 1015 (25), 927 (22), 908 (7), 889 (19), 859 (100), 833 (47), 779 (12), 768 (8), 707 (14), 649 (9), 617 (15), 604 (31), 573 (14), 490 (39), 429 (31), 394 (12), 362 (6), 307 (13), 256 (5), 208 (34), 187 (11), 156 (51), 111 (12) cm^{-1}. MS (DEI$^+$): m/z = 263.1 (3) [M$^+$]. EA ($C_4H_5N_7O_7$, 263.13 g mol^{-1}): calcd C 18.26, H 1.92, N 37.26%; found C 18.35, H 1.94, N 37.47%. Sensitivities (grain size: 100–500 µm): IS: 30 J; FS: > 360 N; ESD: 0.5 J.

1,5-Bis(4-nitrofurazan-3-yl)-1,3,5-trinitrazapentane (45)

1,3-Dichloro-2-nitrazapropane (192 mg, 1.21 mmol) was dissolved in acetone (40 mL) and potassium 4-nitrofurazan-3-nitramide (**43f**) (512 mg, 2.40 mmol) and sodium bromide (132 mg, 1.28 mmol) were added. The mixture was stirred overnight at room temperature. Then the inorganic solid was filtered off and the solvent was removed in vacuo. The crude product was recrystallized from acetonitrile to yield a colorless solid (144 mg, 0.33 mmol,

28%).
DTA (5 °C min^{-1}): T_{melt} = 126 °C, T_{dec} = 150 °C. ^{1}H NMR (400 MHz, acetonitrile-d_3): δ = 6.27 (s, 4H, CH_2) ppm. ^{13}C{^{1}H} NMR (101 MHz, acetonitrile-d_3): δ = 156.8 (C_{fz}), 147.2 (C_{fz}), 66.9 (CH$_2$) ppm. ^{14}N{^{1}H} NMR (29 MHz, acetonitrile-d_3): δ = −36, −37, −43 ppm. IR (ATR): $\tilde{\nu}$ = 3043 (vw), 2992 (vw), 1585 (s), 1568 (s), 1543 (s), 1494 (w), 1437 (w), 1410 (w), 1369 (w), 1334 (w), 1277 (vs), 1248 (m), 1209 (vw), 1139 (m), 1086 (m), 1040 (m), 1002 (m), 910 (m), 897 (m), 856 (w), 829 (m), 781 (w), 771 (w), 750 (w), 708 (m), 656 (vw) cm^{-1}. Raman (1064 nm, 300 mW): $\tilde{\nu}$ = 3042 (18), 2993 (33), 1602 (12), 1592 (14), 1578 (14), 1550 (34), 1439 (12), 1414 (28), 1369 (64), 1337 (34), 1251 (10), 1087 (4), 1051 (5), 1003 (12), 912 (26), 892 (21), 859 (85), 831 (58), 752 (4), 659 (5), 635 (26), 625 (12), 492 (44), 471 (10), 382 (17), 362 (13), 347 (9), 271 (6), 230 (7), 222 (8) cm^{-1}. MS (DEI^{+}): m/z = 436.2 (1) [M^{+}]. EA ($C_6H_4N_{12}O_{12}$, 436.17 g mol^{-1}): calcd C 16.52, H 0.92, N 38.54%; found C 16.60, H 1.04, N 38.43%. Sensitivities (grain size: < 100 µm): IS: 2 J; FS: 324 N; ESD: 50 mJ.

11.5 References

[1] T. M. Klapötke, *Chemistry of High-Energy Materials*, 3rd ed., de Gruyter, Berlin, Germany, **2015**.

[2] E. L. Etnier, *Regul. Toxicol. Pharm.* **1989**, *9*, 147–157.

[3] Agency for Toxic Substances and Disease Registry (ATSDR), *Toxicological Profile for RDX*, www.atsdr.cdc.gov./toxprofiles/tp78.pdf, **2012**.

[4] United States Environmental Protection Agency (EPA), *Technical Fact Sheet – Hexahydro-1,3,5-trinitro-1,3,5-triazine (RDX)*, **2014**.

[5] United States Environmental Protection Agency (EPA), *Technical Fact Sheet – 2,4,6-Trinitrotoluene (TNT)*, **2012**.

[6] R. L. Willer, R. S. Day, D. J. Park, US5460669 **1995**.

[7] I. V. Tselinskii, S. F. Mel'nikova, S. N. Vergizov, *Russ. J. Org. Chem.* **1995**, *31*, 1125–1127.

[8] V. P. Zelenov, A. A. Lobanova, *Russ. Chem. Bull.* **2011**, *60*, 334–338.

[9] R. P. Singh, R. D. Verma, D. T. Meshri, J. M. Shreeve, *Angew. Chem., Int. Ed.* **2006**, *45*, 3584–3601; *Angew. Chem.* **2006**, *118*, 3664–3682.

[10] A. B. Sheremetev, V. O. Kulagina, N. S. Aleksandrova, D. E. Dmitriev, Y. A. Strelenko, V. P. Lebedev, Y. N. Matyushin, *Propellants, Explos., Pyrotech.* **1998**, *23*, 142–149.

[11] R. L. Willer, R. S. Day, R. Gilardi, C. George, *J. Heterocycl. Chem.* **1992**, *29*, 1835–1839.

[12] A. B. Sheremetev, V. O. Kulagina, I. A. Kryazhevskikh, T. M. Mel'nikova, N. S. Aleksandrova, *Russ. Chem. Bull.* **2002**, *51*, 1533–1539.

[13] T. M. Klapötke, A. Penger, C. Pflüger, in *New Trends Res. Energ. Mater., Proceedings Semin.*, 14th, Pardubice, Czech Republic, **2011**, *2*, pp. 753–761.

[14] T. M. Klapötke, A. Penger, C. Pflüger, J. Stierstorfer, M. Sućeska, *Eur. J. Inorg. Chem.* **2013**, 4667–4678.

[15] T. M. Klapötke, A. Penger, C. Pflüger, J. Stierstorfer, *New J. Chem.* **2016**, *40*, 6059–6069.

[16] J. C. Bottaro, R. J. Schmitt, A. M. Petrie, P. E. Penwell, US62555112 **2001**.

[17] T. M. Klapötke, P. C. Schmid, J. Stierstorfer, *Crystals* **2015**, *5*, 418–432.

[18] L. Kürti, B. Czakó, *Strategic Applications of Named Reactions in Organic Synthesis*, 5th ed., Elsevier, London, UK, **2005**.

[19] A. F. Holleman, E. Wiberg, N. Wiberg, *Lehrbuch der Anorganischen Chemie*, 102nd ed., de Gruyter, Berlin, Germany **2007**.

[20] M. J. Frisch, G. W. Trucks, H. B. Schlegel, G. E. Scuseria, M. A. Robb, J. R. Cheeseman, G. Scalmani, V. Barone, B. Mennucci, G. A. Petersson, H. Nakatsuji, M. Caricato, X. Li, H. P. Hratchian, A. F. Izmaylov, J. Bloino, G. Zheng, J. L. Sonnenberg, M. Hada, M. Ehara, K. Toyota, R. Fukuda, J. Hasegawa, M. Ishida, T. Nakajima, Y. Honda, O. Kitao, H. Nakai, T. Vreven, J. J. A. Montgomery, J. E. Peralta, F. Ogliaro, M. Bearpark, J. J. Heyd, E. Brothers, K. N. Kudin, V. N. Staroverov, R. Kobayashi, J. Normand, K. Raghavachari, A. Rendell, J. C. Burant, S. S. Iyengar, J. Tomasi, M. Cossi, N. Rega, J. M. Millam, M. Klene, J. E. Knox, J. B. Cross, V. Bakken, C. Adamo, J. Jaramillo, R. Gomperts, R. E. Stratmann, O. Yazyev, A. J. Austin, R. Cammi, C. Pomelli, J. W. Ochterski, R. L. Martin, K. Morokuma, V. G. Zakrzewski, G. A. Voth, P. Salvador, J. J. Dannenberg, S. Dapprich, A. D. Daniels, O. Farkas, J. B. Foresman, J. V. Ortiz, J. Cioslowski, D. J. Fox, Gaussian 09, Revision A.02, Inc., Wallingford CT, **2009**.

[21] J. S. Murray, P. Lane, P. Politzer, P. R. Bolduc, *Chem. Phys. Lett.* **1990**, *168*, 135–139.

[22] F. J. Owens, K. Jayasuriya, L. Abrahmsen, P. Politzer, *Chem. Phys. Lett.* **1985**, *116*, 434–438.

[23] B. M. Rice, J. J. Hare, *J. Phys. Chem. A* **2002**, *106*, 1770–1783.

[24] J. S. Murray, M. C. Concha, P. Politzer, *Mol. Phys.* **2009**, *107*, 89–97.

[25] J. S. Murray, P. Lane, P. Politzer, *Mol. Phys.* **1995**, *85*, 1–8.

[26] M. Sućeska, *Propellants, Explos., Pyrotech.* **1991**, *16*, 197–202.

[27] M. Sućeska, EXPLO5 program, 6.02 ed., Zagreb, Croatia, **2014**.

Summary and Conclusions

In the course of this work, many novel energetic materials based on 1,2,3-triazoles or open-chain nitramines were synthesized and comprehensively characterized. Most of the compounds show enhanced stability towards outer stimuli in comparison to commonly used explosives, while possessing high detonation performances. Therefore, these materials are mainly classified as secondary (high) explosives suitable for military as well as civil applications. Moreover, several investigated compounds may be used in erosion-reduced low-vulnerability (LOVA) gun propellant mixtures, due to their high nitrogen content and very promising computed combustion performances.

The main part of this thesis are Chapters 2 to 11, whereas each chapter is an enclosed research project including its own abstract, introduction, results and discussion, conclusions, and experimental section. Most chapters deal with heterocyclic linked and ring-fused systems containing a 1,2,3-triazole.

In Chapters 2 and 3 the concept of combining the characteristics of traditional and modern explosives has been investigated for dinitrobenzotriazole derivatives. In Chapter 2 the physicochemical and energetic properties were enhanced by successive amination of the benzene core and the introduction of an *N*-oxide to the 1,2,3-triazole moiety. The properties of these compounds were further improved by derivatization of the acidic heterocyclic NH group either by salt formation or alkylation with an alkylnitramine, thereby inserting another energetic group (Chapter 3). In general, the use of nitrogen-rich cations leads to higher positive enthalpies of formation, which thereby improve the detonation performance. The selected nitrogen-rich cations used in this thesis for the formation of nitrogen-rich salts are depicted in Figure 12.1.

The advantageous combination of the generally more stable 1,2,3-triazole and the more energetic tetrazole rings by a C−C linkage has been investigated in Chapters 4 to 7. In Chapter 4 the synthetic route to 5-(5-amino-1,2,3-triazol-4-yl)tetrazole and the conversion of the amino group to explosophoric groups (e.g. azido, nitro, azo) are presented. Their energetic properties were tailored by salt formation either with nitrogen-rich cations or metal cations for possible applications as secondary and primary explosives, respectively,

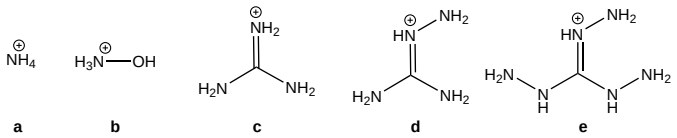

Figure 12.1: Cations **a**–**e** used in this thesis for the formation of nitrogen-rich salts.

as presented in Chapter 5. Furthermore, owing to their nitrogen content, the combustion performances of several nitrogen-rich salts as ingredients in selected LOVA gun propellant mixtures were computed. Chapter 6 reports on the unexpected formation of a diazonium tetrazolyl-1,2,3-triazolate by the attempted nitration of the corresponding amine. The first crystal structure and thorough characterization of a diazo-1,2,3-triazole was accomplished. Chapter 7 presents a comprehensive study of the symmetrically substituted 1,2,3-triazoles, the already known but poorly characterized 4,5-bis(tetrazol-5-yl)-1,2,3-triazole and the novel 4,5-bis(1-hydroxytetrazol-5-yl)-1,2,3-triazole. Nitrogen-rich salts were investigated to improve the surprisingly high impact sensitivities of the parent compounds as well as their detonation performances. Moreover, the toxicity of the heterocyclic systems towards aquatic organisms was determined as well as the combustion behavior of selected nitrogen-rich salts was computed for their potential use in gun propellant mixtures, and metal salts of 4,5-bis(tetrazol-5-yl)-1,2,3-triazole have been investigated regarding their ability to form primary explosives.
The behavior towards high pressure of the bisaminoguanidinium salt of 4,5-bis(tetrazol-5-yl)-1,2,3-triazole, which shows promising energetic properties, has been investigated by Raman spectroscopy using diamond anvil cell technique (Chapter 8).
The combination of 1,2,3-triazoles and 1,2,4-oxadiazoles by means of a C−C linkage to form the first energetic materials composed of these azoles is presented in Chapter 9. In contrast to the tetrazole rings, the oxadiazoles offer the possibility of further tailoring the energetic properties by introduction of various energetic groups at the second carbon atom.
In the last two chapters the focus was turned from the 1,2,3-triazole moiety to open-chain nitramines.
Chapter 10 reports on the investigation of open-chain nitramines as potential TNT replacements as melt-cast explosives. Therefore, various nitro-substituted azoles were alkylated using 1-chloro-2-nitrazapropane to form the corresponding heterocyclic substituted open-chain nitramines.
The concept of improving stability and performance by introduction of another energetic group through alkylation instead of a simple methylation was transferred to the hygroscopic and very sensitive 3-nitramino-4-nitrofurazan (Chapter 11).

Chapter 2 The dinitrobenzotriazole derivatives combine the characteristics of traditional and modern explosives, since they derive their energy from the oxidation of the carbon backbone as well as from the high positive enthalpy of formation of the triazole ring.
The radical mechanism of the amination by a vicarious nucleophilic substitution (VNS) reaction of compounds containing acidic protons using trimethylhydrazinium iodide was confirmed by EPR spectroscopy (Figure 12.2). Furthermore, the preferred positions of the

first aminations could be predicted by quantum mechanical calculations of the spin density population and fit to the experimental results as proven by the crystal structures.
The one and two times aminations of 5,7-dinitrobenzotriazole (**1**) and the zwitterionic 4,6-dinitro-3*H*-benzotriazol-3-ium-1-oxide (**4**) result in successive higher thermal stabilities, lower sensitivities towards outer stimuli such as impact and electrostatic discharge, and improved detonation performances. In general, the considerably more impact sensitive *N*-oxide derivatives **4**–**6** (2 J, 5 J, 20 J, respectively) show higher calculated detonation performances than the corresponding benzotriazoles **1**–**3** (> 40 J, > 40 J, 35 J, respectively). The detonation performances are comparable to TNT ($D = 7241\,\mathrm{m\,s^{-1}}$, $p_{CJ} = 207\,\mathrm{kbar}$).

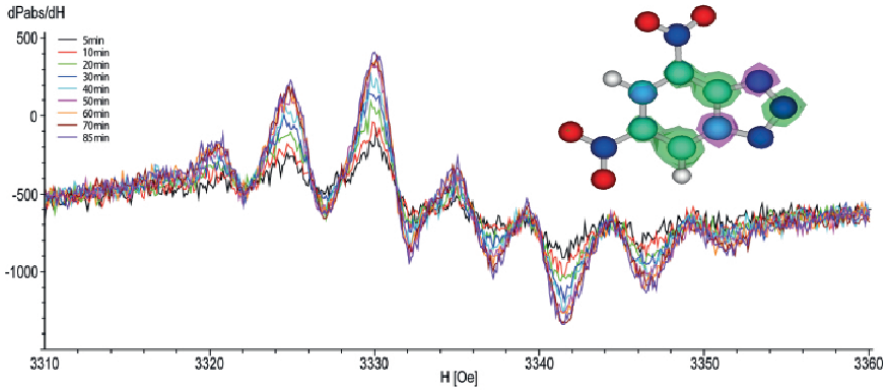

Figure 12.2: EPR spectra of the amination of 5,7-dinitrobenzotriazole (**1**) and calculated spin density population of the radical ion of **1**. Positive spin density population is shown in green and negative spin density population is shown in red.

Chapter 3 The nitrogen-rich salts of **1**, **4**, and 5,7-diamino-4,6-dinitrobenzotriazol-1-oxide (**6**) show, as expected, reduced sensitivities towards outer stimuli and better detonation performances than their nonionic parent compounds. Furthermore, the performance is increased by introduction of the *N*-oxide group and by introduction of the amino groups. Most of the nitrogen-rich salts show high thermal stabilities up to 316 °C.
The acidity of 4,6-diamino-5,7-dinitrobenzotriazole (**3**) was too low to be deprotonated by nitrogen-rich bases, only the potassium salt **3f** could be obtained.
The potassium salt **4f** could be initiated by laser radiation, but unfortunately **4f** as well as the silver salt **4g**·0.5 H_2O are not able to ignite RDX or PETN; the salts **4f** and **4g**·0.5 H_2O only deflagrate and show no transition to a detonation.
The derivatization of the acidic heterocyclic proton by alkylation with 1-chloro-2-nitrazapropane afforded the corresponding isomers of the nitramines **7** and **8**. The crystal structures of the isomers **7x** and **8x** show the main alkylation sites, and furthermore the structure of **8x** reveals its zwitterionic character due to *N*-alkylation instead of *O*-alkylation (Figure 12.3).

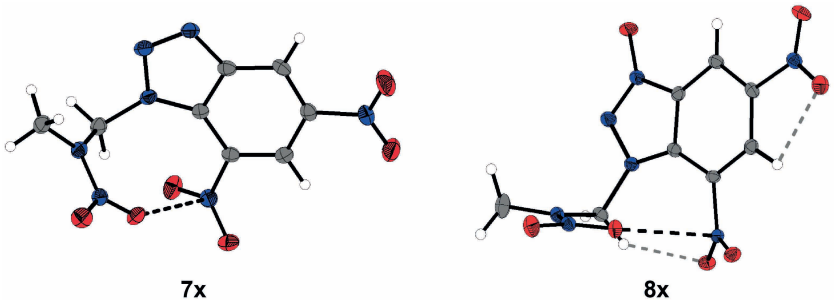

Figure 12.3: Molecular structures of nitramines **7x** and **8x** revealing the main alkylation sites.

The calculated detonation performances of both the nitrogen-rich salts and the nitramines are in between the detonation performances of TNT ($D = 7241\,\mathrm{m\,s^{-1}}$, $p_{CJ} = 207\,\mathrm{kbar}$) and FOX-7 ($D = 8350\,\mathrm{m\,s^{-1}}$, $p_{CJ} = 291\,\mathrm{kbar}$), while the 4,6-dinitrobenzotriazol-1-oxide derivatives show considerably better detonation performances than the 5,7-dinitrobenzotriazole derivatives.

Chapter 4 The goal of this study has been the preparation and thorough characterization of asymmetrically substituted 1,2,3-triazoles combined with a more energetic tetrazole ring by a direct C−C linkage. The introduction of other energetic groups to the second carbon atom of the triazole ring enabled the selective tailoring of the energetic properties.
5-(5-Amino-2*H*-1,2,3-triazol-4-yl)-1*H*-tetrazole (**13**) was prepared from commercially available benzyl chloride in a five step synthesis. The amino group was converted into the explosophoric azido (**14**) and nitro (**15**) groups, as well as a diazene bridge to another molecule (**16**) (Scheme 12.1).
While the amino derivate exhibits a very good thermal stability (241 °C), the more energetic derivatives **14**–**16** are thermally less stable (128 to 188 °C). With the exception of the friction insensitive **13**, the energetic compounds have to be classified as sensitive or even very sensitive to both impact and friction.
Although, compounds **13**–**15** are superior to the commonly used TNT regarding their calculated detonation parameters, the performance of RDX is not reached.
In summary, the compounds **13**–**16** can be considered as nitrogen-rich starting materials for energetic ionic derivatives either in combination with nitrogen-rich cations for applications as secondary explosives (**13**, **15**, and **16**) or with metal cations as primary explosives (**14**) (see Chapter 5). Furthermore, taking into account the high nitrogen contents of 73.66 (**13**), 61.53 (**15**) and 74.65% (**16**) and their highly positive enthalpies of formation, the compounds are of interest as nitrogen-rich salts for gun propellant mixtures.

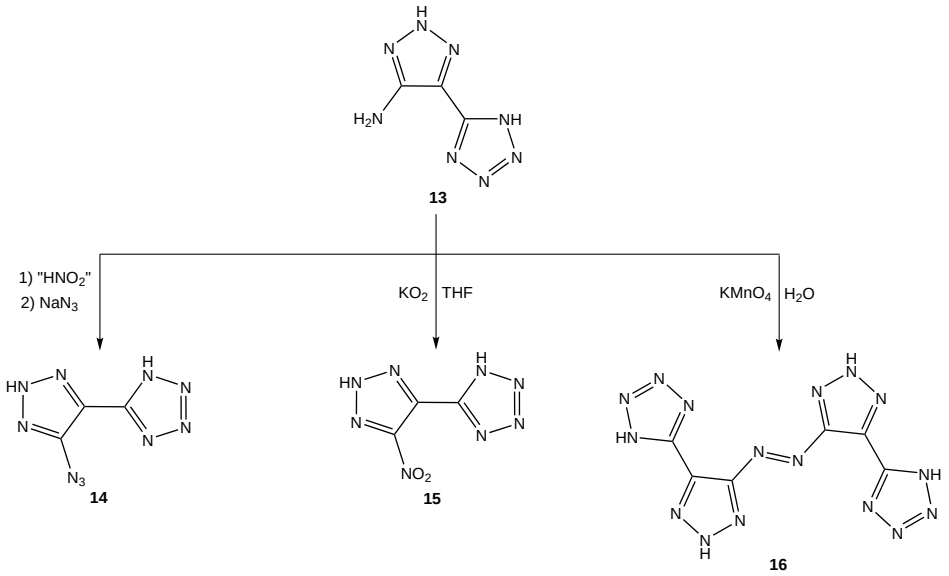

Scheme 12.1: Synthetic route towards the more energetic derivatives 5-(5-azido-2*H*-1,2,3-triazol-4-yl)-1*H*-tetrazole (**14**), 5-(5-nitro-2*H*-1,2,3-triazol-4-yl)-1*H*-tetrazole (**15**) and 1,2-bis(4-(1*H*-tetrazol-5-yl)-2*H*-1,2,3-triazol-5-yl)diazene (**16**).

Chapter 5 The formation of selected metal and nitrogen-rich salts of **13** and its derivatives with an azido group (**14**), a nitro group (**15**), and a diazene bridge (**16**) resulted in the formation of primary and secondary explosives. Deprotonation of the salts of **13** and **15** took place either at the tetrazole ring or the triazole ring, as identified by single-crystal X-ray crystallography (Figure 12.4).

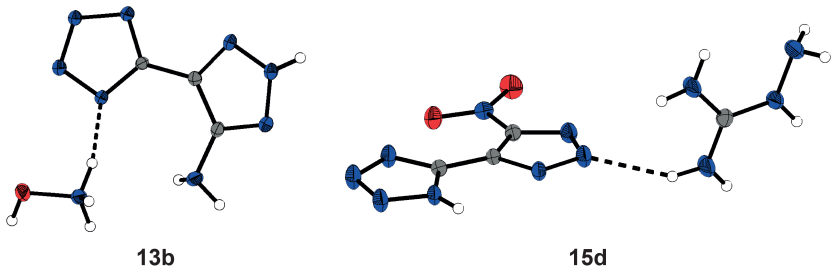

Figure 12.4: Molecular structures of hydroxylammonium 5-(5-amino-2*H*-1,2,3-triazol-4-yl)tetrazolate (**13b**) and aminoguanidinium 5-(5-nitro-1,2,3-triazolate-4-yl)-1*H*-tetrazole (**15d**).

In comparison to the nonionic parent compounds, the nitrogen-rich salts showed reduced sensitivities towards mechanical stimuli such as impact, friction, and electrostatic discharge. Unfortunately, the thermal stabilities were not generally improved by salt formation; however, most salts still show sufficient thermal stability ($>180\,°C$). The calculated detonation performances of the secondary explosives were improved relative to those of the parent molecules. The most promising secondary explosives for potential applications as RDX

replacements are the guanidinium derived salts **13c**–**e** and the doubly deprotonated **16-2d**, which show performances and thermal stabilities similar to those of RDX, while exhibiting better mechanical stabilities (Table 12.1).

Table 12.1: Physical and energetic properties of **13c**–**13e**, **16-2d**, and RDX.

	13c	**13d**	**13e**	**16-2d**	RDX
IS [J][a]	> 40	> 40	25	12.5	7.5
FS [N][b]	> 360	> 360	> 360	> 360	120
T_{dec} [°C][c]	249	232	215	192	204
Calculated detonation parameters (EXPLO5 v. 6.02)					
$-Q_v$ [kJ kg^{-1}][d]	2976	3201	3802	3598	5903
T_{det} [K][e]	2050	2132	2326	2415	3849
p_{CJ} [kbar][f]	241	255	300	253	347
D [m s^{-1}][g]	8706	8926	9571	8740	8854
V_0 [L kg^{-1}][h]	837	855	884	826	785

[a] Impact sensitivity (BAM drophammer 1 of 6). [b] Friction sensitivity (BAM friction tester 1 of 6). [c] Decomposition temperature (DTA, 5 °C min^{-1}). [d] Energy of explosion. [e] Detonation temperature. [f] Detonation pressure. [g] Detonation velocity. [h] Volume of detonation gases.

These four salts were further investigated as potential replacements of the more sensitive bistriaminoguanidinium 5,5′-azobistetrazolate (TAGzT) in nitrogen-rich, thereby erosion-reduced, LOVA gun propellant mixtures HN-1 and HN-2 by calculation of their combustion performances. Their computed combustion performances were at least in the same range as those of the genuine mixtures and in the case of **13e** even improved (Table 12.2). Although their combustion temperatures were higher, they were below the critical temperature (3273 K) to ensure the safety of the gun.
The potassium salt **14f**, the silver salt **14g**, and the cesium salt **14h** were found to be very sensitive true primary explosives with deflagration-to-detonation transitions, and they detonated even if directly burned, similar to lead azide. Specifically, silver salt **14g** was found to be extremely sensitive and could be detonated by the slightest amount of friction when dry. Furthermore, **14h** was able to initiate RDX.

Chapter 6 The unexpected formation of the diazonium compound 5-diazonium-4-(2*H*-tetrazol-5-yl)-1,2,3-triazolate (**17**) was observed by nitration of **13** with mixed acid. The first crystal structure determination of a diazo-1,2,3-triazole reveals a zwitterionic structure with the delocalized negative charge at the triazole ring (Figure 12.5). Further evidence of the zwitterionic structure was supplied by the computed electrostatic potential of the

Table 12.2: Calculated performances of the gun propellant charges based on HN-2 assuming isochoric combustion and loading densities of 0.2 g cm^{-3} with EXPLO5 (v. 6.02).

HN-2[a]	T_C [K][b]	p_{max} [bar][c]	f_E [kJ g^{-1}][d]	b_E [cm^3 g^{-1}][e]	N_2/CO [w/w][f]
TAGzT	2387	2860	0.996	1.517	0.89
13c	2395	2820	0.985	1.506	0.83
13d	2429	2864	1.001	1.504	0.84
13e	2509	2965	1.037	1.501	0.87
16-2d	2496	2896	1.016	1.491	0.84

[a] HN-2: RDX/TAGzT/FOX-12/CAB/BDNPA-F/NC (13.25) 40/20/16/12/8/4. [b] Adiabatic combustion temperature. [c] Pressure in closed vessel. [d] Specific energy. [e] Co-volume of gaseous products. [f] N_2/CO ratio.

molecular surface. The NMR spectroscopic investigation shows an unusual low-field shift of the terminal nitrogen of the diazonium unit, resembling more a diazoalkane situation (Figure 12.5). The diazonium triazolate **17**·H_2O is very sensitive to outer stimuli such as impact (<1 J) and friction (40 N), and is thermally rather stable (141 °C), but nevertheless remarkable stable in comparison to other diazotriazoles.

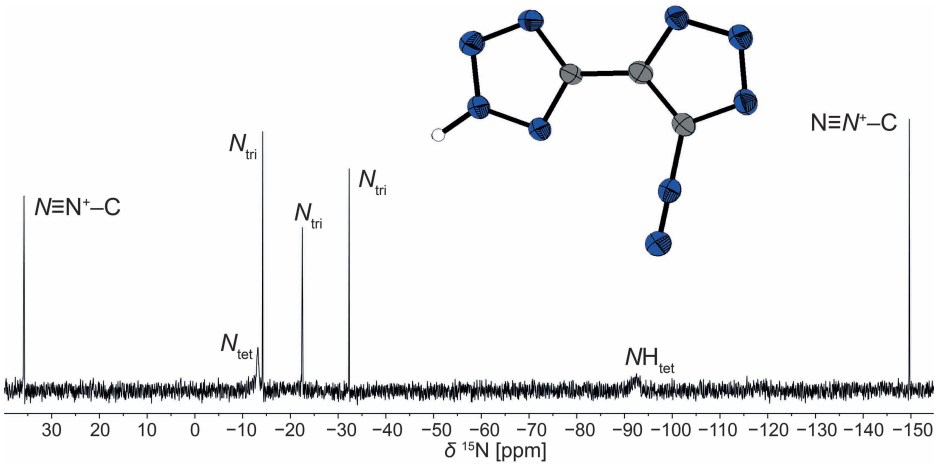

Figure 12.5: Molecular structure and ^{15}N NMR spectrum (in DMSO-d_6) of 5-diazonium-4-(2*H*-tetrazol-5-yl)-1,2,3-triazolate (**17**).

Chapter 7 Similar to the previous chapters, the advantages of linking tetrazole and 1,2,3-triazole rings were combined in symmetrically substituted 1,2,3-triazoles. The syntheses and thorough characterization of the already described, yet poorly characterized 4,5-bis(tetrazol-5-yl)-1,2,3-triazole (**19**) and the novel 4,5-bis(1-hydroxytetrazol-5-yl)-1,2,3-triazole (**23**) were presented (Scheme 12.2).

Nitrogen-rich salts of both compounds **19** and **23** were synthesized to improve their sensitivities and detonation performances. The deprotonation sites of **19d**, one of the

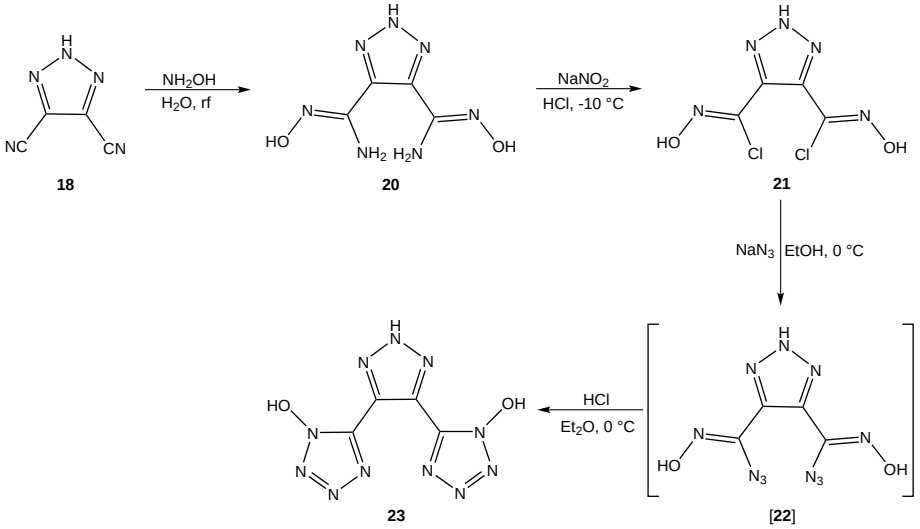

Scheme 12.2: Synthesis of 4,5-bis(1-hydroxytetrazol-5-yl)-2*H*-1,2,3-triazole (**23**).

tetrazole rings and the triazole ring, were revealed by its crystal structure. Selected molecular structures are shown in Figure 12.6. Several metals salts of **19** were investigated to test its ability to form primary explosives, but they were not able to undergo a deflagration-to-detonation transition.

Figure 12.6: Molecular structures of aminoguanidinium 4,5-bis(tetrazol-5-yl)-1,2,3-triazole monohydrate (**19d**·H_2O) and 4,5-bis(1-hydroxytetrazol-5-yl)-2*H*-1,2,3-triazole (**23**).

The molecules **19** and **23** show surprisingly high impact sensitivities of 2 J and 1 J, respectively, whereas their nitrogen-rich salts can be classified as less sensitive or even insensitive. All herein investigated compounds, with the exception of the hydroxylammonium salts **19b** and **23b**, show high thermal stabilities in the temperature range from 215 to 301 °C.
The calculated detonation performances are comparable to common secondary explosives such as RDX (Scheme 12.3). Most promising were the aminoguanidinium salt **19d** and the ammonium salt **23a**, which showed detonation velocities superior to RDX, while possessing lower sensitivities.

Table 12.3: Selected physical and energetic properties of 4,5-bis(tetrazol-5-yl)-1,2,3-triazole (**19**), its aminoguanidinium salt **19d**, and 4,5-bis(1-hydroxytetrazol-5-yl)-1,2,3-triazole (**23**), and its ammonium salt **23a** in comparison to RDX.

	N [%][a]	IS [J][b]	FS [N][c]	T_{dec} [°C][d]	Ω_{CO_2} [%][e]	p_{CJ} [kbar][f]	D [m s^{-1}][g]	V_0 [L kg^{-1}][h]
19	75.11	2	240	277	−74.1	248	8360	733
19d	75.32	> 40	> 360	264	−88.3	263	9022	854
23	64.97	1	240	246	−50.6	260	8277	759
23a	67.14	10	> 360	241	−61.9	288	8991	862
RDX	37.8	7.5	120	205	−21.6	343	8838	786

[a] Nitrogen content. [b] Impact sensitivity (BAM drophammer 1 of 6). [c] Friction sensitivity (BAM friction tester 1 of 6). [d] Decomposition temperature (DTA, 5 °C min^{-1}). [e] Oxygen balance ($\Omega = (x\mathrm{O} - 2y\mathrm{C} - 0.5z\mathrm{H})1600/M$). [f] Detonation pressure. [g] Detonation velocity. [h] Volume of detonation gases.

Due to their high nitrogen content, their potential use in gun propellant mixtures, namely the erosion-reduced HN-1 and HN-2 mixtures, has been investigated by calculation of their combustion parameters. In general, the mixtures containing the tetrazole oxide derivatives show better combustion characteristics.

Additionally, the toxicity to aquatic organisms of the ammonium salt **19a**, due to the insolubility of **19** in water, and **23** have been determined by using the luminescent marine bacterium *Vibrio fischeri*. The half-maximum effective concentrations (EC_{50}) of both **19a** and **23** are higher than the one of RDX, signifying that the two compounds are less toxic than RDX, while **19a** is considerably less toxic than **23**.

Chapter 8 The influence of high-pressure on the structure of bisaminoguanidinium 5-(5-(1*H*-tetrazol-5-yl)-1,2,3-triazolate-4-yl)tetrazolate (**19d**) has been investigated by Raman spectroscopy. The behavior of energetic materials under high-pressure (HP) is of interest regarding structural properties, which affect stability and sensitivities as well as the modeling of the detonative properties with high-pressure equations of state.

In this study structural and molecular changes in structure of the promising nitrogen-rich salt (**19d**) compressed to high pressures up to 19.5 GPa have been investigated using the diamond anvil cell technique.

The Raman spectroscopy reveals that the vibrational bands around 1640 and 1590 cm^{-1} were shifted to higher wavenumbers with increasing pressure. The first change is observed in the Raman spectrum at 1.8 GPa suggesting a transition to a new phase (Figure 12.7).

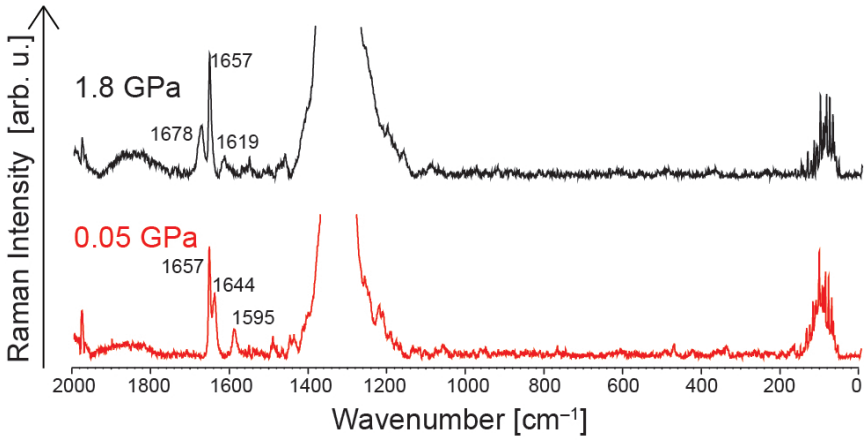

Figure 12.7: HP Raman spectra of **19d** mixed with KBr at 0.05 GPa and 1.8 GPa, respectively, showing the shift of the vibrational bands to higher wavenumbers.

Chapter 9 The cyclization of 5-amino-1,2,3-triazole-4-carboxamidoxime (**27**) and 1,2,3-triazole-4,5-dicarboxamidoxime (**20**) with cyanogen bromide under alkaline conditions to form 1,2,4-oxadiazole rings resulted in the corresponding asymmetrically and symmetrically substituted 1,2,3-triazoles **28** and **29**, respectively. 3,5-Bis(5-amino-2*H*-1,2,3-triazol-4-yl)-1,2,4-oxadiazole (**30**) was synthesized by cyclization of the nitrile **26** and the amidoxime **27** under acidic conditions and elimination of ammonia (Scheme 12.3).

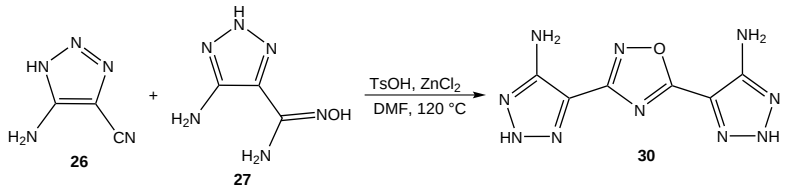

Scheme 12.3: Synthesis of 3,5-bis(5-amino-2*H*-1,2,3-triazole)-1,2,4-oxadiazole (**30**).

The amino-1,2,4-oxadiazole derivatives **28** and **29** are thermally stable up to 163 °C and 180 °C, whereas the thermal stability of **30** is considerably improved to 243 °C. Unfortunately, the oxadiazoles were obtained as monohydrates and dehydration attempts were not successful, thus no calculation of the detonation performances were performed. Nevertheless, for safety issues the sensitivities towards impact, friction, and electrostatic discharge of the oxadiazoles **28**·H_2O (insensitive to impact, >40 J) and **29**·H_2O (impact sensitive, 15 J) were determined.

The presented oxadiazoles are promising backbones for the design of energetic materials due to the possibility of further tailoring their energetic properties by derivatization of the amino group e.g. by nitration or oxidation.

Chapter 10 Numerous efforts to substitute TNT as melt-cast matrix in explosive charges are ongoing due to its low performance and security issues. The straightforward method of derivatization of the heterocyclic N−H function of nitro-substituted azoles, such as 1,2,4-triazoles, imidazoles, and pyrazoles, by alkylation with 1-chloro-2-nitrazapropane yielded various open-chain nitramines as reported herein. The alkylation of 3,4-dinitropyrazole yielded additionally to the desired nitramine **39** the alkylated bipyrazolyl nitramine **40** (Figure 12.8). Prior to this nucleophilic substitution, bipyrazolyl-substituted systems were solely available by *cine*-substitutions.

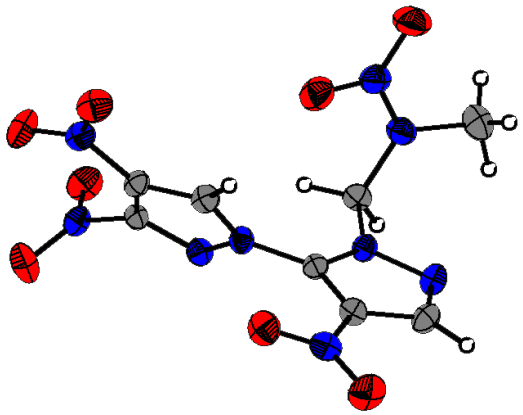

Figure 12.8: Molecular structure of 1-(3,4,4′-trinitro-1,3′-bipyrazol-2′-yl)-2-nitrazapropane (**40**).

The crystal structures of all compounds deliver insights into structural characteristics. A plurality of hydrogen bonds and dipolar C···O and N···O interactions is observed within each crystal structure, which leads to higher densities compared to the known crystal structures of methylated parent compounds and hence improved detonation performances. With exception of **31**, all nitramines melt before decomposition. The decomposition temperatures range from 151 to 264 °C. Nitramines **31**–**42** show calculated detonation velocities in the range from 7788–8482 $\mathrm{m\,s^{-1}}$ and detonation pressures between 237–305 kbar. Their sensitivities are mainly in the range of PETN (IS: 4 J) and TNT (IS: 15 J), or even improved. The most promising potential TNT replacements are nitramines **32**, **36**, **38**, and **41** regarding their syntheses, sensitivities, energetic performance, and especially their thermal behavior, because they possess low melting points ($\leq$ 130 °C) and considerably higher decomposition points (Table 12.4).
For potential applications as energetic materials, apart from melt-cast explosives, the imidazolyl based nitramines **36** and **37** are the most promising materials with regard to their sensitivities and performances.

Table 12.4: Selected physical and energetic properties of the open-chain nitramines 2,4-bis(2-nitrazaprop-1-yl)-3-nitro-1,2,4-triazol-5-one (**32**), 1-(2,4-dinitroimidazol-1-yl)-2-nitrazapropane (**36**), 1-(3,5-dinitropyrazol-1-yl)-2-nitrazapropane (**38**), and 1-(5-chloro-3,4-dinitropyrazol-1-yl)-2-nitrazapropane (**41**) as potential melt-castable replacements for TNT.

	IS [J][a]	FS [N][b]	T_{melt} [°C][c]	T_{dec} [°C][d]	p_{CJ} [kbar][e]	D [m s^{-1}][f]	V_0 [L kg^{-1}][g]
32	> 40	96	117	211	237	7925	798
36	38	120	130	183	263	8046	739
38	19	288	126	210	250	7899	749
41	> 40	288	82	214	256	7788	715
TNT	15	> 360	81	309	207	7241	633

[a] Impact sensitivity (BAM drophammer 1 of 6). [b] Friction sensitivity (BAM friction tester 1 of 6). [c] Melting point (DSC, 5 °C min^{-1}). [d] Decomposition temperature (DSC, 5 °C min^{-1}). [e] Detonation pressure. [f] Detonation velocity. [g] Volume of detonation gases.

Chapter 11 The concept of improving stability and performance by introduction of another energetic group through alkylation instead of a simple methylation was transferred to nitramines, in particular to 3-nitramino-4-nitrofurazan (**43**).

Nitration of 3-amino-4-nitrofurazan with N_2O_5 yielded the corresponding nitramine, which is a very promising explosive regarding detonation performance, but suffers from its hygroscopicity, low thermal stability, and high sensitivities to external stimuli. The introduction of other nitramine groups either by alkylation with 1-chloro-2-nitrazapropane or the combination of two 3-nitramino-4-nitrofurazans by alkylation with 1,3-dichloro-2-nitrazapropane yielded the corresponding thermally more stable and non-hygroscopic open-chain nitramines

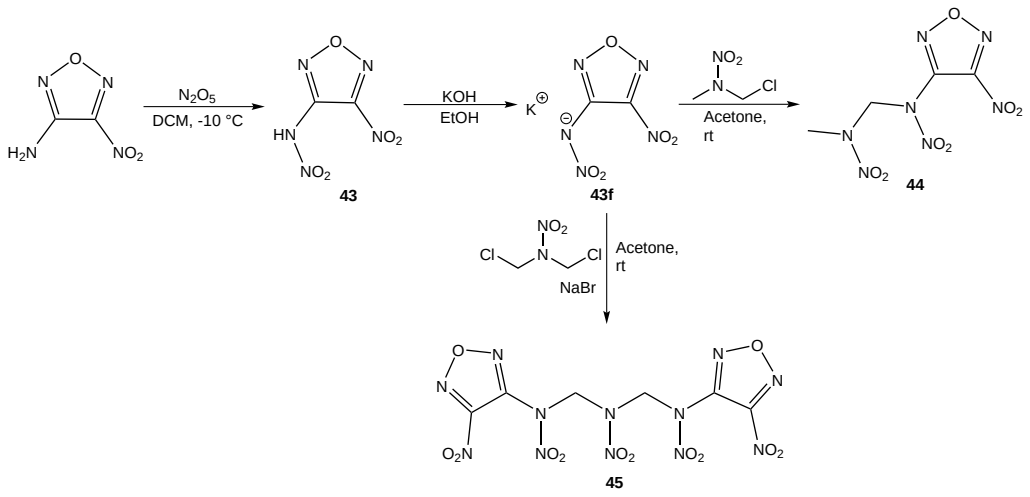

Scheme 12.4: Synthesis of 1-(4-nitrofurazan-3-yl)-1,3-dinitrazabutane (**44**) and 1,5-bis(4-nitrofurazan-3-yl)-1,3,5-trinitrazapentane (**45**).

Table 12.5: Selected physical and energetic properties of 3-nitramino-4-nitrofurazan (**43**) and its nitramines **44** and **45** in comparison to RDX.

	IS [J][a]	FS [N][b]	T_{melt} [°C][c]	T_{dec} [°C][d]	Ω_{CO_2} [%][e]	Ω_{CO} [%][f]	p_{CJ} [kbar][g]	D [m s^{-1}][h]	V_0 [L kg^{-1}][i]
43	4	120	58	65	4.57	22.8	398	9438	733
44	30	> 360	96	108	−21.3	3.0	322	8596	759
45	2	324	128	150	−7.3	14.7	393	9334	728
RDX	7.5	120	204	205	−21.6	0.0	343	8838	786

[a] Impact sensitivity (BAM drophammer 1 of 6). [b] Friction sensitivity (BAM friction tester 1 of 6). [c] Melting point (DTA, 5 °C min^{-1}). [d] Decomposition temperature (DTA, 5 °C min^{-1}). [e] Oxygen balance ($\Omega = (x\mathrm{O} - 2y\mathrm{C} - 0.5z\mathrm{H})1600/M$). [f] Oxygen balance ($\Omega = (x\mathrm{O} - y\mathrm{C} - 0.5z\mathrm{H})1600/M$). [g] Detonation pressure. [h] Detonation velocity. [i] Volume of detonation gases.

44 and **45**, respectively (Scheme 12.4). The impact sensitivities of **44** (30 J) and **45** (2 J) differ strongly, hence their electrostatic potential of the molecular surfaces were computed to reveal possible differences. The more sensitive **45** shows slightly larger and stronger electron-deficient areas above the furazan ring as well as the C−NO_2 bond, which might cause the higher sensitivity.

The nitramines show high calculated detonation performances (Table 12.5). Especially, **45** exhibits excellent detonation parameters superior to RDX but it still suffers from its low thermal stability and high sensitivities, which may prevent any application as explosive filler.

General Conclusion and Outlook In summary, it can be concluded that 1,2,3-triazoles are suitable moieties for the design of new energetic materials composed of linked and fused ring systems. The two carbon atoms as well as the heterocyclic NH group offer various possibilities to introduce functional groups. The introduction of stabilizing (amino, alkyl) or explosophoric (nitro, nitramino, azido, azo) groups and salt formation either with nitrogen-rich or metal cations enables the selective tailoring of the energetic properties, resulting in the formation of primary and secondary explosives.

In general, the formation of nitrogen-rich salts resulted in enhanced sensitivities to mechanical stimuli, but no consistent trend was observed for its influence on the thermal stability. The thermal stabilities of the dinitrobenzotriazole derivatives, the bistetrazolyl and bis(1-hydroxytetrazolyl) substituted 1,2,3-triazoles were improved upon salt formation, whereas the thermal stability of the asymmetrically substituted 1,2,3-triazoles was not increased in principal.

The oxygen balance, which influences the detonation performance, can be improved by the replacement of the tetrazole rings by oxadiazoles and appropriate energetic groups

(nitro, nitramino) as substituents at the second carbon atom of the oxadiazole ring. Further investigations of these compounds are of interest for future work regarding thermal stability, sensitivity, detonation performance and the influence of salt formation thereupon.
The strategy to improve sensitivities and performance of nitro-substituted azoles by alkylation with 1-chloro-2-nitrazapropane resulted in open-chain nitramines as potential replacements for TNT in melt-cast formulation.
The important properties (sensitivity, thermal stability, enthalpies and energies of formation, and detonation performance) of several selected secondary explosives of this thesis as potential RDX replacements are compiled in Table 12.6 in comparison to RDX. Although, the sensitivity and detonation performance of RDX could not be improved in each characteristic parameter, many of the investigated compounds are still of interest for potential applications for example in insensitive munitions, gun propellant or pyrotechnical mixtures.

Table 12.6: Physical and energetic properties of selected herein-investigated secondary explosives in comparison to RDX.

	13b	**13e**	**15e**	**19d**	**23a**	**23d**	**45**	RDX
Formula	$C_2H_7N_9O$	$C_4H_{12}N_{14}$	$C_4H_{10}N_{14}O_2$	$C_6H_{15}N_{19}$	$C_4H_9N_{13}O_2$	$C_6H_{15}N_{19}O_2$	$C_6H_4N_{12}O_{12}$	$C_3H_6N_6O_6$
M [g mol^{-1}]	185.15	256.24	286.21	353.33	271.21	385.32	436.17	316.14
IS [J][a]	25	25	8	>40	10	>40	2	7.5
FS [N][b]	>360	>360	>360	>360	>360	>360	324	120
ESD [mJ][c]	300	400	500	1000	700	1200	50	200
N [%][d]	68.09	76.53	68.51	75.3	67.1	69.07	38.54	37.84
Ω [%][e]	−73.4	−87.4	−61.4	−88.3	−61.9	−72.7	−7.3	−21.6
T_{melt} [°C][f]	–	203	150	–	–	–	128	204
T_{dec} [°C][g]	181	215	174	264	241	215	150	205
ρ [g cm^{-3}][h]	1.70	1.66	1.65	1.66	1.69	1.63	1.90	1.80
$\Delta_f H_m$ [kJ mol^{-1}][i]	540	773	784	846	682	928	603	70
$\Delta_f U$ [kJ kg^{-1}][j]	3032	3140	2725	2515	2625	2523	1463	417
Calculated detonation parameters (EXPLO5 v. 6.02)								
$-Q_{\text{v}}$ [kJ kg^{-1}][k]	4691	3802	4669	3119	4629	4156	6723	5844
T_{det} [K][l]	2871	2326	3001	2104	2989	2677	4725	3815
p_{CJ} [kbar][m]	307	300	280	263	288	266	393	343
D [m s^{-1}][n]	9350	9571	8918	9022	8991	8836	9334	8838
V_0 [L kg^{-1}][o]	860	884	879	854	862	873	728	786

[a] Impact sensitivity (BAM drophammer 1 of 6). [b] Friction sensitivity (BAM friction tester 1 of 6). [c] Electrostatic discharge (OZM Research). [d] Nitrogen content. [e] Oxygen balance ($\Omega = (x\text{O} - 2y\text{C} - 0.5z\text{H})1600/M$). [f] Melting point (DTA, 5 °C min^{-1}). [g] Decomposition temperature (DTA, 5 °C min^{-1}). [h] Density at room temperature. [i] Calculated enthalpy of formation. [j] Calculated energy of formation. [k] Energy of explosion. [l] Detonation temperature. [m] Detonation pressure. [n] Detonation velocity. [o] Volume of detonation gases.

Appendix

A.1 Supporting Information for Chapter 2

EPR Spectra

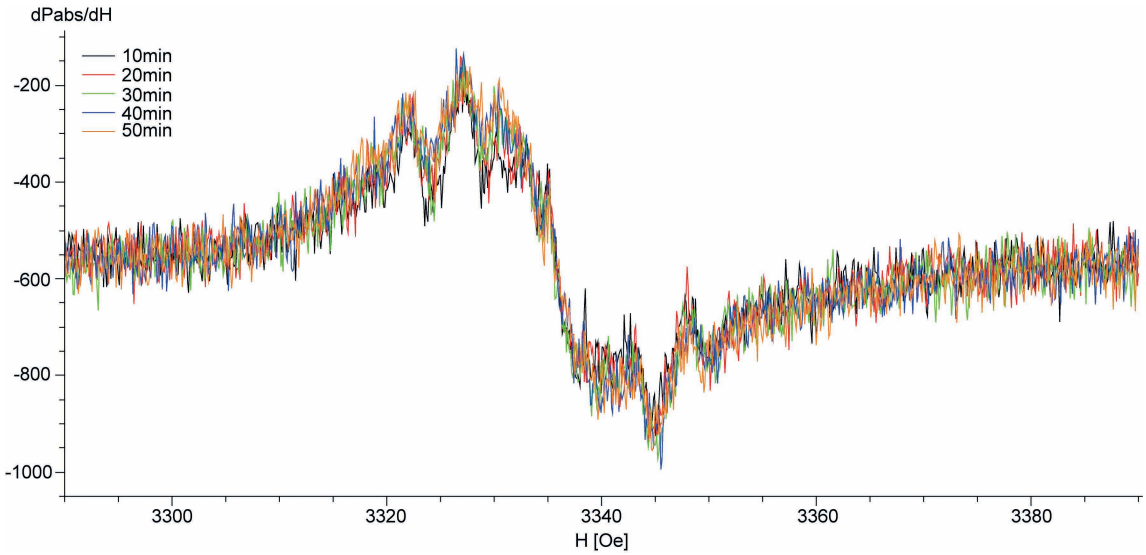

Figure A.1: EPR spectra of the amination reaction of 4,6-dinitrobenzotriazol-1-oxide (**4**) towards 5,7-diamino-4,6-dinitrobenzotriazol-1-oxide (**6**).

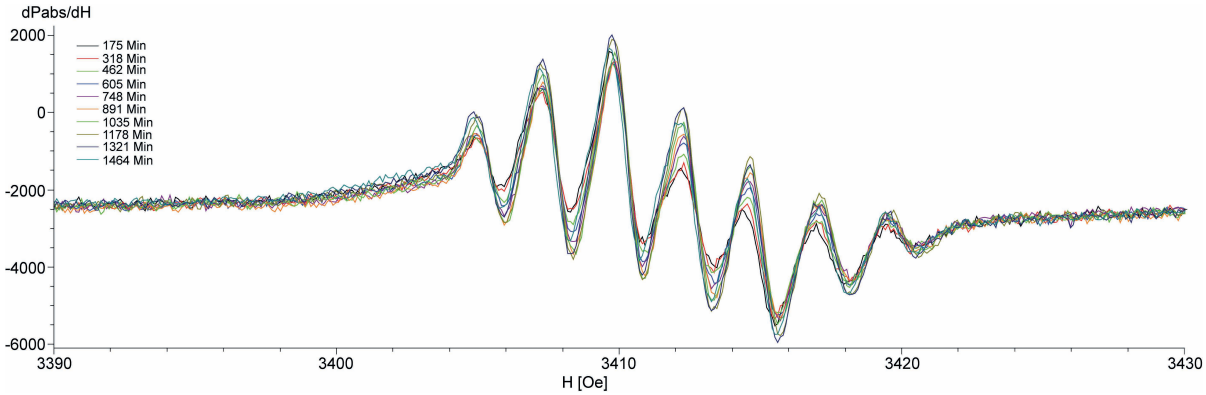

Figure A.2: Selected EPR spectra of the amination reaction of 5,7-dinitrobenzotriazole (**1**) towards 4,6-diamino-5,7-dinitrobenzotriazole (**3**) from 175 min to 1464 min after the reaction started.

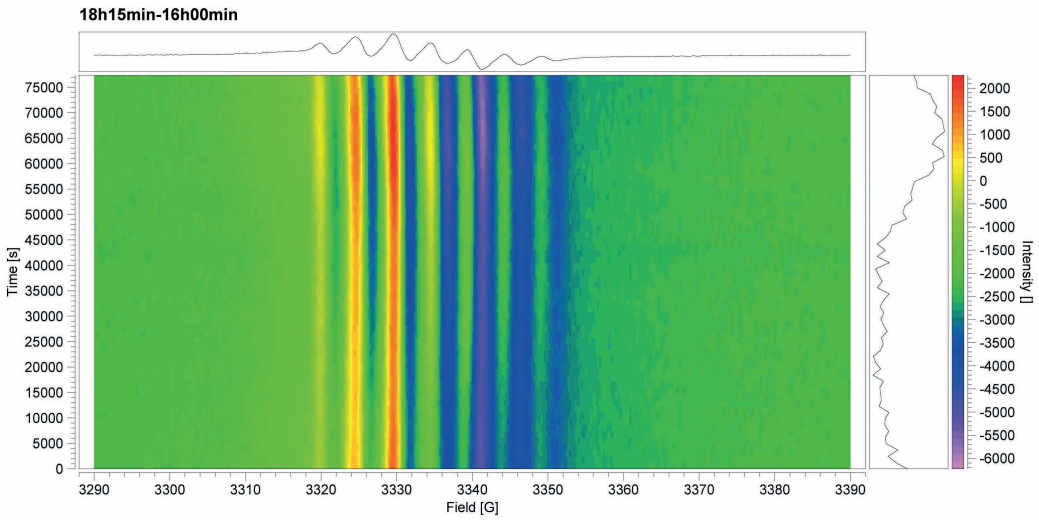

Figure A.3: Time-dependent measurement of the amination reaction progress of 5,7-dinitrobenzotriazole (**1**) over 16 h.

Crystallographic Data

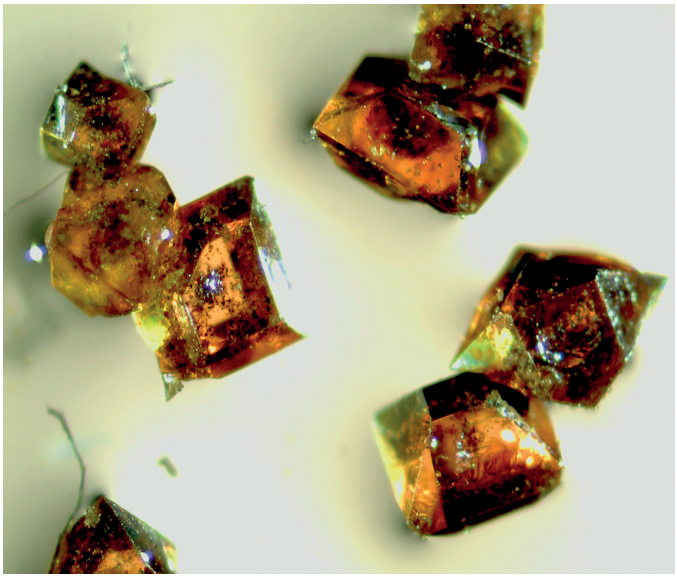

Figure A.4: Microscope photo of the crystals of **4**.

Table A.1: Selected crystallographic data of 5,7-dinitro-1*H*-benzotriazole (**1**) at 293 K and 173 K and 4-amino-5,7-dinitro-1*H*-benzotriazole (**2**).

	1	**1**	**2**
Molecular formula	$C_6H_3N_5O_4$	$C_6H_3N_5O_4$	$C_6H_4N_6O_4 \cdot DMSO$
M [g mol^{-1}]	209.12	209.12	302.27
Color	colorless	colorless	yellow
Habit	block	platelet	platelet
Crystal size [mm]	0.21×0.15×0.12	0.23×0.08×0.03	0.24×0.11×0.04
Crystal system	orthorhombic	orthorhombic	monoclinic
Space group	$Pna2_1$	$Pna2_1$	$P2_1/c$
a [Å]	14.7952(18)	14.480(3)	11.5317(6)
b [Å]	6.3830(7)	6.3394(11)	14.1212(7)
c [Å]	8.9420(9)	8.9352(18)	7.5087(4)
α [°]	90	90	90
β [°]	90	90	101.010(2)
γ [°]	90	90	90
V [Å^3]	844.46(16)	820.2(3)	1200.22(11)
Z	4	4	4
$\rho_{\text{calc.}}$ [g cm^{-3}]	1.645	1.694	1.673
T [K]	293	173	123
$F(000)$	424	424	624
μ [mm^{-1}]	0.142	0.146	0.303
Absorption correction	multi-scan	multi-scan	multi-scan
Index range	$-18 \leq h \leq 19$	$-20 \leq h \leq 14$	$-14 \leq h \leq 14$
	$-8 \leq k \leq 7$	$-9 \leq k \leq 7$	$-17 \leq k \leq 17$
	$-11 \leq l \leq 7$	$-12 \leq l \leq 9$	$-8 \leq l \leq 9$
θ min/max [°]	4.16/27.88	4.19/30.50	2.31/26.37
λ MoK$_\alpha$ [Å]	0.71073	0.71073	0.71073
Measured reflections	4718	4051	29477
Independent reflections	1071	1811	2461
Observed reflections	674	1138	2124
Parameters	140	145	221
R_1 (all data)	0.0794	0.0973	0.0436
R_1 (obs.)	0.0450	0.0514	0.0337
wR_2 (all data)	0.1118	0.0938	0.1087
wR_2 (obs.)	0.0935	0.0806	0.0923
GOF	1.029	1.019	1.189
Res. dens. min. [e Å^{-3}]	−0.15	−0.20	−0.37
Res. dens. max. [e Å^{-3}]	0.21	0.21	0.63
Solution	SIR97	SIR97	SIR97
Refinement	SHELXL-97	SHELXL-97	SHELXL-97
Measurement	hx450	hx527	rv323
CCDC number	1413351	1413353	1413349

Table A.2: Selected crystallographic data of 4,6-dinitro-3*H*-benzotriazol-3-ium-1-oxide (**4**) and 7-amino-4,6-dinitro-3*H*-benzotriazol-3-ium-1-oxide (**5**).

	4	**5**
Molecular formula	$C_6H_3N_5O_5$	$C_6H_4N_6O_5 \cdot H_2O$
M [g mol^{-1}]	225.12	258.15
Color	orange	yellow
Habit	block	needle
Crystal size [mm]	0.39×0.27×0.22	0.15×0.10×0.02
Crystal system	orthorhombic	monoclinic
Space group	$Pbca$	$P2_1/c$
a [Å]	9.0869(3)	9.1531(19))
b [Å]	10.2129(3)	6.2058(12)
c [Å]	18.6989(6)	16.815(5)
α [°]	90	90
β [°]	90	101.784(5)
γ [°]	90	90
V [Å^3]	1735.33(9)	935.0(4)
Z	8	4
$\rho_{\text{calc.}}$ [g cm^{-3}]	1.723	1.834
T [K]	173	100
$F(000)$	912	528
μ [mm^{-1}]	0.153	0.165
Absorption correction	multi-scan	multi-scan
Index range	$-11 \leq h \leq 11$	$-11 \leq h \leq 9$
	$-12 \leq k \leq 12$	$-7 \leq k \leq 7$
	$-23 \leq l \leq 23$	$-13 \leq l \leq 21$
θ min/max [°]	4.14/26.36	4.11/26.37
λ MoK$_\alpha$ [Å]	0.71073	0.71069
Measured reflections	16663	4721
Independent reflections	1768	1904
Observed reflections	1549	1093
Parameters	157	181
R_1 (all data)	0.0356	0.1169
R_1 (obs.)	0.0306	0.0580
wR_2 (all data)	0.0829	0.1109
wR_2 (obs.)	0.0794	0.0903
GOF	1.068	1.002
Res. dens. min. [e Å^{-3}]	−0.25	−0.31
Res. dens. max. [e Å^{-3}]	0.27	0.34
Solution	SIR97	SIR97
Refinement	SHELXL-97	SHELXL-97
Measurement	ix008	ix243
CCDC number	1413352	1413350

A.2 Supporting Information for Chapter 3

Vibrational Spectroscopy

Vibrational spectroscopic studies of all synthesized compounds were performed with IR and Raman spectra and the frequencies were assigned according to literature.[1] For compounds **4d**, **4f**, and **6f** no Raman spectra could be recorded due to their decomposition by laser radiation. The characteristic vibrational frequencies for the asymmetric stretching vibrations of the nitro groups of all presented compounds are in the range of 1542–1507 cm^{-1} and the symmetric ones are observed from 1339–1254 cm^{-1}. The valence vibrations of these aromatic amino groups and the ones of the cations of the salts are seen from 3397 to 3327 cm^{-1}. Additionally, the IR and Raman spectra show some C=N valence vibrations of the aromatic ring system and the nitrogen-rich cations in the range from 1607–1670 cm^{-1}. The aromatic *N*-oxide valence vibrations of **4a**–**4f**, **6a**–**6d**, and **6f** are seen around 1280 cm^{-1} as strong band. The nitramines **7** and **8** show additionally the N=O valence vibrations of the nitramine group, whereby the symmetric one is at lower wavenumbers around 1240 cm^{-1} than the ones of the nitro group bonded to the aromatic carbons. In the Raman spectra the aliphatic CH valence vibrations are observed at lower wavenumbers than the aromatic CH valence vibrations.

Crystallographic Data

Table A.3: Selected interactions within the crystal structure of triaminoguanidinium 5,7-dinitrobenzotriazolate (**1e**).

D−H···A	*d*(D−H) [Å]	*d*(H···A) [Å]	*d*(D···A) [Å]	∠(D−H···A) [°]
N6−H1···N2^{i}	0.87(4)	2.12(4)	2.889(4)	148(3)
N7−H3···N3^{ii}	0.95(4)	2.14(4)	3.078(4)	169(3)
N8−H4···N1	0.79(3)	2.34(3)	2.909(5)	130(3)
N9−H5···N1^{iii}	0.88(3)	2.42(3)	3.291(4)	172(3)
N11−H9···O3^{iv}	0.90(4)	2.34(4)	3.133(5)	146(3)
N10−H7···O1^{v}	0.87(3)	2.25(4)	2.991(5)	143(3)
N9−H6···N9^{vi}	0.88(4)	2.35(4)	3.067(5)	140(3)
N11−H9···O2^{vii}	0.90(4)	2.44(3)	3.161(5)	137(3)
dipolar interactions ΣvdW radii (N···O) < 3.07 Å[2]				
N3···O1 2.828(4) Å				

Symmetry codes: (i) $1-x, 0.5+y, 0.5-z$; (ii) $1-x, -0.5+y, z$; (iii) $x, 1+y, z$; (iv) $1-x, 1-y, -z$; (v) $-1+x, 1+y, z$; (vi) $1-x, 0.5+y, 0.5-z$; (vii) $1+x, 1+y, z$.

Table A.4: Selected interactions within the crystal structure of guanidinium 4,6-dinitrobenzotriazol-1-oxide (**4c**).

D−H···A	d(D−H) [Å]	d(H···A) [Å]	d(D···A) [Å]	∠(D−H···A) [°]
N7−H4···N2	0.86(3)	2.32(2)	3.172(3)	172(2)
N8−H5···O1	0.83(3)	2.11(2)	2.935(2)	174(2)
N6−H1···O1^{i}	0.89(2)	2.03(3)	2.883(3)	158(2)
N7−H3···N2^{ii}	0.80(3)	2.36(3)	3.160(3)	172(3)
N6−H2···O2^{ii}	0.86(3)	2.38(3)	2.929(3)	122(2)
N6−H2···N3^{ii}	0.86(3)	2.18(3)	3.008(3)	161(2)
N7−H3···N3^{ii}	0.80(3)	2.51(3)	3.220(3)	147(3)
C6−H6A···O2^{iii}	1.00(2)	2.62(3)	3.604(3)	167(2)
C4−H4A···O4^{iv}	0.96(2)	2.61(2)	3.599(3)	166(2)
N8−H6···O1^{i}	0.82(3)	2.63(3)	3.266(2)	136(2)
dipolar interactions ΣvdW radii (N···O) < 3.07 Å [2]				
N3···O2 2.803(3) Å				

Symmetry codes: (i) $1-x, 0.5+y, 0.5-z$; (ii) $1-x, 1-y, -z$; (iii) $x, -0.5-y, 0.5+z$; (iv) $-x, 1-y, -z$.

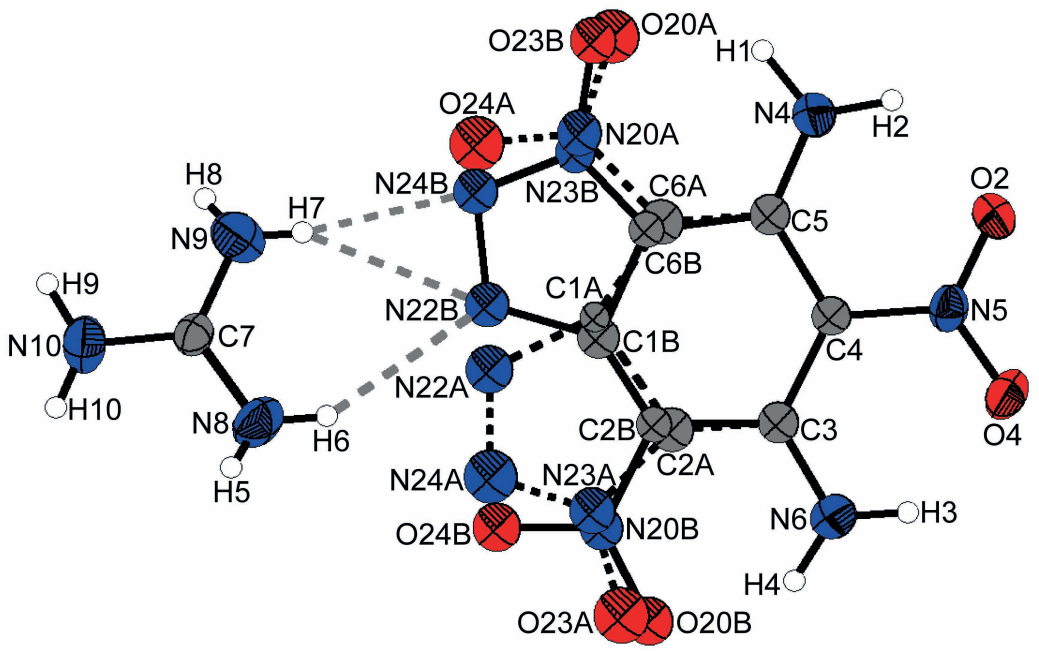

Figure A.5: Disordered molecular structure of guanidinium 5,7-diamino-4,6-dinitrobenzotriazol-1-oxide (**6c**); thermal ellipsoids of non-hydrogen atoms are drawn at the 50% probability level.

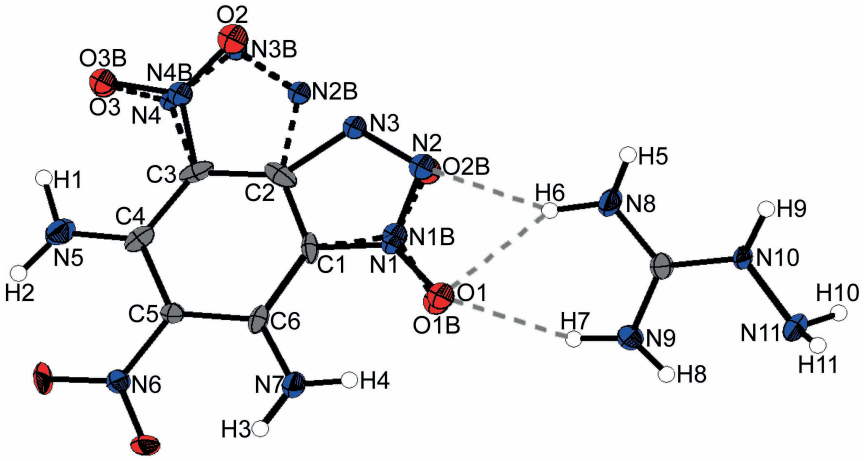

Figure A.6: Disordered molecular structure of aminoguanidinium 5,7-diamino-4,6-dinitrobenzotriazol-1-oxide (**6d**); thermal ellipsoids of non-hydrogen atoms are drawn at the 50% probability level.

Table A.5: Selected interactions within the crystal structure of **7x**.

D−H···A	d(D−H) [Å]	d(H···A) [Å]	d(D···A) [Å]	∠(D−H···A) [°]
C7−H7B···O4	0.9898(19)	2.2367(15)	3.043(2)	137.77(11)
C7−H7A···O5^{i}	0.9898(17)	2.3390(12)	3.325(2)	174.37(10)
C8−H8A···O1^{ii}	0.979(2)	2.3679(17)	3.343(3)	173.44(13)

Symmetry codes: (i) $-1+x, y, z$; (ii) $1.5-x, -y, -0.5+z$.

Table A.6: Selected interactions within the crystal structure of **8x**.

D−H···A	d(D−H) [Å]	d(H···A) [Å]	d(D···A) [Å]	∠(D−H···A) [°]
C7−H7B···O2	0.957(16)	2.230(16)	3.0447(16)	142(1)
C9−H9C···O5^{i}	0.9791(16)	2.8362(11)	3.534(2)	128.9(1)
C6−H6A···O1^{ii}	0.936(19)	2.650(18)	3.4475(16)	144(1)
C9−H9B···O1^{ii}	0.9800(17)	2.6583(11)	3.206(2)	115.63(11)
C7−H7A···O3^{iii}	0.955(18)	2.595(16)	3.1687(16)	119(1)
C7−H7B···O3^{iv}	0.957(16)	2.5770(16)	3.1650(16)	120(1)
dipolar interactions ΣvdW radii (N···O) < 3.07 Å [2] N4···O6 2.7592(14) Å; N1···O4^{iii} 2.9553(16) Å				
dipolar interactions ΣvdW radii (C···O) < 3.22 Å [2] C3···O6 2.9803(16) Å; C2···O6 3.0140(16) Å; C1···O4^{iii} 2.9362(16) Å				

Symmetry codes: (i) $0.5-x, -0.5+y, z$; (ii) $-0.5+x, y, 0.5-z$; (iii) $1+x, y, z$; (iv) $0.5+x, 0.5-y, -z$.

Table A.7: Selected crystallographic data of hydroxylammonium (**1b**), guanidinium (**1c**), and triaminoguanidinium (**1e**) 5,7-dinitrobenzotriazolate.

	1b	**1c**	**1e**
Molecular formula	$C_6H_6N_5O_5 \cdot H_2O$	$C_7H_8N_8O_4$	$C_7H_{11}N_{11}O_4$
M [g mol^{-1}]	260.17	268.19	313.23
Color	yellow	yellow	colorless
Habit	needle	block	needle
Crystal size [mm]	0.40×0.11×0.07	0.35×0.19×0.09	0.31×0.06×0.02
Crystal system	monoclinic	triclinic	monoclinic
Space group	$P2_1$	$P\bar{1}$	$P2_1/c$
a [Å]	7.1807(4)	4.6223(8)	10.946(2)
b [Å]	18.6372(7)	9.736(2)	3.944(1)
c [Å]	7.6276(3)	12.744(2)	29.095(3)
α [°]	90	72.829(16)	90
β [°]	93.170(4)	83.751(13)	94.846(12)
γ [°]	90	80.296(15)	90
V [Å^3]	1019.23(8)	539.05(17)	1251.6(3)
Z	4	2	4
$\rho_{\text{calc.}}$ [g cm^{-3}]	1.695	1.652	1.662
T [K]	173	293	100
$F(000)$	536	276	648
μ [mm^{-1}]	0.152	0.138	0.138
Absorption correction	multi-scan	multi-scan	multi-scan
Index range	$-10 \leq h \leq 10$	$-5 \leq h \leq 5$	$-12 \leq h \leq 13$
	$-28 \leq k \leq 27$	$-5 \leq k \leq 12$	$-4 \leq k \leq 4$
	$-11 \leq l \leq 10$	$-14 \leq l \leq 15$	$-35 \leq l \leq 20$
θ min/max [°]	4.34/33.52	4.27/26.00	4.22/25.50
λ MoK$_\alpha$ [Å]	0.71073	0.71073	0.71073
Measured reflections	8204	2774	3992
Independent reflections	6241	2103	2324
Observed reflections	5507	1556	1394
Parameters	374	204	226
R_1 (all data)	0.0479	0.0735	0.1217
R_1 (obs.)	0.0401	0.0519	0.0646
wR_2 (all data)	0.1042	0.1587	0.1458
wR_2 (obs.)	0.0973	0.1423	0.1184
GOF	1.031	1.166	1.025
Res. dens. min. [e Å^{-3}]	−0.28	−0.20	−0.27
Res. dens. max. [e Å^{-3}]	0.38	0.35	0.32
Solution	SIR97	SIR97	SIR97
Refinement	SHELXL-97	SHELXL-97	SHELXL-97
Measurement	jx149	hx489	ix530
CCDC number	1414368	1414362	1414366

Table A.8: Selected crystallographic data of potassium (**1f**) and 1-(propan-2-ylidene)aminoguanidinium (**1l**) 5,7-dinitrobenzotriazolate and guanidinium 4,6-dinitrobenzotriazol-1-oxide (**4c**).

	1f	**1l**	**4c**
Molecular formula	$C_6H_2KN_5O_4 \cdot 1.5H_2O$	$C_{10}H_{13}N_9O_4$	$C_7H_8N_8O_5$
M [g mol^{-1}]	274.24	323.27	284.19
Color	colorless	yellow	orange
Habit	needle	block	plate
Crystal size [mm]	0.40×0.12×0.07	0.38×0.22×0.13	0.21×0.18×0.05
Crystal system	monoclinic	triclinic	monoclinic
Space group	$P2/n$	$P\bar{1}$	$P2_1/c$
a [Å]	14.4951(9)	8.782(5)	9.1755(8)
b [Å]	4.6676(3)	9.132(6)	7.3381(8)
c [Å]	14.8468(9)	10.480(6)	16.7685(18)
α [°]	90	110.248(6)	90
β [°]	96.865(6)	95.930(5)	104.606(11)
γ [°]	90	113.807(6)	90
V [Å^3]	997.29(11)	691.9(7)	1092.55(19)
Z	4	2	4
$\rho_{\text{calc.}}$ [g cm^{-3}]	1.827	1.552	1.728
T [K]	293	100	100
$F(000)$	556	336	584
μ [mm^{-1}]	0.561	0.124	0.148
Absorption correction	multi-scan	multi-scan	multi-scan
Index range	$-12 \leq h \leq 18$	$-10 \leq h \leq 10$	$-11 \leq h \leq 11$
	$-5 \leq k \leq 5$	$-11 \leq k \leq 11$	$-9 \leq k \leq 9$
	$-18 \leq l \leq 16$	$-13 \leq l \leq 12$	$-20 \leq l \leq 20$
θ min/max [°]	4.22/26.37	4.38/26.36	4.59/26.37
λ MoK$_\alpha$ [Å]	0.71073	0.71069	0.71069
Measured reflections	4973	5369	7063
Independent reflections	2031	2810	2228
Observed reflections	1656	2413	1521
Parameters	174	260	205
R_1 (all data)	0.0416	0.0458	0.0794
R_1 (obs.)	0.0312	0.0380	0.0456
wR_2 (all data)	0.0847	0.1031	0.1113
wR_2 (obs.)	0.0779	0.0972	0.0932
GOF	1.030	1.031	1.047
Res. dens. min. [e Å^{-3}]	−0.19	−0.23	−0.25
Res. dens. max. [e Å^{-3}]	0.33	0.34	0.27
Solution	SIR97	SIR97	SIR97
Refinement	SHELXL-97	SHELXL-97	SHELXL-97
Measurement	hx465	ix529	ix277
CCDC number	1414365	1414364	1414363

Table A.9: Selected crystallographic data of triaminoguanidinium 4,6-dinitrobenzotriazol-1-oxide (**4e**), guanidinium (**6c**), and aminoguanidinium (**6d**) 5,7-diamino-4,6-dinitrobenzotriazol-1-oxide.

	4e	**6c**	**6d**
Molecular formula	$C_7H_{11}N_{11}O_5$	$C_7H_{10}N_{10}O_5$	$C_7H_{11}N_{11}O_5$
M [g mol^{-1}]	329.23	314.25	329.27
Color	red	yellow	yellow
Habit	needle	rod	platelet
Crystal size [mm]	0.30×0.10×0.03	0.40×0.06×0.03	0.12×0.06×0.01
Crystal system	monoclinic	triclinic	monoclinic
Space group	$P2_1/c$	$P\bar{1}$	$C2/c$
a [Å]	14.545(2)	6.8093(14)	26.719(3)
b [Å]	3.7048(4)	8.9150(13)	6.7113(8)
c [Å]	23.175(2)	9.9163(17)	17.743(2)
α [°]	90	84.660(13)	90
β [°]	90.751(9)	73.037(17)	129.182(3)
γ [°]	90	89.139(15)	90
V [Å^3]	1248.7(2)	573.23(18)	2466.2(5)
Z	4	2	8
$\rho_{\text{calc.}}$ [g cm^{-3}]	1.751	1.821	1.774
T [K]	100	173	100
$F(000)$	680	324	1360
μ [mm^{-1}]	0.149	0.155	0.151
Absorption correction	multi-scan	multi-scan	multi-scan
Index range	$-18 \leq h \leq 15$	$-8 \leq h \leq 9$	$-31 \leq h \leq 31$
	$-3 \leq k \leq 4$	$-11 \leq k \leq 11$	$-7 \leq k \leq 7$
	$-28 \leq l \leq 23$	$-13 \leq l \leq 13$	$-20 \leq l \leq 21$
θ min/max [°]	4.47/26.36	4.29/28.28	2.96/25.01
λ MoK$_\alpha$ [Å]	0.71073	0.71073	0.71073
Measured reflections	6179	5210	5171
Independent reflections	2557	2823	2123
Observed reflections	1748	1635	1417
Parameters	250	215	246
R_1 (all data)	0.0848	0.1214	0.0865
R_1 (obs.)	0.0508	0.0698	0.0481
wR_2 (all data)	0.1231	0.2063	0.1154
wR_2 (obs.)	0.1005	0.1706	0.1031
GOF	1.052	1.034	1.023
Res. dens. min. [e Å^{-3}]	−0.33	−0.36	−0.28
Res. dens. max. [e Å^{-3}]	0.31	0.42	0.26
Solution	SIR97	SIR97	SIR97
Refinement	SHELXL-97	SHELXL-2014	SHELXL-97
Measurement	ix085	jx040	rv464
CCDC number	1414367	1414369	1414359

Table A.10: Selected crystallographic data of 1-(5,7-dinitrobenzotriazol-1-yl)-2-nitrazapropane (**7x**) and 1-(4,6-dinitrobenzotriazol-3-ium-1-oxide-3-yl)-2-nitrazapropane (**8x**).

	7x	**8x**
Molecular formula	$C_8H_7N_7O_6$	$C_8H_7N_7O_7 \cdot C_2H_3N$
M [g mol^{-1}]	297.21	354.24
Color	colorless	yellow
Habit	rod	block
Crystal size [mm]	0.14×0.08×0.03	0.40×0.40×0.22
Crystal system	orthorhombic	orthorhombic
Space group	$P2_12_12_1$	$Pbca$
a [Å]	5.7625(2)	6.0273(2)
b [Å]	9.5536(3)	15.5172(5)
c [Å]	20.5353(6)	31.0012(10)
α [°]	90	90
β [°]	90	90
γ [°]	90	90
V [Å^3]	1130.52(6)	2899.44(16)
Z	4	8
$\rho_{\text{calc.}}$ [g cm^{-3}]	1.746	1.623
T [K]	123	100
$F(000)$	608	1456
μ [mm^{-1}]	0.152	0.1391
Absorption correction	multi-scan	multi-scan
Index range	$-7 \leq h \leq 7$	$-7 \leq h \leq 7$
	$-11 \leq k \leq 11$	$-19 \leq k \leq 19$
	$-25 \leq l \leq 25$	$-38 \leq l \leq 38$
θ min/max [°]	2.35/26.37	4.21/26.37
λ MoK$_\alpha$ [Å]	0.71073	0.71073
Measured reflections	30462	27782
Independent reflections	2310	2961
Observed reflections	2207	2666
Parameters	192	255
R_1 (all data)	0.0318	0.0378
R_1 (obs.)	0.0282	0.0337
wR_2 (all data)	0.0984	0.0854
wR_2 (obs.)	0.0870	0.0830
GOF	1.262	1.121
Res. dens. min. [e Å^{-3}]	−0.27	−0.30
Res. dens. max. [e Å^{-3}]	0.25	0.29
Solution	SIR97	SIR97
Refinement	SHELXL-97	SHELXL-97
Measurement	rv071	ix051
CCDC number	1414360	1414361

Ignition Tests

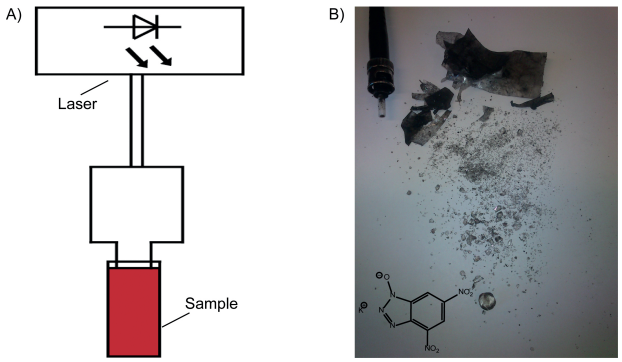

Figure A.7: Laser ignition test of **4f**. A) Schematic setup of the laser ignition test. B) Destroyed glass vessel by a successful laser ignition of potassium 4,6-dinitrobenzotriazol-1-oxide (**4f**).

Potassium (**4f**) or aminoguanidinium (**4d**) 4,6-dinitrobenzotriazol-1-oxide were mixed with 2.5% polyethylene (PE). Therefore, PE was dissolved in hot *n*-hexane and the corresponding salt was added. The precipitate was filtered off after cooling to room temperature while stirring. The samples (∼50 mg) were confined in small glass vials and irradiated with a monopulsed laser beam at 940 nm and a pulse length of 100 µs. The ignation of the potassium salt resulted in the destroyed glass vial, whereas the aminoguanidinium salt only decomposed.

The ignition tests of RDX and PETN with either potassium 4,6-dinitrobenzotriazol-1-oxide (**4f**) or silver 4,6-dinitrobenzotriazol-1-oxide (**4g**·0.5 H_2O) were carried out in a small aluminum tube with a pyrotechnical igniter. At first 300 mg of RDX respective PETN was filled in the tube and slightly compressed. Afterwards 50 mg or 100 mg of the potassium salt was added and also compressed. The pyrotechnical igniter was fixed on the sample and put into a box filled with sand to reduce the noise emission. The same procedure was carried out to test the ignitability of PETN with the silver salt. The potassium salt as well as the silver salt only deflagrate as observed by deformation of the aluminum tubes but they are not able to initiate RDX or PETN (Figure A.8).

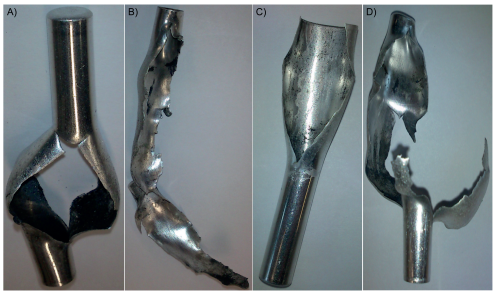

Figure A.8: Ignition tests; A) and B): tube filled with 300 mg of RDX and 50 mg respective 100 mg of potassium 4,6-dinitrobenzotriazol-1-oxide (**4f**). C) and D): tube filled with 300 mg PETN and 50 mg or 100 mg of the potassium salt **4f**.

A.3 Supporting Information for Chapter 4

NMR Spectroscopy

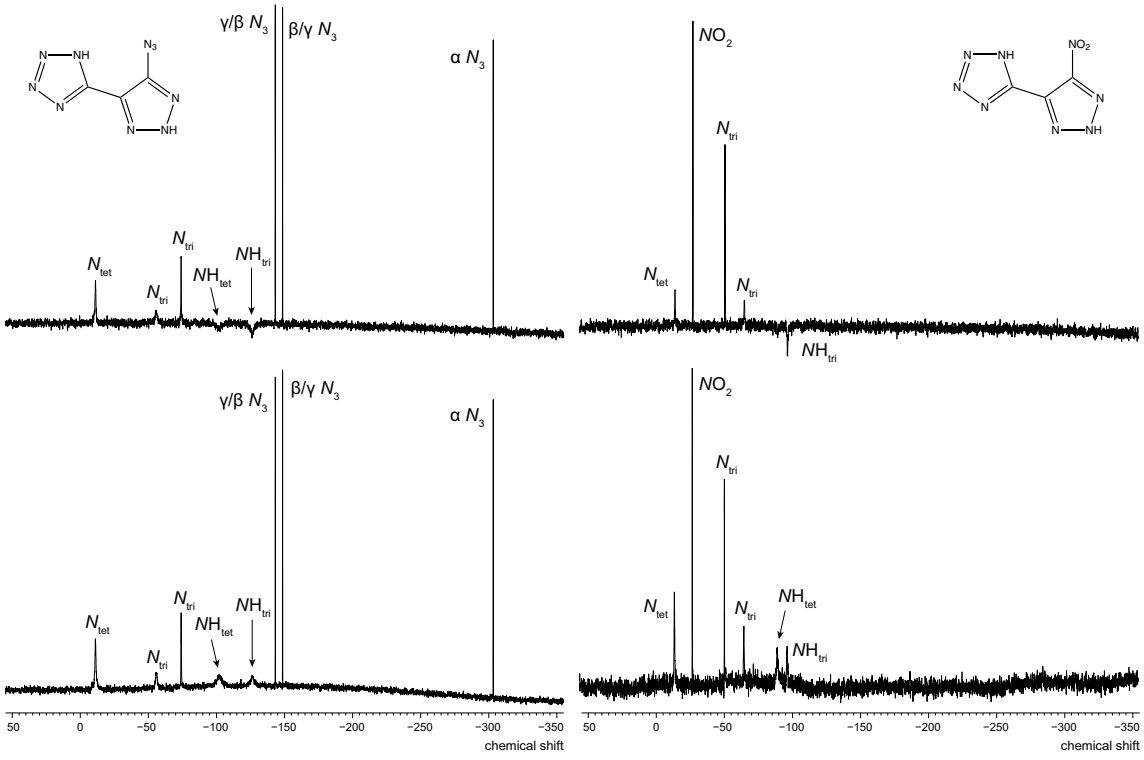

Figure A.9: Proton-decoupled (top) and proton-coupled (bottom) ^{15}N NMR spectra of 5-(5-azido-2*H*-1,2,3-triazol-4-yl)-1*H*-tetrazole (**14**) and 5-(5-nitro-2*H*-1,2,3-triazol-4-yl)-1*H*-tetrazole (**15**) in DMSO-d_6 at room temperature.

Crystallographic Data

Table A.11: Selected crystallographic data of 5-amino-1-benzyl-1,2,3-triazol-4-carboxamide (**10**) and 5-(5-amino-2*H*-1,2,3-triazol-4-yl)-1*H*-tetrazole (**13**).

	10	**13**
Molecular formula	$C_{10}H_{11}N_5O$	$C_3H_4N_8$
M [g mol^{-1}]	217.23	152.14
Color	colorless	colorless
Habit	block	block
Crystal size [mm]	0.27×0.13×0.12	0.08×0.05×0.04
Crystal system	monoclinic	monoclinic
Space group	$P21/c$	$P21/n$
a [Å]	11.731(4)	6.9019(4)
b [Å]	7.423(2)	11.6423(7)
c [Å]	11.188(4)	8.0685(4)
α [°]	90	90
β [°]	93.655(3)	113.881(2)
γ [°]	90	90
V [Å^3]	972.3(5)	592.83(6)
Z	4	4
$\rho_{\text{calc.}}$ [g cm^{-3}]	1.484	1.705
T [K]	173	100
$F(000)$	456	312
μ [mm^{-1}]	0.104	0.131
Absorption correction	multi-scan	multi-scan
Index range	$-14 \leq h \leq 14$	$-8 \leq h \leq 8$
	$-9 \leq k \leq 9$	$-14 \leq k \leq 14$
	$-12 \leq l \leq 13$	$-9 \leq l \leq 10$
θ min/max [°]	4.14/26.37	3.27/26.37
λ MoK$_\alpha$ [Å]	0.71073	0.71073
Measured reflections	6884	6279
Independent reflections	1980	1218
Observed reflections	1738	1057
Parameters	189	116
R_1 (all data)	0.0376	0.0382
R_1 (obs.)	0.0318	0.0323
wR_2 (all data)	0.0802	0.0903
wR_2 (obs.)	0.0758	0.0868
GOF	1.063	1.085
Res. dens. min. [e Å^{-3}]	−0.20	−0.19
Res. dens. max. [e Å^{-3}]	0.24	0.35
Solution	SIR97	SIR97
Refinement	SHELXL-97	SHELXL-2013
Measurement	jx203	tv197
CCDC number	1406925	1413469

A.4 Supporting Information for Chapter 5

Crystallographic Data

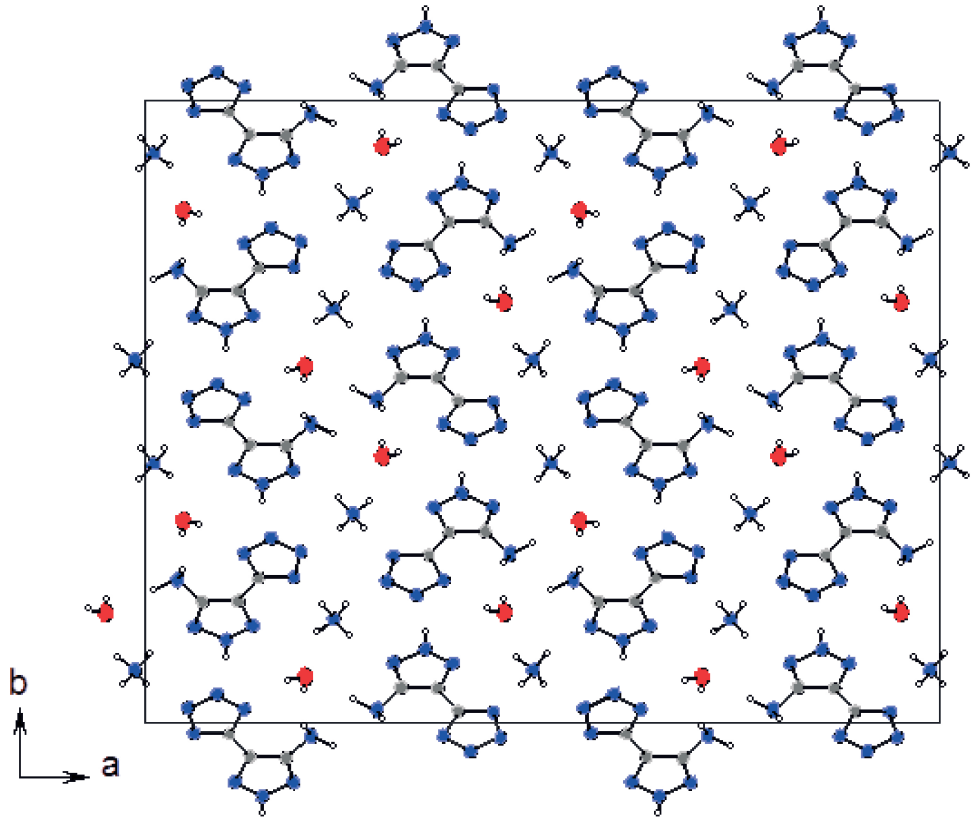

Figure A.10: Unit cell of ammonium 5-(5-amino-2*H*-1,2,3-triazol-4-yl)tetrazolate monohydrate (**13a**·H_2O) along the *c* axis.

Table A.12: Selected hydrogen bonds within the crystal structure of **13a**·H_2O.

D−H···A	*d*(D−H) [Å]	*d*(H···A) [Å]	*d*(D···A) [Å]	∠(D−H···A) [°]	
N8−H3···N4	0.87(3)	2.48(3)	3.027(3)	122(2)	intra
O1−H8···N4	0.80(3)	2.16(4)	2.918(3)	157(3)	inter
O1−H9···N8	0.79(4)	2.16(4)	2.941(3)	167(4)	inter
N6−H1···N3	0.92(3)	1.91(3)	2.819(3)	169(3)	inter
N9−H5···N2	0.95(3)	2.03(3)	2.940(3)	160(3)	inter
N9−H6···N1	0.97(3)	1.96(3)	2.932(3)	173(3)	inter
N9−H4···N7	0.91(2)	2.11(2)	2.996(3)	165(2)	inter
N9−H7···O1	0.94(3)	2.14(3)	2.989(3)	149(3)	inter
N8−H2···O1	0.95(3)	2.07(3)	3.006(3)	171(3)	inter

Table A.13: Selected interactions within the crystal structure of **13b**.

D−H···A	d(D−H) [Å]	d(H···A) [Å]	d(D···A) [Å]	∠(D−H···A) [°]	
N9−H5···N7	0.90(2)	2.24(2)	3.038(2)	147(2)	inter
N9−H6···N4	0.98(2)	1.88(2)	2.851(2)	167(2)	inter
O1−H7···N1	0.90(2)	1.78(2)	2.681(2)	178(2)	inter
N6−H1···N2	0.90(2)	1.94(2)	2.831(2)	172(2)	inter
N8−H2···N3	0.91(2)	2.34(2)	3.222(2)	162(2)	inter
N9−H4···O1	0.93(2)	2.50(2)	2.936(3)	110(1)	inter
N9−H4···N5	0.93(2)	2.11(2)	2.986(2)	158(2)	inter

Table A.14: Selected interactions within the crystal structure of **13c**.

D−H···A	d(D−H) [Å]	d(H···A) [Å]	d(D···A) [Å]	∠(D−H···A) [°]	
N8−H3···N1	0.98(8)	2.50(7)	3.095(7)	119(5)	intra
N8−H2···N2	0.99(5)	2.17(5)	3.105(6)	158(4)	inter
N7−H1···N1	0.96(6)	1.93(6)	2.866(7)	165(5)	inter
N9−H6···N3	0.90(7)	2.21(7)	3.097(7)	166(6)	inter
N9−H7···N5	0.82(6)	2.27(6)	3.045(7)	157(5)	inter
N10−H8···N6	0.82(6)	2.14(6)	2.929(7)	161(6)	inter
N10−H9···N2	0.89(7)	2.16(7)	3.028(7)	168(7)	inter
N11−H4···N4	0.92(7)	2.05(7)	2.939(7)	162(6)	inter
N11−H5···N3	0.94(8)	2.27(8)	3.159(7)	157(7)	inter

Table A.15: Selected hydrogen bonds within the crystal structure of **13e**.

D−H···A	d(D−H) [Å]	d(H···A) [Å]	d(D···A) [Å]	∠(D−H···A) [°]	
N6−H1···N2	0.861(2)	1.949(3)	2.788(4)	164.5(2)	inter
N14−H11···N5	0.907(3)	2.173(2)	3.055(4)	164.0(2)	inter
N14−H12···N1	0.891(3)	2.376(3)	3.114(4)	140.3(2)	inter
N8−H3···N14	0.849(2)	2.387(3)	3.124(4)	145.6(2)	inter
N8−H2···N12	0.877(2)	2.476(2)	3.296(3)	155.9(2)	inter
N10−H5···N3	0.902(2)	2.203(2)	3.089(3)	167.3(2)	inter
N12−H8···N4	0.895(2)	2.393(3)	3.242(4)	158.3(2)	inter
N9−H4···N8	0.848(2)	2.347(2)	3.172(3)	164.6(2)	inter
N11−H7···N7	0.839(2)	2.107(2)	2.869(4)	150.8(2)	inter

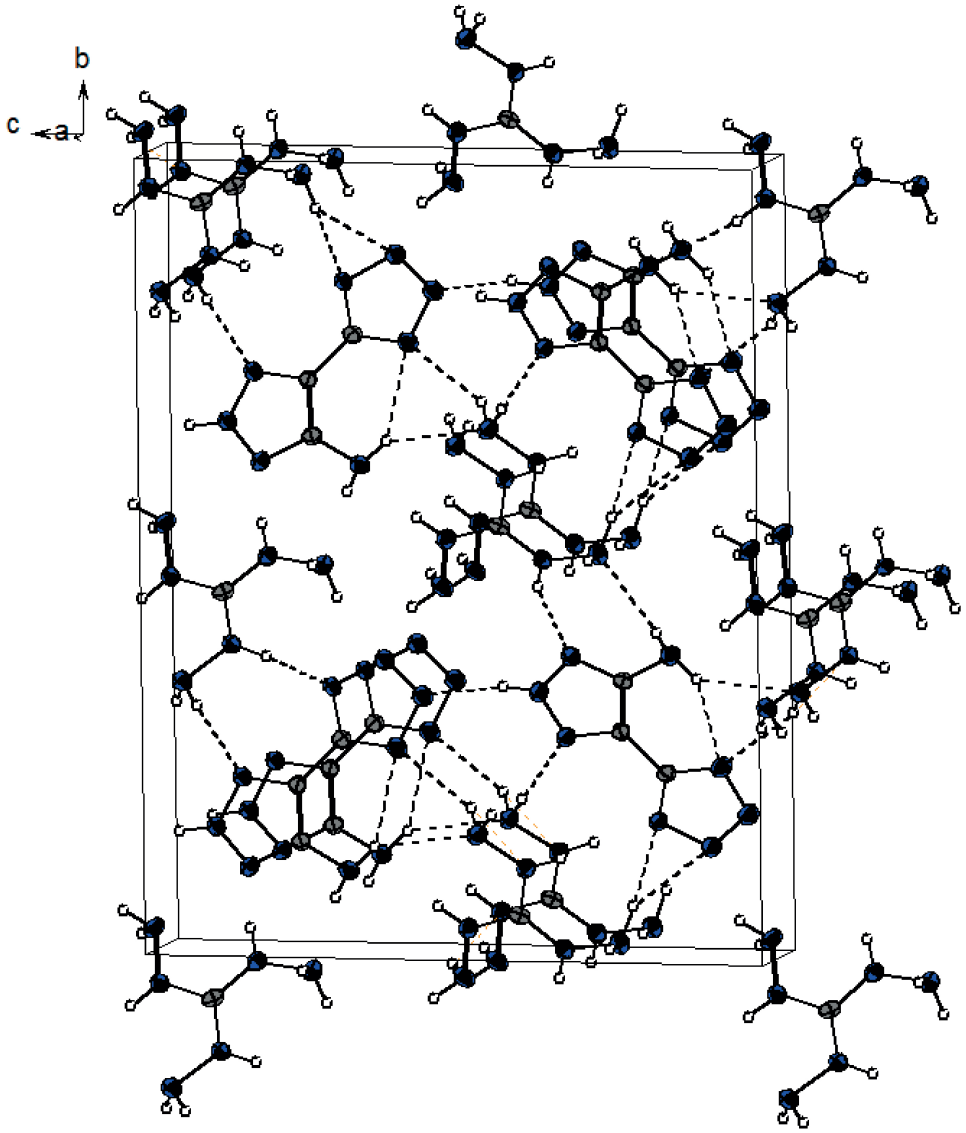

Figure A.11: Crystal structure of triaminoguanidinium 5-(5-amino-2*H*-1,2,3-triazol-4-yl)tetrazolate (**13e**) along the *a* axis. Selected hydrogen bonds are shown black dotted. Thermal ellipsoids are drawn at the 50% probability level.

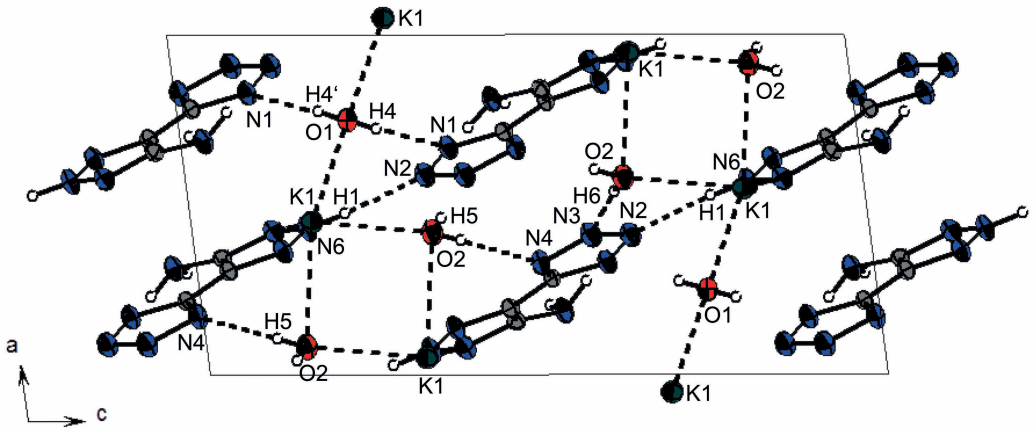

Figure A.12: Unit cell of **13f**·1.5 H_2O along the *b* axis. Selected hydrogen bonds and dipolar interactions are shown black dotted. Thermal ellipsoids are drawn at the 50% probability level.

Table A.16: Selected hydrogen bonds and dipolar interactions within the crystal structure of **15d**.

D−H···A	*d*(D−H) [Å]	*d*(H···A) [Å]	*d*(D···A) [Å]	∠(D−H···A) [°]	
N9−H2···N12	0.90(2)	2.35(2)	2.684(2)	102(1)	intra
N11−H6···N1	0.86(2)	2.17(2)	3.006(2)	164(2)	inter
N10−H5···N2	0.87(2)	2.08(2)	2.936(2)	170(2)	inter
N4−H1···N5	0.86(2)	1.94(2)	2.781(2)	164(2)	inter
N10−H4···N6	0.87(2)	2.20(2)	2.991(2)	150(2)	inter
N12−H7···N7	0.89(2)	2.44(2)	3.133(2)	135(2)	inter
N9−H2···N12	0.90(2)	2.28(2)	3.021(2)	140(1)	inter
dipolar interactions ΣvdW radii (N···O) < 3.07 Å [2] N1···O1^{intra} 2.880(1) Å; N8···O2 2.915(1) Å					
dipolar interactions ΣvdW radii (C···O) < 3.22 Å [2] C1···O1 3.045(1) Å					

Table A.17: Selected crystallographic data of ammonium 5-(5-amino-2*H*-1,2,3-triazol-4-yl)tetrazolate monohydrate (**13a**·H_2O), hydroxylammonium 5-(5-amino-2*H*-1,2,3-triazol-4-yl)tetrazolate (**13b**) and guanidinium 5-(5-amino-1*H*-1,2,3-triazol-4-yl)tetrazolate (**13c**).

	13a	**13b**	**13c**
Molecular formula	$C_3H_7N_9 \cdot H_2O$	$C_3H_7N_9O$	$C_4H_9N_{11}$
M [g mol^{-1}]	187.16	185.15	211.19
Color	yellow	colorless	colorless
Habit	block	rod	plate
Crystal size [mm]	0.40×0.23×0.11	0.30×0.07×0.05	0.32×0.08×0.01
Crystal system	orthorhombic	orthorhombic	monoclinic
Space group	$Fdd2$	$Pbca$	$P2_1$
a [Å]	30.389(2)	6.533(5)	3.5325(10)
b [Å]	23.7798(14)	14.774(5)	10.547(3)
c [Å]	4.4319(3)	14.818(5)	11.363(3)
α [°]	90	90	90
β [°]	90	90	94.08(2)
γ [°]	90	90	90
V [Å^3]	3202.7(4)	1430.2(13)	422.3(2)
Z	16	8	2
$\rho_{calc.}$ [g cm^{-3}]	1.553	1.720	1.661
T [K]	173	173	173
$F(000)$	1568	768	220
μ [mm^{-1}]	0.124	0.139	0.127
Absorption correction	multi-scan	multi-scan	multi-scan
Index range	$-37 \leq h \leq 26$	$-8 \leq h \leq 4$	$-4 \leq h \leq 3$
	$-25 \leq k \leq 29$	$-18 \leq k \leq 18$	$-8 \leq k \leq 13$
	$-5 \leq l \leq 5$	$-10 \leq l \leq 18$	$-14 \leq l \leq 11$
θ min/max [°]	4.35/26.36	4.16/26.37	4.26/26.37
λ MoK$_\alpha$ [Å]	0.71073	0.71073	0.71073
Measured reflections	6422	6000	1665
Independent reflections	928	1460	909
Observed reflections	877	1218	765
Parameters	154	146	173
R_1 (all data)	0.0312	0.0435	0.0677
R_1 (obs.)	0.290	0.0338	0.558
wR_2 (all data)	0.0724	0.0878	0.1345
wR_2 (obs.)	0.0700	0.0827	0.1242
GOF	1.126	1.075	1.089
Res. dens. min. [e Å^{-3}]	−0.19	−0.19	−0.30
Res. dens. max. [e Å^{-3}]	0.20	0.30	0.34
Solution	SIR97	SIR97	SIR97
Refinement	SHELXL-97	SHELXL-2014	SHELXL-97
Measurement	jx209	jx204	jx223
CCDC number	1446641	1446639	1446642

Table A.18: Selected crystallographic data of triaminoguanidinium 5-(5-amino-2*H*-1,2,3-triazol-4-yl)tetrazolate (**13e**), potassium 5-(5-amino-2*H*-1,2,3-triazol-4-yl)tetrazolate sesquihydrate(**13f**·1.5 H_2O) and aminoguanidinium 5-(5-nitro-1,2,3-triazolate-4-yl)-1*H*-tetrazolate (**15d**).

	13e	**13f**	**15d**
Molecular formula	$C_4H_{12}N_{14}$	$C_3H_3KN_8 \cdot 1.5\,H_2O$	$C_4H_8N_{12}O_2$
M [g mol^{-1}]	256.23	217.23	256.19
Color	colorless	colorless	green
Habit	rod	plate	block
Crystal size [mm]	0.15×0.10×0.05	0.32×0.23×0.14	0.40×0.38×0.11
Crystal system	monoclinic	monoclinic	monoclinic
Space group	Cc	$P2/n$	$I2/a$
a [Å]	3.706(2)	7.5899(10)	19.2477(8)
b [Å]	18.391(9)	7.6865(12)	4.7902(2)
c [Å]	14.936(8)	14.987(2)	21.7020(9)
α [°]	90	90	90
β [°]	96.355(5)	97.286(13)	95.088(4)
γ [°]	90	90	90
V [Å^3]	1011.7(14)	867.3(2)	1993.05(14)
Z	4	4	8
$\rho_{\text{calc.}}$ [g cm^{-3}]	1.682	1.664	1.708
T [K]	173	173	173
$F(000)$	536	444	1056
μ [mm^{-1}]	0.130	0.597	0.141
Absorption correction	multi-scan	multi-scan	multi-scan
Index range	$-4 \leq h \leq 4$	$-9 \leq h \leq 9$	$-22 \leq h \leq 24$
	$-24 \leq k \leq 23$	$-9 \leq k \leq 6$	$-5 \leq k \leq 4$
	$-20 \leq l \leq 20$	$-18 \leq l \leq 17$	$-24 \leq l \leq 27$
θ min/max [°]	4.43/28.77	4.14/26.37	4.16/26.37
λ MoK$_\alpha$ [Å]	0.71073	0.71073	0.71073
Measured reflections	3479	3276	7237
Independent reflections	2092	1774	2016
Observed reflections	1753	1432	1805
Parameters	175	141	195
R_1 (all data)	0.0578	0.0548	0.0362
R_1 (obs.)	0.0449	0.0415	0.0323
wR_2 (all data)	0.1002	0.1142	0.0818
wR_2 (obs.)	0.0930	0.0994	0.0784
GOF	1.007	1.054	1.064
Res. dens. min. [e Å^{-3}]	−0.23	−0.40	−0.27
Res. dens. max. [e Å^{-3}]	0.25	1.08	0.21
Solution	SIR97	SIR97	SIR97
Refinement	SHELXL-97	SHELXL-97	SHELXL-97
Measurement	jx205	jx290	jx230
CCDC number	1446640	1446644	1446643

A.5 Supporting Information for Chapter 6

Crystallographic Data

Table A.19: Selected bond lengths and angles in the molecular structure of **17**·H_2O.

Bond lengths [Å]					
C1−N1	1.350(3)	C2−N5	1.330(3)	N8−N9	1.096(3)
N1−N2	1.318(2)	C3−N7	1.353(3)	C3−N8	1.365(3)
N2−N3	1.308(2)	N5−N6	1.365(2)		
N3−N4	1.324(2)	N6−N7	1.317(2)		
C1−N4	1.322(3)	C2−C3	1.388(3)		
C1−C2	1.447(3)				
Bond angles [°]					
C1−N1−N2	105.50(14)	C2−C3−N7	110.05(15)	C3−N8−N9	179.86(19)
C1−N4−N3	101.44(13)	C2−N5−N6	107.39(13)	C2−C3−N8	128.05(16)
N1−N2−N3	106.38(13)	N5−N6−N7	111.52(14)	N7−C3−N8	121.90(18)
N2−N3−N4	114.19(14)	N6−N7−C3	105.09(14)		
N1−C1−C2	124.63(15)	C3−C2−N5	105.95(16)		
N4−C1−C3	122.88(18)				

Table A.20: Selected hydrogen bonds and dipolar interactions within the crystal structure of **17**·H_2O.

D−H···A	d(D−H) [Å]	d(H···A) [Å]	d(D···A) [Å]	∠(D−H···A) [°]
N3−H1···O1^{i}	1.02(3)	1.68(3)	2.643(2)	156(2)
O1−H2···N1^{ii}	0.81(3)	2.08(3)	2.830(2)	154(3)
O1−H3···N7^{iii}	0.84(3)	2.10(3)	2.914(3)	163(2)
dipolar interactions ΣvdW radii (N···O) < 3.07 Å [2] N8···O1^{iv} 2.909(2) Å				
dipolar interactions ΣvdW radii (C···N) < 3.32 Å [2] C1···N6^{v} 3.076(2) Å				
dipolar interactions ΣvdW radii (N···N) < 3.10 Å [2] N2···N9^{vi} 2.884(3) Å				

Symmetry codes: (i) $-x, 2-y, -z$; (ii) $-x, 1-y, -z$; (iii) $-0.5-x, 0.5+y, 0.5-z$, (iv) $1+x, y, z$; (v) $0.5-x, 0.5+y, 0.5-z$; (vi) $0.5+x, 1.5-y, -0.5+z$.

Table A.21: Selected crystallographic data of 5-diazonium-4-(2*H*-tetrazol-5-yl)-1,2,3-triazolate hydrate (**17**·H_2O).

	17·H_2O
Molecular formula	$C_3HN_9 \cdot H_2O$
M [g mol^{-1}]	181.12
Color	yellow
Habit	block
Crystal size [mm]	0.13×0.12×0.06
Crystal system	monoclinic
Space group	$P2_1/n$
a [Å]	8.200(4)
b [Å]	6.899(4)
c [Å]	12.679(8)
α [°]	90
β [°]	102.281(6)
γ [°]	90
V [Å^3]	700.9(7)
Z	4
$\rho_{calc.}$ [g cm^{-3}]	1.716
T [K]	173
$F(000)$	368
μ [mm^{-1}]	0.140
Absorption correction	multi-scan
Index range	$-10 \leq h \leq 10$
	$-7 \leq k \leq 8$
	$-15 \leq l \leq 15$
θ min/max [°]	4.42/26.37
λ MoK$_\alpha$ [Å]	0.71073
Measured reflections	3027
Independent reflections	1431
Observed reflections	1141
Parameters	130
R_1 (all data)	0.0544
R_1 (obs.)	0.0406
wR_2 (all data)	0.1063
wR_2 (obs.)	0.0973
GOF	1.056
Res. dens. min. [e Å^{-3}]	−0.18
Res. dens. max. [e Å^{-3}]	0.30
Solution	SIR97
Refinement	SHELXL-2014
Measurement	jx469
CCDC number	1465295

Vibrational Spectroscopy

In the IR and Raman spectra of **17**, depicted in Figure A.13, the characteristic valence vibration of the diazonium N≡N bond is observed in the expected region as strong bands

at 2206 cm^{-1} and 2210 cm^{-1}, respectively. Furthermore, the vibrations of the triazole and tetrazole moieties, the symmetric and asymmetric N−C−N as well as the N=N, C=N, and C=C vibrations, are observed in the range from 1637 cm^{-1} to 1499 cm^{-1} and further bands in the region of 1312–800 cm^{-1}. In the IR spectrum the stretching vibration of the heterocyclic NH proton and the crystal water molecule, which are involved in hydrogen bonds, are observed at wavenumbers above 3200 cm^{-1}.

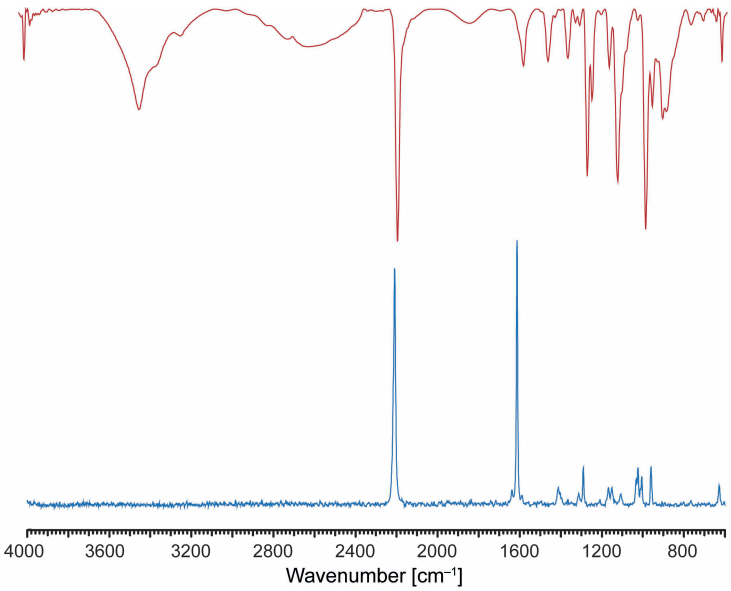

Figure A.13: IR (red) and Raman (blue) spectra of 5-(5-diazonium-1,2,3-triazolat-4-yl)-2*H*-tetrazole monohydrate (**17**·H_2O).

A.6 Supporting Information for Chapter 7

Vibrational Spectroscopy

Vibrational spectroscopic studies of all synthesized compounds were performed with IR and Raman spectra and used for identification of structural elements and functional groups. Absorptions were assigned according to values reported in the literature.[1] Characteristic vibrations of the aromatic heterocyclic system are visible in the spectra of all compounds, such as the tetrazole and triazole framework vibrations, the symmetric and asymmetric N−C−N stretching vibrations, stretching vibrations of N−N and out of plane vibrations of the cyclic C=N bond at 1638–1431 cm^{-1} and in the fingerprint area at 1350–800 cm^{-1}. The NH_2 and NH deformation vibrations, especially from the cations, are also in the range of 1682–1411 cm^{-1} and therefore overlapping with the N−N and C−N stretching vibrations. At the wavenumbers above 3000 cm^{-1} the NH valence vibrations of all compounds and if crystal water or a *N*-hydroxy group are present their OH valence vibrations are

observed, which are involved in hydrogen bonding. The ammonium valence vibrations of the ammonium, hydroxylammonium and guanidinium based cations of **19a**–**19d**, **23a**–**23e** and **23k** could be observed in the range of 2845–2227 cm^{-1}. The N−O valence vibration of the aliphatic *N*-hydroxy group of compounds **20** and **21** is seen around 1000 cm^{-1}, whereas the salts **23a**–**23k** have their strong aromatic N−O valence vibration bands in the range of 1236–1227 cm^{-1}.

Crystallographic Data

Table A.22: Selected hydrogen bonds within the crystal structure of dimethylammonium 5-(4-(1*H*-tetrazol-5-yl)-1*H*-1,2,3-triazol-5-yl)tetrazolate.

D−H···A	*d*(D−H) [Å]	*d*(H···A) [Å]	*d*(D···A) [Å]	∠(D−H···A) [°]
N1−H1···N11	0.874(17)	2.064(17)	2.7928(16)	140.3(15)
N12−H4^{i}···N10	0.977(17)	1.860(17)	2.8316(16)	172.4(15)
N7−H2···N8^{ii}	0.918(17)	1.908(17)	2.8111(16)	167.4(16)
N13−H3···N3^{iii}	0.888(17)	2.125(18)	2.9297(17)	150.3(15)
C6−H6A···N5^{iv}	0.962(17)	2.607(18)	3.401(2)	140.0(14)
C6−H6C···N4^{v}	0.991(17)	2.605(17)	3.373(2)	134.4(13)
C5−H5A···N9^{vi}	1.001(18)	2.604(18)	3.570(2)	162.3(14)

Symmetry codes: (i) $1-x, 1-y, -z$; (ii) $2-x, 0.5+y, 0.5-z$; (iii) $-1+x, 1+y, z$; (iv) $1-x, 0.5+y, 0.5-z$; (v) $x, 1+y, z$; (vi) $2-x, 1-y, -z$.

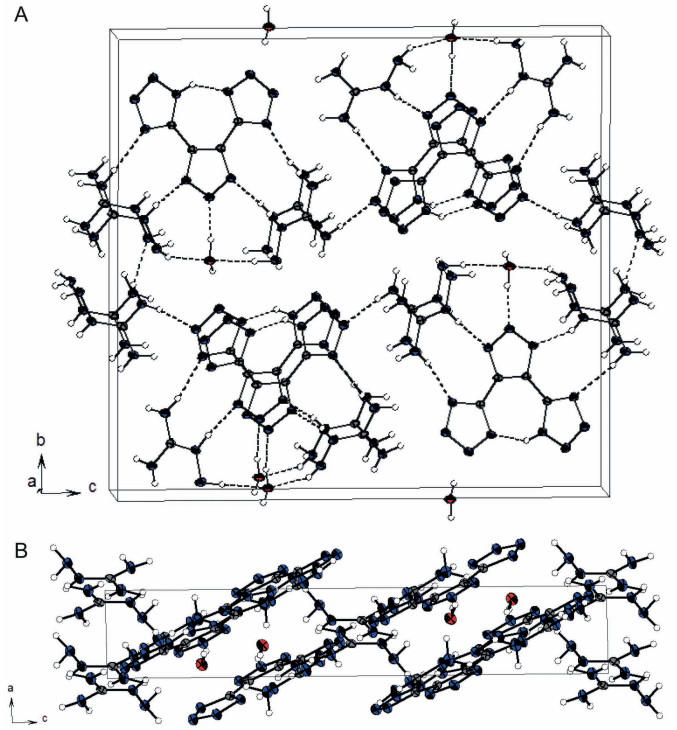

Figure A.14: A) Unit cell of bisaminoguanidinium 5-(4-(1*H*-tetrazol-5-yl)-1,2,3-triazolate-5-yl)tetrazolate **19d**·H_2O. Interactions are shown as dashed lines. B) Diagonal layer structure of **19d**·H_2O along the *b* axis.

Table A.23: Selected hydrogen bonds within the crystal structure of bisaminoguanidinium 5-(4-(1*H*-tetrazol-5-yl)-1,2,3-triazolate-5-yl)tetrazolate (**19d**) monohydrate.

D−H···A	*d*(D−H) [Å]	*d*(H···A) [Å]	*d*(D···A) [Å]	∠(D−H···A) [°]
N11−H1···N14	0.92(3)	1.86(3)	2.671(3)	146.5(23)
N14−H6^{i}···N7	0.86(3)	2.00(3)	2.859(3)	169.8(24)
N15−H8^{i}···O1^{i}	0.94(3)	2.14(3)	3.011(3)	154.5(24)
O1−H16^{i}···N6	0.94(3)	1.83(3)	2.748(2)	165.9(25)
N18−H13···N5	0.88(3)	2.00(3)	2.879(3)	176.0(24)
N16−H9···N1	0.85(3)	2.13(3)	2.962(3)	165.7(24)
N13−H5^{i}···N8	0.84(3)	2.21(3)	3.033(3)	166.5(24)
N12−H3···N2^{ii}	0.88(3)	1.99(3)	2.863(3)	170.2(26)
O1−H17···N2^{iii}	0.83(3)	2.03(3)	2.847(3)	166.5(28)
N17−H11···N9^{iv}	0.90(3)	2.17(2)	3.077(3)	175.8(22)
N17−H12···N10^{iii}	0.80(3)	2.35(3)	3.119(3)	160.8(26)
N19−H15···O1	0.90(3)	2.08(3)	2.973(3)	168.1(24)
N12−H2···N15^{v}	0.90(3)	2.36(3)	3.115(3)	141.8(23)
N16−H10···N13^{vi}	0.89(3)	2.77(2)	3.436(3)	133.2(20)
N15−H7···N6^{i}	0.91(3)	2.55(3)	3.325(3)	143.6(21)

Symmetry codes: (i) $1+x, y, z$; (ii) $1.5+x, 0.5-y, 0.5+z$; (iii) $1.5-x, -0.5+y, 0.5-z$; (iv) $-1.5-x, 0.5-y, -0.5+z$; (v) $3-x, -y, 1-z$; (vi) $-1.5+x, 0.5-y, -0.5+z$.

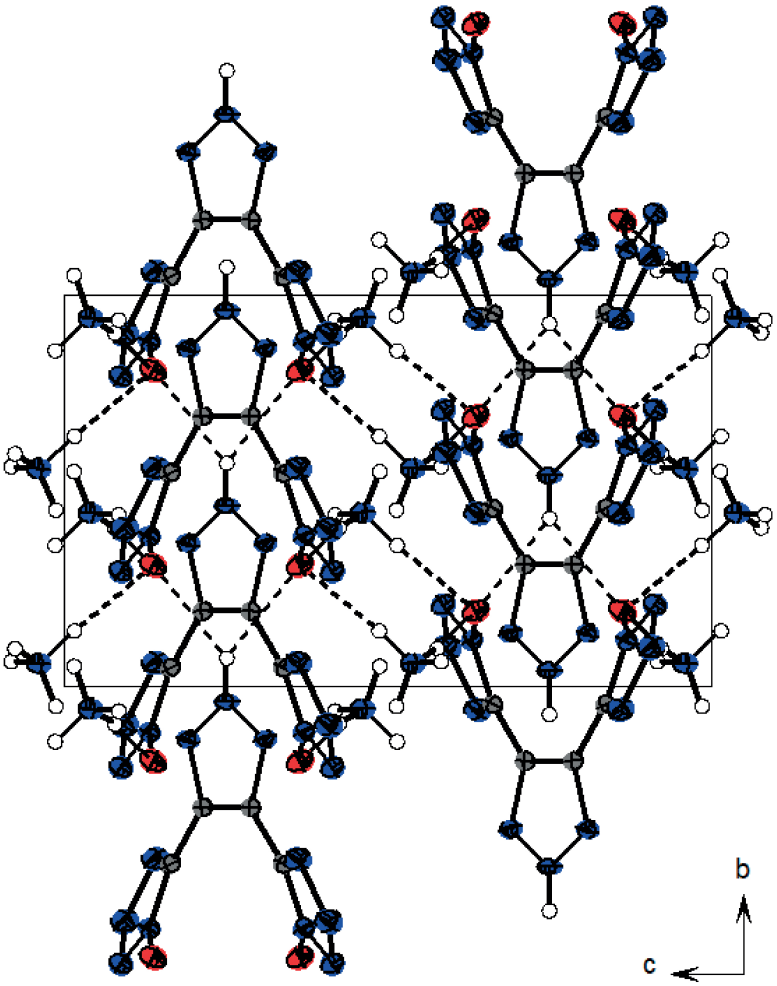

Figure A.15: Unit cell of bisammonium 4,5-bis(tetrazol-1-oxide-5-yl)-2*H*-1,2,3-triazole (**23a**) along the *a* axis. Hydrogen bonds are shown as dashed lines.

Table A.24: Hydrogen bonds within the crystal structure of **23a**.

D−H···A	d(D−H) [Å]	d(H···A) [Å]	d(D···A) [Å]	∠(D−H···A) [°]
N7−H2^{i}···O1	0.93(3)	1.84(3)	2.761(2)	173(3)
N6−H1···O1^{ii}	0.82(4)	2.24(3)	2.923(2)	141.06(4)
N7−H4···N5	0.86(4)	2.20(4)	3.054(3)	168(3)
N7−H5···O1^{iii}	0.92(3)	1.93(3)	2.843(2)	171(2)

Symmetry codes: (i) $-0.5+x, -0.5+y, z$; (ii) $1-x, 1+y, 1.5-z$; (iii) $1-x, -y, 1-z$.

Table A.25: Selected hydrogen bonds within the crystal structure of **23b**.

D−H···A	d(D−H) [Å]	d(H···A) [Å]	d(D···A) [Å]	∠(D−H···A) [°]
N12−H2···O1	0.97(3)	1.83(3)	2.792(2)	171(2)
N13−H6···O2	0.85(4)	2.49(3)	3.018(3)	121(3)
N12−H3^{i}···O1	0.91(2)	1.98(2)	2.811(2)	153(2)
O5−H11^{ii}···O1	0.93(3)	1.78(3)	2.702(2)	174(3)
N13−H7^{iii}···N2	0.92(3)	2.21(3)	3.063(3)	154(2)
N13−H6^{iv}···N3	0.85(4)	2.34(4)	3.102(3)	152(3)
N12−H4^{iv}···N4	0.85(3)	2.18(2)	2.893(2)	141(2)
O3−H5^{v}···N10	1.00(3)	1.72(3)	2.712(2)	174(3)
N7−H1^{vi}···O2	0.90(3)	1.81(3)	2.657(2)	157(2)
O5−H10^{iv}···N6	0.91(3)	1.87(3)	2.754(2)	162(3)
O4−H9^{vii}···O5	1.16(3)	1.45(3)	2.608(2)	174(3)

Symmetry codes: (i) $2-x,-0.5+y,0.5-z$; (ii) $1+x,y,z$; (iii) $x,0.5-y,0.5+z$; (iv) $1-x,-0.5+y,0.5-z$; (v) $-1+x,y,z$; (vi) $1-x,-y,-z$; (vii) $1+x,0.5-y,-0.5+z$.

Table A.26: Hydrogen bonds within the crystal structure of **23k**·H_2O.

D−H···A	d(D−H) [Å]	d(H···A) [Å]	d(D···A) [Å]	∠(D−H···A) [°]
N14−H6···O2	0.87(3)	2.07(2)	2.8229(18)	144(2)
N19−H16^{i}···O1	0.89(2)	2.066(19)	2.9404(16)	168(2)
O3−H20^{ii}···O1	0.88(2)	1.96(2)	2.8348(18)	170(2)
N17−H11^{iii}···N5	0.85(2)	2.149(18)	2.9676(17)	163(2)
N16−H10^{iii}···N6	0.86(2)	2.15(2)	3.0097(19)	173(2)
N12−H2^{iv}···O1	0.84(2)	2.39(2)	3.147(2)	149(2)
N13−H3^{iv}···O1	0.83(2)	2.168(18)	2.9566(16)	158(2)
N13−H4^{v}···N7	0.89(2)	2.130(17)	2.9647(17)	156(2)
N14−H5^{v}···N7	0.86(2)	2.299(2)	3.074(2)	150(2)
N20−H17^{i}···N2	0.90(2)	2.07(2)	2.9638(17)	173(2)
N20−H18^{vi}···N3	0.89(3)	2.14(2)	3.030(2)	177(2)
O3−H19···N4	0.84(2)	2.07(2)	2.8462(18)	154(2)
N15−H7^{v}···N11	0.86(2)	2.35(2)	3.187(2)	167(2)
N17−H12^{v}···N10	0.89(2)	2.18(2)	3.052(2)	164(2)
N16−H9···N9	0.86(3)	2.27(3)	3.105(2)	163(2)
N16−H8···O2	0.90(3)	1.96(3)	2.852(2)	178(2)
N12−H1···O2	0.87(3)	2.05(2)	2.808(2)	145(2)

Symmetry codes: (i) $-1+x,-1+y,z$; (ii) $1-x,-y,-z$; (iii) $x,-1+y,z$; (iv) $1-x,-y,1-z$; (v) $1+x,y,z$; (vi) $1-x,1-y,-z$.

Table A.27: Selected crystallographic data of dimethylammonium 5-(4-(1*H*-tetrazol-5-yl)-1*H*-1,2,3-triazol-5-yl)tetrazolate (Me_2NH_2_BTT), bisaminoguanidinium 5-(4-(1*H*-tetrazol-5-yl)-1,2,3-triazolate-5-yl)tetrazolate (**19d**) and 4,5-bis(1-hydroxytetrazol-5-yl)-2*H*-1,2,3-triazole (**23**).

	Me_2NH_2_BTT	**19d**	**23**
Molecular formula	$C_6H_{10}N_{12}$	$C_6H_{15}N_{19} \cdot H_2O$	$C_4H_3N_{11}O_2 \cdot H_2O$
M [g mol^{-1}]	250.22	371.38	273.21
Color	colorless	colorless	colorless
Habit	block	rod	needle
Crystal size [mm]	0.38×0.19×0.12	0.20×0.04×0.03	0.20×0.08×0.03
Crystal system	monoclinic	monoclinic	orthorhombic
Space group	$P21/c$	$P21/n$	$Pbcn$
a [Å]	5.9531(4)	3.6870(3)	3.674(1)
b [Å]	8.2093(7)	19.7037(16)	13.453(2)
c [Å]	21.8084(16)	20.9271(18)	20.353(3)
α [°]	90	90	90
β [°]	90.960(7)	91.155(2)	90
γ [°]	90	90	90
V [Å^3]	1065.64(14)	1520.0(2)	1006.0(2)
Z	4	4	4
ρ_{calc} [g cm^{-3}]	1.560	1.623	1.804
T [K]	100	100	103
$F(000)$	520	776	560
μ [mm^{-1}]	0.117	0.128	0.157
Absorption correction	multi-scan	multi-scan	multi-scan
Index range	$-7 \leq h \leq 7$	$-4 \leq h \leq 4$	$-4 \leq h \leq 4$
	$-10 \leq k \leq 7$	$-23 \leq k \leq 24$	$-16 \leq k \leq 16$
	$-23 \leq l \leq 27$	$-26 \leq l \leq 26$	$-25 \leq l \leq 25$
θ min/max [°]	4.23/26.37	2.20/26.37	4.27/26.36
λ MoK$_\alpha$ [Å]	0.71073	0.71073	0.71073
Measured reflections	5491	23365	9255
Independent reflections	2175	3113	1033
Observed reflections	1808	2348	790
Parameters	193	286	101
R_1 (all data)	0.0442	0.0688	0.0537
R_1 (obs.)	0.0335	0.0431	0.0362
wR_2 (all data)	0.0860	0.1251	0.0880
wR_2 (obs.)	0.0796	0.1002	0.0806
GOF	1.061	1.128	1.055
Res. dens. min. [e Å^{-3}]	−0.20	−0.28	−0.19
Res. dens. max. [e Å^{-3}]	0.28	0.31	0.27
Solution	SIR97	SIR97	SIR97
Refinement	SHELXL-97	SHELXL-97	SHELXL-97
Measurement	ix384	rv302	gx715
CCDC number	1419889	1419892	1419921

Table A.28: Selected crystallographic data of bisammonium (**23a**) and bishydroxylammonium (**23b**) 4,5-bis(tetrazol-1-oxide-5-yl)-1,2,3-triazole, trisguanidinium 4,5-bis(tetrazol-1-oxide-5-yl)-1,2,3-triazolate (**23k**) and hydroxylammonium 4-(tetrazole-1-oxide-5-yl)-2*H*-1,2,3-triazole-5-carboxamide (**24**)

	23a	**23b**	**23k**	**24**
Molecular formula	$C_4H_9N_{13}O_2$	$C_4N_9N_{13}O_4 \cdot H_2O$	$C_7H_{18}N_{20}O_2 \cdot H_2O$	$C_4H_7N_9O_2$
M [g mol^{-1}]	271.20	321.22	432.37	229.16
Color	colorless	colorless	colorless	yellow
Habit	block	needle	block	block
Crystal size [mm]	0.17×0.11×0.06	0.40×0.02×0.02	0.40×0.34×0.08	0.20×0.15×0.05
Crystal system	monoclinic	monoclinic	triclinic	monoclinic
Space group	$C2/c$	$P2_1/c$	$P\bar{1}$	$P2_1/c$
a [Å]	11.6235(9)	8.4017(7)	8.4186(5)	9.5056(6)
b [Å]	7.3489(3)	6.9752(9)	11.0747(6)	12.8204(6)
c [Å]	13.2578(13)	20.3439(15)	11.6929(8)	6.8935(4)
α [°]	90	90	91.862(5)	90
β [°]	113.614(9)	94.350(7)	109.092(6)	96.683(6)
γ [°]	90	90	111.399(5)	90
V [Å^3]	1037.65(14)	1188.79(17)	944.79(10)	834.37(8)
Z	4	4	2	4
ρ_{calc} [g cm^{-3}]	1.736	1.795	1.520	1.824
T [K]	100	173	173	100
$F(000)$	560	664	452	472
μ [mm^{-1}]	0.143	0.158	0.123	0.155
Absorption correction	multi-scan	multi-scan	multi-scan	multi-scan
Index range	$-14 \leq h \leq 13$ $-9 \leq k \leq 8$ $-12 \leq l \leq 16$	$-11 \leq h \leq 11$ $-9 \leq k \leq 9$ $-26 \leq l \leq 27$	$-10 \leq h \leq 10$ $-13 \leq k \leq 13$ $-14 \leq l \leq 14$	$-12 \leq h \leq 12$ $-16 \leq k \leq 16$ $-8 \leq l \leq 8$
θ min/max [°]	4.09/26.36	4.20/28.28	4.16/26.37	4.19/28.28
λ MoK$_\alpha$ [Å]	0.71073	0.71073	0.71073	0.71069
Measured reflections	2678	10995	9874	5528
Independent reflections	1059	2942	3845	1920
Observed reflections	972	2089	3092	1469
Parameters	105	243	331	173
R_1 (all data)	0.0470	0.0774	0.0470	0.0632
R_1 (obs.)	0.0435	0.0466	0.0339	0.0428
wR_2 (all data)	0.1099	0.1094	0.0873	0.0969
wR_2 (obs.)	0.1075	0.0954	0.0793	0.0855
GOF	1.078	1.034	1.054	1.078
Res. dens. min. [e Å^{-3}]	−0.27	−0.26	−0.23	−0.29
Res. dens. max. [e Å^{-3}]	0.73	0.29	0.23	0.27
Solution	SIR97	SIR97	SIR97	SIR97
Refinement	SHELXL-97	SHELXL-97	SHELXL-97	SHELXL-97
Measurement	ix135	jx170	jx076	ix250
CCDC number	1419887	1419891	1419890	1419888

Luminescent Bacteria Inhibition Test

The luminescent bacteria inhibition test offers a possibility to determine the environmental acceptability of new energetic materials to aquatic organisms whereas the marine bacteria *Vibrio fischeri* NRRL-B-11177 is used as representative. In this test the decrease of luminescence of the liquid-dried bacteria is determined after 15 min and after 30 min at different concentrations of the tested compounds at 15 °C and is compared to a control measurement of a 2% NaCl stock solution. The sample dilution sequence corresponds to DIN 38412 L34, which ranges from 1:2 to 1:32. For a better reproducibility all dilution steps were made in duplicate. The changes of intensity of the bacterial luminescence in the absence (controls) and presence (samples) of the tested compounds after the two different incubation times were recorded with a LUMIStox 300 obtained from Hach Lange GmbH (Düsseldorf, Germany). The controls were measured for calculating the correction factor, which is necessary to consider the normal decrease of luminescence without any toxic effect per time. The EC_{50} value gives the concentration of each compound where the bacterial luminescence is inhibited by 50% and is calculated by plotting Γ against the concentration of the test substance in a diagram with a logarithmic scale, where $\Gamma =$ inhibition (in %)/100−inhibition (in %) and c (concentration of the test sample). The EC_{50} value is identical with the intersection of the resulting graph with the x axis ($\Gamma = 0$). For a better comparison of the determined toxicities the toxic effect of RDX to the bacterial strain under the same conditions is applied for the toxicity assessment of **19a** and **23**. A 2% NaCl stock solution was prepared prior to the measurements using HPLC-grade water to ensure optimal salt conditions for the bacteria. The tested compounds of a known weight are diluted in this stock solution and after complete dissolving were adjusted to a final volume. Dilutions were prepared out of these solutions corresponding to DIN/EN/ISO 11348 without G1 level. RDX was first dissolved in acetone and then diluted in 2% NaCl stock solution to obtain a 1% (vol%) acetone concentration for each dilution. A 1% acetone concentration is not toxic to *Vibrio fischeri*.[3]

A.7 Supporting Information for Chapter 9

Crystallographic Data

Table A.29: Selected crystallographic data of 5-amino-2*H*-1,2,3-triazole-4-carbonitrile (**26**) and 5-amino-2*H*-1,2,3-triazole-4-carboxamidoxime (**27**).

	26	**27**
Molecular formula	$C_3H_3N_5$	$C_3H_6N_6O \cdot H_2O$
M [g mol^{-1}]	109.09	160.15
Color	colorless	colorless
Habit	platelet	needle
Crystal size [mm]	0.21×0.17×0.03	0.40×0.04×0.03
Crystal system	monoclinic	monoclinic
Space group	$P2_1/c$	$P2_1$
a [Å]	7.0064(9)	8.7895(13)
b [Å]	6.2325(5)	3.7291(5)
c [Å]	10.7723(10)	10.3549(12)
α [°]	90	90
β [°]	100.222(11)	91.764(10)
γ [°]	90	90
V [Å^3]	462.93(8)	339.24(8)
Z	4	2
$\rho_{calc.}$ [g cm^{-3}]	1.565	1.568
T [K]	173	173
$F(000)$	224	168
μ [mm^{-1}]	0.116	0.131
Absorption correction	multi-scan	multi-scan
Index range	$-8 \leq h \leq 8$	$-12 \leq h \leq 12$
	$-7 \leq k \leq 7$	$-5 \leq h \leq 5$
	$-10 \leq l \leq 13$	$-15 \leq h \leq 15$
θ min/max [°]	4.41/26.37	4.51/32.32
λ MoK$_\alpha$ [Å]	0.71073	0.71073
Measured reflections	3383	3570
Independent reflections	944	1954
Observed reflections	766	1512
Parameters	85	133
R_1 (all data)	0.0449	0.0737
R_1 (obs.)	0.0347	0.0489
wR_2 (all data)	0.0960	0.1062
wR_2 (obs.)	0.0895	0.0929
GOF	1.049	1.019
Res. dens. min. [e Å^{-3}]	−0.18	−0.23
Res. dens. max. [e Å^{-3}]	0.20	0.29
Solution	SIR97	SIR97
Refinement	SHELXL-2014	SHELXL-2014
Measurement	kx388	lx021
CCDC number	1471558	1471559

A.8 Supporting Information for Chapter 10

IR and Raman Spectroscopy

The IR spectrum of 1-(3-nitro-1*H*-1,2,4-triazol-5-on-4-yl)-2-nitrazapropane (**31**) shows a broad valance stretching mode of the N−H bond in the range of 3162–3096 cm^{-1}. For the two times alkylated **32** the N−H vibration mode disappeared. The C−H vibration bands of compounds **31** and **32** are observed in a range from 3060–2856 cm^{-1} (Raman) and 3062–2852 cm^{-1} (IR). For both NTO derivatives the C=O valence vibration appears as very sharp and intensive band in a range of 1738–1717 cm^{-1} in the IR spectra. The vibrational frequencies for the asymmetric stretching mode of the *C*–bonded nitro group are observed at 1554–1540 cm^{-1}. The symmetric stretching modes are located at lower energy (1354–1340 cm^{-1}). The same trend is observed for the nitramine nitro groups showing the ν_{as} stretching modes at 1586 and 1578 cm^{-1} in the Raman spectra and the ν_{s} stretching modes in a range of 1306–1260 cm^{-1} (IR). For compound **32** an additional vibration mode of the nitramine nitro group is observed, due to the different chemical surroundings of the two nitramine moieties.

The C−H valence vibrations of the 1,2,4-triazole derivatives **33**–**35** are located in the range of 3080–2795 cm^{-1}. The asymmetric and symmetric stretching modes of the nitramine nitro groups are observed at 1644–1552 cm^{-1} and 1300–1237 cm^{-1}, respectively. According to Mel'nikov,[4] the intensive bands at 1440 cm^{-1} and 1380 cm^{-1} of compound **33** respective at 1403 cm^{-1} for **34** and 1492 cm^{-1} for **35** in the Raman spectrum are caused by coupled stretching and bending modes of the ONC respective NCN valence angles of the nitro group and of the fragment of the triazole ring. For the nitro group introduced in the 5-position of **33**, a shift to lower frequencies is observed. Furthermore, the characteristic asymmetric and symmetric IR-intensive stretching modes of the *C*-bonded nitro groups are located in a range of 1540–1496 cm^{-1} and 1334–1306 cm^{-1}, whereas for **33** a splitting of these vibrations into two bands is observed due to a different surrounding of the nitro groups in 3- and 5-position. Additionally, the N−H valence vibrations of **34** are seen at 3428 cm^{-1}.

The dinitroimidazole based compounds **36** and **37** show the same characteristic vibrations of the C−H, nitramine, and *C*-bonded nitro groups as the 1,2,4-triazole derivatives in similar ranges. In addition to the aliphatic C−H vibration modes, aromatic C−H valence vibrations are observed for **36** and **37** at 3146–3126 cm^{-1}.

The aromatic C−H vibrations of nitramines **38**–**40** are seen in the range from 3174–3122 cm^{-1}. The C−H valence vibrations of the 3,5-dinitropyrazole substituted nitramine are shifted to higher wavenumbers compared to the 3,4-dinitropyrazole derivatives. The aliphatic C−H valence vibrations of the nitramine group of **38**–**42** are observed from 3073–2954 cm^{-1}, whereas the vibrations of the methyl group are located at lower wavenum-

bers. The asymmetric and symmetric nitramine N−NO_2 stretching modes are at 1648–1558 cm^{-1} and 1318–1232 cm^{-1}. Furthermore, the characteristic asymmetric and symmetric IR-intensive stretching modes of the *C*-bonded nitro groups are located in a range of 1544–1480 cm^{-1} and 1409–1318 cm^{-1}. Additionally, a C_{ar}−Cl vibration at 1054 cm^{-1} respective N−H valence vibrations at 3489–3383 cm^{-1} could be assigned for nitramines **41** and **42**.

NMR Spectroscopy

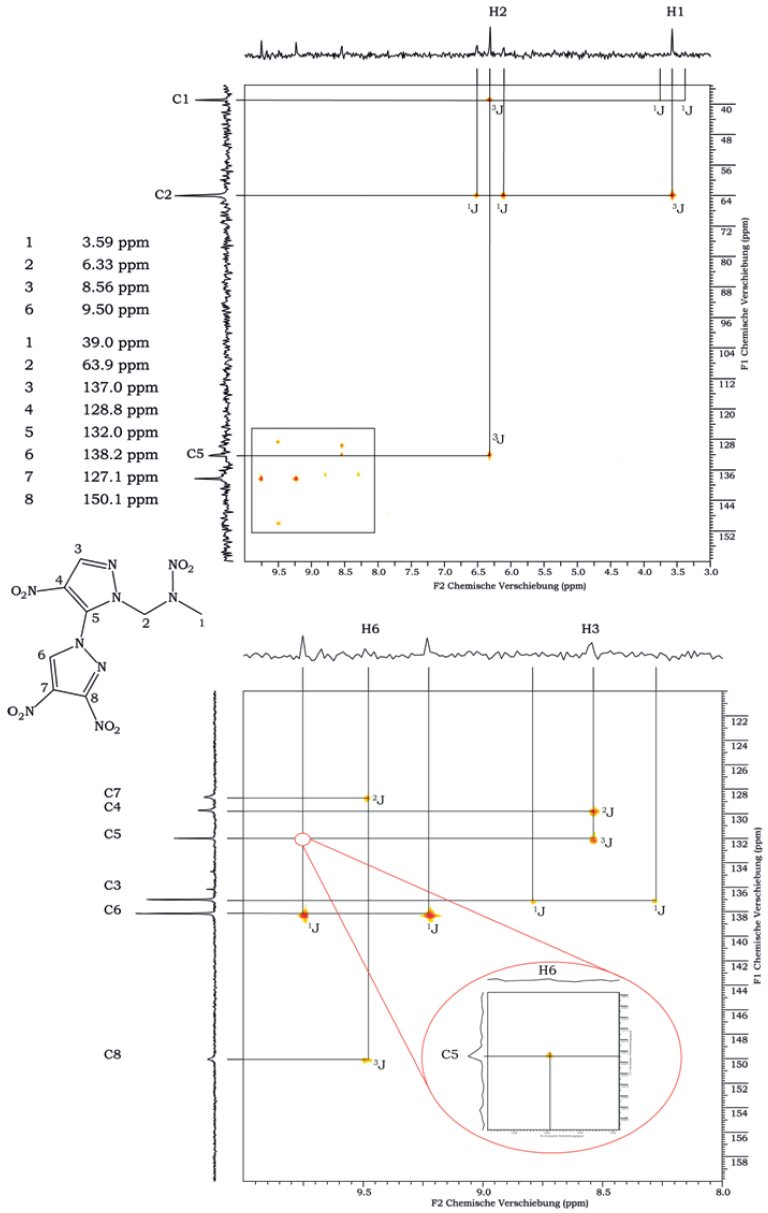

Figure A.16: HMBC NMR spectrum of 1-(3,4,4′-trinitro-1,3′-bipyrazol-2′-yl)-2-nitrazapropane (**40**) in acetone-d_6. (T = 25 °C; c = 5.6×10^{-3} mmol mL^{-1}; 1024 × 1024 Matrix; pulse delay = 1 s; repetition time = 1.9 s) (top), enlarged HMBC section (bottom).

Crystallographic Data

Table A.30: Interactions within the crystal structure of 1-(3-nitro-1*H*-1,2,4-triazol-5-on-4-yl)-2-nitrazapropane (**31**).

D−H···A	d(D−H) [Å]	d(H···A) [Å]	d(D···A) [Å]	∠(D−H···A) [°]	
N1−H1···O5	0.930	1.841	2.755	166.87	inter
C4−H4A···O3	0.996	2.531	3.318	138.77	inter
C3−H3B···O1	0.996	2.545	3.279	130.39	inter
C3−H3A···N2	1.003	2.621	3.535	151.43	inter
C4−H4C···O2	0.987	2.600	3.282	126.25	inter
dipolar interactions ΣvdW radii (N···O) < 3.07 Å [2] N4···O2$^{\text{intra}}$ 2.935 Å; N6···O2$^{\text{inter}}$ 2.970 Å					
dipolar interactions ΣvdW radii (C···O) < 3.22 Å [2] C2···O2$^{\text{intra}}$ 2.869 Å					

Table A.31: Interactions within the crystal structure of 2,4-bis(2-nitrazaprop-1-yl)-3-nitro-1,2,4-triazol-5-one·HNO_3 (**32**·HNO_3).

D−H···A	d(D−H) [Å]	d(H···A) [Å]	d(D···A) [Å]	∠(D−H···A) [°]	
C5−H5B···O2	0.971	2.367	3.013	123.42	intra
O10−H10···O1	0.870	1.747	2.616	176.35	inter
C3−H3B···O5	1.004	2.364	3.320	158.83	inter
C5−H5B···O7	0.971	2.440	3.175	132.20	inter
C6−H6A···O8	0.878	2.491	3.368	176.66	inter
C4−H4A···O7	0.940	2.534	3.137	122.13	inter
C4−H4B···O4	0.910	2.635	3.349	135.91	inter
dipolar interactions ΣvdW radii (N···O) < 3.07 Å [2] N4···O6$^{\text{intra}}$ 2.776 Å; N8···O8$^{\text{inter}}$ 2.850 Å; N7···O8$^{\text{inter}}$ 2.939 Å					
dipolar interactions ΣvdW radii (C···O) < 3.22 Å [2] C2···O6$^{\text{intra}}$ 2.864 Å; C1···O8$^{\text{inter}}$ 2.891 Å; C2···O3$^{\text{inter}}$ 3.075 Å					

Table A.32: Selected interactions within the crystal structure of 1-(3,5-dinitro-1,2,4-triazol-1-yl)-2-nitrazapropane (**33**).

D−H···A	d(D−H) [Å]	d(H···A) [Å]	d(D···A) [Å]	∠(D−H···A) [°]	
C3−H4C···N3	0.957	2.562	3.357	140.63	inter
C4−H4A···O4	0.937	2.476	3.192	133.34	inter
C4−H4B···O5	0.989	2.590	3.414	140.77	inter
C3−H3A···N3	0.946	2.508	3.442	169.34	inter
C4−H4C···O2	0.957	2.602	3.493	155.18	inter
dipolar interactions ΣvdW radii (N···O) < 3.07 Å [2] N5···O5^{inter} 2.924 Å; N5···O1^{inter} 2.950 Å					
dipolar interactions ΣvdW radii (C···O) < 3.22 Å [2] C3···O4^{intra} 2.806 Å; C2···O1^{inter} 2.862 Å; C4···O3^{inter} 3.036 Å					

Table A.33: Selected interactions within the crystal structure of 1-(5-amino-3-nitro-1,2,4-triazol-1-yl)-2-nitrazapropane (**34**).

D−H···A	d(D−H) [Å]	d(H···A) [Å]	d(D···A) [Å]	∠(D−H···A) [°]	
N5−H5A···O2	0.84(2)	2.39(2)	3.046(2)	135.2(17)	intra
C2−H2B···O3	0.96(2)	2.39(2)	3.208(2)	141.8(13)	inter
N5−H5B···N1	0.86(2)	2.18(2)	3.025(2)	167.2(19)	inter
C1−H1B···O3	0.93(3)	2.47(3)	3.238(2)	140(3)	inter
C2−H2A···O4	1.00(2)	2.47(2)	3.395(2)	154.4(14)	inter
N5−H5A···O4	0.84(2)	2.49(2)	3.221(2)	145.6(18)	inter
C1−H1A···O2	0.93(3)	2.539(3)	3.454(2)	171(2)	inter

Table A.34: Selected interactions within the crystal structure of 5,5′-bi(1-(2-nitrazapropan-1-yl)-3-nitro-1,2,4-triazole) (**35**).

D−H···A	d(D−H) [Å]	d(H···A) [Å]	d(D···A) [Å]	∠(D−H···A) [°]	
C3−H3A···N1'	0.95(2)	2.37(2)	3.097(3)	133.8(16)	intra
C4−H4C···O1	0.98(3)	2.52(3)	3.385(4)	146.8(25)	inter
C3−H3B···O1	0.98(2)	2.54(2)	3.473(3)	159.8(16)	inter
C4−H4B···O1	0.95(3)	2.88(3)	3.525(4)	126.6(19)	inter
C4−H4A···O3	0.89(3)	2.59(3)	3.315(3)	139.5(23)	inter
dipolar interactions ΣvdW radii (N···O) < 3.07 Å [2] N3···O3^{intra} 2.935(2) Å; N3···O4^{inter} 2.955(2) Å					
dipolar interactions ΣvdW radii (C···O) < 3.22 Å [2] C1′···O3^{intra} 3.082(2) Å; C3···O4^{inter} 2.920(2) Å					
dipolar interactions ΣvdW radii (C···N) < 3.25 Å [2] C3···N1^{intra} 3.097(3) Å					

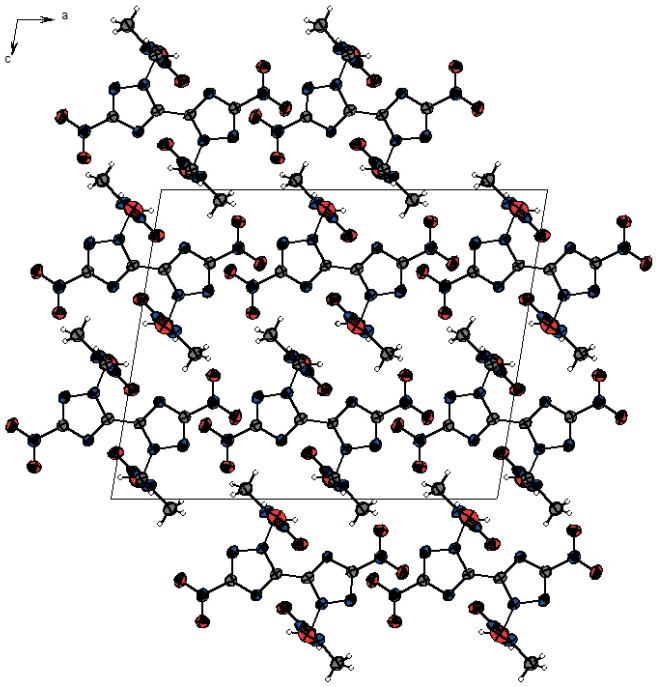

Figure A.17: Crystal structure of 5,5′-bi(1-(2-nitrazapropan-1-yl)-3-nitro-1,2,4-triazole) (**35**) along the *b* axis; thermal ellipsoids of non-hydrogen atoms are drawn at the 50% probability level.

Table A.35: Selected interactions within the crystal structure of 1-(2,4-dinitroimidazol-1-yl)-2-nitrazapropane (**36**).

D−H···A	d(D−H) [Å]	d(H···A) [Å]	d(D···A) [Å]	∠(D−H···A) [°]	
C5−H5A···O1	1.010	2.426	3.113	124.61	intra
C3−H3···O3	0.969	2.579	3.241	125.58	inter
dipolar interactions ΣvdW radii (N···O) < 3.07 Å [2] N6···O2^{inter} 2.886 Å; N5···O2^{inter} 2.901 Å; N6···O6^{inter} 3.028 Å					
dipolar interactions ΣvdW radii (C···O) < 3.22 Å [2] C1···O6^{inter} 2.946 Å; C4···O4^{inter} 3.032 Å; C4···O2^{inter} 3.168 Å					

Table A.36: Selected interactions within the crystal structure of 1-(4,5-dinitroimidazol-1-yl)-2-nitrazapropane (**37**).

D−H···A	d(D−H) [Å]	d(H···A) [Å]	d(D···A) [Å]	∠(D−H···A) [°]	
C4−H4A···O4	0.950	2.339	2.986	124.90	intra
C4−H4B···O5	0.967	2.456	3.398	164.76	inter
C5−H5C···O6	0.975	2.534	3.355	141.73	inter
C5−H5B···N2	1.003	2.589	3.446	143.41	inter
C1−H1A···O1	0.906	2.605	3.482	163.09	inter
C1−H1A···O2	0.906	2.657	3.356	134.66	inter
C4−H4A···O6	0.950	2.691	3.457	138.05	inter
dipolar interactions ΣvdW radii (N···O) < 3.07 Å [2] N4···O6^{inter} 2.963 Å; N6···O1^{inter} 2.992 Å; N5···O4^{inter} 3.005 Å N4···O2^{intra} 3.042 Å; N4···O5^{intra} 2.705 Å					
dipolar interactions ΣvdW radii (C···O) < 3.22 Å [2] C4···O4^{inter} 3.039 Å; C5···O4^{inter} 3.154 Å; C3···O1^{inter} 3.188 Å; C2···O1^{inter} 3.204 Å					

Table A.37: Selected interactions within the crystal structure of 1-(3,5-dinitropyrazol-1-yl)-2-nitrazapropane (**38**).

D−H···A	d(D−H) [Å]	d(H···A) [Å]	d(D···A) [Å]	∠(D−H···A) [°]	
C2−H2B···O7	0.994	2.234	3.194	161.91	inter
C2−H2A···O1	0.992	2.273	2.970	126.31	intra
C7−H7A···O6	0.964	2.322	3.133	141.37	inter
C6−H6···O2	0.916	2.410	3.111	133.33	inter
C7−H7B···O6	0.942	2.667	3.572	161.43	inter
dipolar interactions ΣvdW radii (N···O) < 3.07 Å [2] N6···O9^{inter} 2.913 Å					
dipolar interactions ΣvdW radii (C···O) < 3.22 Å [2] C9···O5^{inter} 2.906 Å; C4···O9^{inter} 3.033 Å; C9···O3^{inter} 3.033 Å C8···O7^{inter} 3.060 Å; C4···O11^{inter} 3.061 Å; C2···O4^{inter} 3.112 Å					

Table A.38: Selected interactions within the crystal structure of 1-(3,4-dinitropyrazol-1-yl)-2-nitrazapropane (**39**).

D−H···A	d(D−H) [Å]	d(H···A) [Å]	d(D···A) [Å]	∠(D−H···A) [°]	
C4−H4B···O2	0.940	2.279	3.155	154.74	inter
C4−H4A···O25	1.073	2.428	3.371	145.99	inter
C24−H24A···O26	0.919	2.444	3.359	173.63	inter
C23−H23···O5	0.909	2.473	3.270	146.50	inter
C24−H24B···O1	0.975	2.478	3.385	154.51	inter
C3−H3A···O29	0.943	2.587	3.444	151.33	inter
dipolar interactions ΣvdW radii (N···O) < 3.07 Å [2] N30···O27$^{\text{inter}}$ 2.817 Å; N3···O4$^{\text{inter}}$ 2.849 Å; N27···O28$^{\text{inter}}$ 2.893 Å					
dipolar interactions ΣvdW radii (C···O) < 3.22 Å [2] C21···O28$^{\text{inter}}$ 3.040 Å; C24···O29$^{\text{inter}}$ 3.086 Å; C3···O6$^{\text{inter}}$ 3.113 Å					

Table A.39: Selected interactions within the crystal structure of 1-(3,4,4′-trinitro-1,3′-bipyrazol-2′-yl)-2-nitrazapropane (**40**).

D−H···A	d(D−H) [Å]	d(H···A) [Å]	d(D···A) [Å]	∠(D−H···A) [°]	
C4−H4···O1	0.953	2.159	3.021	149.81	inter
C2−H2B···N9	0.978	2.463	3.135	125.56	intra
C2−H2A···N9	0.975	2.514	3.279	135.24	inter
C2−H2B···O6	0.978	2.526	3.255	131.26	inter
C1−H1A···O3	0.997	2.621	3.430	138.30	inter
C3−H3A···N2	0.957	2.702	3.416	131.95	inter
dipolar interactions ΣvdW radii (N···O) < 3.07 Å [2] N7···O8$^{\text{inter}}$ 2.921 Å					
dipolar interactions ΣvdW radii (C···O) < 3.22 Å [2] C6···O8$^{\text{inter}}$ 3.114 Å					

Table A.40: Selected interactions within the crystal structure of 1-(5-chloro-3,4-dinitropyrazol-1-yl)-2-nitrazapropane (**41**).

D−H···A	d(D−H) [Å]	d(H···A) [Å]	d(D···A) [Å]	∠(D−H···A) [°]	
C1−H1C···O6	0.911	2.461	3.266	147.32	inter
C2−H2B···O2	0.957	2.550	3.431	153.00	inter
C2−H2A···O5	0.931	2.607	3.062	110.63	inter
C2−H2A···O1	0.931	2.635	3.263	125.33	inter
dipolar interactions ΣvdW radii (N···O) < 3.07 Å [2] N6···O3^{inter} 2.886 Å					
dipolar interactions ΣvdW radii (C···O) < 3.22 Å [2] C2···O5^{inter} 3.062 Å					

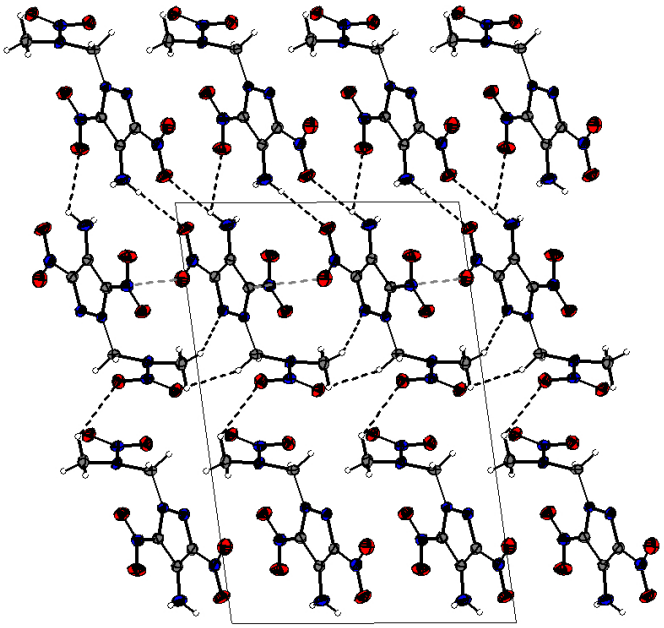

Figure A.18: Unit cell of 1-(4-amino-3,5-dinitropyrazol-1-yl)-2-nitrazapropane (**42**) along the *b* axis; non-classical hydrogen bonds are shown black dotted and dipolar C···O interactions are shown grey dotted; thermal ellipsoids of non-hydrogen atoms are drawn at the 50% probability level.

Table A.41: Selected crystallographic data of nitramines **31**–**34**

	31	**32**	**33**	**34**
Molecular formula	$C_4H_6N_6O_5$	$C_6H_{10}N_8O_7 \cdot HNO_3$	$C_4H_5N_7O_6$	$C_4H_7N_7O_4$
M [g mol^{-1}]	218.13	369.24	247.13	217.14
Color	colorless	colorless	colorless	colorless
Habit	block	block	block	plate
Crystal size [mm]	0.31×0.21×0.19	0.30×0.22×0.16	0.38×0.26×0.17	0.58×0.48×0.05
Crystal system	monoclinic	monoclinic	monoclinic	triclinic
Space group	$P2_1$	$P2_1$	Cc	$P\bar{1}$
a [Å]	6.7610(6)	10.828(2)	15.831(4)	6.3027(8)
b [Å]	5.5064(6)	5.5849(11)	7.0572(7)	6.8628(8)
c [Å]	11.3925(10)	12.363(3)	11.133(3)	10.6253(14)
α [°]	90	90	90	72.876(11)
β [°]	97.072(9)	107.59(3)	132.07(4)	87.968(11)
γ [°]	90	90	90	77.540(11)
V [Å^3]	420.90(7)	712.6(2)	923.3(11)	428.68(10)
Z	2	2	4	2
$\rho_{\text{calc.}}$ [g cm^{-3}]	1.721	1.721	1.778	1.682
T [K]	173	173	173	173
$F(000)$	224	380	504	224
μ [mm^{-1}]	0.157	0.162	0.165	0.148
Absorption correction	multi-scan	multi-scan	multi-scan	multi-scan
Index range	$-4 \leq h \leq 8$	$-13 \leq h \leq 11$	$-21 \leq h \leq 20$	$-7 \leq h \leq 7$
	$-6 \leq k \leq 6$	$-6 \leq k \leq 6$	$-9 \leq k \leq 5$	$-8 \leq k \leq 8$
	$-14 \leq l \leq 13$	$-15 \leq l \leq 12$	$-12 \leq l \leq 14$	$-13 \leq l \leq 13$
θ min/max [°]	4.42/26.30	4.15/26.37	4.81/28.95	4.33/25.99
λ MoK$_\alpha$ [Å]	0.71073	0.71073	0.71073	0.71073
Measured reflections	2241	3846	1895	4326
Independent reflections	1644	2832	1260	1671
Observed reflections	1177	2094	957	1330
Parameters	160	270	174	164
R_1 (all data)	0.0567	0.0529	0.0472	0.0466
R_1 (obs.)	0.0344	0.0349	0.0306	0.0332
wR_2 (all data)	0.0527	0.0611	0.0547	0.0839
wR_2 (obs.)	0.0488	0.0577	0.0515	0.0755
GOF	0.840	0.865	0.895	1.073
Res. dens. min. [e Å^{-3}]	−0.13	−0.16	−0.16	−0.28
Res. dens. max. [e Å^{-3}]	0.17	0.18	0.14	0.05
Solution	SIR92	SIR92	SIR97	SIR92
Refinement	SHELXL-97	SHELXL-97	SHELXL-97	SHELXL-97
Measurement	fx530	fx528	fx408	gx534
CCDC number	1439321	1439320	1439317	1439314

Table A.42: Selected crystallographic data of nitramines **35**–**38**

	35	**36**	**37**	**38**
Molecular formula	$C_8H_{10}N_{12}O_8$	$C_5H_6N_6O_6$	$C_5H_6N_6O_6$	$C_5H_6N_6O_6$
M [g mol^{-1}]	402.28	246.14	246.14	246.14
Color	colorless	colorless	colorless	colorless
Habit	plate	block	block	block
Crystal size [mm]	0.20×0.17×0.08	0.29×0.24×0.13	0.33×0.21×0.18	0.40×0.35×0.15
Crystal system	monoclinic	monoclinic	monoclinic	triclinic
Space group	$C2/c$	$P2_1/c$	Cc	$P\bar{1}$
a [Å]	17.5192(17)	11.4913(12)	5.7787(8)	8.2316(5)
b [Å]	6.4082(6)	6.9525(5)	20.764(3)	9.5937(5)
c [Å]	14.2000(14)	12.8652(11)	7.7190(11)	12.7855(7)
α [°]	90	90	90	93.595(4)
β [°]	99.184(9)	113.537(10)	92.393(12)	102.892(5)
γ [°]	90	90	90	96.844(4)
V [Å^3]	1573.7(3)	942.33(14)	925.4(4)	973.06(9)
Z	4	4	4	4
$\rho_{\text{calc.}}$ [g cm^{-3}]	1.698	1.735	1.767	1.680
T [K]	173	173	173	173
$F(000)$	824	504	504	504
μ [mm^{-1}]	0.151	0.159	0.162	0.154
Absorption correction	multi-scan	multi-scan	multi-scan	multi-scan
Index range	$-17 \leq h \leq 21$	$-14 \leq h \leq 11$	$-7 \leq h \leq 7$	$-10 \leq h \leq 10$
	$-7 \leq k \leq 5$	$-8 \leq k \leq 8$	$-26 \leq k \leq 14$	$-11 \leq k \leq 11$
	$-16 \leq l \leq 17$	$-12 \leq l \leq 16$	$-10 \leq l \leq 8$	$-15 \leq l \leq 15$
θ min/max [°]	4.34/25.57	4.24/26.37	4.43/27.49	4.23/26.37
λ MoK$_\alpha$ [Å]	0.71073	0.71073	0.71073	0.71073
Measured reflections	3779	4194	2573	10170
Independent reflections	1472	1920	1820	3961
Observed reflections	1102	1157	1216	2844
Parameters	147	178	167	356
R_1 (all data)	0.0627	0.0635	0.0653	0.0480
R_1 (obs.)	0.0858	0.0322	0.0388	0.0316
wR_2 (all data)	0.1022	0.0680	0.0834	0.0797
wR_2 (obs.)	0.0895	0.0630	0.0782	0.0755
GOF	1.043	0.835	0.861	0.943
Res. dens. min. [e Å^{-3}]	−0.19	−0.21	−0.30	−0.20
Res. dens. max. [e Å^{-3}]	0.25	0.17	0.19	0.22
Solution	SIR92	SIR92	SIR92	SIR97
Refinement	SHELXL-2014	SHELXL-97	SHELXL-2014	SHELXL-97
Measurement	gx685	fx520	fx488	fx615
CCDC number	1439315	1439319	1439318	1439310

Table A.43: Selected crystallographic data of nitramines **39**–**42**

	39	**40**	**41**	**42**
Molecular formula	$C_5H_6N_6O_6$	$C_8H_7N_9O_8$	$C_5H_5ClN_6O_6$	$C_5H_7N_7O_6$
M [g mol^{-1}]	246.14	357.20	280.58	261.15
Color	colorless	colorless	colorless	yellow
Habit	plate	block	bar	block
Crystal size [mm]	0.40×0.30×0.05	0.25×0.20×0.15	0.60×0.20×0.10	0.15×0.15×0.04
Crystal system	monoclinic	triclinic	monoclinic	monoclinic
Space group	$P2_1/c$	$P\bar{1}$	$P2_1/c$	$P2_1/c$
a [Å]	17.1342(16)	8.5617(9)	5.6441(6)	15.9508(16)
b [Å]	9.3680(8)	9.3986(9)	12.0820(12)	5.6426(7)
c [Å]	12.5388(12)	9.7876(10)	15.3446(15)	10.6832(11)
α [°]	90	113.277(9)	90	90
β [°]	107.400(10)	106.073(9)	98.068(10)	97.579(9)
γ [°]	90	92.266(8)	90	90
V [Å^3]	1920.5(3)	685.23(12)	1036.02(18)	953.13(18)
Z	8	2	4	4
$\rho_{\text{calc.}}$ [g cm^{-3}]	1.703	1.731	1.799	1.820
T [K]	173	173	173	173
$F(000)$	1008	364	568	536
μ [mm^{-1}]	0.156	0.155	0.406	0.165
Absorption correction	multi-scan	multi-scan	multi-scan	multi-scan
Index range	$-20 \leq h \leq 15$	$-10 \leq h \leq 10$	$-7 \leq h \leq 7$	$-18 \leq h \leq 18$
	$-11 \leq k \leq 10$	$-5 \leq k \leq 11$	$-15 \leq k \leq 15$	$-4 \leq k \leq 6$
	$-15 \leq l \leq 14$	$-12 \leq l \leq 11$	$-19 \leq l \leq 19$	$-11 \leq l \leq 12$
θ min/max [°]	4.18/25.35	4.35/26.37	4.21/26.37	4.21/25.00
λ MoK$_\alpha$ [Å]	0.71073	0.71073	0.71073	0.71073
Measured reflections	9206	3705	10410	3330
Independent reflections	3495	2777	2100	1684
Observed reflections	1592	1700	1327	1368
Parameters	332	254	183	143
R_1 (all data)	0.1104	0.0680	0.0647	0.0535
R_1 (obs.)	0.0375	0.0356	0.0335	0.0404
wR_2 (all data)	0.0575	0.0696	0.0723	0.1026
wR_2 (obs.)	0.0492	0.0640	0.0669	0.0910
GOF	0.728	0.822	0.849	1.111
Res. dens. min. [e Å^{-3}]	−0.20	−0.18	−0.20	−0.28
Res. dens. max. [e Å^{-3}]	0.17	0.20	0.27	0.20
Solution	SIR97	SIR92	SIR92	SIR92
Refinement	SHELXL-2014	SHELXL-97	SHELXL-97	SHELXL-2014
Measurement	gx036	gx141	gx173	hx326
CCDC number	1439311	1439312	1439313	1439316

A.9 Supporting Information for Chapter 11

Crystallographic Data

Table A.44: Selected interactions within the crystal structure of 1-(4-nitro-1,2,5-oxadiazol-3-yl)-1,3-dinitrazabutane (**44**).

D−H···A	d(D−H) [Å]	d(H···A) [Å]	d(D···A) [Å]	∠(D−H···A) [°]
C3−H3B···O6^{i}	0.975(19)	2.276(19)	3.2193(16)	162.6(16)
C4−H4C···O4^{ii}	0.92(2)	2.65(2)	3.488(2)	152.1(17)
dipolar interactions ΣvdW radii (N···O) < 3.07 Å [2] N2···O3^{iv} 2.8778(17) Å				
dipolar interactions ΣvdW radii (C···O) < 3.22 Å [2] C2···O6 2.7974(17) Å; C4···O3^{iii} 2.9955(19) Å				

Symmetry codes: (i) $x, 0.5-y, 0.5+z$; (ii) $2-x, -y, 1-z$; (iii) $1+x, y, 1+z$; (iv) $x, y, 1+z$.

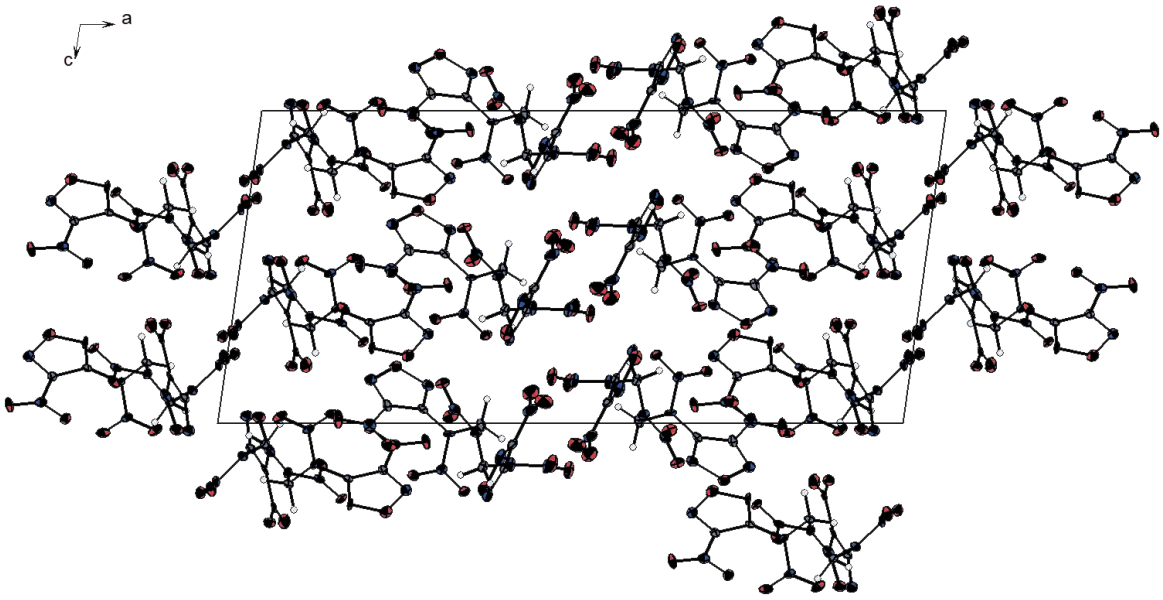

Figure A.19: Unit cell of 1,5-bis(4-nitrofurazan-3-yl)-1,3,5-trinitrazapentane (**45**) along the b axis.

Table A.45: Selected interactions within the crystal structure of 1,5-bis(4-nitrofurazan-5-yl)-1,3,5-trinitrazapentane (**45**).

D−H···A	d(D−H) [Å]	d(H···A) [Å]	d(D···A) [Å]	∠(D−H···A) [°]
C4−H4B···O5	0.991(5)	2.342(4)	3.036(7)	126.4(3)
C10−H10A···O21^{i}	0.990(5)	2.406(4)	3.382(6)	168.4(3)
C10−H10B···O16^{ii}	0.992(5)	2.373(4)	3.223(7)	143.3(3)
C9−H9B···O13^{iii}	0.991(6)	2.459(4)	3.381(7)	154.5(3)
C9−H9B···O14^{iii}	0.991(6)	2.612(5)	3.414(8)	138.1(3)
C3−H3A···O5^{iii}	0.989(6)	2.583(4)	3.531(7)	160.4(3)
C3−H3A···O9^{iv}	0.989(6)	2.596(4)	3.235(7)	122.3(3)
C4−H4A···N23^{v}	0.990(6)	2.563(4)	3.540(7)	169.1(3)
C4−H4B···O12^{v}	0.991(5)	2.526(5)	3.243(7)	129.0(3)
dipolar interactions ΣvdW radii (N···O) < 3.07 Å N2···O19 2.956(6) Å				
dipolar interactions ΣvdW radii (C···O) < 3.22 Å C11···O19 2.864(7) Å				

Symmetry codes: (i) $x, 0.5-y, -0.5+z$; (ii) $2-x, -0.5+y, 1.5-z$; (iii) $x, 1.5-y, 0.5+z$; (iv) $1-x, 1-y, 1-z$; (v) $x, 0.5-y, -0.5+z$.

Table A.46: Selected crystallographic data of **44** and **45**.

	44	**45**
Molecular formula	$C_4H_5N_7O_7$	$C_6H_4N_{12}O_{12}$
M [g mol^{-1}]	263.15	436.21
Color	colorless	colorless
Habit	block	rod
Crystal size [mm]	0.24×0.17×0.05	0.10×0.06×0.05
Crystal system	monoclinic	monoclinic
Space group	$P2_1/c$	$P2_1/c$
a [Å]	9.3960(5)	25.606(1)
b [Å]	18.9399(7)	9.999(4)
c [Å]	5.6677(2)	11.780(6)
α [°]	90	90
β [°]	102.619(4)	97.976(2)
γ [°]	90	90
V [Å^3]	984.26(7)	2987(2)
Z	4	8
$\rho_{\text{calc.}}$ [g cm^{-3}]	1.776	1.940
T [K]	173	100
$F(000)$	536	1760
μ [mm^{-1}]	0.168	0.187
Absorption correction	multi-scan	multi-scan
Index range	$-11 \leq h \leq 11$	$0 \leq h \leq 30$
	$-23 \leq k \leq 23$	$0 \leq k \leq 12$
	$-7 \leq l \leq 7$	$-14 \leq l \leq 14$
θ min/max [°]	4.27/26.37	3.00/26.42
λ MoK$_\alpha$ [Å]	0.71073	0.71073
Measured reflections	14425	6274
Independent reflections	1999	6274
Observed reflections	1722	5843
Parameters	178	542
R_1 (all data)	0.0361	0.0934
R_1 (obs.)	0.0294	0.0756
wR_2 (all data)	0.0796	0.1579
wR_2 (obs.)	0.0756	0.149
GOF	1.032	1.317
Res. dens. min. [e Å^{-3}]	−0.18	−0.47
Res. dens. max. [e Å^{-3}]	0.22	0.46
Solution	SIR97	SIR97
Refinement	SHELXL-97	SHELXL-97
Measurement	kx290	tv456
CCDC number	1451844	1451845

A.10 References

[1] M. Hesse, H. Meier, B. Zeeh, *Spektroskopische Methoden in der organischen Chemie*, 7th ed., Thieme, Stuttgart, Germany, **2005**.

[2] A. Bondi, *J. Phys. Chem.* **1964**, *68*, 441–451.

[3] G. I. Sunhahara, S. Dodard, M. Sarrazin, L. Paquet, G. Ampleman, S. Thiboutot, J. Hawari, A. Y. Renoux, *Ecotox. Environ. Safe.* **1998**, *39*, 185–194.

[4] V. V. Mel'nikov, V. V. Stolpakova, M. S. Pevzner, *Khim. Geterotsikl. Soedin.* **1971**, *3*, 414–417.

A.11 Abbreviations and Formula Symbols

Abbreviations

BAM	*Bundesanstalt für Materialforschung und -prüfung*
br	broad (IR and NMR)
CAB	cellulose acetate butyrate
CJ	Chapman-Jouguet point
CL-20	2,4,6,8,10,12-hexanitrohexaazaisowurtzitane
d	doublet (NMR)
DDT	detonation-to-deflagration transition
DEI	direct electron ionization
DMSO	dimethylsulfoxide
DSC	differential scanning calorimetry
DTA	differential thermal analysis
EA	elemental analysis
EPA	Environmental Protection Agency
EPR	electron paramagnetic resonance
ESD	electrostatic discharge
ESP	electrostatic potential
FAB	fast atom bombardment
FOX-7	1,1-diamino-2,2-dinitroethene
FOX-12	*N*-guanylurea dinitramide (GUDN)
FS	friction sensitivity
GOF	goodness of fit
HE	high (secondary) explosive
HEDM	high energy-dense material
HMX	high melting explosive (1,3,5,7-tetranitro-1,3,5,7-tetrazocane)
HN-1/2	High-Nitrogen 1/2 (gun propellant mixtures)
ICT	Institut für Chemische Technologie
IM	insensitive munition
IR	infrared spectroscopy
IS	impact sensitivity
KDNP	potassium salt of 7-hydroxy-4,6-dinitrobenzofuroxan
LA	lead azide
LOVA	low-vulnerability
LS	lead styphnate
M^+	molecule peak (MS)

M	molar ($\mathrm{mol\,L^{-1}}$)
m	medium (IR), multiplet (NMR)
MF	mercury fulminate
MMH	monomethylhydrazine
MS	mass spectrometry
NMR	nuclear magnetic resonance
PBX	polymer bonded explosive
PE	polyethylene
PETN	pentaerythritol tetranitrate
ppm	parts per million
RDX	royal demolitions explosive (1,3,5-trinitro-1,3,5-triazinane)
s	strong (IR), singlet (NMR)
SII	simple initiating impulse
TAGzT	bistriaminoguanidinium 5,5′-azobistetrazolate
TATB	2,4,6-triamino-1,3,5-trinitrobenzene
TNT	2,4,6-trinitrotoluene
TTA	2,4,6-triazido-1,3,5-triazine
t	triplet (NMR)
UN	United Nations
VNS	vicarious nucleophilic substitution
vs	very strong (IR)
vw	very weak (IR)
w	weak (IR)

Formula Symbols

δ	isotropic chemical shift
D	detonation velocity
${}^{n}J$	coupling constant over n nuclei
m/z	mass per charge
M	molar mass
N	nitrogen content
n	amount of substance
$\tilde{\nu}$	wave number
Ω	oxygen balance
p_{CJ}	detonation pressure
Q_{v}	heat of explosion

ρ	density
T_{dec}	decomposition temperature
T_{dehyd}	dehydration temperature
T_{det}	detonation temperature
T_{ex}	explosion temperature
T_{melt}	melting temperature
V_0	volume of detonation gases

A.12 Bibliography

Peer-reviewed Publications

T. M. Klapötke, B. Krumm, C. Pflüger
"Isolation of a Moderately Stable but Sensitive Zwitterionic Diazonium Tetrazolyl-1,2,3-triazolate"
J. Org. Chem. **2016**, *81*, 6123–6127.

T. M. Klapötke, A. Penger, C. Pflüger, J. Stierstorfer
"Melt-cast Materials: Combining the Advantages of Highly Nitrated Azoles and Open-chain Nitramines"
New J. Chem. **2016**, *40*, 6059–6069.

D. Izsák, T. M. Klapötke, F. H. Lutter, C. Pflüger
"Tailoring the Energetic Properties of 5-(5-Amino-1,2,3-triazol-4-yl)tetrazole and Its Derivatives by Salt Formation: From Sensitive Primary to Insensitive Secondary Explosives"
Eur. J. Inorg. Chem. **2016**, 1720–1729.

A. A. Dippold, D. Izsák, T. M. Klapötke, C. Pflüger
"Combining the Advantages of Tetrazoles and 1,2,3-Triazoles: 4,5-Bis(tetrazol-5-yl)-1,2,3-triazole, 4,5-Bis(1-hydroxy-tetrazol-5-yl)-1,2,3-triazole and Their Energetic Derivatives"
Chem. Eur. J. **2016**, *22*, 1768–1778.

T. M. Klapötke. C. Pflüger, M. W. Reintinger
"Energetic Materials based on 5,7-Dinitrobenzotriazole and 4,6-Dinitrobenzotriazol-3-ium 1-oxide Derivatives"
Eur. J. Inorg. Chem. **2016**, *1*, 138–147.

D. Ehlers, T. M. Klapötke, C. Pflüger
"Investigations of the Vicarious *C*-Aminations of 5,7-Dinitrobenzotriazole and 4,6-Dinitrobenzotriazol-3-ium-1-oxide and Their Energetic Properties"
Chem. Eur. J. **2015**, *21*, 16073–16082.

D. Izsák, T. M. Klapötke, C. Pflüger
"Energetic Derivatives of 5-(5-Amino-2*H*-1,2,3-triazol-4-yl)-1*H*-tetrazole"
Dalton. Trans. **2015**, *44*, 17054–17063.

T. M. Klapötke, A. Penger, C. Pflüger, J. Stierstorfer, M. Sućeska
"Advanced Open-chain Nitramines as Energetic Materials: Heterocyclic-substituted 1,3-Dichloro-2-nitrazapropane"
Eur. J. Inorg. Chem. **2013**, *26*, 4667–4678.

E. Schuh, C. Pflüger, A. Citta, A. Folda, M. P. Rigobello, A. Bindoli, A. Casini, F. Mohr
"Gold(I) Carbene Complexes causing Thioredoxin 1 and Thioredoxin 2 Oxidation as Potential Anticancer Agents"
J. Med. Chem. **2012**, *55*, 5518–5528.

Poster Presentations

D. Izsák, T. M. Klapötke, C. Pflüger
"Energetic Derivatives of 5-(5-Amino-2*H*-1,2,3-triazol-4-yl)-1*H*-tetrazole"
18th New Trends in Research of Energetic Materials, *Proceedings of the Seminar*, Pardubice, Czech Republic, **2015**, *2*, 573–592.

C. Evangelisti, D. Keefer, T. M. Klapötke, C. Pflüger, F. D. Speck
"Characterization and Bomb Calorimetric Studies of Different N-rich Heterocyclic Compounds"
45th International Annual Conference of the Fraunhofer Institute ICT, Karlsruhe, Germany, **2014**, 117/1–117/7.

T. M. Klapötke, C. Pflüger
"Zwitterionic Explosives based on 4,6-Dinitrobenzotriazol-3-ium-1-oxide"
17th New Trends in Research of Energetic Materials, *Proceedings of the Seminar*, Pardubice, Czech Republic, **2014**, *2*, 754–768.

T. M. Klapötke, C. Pflüger, M. W. Reintinger
"Low Sensitivity Secondary Explosives based on 5,7-Dinitrobenzotriazole and 4,6-Diamino-5,7-dinitrobenzotriazole"
16th New Trends in Research of Energetic Materials, *Proceedings of the Seminar*, Pardubice, Czech Republic, **2013**, *2*, 842–856.

Thomas M. Klapötke, Alexander Penger, Carolin Pflüger
"Modified Nitramines with Low Sensitivity"
14th New Trends in Research of Energetic Materials, *Proceedings of the Seminar*, Pardubice, Czech Republic, **2011**, *2*, 753–761.